UNIWERSYTET PRZYRODNICZY WE WROCŁAWIU

mgr inż. Kacper Świechowski

Waloryzacja odpadów i biomasy o niskich wartościach energetycznych w procesie toryfikacji

Valorization of low energy waste and biomass in the torrefaction process

Praca doktorska

wykonana w

Katedrze Biogospodarki Stosowanej

Wydział Przyrodniczo-Technologiczny

pod kierunkiem

promotora prof. dr hab. inż. Andrzeja Białowca

i

promotora pomocniczego dr inż. Sylwii Stegenty-Dąbrowskiej

Wrocław, 2022

Streszczenie

W pracy poddano analizie wpływ trzech kluczowych parametrów technologicznych (temperatury, czasu trwania procesu, ciśnienia) dla siedmiu materiałów odpadowych (drewno odpadowe, osad ściekowy, poferment z biogazowni, borowina, odchody słonia, oraz tworzywa biodegradowalne polilaktyd (PLA) i papier). Na podstawie badań laboratoryjnych uzyskane dane zostały częściowo opisane za pomocą modeli matematycznych. Natomiast pozostałe dane eksperymentalne opracowano poprzez zestawienie w sposób tabelaryczny i graficzny. Dla wszystkich analizowanych materiałów wyznaczono energię aktywacji z wykorzystaniem analizy termograwimetrycznej (TGA), ciepło właściwe oraz efekty cieplne przemian zachodzących w trakcie procesu z wykorzystaniem skaningowej kalorymetrii różnicowej (DSC). Badane materiały poddano toryfikacji w zakresie temperatur od 200°C do 300°C i czasach trwania procesu od 20 min do 60 min. Dodatkowo przeprowadzono toryfikację wybranych odpadów w nadciśnieniu dochodzącym do 10,5 bar z jednoczesnym pomiarem zużycia energii. Na podstawie wyników wykazano, że każdy z przebadanych materiałów charakteryzował się odmiennymi właściwościami paliwowymi. Wartości ciepła spalania nieprzetworzonych materiałów mieściły się w zakresie od 11410 $J \cdot g^{-1}$ do 19420 $J \cdot g^{-1}$, odpowiednio dla odchodów słonia i PLA. Dla większości materiałów, z wyjątkiem PLA i osadu ściekowego, zastosowanie toryfikacji bez nadciśnienia pozwoliło na zwiększenie zagęszczenia energii w toryfikatach od 12% (poferment 280°C i 20 min, borowina 280°C i 40 min, odchody słonia 200°C i 60 min, papier 300°C i 40 min) do 20% (drewno odpadowe 300°C i 40 min) względem nieprzetworzonego materiału. Ponadto zastosowanie nadciśnienia pozwoliło dodatkowo zwiększyć ciepło spalania w zakresie od 1,7% do 7% względem toryfikatów wytworzonych bez nadciśnienia. Wykazano także, że proces toryfikacji nie poprawia właściwości paliwowych PLA, a w przypadku osadu ściekowego zaobserwowano ich pogorszenie. Ponadto na podstawie bilansu masy i energii określono, że suche drewno odpadowe, osad ściekowy, poferment oraz papier można przetworzyć w sposób samowystarczalny energetycznie (w każdych warunkach technologicznych). Natomiast dla borowiny i odchodów słonia, proces może być samowystarczalny energetycznie tylko w przypadku temperatur większych niż 220°C i 240°C. Należy zaznaczyć, że po uwzględnieniu rzeczywistej zawartości wody w przetwarzanych materiałach, jak osad ściekowy, poferment i borowina wykazano, iż wykorzystanie ich w toryfikacji nie pozwala na samowystarczalność energetyczną procesu (bez względu na zastosowane parametry technologiczne). Z kolei drewno odpadowe, odchody słonia oraz papier, ze względu na względnie niską zawartość wilgoci oraz wystarczającą ilość wydzielanych części lotnych i zawartej w nich

energii chemicznej mogą być samowystarczalne energetycznie w temperaturach powyżej odpowiednio 240°C, 263°C i 200°C.

Streszczenie w języku angielskim

The paper determines the influence of technological parameters of the torrefaction of low energy waste and biomass on the amount of torrefied material, its fuel properties, and the energy consumption of the process. The study investigated the impact of the 3 most important technological parameters (temperature, process duration, pressure) on 7 waste materials (waste wood, sewage sludge, biogas digestate, peloid, elephant excrement, and biodegradable polylactide and paper). The effect of the parameters has been described by mathematical models developed from the experimental data and by compiling the experimental data into tables and figures. The research was carried out in laboratory conditions. For all tested materials, the activation energy was determined using thermogravimetric analysis (TGA), also specific heat and thermal effects of changes taking place during the process were determined using differential scanning calorimetry (DSC). The tested materials were torrefied in the temperature range from 200°C to 300°C and the duration of the process from 20 minutes to 60 minutes. In addition, selected wastes were torrefied in an overpressure of up to 10,5 bar with the simultaneous measurement of energy consumption. The results showed that each of the tested materials was characterized by different fuel properties and the requirements of technological parameters ensuring the production of torrefaction with the best fuel properties. The high heating value of raw materials ranged from 11410 $J \cdot g^{-1}$ to 19420 $J \cdot g^{-1}$ for elephant dung and PLA, respectively. For most materials, except for PLA and sewage sludge, the use of torrefaction without overpressure allowed to increase the energy concentration in the torrefied materials by 12% (digestate 280°C and 20 min, peloid 280°C and 40 min, elephant dung 200°C and 60 min, paper 300°C and 40 min) and by 20% (waste wood 300°C and 40 min) relative to the untreated material. Moreover, the use of overpressure allowed to additionally increase the high heating value in the range from 1,7% to 7% concerning torrefied materials produced without overpressure. It has also been shown that the torrefaction process does not improve the fuel properties of PLA, and their deterioration was observed in the case of sewage sludge. Moreover, the performed mass and energy balance showed that dry waste wood, sewage sludge, digestate, and paper can be processed in an energy self-sufficient way in all technological conditions, while for peloid and elephant dung, the process can be energy self-sufficient only at temperatures higher than 220°C and 240°C. However, after taking into account the actual water content in the processed materials, such as sewage sludge, digestate, and peloid, it has been shown that their use in torrefaction does not allow for energy self-sufficiency of the process, regardless of the technological parameters used. On the other hand, waste wood, elephant dung, and paper, due to their relatively low moisture content and a sufficient amount

of released volatile matter and the chemical energy they contain, can be energy self-sufficient at temperatures above 240°C, 263°C, and 200°C, respectively.

Spis treści

1 Wprowadzenie

Wraz z rozwojem gospodarczym zwiększa się ilość wytwarzanych odpadów oraz ich negatywne oddziaływanie na środowisko. Część odpadów może być ponownie wykorzystana w tym poddana recyklingowi, podczas gdy inne odpady, ze względu na swoje właściwości, obecny stan prawny, czynniki ekonomiczne i dostępne technologie poddawane są unieszkodliwianiu [1–3]. Zgodnie z hierarchią postępowania z odpadami zawartą w dyrektywie 2008/98/WE, odpady których produkcji nie udało się uniknąć, należy poddać innym procesom recyklingu, w tym odzysku energii, a jeżeli jest to niemożliwe, procesowi unieszkodliwienia poprzez składowanie na składowisku odpadów [4]. Jednym z procesów, który może służyć do recyklingu jak i przygotowania odpadów do odzysku energii jest toryfikacja. Toryfikacja to proces stosowany pierwotnie do zwiększania wartości energetycznej drewna oraz do produkcji kawy (prażenia kawy). W procesie toryfikacji, materiał jest poddawany oddziaływaniu temperatury z zakresu od 200°C do 300°C w atmosferze gazu inertnego [5]. W efekcie oddziaływania temperatury część materii organicznej ulega rozkładowi i odgazowaniu w postaci palnego niskokalorycznego gazu zwanego torgazem. W rezultacie odgazowania, pierwotna masa materiału poddanego toryfikacji ulega zmniejszeniu o około 30% przy zachowaniu do 90% pierwotnej energii. Produkt procesowy (toryfikat) charakteryzuje się wyższą wartością energetyczną o około 20% względem nieprzetworzonego materiału. Ponadto torgaz stanowiący około 30% pierwotnej masy przetwarzanego materiału i zawierający około 10% pierwotnej energii może zostać wykorzystany jako źródło ciepła niezbędne do przeprowadzenia toryfikacji [6]. Ze względu na fakt, że proces toryfikacji prowadzi do zmniejszenia masy przetwarzanego materiału, zwiększenia zagęszczenia energii oraz właściwości hydrofobowych (materiał chłonie mniej wody), toryfikacja wydaje się być rozwiązaniem, które zmniejszy masę odpadów konieczną do zagospodarowania i zwiększy ich potencjał energetyczny [7]. Jest to szczególnie istotne dla materiałów odpadowych charakteryzujących się niskimi wartościami energetycznymi, których obecne sposoby wykorzystania lub recyklingu są technicznie trudne, bądź ekonomicznie nieuzasadnione. Ponieważ toryfikacja tworzy nowy sposób ich energetycznego zagospodarowania poprzez konwersję w paliwo stałe [8,9].

Proces toryfikacji można podzielić na 5 etapów. Podczas etapu pierwszego, następuje wstępne ogrzanie materiału do 100°C, gdzie wraz z rosnącą temperaturą, z materiału zaczyna odparowywać woda. Gdy temperatura osiągnie 100°C, zaczyna się faza suszenia wstępnego, w której woda jest odparowywana w stałej temperaturze. Następnie, gdy większość wody zostanie usunięta w postaci pary wodnej, temperatura materiału zaczyna rosnąć. Podczas fazy dosuszania

od 100°C do 200°C z materiału poza wodą związaną fizycznie, odparowaniu ulega także część wody związanej chemicznie na skutek niszczenia wiązań chemicznych przetwarzanego materiału. Degradacji termicznej i odgazowaniu zaczynają ulegać również lekkie frakcje związków organicznych. Gdy temperatura materiału osiąga wartość 200°C zaczyna się etap 4 właściwej toryfikacji. Podczas toryfikacji materiał jest przetrzymywany w temperaturze z zakresu od 200°C do 300°C w czasie od kilku minut do kilku godzin. W czasie trwania toryfikacji przetwarzany materiał ulega odgazowaniu i karbonizacji (zagęszczeniu zawartości węgla w suchej masie). Następnie po osiągnięciu wymaganego stopnia konwersji, następuje etap chłodzenia, podczas którego temperatura wytworzonego toryfikatu jest obniżana do temperatury otoczenia [10].

Proces toryfikacji jest wykorzystywany przede wszystkim do waloryzacji właściwości energetycznych biomasy. Można wyróżnić podział procesu na przedziały temperaturowe ze względu na zmiany chemiczne zachodzące w przetwarzanym materiale. W zakresie od 50°C do 150°C następuje suszenie, które nie powoduje zmian w strukturze chemicznej materiału, przy czym powyżej 120°C zaczyna mięknąć lignina. W temperaturach od 150°C do 200°C zaczynają zachodzić nieodwracalne zmiany, następuje rozpad wiązań wodorowych i węglowych. W tej temperaturze dochodzi do depolimeryzacji hemicelulozy oraz częściowej depolimeryzacji lignin. W temperaturach od 200°C do 300°C dochodzi do częściowego odgazowania wynikającego przede wszystkim z termicznego rozkładu hemicelulozy. Dochodzi także do ograniczonej karbonizacji [11].

O ile proces toryfikacji drewna jest znany i został dogłębnie przebadany, znacznie mniej informacji można znaleźć na temat toryfikacji materiałów innych niż ligninocelulozowe z uwzględnieniem materiałów odpadowych [12,13]. Wraz z globalnie rosnącą produkcją odpadów i zwiększoną podażą energii, toryfikację zaczęto uważać za technologię mogącą ujednolicać zróżnicowane właściwości odpadów (np. zmieszanych odpadów komunalnych), celem ułatwienia wykorzystania ich w celach energetycznych. Większość dostępnych prac naukowych opisuje materiały rolnicze oraz określa właściwości paliwowe bez uwzględnienia energochłonności procesu a tym samym zasadności wykorzystania toryfikacji do ich przetwarzania [13]. Ponadto dla materiałów odpadowych brakuje badań nad zastosowaniem nadciśnienia jako dodatkowego czynnika optymalizującego proces toryfikacji [14].

Stąd w niniejszej pracy wybrano 7 materiałów odpadowych i poddano je procesowi toryfikacji (drewno odpadowe, osad ściekowy, poferment z biogazowni, borowina po zabiegowa, odchody słonia, tworzywo biodegradowalne polilaktyd (PLA) i papier). Określono wpływ parametrów technologicznych toryfikacji (temperatury, czasu trwania procesu, ciśnienia) wybranych materiałów na właściwości paliwowe wytwarzanych toryfikatów, przebieg procesu

i jego energochłonność. W celu dostarczenia pełnej wiedzy o wpływie najważniejszych parametrów technologicznych przeprowadzono badania laboratoryjne, które pozwoliły na ilościowe określenie wpływu temperatury, czasu trwania procesu i cieśnienia toryfikacji na ilość i jakość toryfikatu oraz ilość energii zużytej na proces.

2 Problem badawczy, cel pracy i hipotezy

2.1 Problem badawczy

Waloryzacja materiału odpadowego w procesie toryfikacji wymaga nakładu energii w celu uzyskania odpowiedniej temperatury procesu 200-300°C. Energia dostarczana do procesu może pochodzić z zewnętrznego źródła lub z przetwarzanego materiału. Produkty stałe (toryfikat) oraz gazowe (torgaz) mogą być również wykorzystane jako źródło energii. Nakład energii jest wypadkową parametrów technologicznych procesu takich jak temperatura i czas przetrzymywania materiału w reaktorze, właściwości fizyczno-chemicznych materiału oraz jego początkowej wilgotności. Ponieważ na etapie wytwarzania toryfikatu nie ma możliwości wpływu na właściwości fizyczno-chemiczne materiału oraz jego początkową wilgotność, sformułowano problem badawczy dotyczący poszukiwania warunków technologicznych pozwalających na zbilansowanie ilości energii zużytej na proces z ilością energii zachowanej w toryfikacie tak aby stosowanie toryfikacji do waloryzacji odpadów i biomasy było energetycznie uzasadnione.

2.2 Cel pracy

Celem pracy było określenie wpływu parametrów technologicznych toryfikacji odpadów i biomasy: temperatury, czasu trwania procesu i ciśnienia na ilość produkowanego toryfikatu, jego właściwości paliwowe oraz energochłonność procesu.

2.3 Hipotezy

H1 – Wzrost temperatury toryfikacji prowadzi do polepszenia właściwości paliwowych przetwarzanego materiału

H2 – Wydłużenie czasu prowadzenia procesu toryfikacji prowadzi do polepszenia właściwości paliwowych przetwarzanego materiału

H3 – Wzrost ciśnienia procesu toryfikacji prowadzi do polepszenia właściwości paliwowych przetwarzanego materiału

H4 – Toryfikacja w nadciśnieniu skutkuje zmniejszeniem zapotrzebowania energii na proces

H5 – Toryfikacja materiału o większej trwałości termicznej charakteryzuje się wyższym zapotrzebowaniem na energię

3 Struktura rozprawy doktorskiej

3.1 Struktura pracy

Rozprawa doktorska składa się z 6 spójnych tematycznie artykułów naukowych opublikowanych w recenzowanych czasopismach oraz 1 załącznika z danymi nieopublikowanymi. Publikacje charakteryzują się łącznym IF = 17,015 i łączną punktacją Ministerstwa Edukacji i Nauki (MNiSW) = 840 pkt. Średni udział procentowy doktoranta we wskazanych pracach wynosi 42,5%. W skład zbioru artykułów wchodzą publikacje przedstawione w tabeli 1. Publikacje zostały przedstawione w sposób chronologiczny od opublikowanych najwcześniej do opublikowanych najpóźniej. Łączna długość artykułów wynosi 156 stron, a łączna liczba zacytowanych w nich źródeł 350. Natomiast łączna długość niniejszego opracowania bez załączników wynosi 59 stron i zawiera 60 źródeł.

Tabela 1. Zestawienie artykułów wchodzących w skład zbioru publikacji

Nr.	Publikacja	IF, pkt	MNiSW, pkt	Udział, %
A1	**Kacper Świechowski**, Marek Liszewski, Przemysław Bąbelewski, Jacek A. Koziel, Andrzej Białowiec. Oxytree Pruned Biomass Torrefaction: Mathematical Models of the Influence of Temperature and Residence Time on Fuel Properties Improvement. Materials 2019, 12, 2228; doi:10.3390/ma12142228	2,972	140	35
A2	**Kacper Świechowski**, Sylwia Stegenta-Dąbrowska, Marek Liszewski, Przemysław Bąbelewski, Jacek A. Koziel, Andrzej Białowiec. Oxytree Pruned Biomass Torrefaction: Process Kinetics. Materials 2019, 12, 3334; doi:10.3390/ma12203334	2,707	140	40
A3	Paweł Stępień, **Kacper Świechowski**, Martyna Hnat, Szymon Kugler, Sylwia Stegenta-Dąbrowska, Jacek A. Koziel, Piotr Manczarski, Andrzej Białowiec. Waste to Carbon: Biocoal from Elephant Dung as New Cooking Fuel. Energies 2019, 12, 4344; doi:10.3390/en12224344	2,707	140	20
A4	**Kacper Świechowski**, Martyna Hnat, Paweł Stępień, Sylwia Stegenta-Dąbrowska, Szymon Kugler, Jacek A. Koziel, Andrzej Białowiec. Waste to Energy: Solid Fuel Production from Biogas Plant Digestate and Sewage Sludge by Torrefaction-Process Kinetics, Fuel Properties, and Energy Balance. Energies 2020, 13, 3161; doi:10.3390/en13123161	2,002	140	50
A5	**Kacper Świechowski**, Małgorzata Leśniak, Andrzej Białowiec. Medical Peat Waste Upcycling to Carbonized Solid Fuel in the Torrefaction Process. Energies 2021, 14, 6053. doi.org/10.3390/en14196053	3,004	140	50
A6	**Kacper Świechowski**, Christian Zafiu, Andrzej Białowiec. Carbonized Solid Fuel Production from Polylactic Acid and Paper Waste Due to Torrefaction. Materials 2021, 14, 7051. doi.org/10.3390/ma14227051	3,623	140	60

Na rysunku 1 zamieszczono ogólną strukturę pracy wraz z umiejscowieniem publikacji i danych w nich zawartych służących realizacji niniejszej pracy. Aby ułatwić podsumowanie uzyskanych danych doświadczalnych, prace podzielono na dwie części. Pierwsza część wyników dotyczy wyznaczeniu wpływu parametrów technologicznych (temperatura, czas trwania procesu, ciśnienie, właściwości materiału) na ilość i jakość produkowanego toryfikatu. Natomiast druga część wyników dotyczy wpływu parametrów technologicznych na energochłonność toryfikacji. Wyniki z badań dotyczących wpływu temperatury i czasu przebywania materiału w zadanej temperaturze na ilość i jakość wytworzonego toryfikatu przedstawiono w artykułach A1–A6, natomiast wpływ ciśnienia na badane materiały zawarto w załączniku Z1. Z kolei wpływ temperatury na energochłonność procesu przedstawiono w artykułach A4–A6 a wpływ ciśnienia na zużycie energii zawarto w załączniku Z1. Wyniki uzyskane w poszczególnych publikacjach oraz załączniku Z1 pozwoliły na sprawdzenie poprawności postawionych hipotez H1–H5.

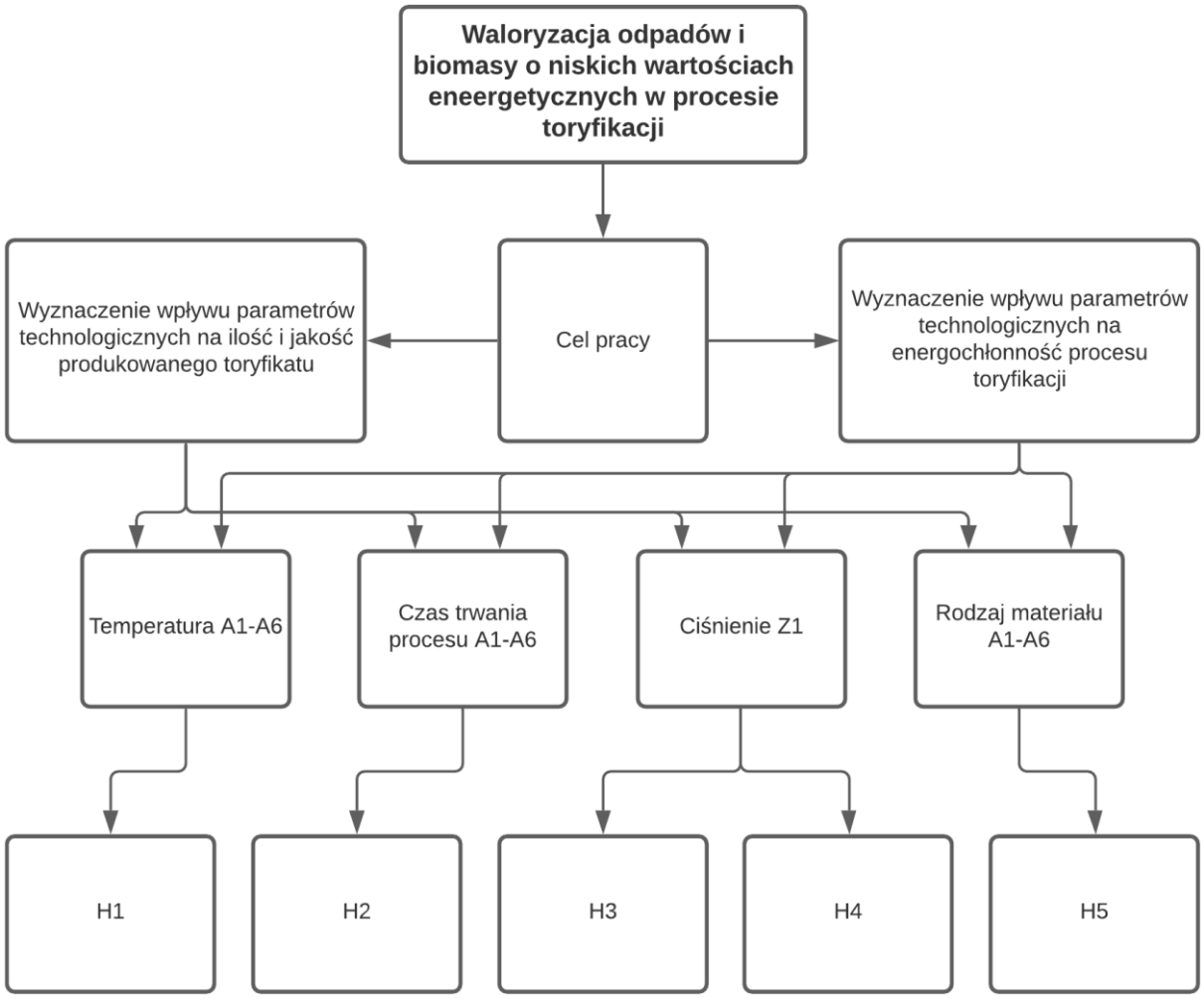

Rysunek 1. Struktura pracy, A1–A6 artykuły wchodzące w skład cyklu publikacji rozprawy doktorskiej, H1–H5 hipotezy postawione w rozprawie doktorskiej

Zawartość poszczególnych publikacji A1-A6, istotną dla realizacji celu rozprawy doktorskiej oraz dyskusje uzyskanych wyników, opisano poniżej w podrozdziale *3.2 Opis zawartości publikacji i załącznika z danymi nieopublikowanymi*. Ponieważ wszystkie publikacje bazują na podobnej metodyce z drobnymi zmianami, metodykę badań i materiały badawcze zostały zebrane i opisane w rozdziale *4 Materiały i metody*. W rozdziale *4.3* opisano proces toryfikacji w nadciśnieniu, którego wyniki zestawiono w załączniku z danymi nieopublikowanymi. Najważniejsze wyniki uzyskane w publikacjach oraz z analizy danych nieopublikowanych zostały zebrane i podsumowane w rozdziale *5 Wyniki badań i dyskusja*. Następnie w rozdziale *6 Wnioski i konkluzje*, dokonano całościowego przedstawienia najważniejszych wyników, sprawdzenia poprawności postawionych hipotez oraz odpowiedzi na postawiony problem badawczym.

3.2 Opis zawartości publikacji i załącznika z danymi nieopublikowanymi

W **publikacji A1** „*Oxytree Pruned Biomass Torrefaction: Mathematical Models of the Influence of Temperature and Residence Time on Fuel Properties Improvement*" [15] przedstawiono część wyników z badań nad toryfikacją drewna odpadowego Oxytree (Paulownia Clon in Vitro 112). Publikacja zawiera uzasadnienie prowadzenia badań nad drewnem odpadowym pochodzącym z zabiegów agrotechnicznych wykonywanych na plantacjach roślin energetycznych/przemysłowych na przykładzie rośliny Oxytree. W pracy przedstawiono metodykę użytą do wyznaczenia modeli empirycznych opisujących wpływ temperatury i czasu przebywania materiału w zadanej temperaturze na ilość i właściwości paliwowe wytworzonych toryfikatów. Publikacja zawiera wartości statystyczne określające dokładność modeli oraz ich graficzną prezentację w postaci wykresów 3D.

W **publikacji A2** „*Oxytree Pruned Biomass Torrefaction: Process Kinetics*" [16] przedstawiono drugą część badań nad drewnem odpadowym Oxytree (Paulownia Clon in Vitro 112). W publikacji opisano metodykę badań dotyczącą sposobu określenia kinetyki procesu toryfikacji. W pracy wyznaczono parametry kinetyczne w warunkach izotermicznych w tym wartość energii aktywacji, współczynnika przed wykładniczego oraz stałe szybkości reakcji. W rezultacie, na podstawie uzyskanych danych, możliwe jest modelowanie ubytku masy (wydajności masowej toryfikatu) w funkcji temperatury i czasu trwania procesu, dokładniej niż ma to miejsce w przypadku modeli zaproponowanych w publikacji [15]. Sposób wykorzystania parametrów kinetycznych przedstawiono w końcowej części publikacji [16], w sekcji Appendix B.

W **publikacji A3** „*Waste to Carbon: Biocoal from Elephant Dung as New Cooking Fuel*" [17] przedstawiono wyniki z badań nad toryfikacją odchodów słonia. Badania zawierały określenie właściwości paliwowych odchodów słonia przed i po jego toryfikacji, określenie parametrów

kinetycznych toryfikacji oraz określenie energochłonności procesu na podstawie danych ze skaningowej kalorymetrii różnicowej (DSC). Wykonano także modele matematyczne określające wpływ temperatury i czasu przebywania materiału w zadanej temperaturze na ilość toryfikatu oraz zmianę właściwości paliwowych w sposób tożsamy do publikacji [15,16] z drobnymi zmianami.

W **publikacji A4** „*Waste to Energy: Solid Fuel Production from Biogas Plant Digestate and Sewage Sludge by Torrefaction-Process Kinetics, Fuel Properties, and Energy Balance*" [18] przedstawiono wyniki z badań nad toryfikacją pofermentu z biogazowni oraz osadów ściekowych. Wykorzystując doświadczenie i metodykę z poprzednich artykułów wyznaczono modele matematyczne opisujące wpływ temperatury i czasu przebywania materiału w zadanej temperaturze na ilość oraz właściwości paliwowe toryfikatów produkowanych z pofermentu oraz osadów ściekowych. Wyznaczono parametry kinetyczne służące do modelowania ubytku masy, wyznaczono energochłonność procesu oraz wyliczono teoretyczny bilans masy i energii procesu toryfikacji. W bilansie uwzględniono ilość energii zawartej w nieprzetworzonym materiale, ilość energii zużytej na proces; ilość energii zachowanej w toryfikacie oraz ilość energii zawartej w torgazie.

W **publikacji A5** „*Medical Peat Waste Upcycling to Carbonized Solid Fuel in the Torrefaction Process*" [19] przedstawiono wyniki z badań nad toryfikacją borowiny pozabiegowej. Badania wykonano na podstawie metodyk opisanych we wcześniejszych artykułach [15–18] z drobnymi zmianami. W pracy wyznaczono właściwości paliwowe borowiny przed i po procesie toryfikacji, na podstawie których wyznaczono modele matematyczne opisujące wpływ temperatury i czasu przebywania materiału w zadanej temperaturze na ilość oraz właściwości paliwowe toryfikatów produkowanych z borowiny pozabiegowej. Wyznaczono również parametry kinetyczne służące do modelowania ubytku masy oraz wyliczono teoretyczny bilans masy i energii procesu toryfikacji. Wykonano bilans masy i energii toryfikacji borowiny pozabiegowej i porównano go z drewnem odpadowym z publikacji [15,16].

W **publikacji A6** „*Carbonized Solid Fuel Production from Polylactic Acid and Paper Waste Due to Torrefaction*" [20] korzystając z metodyk przedstawionych we wcześniejszych pracach zbadano właściwości paliwowe toryfikatów wytwarzanych z PLA oraz papieru jako materiału odniesienia dla PLA. W publikacji wyznaczono modele matematyczne opisujące wpływ temperatury i czasu trwania procesu na ilość oraz właściwości paliwowe toryfikatów. Wyliczono także teoretyczny bilans masy i energii procesu toryfikacji dla badanych materiałów. Nie wyznaczono natomiast parametrów kinetycznych w warunkach izotermicznych,

ponieważ używany termograwimetr nie był w stanie zarejestrować zmian masy badanego PLA (temperatura rozkładu materiału poza zakresem termicznym toryfikacji).

W **załączniku Z1** „*Wyniki z badań toryfikacji w nadciśnieniu*” przedstawiono wyniki z badań w formie tabelarycznej. Wyniki zawierają informacje o masie materiałów poddanych analizie i ilości wytworzonych toryfikatów, właściwościach paliwowych toryfikatów, zużyciu energii na proces toryfikacji oraz charakterystyki zmiany parametrów technologicznych (temperatury płaszcza grzewczego, temperatury wewnątrz reaktora, ciśnienia wewnątrz reaktora) podczas procesu.

4 Materiały i metody badawcze

Na rysunku 2 przedstawiono schemat blokowy przeprowadzonych badań, na podstawie których powstała niniejsza rozprawa doktorska.

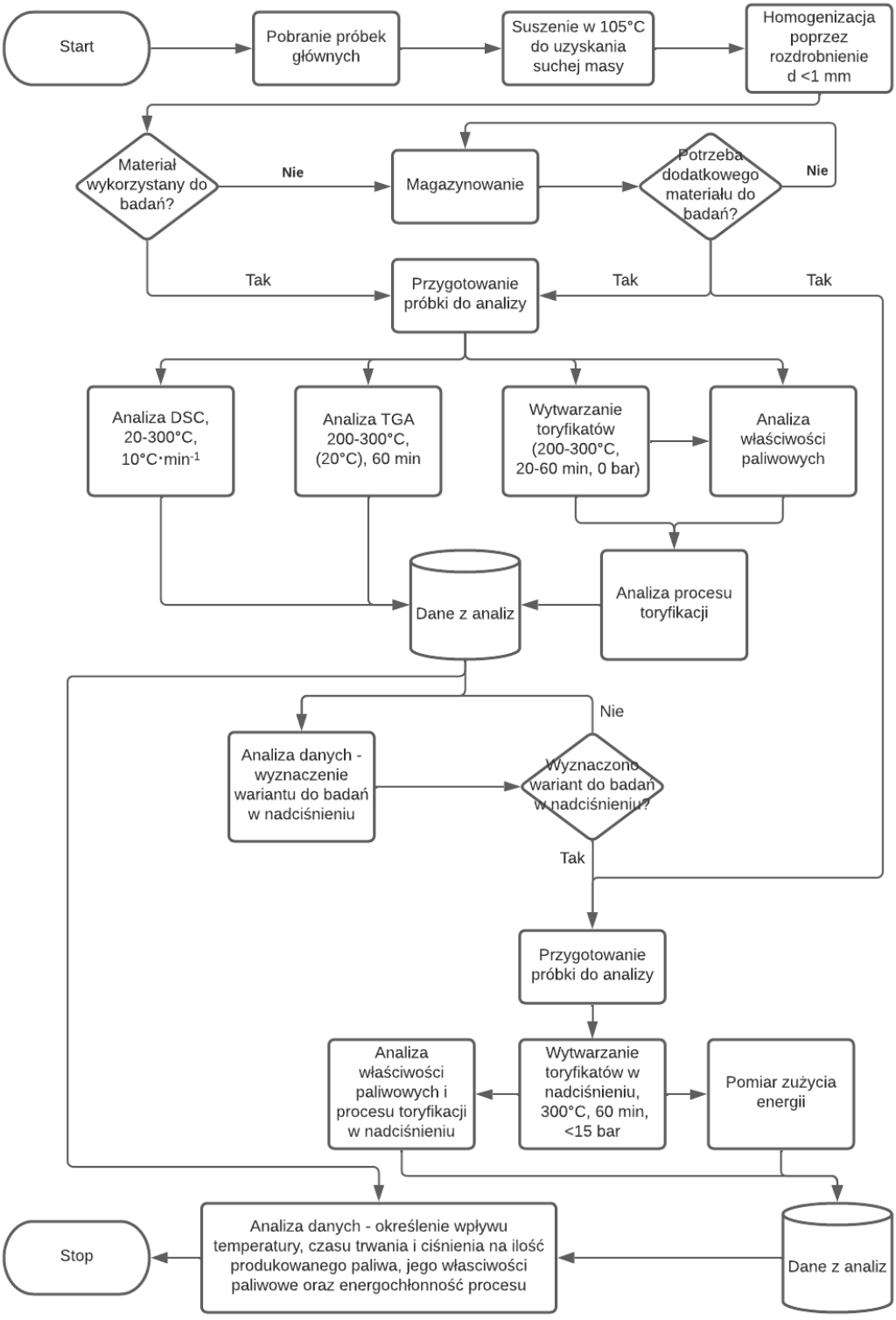

Rysunek 2. Schemat blokowy badań

Na początku zostały wybrane i pozyskane materiały badawcze. Pozyskane materiały (próbki pierwotne) zostały przygotowane do dalszych badań poprzez suszenie, rozdrobnienie, a następnie magazynowanie. Każdy z materiałów został poddany analizie DSC, analizie TGA, określeniu właściwości paliwowych, a następnie poddany procesowi toryfikacji. Wytworzone toryfikaty poddano analizą mającym na celu wyznaczenie właściwości procesu oraz właściwości paliwowych toryfikatów. Na podstawie zebranych i przeanalizowanych danych określono wpływ temperatury oraz czasu trwania procesu na właściwości paliwowe toryfikatów oraz teoretyczną energochłonność procesu dla poszczególnych materiałów. Na podstawie przeanalizowanych danych zdecydowano także, że badania w nadciśnieniu zostaną wykonane w 300°C i 60 min przy nadciśnieniu nieprzekraczającym 15 bar. Głównym powodem wyboru najwyższej możliwej temperatury procesu była idea uzyskania możliwie najwyższego wzrostu nadciśnienia w reaktorze, podczas gdy ograniczenie do 15 bar wynikało z wytrzymałości używanego reaktora. Natomiast długi czas procesu wpływał na lepsze odgazowanie przetwarzanego materiału i dalszy wzrost ciśnienia. Podczas badań w warunkach nadciśnienia mierzono realne zużycie energii na proces, a następnie wyznaczono właściwości paliowe wytworzonych toryfikatów. Dane z badań w warunkach nadciśnienia wykorzystano następnie do określenie wpływu tego parametru na właściwości produkowanego paliwa oraz energochłonność procesu.

4.1 Materiały badawcze

W rozprawie doktorskiej poddano analizie łącznie 7 materiałów o niskich wartościach energetycznych. Wybranymi materiałami badawczymi były drewno odpadowe, osad ściekowy, poferment z biogazowni, borowina po zabiegowa, odchody słonia, tworzywo biodegradowalne polilaktyd (PLA) i papier.

Drewno odpadowe – materiał badawczy reprezentujący drewno odpadowe pochodził z zabiegów agrotechnicznych wykonanych na plantacjach doświadczalnych położonych w Pawłowicach i Psarach (Wrocław, Polska), gdzie uprawiane są drzewa Oxytree (Paulownia Clon in Vitro 112). Materiał badawczy pochodził z przycinki drzew w pierwszym roku wegetacyjnym. Badaniu poddano łącznie 8 próbek drewna odpadowego z przycinki uprawianych na 2 różnych rodzajach gleby oraz 4 wariantów uprawy z wykorzystaniem geowłókniny i systemu nawadniania. Ze względu na fakt, że w publikacji [16] wykazano brak wpływu gleby i sposobu uprawy na kinetykę procesu toryfikacji, wszystkie próbki badawcze traktuje się w tej pracy jako równoważne. Dokładne dane sposobu uprawy są dostępne w publikacji [21].

Osad ściekowy – został pobrany z oczyszczalni ścieków w Janówek (Wrocław, Polska) przetwarzającej 140 000 $m^3 \cdot d^{-1}$ ścieków z Wrocławia. W oczyszczalni Janówek ścieki

są oczyszczane w sposób mechaniczno-biologiczny z dodatkiem związków chemicznych usuwających nadmiar fosforu [22]. Pierwotna próbka osadów ściekowych o masie 20 kg została pobrana ze zbiornika wtórnego przed procesem stabilizacji beztlenowej.

Poferment z biogazowni – Poferment do badań został pobrany z biogazowni Bio-Wat Sp. z o. o. zlokalizowanej w Świdnicy, posiadającej moc zainstalowaną 1 MW_{el} [23]. Na czas poboru próbki pofermentu do produkcji biogazu stosowane były następujące substraty: frakcja organiczna odseparowana ze zmieszanych odpadów komunalnych 34%, kiszonka z kukurydzy 30%, wysłodki buraczane 30%, ciasto drożdżowe 6%. Próbka pierwotna o masie 20 kg została pobrana z komory na poferment.

Borowina po zabiegowa – Borowina do badań została pozyskana z uzdrowiska, Uzdrowisko Kołobrzeg S.A. (Kołobrzeg, Polska). Borowina pochodziła z torfowiska zlokalizowanego około 3,5 km od miasta Kołobrzeg. Próbka pierwotna o masie około 25 kg charakteryzowała się stopniem humifikacji pomiędzy H_4 a H_6 według skali van Posta.

Odchody słonia – Próbka pierwotna odchodów słonia azjatyckiego o masie 5 kg została pobrana z Wrocławskiego ogrodu zoologicznego (Wrocław, Polska).

Polilaktyd (PLA) – Próbka pierwotna PLA została pozyskana poprzez mechaniczne rozdrobnienie kubków jednorazowych wykonanych w 100% z PLA. Kubki zostały zakupione w lokalnym sklepie (Wrocław, Polska).

Papier – Próbka pierwotna papieru została pozyskana poprzez mechaniczne rozdrobnienie kubków jednorazowych wykonanych w 99% z papieru oraz 1% PLA, które zostały zakupione w lokalnym sklepie (Wrocław, Polska).

4.2 Metody badawcze dla toryfikacji w ciśnieniu atmosferycznym

4.2.1 Przygotowanie materiału do badań

Wszystkie próbki pierwotne po dostarczeniu do laboratorium zostały podzielone na mniejsze próbki laboratoryjne. Nadmiar materiału był magazynowany w zamrażarce. Natomiast materiał służący do badań był suszony w 105°C w suszarce laboratoryjnej (WAMED, KBC-65W, Warszawa, Polska) do uzyskania suchej masy, a następnie rozdrobniony przy wykorzystaniu laboratoryjnego młynka nożowego (Testchem, LMN-100, Pszów, Polska) do frakcji mniejszej niż 1 mm. Tak przygotowane do badań materiały były przechowywane w plastikowych pojemnikach bądź workach strunowych w temperaturze pokojowej. Przed każdym badaniem materiał był ponownie suszony, celem usunięcia ewentualnej wilgoci.

4.2.2 Proces toryfikacji (wytwarzanie toryfikatów)

Proces toryfikacji przedstawiony w publikacjach [15–20] odbył się w piecu muflowym (Snol, 8.1/1100, Utena, Litwa), przedstawionym na rysunku 3a. Wysuszony i rozdrobniony materiał badawczy o masie 10-20 g był umieszczany na porcelanowych płaskich tyglach, które następnie były umieszczone w komorze pieca muflowego. Przed włączeniem programu grzewczego, do komory pieca dostarczany był gaz interny CO_2 który tworzył warunki beztlenowe. Po napełnieniu komory gazem, program grzewczy był uruchamiany, przy czym przepływ gazu intratnego był kontynuowany przez cały proces toryfikacji aż do momentu wyjęcia produktu z pieca. Proces toryfikacji był prowadzony w temperaturach w zakresie od 200°C do 300°C z interwałem co 20°C i czasach przebywania materiału w zadanej temperaturze wynoszących odpowiednio 20, 40 i 60 minut. Szybkość ogrzewania (ang. heating rate) pieca była każdorazowo ustawiona na 50°C·min^{-1}, co zapewniało relatywnie szybkie osiągnięcie zadanej temperatury, a także mieściło się w zakresie szybkości ogrzewania stosowanej w procesach toryfikacji [24]. Po zakończeniu procesu grzanie pieca było wyłączane i następował etap samoistnego chłodzenia reaktora. Przykładowa krzywa zmiany temperatury podczas procesu toryfikacji przedstawiono w publikacji [17], oraz jej odpowiedniku na rysunku 3b. Toryfikaty były wyjmowane z pieca, gdy temperatura na etapie chłodzenia wynosiła poniżej 150°C.

a) b)

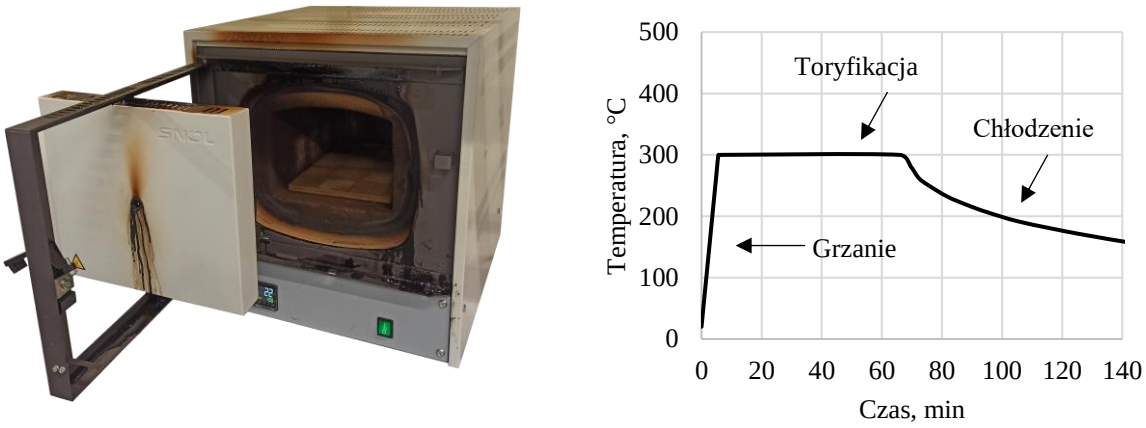

Rysunek 3. a) Piec muflowy (Snol, 8.1/1100, Utena, Litwa) b) Przykładowy przebieg temperatury podczas toryfikacji osadów ściekowych i pofermentu, warunki procesu 300 °C i 60 min, publikacja [17]

4.2.3 Analiza właściwości paliwowych nieprzetworzonych materiałów i toryfikatów

Suche i rozdrobnione materiały badawcze przed i po procesie toryfikacji zostały poddane analizom określającym ich właściwości paliwowe. W przypadku materiałów borowiny, PLA, oraz papieru wyznaczono wszystkie właściwości przedstawione w tabeli 2, natomiast dla pozostałych materiałów nie wyznaczono zawartości części lotnych oraz zawartości węgla związanego.

W skład właściwości określających jakość paliwa wyznaczono:

- wilgotność (ang. moisture content, MC) wyrażoną w %, świadczącą o ilości wody zawartej w badanym materiale. Dane dotyczące wilgotności przedstawione w publikacjach jak i tej pracy odnoszą się do stanu roboczego (ang. as recived basis);
- części lotne (ang. volatile matter, VM) wyrażone w %, świadczące o zawartości substancji ulegających odgazowaniu w temperaturze 950°C w czasie 7 min, wartości w publikacjach i pracy odnoszą się do stanu suchego (ang. dry basis);
- węgiel związany (ang. fixed carbon, FC) wyrażony w %, świadczący o zawartości stałych substancji palnych nieulegających odgazowaniu w temperaturze 950°C w czasie 7 min, wartości w publikacjach i pracy odnoszą się do stanu suchego (ang. dry basis);
- popiół (ang. ash content, AC) wyrażony w %, świadczący o zawartości mineralnej pozostałej po spaleniu paliwa w 815°C, wartości w publikacjach i pracy odnoszą się do stanu suchego (ang. dry basis);
- materie organiczną (ang. volatile solids, VS) świadcząca o ilości masy organicznej która ulega spaleniu w temperaturze 550°C. Zawartość materii organicznej jest wyrażona jako % suchej masy paliwa, a nie całego paliwa (sucha masa + woda);
- części palne (ang. combustible parts, CP) wyrażone w %, świadczące o ilość wszystkich związków organicznych i nieorganicznych które ulegają spaleniu w temperaturze 815°C, wartości w publikacjach i pracy odnoszą się do stanu suchego paliwa (ang. dry basis);
- ciepło spalania (ang. high heating value) wyrażone w dżulach na gram suchej masy paliwa ($J \cdot g^{-1}$), określające ilość energii wydzielonej podczas całkowitego i zupełnego spalenia 1 g suchej masy paliwa.

Tabela 2. Zestawienie analizowanych właściwości paliwowych

Właściwość	Metoda	Aparatura badawcza
Wilgotność (MC)	PN-EN 14346:2011 [25]	Suszarka laboratoryjna (WAMED, KBC-65W, Warszawa, Polska)
Części lotne (VM)	Metoda termograwimetryczna [26]	Termograwimetr (Czylok, RST 40 × 200/100, Jastrzębie-Zdrój, Polska)
Węgiel związany (FC)	Metoda obliczeniowa [26]	-
Popiół (AC)	PN-Z-15008-03:1993 [27]	Piec muflowy (Snol, 8.1/1100, Utena, Litwa)
Materia organiczna (VS)	PN-EN 15169:2011 [28]	
Części palne (CP)	PN-Z-15008-03:1993 [27]	
Ciepło spalania (HHV)	PN EN ISO 18125:2017-07 [29]	Kalorymetr (IKA, C200, Staufen, Niemcy)

4.2.4 Analiza efektywności procesu toryfikacji

Podczas procesu toryfikacji, masa materiału przed i po procesie była mierzona w celu wyznaczenia parametrów charakteryzujących efektywność procesu. Na podstawie masy początkowej i końcowej wyznaczono wydajność masową (ang. mass yield, MY) wyrażoną w %, wskazującą, ile toryfikatu można uzyskać w danym procesie, równanie 1 [21].

$$\mathrm{MY} = \frac{\text{masa materiału po toryfikacji}}{\text{masa materiału przed toryfikacją}} \times 100 \quad (1)$$

Na podstawie wyników ciepła spalania dla toryfikatów i nieprzetworzonych materiałów wyznaczono współczynnik zagęszczenia energii (ang. energy densification rato, EDr). EDr jest wskaźnikiem świadczącym o tym, o ile wzrosła/zmalała wartość ciepła spalania w toryfikacie względem nieprzetworzonego materiału, równanie 2 [21].

$$\mathrm{EDr} = \frac{\text{ciepło spalania materiału po toryfikacji}}{\text{ciepło spalania materiału przed toryfikacją}} \quad (2)$$

Natomiast poprzez połączenie danych otrzymanych z równań (1) i (2) wyznaczono wydajność energetyczną (ang. energy yield, EY) wyrażoną w %, świadczącą o ilości energii zachowanej w toryfikacie względem energii zawartej w materiale wykorzystanym do jego produkcji, równanie 3 [21].

$$\mathrm{EY} = \mathrm{MY} \times \mathrm{EDr} \quad (3)$$

4.2.5 Modelowanie wpływu temperatury i czasu trwania procesu na ilość i właściwości paliwowe toryfikatów

Wyniki dotyczące właściwości paliwowych toryfikatów oraz właściwości procesu toryfikacji zostały poddane analizie regresji wielorakiej, której celem było stworzenie modeli matematycznych opisujących wpływ temperatury procesu i czasu przebywania materiału w zadanej temperaturze na ilość i właściwości paliwowe toryfikatów. We wszystkich publikacjach do przeprowadzenia regresji metodą najmniejszych kwadratów wykorzystano oprogramowanie Statistica 13.3 (StatSoft, Palo Alto, CA, USA). Nie mniej w każdym artykule rozwijano podejście do wykonywanej analizy regresji, co wynikało z zdobywanego doświadczenia i umiejętności w trakcie opracowywania kolejnych modeli.

Metodyka procesu analizy regresji polegała na estymacji współczynników narzuconego równania składającego się z 1 współczynnika kierunkowego (a_1) i do 6 współczynników regresyjnych (a_2-a_7). Następnie, dla wygenerowanego modelu wyliczano współczynnik determinacji R^2 określający stopień dopasowania danych eksperymentalnych do wygenerowanego modelu, gdzie wartość 0 oznaczała brak dopasowania, natomiast 1 idealne dopasowanie. Sprawdzano także istotność oszacowanych współczynników regresji na poziomie istotności 0,05, a gdy wartość $p > 0,05$ zakładano brak istotności statystycznej współczynnika. Następnie z równań usuwano nieistotne współczynniki i przeprowadzano estymacje pozostałych współczynników ponownie. Kolejno dla nowych modeli niezawierających współczynników nieistotnych ponownie wyznaczano współczynnik determinacji. Dodatkowo dla modelu przed i po usunięciu nieistotnych współczynników wyznaczano wartość kryterium informacyjne Akaike (AIC). Kryterium AIC służy jako pomoc do wyboru pomiędzy modelami wielomianowymi o różnej liczbie współczynników, im mniejsza wartość AIC tym lepiej (mniejsza szansa, że model jest przeuczony) [30]. Następnie dokonywano wyboru najlepszego modelu w następujący sposób: na początku wybierano model z największą wartością R^2, w przypadku, gdy modele miały podobną wartość R^2, wybierano model o mniejszej wartości AIC, a gdy wartości AIC były zbliżone, wybierano model niezawierający współczynników nieistotnych statystycznie.

4.2.6 Analiza termograwimetryczna (TGA)

Wszystkie materiały poza PLA i papierem zostały poddane analizie termograwimetrycznej TGA w warunkach izotermicznych. Materiał PLA i papier zostały wykluczone z badań, ponieważ użyty sprzęt, termograwimetr (Czylok, RST 40 × 200/100, Jastrzębie-Zdrój, Polska), nie był w stanie zarejestrować zmian masy PLA w sposób poprawny. Wynikało to z faktu, że po osiągnięciu temperatury topnienia PLA zaczynało wyciekać z tygla, a następnie spływało poniżej strefy grzania.

Pozostałe materiały zostały poddane analizie TGA w temperaturach 200, 220, 240, 260, 280 i 300°C w czasie przebywania materiału w zadanej temperaturze wynoszącym 60 min. Sucha próbka o wadze od 1 do 3 g (w zależności od badanego materiału) była umieszczana w tyglu pomiarowym sprzężonym z wagą o dokładności d = 0,001 g. Następnie na tygiel był opuszczany wygrzany do zadanej temperatury reaktor. W czasie procesu od spodu reaktora był dozowany gaz interny CO_2. Na podstawie wygenerowanych danych (ubytek masy w funkcji czasu) wyznaczono parametry kinetyczne procesu toryfikacji, w tym stałą szybkości reakcji (k), energię aktywacji (E_a) oraz współczynniki przed wykładnicze (A).

Wyznaczenie stałych szybkości reakcji k dla poszczególnych temperatur polegało na dopasowaniu krzywych ubytku masy do równania reakcji pierwszego rzędu z wykorzystaniem estymacji nieliniowej w oprogramowaniu Statistica 13,3 (StatSoft, Palo Alto, CA, USA), metodą najmniejszych kwadratów. Następnie stałe szybkości reakcji wyznaczone dla poszczególnych temperatur naniesiono na wykres Arrheniusa (ln(k) vs 1/T). Kolejno z nachylenia powstałej prostej wyznaczono energię aktywacji korzystając z równania 4 oraz współczynnik przed wykładniczy korzystając z równania 5 [31].

$$E_a = -a \times R \tag{4}$$

$$A = \exp(b) \tag{5}$$

gdzie:

a – współczynniki kierunkowy równania prostej z wykresu Arrheniusa,

b – wyraz wolny równania prostej z wykresu Arrheniusa,

R – uniwersalna stała gazowa.

4.2.7 Skaningowa kalorymetria różnicowa (DSC)

Analizy DSC zostały użyte i opisane w artykułach [17–20]. Do analizy materiałów osad ściekowy, poferment i odchody słonia wykorzystano kalorymetr skaningowo różnicowy (TA Instruments, DSC Q2500, New Castle, DE, USA) a dla materiałów drewna odpadowego, borowiny, PLA oraz papieru, analizator termiczny TGA-DSC (Netzsch, 449 F1 Jupiter, Selb, Germany). Masa suchej próbki użytej w badaniu wynosiła między 3 a 6 mg (w zależności od rodzaju materiału). Analiza DSC była wykonana warunkach nieizotermicznych, gdzie temperatura zwiększała się z temperatury otoczenia do 500-800°C z szybkością 10°C·min^{-1}. Analizy były przeprowadzone w atmosferze gazu N_2. Wyniki z analiz DSC z zakresu temperatur 30-300°C zostały następnie użyte do wyznaczenia ilość energii pochłoniętej przez próbkę w trakcie jej ogrzewania do zadanej temperatury lub wydzielonej w wyniku zachodzących procesów egzotermicznych.

4.2.8 Bilans masy i energii procesu toryfikacji

Bilans masy i energii dla procesu toryfikacji został wyznaczony dla wszystkich badanych materiałów poprzez wykorzystanie danych uzyskanych z wcześniejszych analiz w tym: wartości ciepła spalania (HHV), ilość energii pochłoniętej przez próbkę w trakcie ogrzewania jej do zadanej temperatury (wyniki z analizy DSC), oraz wydajności masowej (MY). Bilans został obliczony w przeliczeniu na ilość masy i energii potrzebnej do wyprodukowania 1 g toryfikatu. W publikacjach, nazwę „toryfikat" zastąpiono nazwą karbonizowanego paliwa stałego „carbonized solid fuel" (CSF). W celu uproszczenia obliczeń przyjęto następujące założenia: przetwarzany materiał nie zawiera wilgoci, MC = 0%; energia do procesu jest dostarczana z zewnętrznego źródła energii z sprawnością 100%; brak strat ciepła z reaktora; wartość energii zawartej w torgazie jest sumą energii chemicznej wynikającej z jego składu chemicznego i posiadanej temperatury (ciepła), w obliczeniach założono, że całe ciepło z procesu trafia do torgazu.

Schemat obliczania bilansu masy i energii przedstawiono na rysunku 4. Na szaro zaznaczono dane wejściowe uzyskane z wspomnianych analiz. Kolorem niebieskim zaznaczono masę i energię materiałów wchodzących do reaktora oraz masę i energię produktów opuszczających reaktor. Natomiast kolorem zielonym oznaczono kolejność wykonywanych obliczeń.

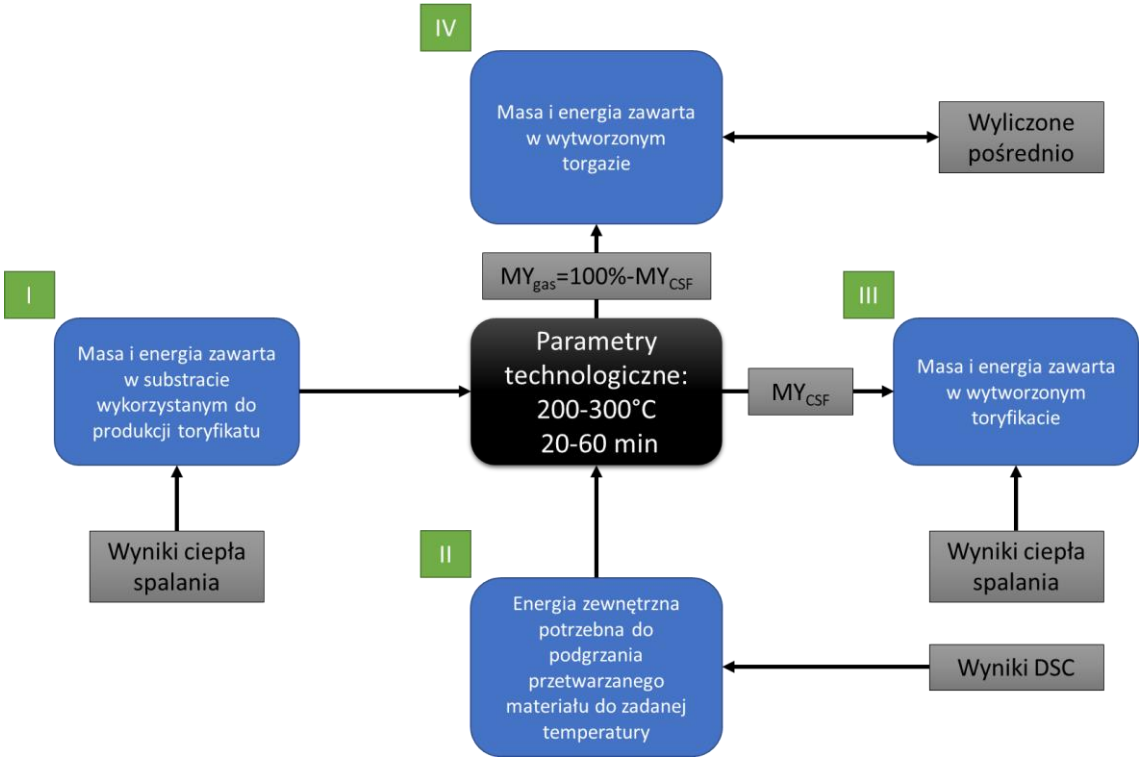

Rysunek 4. Schemat obliczania bilansu masy i energii procesu toryfikacji, publikacja [20]

W pierwszym etapie obliczeń (I) wykorzystano wydajność masową (MY) do wyliczenia ilości materiału potrzebnego do wyprodukowania 1 g toryfikatu (równanie 6), następnie znając masę

potrzebnego materiału oraz jego ciepło spalania (HHV), wyznaczono ilość energii zwartej w przetwarzanym materiale (równanie 7).

W drugim etapie (II) obliczeń wykorzystano wyniki z analizy DSC w celu określenia ilości energii pobranej przez przetwarzany materiał w celu osiągnięcia przez niego zadanej temperatury toryfikacji. Ponieważ wyniki DSC wyrażone są w mocy dostarczonej/wydzielonej z próbki podczas jej ogrzewania ($mW \cdot mg^{-1}$), wartości te zostały przeliczone z mocy na energię poprzez przemnożenie mocy przez czas ($mJ \cdot mg^{-1}$). Następnie uzyskane wyniki zsumowano od temperatury otoczenia do zadanej temperatury toryfikacji uzyskując ilość energii pochłoniętej przez próbkę.

Na trzecim etapie obliczeń (III) założono, że ilość energii w wyprodukowanym toryfikacie odpowiada wyznaczonemu eksperymentalnie ciepłu spalania toryfikatu (HHV).

Na czwartym etapie obliczeń (IV) została wyliczona masa (równanie 8) i energia (równanie 9) torgazu, który powstał podczas produkcji 1 g toryfikatu. Założono, że energia torgazu jest sumą energii chemicznej wynikającej z jego składu chemicznego oraz posiadanego ciepła (posiadanej temperatury).

$$M_S = \frac{Mr_{CSF}}{MY_{CSF}} \tag{6}$$

$$E_S = M_S \times HHV_S \tag{7}$$

$$M_G = (100\% - MY_{CSF}) \times M_S \tag{8}$$

$$E_G = E_Z + E_S - E_{CSF} \tag{9}$$

gdzie:

M_S – masa potrzebnego materiału do wyprodukowania Mr_{CSF} g toryfikatu, g,

Mr_{CSF} – masa toryfikatu jaką chcemy wyprodukować, (tu 1 g), g,

MY_{CSF} – wydajność masowa produkcji toryfikatu, %,

E_S – energia zawarta w materiale użytym do produkcji Mr_{CSF} g toryfikatu, J,

HHV_S – ciepło spalania materiału przed toryfikacją, $J \cdot g^{-1}$.

M_G – masa torgazu wytworzona podczas produkcji toryfikatu, g.

E_G – energia zawarta w wyprodukowanym torgazie, J,

E_Z – energia zewnętrzna dostarczona do procesu wyliczona na II etapie, J,

E_{CSF} – energia zawarta w wyprodukowanym toryfikacie, J.

4.2.9 Analiza statystyczna

Do określenia czy temperatura i czas procesu miały wpływ na proces i zmianę właściwości paliwowych stosowano analizę wariancji. Dla układów, dla których analiza wariancji na poziomie ($p<0,05$) wskazała występowanie istotnych statystycznie różnic, przeprowadzono test post hoc

Tukey-a w celu wyznaczenia pomiędzy którymi średnimi te różnice występują. Analizę wariancji oraz test post hoc wykonano przy wykorzystaniu oprogramowania Statistica 13,3 (StatSoft, Palo Alto, CA, USA).

4.3 Metody badawcze dla toryfikacji w nadciśnieniu

4.3.1 Przygotowanie materiału do badań

Dla 5 z 7 przebadanych materiałów wykonano badania w prototypowym reaktorze ciśnieniowym (WUELS, RBMT2020-1.1, Wrocław, Polska). Toryfikację w nadciśnieniu przeprowadzono dla drewna odpadowego, osadu ściekowego, pofermentu, borowiny oraz PLA. W przypadku odchodów słonia i papieru zabezpieczono niewystarczającą masę materiału do przeprowadzenia badań. Przed procesem toryfikacji materiały badawcze został wysuszone za pomocą suszarki laboratoryjnej (WAMED, KBC-65W, Warszawa, Polska) zgodnie z normą PN-EN 14346:2011. Po wysuszeniu każdy materiał badawczy został podzielony na 5 równych części o łącznej masie ~160–400 g. Tak podzielony materiał był następnie umieszczany w aluminiowych tackach, które następnie zostały szczelnie owinięte folią aluminiową. Tak przygotowany materiał był następnie umieszczany w reaktorze ciśnieniowym.

4.3.2 Budowa reaktora ciśnieniowego

Badania w nadciśnieniu przeprowadzono w prototypowym reaktorze ciśnieniowym (WUELS, RBMT2020-1.1, Wrocław, Polska) przedstawionym na rysunku 5a i 5b. Reaktor składa się z komory reaktora (1) o pojemności całkowitej 22,3 dm^3. Wewnątrz komory na wysokości około 10 cm nad dnem znajduje się kratka stanowiąca miejsce umieszczania materiału badawczego. Celem kratki jest oddzielenie frakcji stałej od frakcji ciekłej wydzielonej podczas toryfikacji i skroplonej wewnątrz reaktora podczas procesu jego chłodzenia, która to zbiera się na dnie pod kratką. Komora reaktora z zewnętrznej strony jest owinięta płaszczem grzewczym o mocy 3 kW, który został owinięty taśmą izolacyjną z włókna szklanego (grubość warstwy izolacyjnej ~7,5 cm, λ ~0,05 $W \cdot m^{-1} \cdot K^{-1}$). Dodatkowo cała komora reaktora z uwzględnieniem płyty dolnej i górnej została zaizolowana z wykorzystaniem wełny mineralnej jednostronnie pokrytej folią aluminiową (grubości 2.5 cm λ ~0,047 $W \cdot m^{-1} \cdot K^{-1}$). Górna płyty reaktora jest połączona z chłodnicą (5), której zadaniem jest schładzanie wydostających się gazów do temperatury poniżej 200°C w celu zapobiegnięcia uszkodzenia manometru (4). Szczelność reaktora można regulować poprzez manualne otwieranie i zamykanie zaworów górnego (1) oraz zaworu dolnego (7). Reaktor został zaprojektowany tak aby prowadzić proces w nadciśnieniu dochodzącym do 15 bar. Powyżej wartości 15 bar dochodzi do samoczynnego otwarcia zaworu bezpieczeństwa.

a) b)

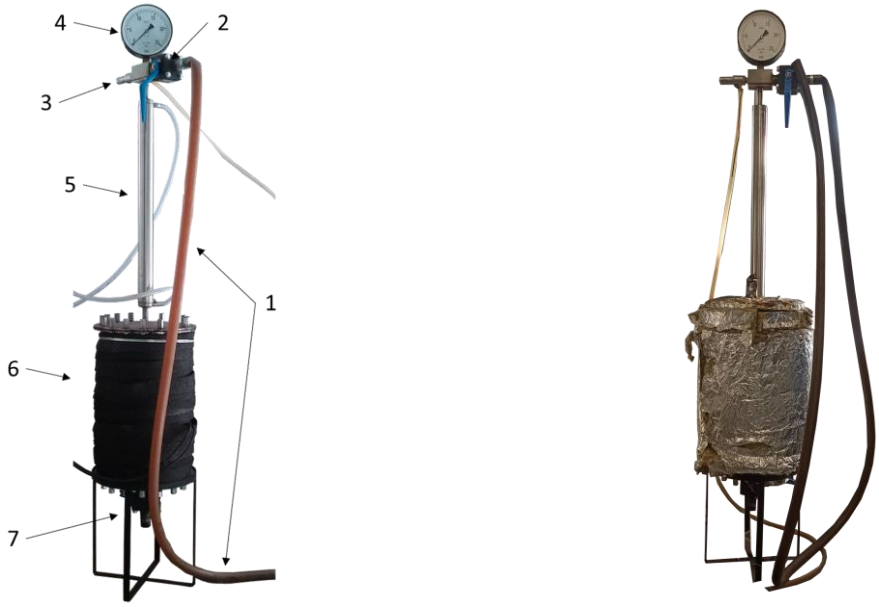

Rysunek 5. Prototyp reaktora ciśnieniowego do toryfikacji, a) reaktor bez dodatkowej izolacji z wełny mineralnej, b) reaktor z dodatkową izolacją. 1 – rura wylotowa, 2 – zawór górny, 3 – zawór bezpieczeństwa, 4 – manometr, 5 – chłodnica, 6 – komora reaktora owinięta matą grzejną i taśmą izolacyjną z włókna szklanego, 7 – zawór dolny [14]

4.3.3 Proces toryfikacji w nadciśnieniu (wytwarzanie toryfikatów)

Dla każdego materiału badawczego wykonano dwa pomiary w zmiennych warunkach ciśnienia. Pierwszy pomiar odniesienia z otwartym zaworem reaktora (O), w który produkowany podczas procesu torgaz swobodnie opuszczał komorę reaktora – ciśnienie normalne. Drugi pomiar, w którym wszystkie zawory były zamknięte (Z) a wzrost temperatury oraz powstający torgaz zwiększał ciśnienie wewnątrz reaktora.

Wysuszony i rozdrobniony materiał badawczy był umieszczany w 5 aluminiowych tackach, które po zawinięciu w aluminiową folię były równomiernie rozkładane w komorze reaktora ciśnieniowego. Po załadowaniu materiału badawczego do reaktora, program grzewczy był uruchamiany. Gaz inertny nie był dozowany do komory reaktora, ponieważ materiał został szczelnie owinięty folią. W przypadku pomiaru pierwszego, powstający torgaz opuszczał komorę rektora swobodnie poprzez otwarty zawór dolny, natomiast w przypadku pomiaru drugiego powstający torgaz pozostawał w komorze reaktora, ponieważ wszystkie zawory były zamknięte. W celu osiągnięcia wewnątrz reaktora temperatury 300°C, temperatura na płaszczu grzewczym była nastawiona na 500°C, a następnie, gdy wartość wewnątrz reaktora osiągała 300°C, temperaturę płaszcza redukowano do 400°C. Po osiągnięciu temperatury 300°C wewnątrz komory reaktora, odliczano 60 minut, po upływie, których płaszcz grzewczy był wyłączany, a reaktor zostawiony do wychłodzenia. W przypadku procesu z zamkniętymi zaworami, po upływie 60 minut zawór dolny był otwierany w celu upuszczenia nadciśnienia panującego w komorze. Materiał badawczy był

wyjmowany z reaktora po jego wychłodzeniu do temperatury otoczenia. Krzywe zmiany temperatur i ciśnienia podczas procesu toryfikacji dla poszczególnych materiałów przedstawiono w załączniku Z1 na rysunkach Z1-Z5 natomiast na rysunku 6 przedstawiono przykładowy przebieg temperatury zewnętrznej (T_z) na płaszczu reaktora oraz temperatury (T_w) i nadciśnienia (p) wewnątrz reaktora.

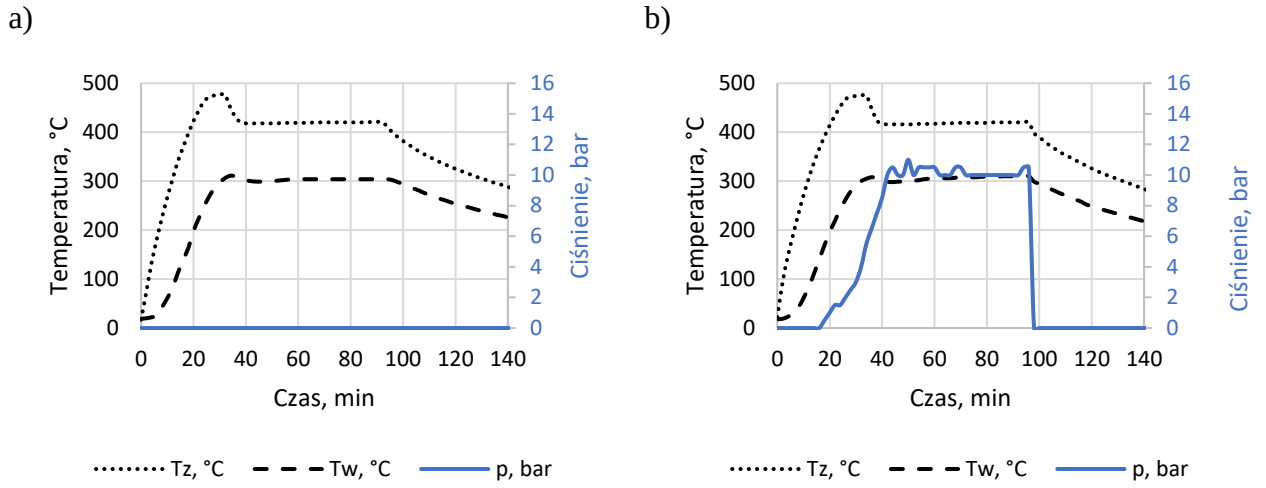

Rysunek 6. Przykładowy przebieg temperatury zewnętrznej (płaszcza grzewczego), wewnętrznej (wewnątrz reaktora) oraz ciśnienia dla borowiny, a) pomiar z zaworem otwartym (O), b) pomiar z zaworami zamkniętymi (Z)

Podczas każdego pomiaru, mierzono ilość energii elektrycznej zużytej przez płaszcz grzewczy reaktora. Ilość zużytej energii została zmierzona za pomocą analizatora jakości sieci energetycznej (Lumel, ND40, Zielona Góra, Polska). Właściwości paliwowe toryfikatów oraz właściwości procesu toryfikacji zostały wyznaczone w sposób tożsamy z opisami w podrozdziałach 4.2.3 i 4.2.4.

4.3.4 Analiza statystyczna

Wyniki pomiarów wykonane w powtórzeniach zostały poddane analizie wariancji dla układów czynnikowych, gdzie zmiennymi zależnymi były właściwości procesu toryfikacji i właściwości paliwowe toryfikatów, a czynnikami jakościowymi rodzaj przetwarzanego materiału oraz rodzaj procesu (toryfikacja z zaworem otwartym i z zaworami zamkniętymi). Dla układów, dla których analiza wariancji na poziomie ($p<0,05$) wskazała występowanie istotnych statystycznie różnic, przeprowadzono test post hoc Tukey-a w celu wyznaczenia pomiędzy którymi średnimi występują różnice. Analizę wariancji oraz test post hoc wykonano przy wykorzystaniu oprogramowania Statistica 13,3 (StatSoft, Palo Alto, CA, USA). Wyniki z analizy wariancji oraz testu post hoc przedstawiono w załączniku Z1 w tabelach Z3-Z12.

5 Wyniki badań i dyskusja

5.1 Wydajność procesu toryfikacji i właściwości paliwowe toryfikatów

Szczegółowe wyniki dotyczące właściwości paliwowych nieprzetworzonych materiałów, toryfikatów, efektywności procesu toryfikacji, kinetyki toryfikacji oraz energii aktywacji procesu, jak również estymacji parametrów modeli opisujących wpływ parametrów technologicznych toryfikacji na właściwości toryfikatów oraz efektywność procesu oraz ich dyskusja zostały zawarte w publikacjach [15–20]. W niniejszej rozprawie w sposób syntetyczny i porównawczy zestawiono uzyskane wyniki. W podrozdziale 5.1.1 omówiono toryfikaty charakteryzujące się najlepszymi właściwościami paliwowymi wytworzonymi w ciśnieniu atmosferycznym, natomiast w podrozdziale 5.1.2 omówiono wpływ nadciśnienia na wydajności procesu toryfikacji oraz zmianę właściwości paliwowych toryfikatów.

5.1.1 Wpływ temperatury i czasu na wydajność procesu i właściwości paliwowe toryfikatów

W tabeli 3 dokonano zestawienia porównawczego właściwości paliwowych nieprzetworzonych materiałów oraz toryfikatów o najwyższym cieple spalania wytworzonych w określonych warunkach technologicznych.

Tabela 3. Zestawienie właściwości procesu toryfikacji oraz właściwości paliwowych dla waloryzowanych materiałów oraz toryfikatów o największej wartości ciepła spalania, publikacje [15,17–20]

Materiał	MY, %	EDr, %	EY, %	MC, %	VM, %	FC, %	AC, %	VS, %	CP, %	HHV, $J \cdot g^{-1}$
Drewno odpadowe	-	-	-	40,0	-	-	8,1	90,2	91,9	18295
Toryfikat 300/40	54,7	1,20	65,9	6,4	-	-	14,0	82,9	85,9	22034
Zmiana, %	-	-	-	17,0	-	-	73,9	-8,2	-6,5	20,44
Osady ściekowe	-	-	-	84,4	-	-	36,3	61,9	63,7	14590
Toryfikat 200/20	96,2	1,02	97,9	4,3	-	-	38,6	59,3	61,4	14854
Zmiana, %	-	-	-	-94,9	-	-	6,3	-4,3	-3,6	1,81
Poferment	-	-	-	85,6	-	-	12,4	86,5	87,6	18087
Toryfikat 280/20	59,3	1,12	66,3	4,0	-	-	17,9	80,9	82,1	20215
Zmiana, %	-	-	-	-95,3	-	-	44,6	-6,5	-6,3	11,77
Borowina	-	-	-	84,8	59,3	26,3	14,4	83,0	85,6	19013
Toryfikat 280/40	79,9	1,12	89,6	0,0	44,6	37,7	17,7	78,8	82,3	21324
Zmiana, %	-	-	-	-100,0	-24,8	43,4	22,9	-5,1	-3,9	12,15
Odchody słonia	-	-	-	49,2	-	-	50,8	48,9	49,3	11410
Toryfikat 200/60	95,6	1,14	108,9	2,4	-	-	42,5	57,4	57,5	13003
Zmiana, %	-	-	-	-95,2	-	-	-16,3	17,3	16,6	13,96
PLA	-	-	-	0,7	100,0	0,0	0,0	100,0	100,0	19420
Toryfikat 220/40	99,6	1,02	101,5	0,5	100,0	0,0	0,0	100,0	100,0	19799
Zmiana, %	-	-	-	-26,1	0,0	-	-	0,0	0,0	1,95
Papier	-	-	-	6,4	88,2	8,7	3,6	96,3	96,4	17525
Toryfikat 300/40	42,4	1,11	47,3	4,4	60,8	31,5	7,7	91,8	92,3	19520
Zmiana, %	-	-	-	-31,5	-31,1	285,9	112,4	-4,7	-4,2	11,38

Dla toryfikatów podano także właściwości opisujące procesu toryfikacji, w których zostały wytworzone. Dane pochodzą z artykułów [15,17–20]. Dla każdego toryfikatu wyznaczono względną wartość (względem materiału nieprzetworzonego) zmiany parametrów paliwowych wynikających z przeprowadzonej toryfikacji.

Do najważniejszych parametrów opisujących proces toryfikacji zalicza się wydajność masową, współczynnik zagęszczenia energii oraz wydajność energetyczną. Wydajność masowa wyrażona w % świadczy o tym, ile toryfikatu powstanie po procesie z każdej jednostki nieprzetworzonego materiału umieszczonego w reaktorze. Wartość ta powinna być zawsze mniejsza niż 100%, ponieważ wartości wyższe niż 100% wskazywałyby, że masa materiału po procesie jest większa niż przed procesem [32]. Współczynnik zagęszczenia energii jest ilorazem wartości ciepła spalania toryfikatu do wartości nieprzetworzonego materiału. Jeżeli wartość współczynnika zagęszczenia energii jest większa niż 1 oznacza to, że toryfikat charakteryzuje się większą wartością energetyczną niż nieprzetworzony materiał. Z kolei wartość niższa niż 1, wskazuje, że toryfikat posiada niższą wartość ciepła spalania niż nieprzetworzony materiał wykorzystany do jego produkcji [32]. Z kolei wydajność energetyczna jest iloczynem wydajności masowej i współczynnika zagęszczenia energii i świadczy o ilości energii pierwotnej zachowanej w toryfikacie. Energię pierwotna rozumie się jako energie chemiczną zawartą w materiale użytym do produkcji toryfikatu. Wartość tego współczynnika, także powinna być mniejsze niż 100%, ponieważ wartości powyżej 100% świadczyłaby, że w wyprodukowanym toryfikacie jest więcej energii niż w materiale wykorzystanym do jego produkcji. Nie mniej jednak, można znaleźć w literaturze wartości wyższe niż 100% co wynika najprawdopodobniej z niedokładności pomiarowej dotyczącej ilości materiału powstałego po procesie toryfikacji oraz niedokładności pomiaru ciepła spalania, na skutek dużej heterogeniczności materiału [33,34]. Wystąpiło to również w przypadku próbek odchodów słonia dla których wartość EY wyniosła 108,9% (tabela 3), co wynikało z dużego zróżnicowania materiału i wysokiej zawartości popiołu. Najprawdopodobniej materiał użyty do oznaczenia ciepła spalania w nieprzetworzonym materiale posiadał więcej popiołu niż materiał wykorzystany do wyprodukowania toryfikatu. W rezultacie toryfikat mógł mieć znacznie wyższą wartość ciepła spalania, która po przemnożeniu przez wydajność masową wykazała większą ilość energii niż ilość energii zawarta w materiale wykorzystanym do jego wyprodukowania.

Wyniki wskazują, że wraz ze wzrostem temperatury i czasu trwania procesu wydajność masowa i energetyczna procesu maleje, przy czym szybkość tego spadku jest zależna od rodzaju przetwarzanego materiału [15,17–20]. Z kolei współczynnik zagęszczenia energii (EDr)

nie wykazuje takiej tendencji i w zależności od rodzaju materiału oraz parametrów technologicznych toryfikacji rośnie bądź maleje po przekroczeniu granicznych wartości temperatury i czasu procesu. Dla przykładu, wartości EDr dla drewna i papieru rosną wraz ze wzrostem temperatury i czasu trwania procesu z około 1,01 dla toryfikatów wytworzonych w 200°C i 20 min odpowiednio do 1,20 i 1,10 dla toryfikatów wytworzonych w 300°C i 60 min [15,20]. Podczas, gdy dla osadu ściekowego trend jest odwrotny i wartość EDr maleje wraz ze wzrostem temperatury i dla toryfikacji w 300°C uzyskuje wartość 0,85 [18]. Z kolei odchody słonia charakteryzowały się wartością współczynnika EDr powyżej 1 dla temperatury 200°C, natomiast powyżej 200°C wartość ta malała podobnie jak w przypadku osadów ściekowych [17]. Ponieważ wartość zagęszczenia energii zależy od ciepła spalania toryfikatu i nieprzetworzonego materiału, jest on dobrym wskaźnikiem jakości toryfikatu pod względem energetycznym. Z tego względu tylko toryfikaty o największej wartości EDr dla poszczególnych materiałów zostały zestawione w tabeli 3. Dzięki wykorzystaniu procesu toryfikacji udało się zwiększyć zagęszczenie energii dla drewna odpadowego do 1,20, odchodów słonia do 1,14, borowiny do 1,12, pofermentu do 1,12, oraz papieru do 1,10. Natomiast dla materiałów takich jak osady ściekowe oraz PLA efekt zwiększenia zagęszczenia energii był znikomy EDr = 1,02 (tabela 3) co świadczy o nieprzydatności procesu toryfikacji do waloryzacji właściwości paliwowych tych materiałów. Ponadto analiza wariancji w publikacji dotyczącej PLA [20] wykazała, że wartości ciepła spalania dla wszystkich przebadanych toryfikatów nie różniły się istotnie od materiału nieprzetworzonego ($p<0,05$).

Znaczący wpływ na efekt procesu toryfikacji miały właściwości badanych materiałów. Badane materiały charakteryzowały się odmiennymi właściwościami paliwowymi. Największą wilgotność w stanie roboczym (na moment pozyskania materiału do badań) posiadał poferment 85,6%, borowina 84,8% oraz osad ściekowy 84,4%. Prawie dwukrotnie mniejszą wilgotność charakteryzowały się odchody słonia 49,2% oraz drewno odpadowe ~ 40%. Pozostałe materiały jak papier i PLA posiadały znacznie niższą wartość wilgotności wynoszącą odpowiednio 6,4% i 0,7% (tabela 3). Pomimo tego, że materiały przed toryfikacją zostały wysuszone, proces suszenia jest nieodzownym elementem toryfikacji i jej przeprowadzenie skutkuje usunięciem wody. Dla wszystkich przedstawionych w tabeli 3 toryfikatów, zawartość wilgoci w stanie powietrzno-suchym po procesie toryfikacji była nie większa niż 6,4%. Dla borowiny natomiast wartość ta wyniosła 0%, co świadczy o wytworzeniu toryfikatu o właściwościach silnie hydrofobowych. Badania nad wilgotnością wytworzonych toryfikatów nie zawierały określenia hydrofobowości, przy czym z danych literaturowych wynika, że wzrost temperatury toryfikacji prowadzi do zmiany właściwości hydrofilowych na hydrofobowe [35]. Temperatura z zakresu 220-240°C może

spowodować zmianę właściwości materiału hydrofilowego na właściwości ekstremalnie hydrofobowe [35]. Wynika to przede wszystkim z termicznego rozkładu hemicelulozy oraz celulozy bogatych w grupy hydroksylowe (-OH), które są uważane za kluczowy czynnik wiążący wodę [36].

W przeprowadzonych badaniach największą początkową zawartością popiołu charakteryzowały się odchody słonia 50,8%, oraz osad ściekowy 36,3%. Znacznie mniejszą zawartość popiołu posiadała borowina 14,4%, poferment 12,4% oraz drewno odpadowe 8,1%. Natomiast najniższą zawartością charakteryzował się papier 3,6% oraz PLA 0,7% (tabele 3). Bez względu na rodzaj odpadu (z wyłączeniem PLA) wzrost temperatury procesu i czasu jej oddziaływania prowadził do zwiększenia zawartości popiołu w toryfikacie [15,17–20]. Dla toryfikatów o najwyższych ciepłach spalania przedstawionych w tabeli 3, także odnotowano wzrost zawartości popiołu względem nieprzetworzonego materiału. Największy procentowy wzrost zawartości popiołu odnotowano dla papieru, odpowiednio 112,4% oraz drewna odpadowego, wzrost o 73,9%. Znaczący wzrost zawartości popiołu odnotowano także dla pofermentu odpowiednio 44,6% oraz borowiny, wzrost o 22,9% (tabela 3). W przypadku PLA nie odnotowano zmiany zawartości popiołu, ponieważ materiał ten charakteryzował się zerową zawartością popiołu. Natomiast zawartość popiołu w toryfikacie wykonanym z odchodów słonia okazała się mniejsza o 16,3% niż w nieprzetworzonym materiale (tabela 3). Zawartość popiołu w toryfikacie zależy bezpośrednio od zawartości popiołu w materiale użytym w procesie. Wzrost zawartości popiołu jest względny, wzrasta na skutek zmniejszenia zawartości części lotnych ulegających odgazowaniu [37]. Zaobserwowane zmniejszenie zawartości popiołu w przypadku odchodów słonia wynika najprawdopodobniej z dużej heterogeniczności materiału pomimo jego homogenizacji przed rozpoczęciem badań. Gdzie najprawdopodobniej materiał użyty do wyprodukowania toryfikatu w 200°C i 60 min (tabela 3) posiadał znacznie mniej części mineralnych niż ten wykorzystany do oznaczenia zawartości popiołu w nieprzetworzonym materiale. Aby uniknąć takiej sytuacji w przyszłości należałoby opracować lub zastosować procedury poboru i homogenizacji próbek materiałów charakteryzujących się dużą heterogenicznością. Przykładem takiej procedury może być zwiększenie masy i ilości pobranych próbek pierwotnych oraz i ich kilkukrotne mieszanie. Pomocne będzie także zwiększenie ilości powtórzeń wykonywanych analiz [38].

Dla borowiny, papieru i PLA oznaczono zawartość części lotnych oraz zawartości węgla związanego. Największą zawartością części lotnych charakteryzował się PLA 100%, następnie papier 88,2% i borowina 59,3%. Tym samym najmniejszą zawartością węgla związanego wynoszącą 0% zmierzono dla PLA, 8,7% dla papieru, oraz 26,3% dla borowiny (tabela 3). Wyniki przedstawione w publikacjach [19,20] wskazują, że niezależnie od przetwarzanego materiału

(z wyłączeniem PLA) wraz ze wzrostem temperatury i czasu trwania procesu w toryfikatach maleje zawartość części lotnych, a rośnie zawartość węgla związanego [19,20]. Jest to efekt pożądany, ponieważ prowadzi do przybliżenia właściwości paliwowych biomasy i odpadów do właściwości węgla wykorzystywanego w energetyce, co ułatwia ich współspalanie. Typowy węgiel energetyczny posiada zawartość części lotnych w zakresie od 21% do 45% [39]. Podczas, gdy w biomasie części lotne stanowią do 80% [40]. W przypadku toryfikatów o największym cieple spalania zestawionych w tabeli 3, zawartość części lotnych wyniosła 44,6% w przypadku borowiny oraz 60,8% w przypadku papieru. W związku z czym toryfikat z borowiny osiągnął zbliżone właściwości do węgli energetycznych, a papier powinien zostać silniej odgazowany poprzez zwiększenie temperatury procesu albo wydłużenie czasu procesu. Substancjami, które w głównej mierze są odpowiedzialne za wysoką zawartość części lotnych w biomasie jak i badanym papierze jest hemiceluloza oraz celuloza, które zawierają odpowiednio 78.6% i 95.2% części lotnych [41].

Badane materiały, poza odchodami słonia oraz osadem ściekowych charakteryzowały się wysoką zawartości materii organicznej oraz zawartości części palnych wynoszących ponad 80% (tabela 3). W przypadku odchodów słonia i osadu ściekowego zawartość materii organicznej wynosiła odpowiednio 48,9% i 61,9%, co wynikało bezpośrednio z wysokiej zawartości popiołu w tych materiałach (tabela 3). Wyniki uzyskane w publikacjach [15,17–20] wykazały, że wraz ze wzrostem temperatury procesu oraz wydłużeniem czasu jej oddziaływania na materiał podczas toryfikacji zachodzi zmniejszenie zawartości materii organicznej i części palnych w produkowanym toryfikacie. Podobnie jak w przypadku części lotnych, podczas termicznej dekompozycji dochodzi do rozkładu i odgazowania związków organicznych, które także stanowią części palne, skutkując zmniejszeniem ich procentowych udziałów w toryfikatach. W przypadku toryfikatów zestawionych w tabeli 3, największy ubytek materii organicznej odnotowano dla odchodów słonia, zmniejszenie udziału materii organicznej o 17,3%, natomiast najmniejszy ubytek materii organicznej wynoszący 4,3% odnotowano dla osadu ściekowego. Różnica w ilości utraconej materii organicznej oraz części palnych, zależy od parametrów procesu w których wyprodukowano toryfikat oraz od właściwości przetwarzanego materiału [15,17–20]. Materiały mniej trwałe termiczne (łatwiej ulegające rozkładowi termicznemu), będą charakteryzowały się większym ubytkiem materii organicznej i części palnych, niż materiały o większej trwałości nawet jeśli będą przetwarzane w tych samych warunkach [15,17–20]. Ciekawym przypadkiem jest natomiast PLA dla którego nie zaobserwowano zmian w zawartości materii organicznej oraz części palnych (tabela 3) co wynika najprawdopodobniej z faktu, że materiał ten w całości składa się z materii organicznej i jej ubytek nie powoduje zmniejszenia względnego udziału materii organicznej i części palnych.

Najważniejszą właściwością paliwa jest jego ciepło spalania. Ciepło spalania wskazuje, ile energii zostanie wydzielone podczas całkowitego i zupełnego spalenia suchego paliwa [42]. Z przebadanych materiałów, najwyższą wartość ciepła spalania posiadał PLA oraz borowina, odpowiednio 19549 $J \cdot g^{-1}$ i 19013 $J \cdot g^{-1}$. Względnie wysoką wartość ciepła spalania posiadało także drewno, poferment oraz papier, których wartości wyniosły odpowiednio 18295 $J \cdot g^{-1}$, 18087 $J \cdot g^{-1}$ i 17525 $J \cdot g^{-1}$. Natomiast najniższą wartość posiadał osad ściekowy oraz odchody słonia, odpowiednio 14590 $J \cdot g^{-1}$ i 11410 $J \cdot g^{-1}$ (tabele 3). Poza osadami ściekowymi i odchodami słonia przebadane materiały wykazywały zbliżoną wartość energetyczną do biomasy odpadowej i roślin energetycznych ~17500-18500 $J \cdot g^{-1}$ [43,44]. Dzięki zastosowaniu toryfikacji, udało się zwiększyć ciepło spalania badanych materiałów. Największy wzrost ciepła spalania wynoszący 20,44% odnotowano dla drewna odpadowego. Wysoki, lecz dwukrotnie mniejszy wzrost wynoszący między 11%, a 13% odnotowano dla pofermentu, borowiny odchodów słonia oraz papieru. Natomiast w przypadku osadów ściekowych oraz PLA wzrost ten wyniósł niecałe 2% (tabela 3). Pomimo wzrostu ciepła spalania dla większości badanych materiałów, uzyskane wartości nadal są relatywnie niskie w porównaniu do węgla wykorzystywane w energetyce ~27000 $J \cdot g^{-1}$ [45]. Materiał po toryfikacji znacznie bardziej nadaje się do współspalania z węglem ponieważ, ma niższą wilgotność, oraz jego rozdrobnienie wymaga mniejszych nakładów energii [46]. Ponadto toryfikat posiada większe zagęszczenie energii niż nieprzetworzony materiał, w związku z powyższym więcej energii w jednostce czasu może być dozowane do komory pieca [46]. Zwiększenie ciepła spalania oraz zmniejszenie objętości toryfikatu jest uzyskiwane poprzez minimalizowanie stosunku tlenu do węgla (O/C) oraz wodoru do węgla (H/C) na skutek odgazowania niskoenergetycznych części lotnych i wody chemicznie związanej zawartej w przetwarzanym materiale [47]. Ponadto relatywnie niska temperatura procesu toryfikacji oraz niska wartość szybkości ogrzewania pozwala uniknąć reakcji karbonizacji, maksymalizując tym samym wydajność masową [47]. Nie mniej jak wykazały przeprowadzone badania, każdy materiał charakteryzuje się odmiennymi parametrami technologicznymi w których uzyskuje największe wartości ciepła spalania, natomiast po przekroczeniu których wartości te zaczynają spadać [15,17–20]. Najprawdopodobniej, początkowy wzrost wartości ciepła spalania wraz ze wzrostem temperatury wynika z odgazowania niskoenergetycznych substancji zawierających znaczące ilości tlenu. Po przekroczeniu granicznej wartości temperatury, odgazowaniu zaczynają ulegać również związki zawierające większą wartość energetyczna np. węgiel elementarny w formie CO lub CO_2. W następstwie skutkuje to zmniejszeniem nominalnej ilości materii palnej, a zwiększeniem względnej ilości popiołu w toryfikacie.

W tabeli 4 przedstawiono dane dotyczące parametrów kinetycznych toryfikacji badanych materiałów pochodzące z publikacji [16–20]. W tabeli zestawiono parametry kinetyczne wykonane w warunkach izotermicznych dla 5 z 7 badanych materiałów. Dla PLA i papieru wyznaczono parametry kinetyczne w warunkach nieizotermicznych. Z tego względu, wartości parametrów kinetycznych dla PLA i papieru nie zostały ujęte. Pełen opis znajduje się natomiast w publikacji [20]. Zmiana metody wynikała z faktu, że materiały te były badane jako ostatnie, i podczas analizy PLA, używany sprzęt okazało się nieodpowiedni. Podczas pomiaru PLA ulegało upłynnieniu pod wpływem temperatury i wyciekało z tygla pomiarowego poniżej strefy grzania. Tabela 4 zawiera średnie wartości stałej szybkości reakcji, dla modelu równania reakcji pierwszego rzędu, energię aktywacji oraz wartość współczynnika przedwykładniczego. Dokładne dane stałych szybkości reakcji dla poszczególnych temperatur są dostępne w publikacjach [16–19]. Wyznaczone wartości energii aktywacji oraz współczynnik przedwykładniczego można wykorzystać do wyznaczenia stałej szybkości reakcji dla dowolnej temperatury i tym samym zamodelować zmianę masy materiału w czasie znacznie dokładnie, niż miało to miejsce z wykorzystaniem wyznaczonej wydajności masowej (MY). MY pełni funkcję łączącą wartości czasu, w którym materiał był ogrzewany do zadanej temperatury, czasu przebywania materiału w zadanej temperaturze oraz czasu chłodzenia materiału po procesie jako jedną wartość. W związku z powyższym może to powodować duże błędy przy stosowaniu modelu wyznaczonego np. na piecu muflowym do instalacji przemysłowej. Natomiast parametry kinetyczne można wykorzystać do modelowania ubytku masy dla dowolnych wartości temperatury i czasu oddziaływania temperatury na materiał. Przykład symulacji z wykorzystaniem parametrów przedstawiono w publikacjach [16,19].

Tabela 4. Zestawienie porównawcze parametrów kinetycznych toryfikacji dla poszczególnych materiałów

Materiał	**k, s^{-1}**	**E_a, $J \cdot mol^{-1}$**	**A, s^{-1}**
Drewno odpadowe	$3{,}90 \times 10^{-5}$	36440	$1{,}53 \times 10^{-1}$
Osad ściekowy	$1{,}93 \times 10^{-5}$	46704	$7{,}48 \times 10^{-1}$
Poferment	$1{,}62 \times 10^{-5}$	52227	$1{,}94 \times 10^{0}$
Borowina	$2{,}23 \times 10^{-5}$	22025	$3{,}41 \times 10^{-3}$
Odchody słonia	$1{,}67 \times 10^{-5}$	17725	$9{,}60 \times 10^{-4}$
PLA	-	-	-
Papier	-	-	-

Z kolei wartości średnie stałych szybkości reakcji można wykorzystać do porównania trwałości termicznej materiałów. Im wyższa wartość k, tym szybciej materiał ulega dekompozycji lub większy stopień odgazowania/konwersji zostanie osiągnięty w tych samych warunkach. Z uzyskanych danych przedstawionych w tabeli 4 wynika, że najłatwiej ulegającym dekompozycji jest drewno odpadowe $3{,}90 \times 10^{-5}$ s^{-1}, oraz borowina $2{,}23 \times 10^{-5}$ s^{-1}. Natomiast znacznie niższe wartości posiadał poferment $1{,}62 \times 10^{-5}$ oraz odchody słonia $1{,}67 \times 10^{-5}$. Na szybkość rozkładu poza

zawiązkami organicznymi wchodzącymi w skład materiał, może mieć wpływ także zawartość popiołu. Badane materiały posiadały znaczne wartości popiołu i niejako wartość k maleje wraz ze wzrostem zawartości popiołu w badanych materiałach (tabela 3 i 4). Wynika to najprawdopodobniej z faktu, że materiał zawierający więcej popiołu posiada mniej materii organicznej, która może ulec dekompozycji pod wpływem temperatury. Wpływa to bezpośrednio na zmniejszenie utraty masy, która jest używana do oszacowania wartości k [48,49].

5.1.2 Wpływ ciśnienia na wydajność procesu i właściwości paliwowe

W tabeli 5 przedstawiono właściwości procesu toryfikacji i właściwości paliwowe toryfikatów wytworzonych w reaktorze ciśnieniowym wraz z wartością maksymalnego nadciśnienia uzyskanego w reaktorze. Proces prowadzono w temperaturze 300°C i trwał 60 min.

Tabela 5. Efektywność toryfikacji i właściwości paliwowe toryfikatów wyprodukowanych w reaktorze ciśnieniowym w temperaturze 300°C, przy czasie przetrzymania materiału w zadanej temperaturze wynoszącym 60 min i nadciśnieniu <15 bar w przypadku procesu z zamkniętym zaworem (Z) i nadciśnieniu 0 bar dla procesu z zaworem otwartym (O)

Materiał	Proces	p, bar	MY, %	EDr, -	EY, %	MC, %	VM, %	FC, %	AC, %	VS, %	CP, %	HHV, $J \cdot g^{-1}$
Drewno odpadowe	O	0	33,8 ± 1,3	1,5 ± 0,0	55,4 ± 2,2	3,5 ± 0,1	30,9 ± 0,1	66,3 ± 0,1	2,8 ± 0,1	96,5 ± 0,2	97,2 ± 0,1	30590 ± 232
	Z	10	36,0 ± 0,9	1,6 ± 0,0	57,2 ± 1,3	3,2 ± 0,0	24,5 ± 1,1	72,8 ± 1,1	2,8 ± 0,1	96,5 ± 0,0	97,2 ± 0,1	31623 ± 59
	Zmiana, %	-	6,7	3,2	3,4	-6,9	-20,7	9,8	-2,5	0,0	0,1	3,4
Osad ściekowy	O	0	61,1 ± 2,3	0,9 ± 0,0	60,8 ± 1,2	2,5 ± 0,0	23,3 ± 0,0	19,9 ± 0,8	56,8 ± 0,2	41,4 ± 0,1	43,2 ± 0,2	13335 ± 216
	Z	7.5	66,5 ± 1,4	0,9 ± 0,0	62,8 ± 1,7	1,6 ± 0,1	21,8 ± 0,4	19,5 ± 0,5	58,7 ± 0,3	39,5 ± 0,2	41,3 ± 0,3	13780 ± 20
	Zmiana, %	-	8,8	3,3	3,3	-35,0	-6,3	-2,0	3,3	-4,6	-4,3	3,3
Poferment	O	0	49,1 ± 2,0	1,2 ± 0,0	58,7 ± 2,6	4,9 ± 0,1	28,3 ± 0,1	47,0 ± 0,2	24,7 ± 0,3	73,3 ± 0,2	75,3 ± 0,3	22280 ± 294
	Z	7.5	47,6 ± 1,3	1,3 ± 0,0	62,7 ± 1,5	4,4 ± 0,0	26,0 ± 0,1	50,8 ± 0,3	23,2 ± 0,4	74,8 ± 0,4	76,8 ± 0,4	23825 ± 170
	Zmiana, %	-	-3,0	7,3	6,9	-9,8	-8,2	8,1	-6,0	2,1	2,0	6,9
Borowina	O	0	69,2 ± 1,4	1,1 ± 0,0	70,3 ± 1,9	5,7 ± 0,1	36,3 ± 0,4	43,6 ± 0,3	20,2 ± 0,7	75,9 ± 0,7	79,8 ± 0,7	21171 ± 122
	Z	10.5	63,2 ± 1,4	1,1 ± 0,0	71,5 ± 2,0	3,9 ± 0,0	30,8 ± 0,6	47,4 ± 0,4	21,8 ± 0,3	74,3 ± 0,3	78,2 ± 0,3	21535 ± 190
	Zmiana, %	-	-8,8	1,8	1,7	-31,7	-15,1	8,9	7,9	-2,1	-2,0	1,7
PLA	O	0	2,0 ± 1,7	1,3 ± 0,0	1,9 ± 2,1	11,3 ± 0,0	71,2 ± 0,0	28,9 ± 0,0	0,0 ± 0,0	100,0 ± 0,0	100,0 ± 0,0	25002 ± 592
	Z	10.5	1,5 ± 0,2	1,7 ± 0,0	2,5 ± 0,3	1,6 ± 0,0	53,7 ± 0,0	42,5 ± 0,0	3,8 ± 0,0	96,0 ± 0,0	96,2 ± 0,0	32939 ± 874
	Zmiana, %	-	-23,6	31,8	31,8	-86,3	-24,6	47,2	-	-4,0	-3,8	31,7

Pierwszy pomiar wykonano z zaworem otwartym, który umożliwiał wydostawanie się powstającego gazu z reaktora (O). Drugi pomiar wykonano przy szczelnie zamkniętym reaktorze,

gdzie wzrost temperatury i powstający torgaz (wydzielające się części lotne) powodowały wzrost ciśnienia (Z). Pierwszy pomiar był pomiarem odniesienia dla pomiaru drugiego, wykonanego w nadciśnieniu.

Dla każdego z przebadanych materiałów ciepło spalania było większe dla procesu prowadzonego w nadciśnieniu, niż gdy nadciśnienie nie było stosowane. Największy wzrost wartości ciepła spalania o ponad 31,7% odnotowano dla PLA, którego wartość w procesie w nadciśnieniu wzrosła aż do 32939 $J \cdot g^{-1}$. Wartość ciepła spalania PLA bez nadciśnienia, także była znacznie wyższa niż w przypadku toryfikacji wykonanej w piecu muflowym wyznaczonym w publikacji [20]. W przypadku pofermentu zastosowanie nadciśnienia spowodowało wzrost ciepła spalania o 6,9%, natomiast dla drewna i osadu ściekowego wzrost o 3,4% i 3,3%. Najmniej podatna na odziaływanie nadciśnienia okazała się borowina, dla której ciepło spalania wzrosło tylko o 1,7% (tabela 5). Podobnie jak w przypadku PLA widoczne są znaczące różnice między wartością ciepła spalania dla toryfikatów wytworzonych bez nadciśnienia w piecu muflowym, a reaktorze ciśnieniowym. Toryfikaty o lepszych właściwościach paliwowych powstawały podczas prowadzenia procesu w reaktorze ciśnieniowym (tabela 3 i 5). Poza zwiększeniem wartości ciepła spalania, zastosowanie nadciśnienia w procesie toryfikacji doprowadziło do zmniejszenia zawartości części lotnych we wszystkich badanych materiałach w zakresie około 6-25%, oraz zwiększenia zawartości węgla związanego o około 8-9% z wyłączeniem osadu ściekowego oraz PLA (tabela 5). Dla osadu ściekowego jako jedynego z badanych materiałów wartość węgla związanego obniżyła się o 2,0% w stosunku do procesu bez nadciśnienia, natomiast dla PLA nastąpił wzrost węgla związanego o 47,2% (tabela 5). Najprawdopodobniej obniżenie zawartości węgla w przypadku osadu ściekowego wynikało z niskiej homogeniczności próbek użytych do przeprowadzenia badań z otwartym i zamkniętym zaworem. W przypadku PLA należy zaznaczyć, że udało się zmierzyć węgiel związany, także dla pomiaru bez nadciśnienia, podczas gdy w przypadku toryfikatu wykonanego w piecu muflowym badania wskazywały brak zawartości węgla związanego w toryfikacie (tabela 3). Sytuacja ta może wynikać z faktu, że w przypadku procesu w reaktorze ciśnieniowym, części lotne przetwarzanego PLA pozostawały dłużej w komorze ulegając reakcją wtórnym, w wyniku których powstał węgiel [50]. Natomiast w przypadku pieca muflowego części lotne były wypłukiwane za pomocą gazu inertnego. Warto podkreślić, że wydajność masowa PLA przetwarzanego w reaktorze wyniosła mniej niż 2% (tabela 5), podczas gdy w przypadku pieca muflowego aż 92% [20]. Różnica ta może wynikać także z teoretycznie wyższej temperatury procesu. W przypadku reaktora ciśnieniowego temperatura wewnątrz reaktora wynosiła 300°C, natomiast ściany zewnętrzne posiadały temperaturę około

400°C (rysunek 6). Efektem tych działań było oddziaływanie na PLA temperatur z zakresu 300-400°C, czyli wyższych niż w przypadku pieca muflowego.

Analiza wyników wykazuje, że dla wszystkich przebadanych materiałów, zastosowanie nadciśnienia spowodowało zwiększenie współczynnika zagęszczenia energii oraz zwiększyło wydajność energetyczną toryfikatu. W przypadku wydajności masowej zastosowanie nadciśnienia doprowadziło do jej zmniejszenia w przypadku pofermentu i borowiny, podczas gdy dla pozostałych materiałów wartość wydajności masowej wzrosła (tabela 5).

Głównym mechanizmem powodującym zwiększenie zagęszczenia energii w toryfikacie jest zmniejszenie udziału tlenu względem zawartości węgla. Przy czym wraz z usuwaniem tlenu usunięciu ulega także część węgla w postaci torgazu zawierającego CO, CO_2 oraz innych kondensujących gazów które przyczyniają się także do zmniejszenia wydajności energetycznej procesu [51]. Z kolei proces prowadzony w nadciśnieniu powoduje uwięzienie powstających części lotnych i zawartych w nich cięższych molekuł i smół w reaktorze. Co skutkuje ich częściowym zwęgleniem i konwersją w węgiel w formie stałej, podnosząc wydajność masową i energetyczną procesu jak również zwiększając wartość ciepła spalania toryfikatu. Ponadto istnieje też możliwość, że cięższe smoły uwięzione w reaktorze po jego wystudzeniu mogą skroplić się na powierzchni toryfikatu zwiększając dodatkowo jego zagęszczenie energii [52]. Dacreis i in. [53] prowadząc toryfikację biomasy w nadciśnieniu dochodzącym do 50 bar zaobserwował wzrost zawartości węgla w stałej pozostałości oraz zmniejszenie stosunku O/C, który spowodował znaczący wzrost ciepła spalania biomasy o 40%. Podczas, gdy tradycyjna toryfikacja zwiększyła ciepło spalania o 10%. Za jedną z przyczyn takiego stanu rzeczy, podano przyspieszenie reakcji dekompozycji i reakcje odtleniania biomasy na skutek zwiększonego ciśnienia [54]. Do podobnych wniosków doszedł Agar i in. [55], którzy przeprowadzili toryfikację drewna dla wartości nadciśnienia od 1 do 21 bar, wykazując, że szybkość reakcji dekompozycji rośnie wraz ze wzrostem ciśnienia. Ponadto materiał poddany wyższemu ciśnieniu, ale w krótszym czasie pomimo takiej samej wartości wydajności masowej posiadał większą zawartość węgla, a tym samym większą wydajność energetyczną [55]. Najprawdopodobniej za zwiększoną zawartością węgla w procesie z zastosowaniem nadciśnienia odpowiadają tak zwane reakcje wtórne, dotyczące uwięzionych części lotnych i zawartych w nich reaktywnych smół. Według modelu zaproponowanego przez Jones i in. [50] smoły zawarte w częściach lotnych można podzielić na niereaktywne, pozostające smołami bez względu na temperaturę, ciśnienie i czas przebywania w reaktorze, oraz smoły reaktywne. Smoły reaktywne mogą, natomiast oddziaływać ze sobą powodując reakcje egzogenne i endogenne oraz reakcje prowadzące do wytworzenia wtórnego węgla w postaci stałej [50].

Wyniki uzyskane w pracy doktorskiej pokrywają się z danymi z literatury i potwierdzają pozytywne oddziaływanie nadciśnienia na polepszenie właściwości paliwowych toryfikatów i ilości produkowanego paliwa. Warto tu podkreślić, że nie tylko nadciśnienie, ale sama zmiana reaktora z pieca muflowego na reaktor ciśnieniowy znacząco podniosła właściwości paliwowe toryfikatów co nasuwa pytanie odnośnie optymalizacji toryfikacji i bezpośredniego porównywania wyników badań opracowanych przez różnych autorów. Podczas toryfikacji w piecu muflowym torgaz był wypłukiwany przez dozowany gaz inertny. Natomiast w reaktorze ciśnieniowym przy otwartym zaworze, torgaz swobodnie opuszczał komorę pod wpływem konwekcji. Ponadto oba urządzenia różniły się także szybkością ogrzewania wsadu oraz czasem jego chłodzenia, co jest związane z efektem skali (reaktor ciśnieniowy był większy). W związku z czym przyszłe badania powinny uwzględniać także te parametry oraz czas przebywania części lotnych w komorze reaktora, ponieważ temperatura i czas toryfikacji może nie być wystarczający do poprawnego opisu procesu.

5.2 Energochłonność procesu toryfikacji

Szczegółowe wyniki dotyczące wpływu zadanej temperatury oraz czasu jej odziaływania na energochłonność procesu oraz ich dyskusja zostały zawarte w publikacjach [17–20]. W niniejszej rozprawie w sposób syntetyczny i porównawczy zestawiono uzyskane wyniki charakteryzujące warianty o najwyższej i najniższej energochłonności w zastawieniu z wariantami, w których uzyskano toryfikaty o najlepszych właściwościach paliwowych w odniesieniu do każdego testowanego materiału. W podrozdziale 5.2.1 przedstawiono wyniki dotyczące wpływu temperatury i czasu trwania procesu na ilość energii zużytej na przetworzenie suchego materiału. Na podstawie wykonanych bilansów masy i energii, wykonano symulację zużycia energii na proces toryfikacji z uwzględnieniem pierwotnej wilgotności materiału. W podrozdziale 5.2.2 przedstawiono wpływ nadciśnienia na energochłonność, natomiast w podrozdziale 5.2.3 przedstawiono wyniki dotyczące wpływu trwałości termicznej przetwarzanego materiału na energochłonność procesu.

5.2.1 Wpływ temperatury i czasu na energochłonność procesu – bilans masy i energii

Wszystkie wyniki dotyczące wpływu zadanej temperatury oraz czasu trwania procesu na energochłonność oraz ich dyskusja zostały zawarte w publikacjach [17–20]. W tabeli 6 zestawiono natomiast parametry technologiczne, dla których uzyskano najniższą i najwyższą energochłonność procesu oraz te, w których toryfikat charakteryzował się najwyższą wartością ciepła spalania. Wartości wyznaczone w bilansie odnoszą się do sytuacji teoretycznej, w której proces przebiega bez strat energii, a materiał poddany procesowi nie zawiera w sobie wilgoci. Założono, że proces toryfikacji może być samowystarczalny energetycznie, gdy ilość energii

w wyprodukowanym torgazie jest większa niż ilość energii potrzebnej do wyprodukowania toryfikatu. Wyniki z publikacji wykazały, że proces toryfikacji może być samowystarczalny dla drewna, osadu ściekowego, pofermentu oraz papieru bez względu na warunki [18–20]. Natomiast dla borowiny i odchodów słonia, proces może być samowystarczalny energetycznie w przypadku temperatur większych niż 220°C i 240°C [17,19]. Przy czym w przypadku odchodów słonia najlepszy toryfikat można wytworzyć w 200°C (tabela 3) co powoduje, że ilość torgazu będzie niewystarczająca do produkcji toryfikatu o najlepszej jakości.

Tabela 6. Zestawienie bilansu masy i energii dla skrajnych wartości

Materiał	Energochłonność	Warunki procesu, °C/min	Masa materiału użyta do produkcji 1 g CSF, g	Energia zawarta w materiale wykorzystanym do produkcji 1 g CSF, J	Energia zewnętrzna potrzebna do produkcji 1 g CSF, J	Energia zawarta w 1 g CSF, J	Masa gazu wytworzonego przy produkcji g CSF, g	Energia zawarta w gazie wytworzonym przy produkcji 1 g CSF, J	Ilość energii zużytej na wyprodukowanie 1 J CSF, J
Drewno odpadowe	Najmniejsza	200/20	1,042	19068	142	18551	0,042	654	0,008
	Największa	300/60	1,831	33493	1058	22002	0,831	12069	0,048
	Najwyższe HHV	300/40	1,829	33454	1057	22034	0,829	11998	0,048
Osad ściekowy	Najmniejsza	200/20	1,04	15167	467	14854	0,04	762	0,031
	Największa	280/60	1,377	20090	844	11884	0,377	8819	0,071
	Najwyższe HHV	200/20	1,04	15167	467	14854	0,04	762	0,031
Poferment	Najmniejsza	200/40	1,022	18482	389	18211	0,022	652	0,021
	Największa	280/40	2,323	42010	1138	18515	1,323	23985	0,061
	Najwyższe HHV	280/20	1,686	30495	826	20215	0,686	10770	0,041
Borowina	Najmniejsza	200/40	1,027	19533	184	19941	0,027	-229	0,009
	Największa	300/60	1,446	27498	915	20873	0,446	7257	0,044
	Najwyższe HHV	280/40	1,252	23809	620	21324	0,252	2980	0,029
Odchody słonia	Najmniejsza	200/60	1,046	11936	364	13003	0,046	-718	0,028
	Największa	300/60	1,879	21444	885	8661	0,879	13255	0,102
	Najwyższe HHV	200/60	1,046	11936	364	13003	0,046	-718	0,028
PLA	Najmniejsza	220/40	1,004	19505	134	19799	0,004	-161	0,007
	Największa	300/60	1,227	23833	562	19571	0,227	4719	0,029
	Najwyższe HHV	220/40	1,004	19505	134	19799	0,004	-161	0,007
Papier	Najmniejsza	200/20	1,054	18475	346	17889	0,054	914	0,019
	Największa	300/60	2,485	43551	2336	19346	1,485	25144	0,121
	Najwyższe HHV	300/40	2,357	41303	2216	19520	1,357	22722	0,114

Na podstawie wykonanych badań i przeprowadzonych obliczeń określono, że każdy z przebadanych materiałów posiada odmienne warunki procesu zapewniające najwyższą możliwą wartość ciepła spalania oraz możliwie najmniejsze zużycie energii (tabela 6). W przypadku drewna, osadu ściekowego oraz papieru, najniższą energochłonność uzyskano dla 200°C i 20 min, podczas gdy dla pozostałych materiałów było to 220°C i 40-60 min oraz 220 °C i 40 min dla PLA (tabela 6). Oczywiste jest, że najniższe wartości energochłonności zostaną uzyskane dla najniższych wartości temperatury i najkrótszych czasów procesu, ponieważ mniej energii jest potrzebne na ogrzanie materiału do zadanej temperatury. W przypadku borowiny, odchodów słonia oraz PLA, dla parametrów technologicznych o najmniejszej energochłonności wyliczone wartości energii zawartej w torgazie okazały się być ujemne, co fizycznie nie jest możliwe. Wartości te wynikają najprawdopodobniej z przyjętego i uproszczonego sposoby wyznaczania energii zawartej w torgazie.

Największe zużycie energii odnotowano natomiast dla najwyższej temperatury i najdłuższych czasów trwania procesu wynoszących od 280°C do 300°C i 60 min (tabela 6). Podobnie jak w przypadku najmniejszej energochłonności, największą energochłonność powinna być uzyskana dla procesów o najwyższych temperaturach. W tych procesach najwięcej energii jest zużywane na podgrzanie materiału do zadanej temperatury (konieczność podgrzania materiału do wyższej temperatury, oraz konieczność podgrzania większej ilości materiału ze względu na większe odgazowanie). Z drugiej strony powyżej 200°C może dochodzić do reakcje endotermicznych i egzotermicznych [56]. W procesach endotermicznych, należy dostarczyć więcej energii, aby reakcja zaszła. Natomiast w przypadku reakcji egzotermicznych, po zajściu reakcji zostaje wyzwolona energia, która może dodatkowo podnieść temperaturę zmniejszając ilość energii potrzebnej do podgrzania materiału [56]. W związku z czym wystąpienie reakcji egzotermicznych może spowodować zmniejszenie energochłonności w przypadku zastosowania wyższej temperatury procesu.

Poza najmniejszą i największą energochłonnością procesu, w tabeli 6 zestawiono wartości energochłonności dla warunków, w których toryfikaty posiadały największe wartości ciepła spalania. Ponadto dodano kolumnę z przeliczeniem ilości dżuli zużytych na wyprodukowanie jednego dżula energii zawartego w toryfikacie. Na podstawie analizy danych wynika, że wraz ze wzrostem temperatury procesu rośnie także ilość energii jaką trzeba zużyć aby wyprodukować 1 J energii w toryfikacie (tabela 6).

Jak wspomniano wcześniej, na podstawie wykonanych badań i przeprowadzonych obliczeń, [15,17–20] każdy z przebadanych materiałów posiada odmienne warunki procesu zapewniające

najwyższą możliwą wartość ciepła spalania oraz możliwie najmniejsze zużycie energii. Dla materiałów takich jak drewno, osad ściekowy, poferment oraz papier proces toryfikacji może być samowystarczalny energetycznie, bez względu na warunki. Dla borowiny i odchodów słonia, proces może być samowystarczalny energetycznie w przypadku temperatur większych niż 220°C i 240°C [15,17–20]. Przy czym w przypadku odchodów słonia najlepszy toryfikat można wytworzyć w 200°C co powoduje, że ilość torgazu będzie niewystarczająca do produkcji toryfikatu o najlepszej jakości. Oczywiście brakującą ilość energii można pozyskać poprzez spalenie część nieprzetworzonego materiału, albo już wyprodukowanego toryfikatu. Jednak prowadzić to będzie do mniejszej wydajności energetycznej procesu. W przypadku PLA nie ma znaczenia ilość zużytej energii na proces, ponieważ toryfikacja nie prowadzi do poprawy zmian właściwości paliwowych. Natomiast w przypadku zastosowania reaktora ciśnieniowego zanotowano znaczący wzrost ciepła spalania, nie mniej wydajność masowa jak i wydajność energetyczna zmalał do wartości poniżej 2,5% (tabela 5) w związku z czym przetwarzanie PLA za pomocą toryfikacji nadal wydaje się być nieodpowiednie.

Dane przedstawione w publikacjach [17–20] i tabeli 6 dotyczą suchego materiału. Wyniki wskazują, że badane materiały nieznacznie różnią się ilością energii, którą trzeba do nich dostarczyć, aby podgrzać je do zadanej temperatury. Wartości te znajdują się w zakresie od 86 J dla PLA podczas toryfikacji w 200°C do 940 J podczas toryfikacji papieru w 300°C [20]. Wartości te pokrywają się częściowo z danymi entalpi dla procesu toryfikacji jakie można znaleźć w literaturze. Wartości te w zależności od rodzaju przetwarzanego materiału, temperatury procesu i sposobu pomiaru przyjmują wartości od -200 $J \cdot g^{-1}$ do +1350 $J \cdot g^{-1}$, gdzie (-) oznacza reakcje egzotermiczne, a (+) reakcje endotermiczne [57]. W związku z powyższym ilość energii potrzebna na podgrzanie suchego materiału jest relatywnie niska w porównaniu do ilości energii potrzebnej do odparowania wody zawartej w materiale. Teoretyczna minimalna ilość energii potrzebna do odparowania 1 g wody wynosi 2257 J (ciepło parowania wody w 100°C). Przy czym rzeczywisty proces suszenia wymaga zazwyczaj o 1,5 razy energii więcej [58], co wynika między innymi z zapotrzebowania na dodatkową energię potrzebną do zerwania wiązań i uwolnienia wilgoci związanej, wyrównania strat ciepła i pokonania oporów przenikania ciepła. W związku z czym dla suszenia konwekcyjnego, można przyjąć zapotrzebowanie energetyczne na poziomie 3500 J na 1 g odparowanej wody. Przy czym zawansowane sposoby suszenia, odzyskujące ukryte ciepło parowania za pomocą pompy ciepła mogą zmniejszyć to zapotrzebowanie nawet do 1000 $J \cdot g^{-1}$ [58].

Na rysunku 5 przedstawiono wyniki uproszczonej symulacji ilości energii potrzebnej na wykonanie toryfikacji materiału znajdującego się w stanie roboczym (zawierającego wilgotność

w momencie pozyskania materiału) względem energii zawartej w torgazie. W symulacji założono, że do odparowania 1 g wilgoci należy doprowadzić 2593 J energii (co wynika z potrzeby ogrzania wody z temperatury otoczenia (20°C) do 100°C i następnie jej odparowania). Wilgotność początkową materiałów przedstawiono na rysunku 5 h.

a) drewno odpadowe

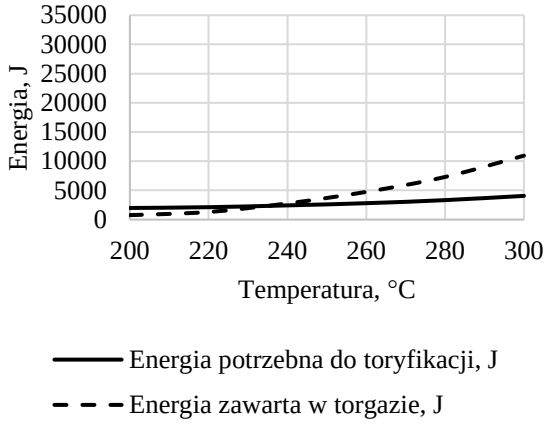

b) osad ściekowy

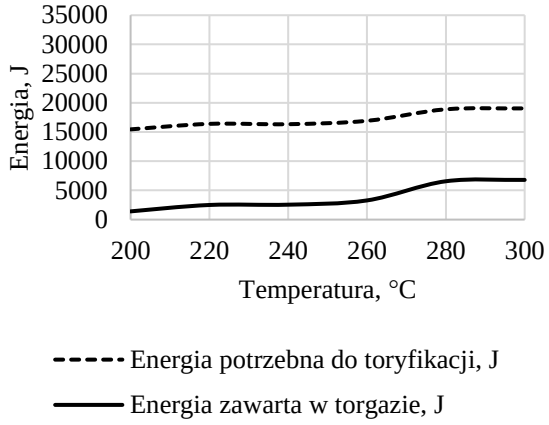

c) poferment

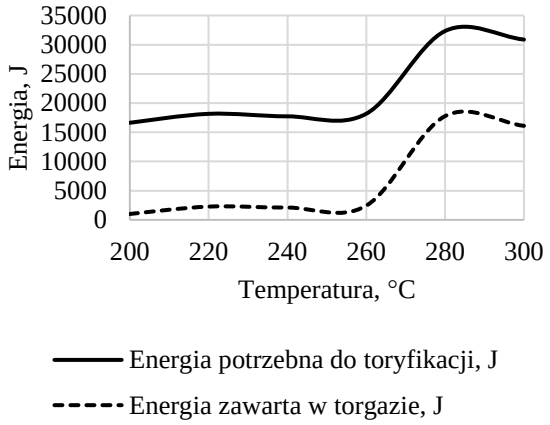

d) borowina

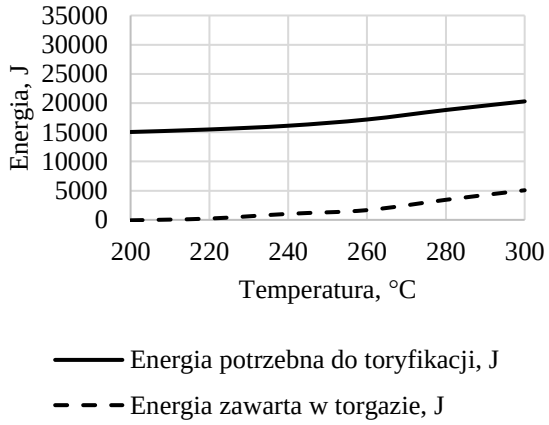

e) odchody słonia

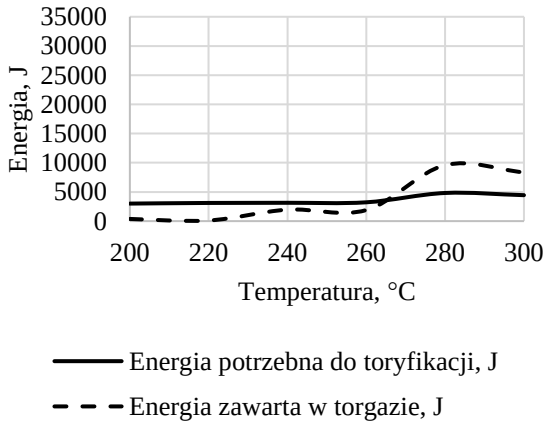

f) PLA

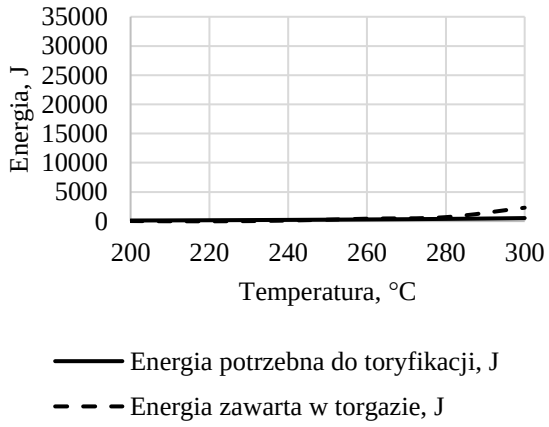

g) Papier

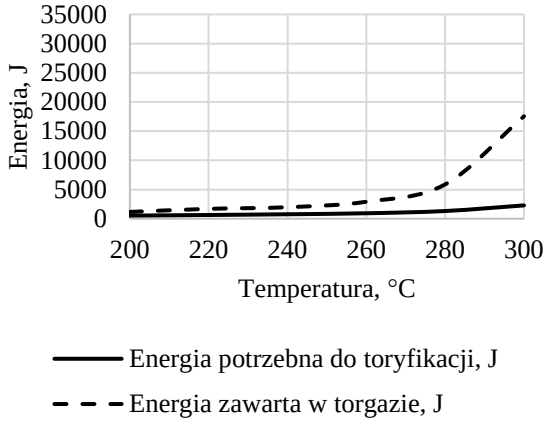

h) wilgotność materiałów

Drewno odpadowe	40,0%
Osad ściekowy	84,4%
Poferment	85,6%
Borowina	84,8%
Odchody słonia	49,2%
PLA	0,69%
Papier	6,40%

Rysunek 7. Średnia wartość energii potrzebnej do wyprodukowania 1 g toryfikatu z mokrego materiału w zależności od temperatury procesu, a) drewno odpadowe, b) osady ściekowe, c) poferment, d) borowina, e) odchody słonia, f) PLA, g) papier, h) wilgotność materiałów

Wykresy przedstawiają uśrednioną ilość energii zawartej w torgazie (na podstawie danych z publikacji [17–20] i ilość energii potrzebnej na proces toryfikacji (odparowanie wilgoci wraz z ogrzaniem mokrego materiału (wody i suchej masy) do zadanej temperatury) podczas produkcji 1 g toryfikatu. Symulacja nie uwzględnia sprawności suszenia oraz dodatkowych nakładów energii na pracę urządzeń suszarniczych. Wyniki symulacji wskazują, że materiały jak osad ściekowy, poferment i borowina ze względu na wysoką początkową wilgotność nie mogą być procesami samowystarczalnymi energetycznie bez względu na zastosowane parametry technologiczne. Natomiast drewno odpadowe, odchody słonia oraz papier, ze względu na względnie niską zawartość wilgoci oraz wystarczającą ilość wydzielanych części lotnych i zawartej w nich energii chemicznej mogą być samowystarczalne w pewnych temperaturach. W przypadku drewna jest to temperatura >240°C, dla odchodów słonia >263°C, a w przypadku papieru >200°C. Oznacza to, że z drewna jak i papieru można wyprodukować toryfikat o najlepszych właściwościach paliwowych (tabela 3) bez nakładów dodatkowej energii, podczas gdy nie jest to możliwe w przypadku odchodów słonia, dla którego najwyższą wartość ciepła spalania osiągnięto w 200°C (tabela 3). Ilość energii zawartej w torgazie wystarczy na przeprowadzenie procesu zależy przede wszystkim od początkowej wilgotności przetwarzanego materiału oraz ilości i kaloryczności wydzielonego torgazu [59]. Przedstawione obliczenia dotyczą procesu toryfikacji przeprowadzonej z sprawnością 100% w piecu muflowym, w związku z czym należy mieć na uwadze, że obliczone wartości energii zawartej w torgazie mogą nie być wystarczające na zapewnienie samowystarczalności energetycznej procesu w pełnoskalowych warunkach rzeczywistych.

5.2.2 Wpływ ciśnienia na energochłonność procesu toryfikacji

W tabeli 7 przedstawiono wyniki zużycia energii z badań przeprowadzonych w reaktorze ciśnieniowym (WUELS, RBMT2020-1.1, Wrocław, Polska). Ilość energii zużytej na proces została przeliczona na ilość energii zużytej do przetworzenia 1 g materiału umieszczonego w reaktorze, a następnie przeliczona na ilość energii zużytej na wyprodukowanie 1 g toryfikatu oraz ilość energii zużytej na wyprodukowanie 1 J energii toryfikatu. Mimo, że reaktor był ogrzewany energią elektryczną, aby zachować zgodność z poprzednią częścią pracy, zużycie energii zostało podane w dżulach, a nie w Wh.

Tabela 7. Ilość energii zużytej na proces toryfikacji przeprowadzonej w reaktorze ciśnieniowym w temperaturze 300°C, przy czasie przetrzymania materiału w zadanej temperaturze wynoszącym 60 min i nadciśnieniu dochodzącym do 15 bar w przypadku procesu z zamkniętym zaworem (Z) i nadciśnieniu 0 bar dla procesu z zaworem otwartym (O)

Materiał	Proces	Masa materiału umieszczona w reaktorze, g	Ilość energii zużytej na proces, J	Ilość energii zużytej na przetworzenie 1 g materiału, $J \cdot g^{-1}$	Ilość energii zużytej na wyprodukowanie 1 g CSF, $J \cdot g^{-1}$	Ilość energii zużytej na wyprodukowanie 1 J CSF, J
Drewno odpadowe	O	174	8 199 000	47 160	139 680	4,6
	Z	180	8 372 160	46 800	129 240	4,1
	Zmiana, %	3,2	2,1	-0,8	-7,5	-10,5
Osad ściekowy	O	230	8 547 480	37 080	60 840	4,6
	Z	231	8 375 040	36 360	54 720	4,0
	Zmiana, %	0,6	-2,0	-1,9	-10,1	-13,0
Poferment	O	205	8 139 600	39 600	81 000	3,6
	Z	213	8 310 960	39 240	82 080	3,4
	Zmiana, %	3,9	2,1	-0,9	1,3	-5,2
Borowina	O	278	8 337 240	29 880	43 200	2,0
	Z	467	8 844 840	19 080	29 880	1,4
	Zmiana, %	67,6	6,1	-36,1	-30,8	-32,0
PLA	O	170	8 287 560	48 960	2 511 360	100,4
	Z	161	8 547 120	53 280	3 576 240	108,6
	Zmiana, %	-5,4	3,1	8,8	42,4	8,1

Do reaktora umieszczano próbki o masie od 160,5 g do 466,7 g. Masa próbki umieszczonej w reaktorze wynikała z jej gęstości nasypowej oraz spodziewanego stopnia odgazowania. Największą dysproporcję w masie próbki zastosowano dla borowiny, gdzie w przypadku procesu w nadciśnieniu zastosowano prawie dwukrotność masy zastosowanej dla procesu z zaworem otwartym. Dla pozostałych materiałów różnice w masie były znacznie mniejsze co wynikało z faktu, że stopień odgazowania tych materiałów był wystarczający do poniesienia ciśnienia w komorze reaktora do wartości około 10 bar. Ponieważ reaktor miał pojemność całkowitą 22 dm^3,

natomiast ilość badanego materiału stanowiła około 0,5 dm^3, znacząca ilość dostarczanej energii była wykorzystywana na podgrzanie elementów reaktora, oraz na pokrywanie strat ciepła wynikających z niedoskonałej izolacji. W związku z czym, uzyskanych danych nie można porównywać i odnosić do wyników z pieca muflowego, które dotyczyły wyłącznie przetwarzanego materiału w warunkach 100% sprawności procesu. Dla wykorzystanego reaktora ilość energii zużytej do przetworzenia 1 g toryfikatu oraz ilość energii zużytej do wyprodukowania 1 g toryfikatu zależała od początkowej ilości wsadu co przedstawiono na rysunku 6. W zawiązku z czym przeprowadzone badanie nie może jednoznacznie wskazać, czy nadciśnienie spowodowało zmniejszeniem zapotrzebowania energetycznego na proces.

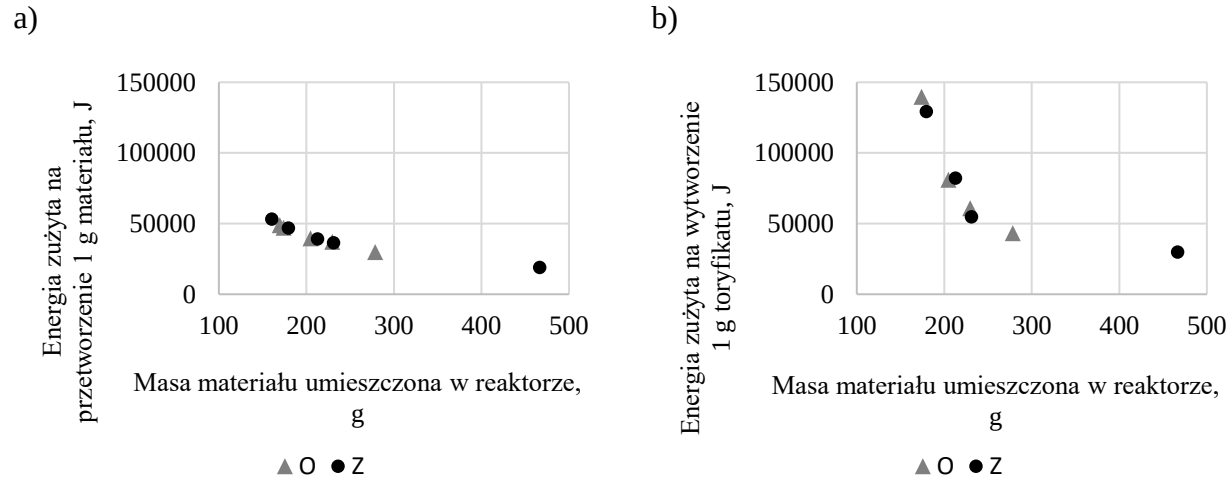

Rysunek 8. Wpływ masy początkowej umieszczonej w reaktorze ciśnieniowym na a) energię zużytą do przetworzenia 1 g materiału, b) energię zużyta do wyprodukowania 1 g toryfikatu

Dla wszystkich materiałów poza PLA, ilość energii zużytej na przetworzenie 1 g materiału była niższa w przypadku procesu prowadzonego w nadciśnieniu, z drugiej jednak strony w przeliczeniu na ilość energii zużytej na wyprodukowanie 1 g toryfikatu, już tylko 3 z 6 przebadanych materiałów charakteryzowały się niższym zużyciem energii poprzez zastosowanie nadciśnienia. Były to drewno odpadowe, osad ściekowy oraz borowina (tabela 7). Z kolei w przeliczeniu na ilość energii wykorzystanej na wyprodukowanie 1 J energii w toryfikacie dla drewna odpadowego, osadu ściekowego, pofermentu i borowiny zaobserwowano zmniejszenie zapotrzebowania na energię odpowiednio o 10,5%, 13,0%, 5,2% oraz 32,0% w przypadku zastosowania nadciśnienia. Jedynie dla PLA nadciśnienie spowodowało wzrost energii potrzebnej do wyprodukowania 1 J energii toryfikatu o 8,1% (tabela 7). W związku z czym zebrane dane nie określają jednoznacznie czy zastosowanie nadciśnienia zmniejsza ilość energii potrzebnej do procesu toryfikacji. Z kolei badania wstępne przeprowadzone na reaktorze [14], przed jego modernizacją wykorzystaną w niniejszej pracy doktorskiej wykazały, że prowadzenie procesu

w nadciśnieniu zmniejszyło ilość zużycia energii elektrycznej średnio o 6% [14]. Jak wynika z danych przedstawionych w tabeli 7 i rysunku 7 na końcowy wynik zużycia energii wpływa rodzaj i ilości przetwarzanego materiału. Z tego względu warto by było przeprowadzić dodatkowe badania na reaktorze przy większej ilości wsadu w oraz w klimatyzowanym pomieszczeniu, które wyeliminuje możliwość utraty ciepła z otoczeniem na skutek niedostatecznie doskonałej izolacji reaktora.

5.2.3 Trwałości termiczna materiału

Jedną z hipotez postawionych w pracy było stwierdzenie, że toryfikacja materiału o większej trwałości termicznej charakteryzuje się wyższym zapotrzebowaniem na energię. W związku z czym na rysunku 8 zestawiono ze sobą wyniki z analizy DSC (zużycie energii potrzebnej do podgrzania materiału do zadanej temperatury) z wynikami z analizy TGA (stałą szybkości reakcji/rozkładu). Jako trwałość termiczną w pracy uznano szybkość rozkładu materiału pod wpływem oddziaływania temperatury opisanej wartością współczynnika k wyznaczonego dla równania reakcji pierwszego rzędu. Wybrano reakcję równania pierwszego rzędu, ponieważ, założenie to jest często wykorzystywane podczas określania parametrów kinetycznych dla reakcji termicznego rozkładu [60]. Dane przedstawione na wykresie pochodzą z publikacji [16–19].

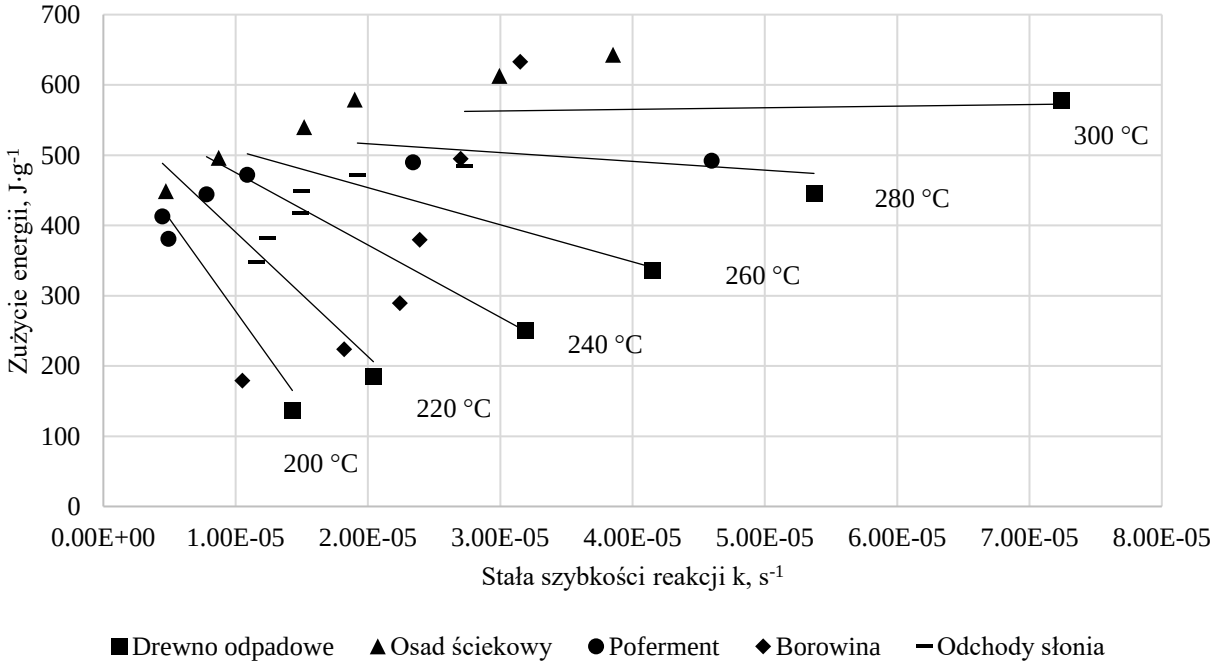

Rysunek 9. Zależność między stałą szybkości reakcji rozkładu a ilością energii zużytej do wyprodukowania 1 g toryfikatu. Liniami trendu zaznaczono pomiary wykonane dla różnych materiałów wykonane w tych samych temperaturach.

Z danych przedstawionych na wykresie wynika, że każdy z badanych materiałów charakteryzuje się odmiennymi właściwościami trwałości termicznej (k) oraz, że wraz z wzrostem

temperatury rośnie wartość współczynnika k. W zakresie temperatur 200-220°C, najmniejszą stałą szybkości reakcji wynoszącą poniżej 1 x 10^{-5} s^{-1} wyznaczono dla osadu ściekowego oraz pofermentu. Natomiast największą wartość k wynosząca ponad 7 x 10^{-5} s^{-1} wyznaczono dla drewna przetwarzanego w temperaturach 300°C. Im większa wartość k tym większa szybkość dekompozycji materiału pod wpływem danej temperatury. Liniami zaznaczono zmierzone wartości k dla poszczególnych temperatur (200-300°C). Z wykresu wynika, że wraz ze wzrostem temperatury procesu linie zaczynają stawać się równoległe względem osi x, co może sugerować, że dla procesu prowadzonego w 280°C i 300°C stałe szybkości nie mają wpływu na ilość energii zużywanej na proces. W temperaturach poniżej 280°C zmierzone wartości k dla poszczególnych materiałów układają się skośnie wskazując, że materiały z większą wartością k potrzebują mniejszą ilość energii do procesu (w odniesieniu do tych samych temperatur). Każdy z materiałów charakteryzuje się odmienną charakterystyką zużycia energii względem trwałości termicznej oraz trendem wzrostu wartości k pod wpływem temperatury. Pomimo tego, że dla każdego materiału ilość potrzebnej energii rośnie wraz ze wzrostem temperatury, to stałe k dla materiałów jak odchody słonia oraz drewna mają trend wzrostu wykładniczego, podczas gdy pozostałe charakteryzuje wzrostu logarytmiczny. Na podstawie danych przedstawionych na wykresie można stwierdzić, że trwałość termiczna może mieć wpływ na zużycie energii w zakresie od 200°C do 260°C, gdyż linie temperatury ukazują zmniejszanie się ilości energii wraz ze wzrostem wartości k. Oznacza to, że w tych temperaturach materiały łatwiej ulegające dekompozycji potrzebują mniej energii. Przyczyną takiego stanu może być fakt, że im większa część materiału zostanie odgazowana w niższej temperaturze, to zmniejsza się masa próbki, którą będzie trzeba następnie podgrzać do wyższej temperatury.

6 Wnioski i konkluzje

Postawiony problem badawczy pracy dotyczył zbadania zasadności stosowania toryfikacji jako metody waloryzacji wybranych materiałów o niskich wartościach energetycznych. W tym celu zaprojektowano badania, które określiły wpływ parametrów toryfikacji (temperatury, czasu trwania procesu, ciśnienia) na zmianę właściwości paliwowych waloryzowanych materiałów oraz ilość energii zużytej na proces.

Analiza wyników przedstawionych w podrozdziale 5.1.1 wykazała, że wraz ze wzrostem temperatury i czasu trwania procesu polepszają się właściwości paliwowe materiałów. Natomiast zbyt wysoka temperatura, bądź zbyt długi czas przebywania materiału w zadanej temperaturze może powodować pogorszenie się właściwości paliwowych i zmniejszenie ilości produkowanego toryfikatu. Na skutek zbyt dużej utraty atomów węgla względem atomów tlenu i rosnącego udziału frakcji mineralnej. W związku z czym hipotezy H1 – *wzrost temperatury toryfikacji prowadzi do polepszenia właściwości paliwowych przetwarzanego materiału* oraz H2 – *wydłużenie procesu toryfikacji prowadzi do polepszenia właściwości paliwowych przetwarzanego materiału* są prawdziwe tylko dla pewnych zakresów temperatur i czasów, które różnią się w zależności od przetwarzanego materiału. Podsumowując, dla przebadanych materiałów z wykluczeniem PLA, wzrost temperatury i czasu trwania procesu powoduję poprawę właściwości energetycznych toryfikatów

- dla drewna odpadowego do 300°C i 40 min o 20%;
- dla osadu ściekowego do 200°C i 20 min o 2%;
- dla pofermentu z biogazowni do 280°C i 40 min o 12%;
- dla borowiny do 280°C i 40 min o 12%;
- dla papieru do 300°C i 40 min o 11%.

W podrozdziale 5.1.2 przedstawiono wpływ zastosowania nadciśnienia na ilość i właściwości paliwowe toryfikatów. Postawiona w pracy hipoteza H3 – *Wzrost ciśnienia procesu toryfikacji prowadzi do polepszenia właściwości paliwowych przetwarzanego materiału* okazała się prawdziwa dla wszystkich badanych materiałów. W przypadku drewna odpadowego, osadu ściekowego i borowiny, nadciśnienie pozytywnie wpłynęło na zwiększenie ciepła spalania od 1,7% do 3,4%, dla pofermentu o 7% natomiast dla PLA aż o 31,7%. Wzrost ciepła spalania podczas zastosowania nadciśnienia wynikał bezpośrednio ze zwiększenia udziału węgla związanego w stosunku do udziału części lotnych. Najprawdopodobniej poprzez uwięzienie części lotnych i substancji smolistych w reaktorze. Zawarte w nich smoły reaktywne pod wpływem ciśnienia i temperatury zostały przekonwertowane do węgla związanego. Natomiast smoły niereaktywne

po ostudzeniu reaktora i skondensowaniu, pokryły dodatkowo wierzchnią warstwę toryfikatu zwiększając dodatkowo udział węgla podnosząc jego wartość kaloryczną.

W podrozdziale 5.2.1 przedstawiono wyniki dotyczące wpływy temperatury procesu i czasu przebywania materiału w zadanej temperaturze na ilość energii zużytej do przeprowadzenia toryfikacji. Najpierw dla suchego materiału, następnie dodatkowo dla materiału w stanie roboczym w celu odpowiedzenia na *problem badawczy*. Wyniki z obliczeń wykazały, że każdy z badanych materiałów będąc w stanie suchym może wytworzyć tyle torgazu, który będzie posiadał wystarczającą ilość energii na podtrzymanie procesu. W przypadku odchodów słonia warunki, w których uzyskuje się najlepszy toryfikat nie pozwalają na samo podtrzymanie procesu poprzez spalenie torgazu. Natomiast przetwarzanie PLA, w żadnym z rozważanych przypadków nie jest uzasadnione ze względu na brak zwiększenia ciepła spalania toryfikatu. Ponadto po uwzględnieniu wilgotności materiału, proces toryfikacji może być samowystarczalny tylko dla drewna odpadowego w temperaturze większej niż 240°C, dla odchodów słonia powyżej 263°C i papieru powyżej 200°C.

W podrozdziale 5.2.2 przedstawiono wyniki dotyczące zużycia energii na proces toryfikacji w nadciśnieniu w celu stwierdzenia poprawności hipotezy H4 – *Toryfikacja w nadciśnieniu skutkuje zmniejszeniem zapotrzebowania energii na proces*. Przeprowadzone badania nie pozwoliły jednoznacznie stwierdzić prawidłowości postawionej hipotezy. Hipoteza w domyśle zakładała, że skoro torgaz nie opuszcza komory reaktora to wraz z nim nie jest odprowadzane ciepło, więc mniej energii potrzeba, aby ogrzać materiał do wyższej temperatury. W przeprowadzonych badaniach relatywnie mała masa próbki w stosunku do wielkości reaktora, a tym samym jego pojemności cieplnej oraz strat ciepła na izolacji uniemożliwiła uzyskanie jednoznacznych wyników. Z jednej strony dla wszystkich materiałów poza PLA, ilość energii zużytej na przetworzenie 1 g materiału była niższa w przypadku procesu prowadzonego w nadciśnieniu, natomiast po przeliczeniu na ilość energii zużytej na wyprodukowanie 1 g toryfikatu, już tylko 3 z 6 przebadanych materiałów charakteryzowały się niższym zużyciem energii w przypadku zastosowania nadciśnienia.

W podrozdziale 5.2.3 przedstawiono wyniki dotyczące wpływu trwałości termicznej przetwarzanego materiału na ilość energii zużytej na proces w celu sprawdzenia poprawności hipotezy H5 – *Toryfikacja materiału o większej trwałości termicznej charakteryzuje się wyższym zapotrzebowaniem na energię*. Hipoteza powstała z domysłem, że materiał trudniej ulegający dekompozycji potrzebuje więcej czasu i wyższej temperatury procesu aby zostać przetworzonym. Przy czym zestawienie wyników TGA i DSC badanych materiałów wykazało, że trwałość termiczna materiału może mieć wpływ na zużycie energii w zakresie od 200°C do 260°C. Uzyskane wyniki

nie określiły jednoznacznie zależności między trwałością termiczną, a zużyciem energii, ponieważ każdy z materiałów charakteryzował się odmienną trwałością termiczną (k) w badanych temperaturach.

Podsumowując, wyniki z przeprowadzonych badań pozwoliły na nieodrzucenie 3 z 5 postawionych hipotez, z czego 2 hipotezy (H1 i H2) zostały przyjęte tylko dla pewnych zakresów temperatury i czasu trwania procesu, natomiast 1 hipotezę (H3) przyjęto w całym zakresie toryfikacji. Dla 2 hipotez (H4 i H5) nie udało się znaleźć jednoznacznej odpowiedzi ze względu na niewystarczające dane. W związku z czym konieczne jest zaprojektowanie dodatkowych badań które to umożliwią . Uzyskane wyniki pozwoliły natomiast na osiągnięcie zakładanego celu pracy, czyli określenia wpływu parametrów technologicznych toryfikacji odpadów i biomasy (temperatury, czasu i ciśnienia) na ilość produkowanego toryfikatu, jego właściwości paliwowe oraz ilość energii zużytej na proces.

Po przeprowadzeniu badań i wykonaniu analizy uzyskanych rezultatów wnioskować należy, że zabrakło pewnych analiz, które umożliwiłyby lepsze zrozumienie zmian zachodzących podczas procesu toryfikacji badanych materiałów oraz ich wpływu na właściwości paliwowe uzyskiwanych toryfikatów. W celu lepszego wyjaśnienia postawionych hipotez H1 i H2 proponuje się, aby w przyszłych badaniach uwzględnić skład elementarny przed i po procesie dla frakcji stałej, wyznaczyć zawartość składu chemicznego torgazu oraz wydzielić i zbadać skład frakcji ciekłej. Dokładna znajomość zmiany udziału związków organicznych jak i pierwiastków elementarnych wyznaczona odrębnie dla wszystkich frakcji pozwoliłaby na określenie wpływu temperatury i czasu na ich migrację w różnych produktach procesu toryfikacji. Ponadto znajomość składu frakcji płynnej będących źródłem smół w procesie toryfikacji, umożliwiłaby sprawdzenie czy to faktycznie smoły miały decydujący wpływ na zwiększenie wydajności masowej i wartości ciepła spalania podczas procesu w nadciśnieniu (H3). Natomiast wykonanie sprzężonych analiz TGA-DSC chrakteryzujących skład chemiczny badanych materiałów oraz czystych substancji budujących poszczególne materiały, pozwoliłyby na określenie ich trwałości termicznej oraz ilość energii potrzebnej na ich rozłożenie. Dodatkowo pozwoliłoby to także na określenie zachodzących interakcji pomiędzy komponentami budującymi poszczególne materiały. Interakcje takie mogą powodować zwiększenie bądź zmniejszenie ilości energii potrzebnej na przetworzenie danego materiału.

7 Bibliografia

1. di Foggia, G.; Beccarello, M. Drivers of Municipal Solid Waste Management Cost Based on Cost Models Inherent to Sorted and Unsorted Waste. *Waste Management* **2020**, *114*, 202–214, doi:10.1016/j.wasman.2020.07.012.
2. Mathioudakis, D.; Papadopoulou, K.; Lytras, G.M.; Pavlopoulos, C.; Niakas, S.; Filippou, K.; Melanitou, E.; Lekkas, D.F.; Lyberatos, G. A Detailed Characterization of Household Municipal Solid Waste. *Waste and Biomass Valorization* **2021**, *12*, 2945–2957, doi:10.1007/s12649-020-01260-6.
3. Weber, K.; Quicker, P.; Hanewinkel, J.; Flamme, S. Status of Waste-to-Energy in Germany, Part I – Waste Treatment Facilities. *Waste Management & Research* **2020**, *38*, 23–44, doi:10.1177/0734242X19894632.
4. Directive 2008/98/EC of the European Parliament and of the Council of 19 November 2008 on Waste and Repealing Certain Directives 2008.
5. Chen, W.-H.; Lin, B.-J.; Lin, Y.-Y.; Chu, Y.-S.; Ubando, A.T.; Show, P.L.; Ong, H.C.; Chang, J.-S.; Ho, S.-H.; Culaba, A.B.; et al. Progress in Biomass Torrefaction: Principles, Applications and Challenges. *Progress in Energy and Combustion Science* **2021**, *82*, 100887, doi:10.1016/j.pecs.2020.100887.
6. Adeleke, A.A.; Odusote, J.K.; Ikubanni, P.P.; Lasode, O.A.; Malathi, M.; Paswan, D. Essential Basics on Biomass Torrefaction, Densification and Utilization. *International Journal of Energy Research* **2021**, *45*, 1375–1395, doi:10.1002/er.5884.
7. Mamvura, T.A.; Danha, G. Biomass Torrefaction as an Emerging Technology to Aid in Energy Production. *Heliyon* **2020**, *6*, e03531, doi:10.1016/j.heliyon.2020.e03531.
8. Rasheed, T.; Anwar, M.T.; Ahmad, N.; Sher, F.; Khan, S.U.-D.; Ahmad, A.; Khan, R.; Wazeer, I. Valorisation and Emerging Perspective of Biomass Based Waste-to-Energy Technologies and Their Socio-Environmental Impact: A Review. *Journal of Environmental Management* **2021**, *287*, 112257, doi:10.1016/j.jenvman.2021.112257.
9. Wijekoon, P.; Wickramasinghe, C.; Athapattu, B.C.L.; Narayana, M.; de Alwis, A.; Vithanage, M. Biomass Valorization and Phytoremediation as Integrated Technology for Municipal Solid Waste Management for Developing Economic Context. *Biomass Conversion and Biorefinery* **2021**, *11*, 363–382, doi:10.1007/s13399-020-00818-7.
10. Negi, S.; Jaswal, G.; Dass, K.; Mazumder, K.; Elumalai, S.; Roy, J.K. Torrefaction: A Sustainable Method for Transforming of Agri-Wastes to High Energy Density Solids

(Biocoal). *Reviews in Environmental Science and Bio/Technology* **2020**, *19*, 463–488, doi:10.1007/s11157-020-09532-2.

11. Shankar Tumuluru, J.; Sokhansanj, S.; Hess, J.R.; Wright, C.T.; Boardman, R.D. A Review on Biomass Torrefaction Process and Product Properties for Energy Applications. *Industrial Biotechnology* **2011**, *7*, 384–401, doi:10.1089/ind.2011.7.384.
12. Su, K.; Qin, Q.; Yang, J.; Li, L.; Deng, S. Recent Advance on Torrefaction Valorization and Application of Biochar from Agricultural Waste for Soil Remediation. *Journal of Renewable Materials* **2022**, *10*, 247–261, doi:10.32604/jrm.2022.018146.
13. Abdulyekeen, K.A.; Umar, A.A.; Patah, M.F.A.; Daud, W.M.A.W. Torrefaction of Biomass: Production of Enhanced Solid Biofuel from Municipal Solid Waste and Other Types of Biomass. *Renewable and Sustainable Energy Reviews* **2021**, *150*, 111436, doi:10.1016/j.rser.2021.111436.
14. Matyjewicz, B.; Świechowski, K.; Koziel, J.A.; Białowiec, A. Proof-of-Concept of High-Pressure Torrefaction for Improvement of Pelletized Biomass Fuel Properties and Process Cost Reduction. *Energies* **2020**, *13*, 4790, doi:10.3390/en13184790.
15. Świechowski, K.; Liszewski, M.; Bąbelewski, P.; Koziel, J.; Białowiec, A. Oxytree Pruned Biomass Torrefaction: Mathematical Models of the Influence of Temperature and Residence Time on Fuel Properties Improvement. *Materials* **2019**, *12*, 2228, doi:10.3390/ma12142228.
16. Świechowski, K.; Stegenta-Dabrowska, S.; Liszewski, M.; Babelewski, P.; Koziel, J.A.; Białowiec, A. Oxytree Pruned Biomass Torrefaction: Process Kinetics. *Materials* **2019**, *12*, doi:10.3390/ma12203334.
17. Stępień, P.; Świechowski, K.; Hnat, M.; Kugler, S.; Stegenta-Dąbrowska, S.; Koziel, J.A.; Manczarski, P.; Białowiec, A. Waste to Carbon: Biocoal from Elephant Dung as New Cooking Fuel. *Energies* **2019**, *12*, 1–32, doi:doi:10.3390/en12224344.
18. Świechowski, K.; Hnat, M.; Stępień, P.; Stegenta-Dąbrowska, S.; Kugler, S.; Koziel, J.A.; Białowiec, A. Waste to Energy: Solid Fuel Production from Biogas Plant Digestate and Sewage Sludge by Torrefaction-Process Kinetics, Fuel Properties, and Energy Balance. *Energies* **2020**, *13*, 3161, doi:10.3390/en13123161.
19. Świechowski, K.; Leśniak, M.; Białowiec, A. Medical Peat Waste Upcycling to Carbonized Solid Fuel in the Torrefaction Process. *Energies* **2021**, *14*, 6053, doi:10.3390/en14196053.
20. Świechowski, K.; Zafiu, C.; Białowiec, A. Carbonized Solid Fuel Production from Polylactic Acid and Paper Waste Due to Torrefaction. *Materials* **2021**, *14*, 7051, doi:10.3390/ma14227051.

21. Świechowski, K.; Liszewski, M.; Bąbelewski, P.; Koziel, J.; Białowiec, A. Fuel Properties of Torrefied Biomass from Pruning of Oxytree. *Data* **2019**, *4*, 55, doi:10.3390/data4020055.
22. MPWiK S.A. We Wrocławiu Available online: https://www.mpwik.wroc.pl/ (accessed on 17 February 2022).
23. Pierwsza Rolnicza Biogazownia w Świdnicy Available online: http://bio-wat.pl/ (accessed on 17 February 2022).
24. Basu, P. Torrefaction. In *Biomass Gasification, Pyrolysis and Torrefaction*; Elsevier, 2018; pp. 93–154.
25. PN-EN 14346:2011 Standard. Waste Characteristics. Calculation of Dry Mass on the Basis of Dry Residue or Water Content.
26. Torquato, L.D.M.; Crnkovic, P.M.; Ribeiro, C.A.; Crespi, M.S. New Approach for Proximate Analysis by Thermogravimetry Using CO2 Atmosphere: Validation and Application to Different Biomasses. *Journal of Thermal Analysis and Calorimetry* **2017**, *128*, doi:10.1007/s10973-016-5882-z.
27. PN-Z-15008-04:1993 Standard. Municipal Solid Waste. Analysis of Combustible and Non-Combustible Content.
28. PN-EN 15169:2011 Standard. Waste Characteristics. Determination of Organic Matter Content for Waste, Slurry and Sludge.
29. *PN EN ISO 18125:2017-07 Solid Biofuels - Determination of Calorific Value*;
30. Stegenta, Sylwia.; Kałdun, Barbara.; Białowiec, Andrzej. Model Selection and Estimation of Kinetic Parameters of Oxygen Consumption during Biostabilization of Under-Size Fraction of Muncipal Solid Waste. *Rocznik Ochrona Środowiska* **2016**, *18*, 800–814.
31. Stępień, P.; Białowiec, A. Kinetic Parameters of Torrefaction Process of Alternative Fuel Produced from Municipal Solid Waste and Characteristic of Carbonized Refuse Derived Fuel. *Detritus* **2018**, *3*, 75–83, doi:10.31025/2611-4135/2018.13702.
32. Zhang, B.; Heidari, M.; Regmi, B.; Salaudeen, S.; Arku, P.; Thimmannagari, M.; Dutta, A. Hydrothermal Carbonization of Fruit Wastes: A Promising Technique for Generating Hydrochar. *Energies* **2018**, *11*, doi:10.3390/en11082022.
33. Dyjakon, A.; Noszczyk, T. Alternative Fuels from Forestry Biomass Residue: Torrefaction Process of Horse Chestnuts, Oak Acorns, and Spruce Cones. *Energies* **2020**, *13*, doi:10.3390/en13102468.
34. Nunes, L.J.R.; Matias, J.C.O.; Loureiro, L.M.E.F.; Sá, L.C.R.; Silva, H.F.C.; Rodrigues, A.M.; Causer, T.P.; DeVallance, D.B.; Ciolkosz, D.E. Evaluation of the Potential of

Agricultural Waste Recovery: Energy Densification as a Factor for Residual Biomass Logistics Optimization. *Applied Sciences* **2020**, *11*, 20, doi:10.3390/app11010020.

35. Dyjakon, A.; Noszczyk, T.; Sobol, Ł.; Misiakiewicz, D. Influence of Torrefaction Temperature and Climatic Chamber Operation Time on Hydrophobic Properties of Agri-Food Biomass Investigated Using the EMC Method. *Energies* **2021**, *14*, 5299, doi:10.3390/en14175299.
36. Dyjakon, A.; Sobol, Ł.; Noszczyk, T.; Mitręga, J. The Impact of Torrefaction Temperature on the Physical-Chemical Properties of Residual Exotic Fruit (Avocado, Mango, Lychee) Seeds. *Energies* **2022**, *15*, 612, doi:10.3390/en15020612.
37. Tumuluru, J.S. Comparison of Chemical Composition and Energy Property of Torrefied Switchgrass and Corn Stover. *Frontiers in Energy Research* **2015**, *3*, doi:10.3389/fenrg.2015.00046.
38. Bachmann, H.J.; Bucheli, T.D.; Dieguez-Alonso, A.; Fabbri, D.; Knicker, H.; Schmidt, H.-P.; Ulbricht, A.; Becker, R.; Buscaroli, A.; Buerge, D.; et al. Toward the Standardization of Biochar Analysis: The COST Action TD1107 Interlaboratory Comparison. *Journal of Agricultural and Food Chemistry* **2016**, *64*, 513–527, doi:10.1021/acs.jafc.5b05055.
39. Ozbayoglu, G. Energy Production From Coal. In *Comprehensive Energy Systems*; Elsevier, 2018; Vol. 3–5, pp. 788–821.
40. Cavalaglio, G.; Cotana, F.; Nicolini, A.; Coccia, V.; Petrozzi, A.; Formica, A.; Bertini, A. Characterization of Various Biomass Feedstock Suitable for Small-Scale Energy Plants as Preliminary Activity of Biocheaper Project. *Sustainability* **2020**, *12*, 6678, doi:10.3390/su12166678.
41. Zhou, H.; Long, Y.; Meng, A.; Chen, S.; Li, Q.; Zhang, Y. A Novel Method for Kinetics Analysis of Pyrolysis of Hemicellulose, Cellulose, and Lignin in TGA and Macro-TGA. *RSC Advances* **2015**, *5*, 26509–26516, doi:10.1039/C5RA02715B.
42. Noushabadi, A.S.; Dashti, A.; Ahmadijokani, F.; Hu, J.; Mohammadi, A.H. Estimation of Higher Heating Values (HHVs) of Biomass Fuels Based on Ultimate Analysis Using Machine Learning Techniques and Improved Equation. *Renewable Energy* **2021**, *179*, 550–562, doi:10.1016/j.renene.2021.07.003.
43. Słupska, M.; Dyjakon, A.; Stopa, R. Determination of Strength Properties of Energy Plants on the Example of Miscanthus-Giganteus, Rosa Multiflora and Salix Viminalis. *Energies* **2019**, *12*, doi:10.3390/en12193660.

44. Morato, T.; Vaezi, M.; Kumar, A. Assessment of Energy Production Potential from Agricultural Residues in Bolivia. *Renewable and Sustainable Energy Reviews* **2019**, *102*, 14–23, doi:10.1016/j.rser.2018.11.032.
45. Jatoi, W.B.; Khokhar, C.M.; Dewani, V.K.; Khaskheli, M.I.; Shar, G.Q.; Jakhrani, M.A.; Sirohi, M.H.; Memon, I.N.; Jatoi, A.H. Proximate Analysis of Lakhra Coal Power Plant and Its Health and Environmental Impact. *Energy Sources, Part A: Recovery, Utilization, and Environmental Effects* **2019**, 1–7, doi:10.1080/15567036.2019.1695980.
46. Sankaran, R.; Show, P.L.; Nagarajan, D.; Chang, J.-S. Exploitation and Biorefinery of Microalgae. In *Waste Biorefinery*; Elsevier, 2018; pp. 571–601.
47. Gent, S.; Twedt, M.; Gerometta, C.; Almberg, E. Introduction to Thermochemical Conversion Processes. In *Theoretical and Applied Aspects of Biomass Torrefaction*; Elsevier, 2017; pp. 1–16.
48. Naqvi, S.R.; Tariq, R.; Hameed, Z.; Ali, I.; Naqvi, M.; Chen, W.-H.; Ceylan, S.; Rashid, H.; Ahmad, J.; Taqvi, S.A.; et al. Pyrolysis of High Ash Sewage Sludge: Kinetics and Thermodynamic Analysis Using Coats-Redfern Method. *Renewable Energy* **2019**, *131*, 854–860, doi:10.1016/j.renene.2018.07.094.
49. Yang, L.; Ran, J.; Zhang, L. Mechanism and Kinetics of Pyrolysis of Coal With High Ash and Low Fixed Carbon Contents. *Journal of Energy Resources Technology* **2011**, *133*, doi:10.1115/1.4004786.
50. Jones, J.R.; Chen, Q.; Ripberger, G.D. Secondary Reactions and the Heat of Pyrolysis of Wood. *Energy Technology* **2020**, *8*, 2000130, doi:10.1002/ente.202000130.
51. Wannapeera, J.; Worasuwannarak, N. Upgrading of Woody Biomass by Torrefaction under Pressure. *Journal of Analytical and Applied Pyrolysis* **2012**, *96*, 173–180, doi:10.1016/j.jaap.2012.04.002.
52. Nhuchhen, D.R.; Basu, P. Experimental Investigation of Mildly Pressurized Torrefaction in Air and Nitrogen. *Energy & Fuels* **2014**, *28*, 3110–3121, doi:10.1021/ef4022202.
53. Dacres, O.D.; Tong, S.; Li, X.; Sun, Y.; Wang, F.; Luo, G.; Liu, H.; Hu, H.; Yao, H. Gas-Pressurized Torrefaction of Biomass Wastes: The Effect of Varied Pressure on Pyrolysis Kinetics and Mechanism of Torrefied Biomass. *Fuel* **2020**, *276*, 118132, doi:10.1016/j.fuel.2020.118132.
54. Dacres, O.D.; Tong, S.; Li, X.; Zhu, X.; Edreis, E.M.A.; Liu, H.; Luo, G.; Worasuwannarak, N.; Kerdsuwan, S.; Fungtammasan, B.; et al. Pyrolysis Kinetics of Biomasses Pretreated by

Gas-Pressurized Torrefaction. *Energy Conversion and Management* **2019**, *182*, 117–125, doi:10.1016/j.enconman.2018.12.055.

55. Agar, D.; DeMartini, N.; Hupa, M. Influence of Elevated Pressure on the Torrefaction of Wood. *Energy & Fuels* **2016**, *30*, 2127–2136, doi:10.1021/acs.energyfuels.5b01352.
56. Syguła, E.; Świechowski, K.; Hejna, M.; Kunaszyk, I.; Białowiec, A. Municipal Solid Waste Thermal Analysis—Pyrolysis Kinetics and Decomposition Reactions. *Energies* **2021**, *14*, 4510, doi:10.3390/en14154510.
57. Bates, R.B.; Ghoniem, A.F. Biomass Torrefaction: Modeling of Reaction Thermochemistry. *Bioresource Technology* **2013**, *134*, 331–340, doi:10.1016/j.biortech.2013.01.158.
58. Yun, H.; Wang, Z.; Wang, R.; Bi, X.; Chen, W.-H. Identification of Suitable Biomass Torrefaction Operation Envelops for Auto-Thermal Operation. *Frontiers in Energy Research* **2021**, *9*, doi:10.3389/fenrg.2021.636938.
59. Cardona, S.; Gallego, L.J.; Valencia, V.; Martínez, E.; Rios, L.A. Torrefaction of Eucalyptus-Tree Residues: A New Method for Energy and Mass Balances of the Process with the Best Torrefaction Conditions. *Sustainable Energy Technologies and Assessments* **2019**, *31*, 17–24, doi:10.1016/j.seta.2018.11.002.
60. Vyazovkin, S.; Burnham, A.K.; Criado, J.M.; Pérez-Maqueda, L.A.; Popescu, C.; Sbirrazzuoli, N. ICTAC Kinetics Committee Recommendations for Performing Kinetic Computations on Thermal Analysis Data. *Thermochimica Acta* **2011**, *520*, 1–19, doi:10.1016/j.tca.2011.03.034.

8 Lista załączników

1. Kacper Świechowski, Załącznik z danymi nieopublikowanymi Z1, Wyniki z badań toryfikacji w nadciśnieniu
2. Kacper Świechowski, Marek Liszewski, Przemysław Bąbelewski, Jacek A. Koziel, Andrzej Białowiec. Oxytree Pruned Biomass Torrefaction: Mathematical Models of the Influence of Temperature and Residence Time on Fuel Properties Improvement. Materials 2019, 12, 2228; doi:10.3390/ma12142228
3. Kacper Świechowski, Sylwia Stegenta-Dąbrowska, Marek Liszewski, Przemysław Bąbelewski, Jacek A. Koziel, Andrzej Białowiec. Oxytree Pruned Biomass Torrefaction: Process Kinetics. Materials 2019, 12, 3334; doi:10.3390/ma12203334
4. Paweł Stępień, Kacper Świechowski, Martyna Hnat, Szymon Kugler, Sylwia Stegenta-Dąbrowska, Jacek A. Koziel, Piotr Manczarski, Andrzej Białowiec. Waste to Carbon: Biocoal from Elephant Dung as New Cooking Fuel. Energies 2019, 12, 4344; doi:10.3390/en12224344
5. Kacper Świechowski, Martyna Hnat, Paweł Stępień, Sylwia Stegenta-Dąbrowska, Szymon Kugler, Jacek A. Koziel, Andrzej Białowiec. Waste to Energy: Solid Fuel Production from Biogas Plant Digestate and Sewage Sludge by Torrefaction-Process Kinetics, Fuel Properties, and Energy Balance. Energies 2020, 13, 3161; doi:10.3390/en13123161
6. Kacper Świechowski, Małgorzata Leśniak, Andrzej Białowiec. Medical Peat Waste Upcycling to Carbonized Solid Fuel in the Torrefaction Process. Energies 2021, 14, 6053. doi.org/10.3390/en14196053
7. Kacper Świechowski, Christian Zafiu, Andrzej Białowiec. Carbonized Solid Fuel Production from Polylactic Acid and Paper Waste Due to Torrefaction. Materials 2021, 14, 7051. doi.org/10.3390/ma14227051

Załącznik z danymi nieopublikowanymi Z1

Temat: Wyniki z badań toryfikacji w nadciśnieniu

Opracował: Kacper Świechowski

1 Zawartość załącznika

W załączniku przedstawiono wyniki z badań w formie tabelarycznej. Wyniki zawierają informacje o masie materiałów poddanych analizie i ilości wytworzonych toryfikatów, właściwościach paliwowych toryfikatów, zużycie energii na proces toryfikacji oraz charakterystyki zmiany parametrów technologicznych (temperatura płaszcza grzewczego, temperatura wewnątrz reaktora, ciśnienie wewnątrz reaktora) podczas procesu.

Spis treści

2 Wyniki badań

W tabeli Z1 i Z2 przedstawiono wyniki wygenerowane podczas procesu toryfikacji jak i na podstawie przeprowadzonych analiz. Tabel Z1 zawiera właściwości paliwowe toryfikatów, natomiast tabela 2 zawiera informacje charakteryzujące proces toryfikacji. W tabelach Z3-Z12 przedstawiono natomiast wyniki z analizy wariancji sprawdzone testem post hoc Tukey ($p<0,05$). Na czerwono zaznaczono wartości różniące się w sposób statystycznie istotny ($p<0,05$). Charakterystykę (przebieg) zmiany temperatury wewnątrz reaktora, temperatury na płaszczu grzewczym, oraz ciśnienia w reaktorze dla poszczególnych procesów przedstawiono na rysunkach Z1-Z5.

Tabela Z1. Właściwości paliwowe wytworzonych toryfikatów, O – pomiar z zaworem otwartym, Z – pomiar z zaworami zamkniętymi

Materiał	Proces	MC, %	VM, %	FC, %	AC, %	VS, %	CP, %	HHV, $J \cdot g^{-1}$
Drewno odpadowe	O	3,62	30,92	66,33	2,76	96,80	97,24	30328
		3,36	30,94	66,19	2,87	96,38	97,13	30952
		3,40	30,74	66,40	2,86	96,46	97,14	30578
	Z	3,23	24,95	72,16	2,89	96,53	97,11	31628
		3,17	25,27	72,12	2,61	96,52	97,39	31593
		3,26	23,20	74,02	2,78	96,58	97,22	31542
Osad ściekowy	O	2,43	23,00	19,98	57,02	41,21	42,98	13055
		2,49	22,50	20,69	56,82	41,38	43,18	13211
		2,47	24,33	19,01	56,66	41,49	43,34	13619
	Z	1,64	22,21	19,22	58,57	39,52	41,43	13786
		1,61	21,44	20,11	58,45	39,65	41,55	13788
		1,54	21,80	19,18	59,02	39,24	40,98	13770
Poferment	O	5,15	29,22	46,04	24,74	73,07	75,26	22049
		5,12	29,10	45,67	25,24	72,62	74,76	22086
		5,04	29,12	45,86	25,01	72,99	74,99	22767
	Z	4,39	25,86	50,42	23,73	74,38	76,27	23824
		4,48	26,04	51,03	22,93	74,86	77,07	23607
		4,44	26,10	50,92	22,98	75,10	77,02	23977
Borowina	O	5,67	36,26	44,03	19,71	76,34	80,29	21171
		5,80	36,90	43,23	19,87	76,23	80,13	21293
		5,76	35,60	43,43	20,97	75,13	79,03	21001
	Z	3,94	31,57	46,80	21,63	74,44	78,37	21334
		3,90	30,06	47,82	22,11	73,98	77,89	21846
		3,93	30,67	47,71	21,62	74,49	78,38	21448
PLA	O	11,32	71,21	28,88	-0,10	100,00	100,00	25553
		-	-	-	-	-	-	24286
		-	-	-	-	-	-	25674
	Z	1,55	53,66	42,50	3,84	95,99	96,16	31475
		-	-	-	-	-	-	33217
		-	-	-	-	-	-	33791

Tabela Z2. Efektywność procesu toryfikacji, O – pomiar z zaworem otwartym, Z – pomiar z zaworami zamkniętymi

Materiał	Proces	MY, %	EDr, -	EY, %	Masa materiału umieszczona w reaktorze, g	Zużycie energii elektrycznej, kWh
Drewno odpadowe	O	33,50	1,52	51,05	174,0	2,2775
		34,91	1,56	54,29		
		35,30	1,54	54,24		
		32,24	1,53	49,36		
		32,89	1,54	50,60		
	Z	36,39	1,59	57,83	179,6	2,3256
		36,43	1,59	57,84		
		37,02	1,58	58,67		
		35,44	1,59	56,45		
		34,81	1,59	55,37		
Osad ściekowy	O	62,28	0,89	55,73	229,6	2,3743
		64,48	0,91	58,39		
		60,28	0,93	56,27		
		59,04	0,91	54,00		
		59,41	0,92	54,75		
	Z	67,81	0,94	64,07	230,9	2,3264
		68,17	0,95	64,42		
		65,57	0,94	61,88		
		65,37	0,95	61,85		
		65,44	0,94	61,68		
Poferment	O	50,07	1,22	61,04	204,7	2,261
		51,38	1,22	62,75		
		49,85	1,26	62,75		
		47,00	1,23	58,05		
		46,75	1,23	57,28		
	Z	49,10	1,32	64,68	212,6	2,3086
		48,92	1,31	63,84		
		46,77	1,33	62,01		
		46,94	1,33	62,30		
		46,47	1,31	60,92		
Borowina	O	70,63	1,11	78,64	278,4	2,3159
		71,06	1,12	79,58		
		67,72	1,10	74,80		
		68,58	1,12	76,75		
		68,59	1,11	76,15		
	Z	64,56	1,12	72,44	466,7	2,4569
		64,99	1,15	74,67		
		61,65	1,13	69,55		
		62,51	1,13	70,73		
		62,52	1,13	70,81		
PLA	O	1,99	1,32	2,61	169,6	2,3021
		4,98	1,25	6,23		
		0,93	1,32	1,23		
		1,20	1,28	1,53		
		1,10	1,27	1,40		
	Z	1,75	1,62	2,84	160,5	2,3742
		1,70	1,71	2,91		
		1,25	1,74	2,17		
		1,39	1,71	2,38		
		1,34	1,70	2,27		

Tabela Z3. Wyniki testu post hoc Tukey dla zawartości wilgotności

Test Tukey dla MC		Drewno odpadowe		Osad ściekowy		Poferment		Borowina	
		O	Z	O	Z	O	Z	O	Z
Drewno odpadowe	O		0,008000	0,000175	0,000175	0,000175	0,000175	0,000175	0,000176
	Z	0,008000		0,000175	0,000175	0,000175	0,000175	0,000175	0,000175
Osad ściekowy	O	0,000175	0,000175		0,000175	0,000175	0,000175	0,000175	0,000175
	Z	0,000175	0,000175	0,000175		0,000175	0,000175	0,000175	0,000175
Poferment	O	0,000175	0,000175	0,000175	0,000175		0,000175	0,000175	0,000175
	Z	0,000175	0,000175	0,000175	0,000175	0,000175		0,000175	0,000175
Borowina	O	0,000175	0,000175	0,000175	0,000175	0,000175	0,000175		0,000175
	Z	0,000176	0,000175	0,000175	0,000175	0,000175	0,000175	0,000175	

Tabela Z4. Wyniki testu post hoc Tukey dla zawartości części lotnych

Test Tukey dla VM		Drewno odpadowe		Osad ściekowy		Poferment		Borowina	
		O	Z	O	Z	O	Z	O	Z
Drewno odpadowe	O		0,000175	0,000175	0,000175	0,071215	0,000175	0,000175	0,999999
	Z	0,000175		0,361719	0,002424	0,000175	0,136624	0,000175	0,000175
Osad ściekowy	O	0,000175	0,361719		0,169166	0,000175	0,001918	0,000175	0,000175
	Z	0,000175	0,002424	0,169166		0,000175	0,000180	0,000175	0,000175
Poferment	O	0,071215	0,000175	0,000175	0,000175		0,000533	0,000175	0,100293
	Z	0,000175	0,136624	0,001918	0,000180	0,000533		0,000175	0,000175
Borowina	O	0,000175	0,000175	0,000175	0,000175	0,000175	0,000175		0,000175
	Z	0,999999	0,000175	0,000175	0,000175	0,100293	0,000175	0,000175	

Tabela Z5. Wyniki testu post hoc Tukey dla zawartości węgla związanego

Test Tukey dla FC		Drewno odpadowe		Osad ściekowy		Poferment		Borowina	
		O	Z	O	Z	O	Z	O	Z
Drewno odpadowe	O		0,000175	0,000175	0,000175	0,000175	0,000175	0,000175	0,000175
	Z	0,000175		0,000175	0,000175	0,000175	0,000175	0,000175	0,000175
Osad ściekowy	O	0,000175	0,000175		0,990218	0,000175	0,000175	0,000175	0,000175
	Z	0,000175	0,000175	0,990218		0,000175	0,000175	0,000175	0,000175
Poferment	O	0,000175	0,000175	0,000175	0,000175		0,000175	0,004301	0,069894
	Z	0,000175	0,000175	0,000175	0,000175	0,000175		0,000175	0,000228
Borowina	O	0,000175	0,000175	0,000175	0,000175	0,004301	0,000175		0,000180
	Z	0,000175	0,000175	0,000175	0,000175	0,069894	0,000228	0,000180	

Tabela Z6. Wyniki testu post hoc Tukey dla zawartości popiołu

Test Tukey dla AC		Drewno odpadowe		Osad ściekowy		Poferment		Borowina	
		O	Z	O	Z	O	Z	O	Z
Drewno odpadowe	O		0,999996	0,000175	0,000175	0,000175	0,000175	0,000175	0,000175
	Z	0,999996		0,000175	0,000175	0,000175	0,000175	0,000175	0,000175
Osad ściekowy	O	0,000175	0,000175		0,000302	0,000175	0,000175	0,000175	0,000175
	Z	0,000175	0,000175	0,000302		0,000175	0,000175	0,000175	0,000175
Poferment	O	0,000175	0,000175	0,000175	0,000175		0,000367	0,000175	0,000175
	Z	0,000175	0,000175	0,000175	0,000175	0,000367		0,000175	0,002453
Borowina	O	0,000175	0,000175	0,000175	0,000175	0,000175	0,000175		0,000840
	Z	0,000175	0,000175	0,000175	0,000175	0,000175	0,002453	0,000840	

Tabela Z7. Wyniki testu post hoc Tukey dla zawartości materii organicznej

Test Tukey dla VS		Drewno odpadowe		Osad ściekowy		Poferment		Borowina	
		O	Z	O	Z	O	Z	O	Z
Drewno odpadowe	O		1,000000	0,000175	0,000175	0,000175	0,000175	0,000175	0,000175
	Z	1,000000		0,000175	0,000175	0,000175	0,000175	0,000175	0,000175
Osad ściekowy	O	0,000175	0,000175		0,000206	0,000175	0,000175	0,000175	0,000175
	Z	0,000175	0,000175	0,000206		0,000175	0,000175	0,000175	0,000175
Poferment	O	0,000175	0,000175	0,000175	0,000175		0,000207	0,000175	0,001420
	Z	0,000175	0,000175	0,000175	0,000175	0,000207		0,011083	0,623588
Borowina	O	0,000175	0,000175	0,000175	0,000175	0,000175	0,011083		0,000486
	Z	0,000175	0,000175	0,000175	0,000175	0,001420	0,623588	0,000486	

Tabela Z8. Wyniki testu post hoc Tukey dla zawartości części palnych

Test Tukey dla CP		Drewno odpadowe		Osad ściekowy		Poferment		Borowina	
		O	Z	O	Z	O	Z	O	Z
Drewno odpadowe	O		0,999996	0,000175	0,000175	0,000175	0,000175	0,000175	0,000175
	Z	0,999996		0,000175	0,000175	0,000175	0,000175	0,000175	0,000175
Osad ściekowy	O	0,000175	0,000175		0,000302	0,000175	0,000175	0,000175	0,000175
	Z	0,000175	0,000175	0,000302		0,000175	0,000175	0,000175	0,000175
Poferment	O	0,000175	0,000175	0,000175	0,000175		0,000367	0,000175	0,000175
	Z	0,000175	0,000175	0,000175	0,000175	0,000367		0,000175	0,002453
Borowina	O	0,000175	0,000175	0,000175	0,000175	0,000175	0,000175		0,000840
	Z	0,000175	0,000175	0,000175	0,000175	0,000175	0,002453	0,000840	

Tabela Z9. Wyniki testu post hoc Tukey dla ciepła spalania

Test Tukey dla HHV		Drewno odpadowe		Osad ściekowy		Poferment		Borowina	
		O	Z	O	Z	O	Z	O	Z
Drewno odpadowe	O		0,003488	0,000175	0,000175	0,000175	0,000175	0,000175	0,000175
	Z	0,003488		0,000175	0,000175	0,000175	0,000175	0,000175	0,000175
Osad ściekowy	O	0,000175	0,000175		0,287412	0,000175	0,000175	0,000175	0,000175
	Z	0,000175	0,000175	0,287412		0,000175	0,000175	0,000175	0,000175
Poferment	O	0,000175	0,000175	0,000175	0,000175		0,000189	0,000747	0,026338
	Z	0,000175	0,000175	0,000175	0,000175	0,000189		0,000175	0,000175
Borowina	O	0,000175	0,000175	0,000175	0,000175	0,000747	0,000175		0,543452
	Z	0,000175	0,000175	0,000175	0,000175	0,026338	0,000175	0,543452	

Tabela Z10. Wyniki testu post hoc Tukey dla wydajności masowej toryfikacji

Test Tukey dla MY		Drewno odpadowe		Osad ściekowy		Poferment		Borowina		PLA	
		O	Z	O	Z	O	Z	O	Z	O	Z
Drewno odpadowe	O		0,366656	0,000158	0,000158	0,000158	0,000158	0,000158	0,000158	0,000158	0,000158
	Z	0,366656		0,000158	0,000158	0,000158	0,000158	0,000158	0,000158	0,000158	0,000158
Osad ściekowy	O	0,000158	0,000158		0,000201	0,000158	0,000158	0,000158	0,430851	0,000158	0,000158
	Z	0,000158	0,000158	0,000201		0,000158	0,000158	0,111722	0,043381	0,000158	0,000158
Poferment	O	0,000158	0,000158	0,000158	0,000158		0,904496	0,000158	0,000158	0,000158	0,000158
	Z	0,000158	0,000158	0,000158	0,000158	0,904496		0,000158	0,000158	0,000158	0,000158
Borowina	O	0,000158	0,000158	0,000158	0,111722	0,000158	0,000158		0,000161	0,000158	0,000158
	Z	0,000158	0,000158	0,430851	0,043381	0,000158	0,000158	0,000161		0,000158	0,000158
PLA	O	0,000158	0,000158	0,000158	0,000158	0,000158	0,000158	0,000158	0,000158		0,999859
	Z	0,000158	0,000158	0,000158	0,000158	0,000158	0,000158	0,000158	0,000158	0,999859	

Tabela Z11. Wyniki testu post hoc Tukey dla współczynnika zagęszczenia energii

Test Tukey dla EDr		Drewno odpadowe		Osad ściekowy		Poferment		Borowina		PLA	
		O	Z	O	Z	O	Z	O	Z	O	Z
Drewno odpadowe	O		0,010970	0,000158	0,000158	0,000158	0,000158	0,000158	0,000158	0,000158	0,000158
	Z	0,010970		0,000158	0,000158	0,000158	0,000158	0,000158	0,000158	0,000158	0,000158
Osad ściekowy	O	0,000158	0,000158		0,292121	0,000158	0,000158	0,000158	0,000158	0,000158	0,000158
	Z	0,000158	0,000158	0,292121		0,000158	0,000158	0,000158	0,000158	0,000158	0,000158
Poferment	O	0,000158	0,000158	0,000158	0,000158		0,000158	0,000158	0,000158	0,002918	0,000158
	Z	0,000158	0,000158	0,000158	0,000158	0,000158		0,000158	0,000158	0,292121	0,000158
Borowina	O	0,000158	0,000158	0,000158	0,000158	0,000158	0,000158		0,853736	0,000158	0,000158
	Z	0,000158	0,000158	0,000158	0,000158	0,000158	0,000158	0,853736		0,000158	0,000158
PLA	O	0,000158	0,000158	0,000158	0,000158	0,002918	0,292121	0,000158	0,000158		0,000158
	Z	0,000158	0,000158	0,000158	0,000158	0,000158	0,000158	0,000158	0,000158	0,000158	

Tabela Z12. Wyniki testu post hoc Tukey dla wydajności energetycznej

Test Tukey dla EY		Drewno odpadowe		Osad ściekowy		Poferment		Borowina		PLA	
		O	Z	O	Z	O	Z	O	Z	O	Z
Drewno odpadowe	O		0,001350	0,039734	0,000158	0,000158	0,000158	0,000158	0,000158	0,000158	0,000158
	Z	0,001350		0,962342	0,000803	0,186024	0,000859	0,000158	0,000158	0,000158	0,000158
Osad ściekowy	O	0,039734	0,962342		0,000167	0,009226	0,000168	0,000158	0,000158	0,000158	0,000158
	Z	0,000158	0,000803	0,000167		0,530244	1,000000	0,000158	0,000158	0,000158	0,000158
Poferment	O	0,000158	0,186024	0,009226	0,530244		0,547516	0,000158	0,000158	0,000158	0,000158
	Z	0,000158	0,000859	0,000168	1,000000	0,547516		0,000158	0,000158	0,000158	0,000158
Borowina	O	0,000158	0,000158	0,000158	0,000158	0,000158	0,000158		0,000810	0,000158	0,000158
	Z	0,000158	0,000158	0,000158	0,000158	0,000158	0,000158	0,000810		0,000158	0,000158
PLA	O	0,000158	0,000158	0,000158	0,000158	0,000158	0,000158	0,000158	0,000158		1,000000
	Z	0,000158	0,000158	0,000158	0,000158	0,000158	0,000158	0,000158	0,000158	1,000000	

a) b)

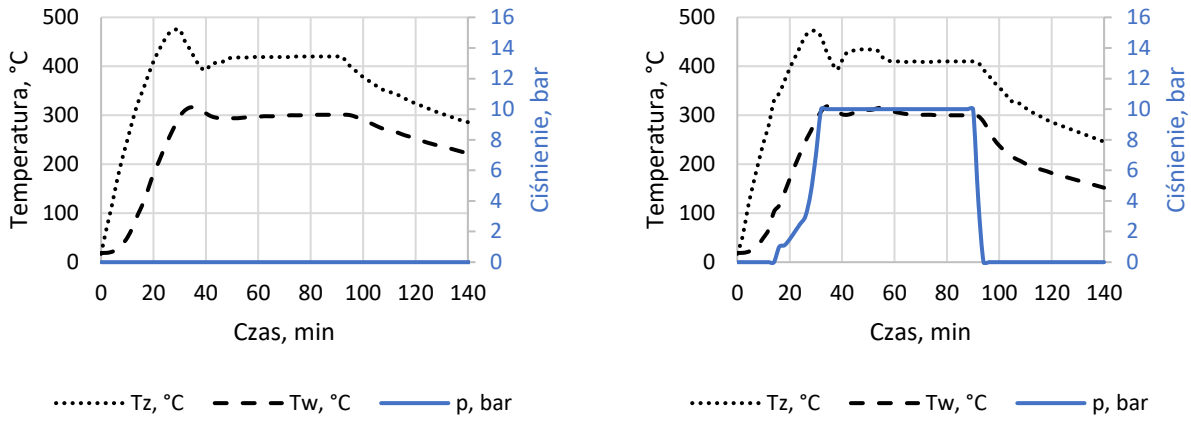

Rysunek Z1. Przebieg zmian temperatury zewnętrznej (płaszcza grzewczego), wewnętrznej (wewnątrz reaktora) oraz ciśnienia dla drewna odpadowego, a) pomiar z zaworem otwartym (O), b) pomiar z zaworami zamkniętymi (Z)

a) b)

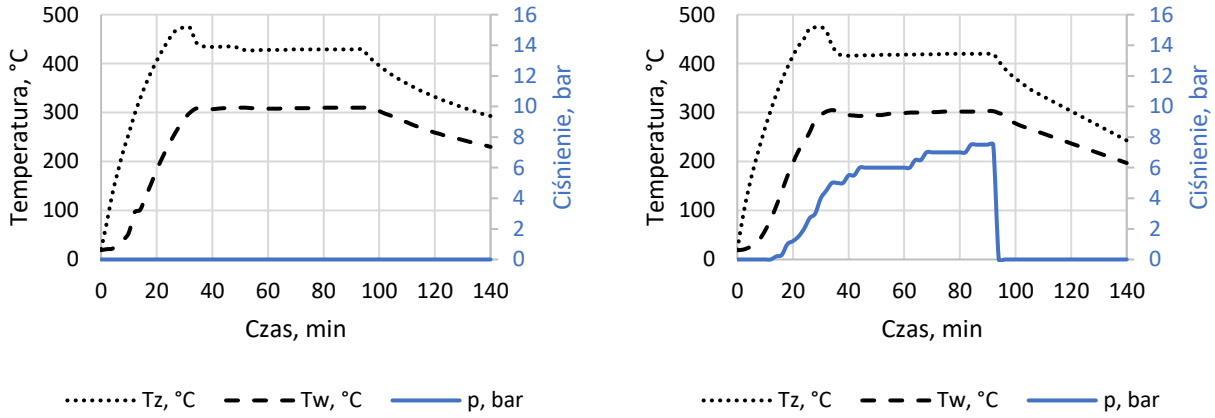

Rysunek Z2. Przebieg zmian temperatury zewnętrznej (płaszcza grzewczego), wewnętrznej (wewnątrz reaktora) oraz ciśnienia dla osadów ściekowych, a) pomiar z zaworem otwartym (O), b) pomiar z zaworami zamkniętymi (Z)

a) b)

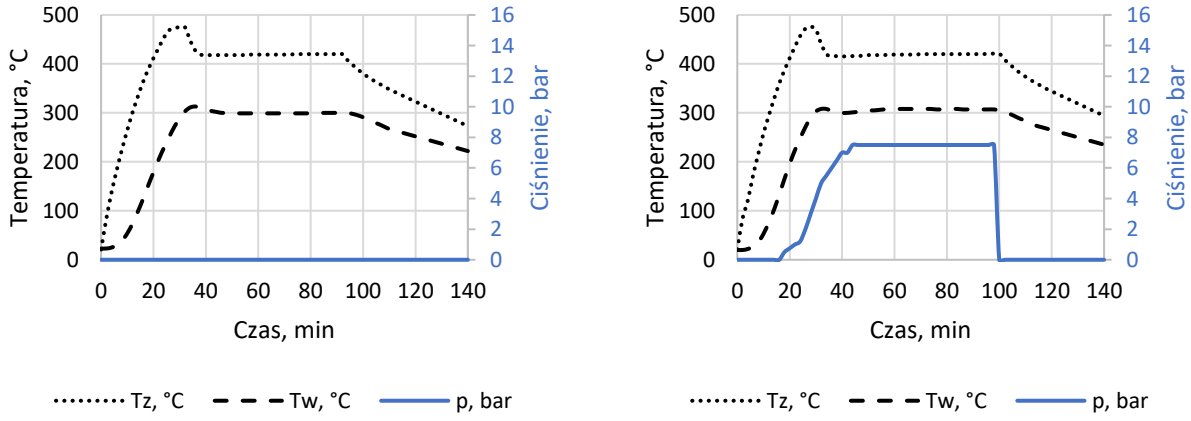

Rysunek Z3. Przebieg zmian temperatury zewnętrznej (płaszcza grzewczego), wewnętrznej (wewnątrz reaktora) oraz ciśnienia dla pofermentu, a) pomiar z zaworem otwartym (O), b) pomiar z zaworami zamkniętymi (Z)

a) b)

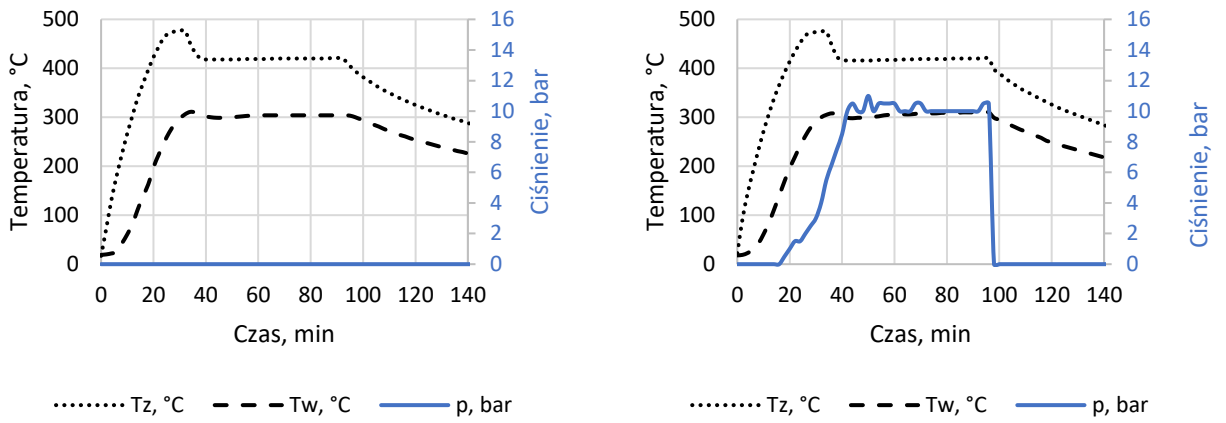

Rysunek Z4. Przebieg zmian temperatury zewnętrznej (płaszcza grzewczego), wewnętrznej (wewnątrz reaktora) oraz ciśnienia dla borowiny, a) pomiar z zaworem otwartym (O), b) pomiar z zaworami zamkniętymi (Z)

a) b)

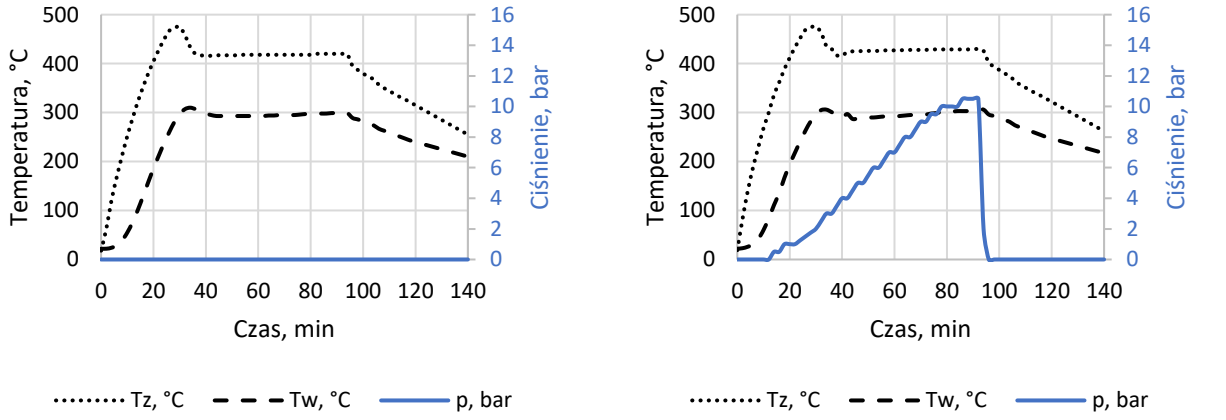

Rysunek Z5. Przebieg zmian temperatury zewnętrznej (płaszcza grzewczego), wewnętrznej (wewnątrz reaktora) oraz ciśnienia dla PLA, a) pomiar z zaworem otwartym (O), b) pomiar z zaworami zamkniętymi (Z)

materials

MDPI

Article

Oxytree Pruned Biomass Torrefaction: Mathematical Models of the Influence of Temperature and Residence Time on Fuel Properties Improvement

Kacper Świechowski [1], Marek Liszewski [2], Przemysław Bąbelewski [3], Jacek A. Koziel [4] and Andrzej Białowiec [1,4,*]

1 Institute of Agricultural Engineering, Faculty of Life Sciences and Technology, Wrocław University of Environmental and Life Sciences, 37/41 Chełmońskiego Str., 51-630 Wrocław, Poland
2 Institute of Agroecology and Plant Production, Faculty of Life Sciences and Technology, Wrocław University of Environmental and Life Sciences, 24A pl. Grunwaldzki Str., 53-363 Wrocław, Poland
3 Department of Horticulture, Faculty of Life Sciences and Technology, Wrocław University of Environmental and Life Sciences, 24A pl. Grunwaldzki Str., 53-363 Wrocław, Poland
4 Department of Agricultural and Biosystems Engineering, Iowa State University, Ames, IA 50011, USA
* Correspondence: andrzej.bialowiec@upwr.edu.pl; Tel.: +48-71-320-5973

Received: 11 June 2019; Accepted: 5 July 2019; Published: 10 July 2019

Abstract: Biowaste generated in the process of Oxytree cultivation and logging represents a potential source of energy. Torrefaction (a.k.a. low-temperature pyrolysis) is one of the methods proposed for the valorization of woody biomass. Still, energy is required for the torrefaction process during which the raw biomass becomes torrefied biomass with fuel properties similar to those of lignite coal. In this work, models describing the influence of torrefaction temperature and residence time on the resulting fuel properties (mass and energy yields, energy densification ratio, organic matter and ash content, combustible parts, lower and higher heating values, CHONS content, *H:C* and *O:C* ratios) were proposed according to the Akaike criterion. The degree of the models' parameters matching the raw data expressed as the determination coefficient (R^2) ranged from 0.52 to 0.92. Each model parameter was statistically significant ($p < 0.05$). Estimations of the value and quantity of the produced torrefied biomass from 1 Mg of biomass residues were made based on two models and a set of simple assumptions. The value of torrefied biomass (€123.4·Mg^{-1}) was estimated based on the price of commercially available coal fuel and its lower heating value (*LHV*) for biomass moisture content of 50%, torrefaction for 20 min at 200 °C. This research could be useful to inform techno-economic analyses and decision-making process pertaining to the valorization of pruned biomass residues.

Keywords: biorenewable energy; pruning biomass; torrefaction; torrefied biomass; fuel properties; Oxytree; model

1. Introduction

The energy demand continues to increase, and researchers continue to develop alternative sources of energy. European Union directives aim to increase the share of renewable energy sources (RES) while lowering overall environmental impact. Renewable energy sources can have a positive impact on the environment and diversify energy supply. To date, ~10% of the total primary energy supply (TPES) is derived from biomass on a global scale [1]. The EU aims to increase the biomass share in the RES up to 50% [1]. By 2050, the share of RES in total energy consumption is expected to increase to 55% to 75% [2]. Thus, the demand for RES, including wood-based biomass is expected to grow. At present, it is not feasible to completely replace fossil fuels with RES in a sustainable manner. There are concerns about the negative impact of increased energy demand from biomass on biodiversity and

food security [3]. However, introducing different biomass as feedstock could improve the biodiversity of energy crops. It is expected that the increase in the share of RES in the EU will lead to an increase in the demand for biomass from trees, which will lead to an increase in forested areas and short-rotation plantations [4].

Oxytree (*Paulownia Clon* in Vitro *112*) has been considered as a relatively new plant suitable for short rotation because of its quick-growing characteristics and the ability to produce a significant amount of biomass. Oxytree biomass yield increases significantly in a relatively short time. For example, the dry mass of the tree can increase tenfold from 0.21 to 2.05 kg d.m. from the first to the second year since planting [5]. Besides rapid growth, Oxytree is also more versatile than other energy crops. Oxytree's wood can be used as a non-construction building material for paper, furniture, instruments, and others [6]. This versatility of end users is of great importance in case of an unexpected drop in the demand for bioenergy; it also allows greater flexibility in meeting the needs of the energy and industrial sectors.

The Oxytree biomass yield depends on many factors, such as stocking density and climate. With estimated stocking of 3300 trees per hectare, the yield in the 5-y period can amount to 80 Mg·ha^{-1} d.m., on average ~16 Mg·ha^{-1} d.m. per year [7]. Warm climates favored by paulownia can produce ~7.2–14.0 Mg·ha^{-1} d.m., with a planting density on a 3 m × 2 m grid, in conversion 1666 ha^{-1} per hectare and 6000 m^3·ha^{-1} of irrigation in Andalusia [8].

Oxytree residues can be additionally utilized for energy purposes, similarly to the concept proposed by Dyjakon [9] for clippings from the apple orchard. The volume of plantation residues can be ~107 m^3 per hectare assuming that clippings consist of ~70% of the total tree volume and that ~250 m^3 of industrial wood can be obtained from 1 ha [10]. The application of torrefaction for the valorization of residual biomass fuel properties may increase the profitability and sustainability of energy production from the Oxytree biomass (Figure 1). To date, pruned biomass is typically left on the field, burned or composted on-site.

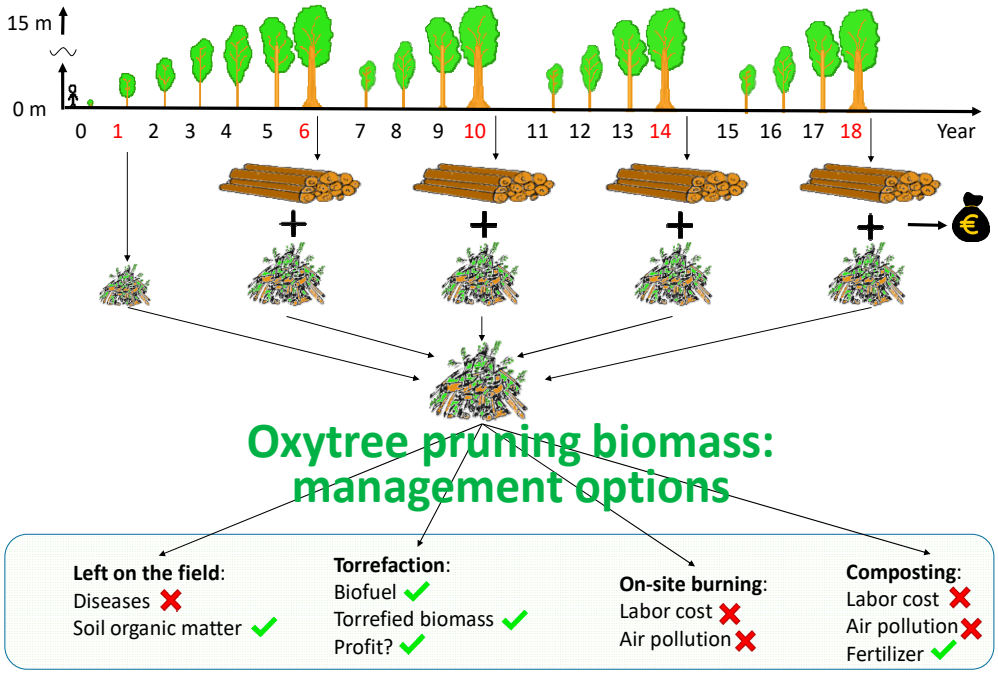

Figure 1. Graphic presentation of the current and proposed utilization of biomass residues on a plantation.

Torrefaction, a.k.a. 'roasting' or 'mild pyrolysis,' is a thermochemical process with a limited amount of oxygen at ~near atmospheric pressure. The biomass is torrefied at a temperature of 200–300 °C at most up to 1 h. The purpose of the process is to obtain a material (called torrefied

biomass) that has improved fuel properties compared with the substrate used for its production. During the biomass torrefaction, gases such as H_2, CO_2, CO, CH_4, C_xH_y, toluene, and benzene are produced in addition to steam, volatile organic compounds, and lipids. During the torrefaction, up to 30% of the mass losses occur while maintaining 90% of the energy content of the substrate. These mass losses result from volatilization of condensable and non-condensable gases products [11,12]. Biomass is pre-treated to produce a high-quality solid biofuel that can be used for combustion or gasification. Torrefaction is based on oxygen removal and decomposing of the reactive hemicellulose using temperature. The quality of obtained solid fuel depends on reaction conditions, such as temperature, inert gas type, reaction time, used feedstock, and others [13]. Although the torrefaction process has been known for a long time, it has only recently become popular again because of the commencement of co-combustion of coal with biomass in some power plants. The torrefied biomass has a higher energy value; it contains less moisture, and it is easier to grind compared with raw biomass. By subjecting the biomass to torrefaction, it is possible to obtain torrefied biomass with fuel properties similar to lignite coal [14]. The energy requirements related to grinding decreased up to ten times (from around 250 to 25 kWh·Mg^{-1}) for forest logging residues [15].

Pyrolyzed biomass is considered as an eco-friendly fuel that could reduce greenhouse gas emissions by sequestrating of atmospheric carbon into the soil. Torrefied biomass or biochar used in this way can help improve soil fertility and soil health. Biochar can also be used as a sorbent for organic and inorganic contamination of water [16] or for upgrade to biological processes, e.g., methane fermentation [17]. Nevertheless, particular ways of utilization depend on different properties of torrefied biomass/biochars, which profoundly changes with the temperature of a process in the range 200–400 °C [18].

Cultivation of the Oxytree is critical to increasing the biomass yield (Figure 1). Pruning the tree at ~0.05 m above the ground in the middle of May (of the second growing season) is practiced to accelerate the growth and bring out a single straight trunk. During pruning, waste biomass is produced in the amount of 0.11–0.16 Mg·ha^{-1} d.m. (assuming 625 trees per ha) [19]. Still, the amount of this biomass (30% by volume) may be too small for the energy-producing industry. However, after torrefaction, pruned biomass may be a source of additional income for growers in retail.

In our previous data article [19] titled "Fuel Properties of Torrefied Biomass from Pruning of Oxytree," raw data describing the process of torrefaction and properties of torrefied biomass were presented. The pruned biomass of the Oxytree obtained from the eight different cultivating conditions was torrefied and examined [19]. For this article, biomass data from all eight cultivating conditions were treated as one set because of small differences in their pre-torrefaction properties. This research aimed at the determination of models for the influence of torrefaction temperature and process residence time on the torrefied biomass properties according to the Akaike criterion. Developed models may be used for the determination of the energetic potential of residues from pruning Oxytree and the techno-economic justification of using torrefaction for biomass valorization. In addition, the proposed models could be used to evaluate fuel properties from residues common in logging and horticulture industry because the pruned biomass is similar to common tree branches.

2. Materials and Methods

Models

The schematic diagram of the experiment and data treatment resulting in polynomial model parameter evaluation is shown in Figure 2. The experiment consisted of four elements: (1) Oxytree cultivation and pruning, (2) pruned biomass torrefaction, (3) determination of fuel properties of resulting torrefied biomasses, and (4) estimation of parameters of a polynomial model describing the influence of torrefaction technological parameters (i.e., temperature, residence time) on fuel properties of torrefied biomasses. The details of the experimental methodology of torrefaction process and

obtained raw data were presented in the previous data article [19]. The data article contains the results of the pruned biomass process, the fuel properties of raw and torrefied biomass.

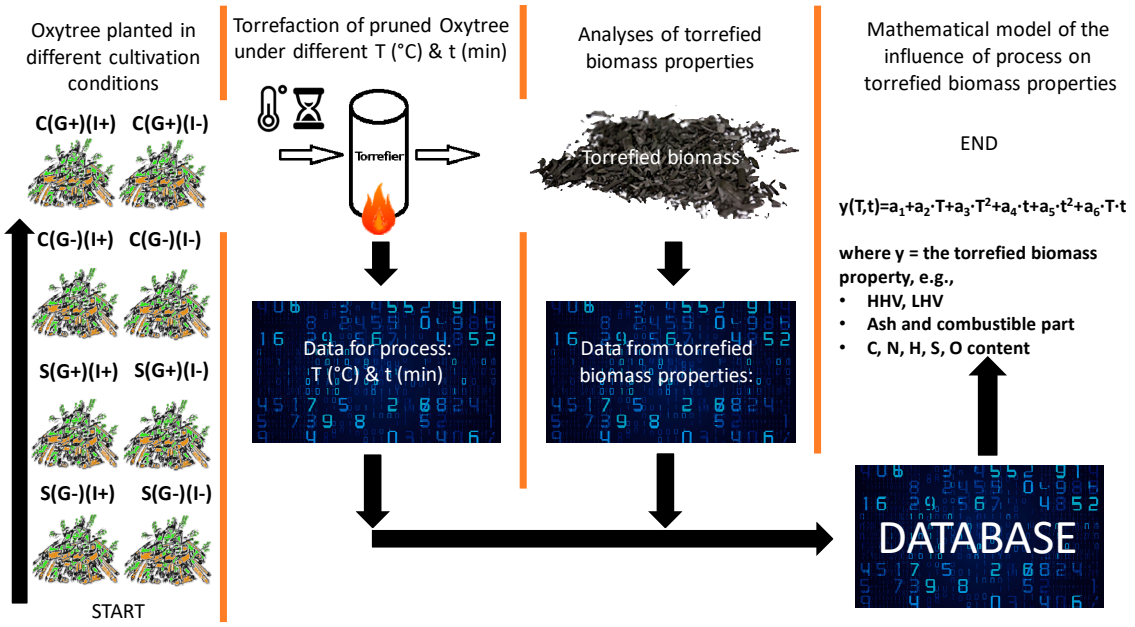

Figure 2. Diagram of experimental design and data evaluation.

The pruned Oxytree biomass was originated from plantations cultivated under 8 different conditions of soil type, irrigation status, and geotextile. Oxytrees were grown on (S) sandy soil (classified as V soil belonging to brunic arenosols) and (C) clay soil (classified as Phaeozems), on which they were irrigated (I+) or not (I−) and had geotextile (G+) or not (G−) (Figure 2). The torrefaction was carried out at temperatures of 200–300 °C with an interval of 20 °C, at residence times 20, 40, and 60 min.

Polynomial models of influence of torrefaction temperature and biomass residence time in the torrefaction reactor on mass and energy efficiency of the torrefaction process, energy densification ratio, organic matter, combustible elements, ash, high heating value, low heating value, and elemental composition of torrefied biomass were built using the raw data (a more detailed description of raw data organized in [19] is presented in Supplementary Materials). The model parameters were estimated due to the non-linear regression analysis. Regression analysis used a 2-degree polynomial with a general form, with intercept (a_1) and 5 regression coefficients ($a_{2–6}$) (Equation (1)). The confidence interval of parameter evaluations ($a_{1–6}$) was 95%. All results for p-value below 0.05 level were assumed to be statistically significant.

$$f(T,t) = a_1 + a_2 \cdot T + a_3 \cdot T^2 + a_4 \cdot t + a_5 \cdot t^2 + a_6 \cdot T \cdot t \quad (1)$$

where:

$f(T, t)$—the torrefied biomass property obtained under T—temperature, and t—residence time conditions,

a_1—intercept;

$a_{2–6}$—regression coefficient;

T—temperature, T = 200–300 °C;

t—residence time, t = 0–60 min.

The standardized regression coefficients (β) for each regression coefficients ($a_{2–6}$) were determined based on Equation (2). The standardized beta β coefficient determines how much (its own) standard

deviations will increase or decrease the dependent variable Y if the independent variable will be changed by one (its own) standard deviation.

$$\beta = \frac{a_n \cdot SD_{Xi}}{SD_{Yi}} \tag{2}$$

where:

β—standardized regression coefficient;
a_n—estimated regression coefficient;
SD_{Xi}—standard deviation of the independent variable x;
x_i—values of subsequent independent variables;
SD_{Yi}—standard deviation of the dependent variable y;
y_i—values of subsequent dependent variables.

The regression analysis was performed using the Statistica 12 software (StatSoft, Inc., TIBCO Software Inc. Palo Alto, CA, USA). For the determination of model parameters, the degree of matching to raw data, the determination coefficient (R^2) was calculated. The backward stepwise regression analysis was used for the reduction of insignificant parameters from the model in case of a lack of statistical significance ($p < 0.05$). Then both models were compared with the Akaike Information Criterion (*AIC*) to propose the simplest model with a similar matching to raw data. *AIC* was determined according to the least-squares method (Equation (3)) [20]:

$$AIC = n \cdot ln\left(\sum_{i=1}^{n} e_i^2\right) + 2 \cdot K \tag{3}$$

where:

AIC—value of Akaike analysis;
n—the number of measurements;
e—the value of the rest of the model for particular measurements point;
K—number of regression coefficients including intercept (a_n) in model.

Generally, models with a larger number of predictors are more accurate but tend to over-fitting. The over-fitted models are good in predictions of data on which they were built but can result in poorer predictions when other data is used. The *AIC* approach can be used in order to preserve good accuracy and a low number of predictors in compared models. When models for a particular variable are compared, a model with a lower *AIC* is better.

3. Results

Models

Data descriptions. All models are firstly presented by a 3D model figure used to a visualization of data. Next, information about a particular model was summarized in a related table. Each table contains the following information:

- The first row contains a model to evaluate the particular properties of torrefied biomass and R^2 value. *AIC* values are also presented in cases where an alternative model (e.g., model 2 or 3) was developed, and the data is presented in Appendix A;
- The first column shows the intercept a_1 and coefficients a_2–a_6;
- The second column presents values for particular intercept/coefficients that are used in the model;
- The third column summarizes standard error calculated for particular intercept/coefficient.
- The fourth column presents p-values (probability value or significance). Statistical significance is assumed when $p < 0.05$).
- The fifth and sixth columns summarize the lower and upper limit of confidence of intercept/coefficient value.

- The seventh column summarizes the value of standardized regression coefficients (β) for each regression coefficients ($a_{2–6}$).

Additional information about data descriptions:

- The name (model 1) in table description presents the original model $f(T,t) = a_1 + a_2{\cdot}T + a_3{\cdot}T^2 + a_4{\cdot}t + a_5{\cdot}t^2 + a_6{\cdot}T{\cdot}t$. The alternative (model 2) and (model 3) stand for improved versions of a model without insignificant coefficients;
- Blue lines with circles present in figures stand for raw data used to nonlinear regression;
- Coefficients with (−) reduce the calculated value of y and coefficients with (+) increase the calculated value of y. The same system is used for standardized regression coefficients (β).

The mass yield (MY) of the Oxytree torrefaction is shown in Figure 3 and Table 1. The MY decreased as the temperature and process time increased ($R^2 = 0.92$). The analysis of data reveals that the increase in temperature is more important to reduce MY than the residence time. The mass yield was ~50% for the torrefaction conditions (T, t) of 300 °C, 60 min. All regression coefficients of the model were statistically significant ($p < 0.05$). In this model, a reduction of MY is caused by predictors T^2 ($\beta = -1.49$), t ($\beta = -0.19$), and $T{\cdot}t$ ($\beta = -0.74$), respectively.

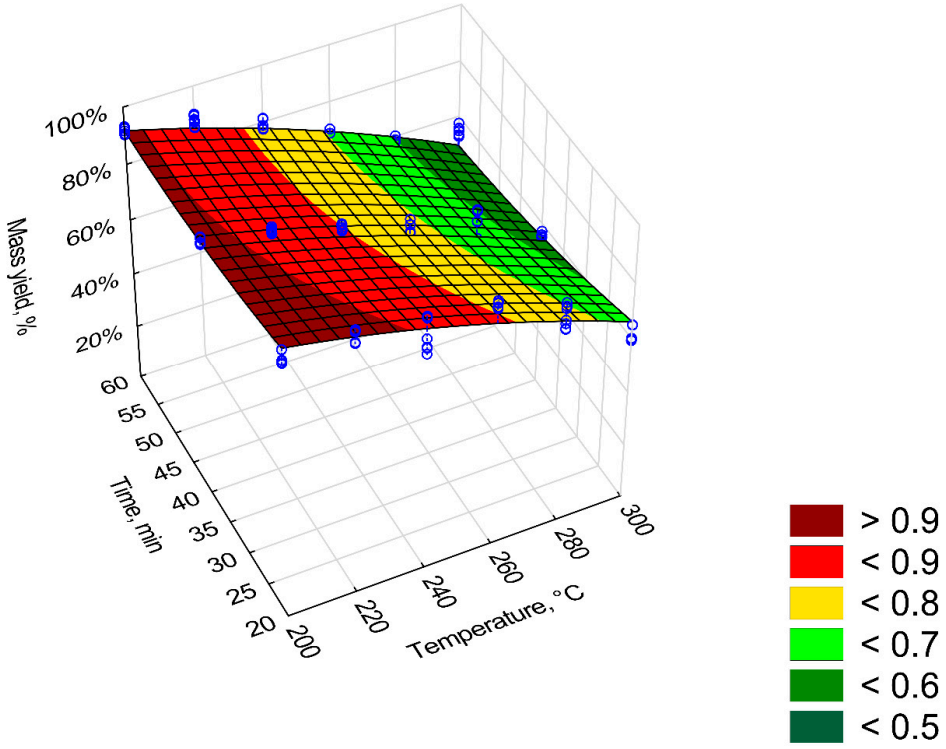

Figure 3. Visualization of 3D model of mass yield (MY) of pruned biomass torrefaction.

Table 1. Statistical evaluation of mass yield (MY) model of pruned biomass torrefaction.

Intercept/ Coefficient	Value of Intercept/ Coefficient	Standard Error	p	Lower Limit of Confidence	Upper Limit of Confidence	Standardized β Coefficient
a_1	0.891816	0.223378	0.000000	0.450129	1.333503	–
a_2	0.003525	0.001746	0.000000	0.000074	0.006977	0.83
a_3	−0.000013	0.000000	0.000000	−0.000013	−0.000013	−1.49
a_4	−0.001684	0.002135	0.000000	−0.005905	0.002538	−0.19
a_5	0.000062	0.000018	0.000000	0.000025	0.000098	0.56
a_6	−0.000025	0.000000	0.000000	−0.000025	−0.000025	−0.74

$MY = a_1 + a_2{\cdot}T + a_3{\cdot}T^2 + a_4{\cdot}t + a_5{\cdot}t^2 + a_6{\cdot}T{\cdot}t$, $R^2 = 0.92$, (model 1).

The torrefaction process led to a reduction in the energy yield (*EY*) of the valorized material (R^2 = 0.88) (Figure 4). As with *MY*, the predictor T^2 had the biggest impact on lowering the energy yield value (Table 2). The lowest value of *EY* (<70%) was achieved at 300 °C and 60 min. Each regression coefficient was statistically significant ($p < 0.05$). The EY value is reduced by predictor *T* ($\beta = -2.35$) and $T \cdot t$ ($\beta = -1.16$). Because the predictor T^2 has the highest negative value, it is reasonable to assume that torrefaction temperature has the biggest impact on decreasing the *EY* (and greater than time).

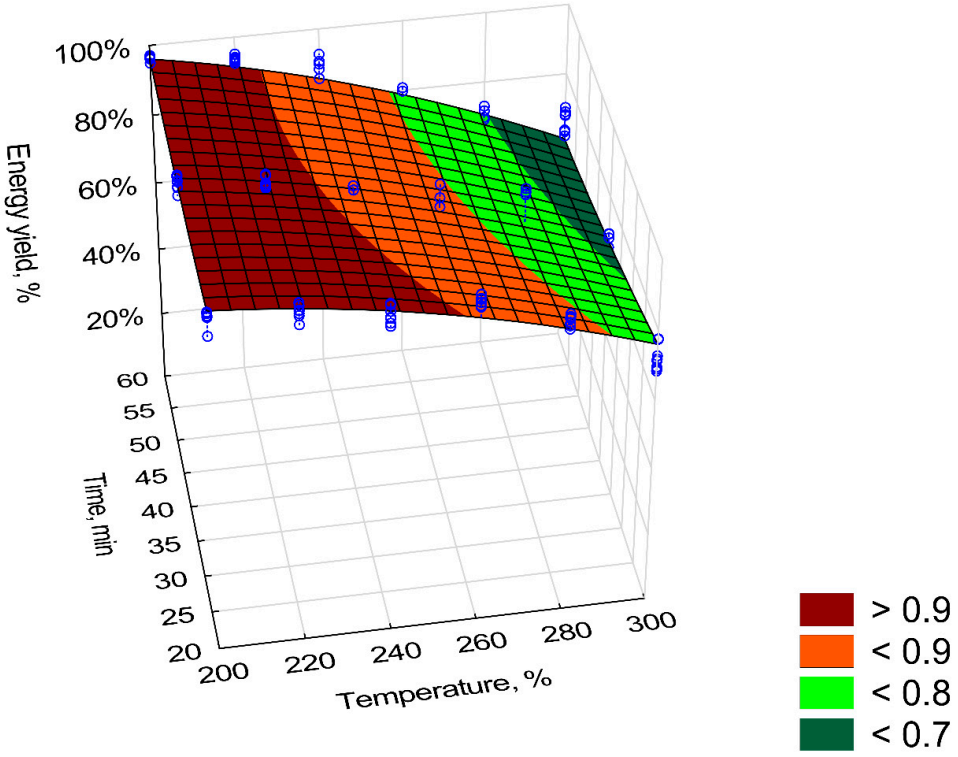

Figure 4. Visualization of 3D model of energy yield (*EY*) of pruned biomass torrefaction.

Table 2. Statistical evaluation of energy yield (*EY*) model of pruned biomass torrefaction.

Intercept/ Coefficient	Value of Intercept/ Coefficient	Standard Error	*p*	Lower Limit of Confidence	Upper Limit of Confidence	Standardized β Coefficient
a_1	0.429884	0.219439	0.000000	−0.004012	0.863781	–
a_2	0.006285	0.001715	0.000000	0.002894	0.009675	1.85
a_3	−0.000016	0.000000	0.000000	−0.000016	−0.000016	−2.35
a_4	0.002472	0.002097	0.000000	−0.001675	0.006619	0.35
a_5	0.000037	0.000018	0.000000	0.000002	0.000073	0.42
a_6	−0.000031	0.000000	0.000000	−0.000031	−0.000031	−1.16

$EY = a_1 + a_2 \cdot T + a_3 \cdot T^2 + a_4 \cdot t + a_5 \cdot t^2 + a_6 \cdot T \cdot t$, $R^2 = 0.88$, (model 1).

The increase in energy densification ratio (*EDr*) in the torrefied biomass is one of the main advantages of the biomass torrefaction process. The *EDr* improves with the increase in the process temperature and its duration (Figure 5). The highest energy densification ratio value was ~1.21 for 300 °C and 60 min (Figure 5). The *EDr* model was characterized by a slightly lower R^2 (0.78) compared with *MY* and *EY*. Regression coefficients of the *EDr* model were statistically significant ($p < 0.05$). The T^2, *t*, and $T \cdot t$ predictors cause the increase of *EDr* (β = 0.93, 0.78, and 0.23 respectively) (Table 3). The *T* and t^2 predictors were negative ($\beta = -0.18$ and −0.7, respectively) (Table 3).

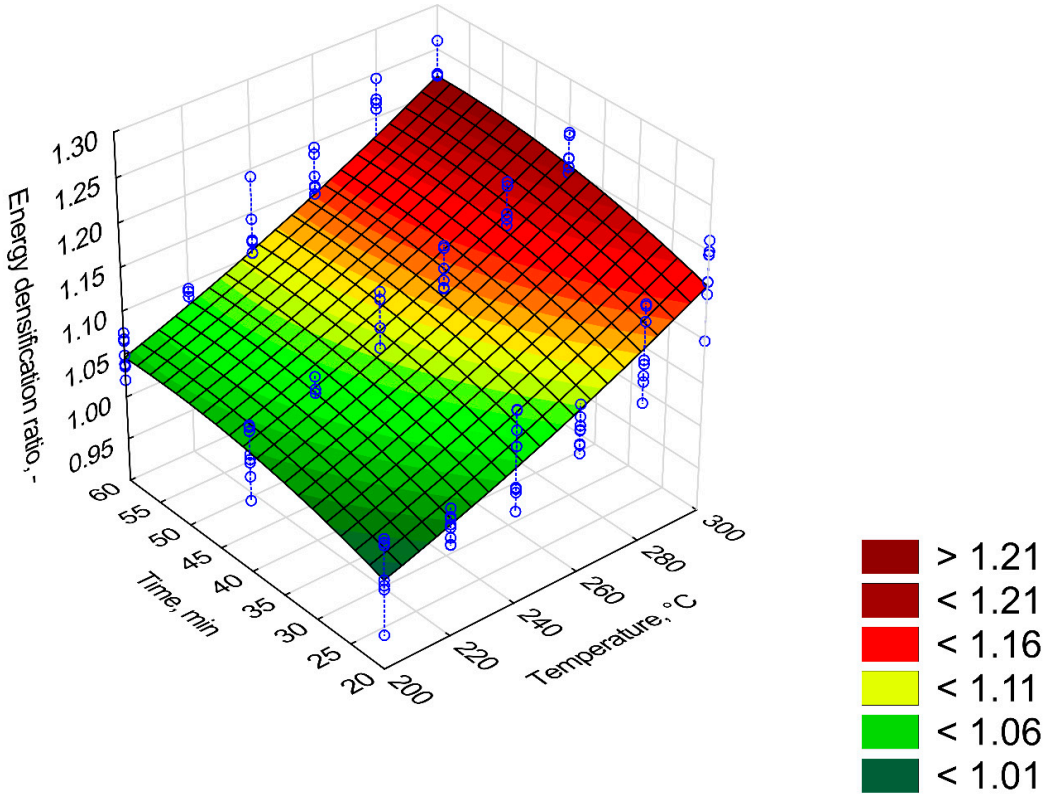

Figure 5. Visualization of 3D model of energy densification ratio (*EDr*) of pruned biomass torrefaction.

Table 3. Statistical evaluation of energy densification ratio (*EDr*) model of pruned biomass torrefaction.

Intercept/ Coefficient	Value of Intercept/ Coefficient	Standard Error	*p*	Lower Limit of Confidence	Upper Limit of Confidence	Standardized β Coefficient
a_1	0.860189	0.182285	0.000000	0.499756	1.220621	–
a_2	−0.000366	0.001424	0.000000	−0.003183	0.002450	−0.18
a_3	0.000004	0.000000	0.000000	0.000004	0.000004	0.93
a_4	0.003294	0.001742	0.000000	−0.000151	0.006739	0.78
a_5	−0.000037	0.000015	0.000000	−0.000066	−0.000007	−0.70
a_6	0.000004	0.000000	0.000000	0.000004	0.000004	0.23

$EDr = a_1 + a_2 \cdot T + a_3 \cdot T^2 + a_4 \cdot t + a_5 \cdot t^2 + a_6 \cdot T \cdot t$, $R^2 = 0.78$, (model 1).

The highest organic matter content (*OM*) occurred in the torrefied biomass with the shortest process time and the lowest temperature of 200 °C (Figure 6). The *OM* content in the tested torrefied biomass ranged from 90% to 82%. Because of the large discrepancy in the results (blue vertical lines), the model has $R^2 = 0.61$. The regression coefficients of the model describing the organic matter are summarized in Table 4. All regression coefficients of the equation were statistically significant ($p < 0.05$). According to the standardized regression coefficient, predictors T, t, and t^2 cause an increase of *OM*, whereas predictors T^2 and $T \cdot t$ cause a decrease of *OM* (Table 4).

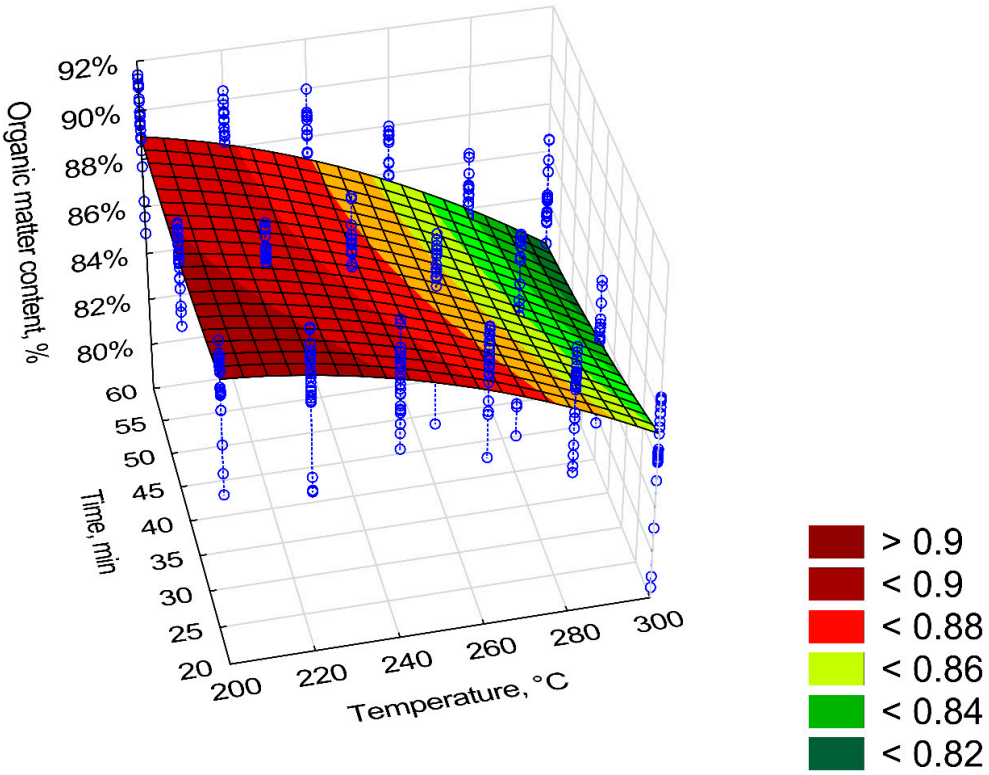

Figure 6. Visualization of 3D model of organic matter (*OM*) content of torrefied pruned biomass.

Table 4. Statistical evaluation of organic matter (*OM*) content model torrefied of pruned biomass.

Intercept/ Coefficient	Value of Intercept/ Coefficient	Standard Error	*p*	Lower Limit of Confidence	Upper Limit of Confidence	Standardized β Coefficient
a_1	0.764595	0.059289	0.000000	0.648061	0.881130	–
a_2	0.001510	0.000463	0.000000	0.000600	0.002421	1.76
a_3	−0.000004	0.000000	0.000000	−0.000004	−0.000004	−2.21
a_4	0.000138	0.000567	0.000000	−0.000976	0.001252	0.08
a_5	0.000008	0.000000	0.000000	0.000008	0.000008	0.35
a_6	−0.000005	0.000000	0.000000	−0.000005	−0.000005	−0.76

$OM = a_1 + a_2 \cdot T + a_3 \cdot T^2 + a_4 \cdot t + a_5 \cdot t^2 + a_6 \cdot T \cdot t$, $R^2 = 0.61$, (model 1).

Combustible part (*CP*) had a similar trend to that of *OM*. The *CP* content in the torrefied biomass decrease with time and process temperature (Figure 7). *CP* in the torrefied biomass decreased from 92% to 86% (Figure 7). The content of *CP* was inversely related to ash content (*AC*), i.e., as *CP* decreased, the *AC* (Figure 8) increased. The torrefied biomass was characterized by a high *AC* of up to 15%. The *CP* and *AC* models had poor fits ($R^2 = 0.53$) because there were significant deviations from mean values of up to 8% (straight blue lines on Figures 7 and 8). The regression coefficients of the *CP* and the *AC* models are presented in Tables 5 and 6, respectively. All regression coefficients of the equation were statistically significant ($p < 0.05$) for both models. The standardized regression coefficients β in the *CP* model had a similar trend as in *OM*; i.e., predictors T^2 and $T \cdot t$ cause decrease of *CP* value (Table 5). In the case of *AC* model, predictors T, t, and t^2 cause the decrease of *AC* value (Table 6).

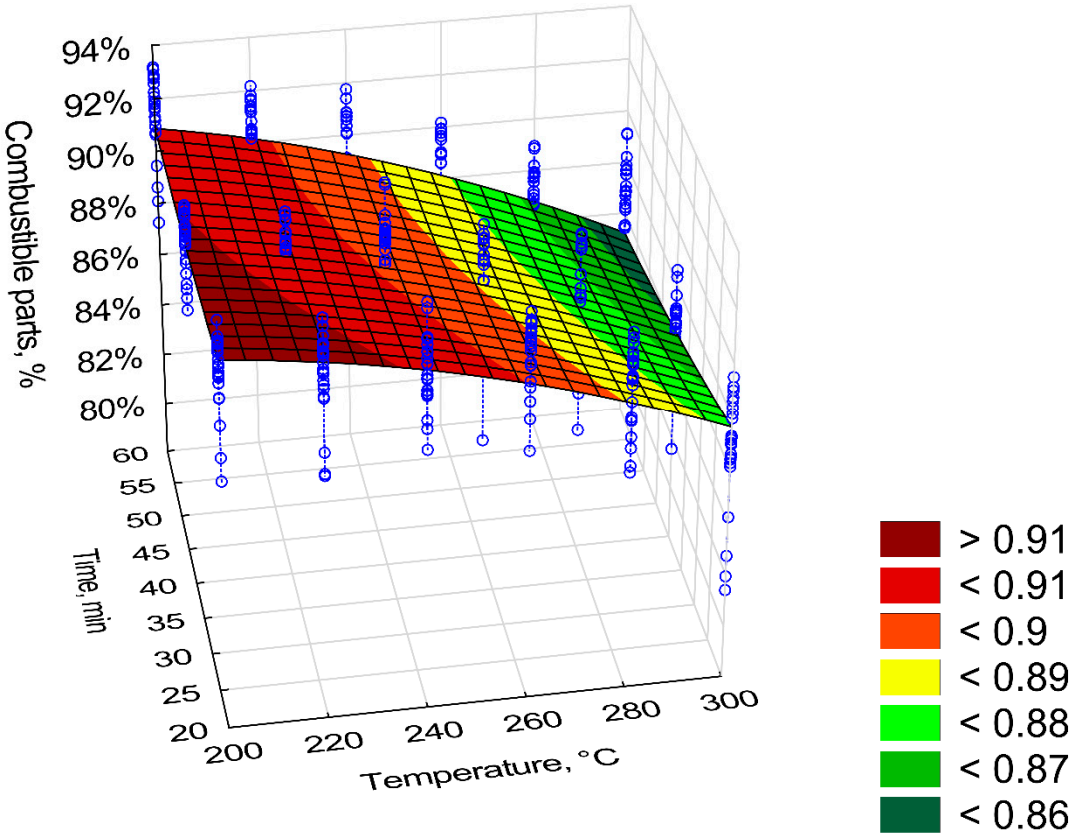

Figure 7. Visualization of 3D model of the combustible part (*CP*) of torrefied pruned biomass.

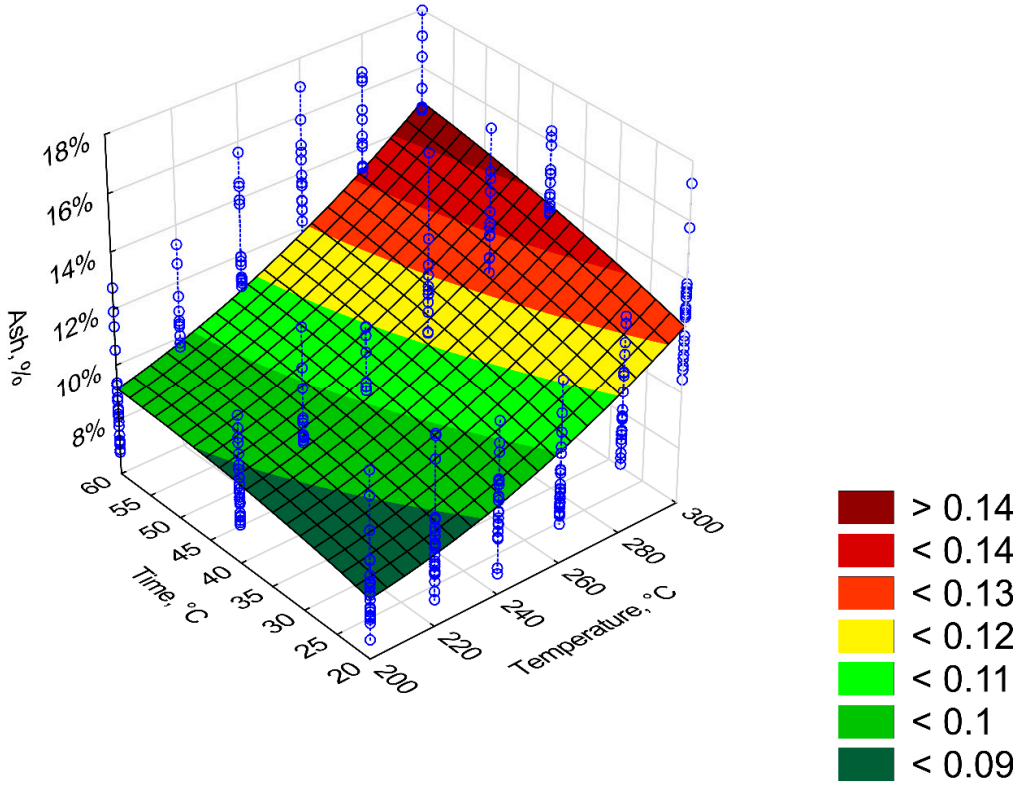

Figure 8. Visualization of 3D model of ash content (*AC*) of torrefied pruned biomass.

Table 5. Statistical evaluation of the combustible part (*CP*) model of torrefied pruned biomass.

Intercept/ Coefficient	Value of Intercept/ Coefficient	Standard Error	*p*	Lower Limit of Confidence	Upper Limit of Confidence	Standardized β Coefficient
a_1	0.838668	0.054980	0.000000	0.730603	0.946733	–
a_2	0.000997	0.000430	0.000000	0.000152	0.001841	1.33
a_3	−0.000003	0.000000	0.000000	−0.000003	−0.000003	−1.81
a_4	0.000029	0.000526	0.000000	−0.001004	0.001062	0.02
a_5	0.000005	0.000000	0.000000	0.000005	0.000005	0.28
a_6	−0.000004	0.000000	0.000000	−0.000004	−0.000004	−0.60

$CP = a_1 + a_2 \cdot T + a_3 \cdot T^2 + a_4 \cdot t + a_5 \cdot t^2 + a_6 \cdot T \cdot t$, $R^2 = 0.53$, (model 1).

Table 6. Statistical evaluation of ash content (*AC*) model of torrefied pruned biomass.

Intercept/ Coefficient	Value of Intercept/ Coefficient	Standard Error	*p*	Lower Limit of Confidence	Upper Limit of Confidence	Standardized β Coefficient
a_1	0.161333	0.054979	0.000000	0.053268	0.269398	–
a_2	−0.000997	0.000430	0.000000	−0.001841	−0.000152	−1.33
a_3	0.000003	0.000000	0.000000	0.000003	0.000003	1.81
a_4	−0.000029	0.000525	0.000000	−0.001062	0.001004	−0.02
a_5	−0.000005	0.000000	0.000000	−0.000005	−0.000005	−0.28
a_6	0.000004	0.000000	0.000000	0.000004	0.000004	0.60

Ash $(AC) = a_1 + a_2 \cdot T + a_3 \cdot T^2 + a_4 \cdot t + a_5 \cdot t^2 + a_6 \cdot T \cdot t$, $R^2 = 0.53$, (model 1).

The high heating value (*HHV*) increased with the process temperature and its duration increase (Figure 9). The highest *HHV* = 23 MJ·kg^{-1} value was recorded at 300 °C and 60 min, whereas the raw biomass had the *HHV* = 18.4 MJ·kg^{-1} [19]. The regression coefficients of the *HHV* model are summarized in Table 7. The a_2 and a_6 regression coefficients were not statistically significant ($p < 0.05$) for $HHV = a_1 + a_2 \cdot T + a_3 \cdot T^2 + a_4 \cdot t + a_5 \cdot t^2 + a_6 \cdot T \cdot t$ (model 1, Table A1). Consequently, they were removed from the analysis and the estimations were made again for the $HHV = a_1 + a_2 \cdot T^2 + a_4 \cdot t + a_5 \cdot t^2$ (model 2, Figure 9). There were practically no differences between model (1) and (2) according to R^2 values. However, the Akaike analysis of both models revealed that the model (2) had the *AIC* lower by 2 compared with the model (1). Therefore, the model (2) with a lower value of *AIC* was chosen. According to standardized regression coefficient β, the T^2 and t predictors cause an increase of *HHV*, whereas predictor $T \cdot t$ a decrease of *HHV* (Table 7).

The lower calorific value (*LHV*) increased with the increase of the process temperature and residence time (Figure 10). The *LHV* was found in torrefied biomass made at 200 °C and 220 °C and ranged from 16 to 20 MJ·kg^{-1}, respectively [19]. The highest *LHV* resulted from torrefied biomass generated at 300 °C and 60 min. The regression coefficients of the *LVH* model are presented in Figure 10. Because in the model $LHV = a_1 + a_2 \cdot T + a_3 \cdot T^2 + a_4 \cdot t + a_5 \cdot t^2 + a_6 \cdot T \cdot t$ the a_2 regression coefficient ($p < 0.05$) was not statistically significant (model 1, Table A2), the alternative model $LHV = a_1 + a_2 \cdot T^2 + a_3 \cdot t + a_4 \cdot t^2 + a_5 \cdot T \cdot t$ was tested (model 2). Again, in this revised model, a_5 was not statistically significant (Table A3), so the model $LHV = a_1 + a_2 \cdot T^2 + a_3 \cdot t + a_4 \cdot t^2$ was tested (model 3). In model 3, all regression coefficients were statistically significant ($p < 0.05$). The R^2 values were almost the same in each model (~0.82). It can be assumed that the third model, compared to the first and second models, had a better fit because of *AIC* value. The first, second, and third models had an *AIC* of 8137, 8135, and 4904, respectively. For model 3, the predictors of *LHV* (Table 8) have similar trends as predictors of *HHV*.

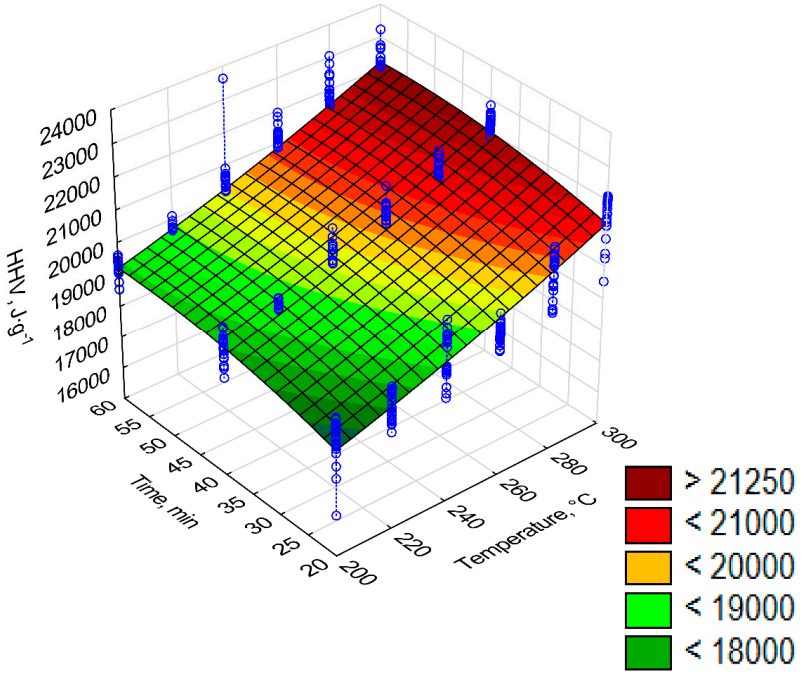

Figure 9. Visualization of 3D model of *HHV* of torrefied pruned biomass (model 2).

Table 7. Statistical evaluation of *HHV* model of torrefied pruned biomass (model 2).

Intercept/ Coefficient	Value of Intercept/ Coefficient	Standard Error	*p*	Lower Limit of Confidence	Upper Limit of Confidence	Standardized β Coefficient
a_1	14,572.93	235.6392	0.000000	14109.78	15,036.09	–
a_2	0.06	0.0016	0.000000	0.06	0.06	0.83
a_3	76.79	12.0003	0.000000	53.20	100.38	1.00
a_4	−0.67	0.1485	0.000009	−0.96	−0.38	−0.70

$HHV = a_1 + a_2 \cdot T^2 + a_3 \cdot t + a_4 \cdot t^2$, $R^2 = 0.79$, (model 2), $AIC = 8126$.

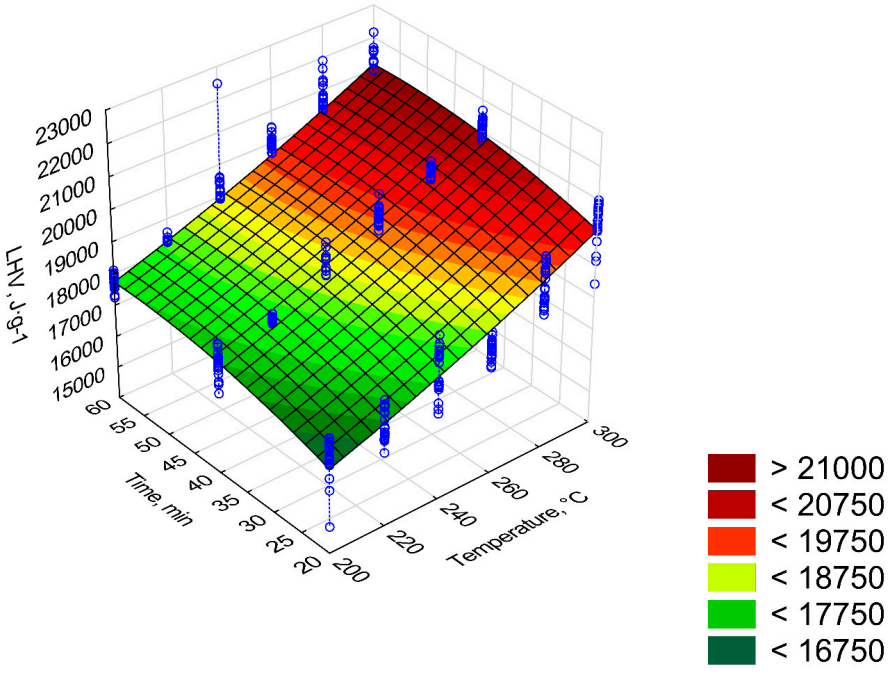

Figure 10. Visualization of 3D model of *LHV* of torrefied pruned biomass (model 3).

Table 8. Statistical evaluation of *LHV* model of torrefied pruned biomass (model 3).

Intercept/ Coefficient	Value of Intercept/ Coefficient	Standard Error	p	Lower Limit of Confidence	Upper Limit of Confidence	Standardized β Coefficient
a_1	12,394.39	238.9256	0.000000	11,924.77	12,864.00	–
a_2	0.07	0.0017	0.000000	0.07	0.07	0.84
a_3	90.68	12.1676	0.000000	66.76	114.59	1.06
a_4	−0.79	0.1505	0.000000	−1.09	−0.50	−0.75

$LHV = a_1 + a_2 \cdot T^2 + a_3 \cdot t + a_4 \cdot t^2$, $R^2 = 0.82$, (model 3), $AIC = 4904$.

Figures 11–15 present models of the C, H, N, S, O content in the torrefied biomass. The C (Figure 11) and N (Figure 13) contents increased with the increase in process temperature and time. The H (Figure 12) and O (Figure 15) contents had the opposite tends. The 3D model of S content (Figure 14) appears insensitive to temperature or time. Visible changes occurred only above 250 °C and 40 min. In Tables 9–13 a statistical evaluation of these models was presented. For these models, R^2 ranged from 0.06 to 0.66. The highest R^2 was for the H model and the lowest for the S model. Relatively high $R^2 = 0.55$ was also noted for the O model. Other models had a coefficient of determination <0.5. All regression coefficients were statistically significant ($p < 0.05$) for each model (Tables 9–13). A common finding for C, H, N, S, and O models was the value of standardized regression coefficients β. Predictors related to temperature (T, T^2) had a higher absolute value than those related to time (t, t^2). However, there was no link where predictors T and T^2 had a positive or negative value.

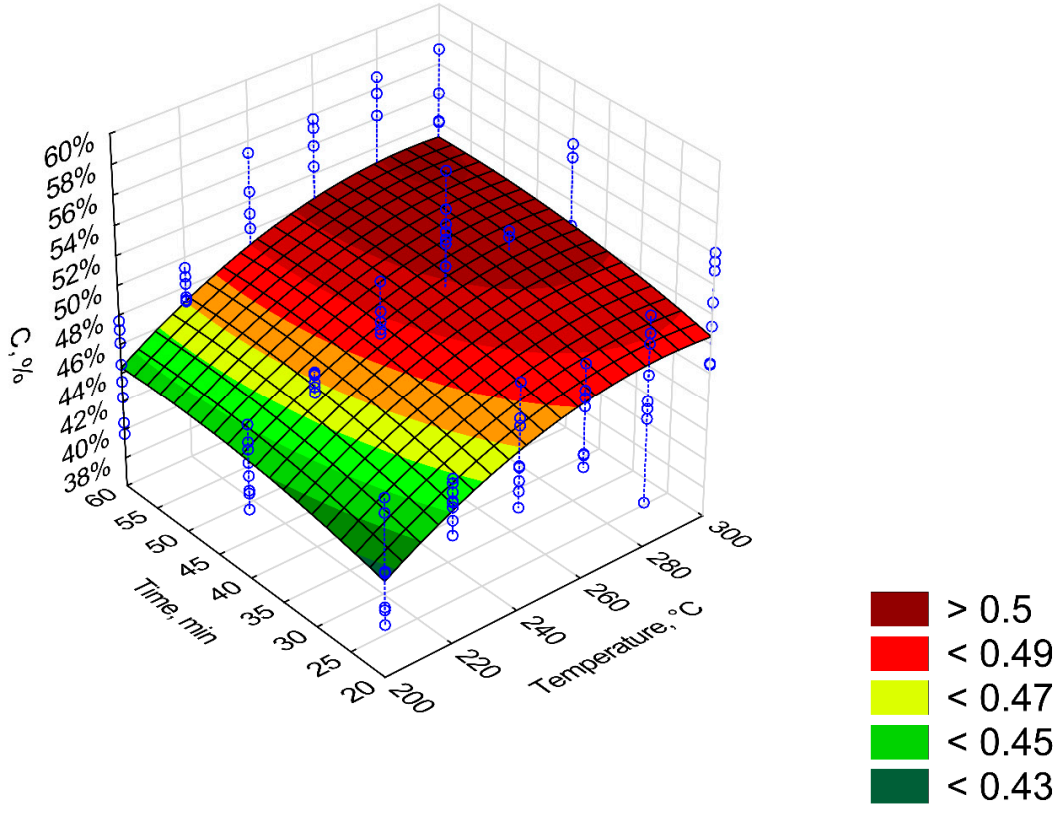

Figure 11. Visualization of 3D model of C content of torrefied pruned biomass.

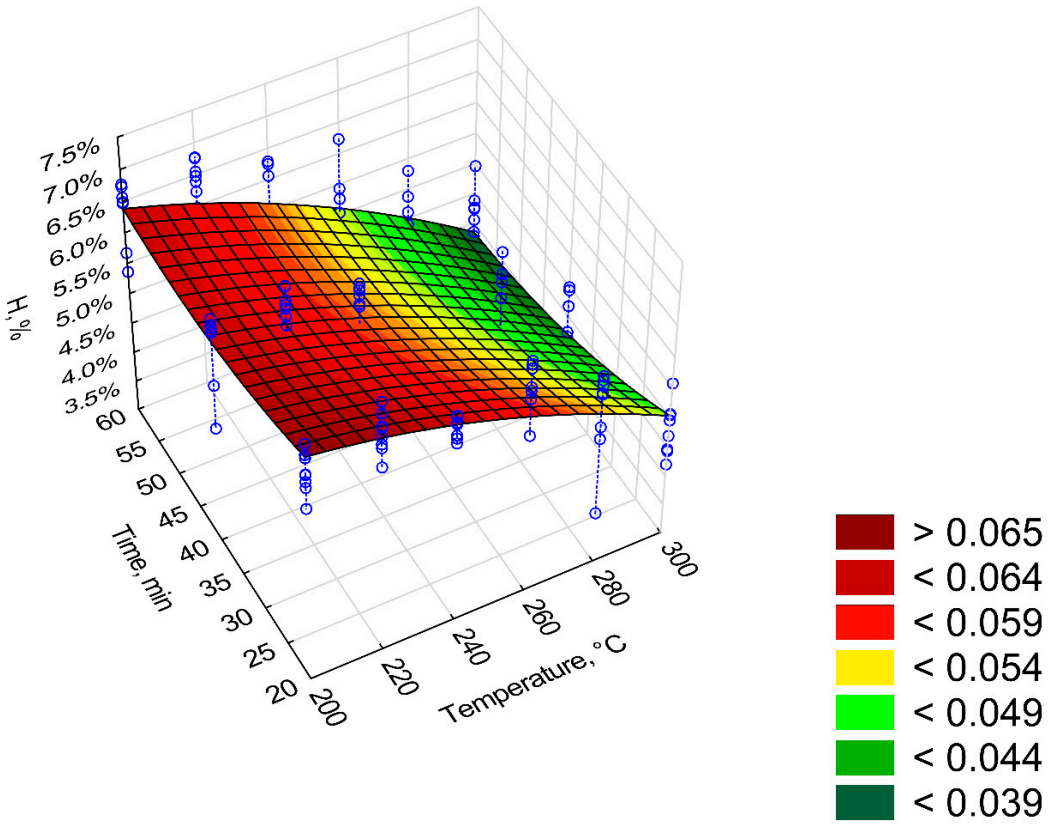

Figure 12. Visualization of 3D model of H content of torrefied pruned biomass.

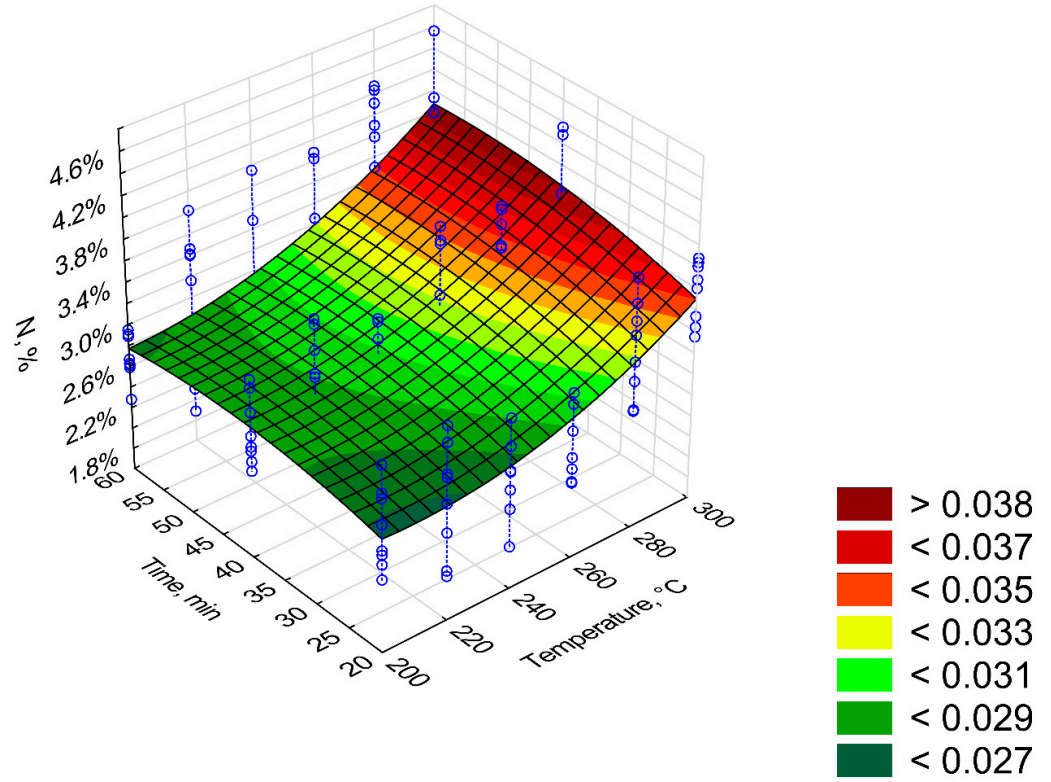

Figure 13. Visualization of 3D model of N content of torrefied pruned biomass.

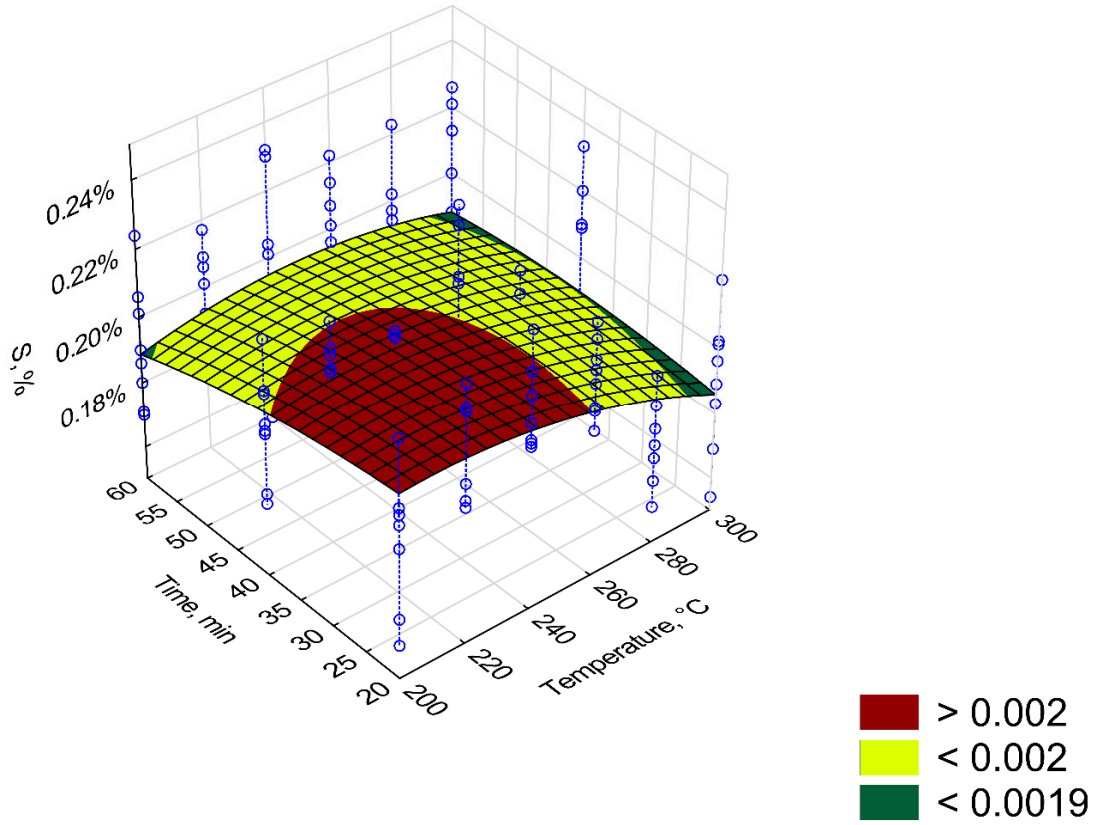

Figure 14. Visualization of 3D model of S content of torrefied pruned biomass.

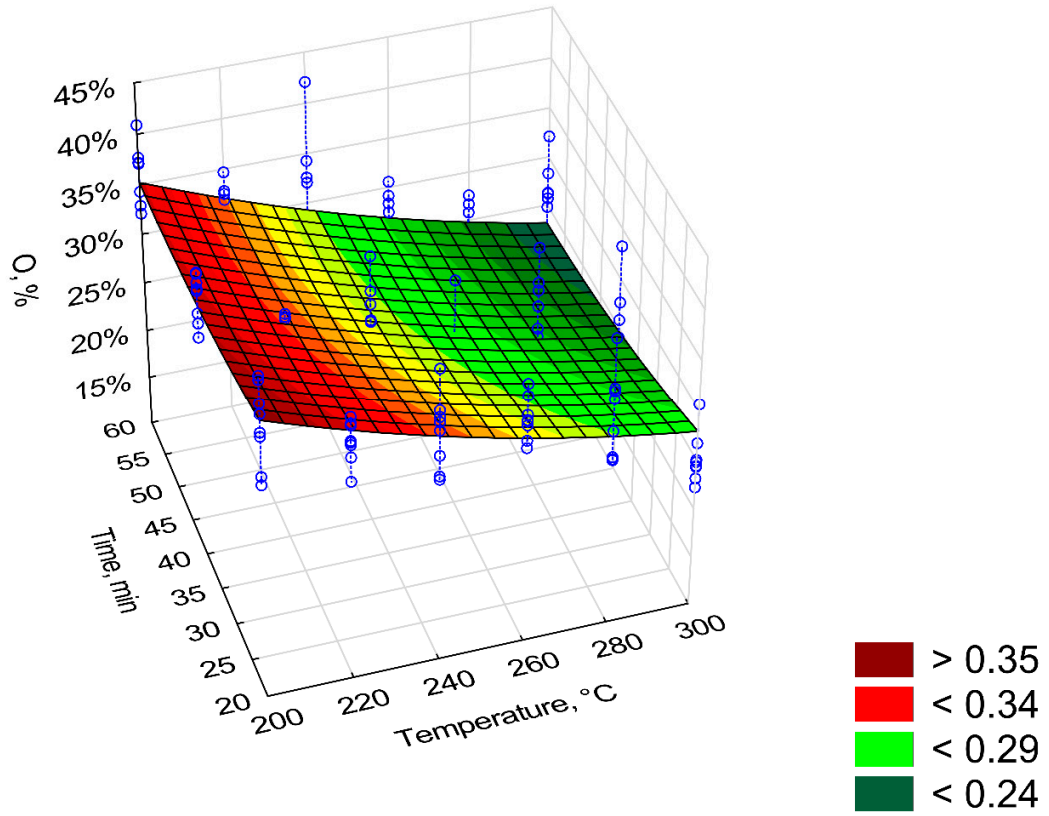

Figure 15. Visualization of 3D model of O content of torrefied pruned biomass.

Table 9. Statistical evaluation of C content model of torrefied pruned biomass.

Intercept/ Coefficient	Value of Intercept/ Coefficient	Standard Error	p	Lower Limit of Confidence	Upper Limit of Confidence	Standardized β Coefficient
a_1	−0.212855	0.188451	0.000000	−0.585480	0.159770	–
a_2	0.004700	0.001473	0.000000	0.001788	0.007612	3.80
a_3	−0.000008	0.000000	0.000000	−0.000008	−0.000008	−3.35
a_4	0.001477	0.001801	0.000000	−0.002084	0.005039	0.57
a_5	−0.000017	0.000015	0.000000	−0.000047	0.000014	−0.52
a_6	0.000002	0.000000	0.000000	0.000002	0.000002	0.16

$C = a_1 + a_2 \cdot T + a_3 \cdot T^2 + a_4 \cdot t + a_5 \cdot t^2 + a_6 \cdot T \cdot t$, $R^2 = 0.35$, (model 1).

Table 10. Statistical evaluation of H content model of torrefied pruned biomass.

Intercept/ Coefficient	Value of Intercept/ Coefficient	Standard Error	p	Lower Limit of Confidence	Upper Limit of Confidence	Standardized β Coefficient
a_1	0.042265	0.032430	0.000000	−0.021858	0.106388	–
a_2	0.000377	0.000253	0.000000	−0.000124	0.000878	1.27
a_3	−0.000001	0.000000	0.000000	−0.000001	−0.000001	−1.74
a_4	−0.000164	0.000310	0.000000	−0.000777	0.000449	−0.27
a_5	0.000006	0.000000	0.000000	0.000006	0.000006	0.75
a_6	−0.000002	0.000000	0.000000	−0.000002	−0.000002	−0.85

$H = a_1 + a_2 \cdot T + a_3 \cdot T^2 + a_4 \cdot t + a_5 \cdot t^2 + a_6 \cdot T \cdot t$, $R^2 = 0.66$, (model 1).

Table 11. Statistical evaluation of N content model of torrefied pruned biomass.

Intercept/ Coefficient	Value of Intercept/ Coefficient	Standard Error	p	Lower Limit of Confidence	Upper Limit of Confidence	Standardized β Coefficient
a_1	0.068473	0.023985	0.000000	0.021047	0.115899	–
a_2	−0.000429	0.000187	0.000000	−0.000800	−0.000059	−2.59
a_3	0.000001	0.000000	0.000000	0.000001	0.000001	3.01
a_4	0.000134	0.000229	0.000000	−0.000319	0.000588	0.39
a_5	−0.000003	0.000000	0.000000	−0.000003	−0.000003	−0.71
a_6	0.000001	0.000000	0.000000	0.000001	0.000001	0.51

$N = a_1 + a_2 \cdot T + a_3 \cdot T^2 + a_4 \cdot t + a_5 \cdot t^2 + a_6 \cdot T \cdot t$, $R^2 = 0.41$, (model 1).

Table 12. Statistical evaluation of S content model of torrefied pruned biomass.

Intercept/ Coefficient	Value of Intercept/ Coefficient	Standard Error	p	Lower Limit of Confidence	Upper Limit of Confidence	Standardized β Coefficient
a_1	0.001055	0.001325	0.000000	−0.001566	0.003676	–
a_2	0.000010	0.000010	0.000000	−0.000010	0.000031	1.41
a_3	2.61×10^{-8}	0.000000	0.000000	0.000000	0.000000	−1.81
a_4	−0.000008	0.000013	0.000000	−0.000033	0.000017	−0.52
a_5	6.77×10^{-8}	0.000000	0.000000	0.000000	0.000000	−0.36
a_6	4.63×10^{-8}	0.000000	0.000000	0.000000	0.000000	0.81

$S = a_1 + a_2 \cdot T + a_3 \cdot T^2 + a_4 \cdot t + a_5 \cdot t^2 + a_6 \cdot T \cdot t$, $R^2 = 0.06$, (model 1).

Table 13. Statistical evaluation of O content model of torrefied pruned biomass.

Intercept/ Coefficient	Value of Intercept/ Coefficient	Standard Error	p	Lower Limit of Confidence	Upper Limit of Confidence	Standardized β Coefficient
a_1	0.873544	0.207078	0.000000	0.464088	1.283001	–
a_2	−0.003199	0.001618	0.000000	−0.006398	0.000001	−1.96
a_3	0.000005	0.000000	0.000000	0.000005	0.000005	1.42
a_4	−0.001367	0.001979	0.000000	−0.005280	0.002547	−0.40
a_5	0.000022	0.000017	0.000000	−0.000011	0.000055	0.52
a_6	−0.000005	0.000000	0.000000	−0.000005	−0.000005	−0.41

$O = a_1 + a_2 \cdot T + a_3 \cdot T^2 + a_4 \cdot t + a_5 \cdot t^2 + a_6 \cdot T \cdot t$, $R^2 = 0.55$, (model 1).

Figures 16 and 17 depict changes in the value of *H:C* and *O:C* ratios depending on the *T* and *t* time. The model of *H:C* ratio (Figure 16) was characterized by high R^2 (0.82), while the *O:C* ratio model had R^2 of 0.48. The first model of *H:C* ratio (model 1) had 3 statistically insignificant regression coefficients ($p < 0.05$), $R^2 = 0.82$, and $AIC = 164$ (Table A4). Non-significant regression coefficients have been removed, and the second model has been proposed (model 2, Figure 16, Table 14). The second model has the same $R^2 = 0.82$ yet with a higher $AIC = 200$ (Figure 16). Elevating the temperature and process time led to a reduction of *H:C* ratio from about 1.5 to 0.9 (%/%) for 300 °C at 20 min and 300 °C at 60 min, respectively (Figure 16). The same change in conditions caused a change in *O:C* ratio from ~0.47 to 0.37 (%/%) (Figure 17). For *H:C* ratio (model 2), the predictor t^2 caused an increase of *H:C* ratio ($\beta = 1.68$) whereas predictor $T{\cdot}t$ a decrease of *H:C* ratio ($\beta = -2.15$). With the *O:C* ratio model, the decrease of *O:C* ratio is caused by predictors *T*, *t* and $T{\cdot}t$ for which $\beta = -3.03$, -0.59, and -0.21 respectively (Table 15).

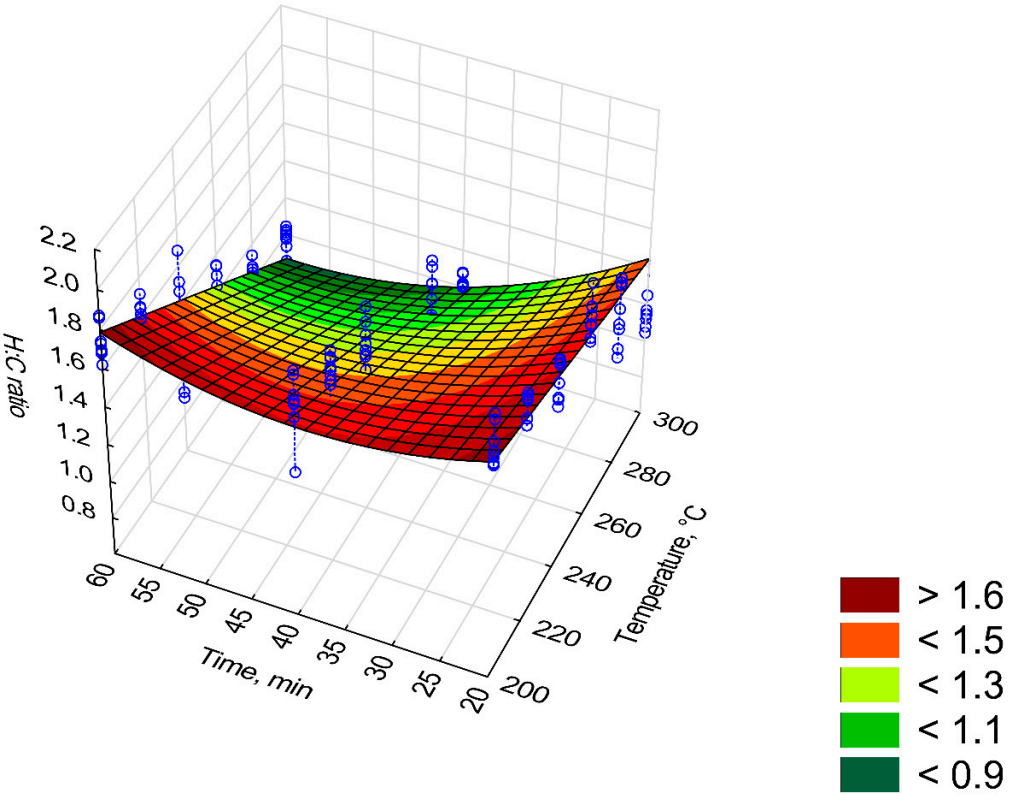

Figure 16. Visualization of 3D model of *H:C* ratio of torrefied pruned biomass (model 2).

Table 14. Statistical evaluation of *H:C* ratio model of torrefied pruned biomass (model 2).

Intercept/ Coefficient	Value of Intercept/ Coefficient	Standard Error	*p*	Lower Limit of Confidence	Upper Limit of Confidence	Standardized β Coefficient
a_1	2.207455	0.044156	0.000000	2.120162	2.294748	–
a_2	0.000394	0.000029	0.000000	0.000338	0.000451	1.68
a_3	−0.000153	0.000000	0.000000	−0.000153	−0.000153	−2.15

$H{:}C = a_1 + a_2{\cdot}t^2 + a_3{\cdot}T{\cdot}t$, $R^2 = 0.82$, (model 2), $AIC = 200$.

Table 15. Statistical evaluation of *O:C* ratio model of torrefied pruned biomass.

Intercept/ Coefficient	Value of Intercept/ Coefficient	Standard Error	*p*	Lower Limit of Confidence	Upper Limit of Confidence	Standardized β Coefficient
a_1	0.022935	0.005095	0.000000	0.012860	0.033010	-
a_2	−0.000114	0.000040	0.000000	−0.000192	−0.000035	−3.03
a_3	1.85×10^{-5}	0.000000	0.000000	0.000000	0.000000	2.47
a_4	−0.000047	0.000049	0.000000	−0.000143	0.000050	−0.59
a_5	5.38×10^{-5}	0.000000	0.000000	0.000001	0.000001	0.55
a_6	-6.26×10^{-5}	0.000000	0.000000	0.000000	0.000000	−0.21

$O{:}C = a_1 + a_2{\cdot}T + a_3{\cdot}T^2 + a_4{\cdot}t + a_5{\cdot}t^2 + a_6{\cdot}T{\cdot}t$, $R^2 = 0.48$.

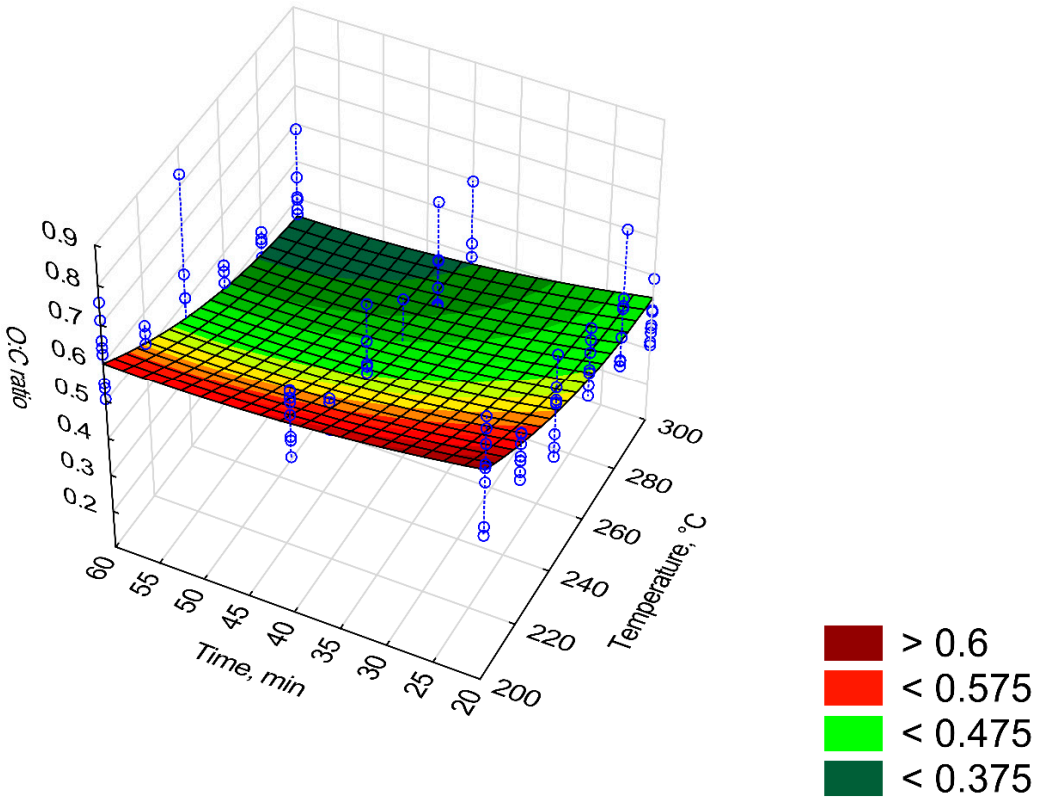

Figure 17. Visualization of 3D model of *O:C* ratio of torrefied pruned biomass.

4. Discussion

4.1. Models

The mass and energy yield (*MY* and *EY*) of the torrefaction process decreased with increasing *T* and *t*. The *MY* and *EY* values for Oxytree were in the range of other torrefied biomass derived from wood. At temperatures of 275 °C and 300 °C (60 min), the *MY* value for spruce was ~70% and ~50% [21], i.e., corresponding to those reported in Figure 1. At temperatures of 275 °C and 300 °C (60 min), the *MY* value for spruce was ~70% and ~50% [16], i.e., corresponding to those reported in Figure 1. For willow torrefied in 15 min at 250 °C, the *MY* was 70% [22]. It is much less than for torrefied pruned biomass of Oxytree for which *MY* at 250 °C, 20 min was 90% (Figure 1). The *MY* and *EY* in the case of torrefied willow at a process temperature of 230–290 °C was 95%–72%, and *EY* was 97%–79% [23]. In the case of Oxytree, these values ranged from 90%–50% and 90%–70%, respectively (Figures 3 and 4). Energy efficiency for spruce torrefaction at 225–300 °C was between 93%–68%, and the *EDr* at 300 °C was 1.2 [24], i.e., the same as for the pruned torrefied Oxytree biomass (Figure 5).

The models for *MY*, *EY*, and *EDr* were characterized by a high determination coefficient R^2 of 0.78–0.92, which means that the proposed models can be considered suitable for describing the torrefaction of pruned biomass from a cultivation treatment.

The content of *OM* in the torrefied Oxytree ranged from 90% to 80%. The model describing the value of *OM* had a relatively low R^2 (0.63). The decrease in the *OM* resulted from the decomposition of organic compounds under the influence of T and their degassing (torgas). The lower fit of the model to the data was likely due to the high variability of empirical data around the average (illustrated with the blue vertical lines). Nevertheless, it showed accurately the trends of the *OM* loss along with the increase of temperature and time.

Similar low coefficients of determination were obtained for the *CP* and *AC* ($R^2 = 0.53$). This was similar, as in the case of *OM*, because of the large variation in measurement data. *CP* is associated with the ash content. As the *CP* decreases, the *AC* increases. Torrefaction causes a decrease in *CP* and an increase in *AC*. It is associated with the degassing of combustibles that are released during the torrefaction process. The *AC* in the torrefied pruned Oxytree biomass ranged from 7% to 1% [19]. This is a much higher value than that found in torrefied wood from torrefied pine 0.15%–0.21% [25] and birch 0.23%–0.38% [26]. The AC values obtained for Oxytree were closer to the corn stover 10%–12% [27]. The model of $HHV = a_1 + a_2 \cdot T^2 + a_4 \cdot t + a_5 \cdot t^2$ form was better than $HHV = a_1 + a_2 \cdot T + a_3 \cdot T^2 + a_4 \cdot t + a_5 \cdot t^2 + a_6 \cdot T \cdot t$ because it had a lower number of parameters, so it was easier to use. In addition, the model had a lower *AIC* value. The differences were insignificant, but the shorter model had an *AIC* of 8126 compared to 8128, whereas the R^2 was almost the same for both.

The *LHV* of the torrefied pruned Oxytree biomass at 270 °C and 30 min was over 21.5 $MJ \cdot kg^{-1}$ (Figure 9) and was comparable with the calorific value of willow torrefied in the same conditions [28]. The calorific value of the torrefaction from the pruned Oxytree biomass generated at 265 °C and 60 min was above 20 $MJ \cdot kg^{-1}$ (Figure 10). This value was ~1–3 $MJ \cdot kg^{-1}$ lower than in the case of torrefied eucalyptus, poplar, and pine at 265 °C and 105 min [29].

Models describing the change in the content of elements suggest that increasing the torrefaction temperature leads to an increase in the C content and a decrease in the content of O and H. An interesting tendency can be observed in the N model, i.e., the amount of N increased with increasing T and t. This finding is opposite to the typical N content [30,31]. The S model had a low $R^2 = 0.06$. According to the S model (Figure 14), the S content decreases from 260 °C, 20 min, and 200 °C, 40 min, nevertheless, the decrease was small. The smallest S content was obtained at 300 °C where S was ~0.19%. In this study, a trend of S changes was not clear because of variability in measurements. Ren et al. [32] reported 30%–80% S loss during torrefaction of herbaceous, crop, and woody biomass, depending on feedstock. Lack of greater decrease of S content in this research was probably caused by the decrease of other more reactive elements. During the torrefaction process, the decrease in O and H content was mainly due to the weakness of bonded structures such as -OH [33]. Similarly, a drop in N content should be observed due to losses of weakly bonded structures, e.g., $-NH_2$ [33]. The increase in the C content resulted likely from slower decomposition in comparison with other elements [34].

The decrease of *O:C* with the *T* rise might be also attributed to the loss of hydrophilic surfaces [35]. In addition, the C losses were smaller than in the case of O. The decrease in *H:C* resulted, similarly to the decrease in the content of *O:C*, from the faster decomposition of substances containing H in relation to C. The lower values of *O:C* or *H:C* ratios cause the higher energy content of fuel feedstock [36]. Torrefied pruned Oxytree biomass produced at 300 °C and 60 min was characterized by the lowest values of *O:C* and *H:C* of 0.9 and 0.375 (%/%), respectively. *O:C* and *H:C* ratios for wood biomass were >1.4 and >0.65, respectively [36]. For bituminous coal *O:C* was 1.2 (%/%)and *H:C* was 0.125 (%/%) [37]. The values for the torrefied pruned Oxytree biomass were similar to the value of *Gmelina arborea*, torrefied in the same conditions (300 °C, 60 min) [36].

The standardized regression coefficients β are challenging to interpret because predictors are correlated in each other. For example, when one predictor related to *T* has a positive impact on the dependent value, the second predictors (e.g., T^2, or $T \cdot t$) not necessarily do. In almost all cases, the

correlated predictors had an opposing impact. One common characteristic which could be observed based on β in most of the presented models is that predictors which depended on temperature had an absolute impact greater than these ones related to the time. Based on this, it can be assumed that temperature has a greater impact on the properties of torrefied pruned biomass of Oxytree.

4.2. Evaluations of the Value of Torrefied Residue Biomass

The common assumption is that the amount of biomass produced during the pruning treatment of the Oxytree plantation is too small to be economically used for energy purposes. Nevertheless, assuming that the material tested in [19] has properties similar to branches (and others residues) that make up waste at Oxytree harvesting (up to 30% of the weight of the tree), a simple model is proposed here for calculating the value of torrefied biomass produced in relation to commercial coal fuel available on the market, depending on the T and the duration of the torrefaction process (Figure 18). The model also theoretically calculates the maximum profit from the waste mass on the plantation. The calculations assume that part of the terrified biomass is used to maintain the torrefaction process. Calculations do not include labor costs, harvesting, transport, processing, and other costs related to the torrefaction process as well as the distribution of produced fuel.

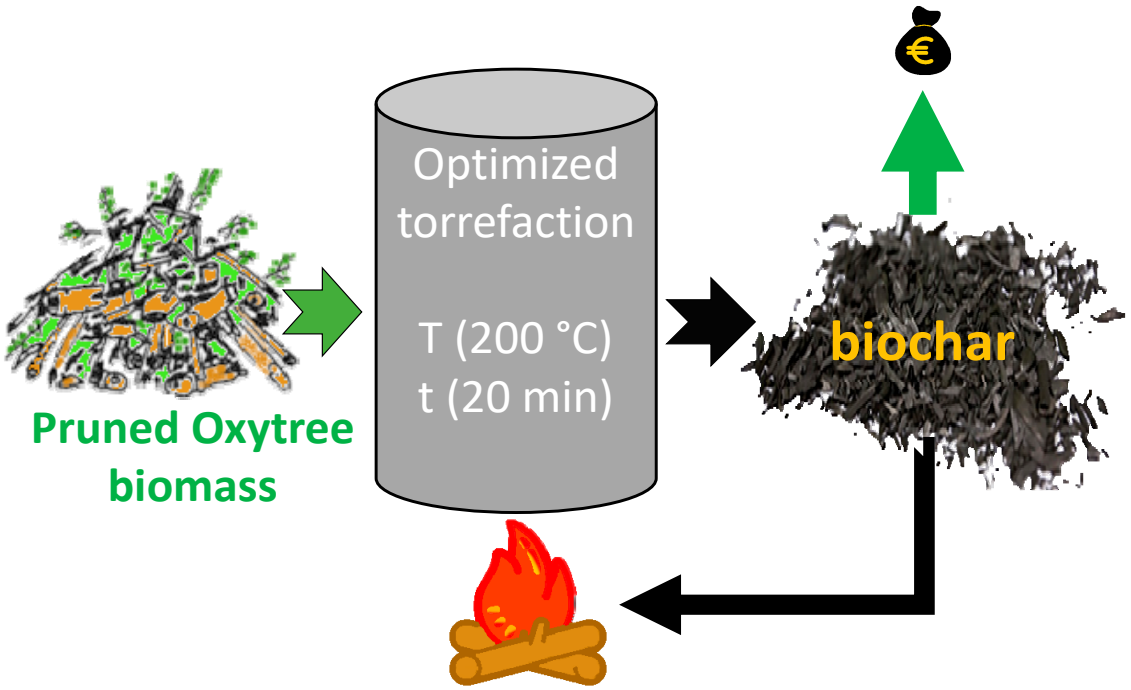

Figure 18. Graphic presentation of the benefits of the pruned Oxytree torrefaction concept.

Data for calculations:

- mass of Oxytree residues, Mg; assumed 1 Mg;
- the moisture content of Oxytree residues, %; assumed 50%;
- torrefaction parameters temperature and time; assumed to be 200 °C and 20 min.

4.2.1. Initial Calculations

The dry mass of Oxytree residues:

$$mr_d = mr_w - mr_w \cdot MC \quad (4)$$

where:

mr_d—dry mass of Oxytree residues, M_g,
mr_w—wet mass of Oxytree residues, M_g,
MC—moisture content of Oxytree residues, %.
Amount of water in Oxytree residues:

$$m_w = mr_w - mr_d \tag{5}$$

where:
m_w—mass of water in Oxytree residues, Mg.

4.2.2. Main Properties of Torrefied Biomass Calculations

Mass yield of torrefaction based on Figure 3

$$MY = 0.891816 + 0.003525 \cdot T - 0.000013 \cdot T^2 - 0.001684 \cdot t + 0.000062 \cdot t^2 - 0.000025 \cdot T \cdot t \tag{6}$$

where:
MY—mass yield of torrefaction process, %;
T—temperature of torrefaction, °C;
t—time of torrefaction, min.
Mass of torrefied biomass after torrefaction

$$mtb = mr_d \cdot MY \tag{7}$$

where:
mtb—mass of torrefied biomass after torrefaction process at T, and t conditions.
LHV of torrefied biomass based on Figure 10

$$LHV_{tb} = \left(12394.39 + 0.07 \cdot T^2 + 90.68 \cdot t - 0.79 \cdot t^2\right)/1000 \tag{8}$$

where:
LHV_{tb}—the low heating value of torrefied biomass depending of torrefaction conditions, $MJ \cdot kg^{-1}$;
1000—conversion of kJ to MJ.
The total energy in torrefied biomass

$$E_{tb} = MY \cdot LHV \cdot 1000 \tag{9}$$

where:
E_{tb}—energy in torrefied biomass, kJ;
1000—conversion of Mg to kg.

4.2.3. Energy Need to Torrefaction Process

Data for calculations [38]:

- T_a—ambient temperature, °C, assumed 15 °C;
- T_b—boiling point of water, 100 °C;
- latent heat of water vaporization, 2500 $kJ \cdot kg^{-1}$ [39] ;
- specific heat of water, 4.18 $kJ \cdot kg^{-1}$ [39];
- specific heat of wood, $kJ \cdot kg^{-1}$, assumed 1.6 $kJ \cdot kg^{-1}$ [40].

The energy needed to heat water contained in Oxytree residues

$$E_w = m_w \cdot Cp_{water} \cdot (T_b - T_a) \tag{10}$$

where:

Ew—energy needed to heat water contained in Oxytree residues, MJ;
Cp_{water}—specific heat of water, 4.18 kJ·kg^{-1}.
The energy needed to water vaporization

$$E_{ev} = m_w \cdot L_h \tag{11}$$

where:

E_{ev}—energy needed to vaporization of water contained in Oxytree residues, MJ;
L_h—latent heat of water vaporization, kJ·kg^{-1}.
The energy needed to heat Oxytree residues during torrefaction

$$E_{hw} = mr_d \cdot Cp_{wood} \cdot (T - T_a) \tag{12}$$

where:

E_{hw}—energy needed to heat Oxytree residues from ambient to torrefaction temperature, MJ;
Cp_{wood}—specific heat of wood, kJ·kg^{-1}.
Total energy needed to torrefied Oxytree residues

$$E = E_w + E_{ev} + E_{hw} \tag{13}$$

where:

E—energy needed to torrefied Oxytree residues

4.2.4. Estimation of the Value of Torrefied Biomass

Estimation was done based on the price of commercial coal fuel available in Poland's market in 2019 and its *LHV*. The value in PLN has been converted to € at the current exchange rate.
Data for calculations:

- Price of commercial coal fuel, €·Mg^{-1}, assumed 170 €·Mg^{-1} [41];
- *LHV* of commercial coal fuel, MJ·kg^{-1}, assumed 23 MJ·kg^{-1} [41].

The estimated value of torrefied biomass

$$V_{tb} = \frac{V_{ccf} \cdot LHV_{tb}}{LHV_{ccf}} \tag{14}$$

where:

V_{tb}—the estimated value of torrefied biomass, €·Mg^{-1};
$Vccf$—value (price) of commercial coal fuel, €·Mg^{-1};
LHV_{ccf}—low heating value of commercial coal fuel, MJ·kg^{-1}.

4.2.5. Profit from Torrefied Oxytree Residues

Mass of torrefied Oxytree residues net (when assumed that part of it is used as fuel to the process of torrefaction)

$$mtb_n = \frac{E_{tb} - E}{LHV_{tb}} \tag{15}$$

where:

mtb_n—a mass of torrefied Oxytree residues net, Mg.

The evaluations of the value of torrefied biomass were completed for 1 Mg of Oxytree wet residues. The moisture content in Oxytree residues was assumed as 50%. Based on Solver a Microsoft Excel add-in program, the best conditions for the torrefaction process (in terms of economics) were

T = 200 °C, and t = 20 min. For these conditions, *MY* of torrefied biomass was 97% and *LHV* of torrefied biomass was 16.7 MJ·kg^{-1}. In these conditions, the calculated value of produced torrefied biomass was 123.38 €·Mg^{-1} d.m., while the net mass obtained after torrefaction was 0.39 Mg d.m. The evaluated value of torrefied biomass from 1 Mg of Oxytree wet residues (containing 50% of moisture) was €44.92.

The presented simple model of evaluation of the value of torrefied Oxytree residues as a fuel is the first step to the evaluation of the profitability of utilization of torrefaction technology to Oxytree residues. The model has been based on simple assumptions, and thus, it cannot be used as a fully-fledged tool to evaluate the economic value of torrefied biomass yet. For prices of fuel such as coal, the impact has many factors, such as ash content, grindability, fraction, etc. Nevertheless, after knowing these factors and their impact on the price of coal, the presented model could be extended and improved. The situation is the same with the estimations of the cost of production of torrefied biomass. A more complete and improved analysis of all types of costs is warranted.

5. Conclusions

In this article, we used raw data of torrefied pruned biomass of Oxytree and developed mathematical models describing torrefied pruned Oxytree properties. Presented models of mass yield, energy yield, energy densification ratio, *HHV*, and *LHV* are characterized by $R^2 > 0.78$. Thus, the newly developed models could be used for describing the process of torrefaction of biomass originating from Oxytree pruning. The other models still describe the process trends well albeit with large standard deviations in the measurement data. The energetic properties of torrefied Oxytree biomass are comparable to other woody biomass. The highest *HHV* of torrefied biomass was 21 MJ·kg^{-1} at 300 °C and 20 min. The study found that the most beneficial economic aspect parameters of torrefaction are 200 °C and 20 min. These parameters provide the greatest profit and the smallest energetic losses.

Supplementary Materials: The following are available online at https://doi.org/10.3390/data4020055, file: data-04-00055-s001.xlsx. This file contains data of fuel properties of torrefied pruned biomass of *Paulownia Clon* in Vitro 112 (Oxytree) the hybrid of *Paulownia elongata* x *Paulownia fortunei*. The "Read me" sheet is a guide on how to read the data with short information about each type of treatment. The second spreadsheet ("Oxytree biomass yield") contains data about the Oxytree biomass yield, energy densification ratio, mass, and energy yield of torrefied biomass. The third spreadsheet ("Oxytree torrefaction TGA") contains raw data from TGA tests. The fourth spreadsheet ("Proximate analyses") contains information about moisture content, organic matter content, combustible content, and ash content in raw and torrefied Oxytree biomass. The fifth spreadsheet ("Ultimate analyses") presents the elemental composition and *H:C*, and *O:C* ratio of raw Oxytree biomass and torrefied biomass, high heating value, low heating value, and high heating value (without ash).

Author Contributions: Conceptualization, K.S. and A.B.; methodology, K.S. and A.B.; software, K.S.; validation, K.S., A.B., and J.K.; formal analysis, K.S.; investigation, K.S., M.L., P.B.; resources, K.S., M.L., P.B., A.B., and J.K.; data curation, K.S.; writing—original draft preparation, K.S.; writing—review and editing, K.S., A.B, J.K.; visualization, K.S.; supervision, A.B. and J.K.; project administration, A.B.; funding acquisition, K.S., A.B., and J.K.

Funding: Authors would like to thank "The PROM Programme—International scholarship exchange of Ph.D. candidates and academic staff" cofinanced by the European Social Fund under the Knowledge Education Development Operational Programme PPI/PRO/2018/1/00004/U/001. Authors would like also to thank the Fulbright Foundation for funding the project titled "Research on pollutants emission from Carbonized Refuse Derived Fuel into the environment," completed at the Iowa State University. In addition, this project was partially supported by the Iowa Agriculture and Home Economics Experiment Station, Ames, Iowa. Project no. IOW05556 (Future Challenges in Animal Production Systems: Seeking Solutions through Focused Facilitation) sponsored by Hatch Act and State of Iowa funds.

Conflicts of Interest: "The authors declare no conflicts of interest."

Appendix A

Appendix A presents models for which some parameters are statistically insignificant at $p < 0.05$. Insignificant parameters are presented in black font, whereas statistically significant by red font (Tables A1–A4). In each table, the first row contains a model to evaluate the particular properties of torrefied biomass, R^2, and *AIC* value. The name (e.g., model 1) presents the original model

$f(T,t) = a_1 + a_2{\cdot}T + a_3{\cdot}T^2 + a_4{\cdot}t + a_5{\cdot}t^2 + a_6{\cdot}T{\cdot}t$. The (model 2) and (model 3) names stand for next (alternative) versions of a model without insignificant coefficients.

Table A1. Statistic evaluation of 3D model parameters of *HHV* (model 1).

Intercept/ Coefficient	Value of Intercept/ Coefficient	Standard Error	*p*	Lower Limit of Confidence	Upper Limit of Confidence	Standardized β Coefficient
a_1	**15,766.51**	**1816.820**	**8.67808**	**0.000000**	**12,195.46**	-
a_2	−6.93	14.197	−0.48833	0.625567	−34.84	−0.19
a_3	**0.07**	**0.028**	**2.46019**	**0.014282**	**0.01**	**0.94**
a_4	**60.04**	**17.365**	**3.45749**	**0.000600**	**25.91**	**0.78**
a_5	**−0.67**	**0.148**	**−4.50308**	**0.000009**	**−0.96**	**−0.70**
a_6	0.07	0.050	1.33485	0.182637	−0.03	0.23

$HHV = a_1 + a_2{\cdot}T + a_3{\cdot}T^2 + a_4{\cdot}t + a_5{\cdot}t^2 + a_6{\cdot}T{\cdot}t$, $R^2 = 0.79$, *AIC* = 8128; **bold** font signifies statistical significance ($p < 0.05$).

Table A2. Statistic evaluation of 3D model parameters of *LHV* (model 1).

Intercept/ Coefficient	Value of Intercept/ Coefficient	Standard Error	*p*	Lower Limit of Confidence	Upper Limit of Confidence	Standardized β Coefficient
a_1	**14,913.84**	**1835.747**	**0.000000**	**11,305.59**	**18,522.09**	–
a_2	−16.21	14.345	0.259123	−44.41	11.99	−0.40
a_3	**0.09**	**0.028**	**0.001152**	**0.04**	**0.15**	**1.14**
a_4	**64.87**	**17.546**	**0.000247**	**30.38**	**99.35**	**0.76**
a_5	**−0.79**	**0.150**	**0.000000**	**−1.09**	**−0.50**	**−0.75**
a_6	**0.10**	**0.051**	**0.042425**	**0.00**	**0.20**	**0.32**

$LHV = a_1 + a_2{\cdot}T + a_3{\cdot}T^2 + a_4{\cdot}t + a_5{\cdot}t^2 + a_6{\cdot}T{\cdot}t$, $R^2 = 0.82$, *AIC* = 8137; **bold** font signifies statistical significance ($p < 0.05$).

Table A3. Statistic evaluation of 3D model parameters of *LHV* (model 2).

Intercept/ Coefficient	Value of Intercept/ Coefficient	Standard Error	*p*	Lower Limit of Confidence	Upper Limit of Confidence	Standardized β Coefficient
a_1	**12,877.28**	**348.9176**	**0.000000**	**12,191.48**	**13,563.09**	–
a_2	**0.06**	**0.0043**	**0.000000**	**0.05**	**0.07**	**0.75**
a_3	**66.89**	**17.4595**	**0.000147**	**32.58**	**101.21**	**0.78**
a_4	**−0.79**	**0.1501**	**0.000000**	**−1.09**	**−0.50**	**−0.75**
a_5	0.10	0.0502	0.058891	0.00	0.19	0.30

$LHV = a_1 + a_2{\cdot}T^2 + a_3{\cdot}t + a_4{\cdot}t^2 + a_5{\cdot}T{\cdot}t$, $R^2 = 0.82$, *AIC* = 8135; **bold** font signifies statistical significance ($p < 0.05$).

Table A4. Statistic evaluation of 3D model parameters of *H:C* (model 1).

Intercept/ Coefficient	Value of Intercept/ Coefficient	Standard Error	*p*	Lower Limit of Confidence	Upper Limit of Confidence	Standardized β Coefficient
a_1	**3.576069**	**0.780513**	**0.000010**	**2.032757**	**5.119380**	–
a_2	−0.007620	0.006099	0.213674	−0.019680	0.004440	−0.84
a_3	0.000004	0.000012	0.731624	−0.000020	0.000028	0.23
a_4	−0.011341	0.007460	0.130728	−0.026092	0.003409	−0.60
a_5	**0.000200**	**0.000064**	**0.002132**	**0.000074**	**0.000326**	**0.85**
a_6	**−0.000044**	**0.000022**	**0.041243**	**−0.000087**	**−0.000002**	**−0.62**

$H{:}C = a_1 + a_2{\cdot}T + a_3{\cdot}T^2 + a_4{\cdot}t + a_5{\cdot}t^2 + a_6{\cdot}T{\cdot}t$, R2 = 0.82, *AIC* = 164; **bold** font signifies statistical significance ($p < 0.05$).

References

1. Baležentis, T.; Streimikiene, D.; Zhang, T.; Liobikiene, G. The role of bioenergy in greenhouse gas emission reduction in EU countries: An Environmental Kuznets Curve modelling. *Resour. Conserv. Recycl.* **2019**, *142*, 225–231. [CrossRef]
2. Paredes-Sánchez, J.P.; López-Ochoa, L.M.; López-González, L.M.; Las-Heras-Casas, J.; Xiberta-Bernat, J. Evolution and perspectives of the bioenergy applications in Spain. *J. Clean. Prod.* **2019**, *213*, 553–568. [CrossRef]
3. Söderberg, C.; Eckerberg, K. Forest Policy and Economics Rising policy conflicts in Europe over bioenergy and forestry. *For. Policy Econ.* **2013**, *33*, 112–119. [CrossRef]
4. Di Fulvio, F.; Forsell, N.; Korosuo, A.; Obersteiner, M.; Hellweg, S. Spatially explicit LCA analysis of biodiversity losses due to different bioenergy policies in the European Union. *Sci. Total Environ.* **2019**, *651*, 1505–1516. [CrossRef] [PubMed]
5. Liszewski, M.; Bąbelewski, P. Oxytree plantation—Second year of research. *Biomasa* **2018**, *8*, 36–38.
6. Jakubowski, M.; Tomczak, A.; Jelonek, T. The use of wood and the possibility of planting trees of the paulownia genus. *Acta Sci. Pol. Silv. Colendar. Ratio Ind. Lignar.* **2018**, *17*, 291–297. [CrossRef]
7. Paulownia Bulletin ≠ 3. Advices And Instructions Paulownia For Biomass Production. Available online: http://paulowniatrees.eu/products/paulownia-planting-material (accessed on 10 March 2019).
8. Hugo Durán Zuazo, V.; Antonio Jiménez Bocanegra, J.; Perea Torres, F.; Rodríguez Pleguezuelo, C.R.; Francia Martínez, J.R. Biomass Yield Potential of Paulownia Trees in a Semi-Arid Mediterranean Environment (S Spain). *Int. J. Renew. Energy Res.* **2013**, *3*.
9. Dyjakon, A. The Influence of Apple Orchard Management on Energy Performance and Pruned Biomass Harvesting for Energetic Applications. *Energies* **2019**, *12*, 632. [CrossRef]
10. Jabłoński, D. Oxytree: Wood for processing in a sawmill 6 years after planting. Available online: https://www.drewno.pl/artykuly/10535,oxytree-drewno-do-przerobu-w-tartaku-w-6-lat-od-posadzenia-drzewa.html (accessed on 12 March 2019).
11. Basu, P. *Biomass Gasification, Pyrolysis and Torrefaction*, 2nd ed.; Academic Press: Cambridge, MA, USA, 2013; pp. 87–145. ISBN 978-0-12-396488-5.
12. Chen, W.H.; Peng, J.; Bi, X.T. A state-of-the-art review of biomass torrfeaction, densification and applications. *Renew. Susr. Energ. Rev.* **2015**, *44*, 847–866. [CrossRef]
13. Van der Stelt, M.J.C.; Gerhauser, H.; Kiel, J.H.A.; Ptasinski, K.J. Biomass upgrading by torrefaction for the production of biofuels: A review. *Biomass Bioenergy* **2011**, *35*, 3748–3762. [CrossRef]
14. Jakubiak, M.; Kordylewski, W. Biomass torrefaction. *Arch. Spalania* **2010**, *10*, 11–25.
15. Phanphanich, M.; Mani, S. Impact of torrefaction on the grindability and fuel characteristics of forest biomass. *Biores. Technol.* **2011**, *102*, 1246–1253. [CrossRef] [PubMed]
16. Ahmed, N.; Rahmana, M.; Won, S.; Shim, S. Biochar properties and eco-friendly applications for climate change mitigation, waste management, and wastewater treatment: A review. *Renew. Sust. Energy Rev.* **2017**, *79*, 255–273. [CrossRef]
17. Dudek, M.; Świechowski, K.; Manczarski, P.; Koziel, J.A.; Białowiec, A. The Effect of Biochar Addition on the Biogas Production Kinetics from the Anaerobic Digestion of Brewers' Spent Grain. *Energies* **2019**, *12*, 1518. [CrossRef]
18. Weber, K.; Quickerbhttps, P. Properties of biochar. *Fuel* **2018**, *217*, 240–261. [CrossRef]
19. Świechowski, K.; Liszewski, M.; Bąbelewski, P.; Koziel, J.A.; Białowiec, A. Fuel Properties of Torrefied Biomass from Pruning of Oxytree. *Data* **2019**, *4*, 55. [CrossRef]
20. Stegenta, S.; Kałdun, B.; Białowiec, A. Model selection and determination of kinetic parameters of respiratory activity of wastes during the aerobic process of biostabilization of municipal solid waste fraction. *Rocz. Ochr. Środowiska* **2016**, *18*, 800–814.
21. Wang, L.; Barta-Rajnai, E.; Skreiberg, O.; Khalil, R.; Czégény, Z.; Jakab, E.; Barta, Z.; Grønli, M. Impact of Torrefaction on Woody Biomass Properties. *Energy Procedia* **2017**, *105*, 1149–1154. [CrossRef]
22. Szymon, S.; Adrian, Ł.; Piersa, P.; Romanowska-Duda, Z.; Grzesik, M.; Cebula, A.; Kowalczyk, S. Renewable Energy Sources: Engineering, Technology, Innovation. *Springer Int. Publ. AG* **2018**, 365–373. [CrossRef]
23. Tumuluru, J.S.; Sokhansanj, S.; Hess, J.R.; Wright, C.T.; Boardman, R.D. A review on biomass torrefaction process and product properties for energy applications. *Ind. Bioterchnol.* **2011**, *7*, 373–384. [CrossRef]

24. Wang, L.; Barta-Rajnai, E.; Skreiberg, Ø; Khalil, R.; Czégény, Z.; Jakab, E.; Barta, Z.; Grønli, M. Effect of torrefaction on physiochemical characteristics and grindability of stem wood, stump and bark. *Appl. Energy* **2018**, *227*, 137–148. [CrossRef]
25. Pach, M.; Zanzi, R.; Bjornbom, E. Torrefied biomass a substitute for wood and charcoal. In Proceedings of the 6th Asia-Pacific International Symposium on Combustion and Energy Utilization, Kuala Lumpur, Malaysia, 20–22 May 2002.
26. Khazraie Shoulaifar, T.; Demartini, N.; Zevenhoven, M.; Verhoeff, F.; Kiel, J.; Hupa, M. Ash-forming matter in torrefied birch wood: Changes in chemical association. *Energy Fuels* **2013**, *27*, 5684–5690. [CrossRef]
27. Tumuluru, J.S. Comparison of Chemical Composition and Energy Property of Torrefied Switchgrass and Corn Stover. *Front. Energy Res.* **2015**, *3*, 1–11. [CrossRef]
28. Grams, J.; Kwapińska, M.; Jędrzejczyk, M.; Rzeźnicka, I.; Leahy, J.J.; Ruppert, A.M. Surface characterization of Miscanthus × giganteus and Willow subjected to torrefaction. *J. Anal. Appl. Pyrolysis* **2019**, *138*, 231–241. [CrossRef]
29. Rodrigues, A.; Loureiro, L.; Nunes, L.J.R. Torrefaction of woody biomasses from poplar SRC and Portuguese roundwood: Properties of torrefied products. *Biomass Bioenergy* **2018**, *108*, 55–65. [CrossRef]
30. Li, S.; Harris, S.; Anandhi, A.; Chen, G. Predicting biochar properties and functions based on feedstock and pyrolysis temperature: A review and data syntheses. *J. Clean. Prod.* **2019**, *215*, 890–902. [CrossRef]
31. Lu, J.J.; Chen, W.H. Product yields and characteristics of corncob waste under various torrefaction atmospheres. *Energies* **2014**, *7*, 13–27. [CrossRef]
32. Ren, X.; Sun, R.; Meng, X.; Vorobiev, N.; Schiemann, M.; Levendis, Y.A. Carbon, sulfur and nitrogen oxide emissions from combustion of pulverized raw and torrefied biomass. *Fuel* **2017**, *188*, 310–323. [CrossRef]
33. Li, S.; Chen, G. Thermogravimetric, thermochemical, and infrared spectral characterization of feedstocks and biochar derived at different pyrolysis temperatures. *Waste Manag.* **2018**, *78*, 198–207. [CrossRef]
34. Li, S.; Barreto, V.; Li, R.; Chen, G.; Hsieh, Y.P. Nitrogen retention of biochar derived from different feedstocks at variable pyrolysis temperatures. *J. Anal. Appl. Pyrolysis* **2018**, *133*, 136–146. [CrossRef]
35. Novak, J.; Lima, I.; Xing, B.; Gaskin, J.W.; Steiner, C.; Das, K.C.; Ahmedna, M.; Rehrah, D.; Watts, D.W.; Busscher, W.J.; et al. Characterization of designer biochar produced at different temperatures and their effects on a loamy sand. *Ann. Environ. Sci.* **2009**, *3*, 195–206.
36. Akanni, A.A.; Kolawole, O.J.; Dayanand, P.; Ajani, L.O.; Madhurai, M. Influence of torrefaction on lignocellulosic woody biomass of Nigerian origin. *J. Chem. Technol. Metall.* **2019**, *54*, 274–285.
37. Markič, M.; Kalan, Z.; Pezdič, J.; Faganeli, J. H/C versus O/C atomic ratio characterization of selected coals in Slovenia. *Geologija* **2011**, *50*, 403–426. [CrossRef]
38. Stępień, P.; Mysior, M.; Bialowiec, A. Technical and techn ological problems and aplicability of waste torrefaction. In *Innovations in Waste Management. Selected Issues*; Białowiec, A., Ed.; Wydawnictwo Uniwersytetu Przyrodniczego we Wrocławiu: Wrocław, Dolnośląskie, 2018; ISBN 9788377172780. [CrossRef]
39. Brusseau, M.L.; Walker, D.B.; Fitzsimmons, K. *Physical-Chemical Characteristics of Water*, 3rd ed.; Elsevier Inc.: Amsterdam, The Netherlands, 2019; ISBN 9780128147191.
40. Radmanović, K.; Đukić, I.; Pervan, S. Specific Heat Capacity of Wood. *Drv. Ind.* **2014**, *65*, 151–157. [CrossRef]
41. Portal Gospodarczy, Coal Prices. Available online: https://www.wnp.pl/gornictwo/notowania/ceny_wegla_pgg/ (accessed on 12 March 2019).

Załącznik nr 3

Kacper Świechowski
imię i nazwisko

WROCŁAW 28.02.2022
(miejscowość i data)

Katedr Biogospodarki Stosowanej
Uniwersytet Przyrodniczy we Wrocławiu
51-630 Wrocław, Chełmońskiego 37a
afiliacja

OŚWIADCZENIE

Oświadczam, że w pracy:

Kacper Świechowski, Marek Liszewski, Przemysław Bąbelewski, Jacek A. Koziel, Andrzej Białowiec. 2019. Oxytree Pruned Biomass Torrefaction: Mathematical Models of the Influence of Temperature and Residence Time on Fuel Properties Improvement. Materials 12, 2228; doi:10.3390/ma12142228

mój udział polegał na:
Opracowaniu wyników z badań pod względem statystycznym przy wykorzystaniu oprogramowania Statistica. Opracowanie polegało na wykorzystaniu danych z eksperymentu toryfikacji Oxytree do wygenerowania modeli matematycznych opisujących wpływ temperatury i czasu toryfikacji na zmianę właściwości paliwowych (z analizy technicznej, elementarnej i ciepła spalania) toryfikatu. Byłem odpowiedzialny za wykonanie opisu i dyskusję otrzymanych wyników. Napisałem wstępną wersję manuskryptu korzystając z pomocy i doświadczenia pozostałych współautorów, wykonałem także grafiki jak i wizualizacje modeli. Brałem udział w pisaniu odpowiedzi dla recenzentów czasopisma.

28.02.2022 Świechowski
data i podpis

Załącznik nr 3

Wrocław, 28.02.2022

(miejscowość i data)

Marek Liszewski
imię i nazwisko

Instytut Agroekologii i Produkcji Roślinnej
Uniwersytet Przyrodniczy we Wrocławiu
50-363 Wrocław, pl. Grunwaldzki 24A
afiliacja

OŚWIADCZENIE

Oświadczam, że w pracy:

Kacper Świechowski, Marek Liszewski, Przemysław Bąbelewski, Jacek A. Koziel, Andrzej Białowiec. 2019. Oxytree Pruned Biomass Torrefaction: Mathematical Models of the Influence of Temperature and Residence Time on Fuel Properties Improvement. Materials 12, 2228; doi:10.3390/ma12142228

mój udział polegał na:

Pozyskaniu i przygotowaniu do dalszych badań materiału badawczego którym był próbki drewna Oxytree pochodzące z plantacji w Pawłowicach. Moje zadanie polegało na posadzeniu drzew Oxytree w Pawłowicach, które były poddawane 4 różnym zabiegom agrotechnicznym, pobraniu próbek drewna, wysuszeniu i ich wstępnym rozdrobnieniu. W manuskrypcie brałem udział w opisywaniu badanych materiałów.

28.02.2022

data i podpis

Załącznik nr 3

Przemysław Bąbelewski
imię i nazwisko

Wrocław 02-03-2022
(miejscowość i data)

Katedra Ogrodnictwa
Uniwersytet Przyrodniczy we Wrocławiu
50-363 Wrocław, pl. Grunwaldzki 24A
afiliacja

OŚWIADCZENIE

Oświadczam, że w pracy:
Kacper Świechowski, Marek Liszewski, Przemysław Bąbelewski, Jacek A. Koziel, Andrzej Białowiec. 2019. Oxytree Pruned Biomass Torrefaction: Mathematical Models of the Influence of Temperature and Residence Time on Fuel Properties Improvement. Materials 12, 2228; doi:10.3390/ma12142228

mój udział polegał na:
Pozyskaniu i przygotowaniu materiału badawczego którym był próbki drewna Oxytree pochodzące z plantacji doświadczalnej w Psarach. Moje zadanie polegało dokonaniu zabiegu agrotechnicznego – przycinania, w wyniku którego powstały 4 próbki drewna użyte w badaniu. Byłem także odpowiedzialny za wstępne przygotowanie materiału, rozdrobnienie, suszenie i dostarczenie do laboratorium. Podczas pisania manuskryptu pomagałem przy opisach dotyczących Oxytree.

Przemysław Bąbelewski
02.03.2022
data i podpis

Załącznik nr 3

Jacek Koziel Ames, 23-2-2022

imię i nazwisko (miejscowość i data)

Department of Agricultural and Biosystems Engineering
Iowa State University
Ames, IA 50011, USA
afiliacja

OŚWIADCZENIE

Oświadczam, że w pracy:

Kacper Świechowski, Marek Liszewski, Przemysław Bąbelewski, Jacek A. Koziel, Andrzej Białowiec. 2019. Oxytree Pruned Biomass Torrefaction: Mathematical Models of the Influence of Temperature and Residence Time on Fuel Properties Improvement. Materials 12, 2228; doi:10.3390/ma12142228

mój udział polegał na:

Pełnieniu opieki merytorycznej nad pracą wykonywaną przez Kacpra Świechowskiego w całym procesie pisania, modyfikowania i recenzowania wyżej wymienionego artykułu. Byłem odpowiedzialny za nadzór nad poprawności przedstawienia koncepcji i metodyki badań w sposób graficzny, odpowiadałem za sprawdzenie i nanoszenie poprawek podczas procesu pisania manuskryptu jak i podczas etapu recenzji. Pozyskałem także część środków niezbędnych do opublikowania artykułu.

data i podpis

Załącznik nr 3

Andrzej Białowiec
imię i nazwisko

Wrocław 26.02.2022
(miejscowość i data)

Katedr Biogospodarki Stosowanej
Uniwersytet Przyrodniczy we Wrocławiu
51-630 Wrocław, Chełmońskiego 37a
afiliacja

OŚWIADCZENIE

Oświadczam, że w pracy:
Kacper Świechowski, Marek Liszewski, Przemysław Bąbelewski, Jacek A. Koziel, Andrzej Białowiec. 2019. Oxytree Pruned Biomass Torrefaction: Mathematical Models of the Influence of Temperature and Residence Time on Fuel Properties Improvement. Materials 12, 2228; doi:10.3390/ma12142228

mój udział polegał na:
Zapewnieniu wsparcia merytorycznego dla piszącego manuskrypt doktoranta, w tym pomagałem stworzyć koncepcje artykułu jak i sprawdziłem poprawność danych przed wysłaniem artykułu do recenzji. Jako autor korespondencyjny byłem odpowiedzialny za prowadzenie dyskusji z recenzentami oraz za wprowadzanie części modyfikacji w manuskrypcie podczas recenzji. Pozyskałem także część finansowania umożliwiającego publikację w open access.

26.02.2022 Białowiec

data i podpis

materials

MDPI

Article

Oxytree Pruned Biomass Torrefaction: Process Kinetics

Kacper Świechowski [1], Sylwia Stegenta-Dąbrowska [1,*], Marek Liszewski [2], Przemysław Bąbelewski [3], Jacek A. Koziel [4] and Andrzej Białowiec [1,4]

1 Faculty of Life Sciences and Technology, Institute of Agricultural Engineering, Wrocław University of Environmental and Life Sciences, 37/41 Chełmońskiego Str., 51-630 Wrocław, Poland; kacper.swiechowski@upwr.edu.pl (K.S.); andrzej.bialowiec@upwr.edu.pl (A.B.)

2 Faculty of Life Sciences and Technology, Institute of Agroecology and Plant Production, Wrocław University of Environmental and Life Sciences, 24A Grunwaldzki Sqr., 53-363 Wrocław, Poland; marek.liszewski@upwr.edu.pl

3 Faculty of Life Sciences and Technology, Department of Horticulture, Wrocław University of Environmental and Life Sciences, 24A Grunwaldzki Sq., 53-363 Wrocław, Poland; przemyslaw.babelewski@upwr.edu.pl

4 Department of Agricultural and Biosystems Engineering, Iowa State University, Ames, IA 50011, USA; koziel@iastate.edu

* Correspondence: sylwia.stegenta@upwr.edu.pl; Tel.: +48-71-320-5973

Received: 27 August 2019; Accepted: 9 October 2019; Published: 12 October 2019

Abstract: Oxytree is a fast-growing energy crop with C4 photosynthesis. In this research, for the first time, the torrefaction kinetic parameters of pruned Oxytree biomass (*Paulownia clon* in Vitro 112) were determined. The influence of the Oxytree cultivation method and soil class on the kinetic parameters of the torrefaction was also investigated. Oxytree pruned biomass from a first-year plantation was subjected to torrefaction within temperature range from 200 to 300 °C and under anaerobic conditions in the laboratory-scale batch reactor. The mass loss was measured continuously during the process. The relative mass loss increased from 1.22% to 19.56% with the increase of the process temperature. The first-order constant rate reaction (k) values increased from 1.26×10^{-5} s^{-1} to 7.69×10^{-5} s^{-1} with the increase in temperature. The average activation energy for the pruned biomass of Oxytree torrefaction was 36.5 kJ·mol^{-1}. Statistical analysis showed no significant ($p < 0.05$) effect of the Oxytree cultivation method and soil class on the k value. The results of this research could be useful for the valorization of energy crops such as Oxytree and optimization of waste-to-carbon and waste-to-energy processes.

Keywords: Oxytree; Paulownia; torrefied biomass; pruned biomass; valorization; renewable energy; fast-growing biomass; energy crops; brownfields; kinetics parameters; activation energy

1. Introduction

It is estimated that the amount of bio-renewable energy in the European Union (EU) will continue to grow by ~22 EJ·year^{-1} from the year 2010 to 2030. This increase is due to the 2009/28/EC directive adopted by the EU [1]. It has been shown that, in 2020, biomass will account for almost 60% of the total renewable energy produced in the EU [2]. The last update of the EU targets and the share of renewable energy sources in the total energy consumption was 27%, contributing to the increasing demand for wooden biomass [3]. The forecasted growth of the biomass share in the energy production balance indicates the importance of the research on new, fast-growing energy crops, especially those which can be cultivated in weak or degraded soils.

To date, short rotation plantations of wood, such as willow, poplar, black locust, alder [4], and aspen [5], were investigated. All mentioned plant species are C3 photosynthesis plants [6,7]. It is

known that a more efficient pathway is photosynthesis C4. It is assumed that, for some plants, successful conversion of the C3 photosynthesis pathway to C4 could result in an increase in crop yield by 50–60% [8,9]. *Paulownia* sp. genus developed the C4 photosynthesis [10]. An additional advantage of *Paulownia* trees is the ability to adapt to different climatic conditions, high mass yield [11,12], and the possibility of establishing plantations on wasteland, brownfields, as well as degraded lands [13].

One of the clones of *Paulownia* is *Paulownia clon* in Vitro 112, which can be characterized by increased biomass, reaching a height of 16 m at the age of 6 y. The Oxytree wood is utilized in construction or furniture-making [14]. *Paulownia clon* in Vitro 112 ranks as class I on Janka's hardness scale—very soft wood [15]. It has been shown that the biochar from *Paulownia* produced at 600 °C is a pure carbon without organic composition, characterized by a pore size from 35.8 to 290.5 µm. Such material, after proper treatment, can be applied as a filtration agent or catalyst [15]. Oxytree can also be utilized for energy purposes. The high heating value in dry mass is 19 470 $J \cdot g^{-1}$, with low ash (1.29%) and chlorine (0.01%) content [16].

Bulky biochar can be pelletized for energy content densification. However, the main limitation of the classic pelletizing is the necessity of biomass drying as well as the high energy demand on its grinding [17]. The problem of moisture and grinding of biomass can be solved by using low-temperature pyrolysis, also known as torrefaction. The resulting solid material is characterized by higher energy content and improved fuel properties, which have been widely described in the case of other types of wooden biomass [18,19]. The additional benefit of torrefaction is the decrease of the energy demand for grinding from approximately 240 $kW \cdot Mg^{-1}$ to 20–80 $kW \cdot Mg^{-1}$ [20]. Torrefaction is a thermochemical pretreatment process that improves biomass utilization values. During torrefaction, the biomass is treated with temperatures of 200–300 °C in an inert condition for up to 1 h [21].

Kinetics are important for biochar valorization. Since biomass is a complex mixture of biopolymers, during the pyrolysis/torrefaction, the thermal decomposition of biomass takes place in multiple steps, which can overlap with each other. Kinetics studies are essential for the understanding of occurring reactions. The term 'kinetics' pertains to kinetics parameters such as the activation energy, pre-exponential factor, reaction rate, and others. The kinetics are used for the design and optimization of reactors, and to establish optimal process conditions. The kinetics of solid torrefied biomass can be obtained in many ways, based on analyses, such as thermogravimetric analysis (TGA), differential thermal analysis (DTA), or differential scanning calorimetry (DSC). The determination of kinetics has two stages. First is an experiment involving one of the analyses mentioned above, and the second stage is based on mathematical analyses of experimental data [22].

Recently, we [23] presented results of the influence of the pruned Oxytree biomass torrefaction temperature and duration on the proximate and ultimate properties of the produced biochar. However, to date, no scientific papers have presented systematic research on the kinetics of torrefaction of *Paulownia*, including the pruned biomass of Oxytree. The kinetics and activation energy of pruned biomass of Oxytree torrefaction is unknown but is essential for modeling the process efficiency and energy demand.

The aim of the study was the determination (for the first time) of the kinetics parameters and the activation energy of torrefaction of pruned biomass of Oxytree corresponding to the agronomic cultivation conditions and soil type. The scheme of the experiment is shown in Figure 1. The TGA analysis in isothermal conditions and first-order reaction models were used to determine the activation energy.

We hypothesized that the soil type and Oxytree cultivation method could impact the torrefaction kinetics as it is generally known that the composition of biomass can be affected by soil or cultivation methods. Thus, this research focuses on pruned Oxytree biomass produced in different soil types and under different cultivation methods (irrigation/no irrigation, and geotextile/no geotextile). Rodrigues et al. [24] showed that soil composition correlated with biomass fuel quality. This means the soil influences biomass chemical composition. Similarly, Achinelli et al. [25] showed that irrigation has a statistically significant impact on the higher heating value (*HHV*) of biomass (willows). On the

other hand, irrigation did not have an impact on ash content, vessel diameter, fiber wall area, and fiber wall thickness [25].

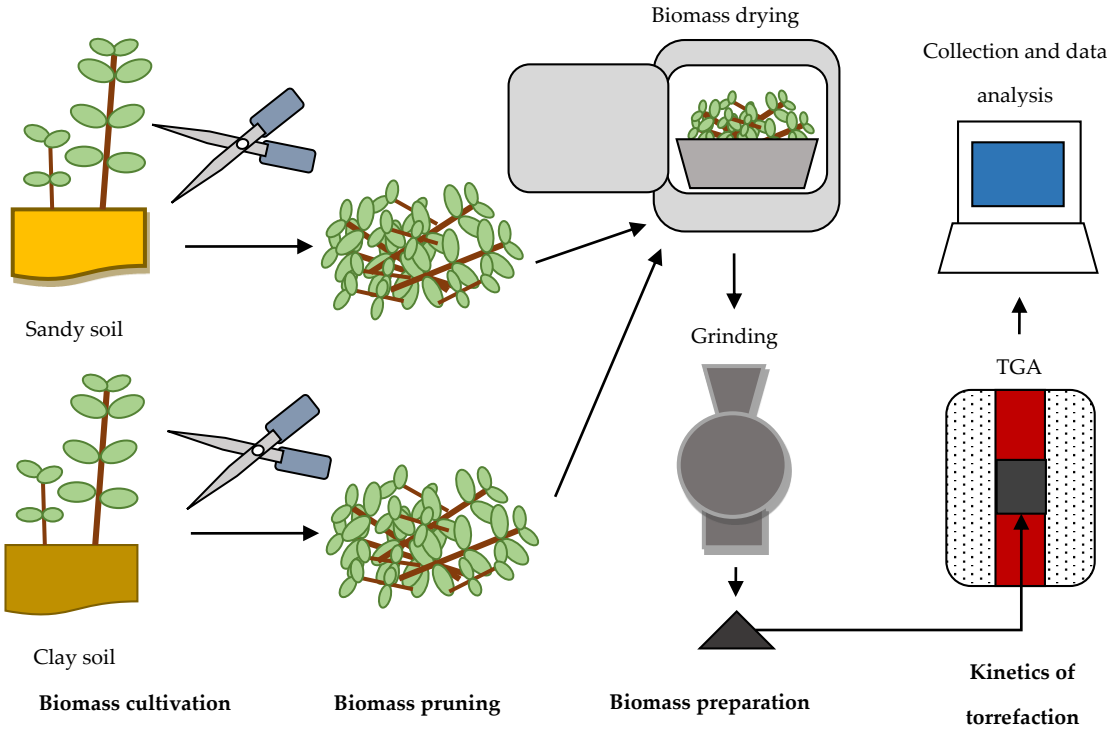

Figure 1. Scheme of experiments to determine the process kinetics of torrefaction for Oxytree prunings.

2. Materials and Methods

2.1. Oxytree Biomass Samples

In a previous data descriptor article [26] titled "Fuel Properties of Torrefied Biomass from Pruning of Oxytree" raw data with descriptions about biomass acquisition, biomass properties, production technology (soil type, mineral fertilization, irrigation), the process of torrefaction, and properties of torrefied biomass were presented in detail. In brief, Oxytree pruned biomass came from two experimental plantations in Poland. The biomasses differed by agro-technical cultivation practices (geotextile and irrigation) and soil type. The cultivation scheme is presented with the following symbols, as is presented below [26]:

- S(G−)(I−),
- S(G+)(I−),
- S(G−)(I+),
- S(G+)(I+),
- C(G+)(I−),
- C(G−)(I−),
- C(G+)(I+),
- C(G−)(I+),

For these symbols, S and C letters stand for the soil type, i.e., S—sandy soil, classified as V soil belonging to brunic arenosols, C—clay soil classified as Phaeozems, respectively, based on the FAO World reference database for soil resources (2014) [27]. The sign (+) stands for cases where geotextile/irrigation, G/I, was used, and (−) for when geotextile/irrigation was not used during cultivation [26].

Oxytree shoots propagated to ~20–40 cm were planted with 4 m × 4 m (16 m^2 per tree) spacing on 19 May 2016. The trees subjected to analysis were pruned on 27 September 2016. The analyzed trees represent pruned biomass after one year of vegetation. A typical agro-technical care treatment takes place 12 months after planting in May, i.e., in the next calendar year. This agro-technical care treatment involves trimming 0.05 m above the pitch to derive one main shoot, which then becomes the main trunk of the tree. The examined biomass samples were about 71% of leaves and 29% of shoots of the total fresh mass, respectively (or 66% and 34%, respectively, on a dry mass basis) [26].

2.2. Ultimate and Proximate Analysis of Samples

The proximate analyses were conducted using standard methods that included:

- Moisture content determined in accordance with [28], using a laboratory dryer (WAMED, model KBC-65W, Warsaw, Poland),
- Organic matter determined in accordance with [29], using a muffle furnace (SNOL, 8.1/1100, Utena, Lithuania).
- Combustibles and ash content determined in accordance with [30], using a muffle furnace (SNOL, 8.1/1100, Utena, Lithuania),
- Higher heating value (*HHV*) and low heating value (*LHV*) determined in accordance with [31] using calorimeters (IKA POL, model C 200, Warsaw, Poland).

The ultimate analyses were the determination of elemental composition (C, H, N, S, O). Carbon, H, and N contents were determined with an elemental CHNS analyzer (CE Instruments Ltd., Manchester, UK). Sulfur was determined by the atomic emission spectrometry method with excitation in inductively-coupled plasma (ICP-AES) after microwave mineralization, using an atomic emission spectrometer (iCAP 7400 ICP-OES, Thermo Fisher Scientific, Waltham, MA, USA).

2.3. Thermogravimetric Analysis—Experimental Design and Procedure

The thermogravimetric analysis (TGA) was carried out using a stand-mounted tubular furnace (Czylok, RST 40x200/100, Jastrzębie-Zdrój, Poland) previously described by Stępień et al. [32].

The mass losses during the torrefaction process were tested under isothermal conditions at 200 °C, 220 °C, 240 °C, 260 °C, 280 °C, and 300 °C with a residence time of 60 min and a CO_2 flow rate of 10 $dm^3 \cdot h^{-1}$ to ensure anaerobic conditions. Three repetitions for each temperature and cultivation type were completed. The materials before the tests were dried in a laboratory dryer (WAMED, model KBC-65W, Warsaw, Poland) for 24 h at 105 °C. Before the experiment was started, the empty tubular furnace was heated to the desired temperature. The samples, with a weight of 3 g, were placed in the steel crucible, which was placed in the heated tubular furnace for 1 h. The measurement of mass loss for each temperature was made using a balance coupled to a cuvette with a biomass sample. The measurement of mass loss took place with a 10 s interval and 0.01 g accuracy.

2.4. Data Analysis

The obtained TGA data were used to determine the constant reaction rate (k, or k value) for particular torrefaction temperatures and Oxytree cultivation types. The k values were estimated according to [33] to the first-order reaction, Equation (1):

$$m_s = m_o \cdot e^{-k \cdot t} \quad (1)$$

where:

m_s—mass after torrefaction time t, g;
m_o—initial mass, g;
k—a constant rate of the reaction, s^{-1};
t—time, s.

The estimation of k values was completed by nonlinear regression and the Statistica 13.3 software (StatSoft, Inc., TIBCO Software Inc., Palo Alto, CA, USA). Then, Arrhenius plots [34] were created, i.e., $\ln(k)[T]$ vs. $1/T$, where k is a constant rate of the reaction, s^{-1}, T is the torrefaction temperature, K. A linear trend line was then obtained for Arrhenius plots:

$$y = a \cdot x + b \quad (2)$$

Then, the activation energy (E_a) values [33] were determined using coefficient 'a' from Equation (2):

$$E_a = a \cdot R \quad (3)$$

where:

E_a—activation energy, $J \cdot mol^{-1}$;
a—the slope coefficient of the linear Equation (2), k;
R—gas constant, $J \cdot mol^{-1} \cdot K^{-1}$.

2.5. Statistical Analysis

The study of the normality of the relative mass loss (Δm) and k values distribution was performed graphically using a quantile chart (Q-Q) and Shapiro–Wilk (S.W.) and Kolmogorov–Smirnov (K.S.) tests along with the Lilliefors correction for a confidence level of $\alpha = 0.05$. Since the Δm and k values were not normally distributed, the analysis of variance was carried out with the non-parametric Kruskal–Wallis (K.W.) test at the $\alpha = 0.05$ level of confidence for the following groups:

- Δm and k—the variable grouping by the cultivation type;
- Δm and k—the variable grouping by torrefaction temperatures;
- Δm—the variable grouping by the torrefaction time.

The post-hoc tests were performed for each K.W. test. A lack of statistically significant differences was marked with the same letters on a box plot. All results of statistical evaluation and interpretation are presented in Appendix A (Figures A1–A9).

3. Results

3.1. Oxytree Biomass Characterization

The organic matter content for Oxytree was 89.22–91.46% d.m. The flammable fraction accounted for 91.22–93.05% d.m. The *HHV* was >17,900 $J \cdot g^{-1}$, with the highest value for S(G+)(I−) being 18,577 $J \cdot g^{-1}$ (Table 1).

Table 1. Proximate analysis of pruned Oxytree biomass; mean values ± standard deviation.

Cultivation Type Symbol, -	Moisture Content, %	Organic Matter Content in d.m., %	Combustible Content in d.m., %	Ash in d.m., %	HHV, J·g d.m.$^{-1}$	LHV, J·g d.m.$^{-1}$
S(G−)(I−)	4.64 ± 0.09	89.22 ± 0.39	91.22 ± 0.38	8.78 ± 0.38	18,251 ± 90	16,666 ± 90
S(G+)(I−)	5.84 ± 0.04	90.36 ± 0.07	92.26 ± 0.09	7.74 ± 0.09	18,577 ± 195	17,135 ± 195
S(G−)(I+)	5.96 ± 0.02	90.10 ± 0.33	91.91 ± 0.29	8.09 ± 0.29	18,407 ± 199	16,762 ± 199
S(G+)(I+)	5.77 ± 0.05	90.06 ± 0.44	91.56 ± 0.44	8.44 ± 0.44	18,499 ± 69	16,858 ± 69
C(G+)(I−)	5.22 ± 0.01	91.00 ± 0.33	92.61 ± 0.29	7.39 ± 0.29	18,453 ± 135	16,920 ± 135
C(G−)(I−)	5.04 ± 0.01	89.75 ± 0.22	91.55 ± 0.21	8.45 ± 0.21	18,099 ± 441	16,463 ± 441
C(G+)(I+)	5.62 ± 0.04	89.86 ± 0.30	91.32 ± 0.31	8.68 ± 0.31	17,910 ± 407	16,430 ± 407
C(G−)(I+)	5.57 ± 0.01	91.46 ± 0.28	93.05 ± 0.18	6.95 ± 0.18	18,167 ± 377	16,450 ± 377
Mean	5.46 ± 0.43	90.23 ± 0.73	91.93 ± 0.67	8.07 ± 0.67	18,295 ± 317	16,711 ± 336

The Oxytree biomass was characterized by an average C (43.76%), H (6.65%), N (2.3%), S (0.2%), and O (37.32%) content, respectively (Table 2). The highest C content was measured in C(G−)(I+) 45.7%, and the lowest S content in S(G−)(I−) 0.17%.

Table 2. Ultimate analysis of pruned Oxytree biomass, mean values ± standard deviation.

Cultivation Type Symbol, -	C, %	H, %	N, %	S, %	O, %
S(G−)(I−)	44.20	6.74	2.05	0.17	36.06
S(G+)(I−)	44.10	5.95	1.95	0.20	38.16
S(G−)(I+)	44.90	6.87	2.22	0.21	35.90
S(G+)(I+)	45.10	6.87	2.83	0.20	35.06
C(G+)(I−)	44.10	6.44	2.72	0.21	37.53
C(G−)(I−)	40.20	6.93	2.46	0.22	39.95
C(G+)(I+)	41.80	6.15	2.06	0.19	39.66
C(G−)(I+)	45.70	7.24	2.09	0.19	36.23
Mean	43.76 ± 1.84	6.65 ± 0.43	2.30 ± 0.33	0.20 ± 0.02	37.32 ± 1.81

3.2. Relative Mass Loss During Torrefaction of Oxytree

A loss of mass occurred during torrefaction for all examined Oxytree samples (Table 3). An increase in mass loss corresponded to the increase of the torrefaction temperature. The smallest Δm values of 0.1% were recorded at 200 °C (lowest temperature) and 10 min (shortest time) for S(G−)(I−), C(G+)(I−), C(G−)(I−) and C(G−)(I+) samples. The data show the increasing Δm value with temperature and process time to 19.6% (S(G+)(I+), 300 °C and 60 min). Post−hoc tests showed that there was no impact of cultivation type on mass loss ($p < 0.05$) (Figure A7). However, the torrefaction temperature had a significant effect on each T tested ($p < 0.05$) (Figure A8). The increasing torrefaction time led (initially) to a significant increase ($p < 0.05$) of relative mass loss (Figure A9). In addition, the detailed raw results of TGA tests may be found in [26]. It has been shown that increasing the torrefaction time and temperature increases weight loss. The use of irrigation allowed for a 1.5% lower weight loss in sandy soil, compared to *Paulownia* grown in clay soil. The highest weight loss was always obtained in the variant S(G+)(I+) regardless of the torrefaction temperature.

Table 3. Relative mass loss (Δm) of pruned Oxytree biomass during torrefaction.

Temperature, °C	Time, min	Relative Mass Loss, %							
		S(G−)(I−)	S(G+)(I−)	S(G−)(I+)	S(G+)(I+)	C(G+)(I−)	C(G−)(I−)	C(G+)(I+)	C(G−)(I+)
200	10	0.1 ± 0.2	0.2 ± 0.2	0.2 ± 0.2	0.4 ± 0.2	0.1 ± 0.2	0.1 ± 0.2	0.2 ± 0.2	0.1 ± 0.2
	20	0.2 ± 0.4	0.3 ± 0.0	0.4 ± 0.2	0.9 ± 0.2	0.4 ± 0.2	0.4 ± 0.2	0.6 ± 0.2	0.4 ± 0.2
	30	0.4 ± 0.5	0.7 ± 0.0	0.7 ± 0.3	1.3 ± 0.3	0.6 ± 0.2	0.8 ± 0.2	0.9 ± 0.2	0.8 ± 0.2
	40	0.8 ± 0.5	0.9 ± 0.2	1.0 ± 0.3	1.8 ± 0.2	0.8 ± 0.2	1.0 ± 0.0	1.0 ± 0.0	1.0 ± 0.0
	50	1.0 ± 0.7	1.0 ± 0.0	1.2 ± 0.5	2.1 ± 0.5	1.0 ± 0.0	1.2 ± 0.2	1.3 ± 0.2	1.2 ± 0.2
	60	1.2 ± 0.5	1.3 ± 0.0	1.4 ± 0.7	2.4 ± 0.5	1.2 ± 0.2	1.3 ± 0.0	1.6 ± 0.0	1.4 ± 0.2
220	10	0.0 ± 0.0	0.3 ± 0.3	0.2 ± 0.2	0.3 ± 0.2	0.4 ± 0.2	0.2 ± 0.2	0.4 ± 0.2	0.3 ± 0.0
	20	0.1 ± 0.2	0.8 ± 0.7	0.7 ± 0.3	1.2 ± 0.2	1.2 ± 0.2	0.8 ± 0.7	1.1 ± 0.2	1.2 ± 0.2
	30	0.6 ± 0.7	1.6 ± 0.8	1.3 ± 0.3	2.1 ± 0.2	1.9 ± 0.2	1.8 ± 0.7	2.0 ± 0.3	2.0 ± 0.3
	40	1.3 ± 0.9	2.2 ± 0.8	1.9 ± 0.5	2.8 ± 0.2	2.3 ± 0.0	2.6 ± 0.8	2.8 ± 0.2	3.0 ± 0.3
	50	2.0 ± 0.9	2.9 ± 0.8	2.3 ± 0.3	3.4 ± 0.2	2.9 ± 0.2	3.2 ± 0.8	3.2 ± 0.2	3.6 ± 0.4
	60	2.7 ± 1.2	3.3 ± 0.7	2.7 ± 0.3	4.0 ± 0.0	3.2 ± 0.2	3.7 ± 0.6	3.7 ± 0.3	4.1 ± 0.5
240	10	0.3 ± 0.0	0.8 ± 0.2	0.4 ± 0.0	0.8 ± 0.2	0.6 ± 0.4	0.9 ± 0.2	0.7 ± 0.0	0.4 ± 0.4
	20	1.4 ± 0.2	2.2 ± 0.2	1.8 ± 0.2	2.7 ± 0.2	1.9 ± 1.0	2.6 ± 0.5	2.2 ± 0.2	2.0 ± 0.9
	30	2.9 ± 0.2	4.0 ± 0.3	3.3 ± 0.2	4.7 ± 0.3	3.7 ± 1.5	4.3 ± 0.7	4.2 ± 0.2	3.9 ± 0.8
	40	4.2 ± 0.2	5.3 ± 0.3	4.8 ± 0.2	6.0 ± 0.3	4.9 ± 1.3	5.7 ± 0.7	5.3 ± 0.3	5.3 ± 0.3
	50	5.2 ± 0.2	6.2 ± 0.2	5.9 ± 0.2	7.0 ± 0.2	5.8 ± 1.1	6.3 ± 0.7	6.0 ± 0.3	6.4 ± 0.2
	60	5.9 ± 0.2	6.8 ± 0.2	6.6 ± 0.2	7.4 ± 0.2	6.3 ± 0.8	6.8 ± 0.8	6.4 ± 0.4	7.0 ± 0.3
260	10	0.3 ± 0.3	1.2 ± 0.2	1.2 ± 0.2	1.0 ± 0.7	1.1 ± 0.4	1.8 ± 0.2	1.1 ± 0.4	1.2 ± 0.2
	20	1.7 ± 0.9	4.2 ± 0.2	4.3 ± 0.3	3.9 ± 1.4	4.1 ± 0.4	6.0 ± 0.3	4.4 ± 0.4	5.1 ± 0.2
	30	4.1 ± 1.5	7.2 ± 0.2	7.4 ± 0.4	6.9 ± 1.3	6.7 ± 0.3	8.8 ± 0.2	6.8 ± 0.4	7.8 ± 0.2
	40	5.7 ± 1.5	8.7 ± 0.0	9.0 ± 0.3	8.3 ± 1.2	8.0 ± 0.0	10.3 ± 0.3	8.0 ± 0.3	9.1 ± 0.2
	50	6.7 ± 1.5	9.6 ± 0.2	9.9 ± 0.5	9.4 ± 1.0	8.7 ± 0.0	11.3 ± 0.3	8.7 ± 0.3	9.9 ± 0.4
	60	7.4 ± 1.6	10.0 ± 0.0	10.3 ± 0.3	10.1 ± 0.7	9.2 ± 0.2	12.2 ± 0.4	9.1 ± 0.2	10.4 ± 0.2
280	10	0.8 ± 0.2	1.3 ± 0.9	2.1 ± 0.4	2.2 ± 0.2	2.1 ± 0.2	2.4 ± 0.2	1.9 ± 0.8	2.1 ± 0.4
	20	4.7 ± 0.0	6.7 ± 2.0	8.2 ± 0.5	8.2 ± 0.5	7.7 ± 0.3	8.7 ± 0.0	7.6 ± 1.3	8.3 ± 0.3
	30	8.4 ± 0.4	10.0 ± 1.2	11.3 ± 0.3	11.3 ± 0.3	10.4 ± 0.2	11.3 ± 0.0	10.1 ± 1.3	11.2 ± 0.4
	40	10.0 ± 0.3	11.7 ± 0.9	12.9 ± 0.2	12.8 ± 0.5	12.0 ± 0.3	12.6 ± 0.2	11.7 ± 1.2	12.8 ± 0.2
	50	11.1 ± 0.4	12.7 ± 0.7	14.0 ± 0.3	13.8 ± 0.5	13.0 ± 0.3	13.6 ± 0.2	12.6 ± 1.1	13.7 ± 0.3
	60	11.6 ± 0.5	13.3 ± 0.7	14.7 ± 0.3	14.3 ± 0.3	13.7 ± 0.3	14.2 ± 0.2	13.3 ± 0.9	14.3 ± 0.3
300	10	1.3 ± 0.9	2.9 ± 0.2	3.4 ± 0.2	3.6 ± 0.7	3.1 ± 1.3	3.4 ± 0.7	3.3 ± 0.0	2.9 ± 1.6
	20	8.3 ± 1.2	11.3 ± 0.3	12.0 ± 0.3	12.1 ± 0.5	10.7 ± 1.5	11.4 ± 0.7	11.1 ± 0.2	11.2 ± 1.9
	30	12.2 ± 1.1	14.7 ± 0.3	15.7 ± 0.3	15.7 ± 0.3	14.0 ± 1.2	14.9 ± 0.5	14.4 ± 0.2	14.7 ± 1.7
	40	14.3 ± 1.2	16.4 ± 0.4	17.7 ± 0.3	17.4 ± 0.4	15.8 ± 1.8	16.6 ± 0.5	16.1 ± 0.2	16.6 ± 1.6
	50	15.7 ± 1.2	17.7 ± 0.3	19.0 ± 0.3	18.8 ± 0.4	16.9 ± 0.8	17.7 ± 0.3	17.3 ± 0.3	17.9 ± 1.3
	60	16.6 ± 1.2	18.3 ± 0.3	19.8 ± 0.5	19.6 ± 0.2	17.7 ± 0.7	18.4 ± 0.4	18.0 ± 0.3	18.8 ± 1.3

3.3. Oxytree Torrefaction Kinetics

The k values significantly ($p < 0.05$) increased with the torrefaction temperature. The lowest k value ($k = 1.25 \times 10^{-5}$ s^{-1}) was observed for 200 °C and in the C(G+)(I−) material, and the highest ($k = 1.82 \times 10^{-5}$ s^{-1}) for S(G+)(I+) (Table 4). In general, the lowest k was observed for the C(G+)(I+) material, i.e., 1.77×10^{-5} s^{-1}, 2.72×10^{-5} s^{-1}, and 3.46×10^{-5} s^{-1}, at 220 °C, 240 °C, and 260 °C, respectively. The lowest k value at 260 °C was associated with the S(G−)(I−) material, regardless of torrefaction time. Also, the S(G−)(I−) material in the temperature range of 260–300 °C had the lowest k values of 3.24×10^{-5} s^{-1}, 4.69×10^{-5} s^{-1}, and 6.42×10^{-5} s^{-1}, respectively.

The highest values of the constant rate k for the 220–260 °C range were recorded for the C(G−)(I−) material and were 2.3×10^{-5} s^{-1}, 3.44×10^{-5} s^{-1}, and 4.63×10^{-5} s^{-1} respectively. The highest k value at 280 °C was observed for S(G−)(I+), and at 300 °C for S(G+)(I+). Post-hoc tests showed that there were no statistically significant differences ($p < 0.05$) between the impact of a particular cultivation type and resulting k value. The statistical significance ($p < 0.05$) is marked with letters in Figure A4.

The S(G+)(I+) material had the highest observed activation energy value of E_a = 39,282 J·mol^{-1}, while the smallest (Ea = 33,369 J·mol^{-1}) was associated with the S(G+)(I−) material. The average value of E_a for all type of pruned Oxytree was 36,510 J·mol^{-1}. The coefficient of determination R^2 for each E_a value was >0.98, which indicates a high matching degree of the estimated parameters to the experimental data. Since the cultivation type did not have an impact on the k value, it can be assumed that cultivation type did not have an impact on the energy activation, and there are no statistically significant differences in the determined energy activation ($p < 0.05$).

The Arrhenius plots for each cultivation type are presented in Appendix B. Figures A15–A22 illustrate linear models for the activation energy estimation. The plots of mass loss at setpoint temperatures are presented in Figures A23–A28 as the comparison between experimental and model kinetics. No apparent differences (>5%) were observed between the experimental and calculated mass loss.

Table 4. Kinetic parameters of torrefaction of pruned biomass of Oxytree.

Cultivation Type Symbol	Process Temperature		Constant Rate of the Reaction	Arrhenius Plot Parameters		Activation Energy	Determination Coefficient
-	T, °C	T, K	k, s^{-1}	1/T, K^{-1}	ln(k), s^{-1}	Ea, J·mol^{-1}	R^2, -
S(G−)(I−)	200	473	1.30×10^{-5}	2.11×10^{-3}	−11.3	35,028	0.98
	220	493	1.95×10^{-5}	2.03×10^{-3}	−10.9		
	240	513	2.99×10^{-5}	1.95×10^{-3}	−10.4		
	260	533	3.24×10^{-5}	1.88×10^{-3}	−10.3		
	280	553	4.69×10^{-5}	1.81×10^{-3}	−9.97		
	300	573	6.64×10^{-5}	1.75×10^{-3}	−9.62		
S(G+)(I−)	200	473	1.59×10^{-5}	2.11×10^{-3}	−11.1	33,369	0.99
	220	493	2.21×10^{-5}	2.03×10^{-3}	−10.7		
	240	513	3.42×10^{-5}	1.95×10^{-3}	−10.3		
	260	533	4.29×10^{-5}	1.88×10^{-3}	−10.1		
	280	553	5.16×10^{-5}	1.81×10^{-3}	−9.87		
	300	573	7.21×10^{-5}	1.75×10^{-3}	−9.54		
S(G−)(I+)	200	473	1.44×10^{-5}	2.11×10^{-3}	−11.2	39,407	0.99
	220	493	1.97×10^{-5}	2.03×10^{-3}	−10.8		
	240	513	3.09×10^{-5}	1.95×10^{-3}	−10.4		
	260	533	4.56×10^{-5}	1.88×10^{-3}	−10.0		
	280	553	6.19×10^{-5}	1.81×10^{-3}	−9.69		
	300	573	7.70×10^{-5}	1.75×10^{-3}	−9.47		

Table 4. *Cont.*

Cultivation Type Symbol	Process Temperature		Constant Rate of the Reaction	Arrhenius Plot Parameters		Activation Energy	Determination Coefficient
-	T, °C	T, K	k, s^{-1}	1/T, K^{-1}	ln(k), s^{-1}	Ea, $J \cdot mol^{-1}$	R^2, -
S(G+)(I+)	200	473	1.82×10^{-5}	2.11×10^{-3}	−10.9	34,282	0.99
	220	493	2.13×10^{-5}	2.03×10^{-3}	−10.8		
	240	513	3.26×10^{-5}	1.95×10^{-3}	−10.3		
	260	533	4.28×10^{-5}	1.88×10^{-3}	−10.1		
	280	553	5.85×10^{-5}	1.81×10^{-3}	−9.75		
	300	573	7.96×10^{-5}	1.75×10^{-3}	−9.44		
C(G+)(I−)	200	473	1.26×10^{-5}	2.11×10^{-3}	−11.3	38,436	0.98
	220	493	1.81×10^{-5}	2.03×10^{-3}	−10.9		
	240	513	3.22×10^{-5}	1.95×10^{-3}	−10.3		
	260	533	4.15×10^{-5}	1.88×10^{-3}	−10.1		
	280	553	5.15×10^{-5}	1.81×10^{-3}	−9.87		
	300	573	6.86×10^{-5}	1.75×10^{-3}	−9.59		
C(G−)(I−)	200	473	1.39×10^{-5}	2.11×10^{-3}	−11.2	36,210	0.98
	220	493	2.31×10^{-5}	2.03×10^{-3}	−10.7		
	240	513	3.44×10^{-5}	1.95×10^{-3}	−10.3		
	260	533	4.63×10^{-5}	1.88×10^{-3}	−9.98		
	280	553	5.37×10^{-5}	1.81×10^{-3}	−9.83		
	300	573	7.36×10^{-5}	1.75×10^{-3}	−9.52		
C(G+)(I+)	200	473	1.34×10^{-5}	2.11×10^{-3}	−11.2	36,442	0.99
	220	493	1.78×10^{-5}	2.03×10^{-3}	−10.9		
	240	513	2.72×10^{-5}	1.95×10^{-3}	−10.5		
	260	533	3.46×10^{-5}	1.88×10^{-3}	−10.3		
	280	553	4.95×10^{-5}	1.81×10^{-3}	−9.91		
	300	573	6.66×10^{-5}	1.75×10^{-3}	−9.62		
C(G−)(I+)	200	473	1.29×10^{-5}	2.11×10^{-3}	−11.3	38,907	0.99
	220	493	2.17×10^{-5}	2.03×10^{-3}	−10.7		
	240	513	3.39×10^{-5}	1.95×10^{-3}	−10.3		
	260	533	4.57×10^{-5}	1.88×10^{-3}	−9.99		
	280	553	5.61×10^{-5}	1.81×10^{-3}	−9.79		
	300	573	7.57×10^{-5}	1.75×10^{-3}	−9.49		

4. Discussion

4.1. Oxytree Biomass Sample Characterization

Woody biomass is composed of three basic elements (C, 52%; H, 6%; O, 42%) [35]. This means that the tested Oxytree biomass has a lower content of C and O by ~8% and ~5%, respectively. The C and H content in the fuel positively influences the energy value of biomass. Oxygen contained in biomass favors burning processes. On the other hand, it reduces its energy value [36].

Pruned biomass of Oxytree was characterized by the organic matter content of ~90%, combustibles content of ~92%, ash ~8%, and the *HHV* 18.3 $MJ \cdot kg^{-1}$ (Table 1). As for woody biomass, the material tested had a high ash content and it is desired for energy crops to be low. For example, in the case of willow and poplar, ash accounts for 0.5–1.2% [37]. Previous research showed that *Paulownia tomentosa* has a 0.19–6% ash content depending on the plant part, with 6% in the leaves and 0.23% in the wood [38]. High ash content in the tested Oxytree material can be caused by a high leaf content of 66% compared to 34% being shoots.

The examined pruned biomass of Oxytree had about 4% more combustibles, compared to the *Paulownia tomentosa* wood from a research forest of Kangwon National University, Republic of Korea [38].

The mean *HHV* was 18,295 ± 31; slightly below values in the literature. The *HHV* depends on the *Paulownia* species (grown in Croatia) with an average of ~19 MJ·kg^{-1} [39]. For comparison, the *HHV* of willow and poplar (at a plantation located in Northeastern Poland) is about 19.5 MJ·kg^{-1} [40] and 18.5–19.1 MJ·kg^{-1}, respectively [41]; confirming that Oxytree energy concent is comparable to conventional woody biomass considered for energy crops.

The determined mean concentrations of elements of the studied Oxytree were similar to those reported for other *Paulownia* species. *Paulownia elongata* (at a plantation located in the West Black Sea region of Turkey) had 45.8% C, 6.3% H, and 0.4% N content [42]. The tested biomass was characterized by a higher N content of 2.3% (Table 2), which can be an effect of N mineral fertilization applied 40 kg·ha^{-1} (pre-planting) and doses of 20 kg·ha^{-1}, supplied monthly [26]. Vusić et al. [39] tested three *Paulownia* species which showed similar contents of C, H, N, S, and O at 49% C, 5.8% H, 0.2% N, 0.05% S, and 44% O, respectively. In comparison to these data, the Oxytree tested here had ~5% less C and ~12% O. Noticeable discrepancies in the results observed by other authors may be results of differing conditions of plant growth in different climates.

The application of the soil cultivation method that is appropriate to the soil type significantly influences ($p < 0.05$) the content of organic matter in both sandy and clay soils (Figure A10). The content of organic substances was the lowest in variants without the support of soil cultivation and was lower by ~1% compared to other variants, and very similar in both soil types at ~89.5% d.m. The highest content of organic matter content was noted in clay soil without geotextile (C(G-)(I+)); however, the use of irrigation had a significant difference ($p < 0.05$) compared with other variants (Figure A10).

The lowest ash content was obtained by cultivating *Paulownia* in clay soil (7.87% d.m.) than in sandy soil (8.26% d.m.). However, the highest ash content was obtained for the variant of clay soil without geotextile and with irrigation (C(G-)(I+))—statistically different ($p < 0.05$) from the other variants (Figure A11). Similar results were obtained in the case of combustible content. The best variant was cultivation in clay soil with a geotextile and no irrigation (C(G+)(I−)), i.e., 93.25% combustible content (Figure A12). This result could be explained by the high compactness of such (clayey) soils, where the irrigation procedure improves the oxygenation of the roots, allowing better plant growth [26].

Although the best conditions for the production of biomass are cultivated in clay soil, it was noted that the highest values of *HHV* and *LHV* were obtained in the sandy soil variant with geotextile and no irrigation (S(G+)(I−)). However, no statistically significant ($p < 0.05$) difference was found between the variants (Figures A13 and A14). The obtained biomass properties are much higher than in the case of *Paulownia* biomass cultivated in Turkey, where the content of moisture and organic substances was lower (by ~3.5%), with much lower ash content of 1.05% d.m. [42], at 5–6% moisture and 8–9% d.m. ash obtained in this study [26].

4.2. Mass Loss During Torrefaction of Oxytree

Due to the novelty of the examined materials, there are no existing data to directly compare with (i.e., torrefaction of *Paulownia*). Nevertheless, the *Paulownia clon* in Vitro 112 prunings are an example of woody biomass, and they can be compared to other published data. The increase of relative mass loss due to the increase of torrefaction temperature and time is obvious and expected based on the literature [43,44]. For the examined Oxytree material, the visually noticeable mass loss started after ~10 min. Examined materials after torrefaction at 200–220 °C for 60 min had mass losses in the range 1.2–4.1% (Table 3). The mass losses were between 5.9% and 7.4% for temperatures 240–260 °C. Tested materials at 280–300 °C had mass losses of 11.6–19.8%. The average relative mass loss for tested biomass at temperatures of 260, 280, and 300 °C, and a time of 30 min was 7.0%, 10.5%, and 14.5%, respectively. For the same temperatures and time of 60 min, these values were 9.8%, 13.7%, and 18.4%, respectively (Table 3).

For comparison, torrefaction of Douglas fir sawdust for 30 min and temperatures of 250, 275, and 300 °C caused a relative mass loss of approximately 9%, 19%, and 35%, respectively. For the same temperatures and time in the 60 min process, Douglas fir has losses of 11%, 25%, 48% [45]. Becker

and Scherer [46] presented mass losses for pine and beech at temperatures of 240, 270, and 300 °C for 25 min. For pine, these values are 3%, 7%, and 14%, and for beech, 3%, 13%, and 20%, respectively. The presented data show that the tested biomass of *Paulownia clon* in Vitro 112 is characterized by a relatively low value of Δm for a time of 60 min. In the 30 min case, the values of Δm are close to the values from the work of Becker and Scherer [46].

In another study, the relative mass losses during the torrefaction of spruce sawdust at temperatures of 230, 250, 270, and 300 °C, were 14%, 23%, 32%, and 53%, respectively [47]. Similarly, high mass losses of 10%, 21%, 32%, and 44% were also noted for beechwood in 30 min torrefaction under temperatures of 240, 260, 280, and 300 °C, respectively [48]. Observed higher Δm by Wang et al. [47] and Gucho et al. [48] probably resulted from the methodology of the conducted research. In [47] and [48], the 'time' refers to the time of active heating (i.e., it does not include cooling time). In this study, measurements of mass losses were stopped after 60 min of active heating, and mass loss during cooling was not measured. It is important to mention that the torrefaction process is still ongoing during cooling until the temperature falls below ~200 °C. This is because the temperature inside of torrefied materials is still higher than ambient temperature [49] and, therefore, the process does not end immediately. Bridgeman et al. [50] included the cooling period in the total time of the torrefaction process.

The noticeable loss of mass in the material started after about 10 min. This means that the tested materials needed ~10 min to warm up in their entire volume. This is a long period if the weight of the sample (3 g) is taken into account. For determination of the influence of the sample mass on the heat transport within the biomass, additional tests of the *Paulownia* heat conductance are warranted. It would be necessary for scaling up the Oxytree torrefaction process.

The statistical tests (K.W.) showed that cultivation type had no effect on the Δm ($p < 0.05$) (Figure A7). The temperature had a significant effect on the Δm value ($p < 0.05$); the post-hoc test showed that the differences occur for each temperature interval (Figure A8). Time also had a significant impact ($p < 0.05$) on the Δm value; the post-hoc test showed that significant differences did not occur between 30 and 50 min and between 40 and 60 min (Figure A9).

4.3. Oxytree Torrefaction Kinetics

The statistical tests (K.W.) showed that the cultivation method and soil type had no effect on the k value ($p < 0.05$) (Figure A3). The temperature had a significant effect on the k value ($p < 0.05$); the post-hoc test showed that the differences did not occur for any of the temperature intervals. There were no significant differences between 200 and 220 °C, 220 and 240 °C, 240 and 260 °C, 260 and 280 °C, and 280 and 300 °C. This also means that a statistically significant increase in k values occurred every 40 °C (Figure A4).

The K.W. tests indicated that there was no statistically significant ($p < 0.05$) effect of the cultivation method and soil class on the value of relative mass loss (Figure A7) and the constant rate of the reaction k for *Paulownia clon* in Vitro 112 (Figure A3). It can, therefore, be assumed that the cultivation method and soil class does not significantly affect the torrefaction activation energy of pruned biomass. This is a very important observation, from a practical point of view, which shows that similar technological parameters of torrefaction could be applied for different Oxytree pruned biomasses. This aspect requires further research in the pilot- and full-scale experiments.

The average k values for the examined temperature range of 200–300 °C, with intervals at 20 °C were 1.43×10^{-5} s^{-1}, 2.04×10^{-5} s^{-1}, 3.19×10^{-5} s^{-1}, 4.15×10^{-5} s^{-1}, 5.37×10^{-5} s^{-1}, and 7.25×10^{-5} s^{-1}, respectively. A general trend of the increase in the k value was observed along with the increase of the process temperature (Table 4). The same dependence is also reported by Dhanavath et al. [51] for the torrefaction of biomass in general. However, the increase in k for Oxytree as a function of temperature was not constant. The largest ($p < 0.05$) differences in k values were observed between 280 °C and 300 °C, of 1.88×10^{-5} s^{-1}, and the smallest between 200 °C and 220 °C, of 6.16×10^{-6} s^{-1}, but both differences were not statistically significant ($p < 0.05$) (Figure A4).

The value of k for Oxytree is challenging to compare with the literature because it depends to a large extent on the kinetic model used to determine it. For example, depending on the test method, the k value for 300 °C for oak wood was in the range from 31×10^{-5} s^{-1} to 121×10^{-5} s^{-1} [52]. Similarly, the activation energy is estimated for the whole torrefaction process [53,54]. The average activation energy (E_a) for the tested pruned biomass of *Paulownia clon* in Vitro was 36.5 kJ·mol^{-1}. Díaz et al. [55] determined the values of activation energy for the individual constituents of *Paulownia* biomass. The E_a values of cellulose, lignin, and hemicellulose were 10.4 kJ·mol^{-1}, 17.2 kJ·mol^{-1}, and 23.5 kJ·mol^{-1}, respectively. Nevertheless, these values were determined for a wider (and higher) temperature range of 200–700 °C [55,56]. The obtained E_a value for Oxytree is low in comparison with other types of woody biomass. For example, E_a values for beech and spruce were 150 kJ·mol^{-1} and 155 kJ·mol^{-1} [48], 46–152 kJ·mol^{-1} for willow [57], 131 kJ·mol^{-1} for pine, and 128 kJ·mol^{-1} for fir [58]. Bach et al. [59] tested biomass fuels (Norwegian spruce and birch) in isothermal conditions at 230–280 °C (interval 10 °C) for 4 h, and used a two-step kinetic model. At first step, E_a was 48.1 kJ·mol^{-1} and 55.1 kJ·mol^{-1}, for spruce and birch, respectively, whereas, at the second step, E_a was much higher, i.e., 99.2 kJ·mol^{-1} and 94.4 kJ·mol^{-1}, respectively [59]. The *Paulownia* wood was co-pyrolysed with plastic waste by Chen et al. [60]. The use of the Kissinger–Akahira–Sunose (KAS) and Flynn–Wall–Ozawa (FWO) methods resulted in E_a ranging from 167 to 189 kJ·mol^{-1}. However, these E_a values were determined by different methods and models. Thus, there is a need for a more unified approach to methods and reporting.

The same methodology of kinetics parameters determination as reported in this manuscript was used previously by Pulka et al. [61] and Syguła et al. [62] for sewage sludge and spent mushroom compost (MSC), respectively. For these materials, E_a was 12 kJ·mol^{-1} and 22.2 kJ·mol^{-1}, and k values ranged from 4.02×10^{-5} to 6.71×10^{-5} s^{-1} and 1.7×10^{-5} to 6.3×10^{-5} s^{-1} for sludge and MSC, respectively.

The kinetic model used in this research is a generic model. This model only allows estimating the yield at a specific temperature and time of the process. Additional studies on the kinetics of the process with a more complex model (e.g., incorporating improved mass and energy balance, gases and tars formed in the process) is warranted. Such information will allow scaling up and designing the technological line for the *Paulownia clon* in Vitro 112 torrefaction.

5. Conclusions

Research on the torrefaction kinetics of pruned biomass of Oxytree allowed us to conclude that:

- the cultivation method and soil type did not have an effect on the relative mass loss, k value, and energy activation ($p < 0.05$);
- the relative mass loss increased with the torrefaction temperature increase (as it is commonly reported for other types of biowaste torrefaction). The smallest relative mass loss was recorded at 200 °C, 10 min and the highest at 300 °C, 60 min, respectively 0.1% and 19.6% ($p < 0.05$);
- the constant reaction rate (k value) significantly increased with the torrefaction temperature increase. The smallest k value was 1.26×10^{-5} s^{-1}, while the largest was 7.96×10^{5} s^{-1} at 200 °C and 300 °C, respectively;
- the average energy activation of the torrefaction in 200–300 °C was 36.5 kJ·mol^{-1}.

The cultivation method (soil type, irrigation, geotextile use) makes no difference for the torrefaction process (lack of statistical differences for E_a and k value at $p < 0.05$). Thus, Oxytree growers can focus on cultivation practices resulting in the most significant biomass yield. The results of this research, especially the kinetics parameters, make it possible to calculate the mass yield of a reliable biochar product for any process temperature and time, which is very useful from a practical point of view—the best biomass properties on sandy soil were with geotextile and without irrigation, on clay soil without geotextile and with irrigation.

Results of this work are complementary with previous articles [23,26] and, taken together, provide essential data about the torrefaction process of pruned Oxytree biomass. The next research questions are with respect to the gas products emitted from the torrefaction process and improved economics and environmental impact analyses.

Author Contributions: Conceptualization: K.Ś. and A.B.; methodology: K.Ś. and A.B.; software: K.Ś.; validation: K.S., S.S.-D., A.B., and J.L.; formal analysis: K.Ś.; investigation: K.Ś., S.S.-D., M.L., and P.B.; resources: K.Ś., S.S.-D., M.L., P.B., A.B., and J.A.K.; data curation: A.B.; writing—original draft preparation: K.Ś.; writing—review and editing: K.Ś., S.S.-D., A.B., and J.A.K.; visualization: K.Ś.; supervision: A.B., J.A.K., and S.S.-D.; project administration: A.B.; funding acquisition: A.B. and J.A.K.

Funding: Authors would like to thank the Fulbright Foundation for funding the project titled "Research on Pollutants Emission from Carbonized Refuse Derived Fuel into the Environment," completed at Iowa State University. In addition, this project was partially supported by the Iowa Agriculture and Home Economics Experiment Station, Ames, Iowa, project no. IOW05556 (Future Challenges in Animal Production Systems: Seeking Solutions through Focused Facilitation) sponsored by Hatch Act and State of Iowa funds.

Conflicts of Interest: The authors declare no conflict of interest.

Appendix A

Appendix A.1. Statistical Evaluation of the k Value

Appendix A.1.1. Results of Distribution Normality Evaluation

The study of the normality of the distribution of k values was performed graphically using a normality plot (Figure A1) and Shapiro–Wilk (S.W.) and Kolmogorov–Smirnov (K.S.) statistical tests, along with the Lilliefors correction for $\alpha = 0.05$ (Figure A2). The following hypotheses were assumed for both tests:

Hypothesis 0 (H0). *The distribution of k values is a normal distribution.*

Hypothesis 1 (H1). *The k value does not have a normal distribution.*

Appendix A.1.2. Analysis of Variance

Since the distribution of k values was not a normal distribution, the analysis of variance was carried out with the non-parametric Kruskal–Wallis test (K.W.). Two non-parametric tests (K.W.) were carried out at the level of $\alpha = 0.05$:

- k relative to the variable grouping the cultivation type;
- k relative to the variable that groups the process temperature.

The tests assumed hypotheses 0 showing no influence of the grouping variable on the value of k and hypothesis 1 showing the influence of the grouping variable on the k value. Multiple comparisons (post-hoc test) were performed to determine which groups had statistically significant differences. The lack of significant differences was marked with the same letters on the box plots.

Appendix A.1.3. Results and Interpretation

The k values did not have a normal distribution because the points did not lie in one line, as shown on the normality plot (Figure A1). Results of the S.W. test show that that $p = 0.00002$ and $< \alpha = 0.05$ so hypothesis 0 on the normality of the distribution should be rejected. The K.S. test (Figure A2) shows that the distribution was normal, because $p = 0.15 > \alpha = 0.05$. On the other hand, the Lilliefors amendment (Figure A2), which takes into account the lack of knowledge of the mean value and standard deviation of the population, shows that hypothesis 0 should be rejected because $p = 0.01$ and $<\alpha = 0.05$.

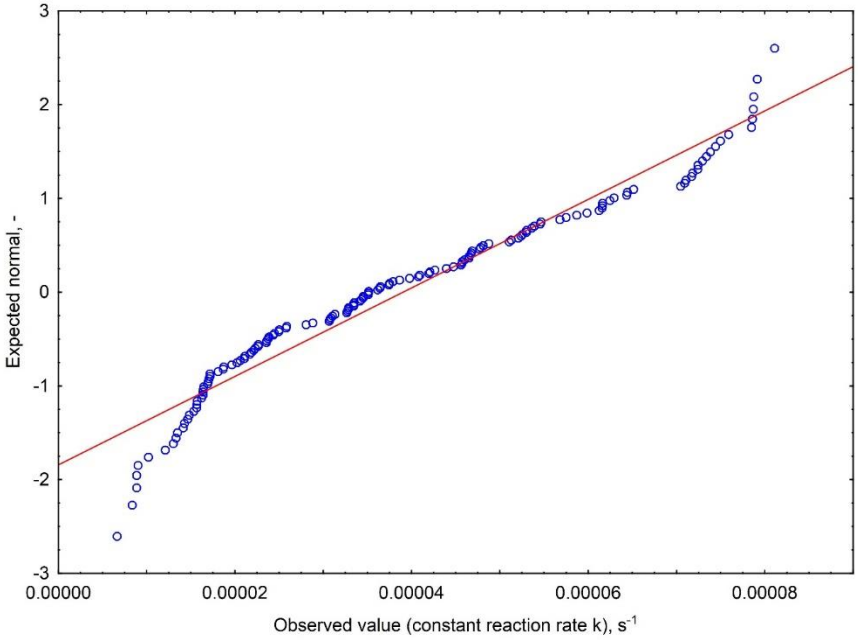

Figure A1. Normality plot of constant reaction rate *k*.

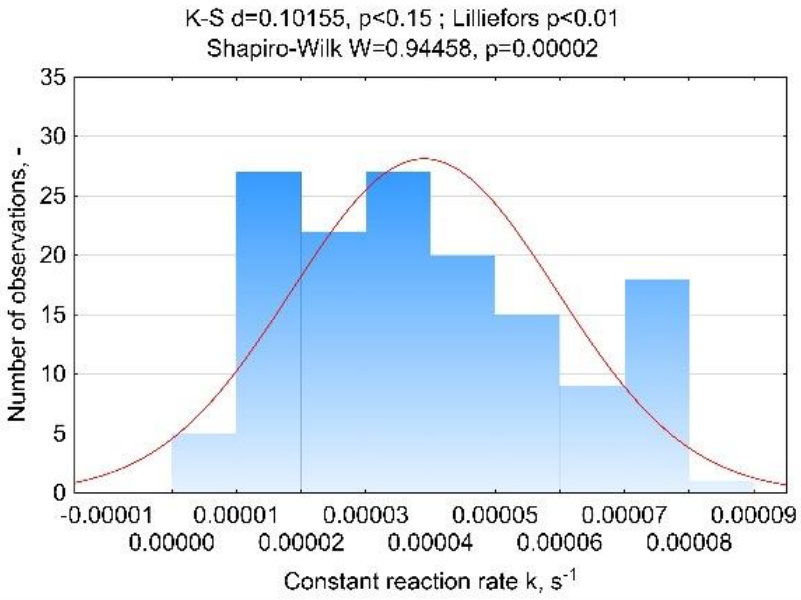

Figure A2. Histogram and the values of K.S., K.S. with the Lilliefors amendment, and S.W. tests for *k*.

The test value (K.W.) for *k* relative to the variable grouping for the cultivation type was $H = 2.689$ and $p = 0.912$. Since $p = 0.912 > \alpha = 0.05$ should be considered a valid hypothesis 0, this means that the cultivation type *Paulownia clon* in Vitro 112 did not have a statistically significant impact on the *k* value. The lack of statistical differences obtained from the K.W. test is illustrated by the same letters in Figure A3. Figure A3 presents the average *k* values for individual cultivation types with the standard deviation and the standard error. The highest average value of *k* was determined for the S(G+)(I−) and S(G−)(I+) materials, and the lowest *k* for S(G−)(I−) (not significantly different).

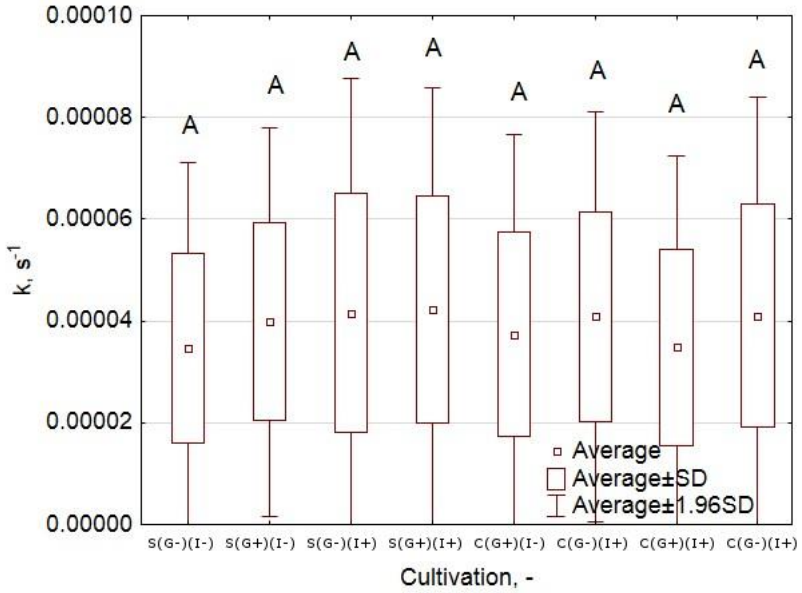

Figure A3. Box plot of k in relation to Oxytree cultivation type. Letters present a lack of statistically significant differences ($p < 0.05$) between the studied groups.

The K.W. test value for k in relation to the variable grouping for the temperature was $H = 133.386$ and $p = 0.000$. Since $p = 0.000 < \alpha = 0.05$, hypothesis 1 stands. This means that the process temperature had a statistically significant impact on the k value. The statistical differences obtained from the K.W. test are illustrated by different letters in Figure A4. The graph presents the mean values of k with respect to temperature (Figure A4). The lowest average k value was recorded at 200 °C, i.e., $<2 \times 10^{-5}$ s^{-1}, and the highest at 300 °C, i.e., $>7 \times 10^{-5}$ s^{-1}. The post-hoc test showed that statistically significant differences occurred approximately every 40 °C. The lack of significant differences ($p < 0.05$) is marked with the same letters.

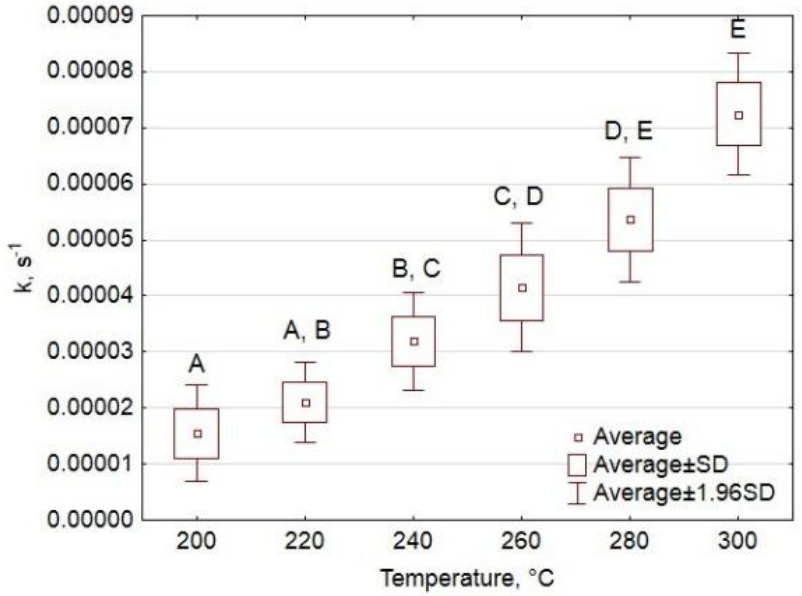

Figure A4. Box plot of k in relation to torrefaction temperature. Letters present statistical significance ($p < 0.05$) of differences between the studied groups.

Appendix A.2. Relative Mass Loss Δm, %

Appendix A.2.1. Results of the Distribution Normality Evaluation

The study of Δ*m* distribution was performed graphically using a normality plot (Figure A5) and statistical tests of S.W. and K.S. along with the Lilliefors correction for $\alpha = 0.05$ (Figure A6). The following hypotheses were assumed for both tests:

Hypothesis 0 (H0). *The distribution of Δm values was a normal distribution.*

Hypothesis 1 (H1). *The Δm value did not have a normal distribution.*

Since the distribution of Δ*m* did not have a normal distribution, the analysis of variance was carried out with the non-parametric K.W. test.

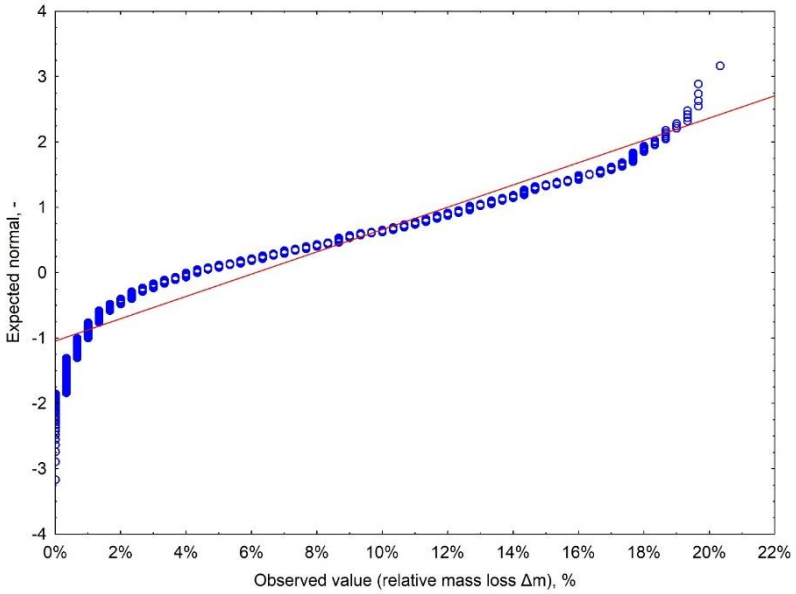

Figure A5. Quantile-quantile plot for Δ*m* during torrefaction of Oxytree.

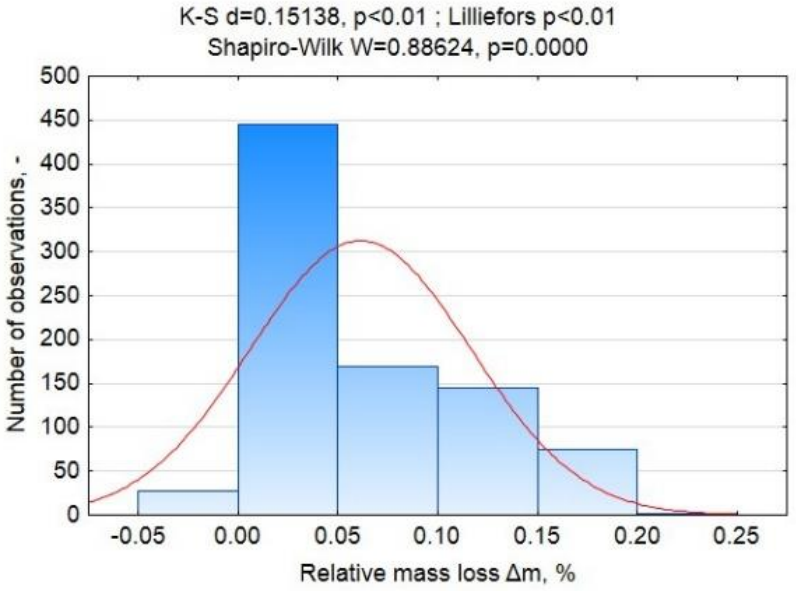

Figure A6. Histogram and the values of K.S., K.S. with the Lilliefors amendment, and S.W. tests for Δ*m* during torrefaction of Oxytree.

Appendix A.2.2. Analysis of Variance

Three non-parametric tests (K.W.) were carried out at the level of $\alpha = 0.05$:

- Δm relative to the variable grouping the cultivation type;
- Δm relative to the variable grouping process temperatures;
- Δm relative to the variable that groups the process time.

Appendix A.2.3. Results and Interpretation

The Δm values did not have a normal distribution because the points did not lie in one line (Figure A5). The S.W. test showed that $p = 0.0000 < \alpha = 0.05$, so hypothesis 0 on the normality of the distribution was rejected. The K.S. test showed that the distribution was not normal because $p = 0.01 > \alpha = 0.05$. Lilliefors' test also confirmed that hypothesis 0 should be rejected because $p = 0.01 < \alpha = 0.05$ (Figure A6).

The K.W. test value for Δm relative to the grouping variable of the cultivation type was $H = 12.299$ and $p = 0.0912$. Since $p = 0.0912 > \alpha = 0.05$, the null hypothesis should be considered as the correct one. This means that the cultivation type had no statistically significant effect on Δm during torrefaction. Figure A7 presents the average Δm values for particular cultivation types along with the standard deviation. The highest mean Δm was measured for S(G-)(I+), S(G+)(I+) and C(G-)(I-), and the smallest for S(G-)(I-). As the K.W. test showed, these differences were not statistically significant ($p < 0.05$).

The K.W. test value for Δm relative to the variable grouping the process temperature was $H = 543.953$ and $p = 0.000$. Because $p = 0.000 < \alpha = 0.05$, hypothesis 1 should be considered the correct one. It means that the process temperature affected the Δm. The post-hoc test showed that statistically significant differences existed between all torrefaction temperature setpoints used in the study ($p < 0.05$). The average Δm values for individual temperatures are shown in Figure A8. The lowest Δm occurred at 200 °C (0%–2%), and the highest at 300 °C (8%–19%), depending on the torrefaction time.

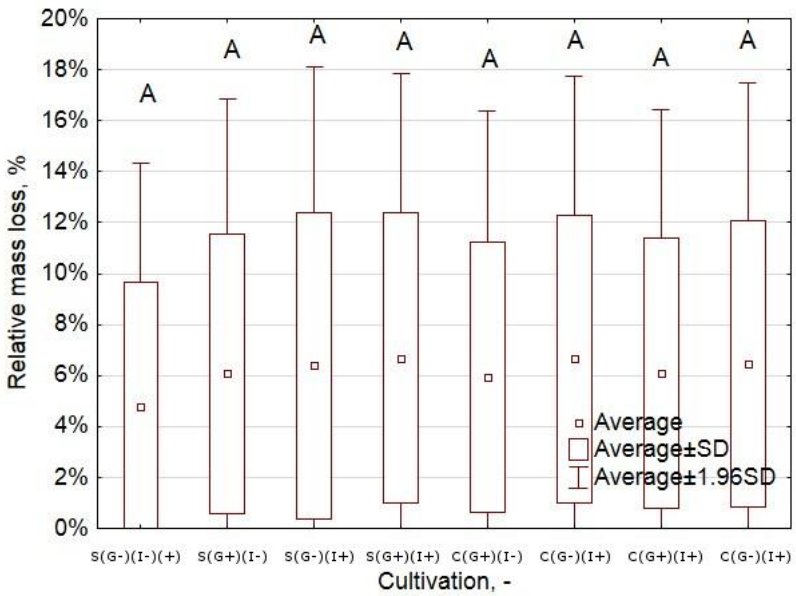

Figure A7. Box plot of Δm during torrefaction in relation to Oxytree cultivation types. Identical letters (A) represent a lack of statistically significant differences ($p < 0.05$) between the studied groups.

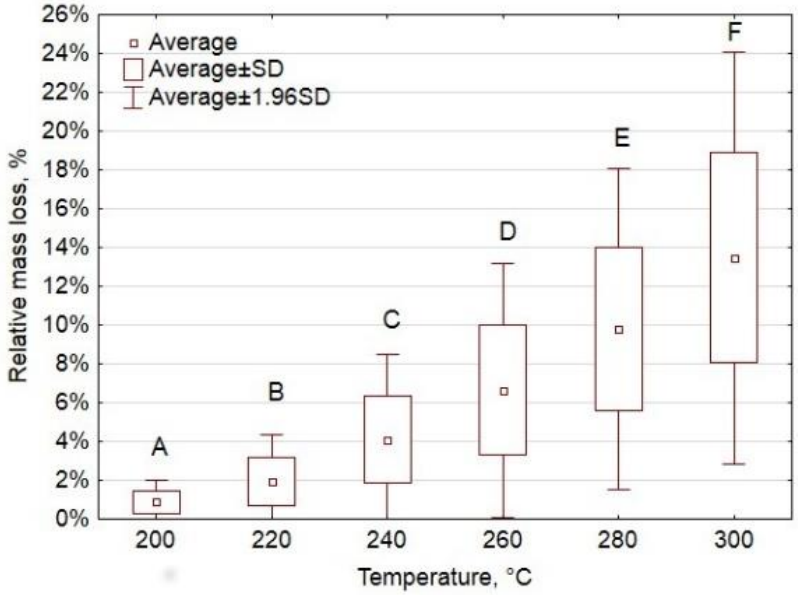

Figure A8. Box plot of Δm during torrefaction in relation to process temperature. Letters present a statistically significance ($p < 0.05$) of differences between the studied groups.

The K.W. test value for Δm relative to the variable grouping the process time was $H = 258.684$ and $p = 0.000$. Since $p = 0.000 < \alpha = 0.05$, hypothesis 1 should be considered as the correct one. This means that the torrefaction time affected Δm. The post-hoc test showed that statistically significant differences did not exist between any of the time groups. Groups with no statistically significant differences ($p < 0.05$) were marked with the same letter in Figure A9. Time had a significant effect on Δm for up to 30 min of torrefaction. The average Δm values did not differ significantly from 30 to 50 min. The value of Δm at 30 min was significantly different from the value of Δm at 60 min, while the values in 40 and 50 min did not differ significantly from the values obtained at 60 min.

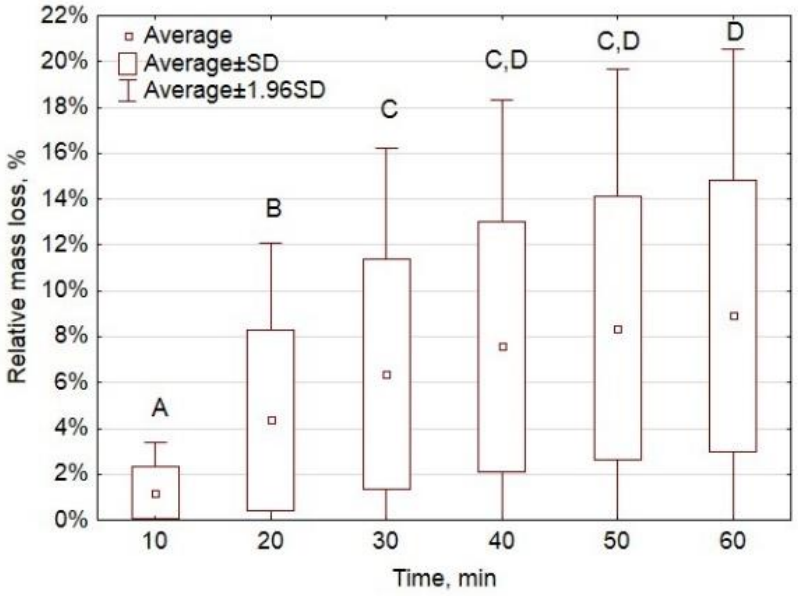

Figure A9. Box plot of Δm during torrefaction in relation to the process time. Letters present statistical significance ($p < 0.05$) of differences between the studied groups.

Appendix A.3. Oxytree Biomass Characterization

Appendix A.3.1. Results of the Distribution Normality Evaluation

Due to the fact that only three replicates were completed to determine each parameter, there was no reason to check the distribution of normality (too small of a sample group). Thus, the lack of normality distributions was assumed, similarly as in previous parameters (presented above).

Appendix A.3.2. Analysis of Variance

Three non-parametric K.W. tests were carried out at the level of $\alpha = 0.05$;

- Organic matter content relative to the variable grouping of the cultivation type;
- Ash relative to the variable grouping of the cultivation type;
- Combustible content relative to the variable grouping of the cultivation type;
- High heating value relative to the variable grouping of the cultivation type; and
- Low heating value relative to the variable grouping of the cultivation type.

In the tests, it was assumed that:

- Hypotheses 0 showed that the grouping variable does not affect the Δm; and
- Hypothesis 1 tests the influence of the grouping variable on the Δm value.

In order to determine which variable groupings had statistically significant differences, multiple comparisons (post-hoc tests) were performed. The lack of significant differences was marked with the same letters on the box plot.

Appendix A.3.3. Results and Interpretation

The post-hoc K.W. tests were carried out in relation to basic biomass parameters obtained on different cultivation methods. The tests showed differences between the effects of the cultivation method on organic matter content (Figure A10), combustible content (Figure A11), and ash content (Figure A12). No statistical differences were observed with respect to *LHV* and *HHV* (Figures A13 and A14).

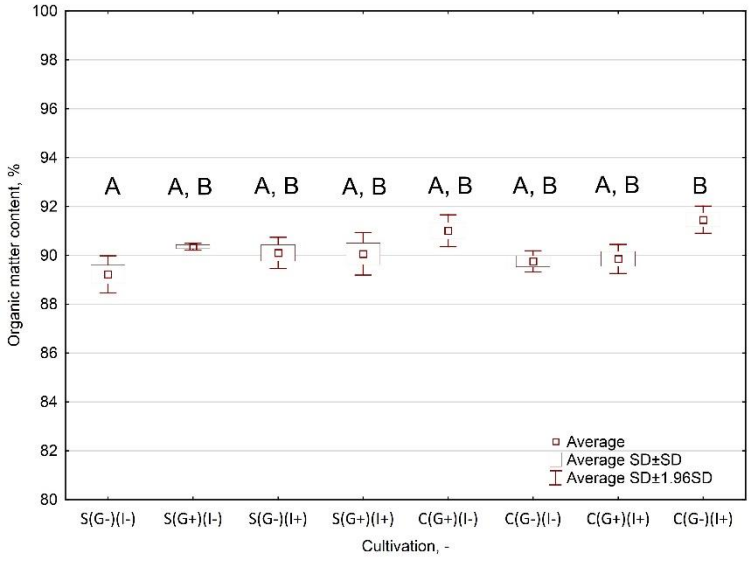

Figure A10. Box plot of organic matter content in raw Oxytree as a function of the cultivation method. Letters present statistical significance ($p < 0.05$) of differences between the studied groups.

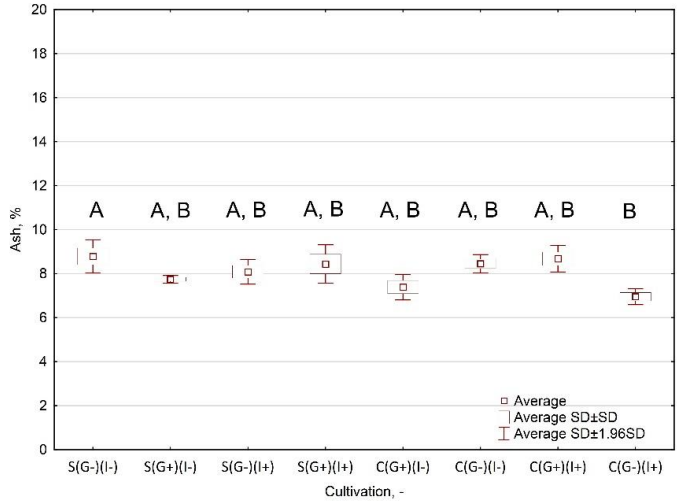

Figure A11. Box plot of ash content in raw Oxytree. Letters present statistical significance ($p < 0.05$) of differences between the studied groups.

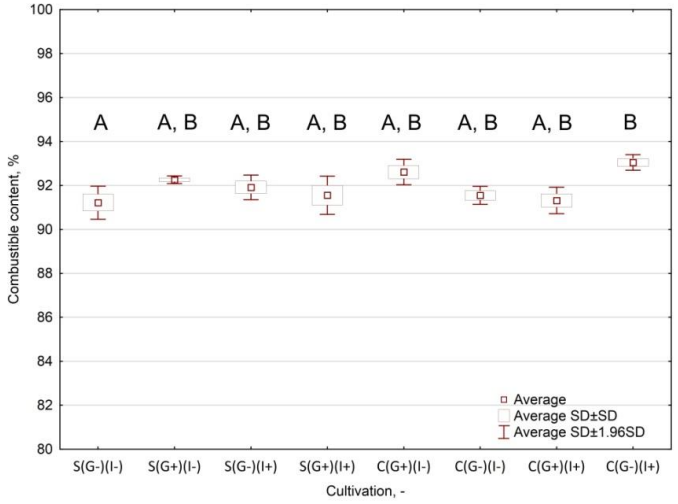

Figure A12. Box plot of combustible content in raw material depending on the cultivation method. Letters present the statistical significance of differences ($p < 0.05$) between the studied groups.

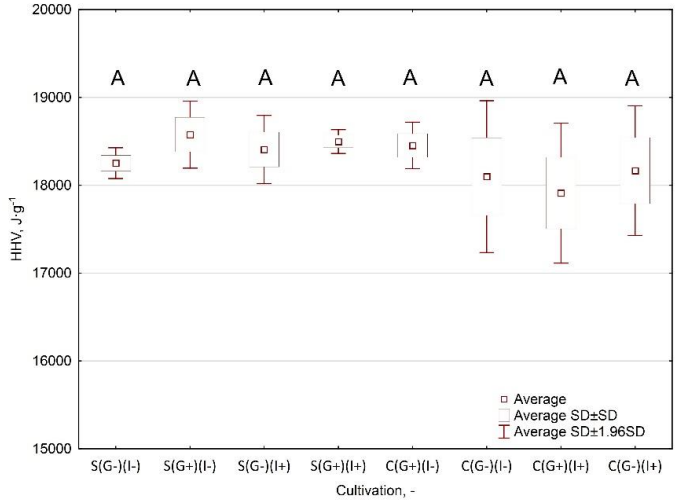

Figure A13. Box plot of *HHV* in raw material depending on the cultivation method. Letters present a lack of statistically significant differences ($p < 0.05$) between the studied groups.

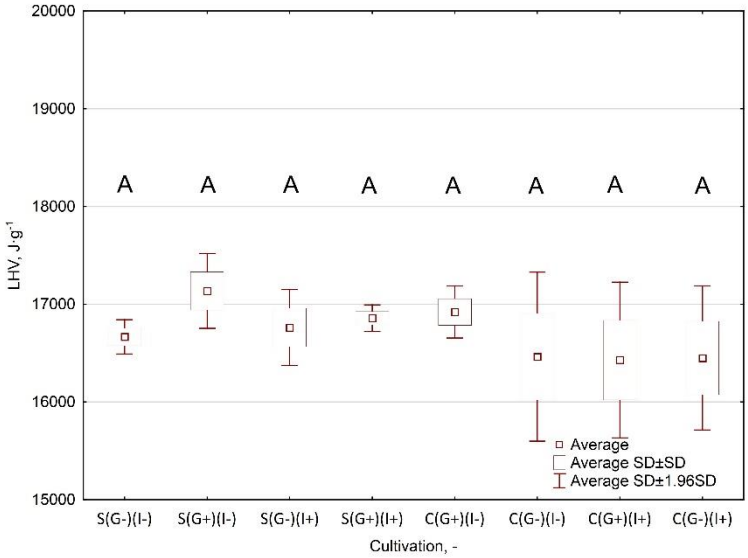

Figure A14. Box plot of *LHV* in raw Oxytree depending on the cultivation method. Letters present a lack of statistically significant differences ($p < 0.05$) between the studied groups.

Appendix B

The Arrhenius plots (Figures A15–A22) for each tested material are presented. The figures illustrate the linear model with a determination coefficient (R^2). The activation energy was determined based on the slope coefficient.

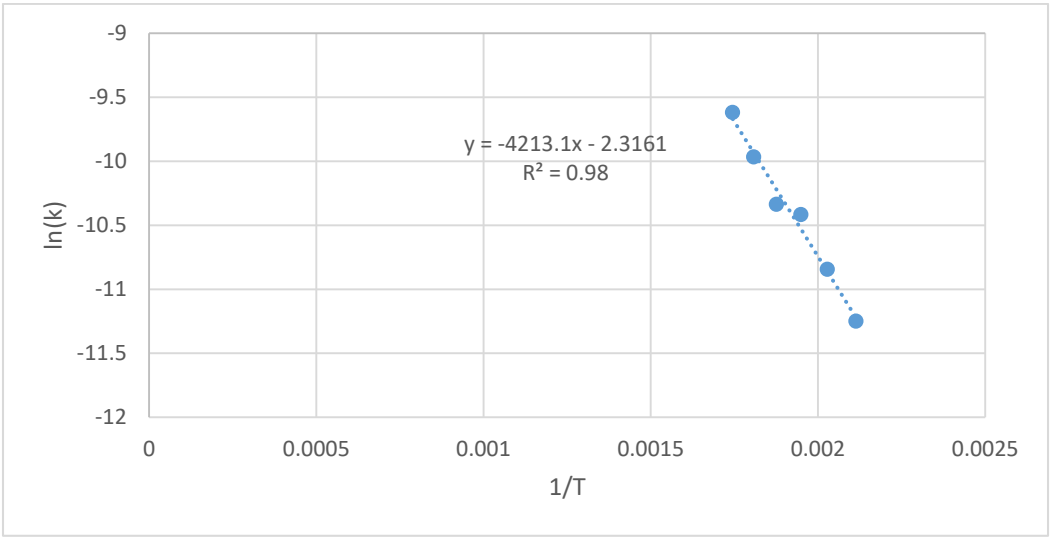

Figure A15. Arrhenius plot for S(G−)(I−).

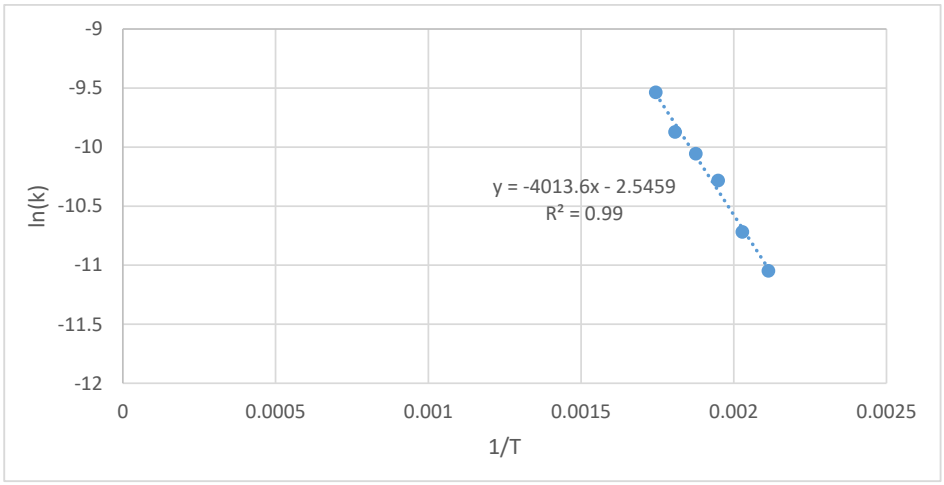

Figure A16. Arrhenius plot for S(G +)(I−).

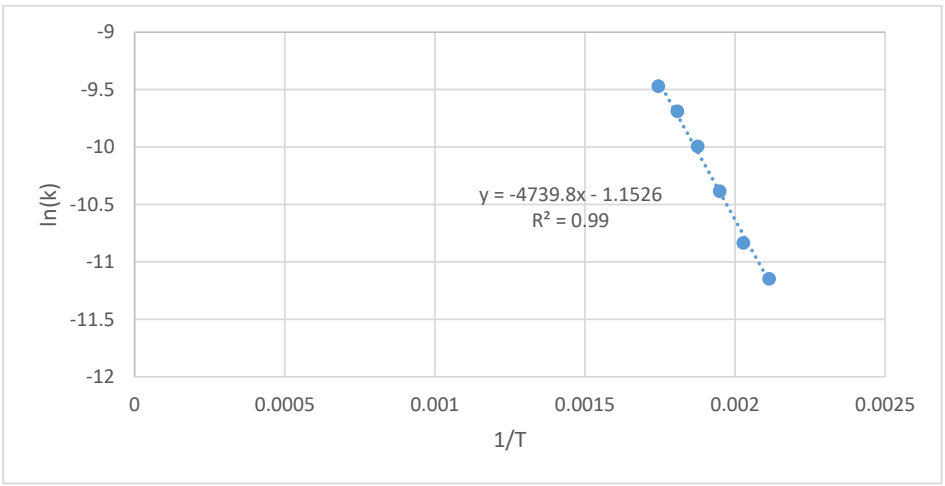

Figure A17. Arrhenius plot for S(G−)(I +).

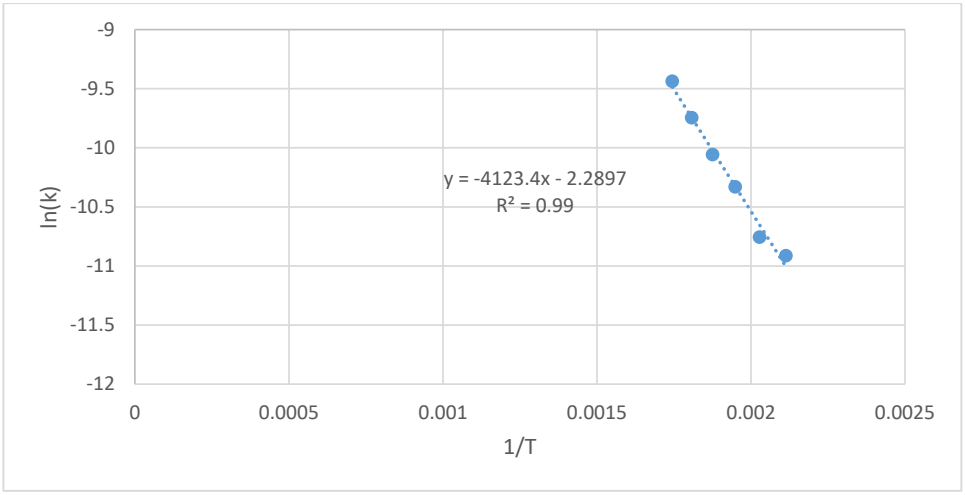

Figure A18. Arrhenius plot for S(G +)(I +).

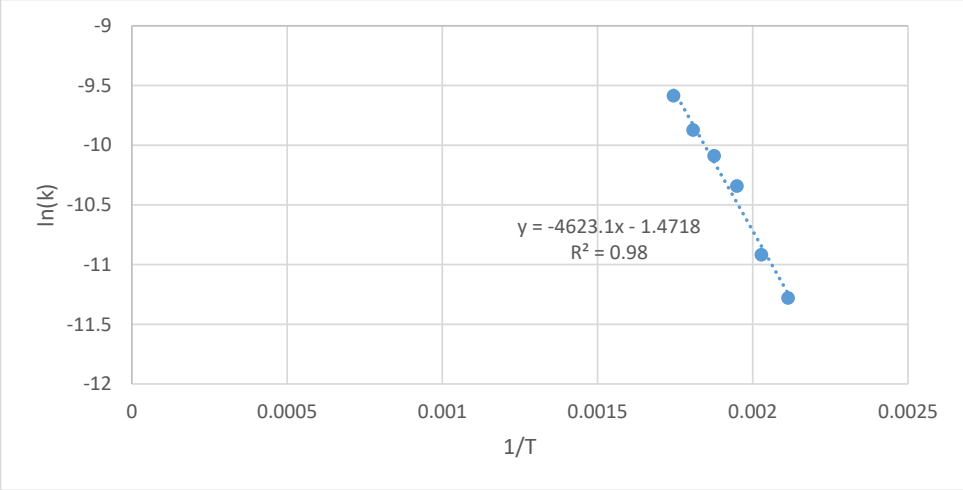

Figure A19. Arrhenius plot for C(G +)(I−).

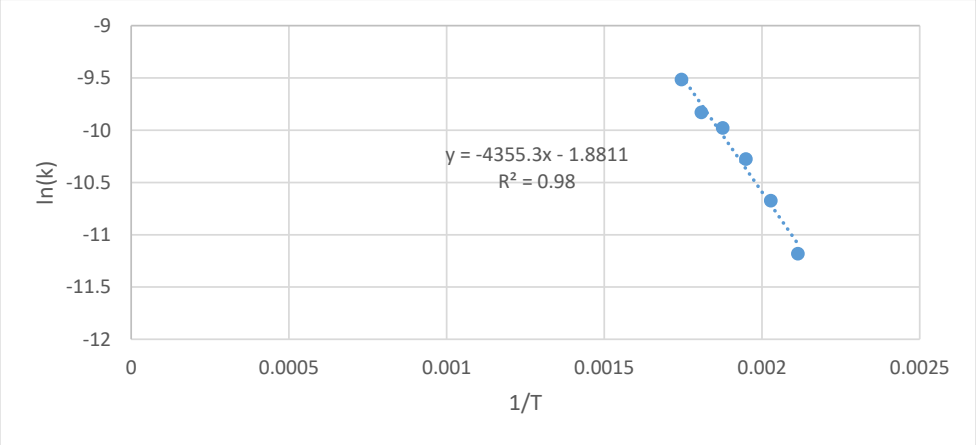

Figure A20. Arrhenius plot for C(G−)(I−).

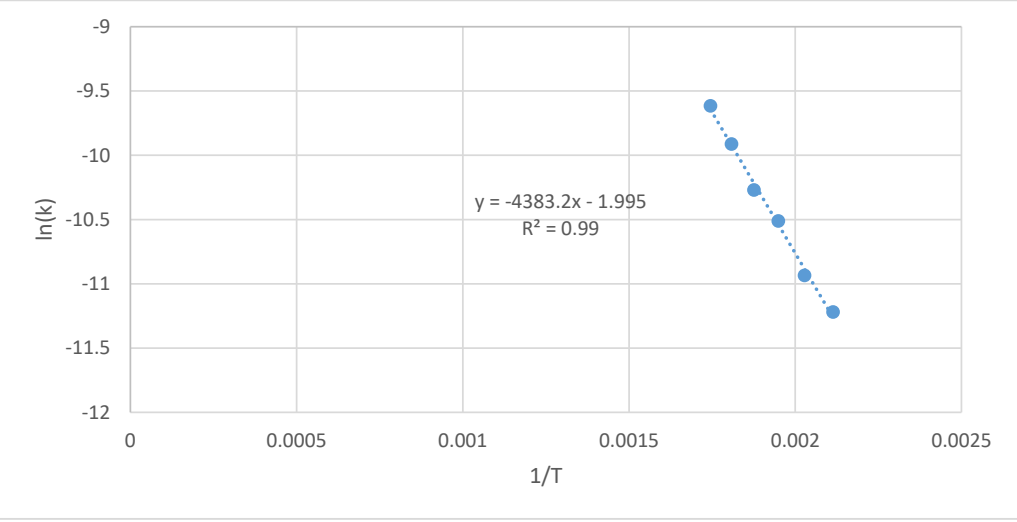

Figure A21. Arrhenius plot for C(G +)(I−).

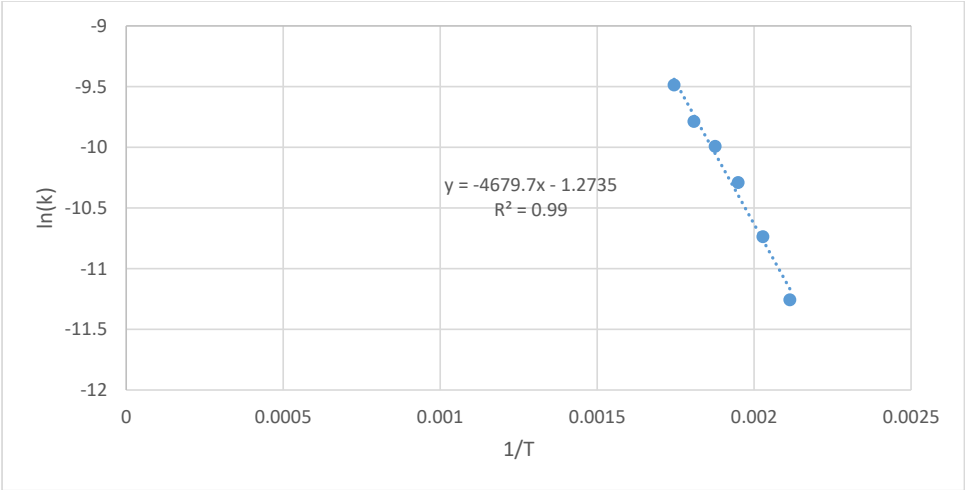

Figure A22. Arrhenius plot for C(G−)(I +).

Figures A23–A28 present differences between experimental (exp) and calculated (mod) mass loss during torrefaction at setpoint temperatures.

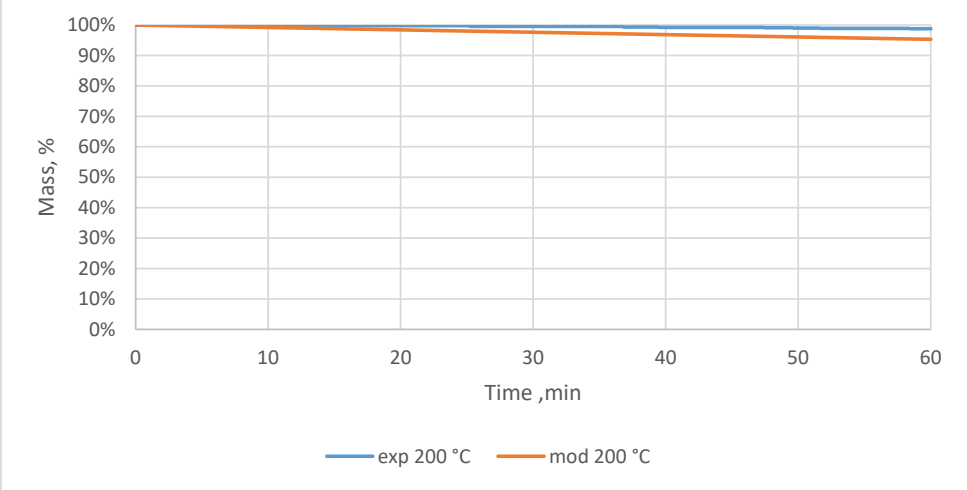

Figure A23. Mass losses during torrefaction at 200 °C; material S(G−)(I−).

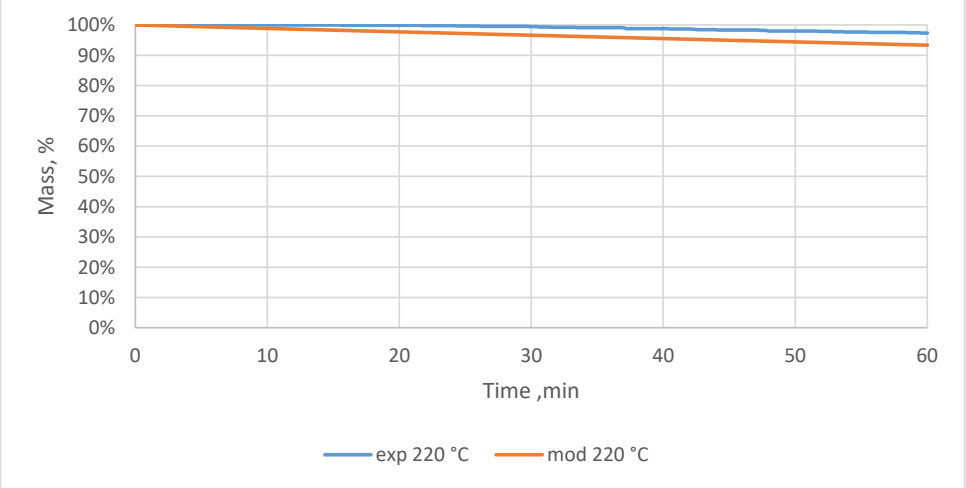

Figure A24. Mass losses during torrefaction at 220 °C; material S(G−)(I−).

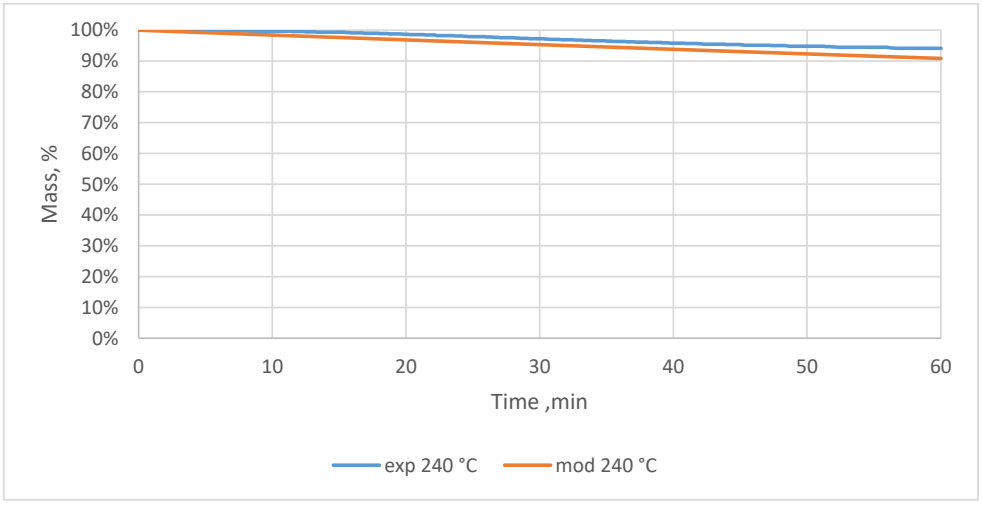

Figure A25. Mass losses during torrefaction at 240 °C; material S(G−)(I−).

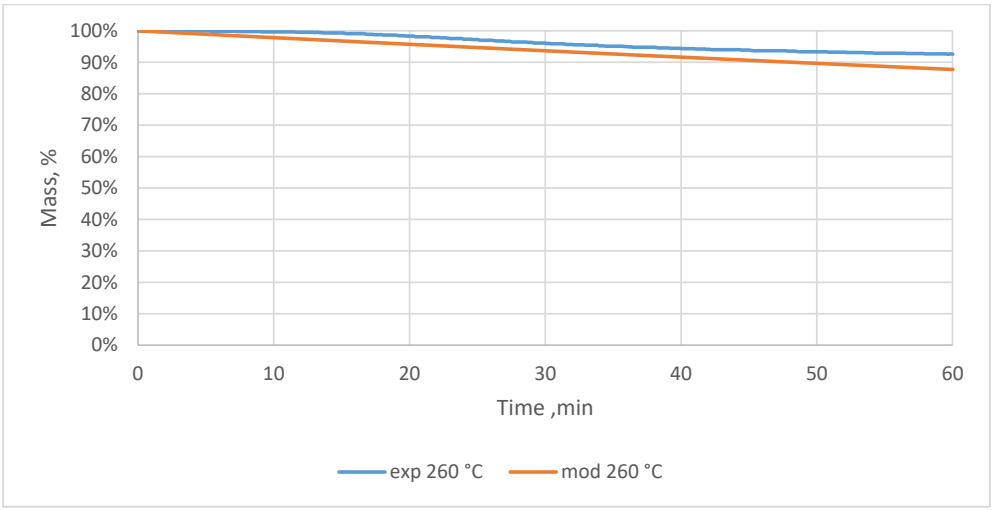

Figure A26. Mass losses during torrefaction at 260 °C; material S(G−)(I−).

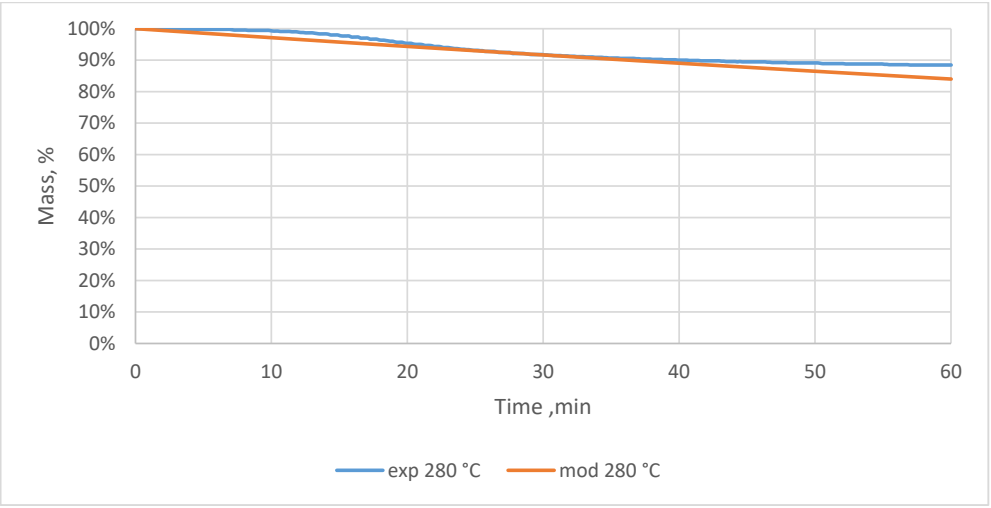

Figure A27. Mass losses during torrefaction at 280 °C; material S(G−)(I−).

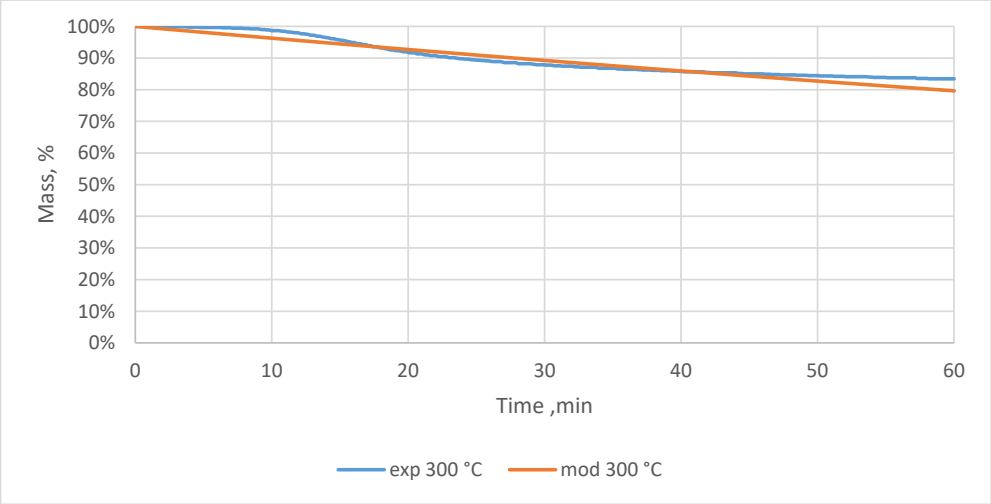

Figure A28. Mass losses during torrefaction at 300 °C; material S(G−)(I−).

References

1. Bentsen, N.S.; Felby, C. Biomass for energy in the European Union - a review of bioenergy resource assessments. *Biotechnol. Biofuels* **2012**, *5*, 25. [CrossRef] [PubMed]
2. Scarlat, N.; Dallemand, J.-F.; Monforti-Ferrario, F.; Banja, M.; Motola, V. Renewable energy policy framework and bioenergy contribution in the European Union—An overview from National Renewable Energy Action Plans and Progress Reports. *Renew. Sustain. Energy Rev.* **2015**, *51*, 969–985. [CrossRef]
3. Di Fulvio, F.; Forsell, N.; Korosuo, A.; Obersteiner, M.; Hellweg, S. Spatially explicit LCA analysis of biodiversity losses due to different bioenergy policies in the European Union. *Sci. Total Environ.* **2019**, *651*, 1505–1516. [CrossRef] [PubMed]
4. Tuskan, G. Short-rotation woody crop supply systems in the United States: What do we know and what do we need to know? *Biomass Bioenergy* **1998**, *14*, 307–315. [CrossRef]
5. Tullus, A.; Rytter, L.; Tullus, T.; Weih, M.; Tullus, H. Short-rotation forestry with hybrid aspen (Populus tremulaL.×P. tremuloidesMichx.) in Northern Europe. *Scand. J. For. Res.* **2012**, *27*, 10–29. [CrossRef]
6. Sage, R.F.; Sultmanis, S. Why are there no C 4 forests? *J. Plant Physiol.* **2016**, *203*, 55–68. [CrossRef]
7. Wang, D.; Jaiswal, D.; Lebauer, D.S.; Wertin, T.M.; Bollero, G.A.; Leakey, A.D.B.; Long, S.P. A physiological and biophysical model of coppice willow (*Salix* spp.) production yields for the contiguous USA in current and future climate scenarios. *Plant Cell Environ.* **2015**, *38*, 1850–1865. [CrossRef]
8. Covshoff, S.; Hibberd, J.M. Integrating C4 photosynthesis into C3 crops to increase yield potential. *Curr. Opin. Biotechnol.* **2012**, *23*, 209–214. [CrossRef]
9. Wang, P.; Vlad, D.; Langdale, J.A. Finding the genes to build C4 rice. *Curr. Opin. Plant Boil.* **2016**, *31*, 44–50. [CrossRef]
10. Icka, P.; Damo, R.; Icka, E. Paulownia Tomentosa, a Fast Growing Timber. *Ann. Valahia Univ. Targoviste Agric.* **2016**, *10*, 14–19. [CrossRef]
11. Moreno, J.L.; Bastida, F.; Ondoño, S.; García, C.; Andrés-Abellán, M.; López-Serrano, F.R. Agro-forestry management of Paulownia plantations and their impact on soil biological quality: The effects of fertilization and irrigation treatments. *Appl. Soil Ecol.* **2017**, *117*, 46–56. [CrossRef]
12. Woods, V.B. Paulownia as a Novel Biomass Crop for Northern Ireland? In *A Review of Current Knowledge*, 7th ed.; Agri-Food and Biosciences Institute: Belfast, Northern Ireland, 2008. Available online: https://www.doc-developpement-durable.org/file/Arbres-Bois-de-Rapport-Reforestation/FICHES_ARBRES/Paulownia/Paulownia%20as%20a%20novel%20biomass%20crop_Ireland.pdf (accessed on 22 July 2019).
13. Huseinovic, S. Paulownia elongata sy hu in function of improving the quality of the environment. *Period. Eng. Nat. Sci. (PEN)* **2017**, *5*, 117–123. [CrossRef]

14. Bortniak, M.; Sekutowski, T.R.; Zajączkowska, O.; Kucharski, M. Influence of the soil from Oxytree [Paulownia elongata S. Y. Hu × Paulownia fortunei (Seem.) Hemsl.] plantation on germination and initial growth of winter wheat and winter rape. *Prog. Plant Prot.* **2018**, *58*, 247–250. [CrossRef]
15. Lisiecka, B.; Bokůvka, O.; Tański, T.; Krzemiński, Ł.; Jambor, M. Obtaining of biomorphic composites based on carbon materials. *Prod. Eng. Arch.* **2018**, *19*, 22–25. [CrossRef]
16. Paulownia112.com. Available online: https://www.paulownia112.com/wp-content/uploads/2015/10/informe-de-resultados-ms344-analisis-biomasa-clon-in-vitro-112r.pdf (accessed on 15 December 2018).
17. Pradhan, P.; Mahajani, S.M.; Arora, A. Production and utilization of fuel pellets from biomass: A review. *Fuel Process. Technol.* **2018**, *181*, 215–232. [CrossRef]
18. Kihedu, J. Torrefaction and Combustion of Ligno-Cellulosic Biomass. *Energy Procedia* **2015**, *75*, 162–167. [CrossRef]
19. Poudel, J.; Oh, S.C. Effect of Torrefaction on the Properties of Corn Stalk to Enhance Solid Fuel Qualities. *Energies* **2014**, *7*, 5586–5600. [CrossRef]
20. Phanphanich, M.; Mani, S. Impact of torrefaction on the grindability and fuel characteristics of forest biomass. *Bioresour. Technol.* **2011**, *102*, 1246–1253. [CrossRef]
21. Bates, R.B.; Ghoniem, A.F. Bioresource Technology Biomass torrefaction: Modeling of volatile and solid product evolution kinetics. *Bioresour. Technol.* **2012**, *124*, 460–469. [CrossRef]
22. Dhyani, V.; Bhaskar, T. *Kinetic Analysis of Biomass Pyrolysis*; Elsevier BV: Amsterdam, The Netherlands, 2018; pp. 39–83.
23. Świechowski, K.; Liszewski, M.; Bąbelewski, P.; Koziel, J.A.; Białowiec, A. Oxytree Pruned Biomass Torrefaction: Mathematical Models of the Influence of Temperature and Residence Time on Fuel Properties Improvement. *Materials* **2019**, *12*, 2228. [CrossRef]
24. Rodrigues, A.; Vanbeveren, S.P.; Costa, M.; Ceulemans, R. Relationship between soil chemical composition and potential fuel quality of biomass from poplar short rotation coppices in Portugal and Belgium. *Biomass Bioenergy* **2017**, *105*, 66–72. [CrossRef]
25. Achinelli, F.G.; Doffo, G.; Barotto, A.J.; Luquez, V.; Monteoliva, S. Effects of irrigation, plantation density and clonal composition on woody biomass quality for bioenergy in a short rotation culture system with willows (*Salix* spp.). *Revista Árvore* **2018**, *42*, 42. [CrossRef]
26. Świechowski, K.; Liszewski, M.; Bąbelewski, P.; Koziel, J.A.; Białowiec, A. Fuel Properties of Torrefied Biomass from Pruning of Oxytree. *Data* **2019**, *4*, 55. [CrossRef]
27. FAO World Reference Base for Soil Resources 2014 International Soil Classification System for Naming Soils and Creating Legends for Soil Maps. 2015. Available online: http://www.fao.org/3/i3794en/I3794en.pdf (accessed on 22 July 2019).
28. Polish Committee for Standardization. PN-EN 14346:2011 Standard. Waste characteristics. Calculation of Dry Mass on the Basis of Dry Residue or Water Content. Available online: https://infostore.saiglobal.com/enau/Standards/pn-en-14346-2011-932471_saig_pkn_pkn_2197939/ (accessed on 22 July 2019).
29. Polish Committee for Standardization. PN-EN 15169:2011 Standard. Waste characteristics. Determination of Organic Matter Content for Waste, Slurry and Sludge. Available online: http://sklep.pkn.pl/pn-en-15169-2011p.html (accessed on 22 July 2019).
30. Polish Committee for Standardization. PN-Z-15008-04:1993 Standard. Municipal Solid Waste. Analysis of Combustible and Non-Combustible Content. Available online: http://sklep.pkn.pl/pn-z-15008-04-1993p.html (accessed on 22 July 2019).
31. Polish Committee for Standardization. PN-G-04513:1981 Standard. Solid Fuels. Determination of the Higher Heating Value and the Lower Heating Value. Available online: http://sklep.pkn.pl/pn-g-04513-1981p.html (accessed on 22 July 2019).
32. Stępień, P.; Pulka, J.; Serowik, M.; Białowiec, A. Thermogravimetric and Calorimetric Characteristics of Alternative Fuel in Terms of Its Use in Low-Temperature Pyrolysis. *Waste Biomass Valorization* **2018**, *10*, 1669–1677. [CrossRef]
33. Stępień, P.; Białowiec, A. Kinetic parameters of torrefaction process of alternative fuel produced from municipal solid waste and characteristic of carbonized refuse derived fuel. *Detritus* **2018**, *3*, 75–83. [CrossRef]
34. Peleg, M.; Normand, M.D.; Corradini, M.G. The Arrhenius Equation Revisited. *Crit. Rev. Food Sci. Nutr.* **2012**, *52*, 830–851. [CrossRef]

35. Liaqat, F. Effects of Storage and Geographical Location on Fuel Quality of Norway Spruce Forest Residues, Swedish University of Agricultural Sciences Examensarbete. 2011. Available online: https://stud.epsilon.slu.se/3174/4/liaqat_f_110826.pdf (accessed on 22 July 2019).
36. Chen, W.-H.; Peng, J.; Bi, X.T. A state-of-the-art review of biomass torrefaction, densification and applications. *Renew. Sustain. Energy Rev.* **2015**, *44*, 847–866. [CrossRef]
37. Klasnja, B.; Kopitovic, S.; Orlovic, S. Wood and bark of some poplar and willow clones as fuelwood. *Biomass Bioenergy* **2002**, *23*, 427–432. [CrossRef]
38. Qi, Y.; Yang, C.; Hidayat, W.; Jang, J.-H.; Kim, N.-H. Solid Bioenergy Properties of Paulownia tomentosa Grown in Korea. *J. Korean Wood Sci. Technol.* **2016**, *44*, 890–896. [CrossRef]
39. Vusić, D.; Migalić, M.; Željko, Z.; Trkmić, M.; Bešlić, A.; Drvodelić, D. Fuel properties of paulownia biomass. *Nat. Resour. Green Technol. Sustain. Dev.* **2018**, 126–130. Available online: https://pdfs.semanticscholar.org/3275/d126918947d36a46da5cd3337f1a3cd1b121.pdf (accessed on 22 July 2019).
40. Krzyżaniak, M.; Stolarski, M.J.; Waliszewska, B.; Szczukowski, S.; Tworkowski, J.; Załuski, D.; Śnieg, M. Willow biomass as feedstock for an integrated multi-product biorefinery. *Ind. Crop. Prod.* **2014**, *58*, 230–237. [CrossRef]
41. Fang, S.; Zhai, X.; Wan, J.; Tang, L. Clonal variation in growth, chemistry and calorific value of new poplar hybrids at nursery stage. *Biomass Bioenergy* **2013**, *54*, 303–311. [CrossRef]
42. Yorgun, S.; Yıldız, D. Preparation and characterization of activated carbons from Paulownia wood by chemical activation with H3PO4. *J. Taiwan Inst. Chem. Eng.* **2015**, *53*, 122–131. [CrossRef]
43. Campbell, W.A.; Evitts, R.W. Determining the Severity of Torrefaction for Multiple Biomass Types Using Carbon Content. *Energy Fuels* **2018**, *32*, 9448–9458. [CrossRef]
44. Ribeiro, J.M.C.; Godina, R.; Matias, J.C.D.O.; Nunes, L.J.R. Future Perspectives of Biomass Torrefaction: Review of the Current State-Of-The-Art and Research Development. *Sustainability* **2018**, *10*, 2323. [CrossRef]
45. Ren, S.; Lei, H.; Wang, L.; Bu, Q.; Chen, S.; Wu, J. Thermal behaviour and kinetic study for woody biomass torrefaction and torrefied biomass pyrolysis by TGA. *Biosyst. Eng.* **2013**, *116*, 420–426. [CrossRef]
46. Becker, A.; Scherer, V. A comparison of the torrefaction behavior of wood, miscanthus and palm kernel shells: Measurements on single particles with geometries of technical relevance. *Fuel* **2018**, *224*, 507–520. [CrossRef]
47. Wang, L.; Barta-Rajnai, E.; Skreiberg, Ø.; Khalil, R.; Czégény, Z.; Jakab, E.; Barta, Z.; Grønli, M. Effect of torrefaction on physiochemical characteristics and grindability of stem wood, stump and bark. *Appl. Energy* **2018**, *227*, 137–148. [CrossRef]
48. Gucho, E.M.; Shahzad, K.; Bramer, E.A.; Akhtar, N.A.; Brem, G. Experimental Study on Dry Torrefaction of Beech Wood and Miscanthus. *Energies* **2015**, *8*, 3903–3923. [CrossRef]
49. Basu, P.; Rao, S.; Dhungana, A. An investigation into the effect of biomass particle size on its torrefaction. *Can. J. Chem. Eng.* **2013**, *91*, 466–474. [CrossRef]
50. Bridgeman, T.; Jones, J.; Shield, I.; Williams, P.; Jones, J. Torrefaction of reed canary grass, wheat straw and willow to enhance solid fuel qualities and combustion properties. *Fuel* **2008**, *87*, 844–856. [CrossRef]
51. Dhanavath, K.N.; Bankupalli, S.; Bhargava, S.K.; Parthasarathy, R. An experimental study to investigate the effect of torrefaction temperature on the kinetics of gas generation. *J. Environ. Chem. Eng.* **2018**, *6*, 3332–3341. [CrossRef]
52. Carrasco, J.C.; Oporto, G.S.; Zondlo, J.; Jingxin, W. Torrefaction Kinetics of Red Oak (Quercus rubra) in a Fluidized Reactor. *BioResources* **2013**, *8*, 5067–5082. [CrossRef]
53. Walkowiak, M.; Bartkowiak, M. The kinetics of the thermal decomposition of the willow wood (*Salix viminalis* L.) exposed to the torrefaction process. *Drewno* **2012**, *55*, 37–49. Available online: http://drewno-wood.pl/pobierz-55 (accessed on 22 July 2019).
54. Saddawi, A.; Jones, J.M.; Williams, A.; Wójtowicz, M.A. Kinetics of the Thermal Decomposition of Biomass. *Energy Fuels* **2010**, *24*, 1274–1282. [CrossRef]
55. Diaz, I.; Rodriguez, M.; Arnaiz, C.; Miguel, G.S.; Dominguez, M. Biomass pyrolysis kinetics through thermogravimetric analysis. *Comput. Aided Chem. Eng.* **2013**, *32*, 1–6.
56. Roesler, J.F.; Sanz, E.; Nastoll, W.; Lu, P. Exothermicity in Wood Torrefaction and its Impact on Product Mass Yields: From Micro to Pilot Scale. *Can. J. Chem. Eng.* **2015**, *93*, 331–339. [CrossRef]
57. Prins, M.J.; Ptasinski, K.J.; Janssen, F.J.J.G. Torrefaction of wood: Part 1. Weight loss kinetic. *J. Anal. Appl. Pyrolysis* **2006**, *77*, 28–34. [CrossRef]

58. Peng, J.H. A Study of Softwood Torrefaction and Densification for the Production of High Quality Wood Pellets, The University of British Columbia. 2012. Available online: https://www.collectionscanada.gc.ca/obj/thesescanada/vol2/BVAU/TC-BVAU-42654.pdf (accessed on 22 July 2019).
59. Bach, Q.; Khalil, R.A.; Tran, K.; Skreiberg, Ø. Torrefaction Kinetics of Norwegian Biomass Fuels. *Chem. Eng. Trans.* **2014**, *37*, 49–54. [CrossRef]
60. Chen, L.; Wang, S.; Meng, H.; Wu, Z.; Zhao, J. Synergistic effect on thermal behavior and char morphology analysis during co-pyrolysis of paulownia wood blended with different plastics waste. *Appl. Therm. Eng.* **2017**, *111*, 834–846. [CrossRef]
61. Pulka, J.; Manczarski, P.; Koziel, J.A.; Białowiec, A. Torrefaction of Sewage Sludge: Kinetics and Fuel Properties of Biochars. *Energies* **2019**, *12*, 565. [CrossRef]
62. Syguła, E.; Koziel, J.A.; Białowiec, A. Proof-of-Concept of Spent Mushrooms Compost Torrefaction—Studying the Process Kinetics and the Influence of Temperature and Duration on the Calorific Value of the Produced Biocoal. *Energies* **2019**, *12*, 3060. [CrossRef]

Załącznik nr 3

Kacper Świechowski
imię i nazwisko

WROCŁAW 28.02.2022
(miejscowość i data)

Katedr Biogospodarki Stosowanej
Uniwersytet Przyrodniczy we Wrocławiu
51-630 Wrocław, Chełmońskiego 37a
afiliacja

OŚWIADCZENIE

Oświadczam, że w pracy:

Kacper Świechowski, Sylwia Stegenta-Dąbrowska, Marek Liszewski, Przemysław Bąbelewski, Jacek A. Koziel, Andrzej Białowiec. 2019. Oxytree Pruned Biomass Torrefaction: Process Kinetics. Materials, 12, 3334; doi:10.3390/ma12203334

mój udział polegał na:

Przeprowadzeniu eksperymentu i opracowaniu wyników z badań pod względem statystycznym przy wykorzystaniu oprogramowania Statistica. Opracowanie polegało na wykorzystaniu danych z eksperymentu TGA próbek Oxytree. Celem opracowania było wyznaczenia parametrów kinetycznych dla procesu toryfikacji dla 8 badanych próbek, a następnie wykorzystanie ich do zamodelowania procesu toryfikacji. Analiza statystyczna obejmowała także sprawdzenie wpływu sposobu uprawy Oxytree na wartości kinetyczne. Podczas pisania manuskryptu byłem odpowiedzialny za napisanie pierwszej wersji tekstu, w szczególności metodyki, wyników i dyskusji. Podczas procesu recenzji stworzyłem pierwszą wersję odpowiedzi dla recenzentów i wykonywałem poprawki w manuskrypcie.

28.02.2022 Świechowski
data i podpis

Załącznik nr 3

Sylwia Stegenta-Dąbrowska
imię i nazwisko

Wrocław, 24.02.2022
(miejscowość i data)

Katedr Biogospodarki Stosowanej
Uniwersytet Przyrodniczy we Wrocławiu
51-630 Wrocław, Chełmońskiego 37a
afiliacja

OŚWIADCZENIE

Oświadczam, że w pracy:

Kacper Świechowski, Sylwia Stegenta-Dąbrowska, Marek Liszewski, Przemysław Bąbelewski, Jacek A. Koziel, Andrzej Białowiec. 2019. Oxytree Pruned Biomass Torrefaction: Process Kinetics. Materials, 12, 3334; doi:10.3390/ma12203334

mój udział polegał na:

Jako promotor pomocniczy pomagałam doktorantowi zmodyfikować pierwszą wersję manuskryptu w szczególności rozdział dotyczący analizy i dyskusji uzyskanych wyników badań, szczególnie w zakresie charakterystyki uzyskanego materiału. Przygotowałam abstrakt graficzny. W trakcie recenzji uczestniczyłam w udzielaniu odpowiedzi do recenzentów oraz nanoszeniu poprawek do manuskryptu.

24.02.2022, Sylwia Stegenta-Dąbrowska
data i podpis

Załącznik nr 3

Wrocław, 28.02.2022

(miejscowość i data)

Marek Liszewski
imię i nazwisko

Instytut Agroekologii i Produkcji Roślinnej
Uniwersytet Przyrodniczy we Wrocławiu
50-363 Wrocław, pl. Grunwaldzki 24A
afiliacja

OŚWIADCZENIE

Oświadczam, że w pracy:
Kacper Świechowski, Sylwia Stegenta-Dąbrowska, Marek Liszewski, Przemysław Bąbelewski, Jacek A. Koziel, Andrzej Białowiec. 2019. Oxytree Pruned Biomass Torrefaction: Process Kinetics. Materials, 12, 3334; doi:10.3390/ma12203334

mój udział polegał na:
Przygotowaniu materiału badawczego którym były próbki drewna Oxytree pochodzące z plantacji w Pawłowicach. Moje zadanie polegało na posadzeniu drzew Oxytree w Pawłowicach, które były poddawane 4 różnym zabiegom agrotechnicznym, pobraniu próbek drewna, wysuszeniu i ich wstępnym rozdrobnieniu. Brałem także udział w opisie badanych materiałów w manuskrypcie.

28.02.2022

data i podpis

Załącznik nr 3

Przemysław Bąbelewski
imię i nazwisko

Wrocław 02.03.2022
(miejscowość i data)

Katedra Ogrodnictwa
Uniwersytet Przyrodniczy we Wrocławiu
50-363 Wrocław, pl. Grunwaldzki 24A
afiliacja

OŚWIADCZENIE

Oświadczam, że w pracy:
Kacper Świechowski, Sylwia Stegenta-Dąbrowska, Marek Liszewski, Przemysław Bąbelewski, Jacek A. Koziel, Andrzej Białowiec. 2019. Oxytree Pruned Biomass Torrefaction: Process Kinetics. Materials, 12, 3334; doi:10.3390/ma12203334

mój udział polegał na:
Przygotowaniu materiału badawczego którym był 4 próbki drewna Oxytree pochodzące z plantacji doświadczalnej w Psarach. Byłem także odpowiedzialny za wstępne przygotowanie materiału badawczego, jego rozdrobnienie, wysuszenie i dostarczenie do laboratorium. Podczas pisania manuskryptu pomagałem przy opisach dotyczących Oxytree.

Przemysław Bąbelewski
02.03.2022
data i podpis

Załącznik nr 3

Jacek Koziel
imię i nazwisko

Department of Agricultural and Biosystems Engineering
Iowa State University
Ames, IA 50011, USA
afiliacja

Ames, 23-2-2022…….
(miejscowość i data)

OŚWIADCZENIE

Oświadczam, że w pracy:
Kacper Świechowski, Sylwia Stegenta-Dąbrowska, Marek Liszewski, Przemysław Bąbelewski, Jacek A. Koziel, Andrzej Białowiec. 2019. Oxytree Pruned Biomass Torrefaction: Process Kinetics. Materials, 12, 3334; doi:10.3390/ma12203334

mój udział polegał na:
Pełnieniu opieki merytorycznej nad pracą wykonywaną przez Kacpra Świechowskiego w całym procesie pisania, modyfikowania i recenzowania artykułu. Byłem odpowiedzialny za nadzór nad poprawności przedstawienia koncepcji i metodyki badań. Odpowiadałem za sprawdzenie poprawności manuskrypty pod względem merytorycznym i redaktorskim. Brałem udział w modyfikowaniu manuskryptu na etapie recenzji. Pozyskałem także część środków na potrzeby publikacji artykułu.

data i podpis

Załącznik nr 3

Andrzej Białowiec Wrocław, 26.02.2022

imię i nazwisko (miejscowość i data)

Katedr Biogospodarki Stosowanej
Uniwersytet Przyrodniczy we Wrocławiu
51-630 Wrocław, Chełmońskiego 37a
afiliacja

OŚWIADCZENIE

Oświadczam, że w pracy:
Kacper Świechowski, Sylwia Stegenta-Dąbrowska, Marek Liszewski, Przemysław Bąbelewski, Jacek A. Koziel, Andrzej Białowiec. 2019. Oxytree Pruned Biomass Torrefaction: Process Kinetics. Materials, 12, 3334; doi:10.3390/ma12203334

mój udział polegał na:
Zapewnieniu wsparcia merytorycznego dla piszącego manuskrypt doktoranta, w tym pomagałem stworzyć koncepcje artykułu jak i sprawdziłem poprawność danych i naniosłem poprawki przed wysłaniem artykułu do recenzji. W trakcie recenzji uczestniczyłem w udzielaniu odpowiedzi do recenzentów oraz nanoszeniu poprawek do manuskryptu. Pozyskałem także część finansowania umożliwiającego publikację w open access.

26.02.2022 Bi Tooni

data i podpis

energies

MDPI

Article

Waste to Carbon: Biocoal from Elephant Dung as New Cooking Fuel

Paweł Stępień [1], Kacper Świechowski [1], Martyna Hnat [1], Szymon Kugler [2], Sylwia Stegenta-Dąbrowska [1,*], Jacek A. Koziel [3], Piotr Manczarski [4] and Andrzej Białowiec [1,3]

1 Institute of Agricultural Engineering, Faculty of Life Sciences and Technology, Wroclaw University of Environmental and Life Sciences, 37a Chełmońskiego Str., 51-630 Wroclaw, Poland; pawel.stepien@upwr.edu.pl (P.S.); kacper.swiechowski@upwr.edu.pl (K.Ś.); hnat.martyna@gmail.com (M.H.); andrzej.bialowiec@upwr.edu.pl (A.B.)

2 Polymer Institute, Faculty of Chemical Technology and Engineering, West Pomeranian University of Technology, 10 Pułaskiego Str., 70-322 Szczecin, Poland; szymon.kugler@zut.edu.pl

3 Department of Agricultural and Biosystems Engineering, Iowa State University, Ames, IA 50011-3270, USA; koziel@iastate.edu

4 Department of Environmental Engineering, Hydro and Environmental Engineering, Faculty of Building Services, Warsaw University of Technology, 00-661 Warszawa, Poland; piotr.manczarski@pw.edu.pl

* Correspondence: sylwia.stegenta@upwr.edu.pl; Tel.: +48-71-320-5811

Received: 10 September 2019; Accepted: 12 November 2019; Published: 14 November 2019

Abstract: The paper presents, for the first time, the results of fuel characteristics of biochars from torrefaction (a.k.a., roasting or low-temperature pyrolysis) of elephant dung (manure). Elephant dung could be processed and valorized by torrefaction to produce fuel with improved qualities for cooking. The work aimed to examine the possibility of using torrefaction to (1) valorize elephant waste and to (2) determine the impact of technological parameters (temperature and duration of the torrefaction process) on the waste conversion rate and fuel properties of resulting biochar (biocoal). In addition, the influence of temperature on the kinetics of the torrefaction and its energy consumption was examined. The lab-scale experiment was based on the production of biocoals at six temperatures (200–300 °C; 20 °C interval) and three process durations of the torrefaction (20, 40, 60 min). The generated biocoals were characterized in terms of moisture content, organic matter, ash, and higher heating values. In addition, thermogravimetric and differential scanning calorimetry analyses were also used for process kinetics assessment. The results show that torrefaction is a feasible method for elephant dung valorization and it could be used as fuel. The process temperature ranging from 200 to 260 °C did not affect the key fuel properties (high heating value, HHV, HHV_{daf}, regardless of the process duration), i.e., important practical information for proposed low-tech applications. However, the higher heating values of the biocoal decreased above 260 °C. Further research is needed regarding the torrefaction of elephant dung focused on scaling up, techno-economic analyses, and the possibility of improving access to reliable energy sources in rural areas.

Keywords: torrefaction; biorenewable energy; biowaste; biocoal; alternative fuel; waste management; manure; thermal valorization; thermogravimetric analysis; differential scanning calorimetry

1. Introduction

It is estimated that there are around~450,000 elephants today, of which 400,000 are in Africa and 50,000 in Asia. In Africa, these mammals live in 34 countries (Angola, Benin, Botswana, Burkina Faso, Cameroon, Central African Republic, Chad, Congo, Ivory Coast, Equatorial Guinea, Eritrea, Ethiopia,

Gabon, Gana, Guinea, Bissau, Kenya, Liberia, Malawi, Mali, Mozambique, Namibia, Niger, Nigeria, Rwanda, Senegal, Sierra Leone, Somalia, South Africa, Sudan, Tanzania, Togo, Uganda, Zambia, Zimbabwe), and on the Asian continent they can be found in 15 countries (India, Nepal, Bhutan and Bangladesh, China, Burma, Thailand, Cambodia, Laos, Vietnam, Malaysia, Andaman Islands, Sri Lanka, Sumatra, Borneo) [1]. The daily amount of dung produced by one elephant is 100–150 kg. The weight of elephant excrement depends on the amount of consumed water [2–4]. Thus, taking into consideration the conservative estimate of the minimum dung weight (100 kg), the daily and annual dung production on a global scale is 45,000 Mg and more than 16 million Mg, respectively, i.e., a large amount of biowaste that could be valorized [2–4].

From an ecological point of view, untreated animal waste or handling, air-drying and combustion without prior treatment can be problematic due to health and environmental concerns, such as elevated risk of contamination with pathogens, contamination of drinking water sources, gaseous emissions of odor, hydrogen sulfide, ammonia, and other toxic gases [5,6]. In addition, the loss of nutrients from dung associated with current practices can also represent economic losses due to its lower value as a fertilizer [5].

We propose a solution to these problems with the introduction of the torrefaction process to manage and valorize the elephant dung. Resulting biocoal can be used as a fuel with a useful high heating value (*HHV*). Research with slow pyrolysis and hydrothermal carbonization of other types of livestock manure resulted in HHVs ranging from 15.8 to 18.4 MJ/kg [7]. Qambrani et al. [8] showed that biocoal from animal manure contains more N compared to biochar from plant residues. Although the pore structure is more organized in biochar from plant sources, the fertilizer quality and heavy metal adsorbability were found to be excellent in manure biochars. On the other hand, some raw waste types (such as poultry manure or sewage sludge) can contain a large amount of copper and zinc, which limits its use as a fertilizer. The proposed concept to valorize elephant manure can provide new technologies for using the torrefaction process in rural areas, which can be used to obtain better quality fuel and fertilizer.

To date, several methods to valorize elephant dung have been proposed. Vermicomposting is a biological process in which the organic fraction of dung is decomposed by microorganisms and earthworms under controlled environmental conditions to a level when it can be applied on arable land. This method can be ecological and economically profitable [9]. Vermicomposting of animal dung from the zoo was investigated in pilot-scale by a team of scientists in Mexico [6]. Elephant dung was also used for research by scientists in Thailand for the production of biogas in co-fermentation with water hyacinth and fermentation on a laboratory scale. In the case of co-fermentation, the calorific value of biogas was 15.05 $MJ \cdot m^{-3}$ [10,11].

Biohydrogen production through anaerobic mixed cultures of microorganisms found in elephant dungs was also researched in laboratory conditions. It is based on simultaneous saccharification and fermentation of cellulose. The bacteria break down the cellulose to glucose, and then non-cellulolytic bacteria from the formed glucose produces hydrogen [12,13]. The microorganism's culture from elephant dung stimulated the production of H_2 from cellulose. It was assumed that cellulolytic bacteria in the dung originate from the plant diet of the elephant. Animal manure, including elephant dung, was also the subject of research conducted in Thailand on cellulolytic bacteria for the direct production of butanol from cellulose, which could be an alternative to fuel obtained from petroleum [14].

The knowledge about practical considerations for the valorization of elephant dung and the progression from lab to full-scale (e.g., costs of construction and operation) is limited. There are also questions about the storage and distribution of finished products (e.g., fuel briquettes for cooking), which could be prohibitively expensive for long-range transport. Life-cycle analyses could be useful to assess the critical transport range [15]. It is equally important to consider managing the residues (e.g., raw dung and sludge), which may require specialized collection, storage, treatment, and disposal. It has not been described yet how existing or developing technologies (anaerobic digestion, biohydrogen production) could be used for waste management, especially in rural regions in which elephant dung is

available in large quantities. Thus, there is a need to find local-scale solutions suited for these regions, which should be safe, inexpensive, simple to build, use and maintain, dependable, and not generating another waste stream to manage.

We propose an alternative solution for elephant dung management via torrefaction (Figure 1). Torrefaction (a.k.a., 'roasting' or low-temperature pyrolysis) is a thermochemical process occurring at 200–300 °C without the presence of an oxidant. Jia et al. [16] described the possibility of using a co-gasification of woody biomass and animal manure as a useful technology to utilize organic waste, which could be practical in the case of elephant dung as well. The elephant dung fuel produced may be an attractive source of rural fuel. For example, in India alone, 6.3% of all households use the so-called 'dung cake' to produce the energy needed for cooking [17]. Assuming 1.34 billion people in India in 2018 [18] and that one household comprises 10 people, as many as ~8.4 million households use dung cake for energy production. Although the torrefaction process requires some energy, it is also the most promising technology for organic waste treatment for its highest greenhouse gas mitigation potential [19]. The produced biocoal, especially when pelletized, poses a lower environmental risk during transport, storage, and combustion, in addition to lowering the risks of sanitary and aquatic pollution [20,21]. Therefore, torrefaction could be one of the potential technologies for elephant dung utilization that are sustainable.

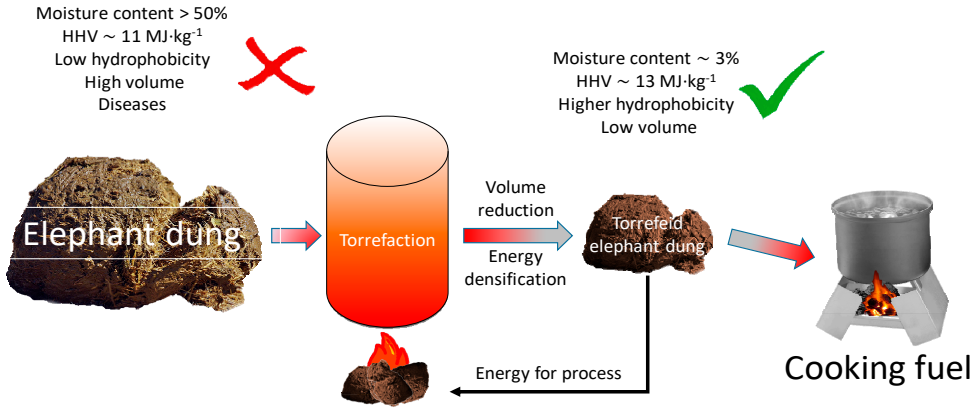

Figure 1. The proposed valorization of elephant dung (manure) via torrefaction.

To date, no work has been carried out on the torrefaction of elephant dung as a method for the production of fuel. Local-scale torrefaction can address challenges with dung management, through its valorization, while improving the socio-economic situation in rural households. Therefore, the research carried out was aimed at determining:

- Whether torrefaction can be used as a method of preliminary valorization of elephant dung;
- Whether the duration of the torrefaction process at a given temperature affects the dung conversion rate (e.g., mass loss, energy densification, and improved fuel properties);
- Whether energy consumption is needed for the torrefaction of elephant dung.

2. Materials and Methods

2.1. Feedstock

The study used Asian elephant dung from the Zoological Garden, located in Wrocław, Poland. The 5 kg sample was dried at 105 °C for 24 h in a laboratory dryer, followed by milling to the grain size of ≤0.425 mm with the laboratory knife mill (TESTCHEM, model LMN-100, Pszów, Poland) to make the sample homogeneous. Samples were frozen at −15 °C for further testing.

2.2. Biocoal Production Method via Torrefaction

A scheme of the experiment is shown in Figure 2. The biocoal production process was carried out in triplicates according to the methodology presented by [22] at six temperatures from 200 to 300 °C (20 °C intervals) at 20, 40, 60 min for each interval, followed by the cooling phase. The biocoals were generated using a muffle furnace (Snol, model 8.1/1100, Utena, Lithuania). CO_2 inert gas was provided to the furnace to ensure non-oxidative conditions. The elephant dung samples were heated from 20 °C to set point at 50 °C·min^{-1}. The cooling times were 38 min, 33 min, 29 min, 23 and 13.5 min, from torrefaction setpoints of 300 °C, 280 °C, 260 °C, 240 °C, and 220 °C to 200 °C, respectively. After the CO_2 supply was cut off, the biocoals were removed from the furnace when the interior temperature was <200 °C. The mass of the sample was determined before and after the cooling process in order to calculate the mass loss. Dung samples of 10 ± 0.5 g (dry mass, d.m.) were used to produce biocoal.

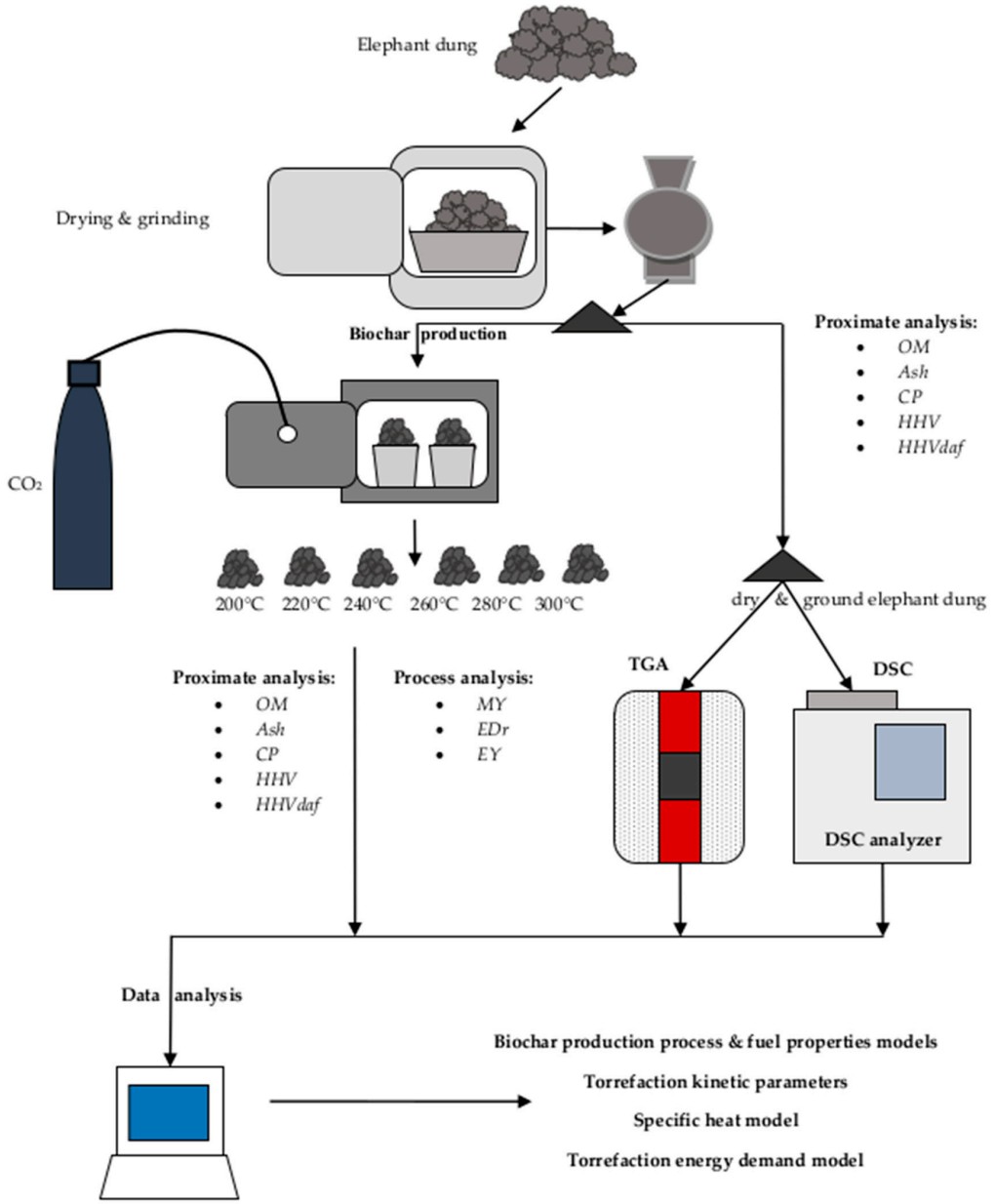

Figure 2. Scheme of experiments – biocoal production via torrefaction of elephant dung to determine the process kinetics with thermogravimetric analyses (TGA) and differential scanning calorimetry (DSC).

2.3. Proximate Analysis of Raw and Torrefied Elephant Dung

Physical and chemical properties were subjected to raw material and produced biocoals. The following tests were made in three replicates using the following standard methods:

- Moisture content (*MC*) by means of a laboratory dryer (WAMED, model KBC-65W, Warsaw, Poland) at temperature 105 °C, time 24 h, in accordance with the PN-EN 14346:2011 standard [23],
- Organic matter content (*OM*) by means of a laboratory dryer (WAMED, model KBC-65W, Warsaw, Poland) at temperature 550 °C, time 4 h, in accordance with the PN-EN 15169:2011 standard [24],
- ash and combustible parts (*CP*) by means of a laboratory dryer (WAMED, model KBC-65W, Warsaw, Poland) at temperature 815 °C, time 4 h in accordance with the PN-Z-15008-04:1993 standard [25],
- High heating value (*HHV*) by means of the IKA C2000 Basic calorimeter, at 17–25 °C, 30 bar pressure in accordance with the PN-G-04513:1981 standard [26].

2.4. Thermogravimetric Analysis (TGA) of Elephant Dung

Thermogravimetric analyses (TGA) were first performed in isothermal conditions to determine the kinetics parameters (k—reaction rate constants and E_a—activation energy) of the torrefaction process of elephant dung. Reaction rate constants were determined for the following temperatures: 200 °C, 220 °C, 240 °C, 260 °C, 280 °C, and 300 °C in accordance with the methodology and reactor set-up presented elsewhere [22]. First, the empty furnace was pre-heated to the set point. Then, 3 g of dry dung was placed in the steel crucible and placed in the furnace for 1 h. Measurement of mass loss was performed using a balance coupled to a steel crucible at 10 s intervals with 0.01 g accuracy. The calculating methodology for the kinetic parameters is presented in Section 2.6.2. The kinetics parameters (reaction rate and activation energy) were calculated.

TGA analyses were also completed in non-isothermal conditions to obtain more comprehensive data on the thermal degradation of elephant dung. These TGA analyses were performed at rising temperatures (from 20 °C to 850 °C) at a heating rate of 650 °C·h^{-1} (10.83 °C·min^{-1}). The sample was heated for 2 min after reaching a set point. The study of kinetic parameters and thermal degradation was performed using the stand-mounted tubular furnace (Czylok, RST 40x200/100, Jastrzębie-Zdrój, Poland).

2.5. Differential Scanning Calorimetry (DSC) of Raw Elephant Dung

Differential scanning calorimetry (DSC) analysis was carried out using a differential scanning calorimeter (TA Instruments, DSC Q2500, New Castle, DE, USA). Approximately 6 mg of the tested material was weighed into the aluminum hermetic crucible. Each sample (n = 1) was then placed in the analyzer and heated from 10 °C to 300 °C at a heating rate of 10 °C·min^{-1}. The N_2 inert gas was supplied at 3 dm^3·h^{-1} flowrates. The analysis provided information on endothermic and exothermic changes during torrefaction.

2.6. Data-Processing Calculation Methods

2.6.1. Mass Yield, Energy Densification Ratio, and Energy Yield

The mass yield, energy densification ratio, and energy yield of each of the variants were determined based on Equations (1)–(3), respectively [27]:

$$MY = \frac{m_b}{m_a} \cdot 100 \quad (1)$$

where:

MY—mass yield, %

m_a—the mass of dry elephant dung before torrefaction, g,
m_b—the mass of dry biocoal after torrefaction, g.

$$EDr = \frac{HHV_b}{HHV_a} \tag{2}$$

where:

EDr—energy densification ratio, -,
HHV_b—the high heating value of biocoal, J·g^{-1},
HHV_a—the high heating value of raw elephant dung, MJ·kg^{-1}.

$$EY = MY{\cdot}ED_r \tag{3}$$

where:

EY—nergy yield, %,
MY—mass yield, %
ED_r—energy densification ratio, -,

The ash-free value of the HHV was determined based on [28]:

$$HHV_{daf} = \frac{HHV}{M_f - M_{ash}} \tag{4}$$

where:

HHV_{daf}—high heating value on dry and ash-free base, MJ·kg^{-1},
HHV—high heating value, MJ·kg^{-1},
M_f—dry mass of fuel, kg,
M_{ash}—the mass of ash in fuel, kg.

2.6.2. Calculation of Kinetics Parameters (Reaction Rate and Activation Energy)

The data obtained from isothermal TGA analysis were used to determine the reaction rate (k) constant for each temperature, based on the first-order model [22]:

$$m_s = m_o{\cdot}e^{-k{\cdot}t} \tag{5}$$

where:

m_s—mass after time t, g,
m_o—initial mass, g,
k—the reaction rate constant, s^{-1},
t—time, s.

The nonlinear estimation of k in Equation (5) for each temperature was made with the Statistica 13.3 software (StatSoft, Inc., TIBCO Software Inc. Palo Alto, CA, USA). The Arrhenius plot was created ($\ln(k)(T)$ vs. $1/T$) on the basis of k values for individual temperatures [29], and a trend line was found:

$$y = a{\cdot}x + b \tag{6}$$

Then, the activation energy (E_a) values [22] were determined as follows:

$$E_a = -(a{\cdot}R) \tag{7}$$

where:

E_a—activation energy, J·mol^{-1},
a—the coefficient from Equation (6), K,
R—gas constant, J·mol^{-1}·K^{-1}.

2.6.3. Calculation of Energy Demand for Torrefaction of Elephant Dung

The results from the DSC and TGA analyses were used to calculate the actual energy demand in processing dry elephant dung (to heat dung from 20 °C to 300 °C) in accordance with the methodology presented in a previous paper [30]. The lack of TGA analysis causes overestimated energy amount needed to process the material, due to the decreasing amount of material during torrefaction caused by its devolatilization. The following is an example of the model use where the calculation for 1 g of the raw elephant dung torrefied at 300 °C was considered. The total amount of energy needed to processing raw elephant dung was calculated by adding the energy needed to evaporate water from raw elephant dung to the result from the model of dry elephant dung. The energy needed to evaporate water was calculated by Equation (8) [31]:

$$Q = m \cdot \Delta T \cdot cp + m \cdot co \tag{8}$$

where:

Q—the total amount of heat needed to heat and evaporate water, J,
m—the mass of water in the sample, g,
ΔT—the temperature difference between ambient temperature (20 °C) and boiling point (100 °C), under normal pressure conditions, °C,
cp—specific heat of water, 4.2 J·(g·°C)$^{-1}$,
co—the heat of water evaporation, 2257 J·g^{-1}.

2.6.4. Modeling of Torrefaction Process and Biocoal Fuel Properties

Polynomial models of the influence of torrefaction temperature and time on torrefaction process and biocoals fuel parameters were developed. These models were based on measured data from the torrefaction process, and biocoal properties for a particular temperature and time using a similar modeling approach described in our previous work [32]. Equations describing MY, EDr, EY, organic matter content, combustible parts, ash, HHV, and HHV_{daf} for biocoal were developed. The general form of the applied polynomial equation was:

$$f(T,t) = a_1 + a_2 \cdot T + a_3 \cdot T^2 + a_4 \cdot t + a_5 \cdot t^2 + a_6 \cdot T \cdot t + a_7 \cdot T^2 \cdot t^2 \tag{9}$$

where:

$f(T,t)$—the property (T, t, & combinations) being analyzed,
a_1—intercept,
a_2–a_7—regression coefficient,
T—process temperature, °C,
t—process time, min.

Regression analysis used a 2-degree polynomial with a general form, with intercept (a_1) and six regression coefficients (a_2–a_7). The confidence interval of the parameter evaluations (a_1–a_7) was 95%. All parameters for which the results of p-value were <0.05, were assumed to be statistically significant. The results of the analysis are presented in the form of equations. as well as the correlation coefficients (R) and determination coefficients (R^2). The results of the DSC analysis were also subjected to polynomial regression analysis in order to determine a useful model of the specific heat (SH) of elephant dung for 200–300 °C. The polynomial regression analysis was used because the torrefaction

process has a non-linear character. The results were presented in the form of an equation describing the dependence of the change of specific heat of elephant dung as a function of temperature. The general form of the polynomial used is in the form of Equation (10). Nine regression coefficients were used to provide a higher level of matching model to raw data.

$$SH = a_1 + a_2 \cdot T + a_3 \cdot T^2 + a_4 \cdot T^3 + a_5 \cdot T^4 + a_6 \cdot T^5 + a_7 \cdot T^6 + a_8 \cdot T^7 + a_9 \cdot T^8 \quad (10)$$

where:

SH—specific heat of elephant dung as a function of temperature, J·(kg·°C)$^{-1}$,
a_1—intercept,
a_2–a_9—regression coefficient,
T—torrefaction temperature, °C.

Nonlinear regression and evaluation of intercepts and regressions coefficients ($p < 0.05$) were completed with Statistica software (13.3, StatSoft, Palo Alto, CA, USA).

2.6.5. Statistical Analysis

An analysis of variance (ANOVA) evaluation of differences between mean values was performed with the application of post-hoc Tuckey's test, at the $p < 0.05$ significance level. For statistical data evaluation, the Statistica software (13.3, StatSoft, Palo Alto, CA, USA) was used.

3. Results

3.1. Result of the Torrefaction Process

The mass yields (MY) for elephant dung biocoals (Figure 3) showed a downward trend with the increase of process temperature. The highest mass yields values were obtained for biocoal generated at 200 °C and were above 90%. The lowest *MY* was for 300 °C, in this case, the mass yield decreased to 66%. All regression coefficients were statistically significant ($p < 0.05$) in the *MY* model, ($R^2 = 0.75$) (Table 1). Detailed *MY* data are shown in Table A2.

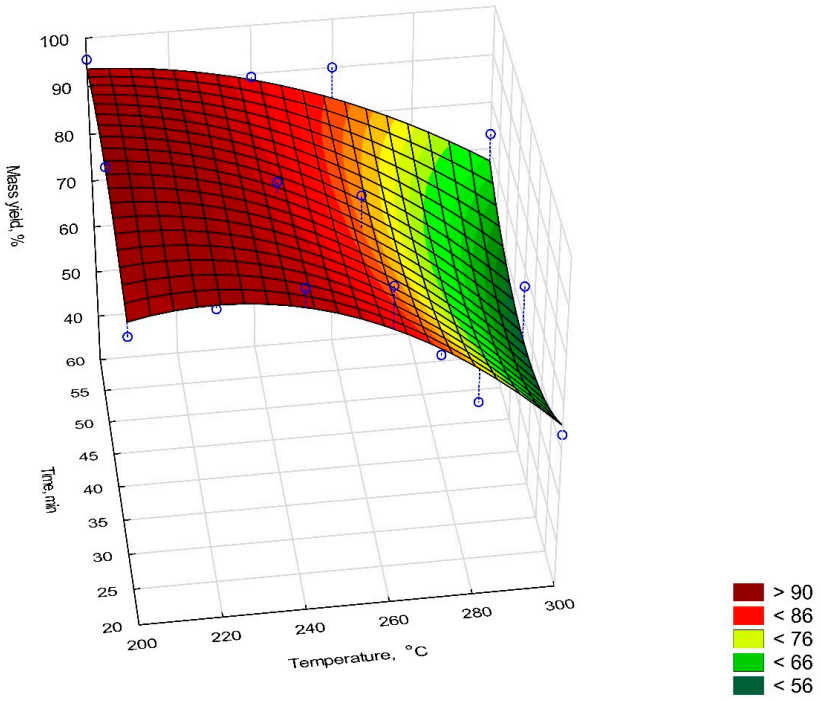

Figure 3. The influence of temperature and time on the mass yield of biocoal from elephant dung.

Table 1. Statistical evaluation of mass yield of biocoal from elephant dung.

Intercept/ Coefficient	Value of Intercept/ Coefficient	Standard Error	*p*	Lower Limit of Confidence	Upper Limit of Confidence
a_1	-2.58×10^2	2.18×10^2	0.00	-7.38×10^2	2.22×10^2
a_2	2.72×10^0	1.44×10^0	0.00	$-4.52 \times 10^{--1}$	5.89×10^0
a_3	-5.12×10^{-3}	2.39×10^{-3}	0.00	-1.04×10^{-2}	1.41×10^{-4}
a_4	6.91×10^0	6.19×10^0	0.00	-6.71×10^0	2.05×10^1
a_5	-4.22×10^{-2}	4.01×10^{-2}	0.00	-1.30×10^{-1}	4.61×10^{-2}
a_6	-3.01×10^{-2}	2.45×10^{-2}	0.00	-8.40×10^{-2}	2.38×10^{-2}
a_7	7.70×10^{-7}	0.00×10^0	0.00	7.70×10^{-7}	7.70×10^{-7}

$MY = a_1 + a_2 \cdot T + a_3 \cdot T^2 + a_4 \cdot t + a_5 \cdot t^2 + a_6 \cdot t + a_7 \cdot T^2 \cdot t$, $R^2 = 0.75$, R = 0.87; T* ranged from 200 °C to 300 °C, t* ranged from 20 min to 60 min; * more information in Section 2.2.

The energy yield (*EY*) of the biochar from elephant dung (Figure 4) also decreased with the increase of temperature and did not change with time. The biocoals produced at 200 °C resulted in more than 105% *EY* compared to raw material. However, the *EY* dropped below 68% for torrefaction at 300 °C. All regression coefficients were statistically significant ($p < 0.05$) for the *EY* model ($R^2 = 0.85$) (Table 2).

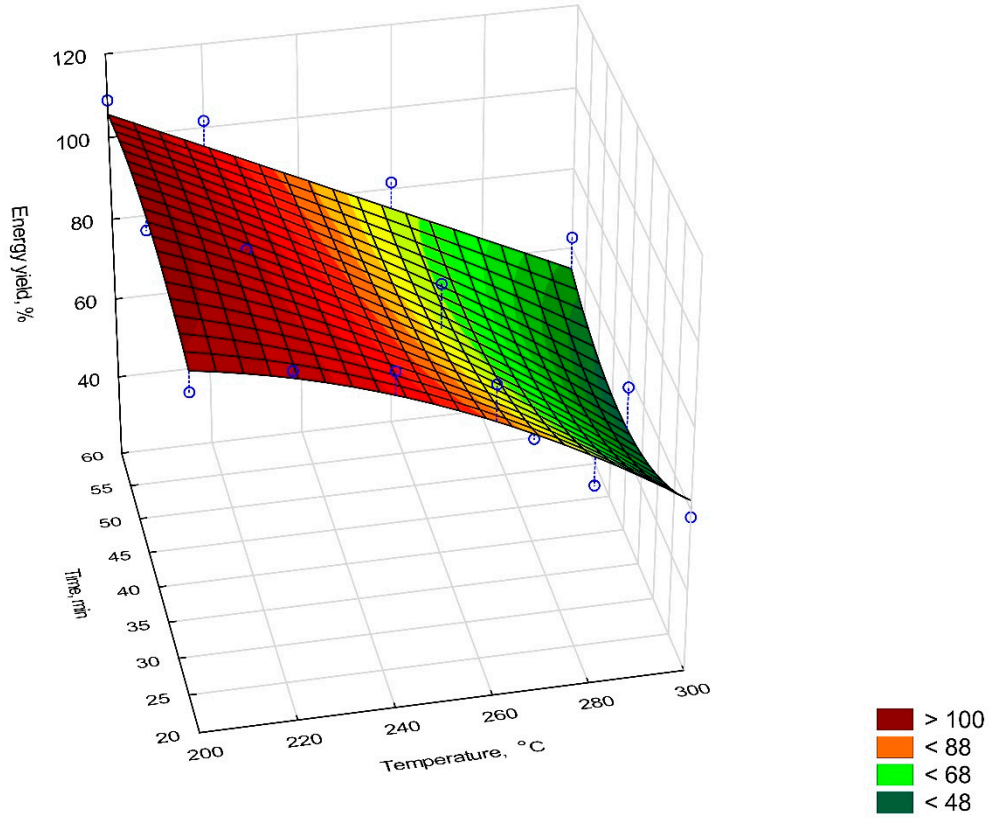

Figure 4. The influence of temperature and time on the energy yield in biocoal from elephant dung.

The energy densification ratio (*EDr*) in biocoals generated from elephant dung (Figure 5) decreased with increasing temperature and did not change much with time. Biocoals produced at 200 °C had the highest *EDr* of ~1.1, while biocoals generated at 300 °C had the lowest *EDr* (~0.9). All regression coefficients were statistically significant ($p < 0.05$) for the *EDr* model ($R^2 = 0.83$) (Table 3).

Table 2. Statistical evaluation of energy yield of biocoal from elephant dung.

Intercept/ Coefficient	Value of Intercept/ Coefficient	Standard Error	*p*	Lower Limit of Confidence	Upper Limit of Confidence
a_1	-1.19×10^2	2.48×10^2	0.00	-6.65×10^2	4.27×10^2
a_2	1.69×10^0	1.64×10^0	0.00	-1.91×10^0	5.30×10^0
a_3	-3.17×10^{-3}	2.72×10^{-3}	0.00	-9.16×10^{-3}	2.82×10^{-3}
a_4	8.26×10^0	7.04×10^0	0.00	-7.23×10^0	2.38×10^1
a_5	-4.74×10^{-2}	4.56×10^{-2}	0.00	-1.48×10^{-1}	5.30×10^{-2}
a_6	-3.65×10^{-2}	2.79×10^{-2}	0.00	-9.78×10^{-2}	2.48×10^{-2}
a_7	8.73×10^{-7}	0.00×10^0	0.00	8.73×10^{-7}	8.73×10^{-7}

$EY = a_1 + a_2 \cdot T + a_3 \cdot T^2 + a_4 \cdot t + a_5 \cdot t^2 + a_6 \cdot T \cdot t + a_7 \cdot T^2 \cdot t$, $R^2 = 0.85$, R = 0.92; T* ranged from 200 °C to 300 °C, t* ranged from 20 min to 60 min; * more information in Section 2.2.

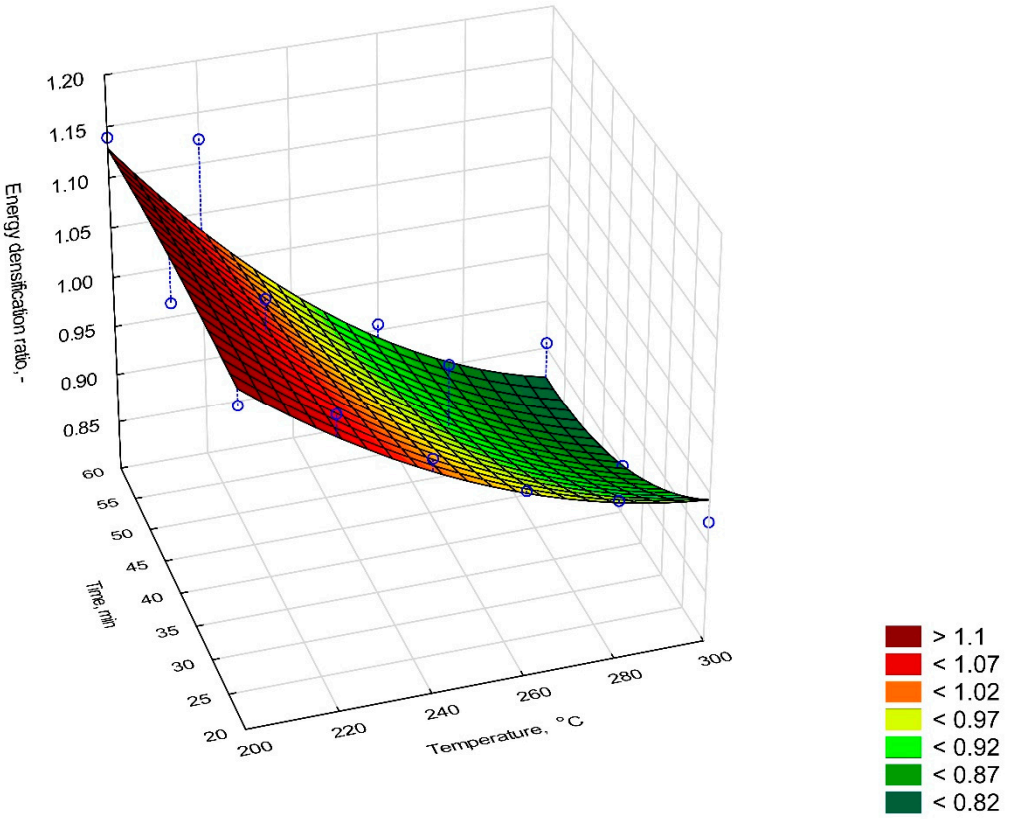

Figure 5. The influence of temperature and time on the energy densification ratio in biocoal from elephant dung.

Table 3. Statistical evaluation of energy densification ratio of biocoal from elephant dung.

Intercept/ Coefficient	Value of Intercept/ Coefficient	Standard Error	*p*	Lower Limit of Confidence	Upper Limit of Confidence
a_1	1.99×10^0	1.38×10^0	0.00	-1.05×10^0	5.04×10^0
a_2	-7.21×10^{-3}	9.14×10^{-3}	0.00	-2.73×10^{-2}	1.29×10^{-2}
a_3	1.41×10^{-5}	1.52×10^{-5}	0.00	-1.93×10^{-5}	4.75×10^{-5}
a_4	2.23×10^{-2}	3.93×10^{-2}	0.00	-6.41×10^{-2}	1.09×10^{-1}
a_5	-9.11×10^{-5}	2.54×10^{-4}	0.00	-6.51×10^{-4}	4.69×10^{-4}
a_6	-1.06×10^{-4}	1.55×10^4	0.00	-4.48×10^{-4}	2.36×10^{-4}
a_7	1.90×10^{-9}	0.00×10^0	0.00	1.90×10^{-9}	1.90×10^{-9}

$EDr = a_1 + a_2 \cdot T + a_3 \cdot T^2 + a \cdot t + a_5 \cdot t^2 + a_6 \cdot t + a_7 \cdot T^2 t$, $R^2 = 0.83$, R = 0.91; T* ranged from 200 °C to 300 °C, t* ranged from 20 min to 60 min; * more information in Section 2.2.

3.2. Result of Proximate Analysis of Raw and Torrefied Elephant Dung

The content of organic matter (*OM*) decreased as the temperature and the retention time increased. The lowest *OM* value was 28.26% for torrefaction at 280 °C and 60 min, and for torrefaction at 300 °C in time 20 min and 40 min (Figure 6, Table A1). Analysis of variance showed that statistically significant differences occur between the results obtained at 260 °C, 280 °C, and 300 °C, ($p < 0.05$) (Figure A1, Table A3). All regression coefficients were statistically significant ($p < 0.05$) for the *OM* model ($R^2 = 0.83$) (Table 4).

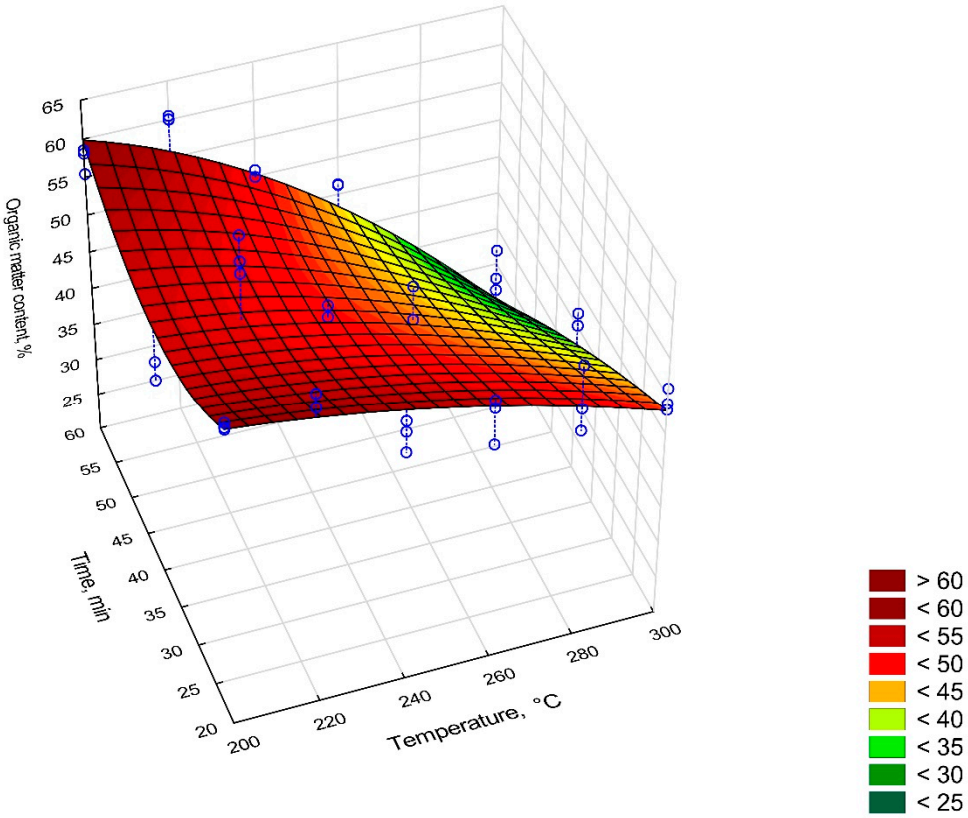

Figure 6. The influence of temperature and time on the organic matter content in biocoal from elephant dung.

Table 4. Statistical evaluation of organic matter content of biocoal from elephant dung.

Intercept/ Coefficient	Value of Intercept/ Coefficient	Standard Error	*p*	Lower Limit of Confidence	Upper Limit of Confidence
a_1	9.74×10^{1}	6.33×10^{1}	0.00	-3.00×10^{1}	2.25×10^{2}
a_2	1.24×10^{-2}	4.18×10^{-1}	0.00	-8.29×10^{-1}	8.54×10^{-1}
a_3	-4.95×10^{-4}	6.95×10^{-4}	0.00	-1.89×10^{-3}	9.03×10^{-4}
a_4	-3.25×10^{0}	1.80×10^{0}	0.00	-6.87×10^{0}	3.62×10^{-1}
a_5	3.20×10^{-2}	1.16×10^{-2}	0.00	8.53×10^{3}	5.54×10^{-2}
a_6	9.62×10^{-3}	7.11×10^{-3}	0.00	-4.69×10^{-3}	2.39×10^{-2}
a_7	-3.85×10^{-7}	0.00×10^{0}	0.00	-3.85×10^{-7}	-3.85×10^{7}

$OM = a_1 + a_2 \cdot T + a_3 \cdot T^2 + a_4 \cdot t + a_5 \cdot t^2 + a_6 \cdot T \cdot t + a_7 \cdot T^2 \cdot t$, $R^2 = 0.83$, $R = 0.91$; T^* ranged from 200 °C to 300 °C, t^* ranged from 20 min to 60 min; * more information in Section 2.2.

The ash content was inversely proportional to the *OM* content and increased to over 71% in comparison to 50.81% for raw dung (Table A1) in biocoal produced at 280 and 300 °C at 60 min (Figure 7). Analysis of variance showed statistically significant differences between the results for

temperatures 260 °C, 280 °C, and 300 °C ($p < 0.05$), (Figure A2, Table A4). All regression coefficients were statistically significant ($p < 0.05$) for the ash content model ($R^2 = 0.83$) (Table 5).

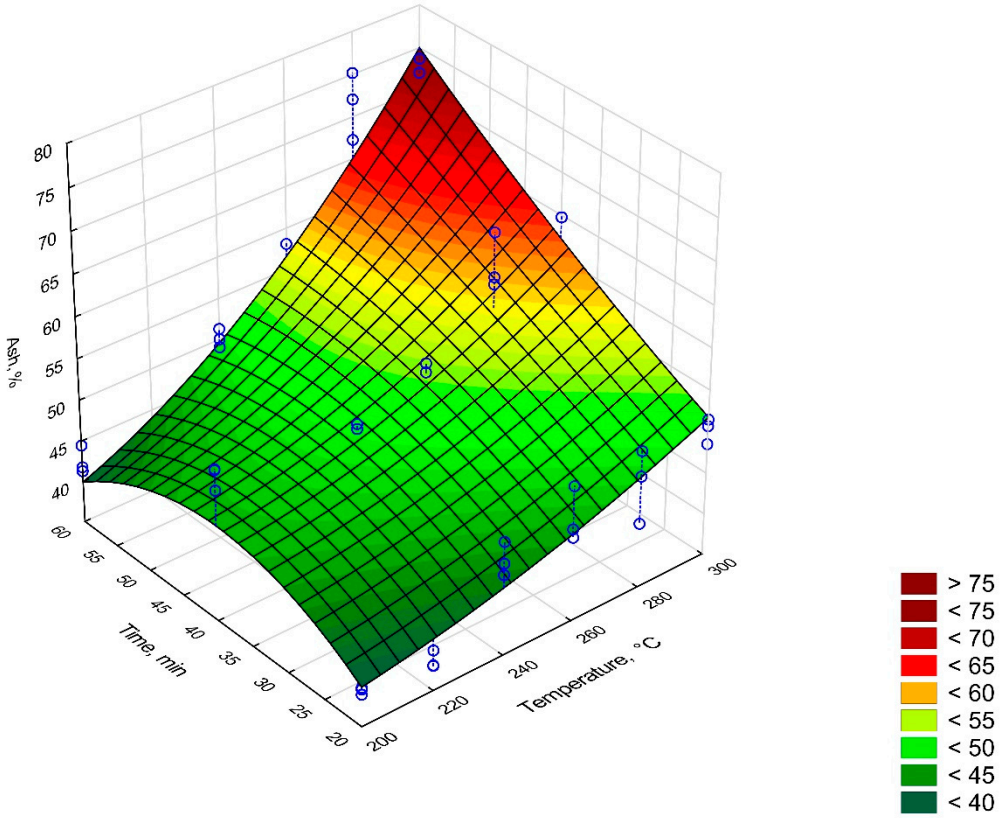

Figure 7. The influence of temperature and time on the ash content in biocoal from elephant dung.

Table 5. Statistical evaluation of ash content of biocoal from elephant dung.

Intercept/ Coefficient	Value of Intercept/ Coefficient	Standard Error	*p*	Lower Limit of Confidence	Upper Limit of Confidence
a_1	-2.82×10^{0}	6.34×10^{1}	0.00	-1.30×10^{2}	1.25×10^{2}
a_2	2.76×10^{-2}	4.19×10^{-1}	0.00	-8.15×10^{-1}	8.70×10^{-1}
a_3	4.22×10^{-4}	6.95×10^{-4}	0.00	-9.76×10^{-4}	1.82×10^{-3}
a_4	3.32×10^{0}	1.80×10^{0}	0.00	-3.01×10^{-1}	6.94×10^{0}
a_5	-3.24×10^{-2}	1.17×10^{-2}	0.00	-5.58×10^{-2}	-8.93×10^{-3}
a_6	-9.87×10^{-3}	7.12×10^{-3}	0.00	-2.42×10^{-2}	4.44×10^{-3}
a_7	3.91×10^{-7}	0.00×10^{0}	0.00	3.91×10^{-7}	3.91×10^{-7}

$Ash = a_1 + a_2 \cdot T + a_3 \cdot T^2 + a_4 \cdot t + a_5 \cdot t^2 + a_6 \cdot T \cdot t + a_7 \cdot T^2 \cdot t$, $R^2 = 0.83$, $R = 0.91$; T* ranged from 200 °C to 300 °C, t* ranged from 20 min to 60 min; * more information in Section 2.2.

The content of combustible parts (*CP*) decreased with time and the rise of the process temperature. Raw elephant dung had a *CP* = 48.9% (Table A1). During the torrefaction, the *CP* decreased to 28.6% at 60 min and 300 °C (Table A1, Figure 8). The analysis of variance showed numerous statistically significant differences, the majority of which occurred between 260 °C, 280 °C, and 300 °C (Table A5, Figure A3). All regression coefficients were statistically significant ($p < 0.05$) for the *CP* model ($R^2 = 0.67$) (Table 6).

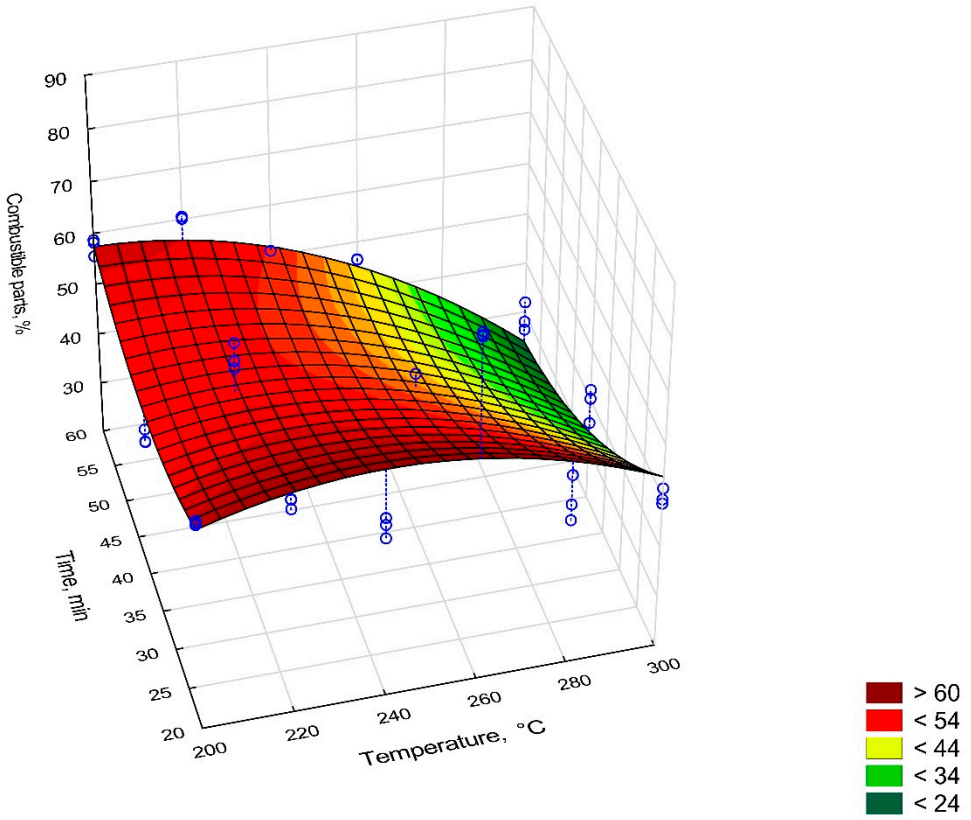

Figure 8. The influence of temperature and time on the combustible parts in biocoal from elephant dung.

Table 6. Statistical evaluation of ash content of biocoal from elephant dung.

Intercept/ Coefficient	Value of Intercept/ Coefficient	Standard Error	*p*	Lower Limit of Confidence	Upper Limit of Confidence
a_1	-1.19×10^2	1.14×10^2	0.00	-3.48×10^2	1.11×10^2
a_2	1.61×10^0	7.54×10^{-1}	0.00	9.02×10^{-2}	3.12×10^0
a_3	-3.10×10^{-3}	1.25×10^{-3}	0.00	-5.62×10^{-3}	-5.79×10^{-4}
a_4	-2.38×10^{-1}	3.24×10^0	0.00	-6.75×10^0	6.28×10^0
a_5	1.73×10^{-2}	2.10×10^{-2}	0.00	-2.49×10^{-2}	5.95×10^{-2}
a_6	-5.28×10^{-3}	1.28×10^{-2}	0.00	-3.11×10^{-2}	2.05×10^{-2}
a_7	-4.29×10^{-8}	0.00×10^0	0.00	-4.29×10^{-8}	-4.29×10^{-9}

$CP = a_1 + a_2 \cdot T + a_3 \cdot T^2 + a_4 \cdot t + a_5 \cdot t^2 + a_6 \cdot T \cdot t + a_7 \cdot T^2 \cdot t$, $R^2 = 0.67$, $R = 0.82$; T^* ranged from 200 °C to 300 °C, t^* ranged from 20 min to 60 min; * more information in Section 2.2.

The decrease in the *HHV* of the biocoals produced from the elephant dung was observed along with the increase of temperature and time (Figure 9, Table A1, Figure A4). The highest *HHV* was obtained for the biocoal generated at 200 °C and 60 min. A similar trend was discovered by Li et al., [33]. They explained this phenomenon by the effect of specific biocoal properties (pH; C, H, N, S, O content; specific surface area) and noticed also a possibility of predicting the biocoal yield of a group of feedstocks with similar physiochemical properties.

The average *HHV* was 13 MJ·kg^{-1} and was higher than the *HHV* of raw elephant dung (by 1.59 MJ·kg^{-1}) and higher than the lowest *HHV* for the biocoal obtained at 300 °C and 60 min (by 6.51 MJ·kg^{-1}). The *HHV* is affected by the high ash content in the biocoals and raw material. Thus, it was decided to estimate the value of *HHV* on an ash-free basis (HHV_{daf}). The highest average HHV_{daf} was obtained for the biocoal generated at 280 °C and for 60 min (27.20 MJ·kg^{-1}) (Figure 10, Table A1). Regression coefficients for the *HHV* and HHV_{daf} were statistically significant ($p < 0.05$), the proposed model worked well for *HHV* but was less representative for HHV_{daf} (R^2 were 0.74 and 0.21,

respectively) (Tables 7 and 8). Analysis of the variance of average values of *HHV* showed statistically significant differences between the results for 280 °C and 300 °C and 40 & 60 min ($p < 0.05$) (Figure A4, Table A6). This result has practical implications for the collection and initial processing of elephant dung to minimize mineral ash content and impurities and to maximize the *HHV*.

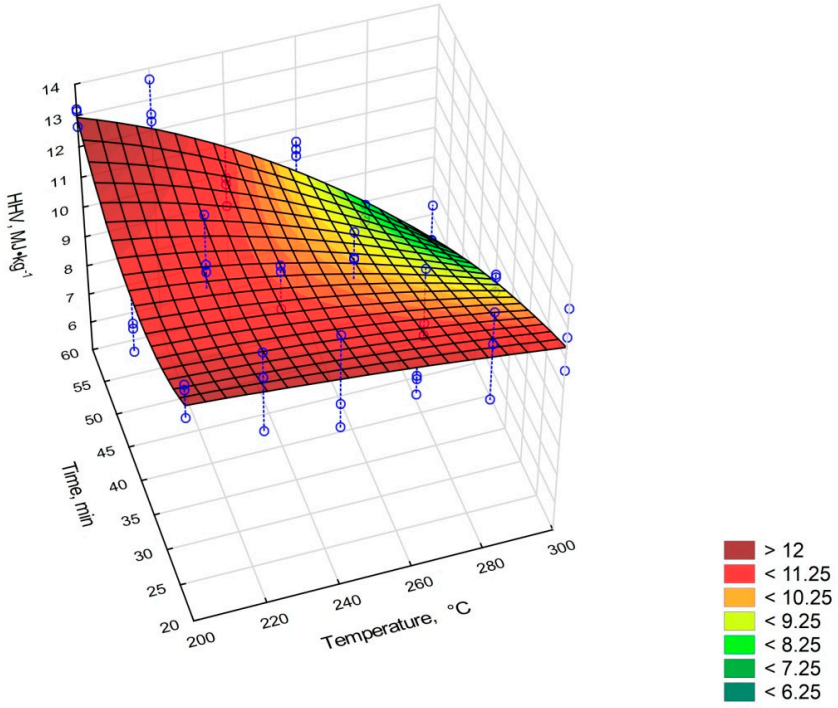

Figure 9. The influence of temperature and time on the high heating value *(HHV)* in biocoal from elephant dung.

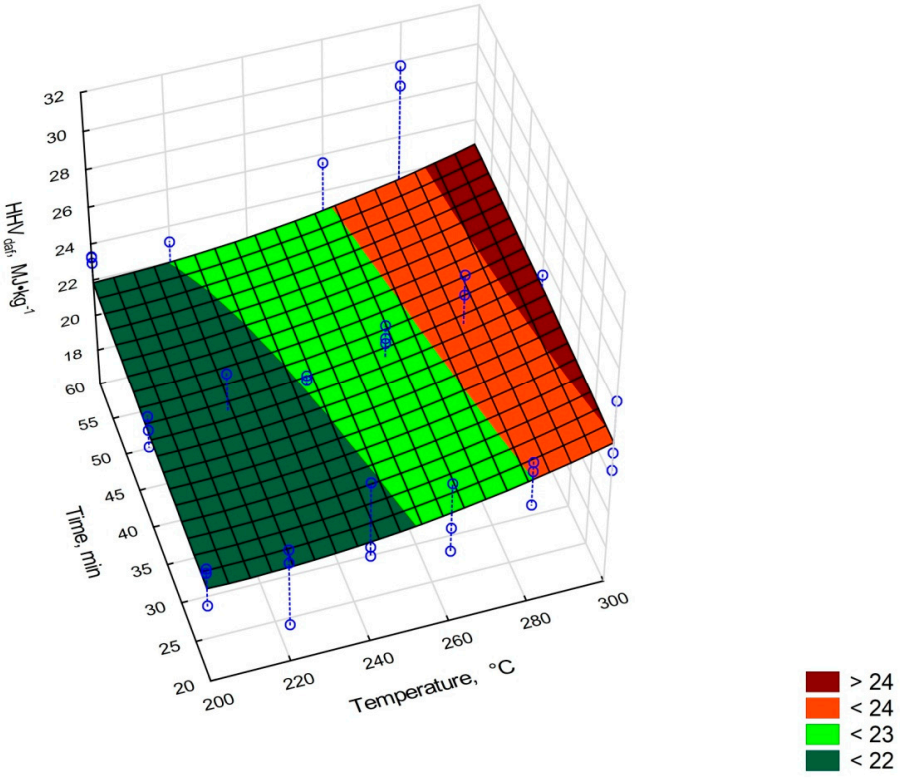

Figure 10. The influence of temperature and time on the HHV_{daf} in biocoal from elephant dung.

Table 7. Statistical evaluation of the high heating value of biocoal from elephant dung.

Intercept/ Coefficient	Value of Intercept/ Coefficient	Standard Error	*p*	Lower Limit of Confidence	Upper Limit of Confidence
a_1	2.25×10^{1}	1.50×10^{1}	0.00	-7.67×10^{0}	5.27×10^{1}
a_2	-3.04×10^{-2}	9.92×10^{-2}	0.00	-2.30×10^{-1}	1.69×10^{-1}
a_3	-2.45×10^{-6}	1.65×10^{-4}	0.00	-3.34×10^{-4}	3.29×10^{-4}
a_4	-6.30×10^{-1}	4.26×10^{-1}	0.00	-1.49×10^{0}	2.27×10^{-1}
a_5	6.68×10^{-3}	2.76×10^{-3}	0.00	1.12×10^{-3}	1.22×10^{-2}
a_6	1.84×10^{-3}	1.69×10^{-3}	0.00	-1.55×10^{-3}	5.23×10^{-3}
a_7	-8.13×10^{-8}	0.00×10^{0}	0.00	-8.13×10^{-8}	-8.13×10^{-8}

$HHV = a_1 + a_2 \cdot T + a_3 \cdot T^2 + a_4 \cdot t + a_5 \cdot t^2 + a_6 \cdot T \cdot t + a_7 \cdot T^2 \cdot t$, $R^2 = 0.74$, R = 0.86; T* ranged from 200 °C to 300 °C, t* ranged from 20 min to 60 min; * more information in Section 2.2.

Table 8. Statistical evaluation of high heating value on the dry ash-free basis of biocoal from elephant dung.

Intercept/ Coefficient	Value of Intercept/ Coefficient	Standard Error	*p*	Lower Limit of Confidence	Upper Limit of Confidence
a_1	3.54×10^{1}	2.99×10^{1}	0.00	-2.48×10^{1}	9.56×10^{1}
a_2	-1.28×10^{-1}	1.98×10^{-1}	0.00	-5.25×10^{-1}	2.70×10^{-1}
a_3	2.91×10^{-4}	3.28×10^{-4}	0.00	-3.69×10^{-4}	9.52×10^{-4}
a_4	-1.04×10^{-1}	8.49×10^{-1}	0.00	-1.81×10^{0}	1.60×10^{0}
a_5	6.68×10^{-4}	5.50×10^{-3}	0.00	-1.04×10^{-2}	1.17×10^{-2}
a_6	4.75×10^{-4}	3.36×10^{-3}	0.00	-6.29×10^{-3}	7.23×10^{-3}
a_7	-1.03×10^{-8}	0.00×10^{0}	0.00	-1.03×10^{-8}	-1.03×10^{-8}

$HHV_{daf} = a_1 + a_2 \cdot T + a_3 \cdot T^2 + a_4 \cdot t + a_5 \cdot t^2 + a_6 \cdot T \cdot t + a_7 \cdot T^2 \cdot t$, $R^2 = 0.21$, R = 0.45; T* ranged from 200 °C to 300 °C, t* ranged from 20min to 60 min; * more information in Section 2.2.

3.3. Result of the Thermogravimetric Analysis (TGA) of Elephant Dung

Table 9 summarizes kinetics parameters based on the TGA analyses and the mass loss data.

Table 9. The values of reaction rate constants and activation energy for elephant dung torrefaction.

T, °C	T^{-1}, °C^{-1}	k, s^{-1}	ln(k), s^{-1}	Ea, J·mol^{-1}
200	2.11×10^{-3}	1.16×10^{-5} a	−11.40	17,700
220	2.03×10^{-3}	1.24×10^{-5} a	−11.30	
240	1.95×10^{-3}	1.49×10^{-5} a	−11.10	
260	1.88×10^{-3}	1.50×10^{-5} a	−11.10	
280	1.81×10^{-3}	1.92×10^{-5} a,b	−10.90	
300	1.75×10^{-3}	2.73×10^{-5} b	−10.50	

a, *b*—letters present a lack of statistically significant differences between k values ($p < 0.05$).

The obtained values of k were analyzed by ANOVA, which showed that there were statistically significant differences ($p < 0.05$) for biocoal produced at 300 °C, and those obtained at 200 °C, 220 °C, 240 °C, and 260 °C, respectively. There were no statistical differences between k for 280 and 300 °C and k for 200–260 °C range. Kim et al. indicated that different optimal temperatures should be selected for different types of manure to maximize the energetic retention efficiency [34]. The energy yield of hydrochar (48.0–71.9%) is higher than that of pyrolysis char (31.5–52.4%), implying that the carbonization process, rather than the reaction temperature, is also a key factor that affects the energy yield of manure [35]. The TGA analysis showed the most substantial mass decrease in the first repetition to 54% of the initial mass of the sample, while in the second and third repetitions, the mass decreased to 64% and 62%. The loss of mass began at a temperature of ~300 °C, and it started to stabilize after exceeding ~600 °C (Figure 11).

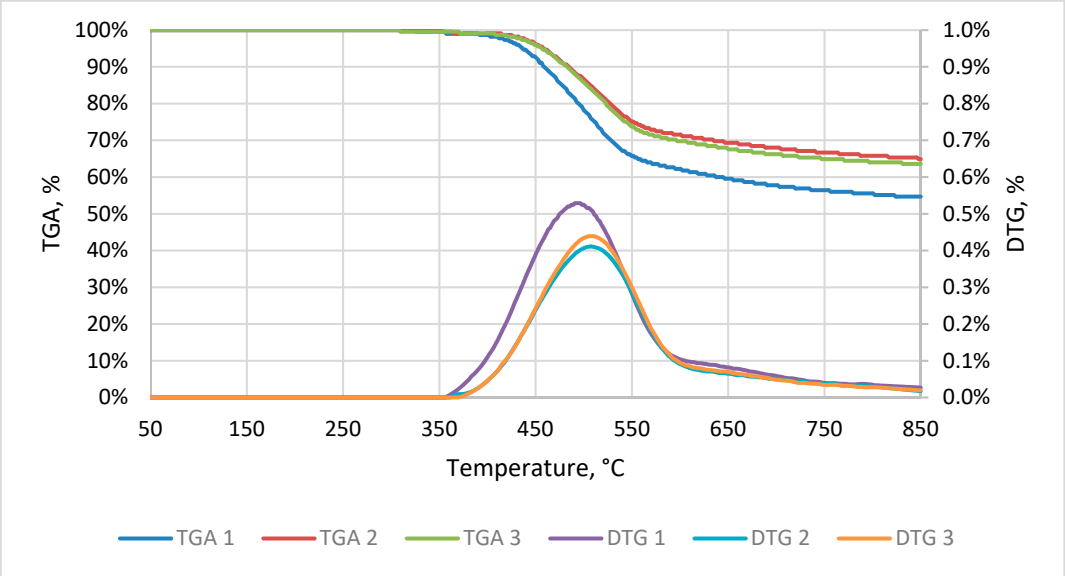

Figure 11. The thermogravimetric characteristic of elephant dung.

New knowledge on the substrates of elephant dung was gained from the TGA analyzes. There was a characteristic peak start at ~330 °C with a maximum at ~500 °C, most likely related to the decomposition of undigested (by elephant) cellulose and lignin from consumed biomass. The decomposition of cellulose and lignin takes place at 305–375 °C and 250–500 °C, respectively [36]. No degradation of hemicellulose was observed based on the DTG (derivative thermogravimetry) analysis. The decomposition of hemicellulose takes place at 225–325 °C [36]. However, the apparent lack of mass change in this temperature range (Figure 11) does not necessarily indicate a lack of hemicelluloses content. It is also likely that particular decompositions could be superimposed [36] and could not be detected by the lack of precision of the used thermogravimetric analyzer.

3.4. Differential Scanning Calorimetry (DSC) of Elephant Dung

DSC analysis showed that during heating, two endoenergetic transformations occurred (Figure 12).

At the beginning of the experiment, the energy was supplied to the sample to raise the temperature of the system. The first observation was that transformation began at 37 °C. Here, the energy was delivered to heat a sample and to initiate its transformation, which reached its maximum value at 80 °C and ended at 146 °C. The total energy demand for this first transformation was 66.17 $J \cdot g^{-1}$. After the first transformation ended, the energy needed only for heating the sample was supplied to the system (146–158 °C). The second transformation began at 158 °C, reached its maximum at 216 °C, and ended at 252 °C, requiring only 9.76 $J \cdot g^{-1}$. After the second transformation occurred, the energy required for heating decreased significantly. After T > 252 °C the exothermic reaction occurred.

The total energy demand for the whole process including heating and transformations of dry elephant dung was 485.37 $kJ \cdot kg^{-1}$ for the −20 to 300 °C range. The estimate for process energy demand calculated by model for torrefaction [30] decreased to 484.81 $kJ \cdot kg^{-1,}$ and it was due to mass loss during the process. In addition, the heating and evaporation of the water contained in raw elephant dung (moisture content 49.19%), results in the additional 1275.49 $kJ \cdot kg^{-1}$ (Equation (8)) energy demand. Thus, the total energy demand for processing of raw elephant dung (heating, moisture evaporation, and torrefaction) is 1760.30 $kJ \cdot kg^{-1}$.

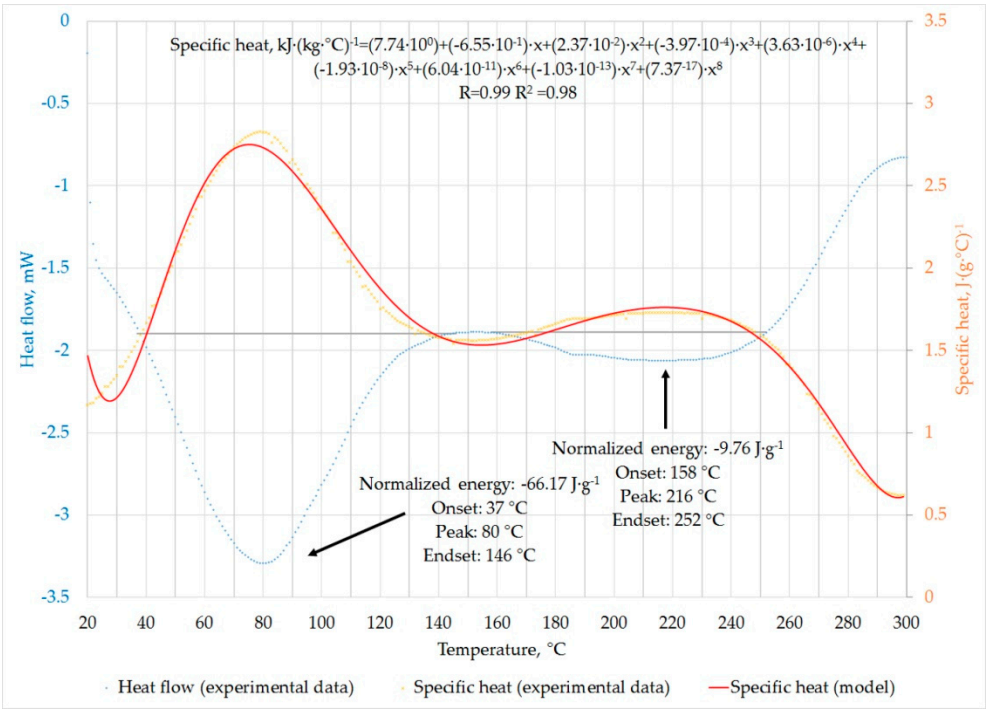

Figure 12. The differential scanning calorimetry (DSC) characteristic of elephant dung.

4. Discussion

4.1. The Impact of Technological Parameters on the Efficiency of the Process

A related torrefaction study carried out on cow manure showed that the *MY* of torrefaction decreased with the increase of the process temperature [37], similar to the finding in this research. The torrefied elephant dung (200–300 °C at 40 min) had the *MY* of 100–68%, whereas it was 90–55% for cow manure at the same process conditions [37]. Differences in *MY* could be explained by a greater decomposition of biodegradable substrates at lower temperatures. Also, elephant dung had higher moisture and *OM* content compared with the cow manure. In addition, it has been reported that it is possible to change specific surface area (SSA) as a result of morphological changes due to thermal condensation, and it could be exploited in different materials [38]. The energy yield of torrefaction of cow manure decreased from around 92% at 200 °C to approximately 57% at 300 °C, whereas elephant dung were of 110% and 60%, respectively. The *EDr* ratio for cow manure had the same downtrend as elephant dung [37]. It was also noticed that there are different degradation processes in the studied range of 200–300 °C. Lignocellulose degradation occurs at approximately 120 °C; hemicellulose degradation occurs at 200–260 °C; cellulose degradation occurs at 240–350 °C; while lignin degradation occurs at 280–350 °C [39], which due to the observation of narrow temperature ranges could have affected the lack of a decrease or increase trend in the case of obtained moisture and *MY*.

4.2. Proximate Analyses of Elephant Dung and Biocoals

The average moisture content in the elephant dung was 49.19%. The moisture content of dung depends on the amount of water consumed by the animal. For example, pig manure could have a moisture content of ~35–82%, whereas cow manure is of ~66–97% [40–42]. In the case of poultry manure, moisture content ranges from ~5 to 40% [40]. The *OM* content in the studied elephant dung was 48.09% (d.m.). For comparison, the *OM* content for Indian elephant and rhinoceros were 52% and 56%, respectively [43]. For yet another case of the cattle manure, an *OM* content was ~74% [44].

These *OMs* are much lower than those reported in related torrefaction studies for pruned biomass of Paulownia (90%) [45], or brewery spent grain (96%) [46].

The elephant dung had a higher ash content (50.81%, d.m.) than the maximum content of ash in pig manure (21.4% d.m.), cow manure (32.8% d.m.) and chicken manure (34% d.m.) [40,47]. The *HHV* of elephant dung was 11.41 MJ·kg^{-1} and was lower than *HHV* in chicken manure (13 MJ·kg^{-1}), cow manure (12.7–17.2 MJ·kg^{-1}), or pig manure (18.1–19.5 MJ·kg^{-1}) [37,40,41,48]. The low value of *HHV* is likely caused by high ash content, i.e., the calculated ash-free *HHV* was as high as 23 MJ·kg^{-1}.

The *HHV* of the torrefied dung was not much higher than the raw sample (Table A1). For biocoal, the highest *HHV* was 13 MJ·kg^{-1} (260 °C, 60 min), and a further increase in temperature and time caused a decrease in its value. The low increase of *HHV* in comparison to the raw base for cow dung was reported by Pahla et al. [37] and *HHV* increased from 16.78 to 18.64 MJ·kg^{-1} (at 300 °C). A small increase of *HHV* in dung biocoal is directly affected by a low amount of fixed carbon (high amount of ash content). During torrefaction, fixed carbon is enhanced by thermal degradation of hemicellulose and part of cellulose and lignin [49]. The decomposition of these constituents results in releases of compounds with low energy content, leaving organic compounds with higher energy content [50]. Cow manure, similarly to elephant dung did not experience high *HHV* enhancement likely because it had less *OM* and more ash content. Pulka et al. [28] tested sewage sludge via torrefaction and met the same problem—the highest value of *HHV* for biocoal generated at 260 °C, 60 min, and further temperature increase decreased *HHV*. Therefore, it may be assumed that at a temperature > 260 and time > 60 min, some organic components from elephant dung and sewage sludge start to decompose and release volatiles with higher energy content.

There was no observed relationship between the moisture content and the process temperature and time for the biocoals from elephant dung. This is likely because dry material was used for the torrefaction process. Small differences in the moisture content of biocoals can result from the time between their generation and the determination of the moisture content experiment. Stored biocoals can adsorb moisture (e.g., from the air), making biomass-derived fuels less advantageous compared with coal [50].

There was a sharp drop in the *OM* and the simultaneous increase in ash content for torrefaction above 260 °C. This also caused a decrease of *HHV* and an increase in the $HHV_{daf,}$ especially in the biocoals produced at 260 °C and 300 °C. A practical implication is that the torrefaction process conducted at temperatures from 200 °C to 260 °C (regardless of time) will have a small impact on the decrease of *HHV* of biocoals.

Furthermore, it could be recommended that torrefaction at 200 °C for 20 min (lowest temperature and shortest time) is needed for the maximization of the *HHV* and minimization of the cost of the torrefaction process. In addition, a lack of significant differences ($p < 0.05$) in 200–260 °C allows us to use torrefaction of elephant dung as a low-tech technology, i.e., one that can be controlled without an accurate measurement system. It is especially important for rural areas. Also, during torrefaction of a more substantial amount of the dung, it would be challenging to evenly heat and then cool down fast all the processed material. However, based on the apparent lack of effect in this research, the risk of generating substandard biocoals appears to be relatively low.

The highest HHV_{daf} value (27.2·MJ·kg^{-1}) was observed for 280 °C, 60 min (Table A1). This value is theoretical, and it is worth considering ways of reducing the ash content in the elephant dung, because it may have a high energetic potential after processing. Considering ash-free elephant dung after torrefaction, it is possible to obtain better solid fuel than commercially-available pellets. For example, pellets made from pine sawdust, wheat straw, corn settlements, agricultural residues have *HHV* of 19.5, 17.5, 18.8, 18.1 MJ·kg^{-1}, (HHV_{daf} 19,6, 19.0, 19.0, 19.8 MJ·kg^{-1}) (Table A8) respectively [51]. These values are still relatively low when compared to ash-free biocoal from elephant dung of 27.2 MJ·kg^{-1}.

The ash in elephant dung is derived from two primary sources, (1) ash introduced during collecting, transporting, storing, and processing, (2) biogenic ash inside plant tissue consumed by an elephant. The sum of these sources is referred to as ash content. Biogenic ash could be removed from biomass

using air separation. For woody pine forest residue, air separation costs ~2.23 $\$\cdot Mg^{-1}$ of biomass to reduce 40% of total biogenic ash to <7% of total biomass [52]. Ash could also be removed from biomass cells via chemical pre-processing that solubilize it. Here, knowledge of the exact morphology and chemical state of the ash is needed to determine the most effective removal methods [52]. From a practical point of view, elephant dung should be collected with the least soil impurities as possible. Next, during transportation, drying, etc. the dung should not be exposed to dust. If prevention is not enough, air separation could be considered, due to its relatively low operational cost. Nevertheless, dung morphology is important factor for air separation. Dung is much more brittle and lighter than wood. Because of this, chipped particles of dung could be lighter than mineral impurities causing the different share of ash in particular fractions than in the case of wood. Although some chemical pre-processing technologies have a high level of ash removal (over 90% removal of alkaline earth and alkali metals) [52], their technological infrastructure and cost would be difficult to adopt in underserved areas.

Another important aspect is the issues related to the supply chain, which may influence the quality of biocoal and efficiency of the process. The collection of elephant dung has a dispersed character with a random accumulation ratio in one specific localization, especially when elephants live in natural habitats. The dung usually is collected directly from the ground, which may increase the ash content. However, when dung is exposed to climatic conditions (especially to wind and sun), the overall effect might be beneficial to drying, which brings benefits related to transportation and torrefaction efficiency. Pre-dried material is more suitable for collection, transportation (less water to be transported), and is less prone to decay. In the case of breeding of elephants or using them as work animals (as practiced in South-East Asia), the accumulation of dung in one specific area is more likely. Natural drying maybe not be sufficient. Therefore, one solution could be pre-drying in the dedicated dryer, which could use a warm air stream for water removal. Solar energy could be used as a heat source. Such solution could solve several practical problems: i) the long-range transport of untreated and wet dung to processing sites that is energy inefficient, while a significant portion of the transportation costs are being used to transport water [5]; ii) the long-term storage of raw biomass can be problematic and impractical because the piled biomass can decompose over time resulting in the decrease of useful *HHV* [7].

4.3. Thermogravimetric Analysis of Raw Material and Kinetic Parameters of Torrefaction

Reported TGA analyses of elephant dung are the first of their kind in the literature. A comparison of kinetic parameters with the literature is then confounded because of the variety of determination methods used for other materials. For this reason, we discuss the kinetics of a subset of the most common and related substrates. We considered the elephant diet consisting mostly of grasses, and the activation energy for some grass plants is available. The activation energy of wheat straw and sorghum determined for the 250–450 °C range was 176 $kJ\cdot mol^{-1}$ and $kJ\cdot mol^{-1}$, respectively [53]. For comparison, lignocellulose materials (eg., woody biomass) have an E_a of 103–165 $kJ\cdot mol^{-1}$ [54,55]. The values presented in this paper were obtained for non-isothermal conditions and pyrolysis temperature range.

In this work, the E_a and the reaction rate constants were determined in isothermal conditions and a temperature range of 200–300 °C. The same conditions and temperatures were used previously by Pulka et al. [56], who tested sewage sludge (SS) with high ash content, and Syguła et al. [57] who tested spent mushroom compost (MSC). The E_a for torrefaction process of elephant dung was 18 $kJ\cdot mol^{-1}$, and k values were increasing with process temperature from $1.16 \times 10^{-5}\cdot s^{-1}$ to $2.73 \times 10^{-5}\cdot s^{-1}$ (from 200 to 300 °C), respectively. In the case of SS, the E_a was 12 $kJ\cdot mol^{-1}$, and the k value increased from $4.02 \times 10^{-5}\cdot s^{-1}$ to $6.71 \times 10^{-5}\cdot s^{-1}$ (from 200 to 300 °C), respectively [56]. In the case of MSC, the E_a was 22.2 $kJ\cdot mol^{-1}$, and the k value increased from $1.7 \times 10^{-5}\cdot s^{-1}$ to $4.6 \times 10^{-5}\cdot s^{-1}$ (from 200 to 300 °C), respectively [57]. Differences could be a result of biomass origin, and organic matter content. *OM* in SS was 56% d.m. [56], 76% d.m. in MSC [57], and 50% d.m. in elephant dung—Table A1).

It should also be noted that the greatest E_a was determined for MSC, which had the highest *OM* content, and much smaller during the torrefaction of elephant dung and SS, where *OM* contents were

lower by ~20%. An opposite trend was observed in the case of the *k* value, which was the highest during the torrefaction of SS, followed by MSC and elephant dung. This may indicate that the content of *OM* is one of the critical drivers of the waste's kinetic properties, such as the *Ea* and possibly *k*.

4.4. Differential Scanning Calorimetry of Raw Material

DSC analysis showed that two endothermic reactions (37–146 °C and 158–252 °C) and one exothermic reaction (252–300 °C) occur during the torrefaction process (Figure 12). The first transformation observed on DSC plot may be attributed to water evaporation. Interestingly, the elephant dung was dried at 105 °C before the DSC test. Thus, the presence of water in a previously dried sample could be due to the hygroscopicity (the sample absorbed some water from the atmosphere before the test; i.e., biocoals are known to be affected by this phenomenon) [58]. The first transformation ended above drying temperature (105 °C), so it is probably associated with bound water evaporation. The nature of the second endothermic transformation is unknown. To our knowledge, there are no DSC data of elephant dung to compare. This transformation may be related to residue hemicellulose degradation. Degradation of hemicellulose takes place at a lower temperature range (225–325 °C) than the degradation of cellulose (305–375 °C) [36]. After the second endothermic transformation ended, the heat flow starts to decrease, which is related to an exothermic reaction (253–300 °C). This exothermic reaction corresponds to mass loss observed on TG/DTG plot observed at the beginning of the process (Figure 11). Interestingly, neither of the endothermic reactions were apparerent in the TG/DTG plot (Figure 11). This might be a result of insufficient precision in the use of the laboratory balance, or due to transformations that were not related to mass loss. In general, endothermal reactions are related to depolymerization and volatilization process, whereas exothermic transformations are due to the charring process [59] phenomenon, the DSC plot shows that the elephant dung torrefaction is an (overall) endothermic process and it requires energy delivery. Some energy cost savings might be realized by using the torrefied elephant dung as a fuel for the torrefaction process (Figure 1).

High ash content 50.81% (Table A1) is not without significance. It makes measurements of TGA and DSC less accurate because smaller mass loses in organic compounds were measured. In the case of DSC, the endothermic reactions of <200 °C that were found could also be associated with water evaporation from components of ash such as chlorine and potassium [60]. The growth of the mineral fraction lowers the activation energy of the pyrolysis reaction, and accelerates exothermic thermochemical conversion reactions [61].

5. Conclusions

Initial valorization of elephant dung by torrefaction is proposed as a possible low-tech fuel production in rural areas with abundant supply. Proposed valorization could be used in households for cooking and heating. These studies have expanded knowledge on the possibilities of torrefaction of elephant dung and provided practical knowledge about the fuel properties of torrefied elephant dung, as high heating value, combustible parts, ash content, and organic matter content. Based on the results, models of torrefaction of elephant dung with kinetics parameter evaluation have been proposed. The following conclusions arise from this research:

- Torrefaction improves the higher heating value of elephant dung. The torrefied elephant dung has an HHV = 13 MJ·kg^{-1} compared to the HHV = 11.41 MJ·kg^{-1} for unprocessed dung.
- Minimal process controls appear to be needed, and thus, scaling the torrefaction up to larger batches of dung is feasible, but due to lack of data, these options need more tests on a technical scale. Biocoals with similar quality are obtained for 200 °C to 260 °C range regardless of the duration of the process (20 to 60 min).
- The recommended temperature of the torrefaction for elephant dung is 200 °C, due to the lack of significant improvements in fuel properties with increasing process temperature.

- The activation energy for torrefaction of elephant dung at 200~300 °C was 17.7 J·mol$^{-1,}$ and the reaction rate constant increased from 1.16×10^{-5}·s^{-1} to 2.73×10^{-5}·s^{-1}.
- The total energy needed to heat the dry elephant dung from 20 °C to 300 °C was approximately 485 kJ·kg^{-1} (obtained in laboratory conditions), and 484.81 kJ·kg^{-1} (obtained from calculations) after the mass loss during the process is factored in. The total energy demand for drying and torrefaction was the total amount of energy for processing (heating, moisture evaporation, and torrefaction) was 1760.30 kJ·kg^{-1}.

This research has shown that there is a potential in using elephant dung as a substrate for torrefaction and its valorization as an improved fuel source. The next step should be to identify the technological parameters for the torrefaction of elephant dung. This is important for investment analysis and technology design, particularly in rural areas.

Author Contributions: Conceptualization, P.S., M.H. and K.Ś.; methodology, M.H.; software, P.S., S.K., and K.Ś.; validation, P.S., K.Ś., and M.H.; formal analysis, M.H.; investigation, M.H. and S.K.; resources, M.H. and A.B.; data curation, P.S., K.Ś., A.B. and J.A.K.; writing—original draft preparation, P.S., M.H. and K.Ś.; writing—review and editing, P.S., K.Ś., S.S.-D., J.A.K.; visualization, P.S. and K.Ś.; supervision, A.B., J.A.K., and P.M.; project administration, P.S.; funding acquisition, P.S., A.B., and J.A.K.

Funding: The research was funded by the Polish Ministry of Science and Higher Education (2015–2019), the Diamond Grant program # 0077/DIA/2015/14. "The PROM Programme - International scholarship exchange of Ph.D. candidates and academic staff" is co-financed by the European Social Fund under the Knowledge Education Development Operational Programme PPI/PRO/2018/1/00004/U/001. The authors would like to thank the Fulbright Foundation for funding the project titled "Research on pollutants emission from Carbonized Refuse Derived Fuel into the environment", completed at Iowa State University. In addition, this project was partially supported by the Iowa Agriculture and Home Economics Experiment Station, Ames, Iowa. Project no. IOW05556 (Future Challenges in Animal Production Systems: Seeking Solutions through Focused Facilitation) sponsored by Hatch Act and State of Iowa funds.

Conflicts of Interest: The authors declare no conflict of interest.

Appendix A

Table A1. Summary of proximate analysis of the tested elephant dung and biocoals resulting from its torrefaction.

Sample		Moisture, %	Organic Matter Content, %	Ash, %	*HHV*, MJ·kg^{-1}	HHV_{daf}, MJ·kg^{-1}
Elephant dung		49.19 ± 5.84	48.90 ± 5.79	50.81 ± 5.84	11.41 ± 1.34	23.18 ± 2.39
200 °C	20 min	3.33 ± 0.08	60.44 ± 0.46	39.37 ± 0.44	12.75 ± 0.58	21.75 ± 1.15
	40 min	1.14 ± 0.02	47.50 ± 1.42	52.40 ± 1.42	10.14 ± 0.51	21.56 ± 0.87
	60 min	2.35 ± 0.08	57.35 ± 1.69	42.51 ± 1.70	13.00 ± 0.31	23.16 ± 0.19
220 °C	20 min	2.11 ± 0.15	61.23 ± 1.04	38.65 ± 1.05	12.47 ± 1.31	20.77 ± 2.30
	40 min	2.15 ± 0.05	60.22 ± 2.52	39.77 ± 2.50	12.34 ± 1.01	21.00 ± 2.48
	60 min	1.90 ± 0.06	60.21 ± 0.27	39.76 ± 0.24	12.82 ± 0.72	21.70 ± 1.24
240 °C	20 min	2.11 ± 0.12	53.57 ± 2.09	46.50 ± 2.01	11.80 ± 1.56	22.48 ± 2.24
	40 min	1.03 ± 0.04	49.91 ± 1.12	50.03 ± 1.08	10.74 ± 0.79	21.71 ± 1.27
	60 min	0.96 ± 0.05	49.79 ± 1.11	50.11 ± 1.13	9.51 ± 0.50	19.24 ± 0.59
260 °C	20 min	3.20 ± 0.06	52.96 ± 3.14	47.52 ± 3.30	11.39 ± 0.33	21.79 ±1.93
	40 min	0.88 ± 0.10	47.63 ± 2.92	52.24 ± 2.97	11.25 ± 0.50	23.77 ± 0.51
	60 min	1.07 ± 0.04	44.82 ± 2.58	55.07 ± 2.62	10.34 ± 0.24	23.33 ± 1.93
280 °C	20 min	2.23 ± 0.15	52.21 ± 4.41	47.60 ± 4.45	11.80 ± 1.45	23.00 ± 1.25
	40 min	2.85 ± 0.26	37.23 ± 3.26	62.59 ± 3.31	8.66 ± 1.22	23.87 ± 2.92
	60 min	1.64 ± 0.26	28.26 ± 3.97	71.48 ± 3.99	7.54 ± 0.32	27.20 ± 3.57
300 °C	20 min	2.61 ± 0.25	49.47 ± 1.47	50.21 ± 1.53	11.64 ± 1.02	24.01 ± 1.99
	40 min	1.99 ± 0.26	39.09 ± 3.47	60.89 ± 3.46	9.05 ± 0.32	23.69 ± 1.25
	60 min	1.24 ± 0.14	28.66 ± 2.92	71.25 ± 2.92	6.49 ± 0.71	22.86 ± 0.79

Table A2. Values of mass yield, energy yield, and energy densification ratio for biocoals.

Sample		Mass Yield, %	Energy Yield, %	Energy Densification Ratio, %
200 °C	20 min	91.42	102.11	1.12
	40 min	98.65	107.78	1.09
	60 min	95.59	108.91	1.13
220 °C	20 min	95.43	104.25	1.09
	40 min	93.16	100.74	1.08
	60 min	90.43	101.62	1.12
240 °C	20 min	98.12	101.43	1.03
	40 min	92.78	87.33	0.94
	60 min	89.36	74.46	0.83
260 °C	20 min	97.07	95.66	0.99
	40 min	88.63	87.34	0.99
	60 min	90.01	81.55	0.90
280 °C	20 min	71.83	68.89	0.96
	40 min	53.21	46.29	0.87
	60 min	63.33	51.59	0.81
300 °C	20 min	63.28	58.28	0.92
	40 min	66.58	56.50	0.85
	60 min	73.18	62.58	0.86

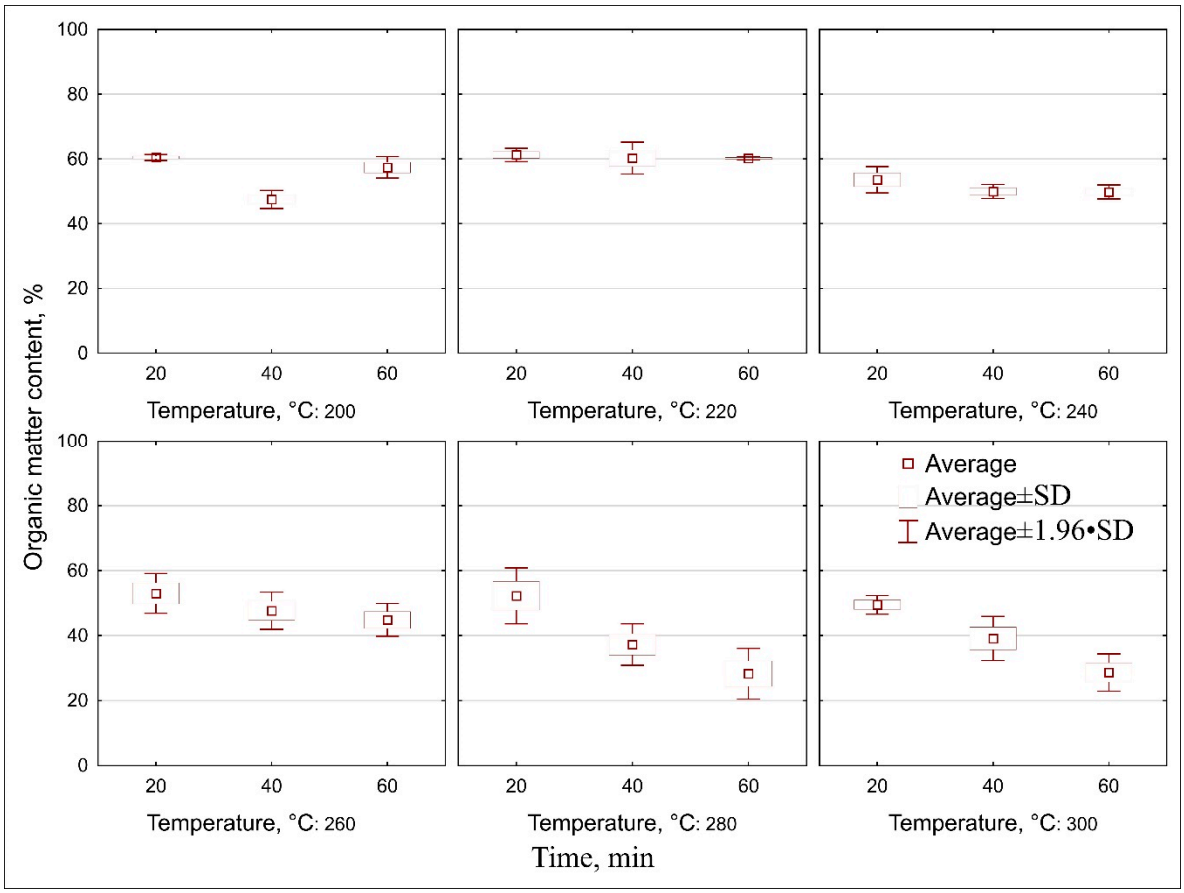

Figure A1. Presentation of differences in individual groups (of torrefaction time) for organic matter content in biocoals from elephant dung.

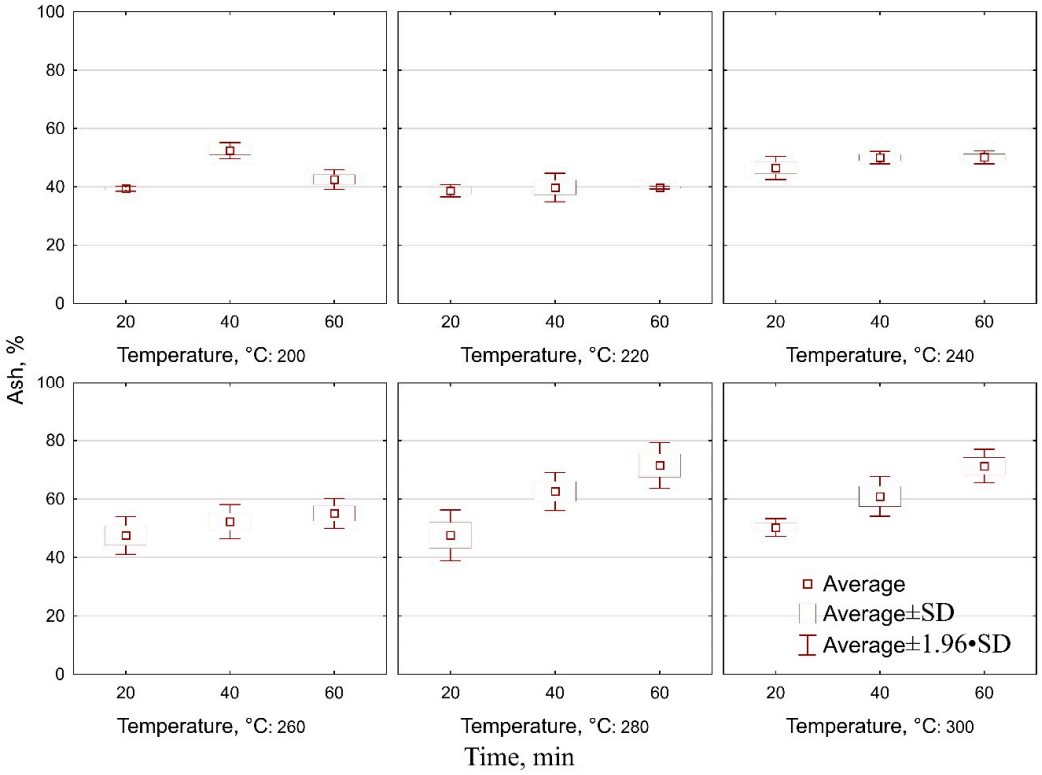

Figure A2. Presentation of differences in individual groups (of torrefaction time) for ash content in biocoals from elephant dung.

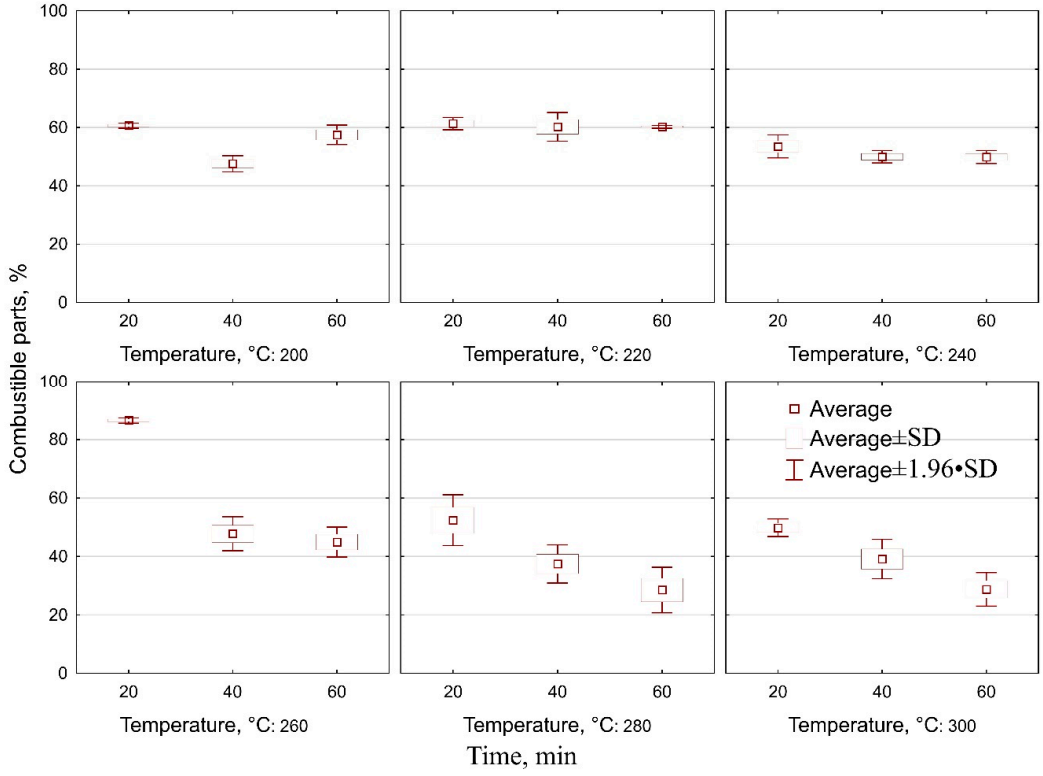

Figure A3. Presentation of differences in individual groups (of torrefaction time) for combustible parts in biocoals from elephant dung.

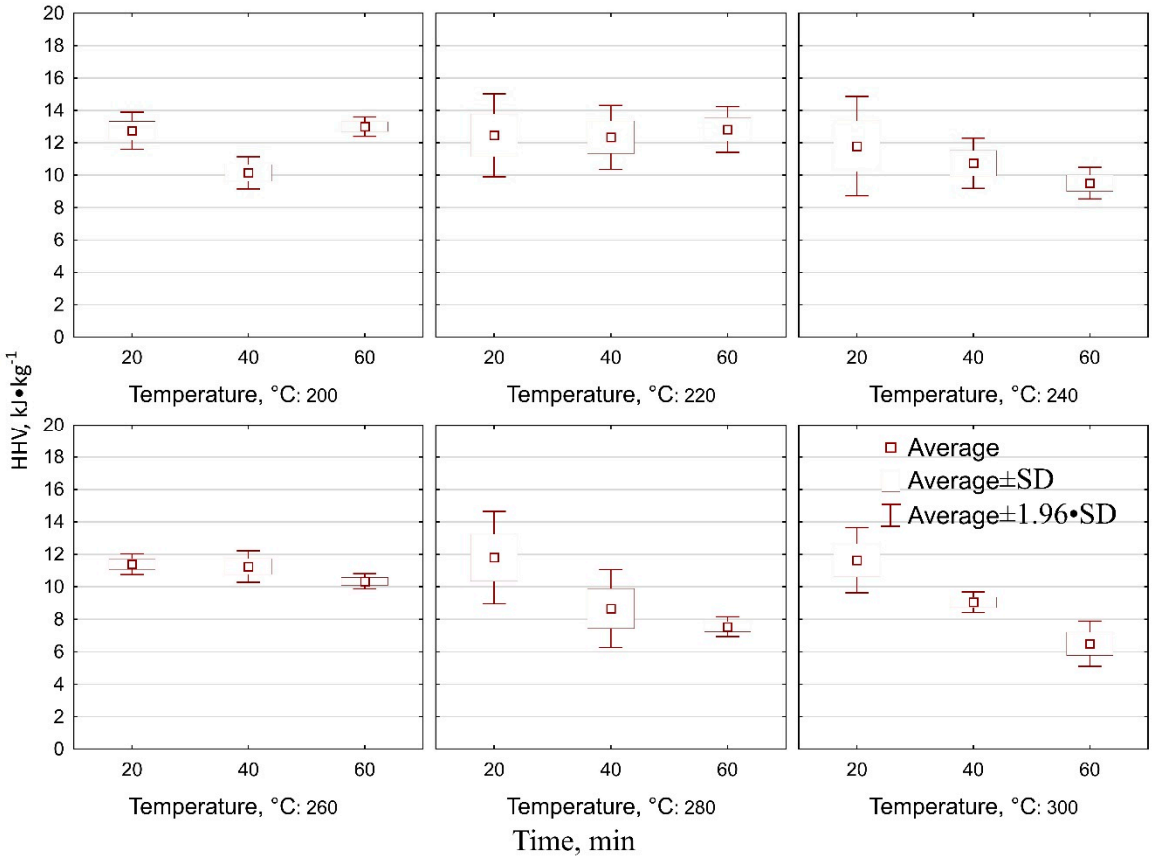

Figure A4. Presentation of differences in individual groups (of torrefaction time) for the high heating value of biocoals from elephant dung.

Table A3. Analysis of variance for organic matter (*OM*) content.

Tukey Test for *OM*; a Bold Font Signifies Statistically Significant Difference ($p < 0.05$)		**200**	**200**	**200**	**220**	**220**	**220**	**240**	**240**	**240**	**260**	**260**	**260**	**280**	**280**	**280**	**300**	**300**	**300**
		20	**40**	**60**	**20**	**40**	**60**	**20**	**40**	**60**	**20**	**40**	**60**	**20**	**40**	**60**	**20**	**40**	**60**
200	20		**0.00**	0.98	1.00	1.00	1.00	0.12	**0.00**	**0.00**	0.06	**0.00**	**0.00**	**0.03**	**0.00**	**0.00**	**0.00**	**0.00**	**0.00**
200	40	**0.00**		**0.00**	**0.00**	**0.00**	**0.00**	0.27	1.00	1.00	0.43	1.00	1.00	0.68	**0.00**	**0.00**	1.00	**0.02**	**0.00**
200	60	0.98	**0.00**		0.90	0.99	0.99	0.91	0.07	0.06	0.77	**0.00**	**0.00**	0.53	**0.00**	**0.00**	**0.04**	**0.00**	**0.00**
220	20	1.00	**0.00**	0.90		1.00	1.00	0.05	**0.00**	**0.00**	**0.02**	**0.00**	**0.00**	**0.01**	**0.00**	**0.00**	**0.00**	**0.00**	**0.00**
220	40	1.00	**0.00**	0.99	1.00		1.00	0.15	**0.00**	**0.00**	0.08	**0.00**	**0.00**	**0.03**	**0.00**	**0.00**	**0.00**	**0.00**	**0.00**
220	60	1.00	**0.00**	0.99	1.00	1.00		0.16	**0.00**	**0.00**	0.08	**0.00**	**0.00**	**0.03**	**0.00**	**0.00**	**0.00**	**0.00**	**0.00**
240	20	0.12	0.27	0.91	0.05	0.15	0.16		0.93	0.91	1.00	0.30	**0.01**	1.00	**0.00**	**0.00**	0.85	**0.00**	**0.00**
240	40	**0.00**	1.00	0.07	**0.00**	**0.00**	**0.00**	0.93		1.00	0.99	1.00	0.55	1.00	**0.00**	**0.00**	1.00	**0.00**	**0.00**
240	60	**0.00**	1.00	0.06	**0.00**	**0.00**	**0.00**	0.91	1.00		0.98	1.00	0.59	1.00	**0.00**	**0.00**	1.00	**0.00**	**0.00**
260	20	0.06	0.43	0.77	**0.02**	0.08	0.08	1.00	0.99	0.98		0.47	**0.03**	1.00	**0.00**	**0.00**	0.95	**0.00**	**0.00**
260	40	**0.00**	1.00	**0.00**	**0.00**	**0.00**	**0.00**	0.30	1.00	1.00	0.47		0.99	0.72	**0.00**	**0.00**	1.00	**0.02**	**0.00**
260	60	**0.00**	1.00	**0.00**	**0.00**	**0.00**	**0.00**	**0.01**	0.55	0.59	**0.03**	0.99		0.07	0.06	**0.00**	0.70	0.35	**0.00**
280	20	**0.03**	0.68	0.53	**0.01**	**0.03**	**0.03**	1.00	1.00	1.00	1.00	0.72	0.07		**0.00**	**0.00**	1.00	**0.00**	**0.00**
280	40	**0.00**	**0.00**	**0.00**	**0.00**	**0.00**	**0.00**	**0.00**	**0.00**	**0.00**	**0.00**	**0.00**	0.06	**0.00**		**0.01**	**0.00**	1.00	**0.02**
280	60	**0.00**	**0.00**	**0.00**	**0.00**	**0.00**	**0.00**	**0.00**	**0.00**	**0.00**	**0.00**	**0.00**	**0.00**	**0.00**	**0.01**		**0.00**	**0.00**	1.00
300	20	**0.00**	1.00	**0.04**	**0.00**	**0.00**	**0.00**	0.85	1.00	1.00	0.95	1.00	0.70	1.00	**0.00**	**0.00**		**0.00**	**0.00**
300	40	**0.00**	**0.02**	**0.00**	**0.00**	**0.00**	**0.00**	**0.00**	**0.00**	**0.00**	**0.00**	**0.02**	0.35	**0.00**	1.00	**0.00**	**0.00**		**0.00**
300	60	**0.00**	**0.00**	**0.00**	**0.00**	**0.00**	**0.00**	**0.00**	**0.00**	**0.00**	**0.00**	**0.00**	**0.00**	**0.00**	**0.02**	1.00	**0.00**	**0.00**	

Table A4. Analysis of variance for ash content.

Tukey Test for Ash Content; a Bold Font Signifies Statistically Significant Difference ($p < 0.05$)		**200**	**200**	**200**	**220**	**220**	**220**	**240**	**240**	**240**	**260**	**260**	**260**	**280**	**280**	**280**	**300**	**300**	**300**
		20	**40**	**60**	**20**	**40**	**60**	**20**	**40**	**60**	**20**	**40**	**60**	**20**	**40**	**60**	**20**	**40**	**60**
200	20		**0.00**	0.98	1.00	1.00	1.00	0.10	**0.00**	**0.00**	**0.03**	**0.00**	**0.00**	**0.03**	**0.00**	**0.00**	**0.00**	**0.00**	**0.00**
200	40	**0.00**		**0.00**	**0.00**	**0.00**	**0.00**	0.32	1.00	1.00	0.64	1.00	1.00	0.66	**0.00**	**0.00**	1.00	**0.02**	**0.00**
200	60	0.98	**0.00**		0.91	1.00	1.00	0.88	0.06	0.06	0.60	**0.00**	**0.00**	0.57	**0.00**	**0.00**	0.05	**0.00**	**0.00**
220	20	1.00	**0.00**	0.91		1.00	1.00	**0.04**	**0.00**	**0.00**	**0.01**	**0.00**	**0.00**	**0.01**	**0.00**	**0.00**	**0.00**	**0.00**	**0.00**
220	40	1.00	**0.00**	1.00	1.00		1.00	0.15	**0.00**	**0.00**	0.05	**0.00**	**0.00**	**0.05**	**0.00**	**0.00**	**0.00**	**0.00**	**0.00**
220	60	1.00	**0.00**	1.00	1.00	1.00		0.15	**0.00**	**0.00**	**0.05**	**0.00**	**0.00**	**0.04**	**0.00**	**0.00**	**0.00**	**0.00**	**0.00**
240	20	0.10	0.32	0.88	**0.04**	0.15	0.15		0.95	0.94	1.00	0.37	**0.02**	1.00	**0.00**	**0.00**	0.93	**0.00**	**0.00**
240	40	**0.00**	1.00	0.06	**0.00**	**0.00**	**0.00**	0.95		1.00	1.00	1.00	0.59	1.00	**0.00**	**0.00**	1.00	**0.00**	**0.00**
240	60	**0.00**	1.00	0.06	**0.00**	**0.00**	**0.00**	0.94	1.00		1.00	1.00	0.61	1.00	**0.00**	**0.00**	1.00	**0.00**	**0.00**
260	20	**0.03**	0.64	0.60	**0.01**	0.05	**0.05**	1.00	1.00	1.00		0.69	0.06	1.00	**0.00**	**0.00**	1.00	**0.00**	**0.00**
260	40	**0.00**	1.00	**0.00**	**0.00**	**0.00**	**0.00**	0.37	1.00	1.00	0.69		0.99	0.71	**0.00**	**0.00**	1.00	**0.02**	**0.00**
260	60	**0.00**	1.00	**0.00**	**0.00**	**0.00**	**0.00**	**0.02**	0.59	0.61	0.06	0.99		0.07	0.06	**0.00**	0.65	0.35	**0.00**
280	20	**0.03**	0.66	0.57	**0.01**	**0.05**	**0.04**	1.00	1.00	1.00	1.00	0.71	0.07		**0.00**	**0.00**	1.00	**0.00**	**0.00**
280	40	**0.00**	**0.00**	**0.00**	**0.00**	**0.00**	**0.00**	**0.00**	**0.00**	**0.00**	**0.00**	**0.00**	0.06	**0.00**		**0.01**	**0.00**	1.00	**0.02**
280	60	**0.00**	**0.00**	**0.00**	**0.00**	**0.00**	**0.00**	**0.00**	**0.00**	**0.00**	**0.00**	**0.00**	**0.00**	**0.00**	**0.01**		**0.00**	**0.00**	1.00
300	20	**0.00**	1.00	0.05	**0.00**	**0.00**	**0.00**	0.93	1.00	1.00	1.00	1.00	0.65	1.00	**0.00**	**0.00**		**0.00**	**0.00**
300	40	**0.00**	**0.02**	**0.00**	**0.00**	**0.00**	**0.00**	**0.00**	**0.00**	**0.00**	**0.00**	**0.02**	0.35	**0.00**	1.00	**0.00**	**0.00**		**0.00**
300	60	**0.00**	**0.00**	**0.00**	**0.00**	**0.00**	**0.00**	**0.00**	**0.00**	**0.00**	**0.00**	**0.00**	**0.00**	**0.00**	**0.02**	1.00	**0.00**	**0.00**	

Table A5. Analysis of variance for combustible parts (*CP*).

Tukey Test for *CP*; a Bold Font Signifies Statistically Significant Difference ($p < 0.05$)		**200**	**200**	**200**	**220**	**220**	**220**	**240**	**240**	**240**	**260**	**260**	**260**	**280**	**280**	**280**	**300**	**300**	**300**
		20	**40**	**60**	**20**	**40**	**60**	**20**	**40**	**60**	**20**	**40**	**60**	**20**	**40**	**60**	**20**	**40**	**60**
200	20		**0.00**	0.97	1.00	1.00	1.00	0.07	**0.00**	**0.00**	**0.00**	**0.00**	**0.00**	**0.02**	**0.00**	**0.00**	**0.00**	**0.00**	**0.00**
200	40	**0.00**		**0.00**	**0.00**	**0.00**	**0.00**	0.25	1.00	1.00	**0.00**	1.00	0.99	0.58	**0.00**	**0.00**	1.00	**0.01**	**0.00**
200	60	0.97	**0.00**		0.87	0.99	0.99	0.84	**0.04**	**0.04**	**0.00**	**0.00**	**0.00**	**0.49**	**0.00**	**0.00**	**0.03**	**0.00**	**0.00**
220	20	1.00	**0.00**	0.87		1.00	1.00	**0.03**	**0.00**	**0.00**	**0.00**	**0.00**	**0.00**	**0.01**	**0.00**	**0.00**	**0.00**	**0.00**	**0.00**
220	40	1.00	**0.00**	0.99	1.00		1.00	0.11	**0.00**	**0.00**	**0.00**	**0.00**	**0.00**	**0.03**	**0.00**	**0.00**	**0.00**	**0.00**	**0.00**
220	60	1.00	**0.00**	0.99	1.00	1.00		0.11	**0.00**	**0.00**	**0.00**	**0.00**	**0.00**	**0.03**	**0.00**	**0.00**	**0.00**	**0.00**	**0.00**
240	20	0.07	0.25	0.84	**0.03**	0.11	0.11		0.93	0.92	**0.00**	0.29	**0.01**	1.00	**0.00**	**0.00**	0.90	**0.00**	**0.00**
240	40	**0.00**	1.00	**0.04**	**0.00**	**0.00**	**0.00**	0.93		1.00	**0.00**	1.00	0.51	1.00	**0.00**	**0.00**	1.00	**0.00**	**0.00**
240	60	**0.00**	1.00	**0.04**	**0.00**	**0.00**	**0.00**	0.92	1.00		**0.00**	1.00	0.53	1.00	**0.00**	**0.00**	1.00	**0.00**	**0.00**
260	20	**0.00**	**0.00**	**0.00**	**0.00**	**0.00**	**0.00**	**0.00**	**0.00**	**0.00**		**0.00**	**0.00**	**0.00**	**0.00**	**0.00**	**0.00**	**0.00**	**0.00**
260	40	**0.00**	1.00	**0.00**	**0.00**	**0.00**	**0.00**	0.29	1.00	1.00	**0.00**		0.99	0.64	**0.00**	**0.00**	1.00	**0.01**	**0.00**
260	60	**0.00**	0.99	**0.00**	**0.00**	**0.00**	**0.00**	**0.01**	0.51	0.53	**0.00**	0.99		**0.04**	**0.04**	**0.00**	0.57	0.27	**0.00**
280	20	**0.02**	0.58	0.49	**0.01**	**0.03**	**0.03**	1.00	1.00	1.00	**0.00**	0.64	**0.04**		**0.00**	**0.00**	1.00	**0.00**	**0.00**
280	40	**0.00**	**0.00**	**0.00**	**0.00**	**0.00**	**0.00**	**0.00**	**0.00**	**0.00**	**0.00**	**0.00**	**0.04**	**0.00**		**0.01**	**0.00**	1.00	**0.01**
280	60	**0.00**	**0.00**	**0.00**	**0.00**	**0.00**	**0.00**	**0.00**	**0.00**	**0.00**	**0.00**	**0.00**	**0.00**	**0.00**	**0.01**		**0.00**	**0.00**	1.00
300	20	**0.00**	1.00	**0.03**	**0.00**	**0.00**	**0.00**	0.90	1.00	1.00	**0.00**	1.00	0.57	1.00	**0.00**	**0.00**		**0.00**	**0.00**
300	40	**0.00**	**0.01**	**0.00**	**0.00**	**0.00**	**0.00**	**0.00**	**0.00**	**0.00**	**0.00**	**0.01**	0.27	**0.00**	1.00	**0.00**	**0.00**		**0.00**
300	60	**0.00**	**0.00**	**0.00**	**0.00**	**0.00**	**0.00**	**0.00**	**0.00**	**0.00**	**0.00**	**0.00**	**0.00**	**0.00**	**0.01**	1.00	**0.00**	**0.00**	

Table A6. Analysis of variance for high heating value (*HHV*).

Tukey Test for *HHV*; a Bold Font Signifies Statistically Significant Difference ($p < 0.05$)		**200**	**200**	**200**	**220**	**220**	**220**	**240**	**240**	**240**	**260**	**260**	**260**	**280**	**280**	**280**	**300**	**300**	**300**
		20	**40**	**60**	**20**	**40**	**60**	**20**	**40**	**60**	**20**	**40**	**60**	**20**	**40**	**60**	**20**	**40**	**60**
200	20		0.05	1.00	1.00	1.00	1.00	0.99	0.31	**0.00**	0.87	0.76	0.10	0.99	**0.00**	**0.00**	0.97	**0.00**	**0.00**
200	40	0.05		**0.02**	0.13	0.18	**0.04**	0.62	1.00	1.00	0.93	0.97	1.00	0.62	0.78	**0.05**	0.77	0.98	**0.00**
200	60	1.00	**0.02**		1.00	1.00	1.00	0.95	0.15	**0.00**	0.66	0.52	**0.04**	0.95	**0.00**	**0.00**	0.87	**0.00**	**0.00**
220	20	1.00	0.13	1.00		1.00	1.00	1.00	0.55	**0.01**	0.98	0.94	0.22	1.00	**0.00**	**0.00**	1.00	**0.00**	**0.00**
220	40	1.00	0.18	1.00	1.00		1.00	1.00	0.68	**0.02**	0.99	0.98	0.31	1.00	**0.00**	**0.00**	1.00	**0.00**	**0.00**
220	60	1.00	**0.04**	1.00	1.00	1.00		0.99	0.25	**0.00**	0.82	0.69	0.07	0.99	**0.00**	**0.00**	0.95	**0.00**	**0.00**
240	20	0.99	0.62	0.95	1.00	1.00	0.99		0.98	0.14	1.00	1.00	0.80	1.00	**0.01**	**0.00**	1.00	**0.03**	**0.00**
240	40	0.31	1.00	0.15	0.55	0.68	0.25	0.98		0.94	1.00	1.00	1.00	0.98	0.25	**0.01**	1.00	0.59	**0.00**
240	60	**0.00**	1.00	**0.00**	**0.01**	**0.02**	**0.00**	0.14	0.94		0.41	0.54	1.00	0.14	1.00	0.33	0.22	1.00	**0.01**
260	20	0.87	0.93	0.66	0.98	0.99	0.82	1.00	1.00	0.41		1.00	0.98	1.00	**0.03**	**0.00**	1.00	0.12	**0.00**
260	40	0.76	0.97	0.52	0.94	0.98	0.69	1.00	1.00	0.54	1.00		1.00	1.00	0.05	**0.00**	1.00	0.18	**0.00**
260	60	0.10	1.00	**0.04**	0.22	0.31	0.07	0.80	1.00	1.00	0.98	1.00		0.79	0.60	**0.02**	0.90	0.91	**0.00**
280	20	0.99	0.62	0.95	1.00	1.00	0.99	1.00	0.98	0.14	1.00	1.00	0.79		**0.01**	**0.00**	1.00	**0.03**	**0.00**
280	40	**0.00**	0.78	**0.00**	**0.00**	**0.00**	**0.00**	**0.01**	0.25	1.00	**0.03**	0.05	0.60	**0.01**		0.97	**0.01**	1.00	0.20
280	60	**0.00**	**0.05**	**0.00**	**0.00**	**0.00**	**0.00**	**0.00**	**0.01**	0.33	**0.00**	**0.00**	**0.02**	**0.00**	0.97		**0.00**	0.75	0.98
300	20	0.97	0.77	0.87	1.00	1.00	0.95	1.00	1.00	0.22	1.00	1.00	0.90	1.00	**0.01**	**0.00**		0.05	**0.00**
300	40	**0.00**	0.98	**0.00**	**0.00**	**0.00**	**0.00**	**0.03**	0.59	1.00	0.12	0.18	0.91	**0.03**	1.00	0.75	0.05		0.06
300	60	**0.00**	**0.00**	**0.00**	**0.00**	**0.00**	**0.00**	**0.00**	**0.00**	**0.01**	**0.00**	**0.00**	**0.00**	**0.00**	0.20	0.98	**0.00**	0.06	

Table A7. Statistical evaluation of specific heat of elephant dung.

Intercept/ Coefficient	Value of Intercept/ Coefficient	Standard Error	*p*	Lower Limit of Confidence	Upper Limit of Confidence
a_1	7.74×10^{0}	2.64×10^{-1}	0.00	6.59×10^{0}	7.62×10^{0}
a_2	-6.55×10^{-1}	2.37×10^{-2}	0.00	-6.55×10^{-1}	-5.62×10^{-1}
a_3	2.37×10^{-2}	8.21×10^{-4}	0.00	2.09×10^{-2}	2.41×10^{-2}
a_4	-3.97×10^{-4}	1.45×10^{-5}	0.00	-4.11×10^{-4}	-3.54×10^{-4}
a_5	3.63×10^{-6}	0.00×10^{0}	0.00	3.53×10^{-6}	3.53×10^{-6}
a_6	-1.93×10^{-8}	0.00×10^{0}	0.00	-1.90×10^{-8}	-1.90×10^{-8}
a_7	6.04×10^{-11}	0.00×10^{0}	0.00	5.97×10^{-11}	5.97×10^{-11}
a_8	-1.03×10^{-13}	0.00×10^{0}	0.00	-1.02×10^{-13}	-1.02×10^{-13}
a_9	7.37×10^{-17}	0.00×10^{0}	0.00	7.37×10^{-17}	7.37×10^{-17}

$SH = a_1 + a_2 \cdot T + a_3 \cdot T^2 + a_4 \cdot T^3 + a_5 \cdot T^4 + a_6 \cdot T^5 + a_7 \cdot T^6 + a_8 \cdot T^7 + a_9\, T^8$, $R^2 = 0.98$, R = 0.99.

Table A8. Evaluation of commercial pellet HHV_{daf}, based on [51].

Type of Pellet	*Ash*, %	*HHV*, MJ·kg^{-1}	HHV_{daf} *, MJ·kg^{-1}
Pine sawdust	0.66	19.52	19.65
Wheat straw	7.27	17.57	18.95
Corn settlements	1.27	18.80	19.04
Agricultural residues	8.27	18.13	19.76

* HHV_{daf} has been calculated based on Equation (4).

References

1. Brown, J.L.; Paris, S.; Prado-Oviedo, N.A.; Meehan, C.L.; Hogan, J.N.; Morfeld, K.A.; Carlstead, K. Reproductive Health Assessment of Female Elephants in North American Zoos and Association of Husbandry Practices with Reproductive Dysfunction in African Elephants (Loxodonta africana). *PLoS ONE* **2016**, *11*, e0145673. [CrossRef] [PubMed]
2. Farah, N.; Amna, M.; Naila, Y.; Ishtiaq, R. Processing of Elephant Dung and its Utilization as a Raw Material for Making Exotic Paper. *Res. J. Chem. Sci.* **2014**, *4*, 94–103.
3. Sannigrahi, A.K. Beneficial Utilization Of Elephant Dung Through Vermicomposting. *Int. J. Recent Sci. Res.* **2015**, *6*, 4814–4817.
4. Elephants for Africa. Available online: http://www.elephantsforafrica.org/elephant-facts/ (accessed on 18 August 2019).
5. Schröder, J.J.; Scholefield, D.; Cabral, F.; Hofman, G. The effects of nutrient losses from agriculture on ground and surface water quality: The position of science in developing indicators for regulation. *Environ. Sci. Policy* **2004**, *7*, 15–23. [CrossRef]
6. Pérez-Godínez, E.A.; Lagunes-Zarate, J.; Corona-Hernández, J.; Barajas-Aceves, M. Growth and reproductive potential of Eisenia foetida (Sav) on various zoo animal dungs after two methods of pre-composting followed by vermicomposting. *Waste Manag.* **2017**, *64*, 67–78. [CrossRef]
7. Zhou, S.; Liang, H.; Han, L.; Huang, G.; Yang, Z. The influence of manure feedstock, slow pyrolysis, and hydrothermal temperature on manure thermochemical and combustion properties. *Waste Manag.* **2019**, *88*, 85–95. [CrossRef]
8. Qambrani, N.A.; Rahman, M.M.; Won, S.; Shim, S.; Ra, C. Biochar properties and eco-friendly applications for climate change mitigation, waste management, and wastewater treatment: A review. *Renew. Sustain. Energy Rev.* **2017**, *79*, 255–273. [CrossRef]
9. Aira, M.; Monroy, F.; Domínguez, J.; Mato, S. How earthworm density affects microbial biomas and activity in pig manure. *Eur. J. Soil Biol.* **2002**, *38*, 7–10. [CrossRef]
10. Sukasem, N.; Khanthi, K.; Prayoonkham, S. Biomethane Recovery from Fresh and Dry Water Hyacinth Anaerobic Co-Digestion with Pig Dung, Elephant Dung and Bat Dung with Different Alkali Pretreatments. *Energy Procedia* **2017**, *138*, 294–300. [CrossRef]
11. Klasson, K.T.; Nghiem, N. *Energy Production from Zoo Animal Wastes*; Oak Ridge National Laboratory: Oak Ridge, TN, USA, 2003; Volume 3, pp. 1–8. [CrossRef]

12. Fangkum, A.; Reungsang, A. Simultaneous saccharification and fermentation of cellulose for bio-hydrogen production by anaerobic mixed cultures in elephant dung. *Int. J. Hydrogen Energy* **2014**, *39*, 9028–9035. [CrossRef]
13. Fangkum, A.; Reungsang, A. Biohydrogen production from mixed xylose/arabinose at thermophilic temperature by anaerobic mixed cultures in elephant dung. *Int. J. Hydrogen Energy* **2011**, *36*, 13928–13938. [CrossRef]
14. Moosophin, K.; Phachan, N.; Apiraksakorn, J. Screening of cellulolytic clostridia from animal dung and compost for direct butanol production from cellulosic materials. *Curr. Opin. Biotechnol.* **2013**, *24*, 48–143. [CrossRef]
15. Li, J.; Xiao, F.; Zhang, L.; Amirkhanian, S.N. Life cycle assessment and life cycle cost analysis of recycled solid waste materials in highway pavement: A review. *J. Clean. Prod.* **2019**, *233*, 1182–1206. [CrossRef]
16. Jia, J.; Shu, L.; Zang, G.; Xu, L.; Abudula, A.; Ge, K. Energy analysis of a co-gasification of woody biomass and animal manure, solid oxide fuel cells and micro gas turbine hybrid system. *Energy* **2018**, *149*, 750–761. [CrossRef]
17. Das, K.; Hiloidhari, M.; Baruah, D.C.; Nonhebel, S. Impact of Time Expenditure on Household Preferences for Cooking Fuels. *Energy* **2018**, *151*, 309–316. [CrossRef]
18. International Monetary Fund Report for Selected Countries and Subjects. Available online: https://data.worldbank.org/indicator/SP.POP.TOTL?name_desc=false (accessed on 23 August 2019).
19. Ji, C.; Cheng, K.; Nayak, D.; Pan, G. Environmental and economic assessment of crop residue competitive utilization for biochar, briquette fuel and combined heat and power generation. *J. Clean. Prod.* **2018**, *192*, 916–923. [CrossRef]
20. Kamara, J.; Galukande, M.; Maeda, F.; Luboga, S.; Renzaho, A. Understanding the Challenges of Improving Sanitation and Hygiene Outcomes in a Community Based Intervention: A Cross-Sectional Study in Rural Tanzania. *Int. J. Environ. Res. Public Health* **2017**, *14*, 602. [CrossRef]
21. Białowiec, A.; Micuda, M.; Szumny, A.; Łyczko, J.; Koziel, J.A. Waste to Carbon: Influence of Structural Modification on VOC Emission Kinetics from Stored Carbonized Refuse-Derived Fuel. *Sustainability* **2019**, *11*, 935. [CrossRef]
22. Stępień, P.; Białowiec, A. Kinetic Parameters of Torrefaction Process of Alternative Fuel Produced From Municipal Solid Waste and Characteristic of Carbonized Refuse Derived Fuel. *Detritus* **2018**, *3*, 75–83. [CrossRef]
23. Waste Characteristics. Calculation of Dry Mass on the Basis of Dry Residue or Water Content. Polish standard PN-EN 14346:2011. Available online: https://infostore.saiglobal.com/enau/Standards/PN-EN-14346-2011-932471_SAIG_PKN_PKN_2197939/ (accessed on 23 August 2019).
24. Waste Characteristics. Content of Organic Matter. Polish Standard PN-EN 15169:2011. Available online: http://sklep.pkn.pl/pn-en-15169-2011p.html (accessed on 23 August 2019).
25. Municipal Solid Waste. Combustible and Non-Combustible Content. Polish Standard PN-Z-15008-04:1993. Available online: http://sklep.pkn.pl/pn-z-15008-04-1993p.html (accessed on 23 August 2019).
26. Solid Fuels. Determination of the Higher Heating Value and the Lower Heating Value. Polish Standard PN-G-04513:1981. Available online: http://sklep.pkn.pl/pn-g-04513-1981p.html (accessed on 23 August 2019).
27. Chin, K.L.; H'ng, P.S.; Go, W.Z.; Wong, W.Z.; Lim, T.W.; Maminski, M.; Paridah, M.T.; Luqman, A.C. Optimization of torrefaction conditions for high energy density solid biofuel from oil palm biomass and fast growing species available in Malaysia. *Ind. Crops Prod.* **2013**, *49*, 768–774. [CrossRef]
28. Pulka, J.; Wiśniewski, D.; Gołaszewski, J.; Białowiec, A. Is the biochar produced from sewage sludge a good quality solid fuel? *Arch. Environ. Prot.* **2016**, *42*, 125–134. [CrossRef]
29. Peleg, M.; Normand, M.D.; Corradini, M.G. The Arrhenius Equation Revisited. *Crit. Rev. Food Sci. Nutr.* **2012**, *52*, 830–851. [CrossRef] [PubMed]
30. Stępień, P.; Serowik, M.; Koziel, J.A.; Białowiec, A. Waste to carbon energy demand model and data based on the TGA and DSC analysis of individual MSW components. *Data* **2019**, *4*, 53. [CrossRef]
31. Stępień, P.; Mysior, M.; Białowiec, A. Technical and technological problems and potential application waste torrefaction. In *Innovations in Waste Management—Selected Issues*; Manczarski, P., Ed.; Wydawnictwo Uniwersytetu Przyrodniczego: Wrocław, Poland, 2018; Volume 1, pp. 59–78. Available online: https://www.researchgate.net/publication/325367684_Innowacje_w_gospodarce_odpadami_Zagadnienia_wybrane (accessed on 23 August 2019).

32. Świechowski, K.; Liszewski, M.; Bąbelewski, P.; Koziel, J.A.; Białowiec, A. Oxytree Pruned Biomass Torrefaction: Mathematical Models of the Influence of Temperature and Residence Time on Fuel Properties Improvement. *Materials* **2019**, *12*, 2228. [CrossRef] [PubMed]
33. Li, S.; Harris, S.; Anandhi, A.; Chen, G. Predicting biochar properties and functions based on feedstock and pyrolysis temperature: A review and data syntheses. *J. Clean. Prod.* **2019**, *215*, 890–902. [CrossRef]
34. Kim, D.; Lee, K.; Park, K.Y. Upgrading the characteristics of biochar from cellulose, lignin, and xylan for solid biofuel production from biomass by hydrothermal carbonization. *J. Ind. Eng. Chem.* **2016**, *42*, 95–100. [CrossRef]
35. Gascó, G.; Paz-Ferreiro, J.; Álvarez, M.L.; Saa, A.; Méndez, A. Biochars and hydrochars prepared by pyrolysis and hydrothermal carbonisation of pig manure. *Waste Manag.* **2018**, *79*, 395–403. [CrossRef]
36. Van der Stelt, M.J.C. *Chemistry and Reaction Kinetics of Biowaste Torrezfaction*; Technische Universiteit Eindhoven: Eindhoven, The Netherlands, 2011. [CrossRef]
37. Pahla, G.; Mamvura, T.A.; Ntuli, F.; Muzenda, E. Energy densification of animal waste lignocellulose biomass and raw biomass. *S. Afr. J. Chem. Eng.* **2017**, *24*, 168–175. [CrossRef]
38. Higgins, M.J.; Adams, G.; Chen, Y.-C.; Erdal, Z.; Forbes, R.H.; Glindemann, D.; Hargreaves, J.R.; McEwen, D.; Murthy, S.N.; Novak, J.T.; et al. Role of protein, amino acids, and enzyme activity on odor production from anaerobically digested and dewatered biosolids. *Water Environ. Res.* **2008**, *80*, 127–135. [CrossRef]
39. Lehmann, J.; Joseph, S. *Biochar for Environmental Management: Science and Technology*; Earthscan: London, UK, 2009; ISBN 184407658X.
40. Ro, K.S.; Libra, J.A.; Bae, S.; Berge, N.D.; Flora, J.R.V.; Pecenka, R. Combustion Behavior of Animal-Manure-Based Hydrochar and Pyrochar. *ACS Sustain. Chem. Eng.* **2019**, *7*, 470–478. [CrossRef]
41. Avellone, E.A.; Baumeister, T.; Saunders, H. *Marks Standard Handbook for Mechanical Engineers*; McGraw-Hill Education: New York, NY, USA, 2008; pp. 101–105.
42. Oshita, K.; Toda, S.; Takaoka, M.; Kanda, H.; Fujimori, T.; Matsukawa, K.; Fujiwara, T. Solid fuel production from cattle manure by dewatering using liquefied dimethyl ether. *Fuel* **2015**, *159*, 7–14. [CrossRef]
43. Dębska, A.; Koziołek, S.; Bieniek, J.; Białowiec, A. Potencjał produkcji biogazu z odpadów we wrocławskim Ogrodzie Zoologicznym. *Annu. Set Environ. Prot.* **2016**, *18*, 337–351.
44. Matthiessen, M.K.; Larney, F.J.; Selinger, L.B.; Olson, A.F. Influence of Loss-on-Ignition Temperature and Heating Time on Ash Content of Compost and Manure. *Commun. Soil Sci. Plant Anal.* **2005**, *36*, 2561–2573. [CrossRef]
45. Świechowski, K.; Koziel, J.A.; Liszewski, M.; Bąbelewski, P.; Białowiec, A. Fuel Properties of Torrefied Biomass from Pruning of Oxytree. *Data* **2019**, *4*, 55. [CrossRef]
46. Dudek, M.; Świechowski, K.; Manczarski, P.; Koziel, J.A.; Białowiec, A. The Effect of Biochar Addition on the Biogas Production Kinetics from the Anaerobic Digestion of Brewers' Spent Grain. *Energies* **2019**, *12*, 1518. [CrossRef]
47. Gautam, S.; Edwards, R.; Yadav, A.; Weltman, R.; Pillarsetti, A.; Arora, N.K.; Smith, K.R. Probe-based measurements of moisture in dung fuel for emissions measurements. *Energy Sustain. Dev.* **2016**, *35*, 1–6. [CrossRef]
48. Lang, Q.; Guo, Y.; Zheng, Q.; Liu, Z.; Gai, C. Co-hydrothermal carbonization of lignocellulosic biomass and swine manure: Hydrochar properties and heavy metal transformation behavior. *Bioresour. Technol.* **2018**, *266*, 242–248. [CrossRef]
49. Rousset, P.; Aguiar, C.; Labbé, N.; Commandré, J.-M. Enhancing the combustible properties of bamboo by torrefaction. *Bioresour. Technol.* **2011**, *102*, 8225–8231. [CrossRef]
50. Bach, Q.-V.; Skreiberg, Ø. Upgrading biomass fuels via wet torrefaction: A review and comparison with dry torrefaction. *Renew. Sustain. Energy Rev.* **2016**, *54*, 665–677. [CrossRef]
51. Dyjakon, A.; Noszczyk, T. The Influence of Freezing Temperature Storage on the Mechanical Durability of Commercial Pellets from Biomass. *Energies* **2019**, *12*, 2627. [CrossRef]
52. Lacey, J.A.; Aston, J.E.; Westover, T.L.; Cherry, R.S.; Thompson, D.N. Removal of introduced inorganic content from chipped forest residues via air classification. *Fuel* **2015**, *160*, 265–273. [CrossRef]
53. Várhegyi, G.; Bobály, B.; Jakab, E.; Chen, H. Thermogravimetric study of biomass pyrolysis kinetics. A distributed activation energy model with prediction tests. *Energy Fuels* **2011**, *25*, 24–32. [CrossRef]
54. Bach, V.; Tran, K.-Q. Dry and wet torrefaction of woody biomass—A comparative study on combustion kinetics. *Energy Proceedia* **2015**, *75*, 150–155. [CrossRef]

55. Soria-Verdugo, A.; Goos, E.; García-Hernando, N. Effect of the number of TGA curves employed on the biomass pyrolysis kinetics results obtained using the Distributed Activation Energy Model. *Fuel Process. Technol.* **2015**, *134*, 360–371. [CrossRef]
56. Pulka, J.; Manczarski, P.; Koziel, J.A.; Białowiec, A. Torrefaction of Sewage Sludge: Kinetics and Fuel Properties of Biochars. *Energies* **2019**, *12*, 565. [CrossRef]
57. Syguła, E.; Koziel, J.A.; Białowiec, A. Proof-of-Concept of Spent Mushrooms Compost Torrefaction—Studying the Process Kinetics and the Influence of Temperature and Duration on the Calorific Value of the Produced Biocoal. *Energies* **2019**, *12*, 3060. [CrossRef]
58. Basak, S.; Samanta, K.K. Thermal behaviour and the cone calorimetric analysis of the jute fabric treated in different pH condition. *J. Therm. Anal. Calorim.* **2019**, *135*, 3095–3105. [CrossRef]
59. Wang, J.; Wang, G.; Zhang, M.; Chen, M.; Li, D.; Min, F.; Chen, M.; Zhang, S.; Ren, Z.; Yan, Y. A comparative study of thermolysis characteristics and kinetics of seaweeds and fir wood. *Process Biochem.* **2006**, *41*, 1883–1886. [CrossRef]
60. Said, N.; Abdel daiem, M.M.; García-Maraver, A.; Zamorano, M. Reduction of Ash Sintering Precursor Components in Rice Straw by Water Washing. *BioResources* **2014**, *9*, 6756–6764. [CrossRef]
61. Burhenne, L.; Messmer, J.; Aicher, T.; Laborie, M.-P. The effect of the biomass components lignin, cellulose and hemicellulose on TGA and fixed bed pyrolysis. *J. Anal. Appl. Pyrolysis* **2013**, *101*, 177–184. [CrossRef]

Załącznik nr 3

Paweł Stępień
imię i nazwisko

Wrocław, 28.02.2022
(miejscowość i data)

Instytut Inżynierii Rolniczej
Uniwersytet Przyrodniczy we Wrocławiu
51-630 Wrocław, Chełmońskiego 37
afiliacja

OŚWIADCZENIE

Oświadczam, że w pracy:
Paweł Stępień, Kacper Świechowski, Martyna Hnat, Szymon Kugler, Sylwia Stegenta-Dąbrowska, Jacek A. Koziel, Piotr Manczarski, Andrzej Białowiec. 2019. Waste to Carbon: Biocoal from Elephant Dung as New Cooking Fuel. Energies, 12, 4344; doi:10.3390/en12224344

mój udział polegał na:
Na częściowym opracowaniu pierwszej wersji manuskryptu w szczególności wstępu. Odpowiedzialny byłem także za opisanie metodyki w zakresie analizy DSC, oraz za opis i opracowanie wyników uzyskanych z analizy DSC.

28.02.2022
data i podpis

Załącznik nr 3

Kacper Świechowski
imię i nazwisko

WROCŁAW 28.02.2022
(miejscowość i data)

Katedr Biogospodarki Stosowanej
Uniwersytet Przyrodniczy we Wrocławiu
51-630 Wrocław, Chełmońskiego 37a
afiliacja

OŚWIADCZENIE

Oświadczam, że w pracy:

Paweł Stępień, Kacper Świechowski, Martyna Hnat, Szymon Kugler, Sylwia Stegenta-Dąbrowska, Jacek A. Koziel, Piotr Manczarski, Andrzej Białowiec. 2019. Waste to Carbon: Biocoal from Elephant Dung as New Cooking Fuel. Energies, 12, 4344; doi:10.3390/en12224344

mój udział polegał na:

Opracowaniu wyników z badań pod względem statystycznym przy wykorzystaniu oprogramowania Statistica. Opracowanie polegało w szczególności na wyznaczeniu modeli wpływu parametrów technologicznych (czasu i temperatury) toryfikacji na zmianę właściwości paliwowych odchodów słonia, wyznaczeniu parametrów kinetycznych toryfikacji w warunkach izotermicznych, wyznaczeniu ilości energii potrzebnej do toryfikacji. Ponadto byłem odpowiedzialny za napisanie pierwszej wersji manuskryptu, w szczególności metodyki oraz opisu i dyskusji wyników. Podczas procesu recenzji stworzyłem pierwszą wersję odpowiedzi dla recenzentów i wykonywałem poprawki w manuskrypcie.

28.02.2022 Świechowski
data i podpis

Załącznik nr 3

Głogów, 25.02.22r.
(miejscowość i data)

Martyna Hnat
imię i nazwisko

Instytut Inżynierii Rolniczej
Uniwersytet Przyrodniczy we Wrocławiu
51-630 Wrocław, Chełmońskiego 37
afiliacja

OŚWIADCZENIE

Oświadczam, że w pracy:
Paweł Stępień, Kacper Świechowski, Martyna Hnat, Szymon Kugler, Sylwia Stegenta-Dąbrowska, Jacek A. Koziel, Piotr Manczarski, Andrzej Białowiec. 2019. Waste to Carbon: Biocoal from Elephant Dung as New Cooking Fuel. Energies, 12, 4344; doi:10.3390/en12224344

mój udział polegał na:
Pozyskaniu materiału badawczego – odchodów słonia i przygotowaniu ich do dalszych badań (suszenie, rozdrobnienie). Do wykonanych przeze mnie badań należało wykonanie biowęgli i poddanie ich wraz z nieprzetworzonymi odchodami słonia analizie technicznej oraz analizie TGA w warunkach izotermicznych i nieizotermicznych.

Hnat Martyna 25.02.22r.
data i podpis

Załącznik nr 3

Szymon Kugler Szczecin, 26.02.2022

imię i nazwisko (miejscowość i data)

Wydział Technologii i Inżynierii Chemicznej
Zachodniopomorski Uniwersytet Technologiczny w Szczecinie
71-065 Szczecin, al. Piastów 42
afiliacja

OŚWIADCZENIE

Oświadczam, że w pracy:

Paweł Stępień, Kacper Świechowski, Martyna Hnat, Szymon Kugler, Sylwia Stegenta-Dąbrowska, Jacek A. Koziel, Piotr Manczarski, Andrzej Białowiec. 2019. Waste to Carbon: Biocoal from Elephant Dung as New Cooking Fuel. Energies, 12, 4344; doi:10.3390/en12224344

mój udział polegał na:

Wykonaniu analizy skaningowej kalorymetrii różnicowej (DSC) przy wykorzystaniu analizatora DSC Q2500 (TA Instruments, New Castle, DE, USA).

Szymon Kugler

Elektronicznie podpisany przez Szymon Kugler
Data: 2022.02.26 15:35:29 +01'00'

……
data i podpis

Załącznik nr 3

Sylwia Stegenta-Dąbrowska
imię i nazwisko

Wrocław 24.02.2022
(miejscowość i data)

Katedr Biogospodarki Stosowanej
Uniwersytet Przyrodniczy we Wrocławiu
51-630 Wrocław, Chełmońskiego 37a
afiliacja

OŚWIADCZENIE

Oświadczam, że w pracy:
Paweł Stępień, Kacper Świechowski, Martyna Hnat, Szymon Kugler, Sylwia Stegenta-Dąbrowska, Jacek A. Koziel, Piotr Manczarski, Andrzej Białowiec. 2019. Waste to Carbon: Biocoal from Elephant Dung as New Cooking Fuel. Energies, 12, 4344; doi:10.3390/en12224344

mój udział polegał na:
Jako promotor pomocniczy pomagałam doktorantowi zmodyfikować pierwszą wersję manuskryptu w szczególności rozdział dotyczący wprowadzenia, metodyki oraz dyskusji uzyskanych wyników badań. W trakcie recenzji uczestniczyłam w udzielaniu odpowiedzi do recenzentów oraz nanoszeniu poprawek do manuskryptu. Pomagałam także w wykonaniu abstraktu graficznego oraz tworzeniu rysunków opisujących metodykę wykonanych badań.

24.02.2022 Sylwia Stegenta-Dąbrowska
data i podpis

Załącznik nr 3

Jacek Koziel
imię i nazwisko

Ames, 23-2-2022…….
(miejscowość i data)

Department of Agricultural and Biosystems Engineering
Iowa State University
Ames, IA 50011, USA
afiliacja

OŚWIADCZENIE

Oświadczam, że w pracy:
Paweł Stępień, Kacper Świechowski, Martyna Hnat, Szymon Kugler, Sylwia Stegenta-Dąbrowska, Jacek A. Koziel, Piotr Manczarski, Andrzej Białowiec. 2019. Waste to Carbon: Biocoal from Elephant Dung as New Cooking Fuel. Energies, 12, 4344; doi:10.3390/en12224344

mój udział polegał na:
Sprawdzeniu i naniesieniu poprawek na pierwszą wersję manuskryptu przed wysłaniem jej do recenzji. Uczestniczyłem w procesie recenzji jak i związanych z nim tworzeniu modyfikacji manuskryptu. Uczestniczyłem także w tworzeniu koncepcji grafik przedstawiających koncepcję badań jak i zastosowaną metodykę badań. Pozyskałem także część środków na opublikowanie artykułu.

23-2-2022……..
data i podpis

Załącznik nr 3

Piotr Manczarski
imię i nazwisko

Warszawa, 20.02.2022 r.
(miejscowość i data)

Wydział Instalacji Budowlanych Hydrotechniki i Inżynierii Środowiska
Politechnika Warszawska
00-653 Warszawa, Nowowiejska 20
afiliacja

OŚWIADCZENIE

Oświadczam, że w pracy:
Paweł Stępień, Kacper Świechowski, Martyna Hnat, Szymon Kugler, Sylwia Stegenta-Dąbrowska, Jacek A. Koziel, Piotr Manczarski, Andrzej Białowiec. 2019. Waste to Carbon: Biocoal from Elephant Dung as New Cooking Fuel. Energies, 12, 4344; doi:10.3390/en12224344

mój udział polegał na:
Zapewnieniu wsparcia merytorycznego podczas opracowywania wyników z doświadczeń oraz sprawdzeniu pierwszej wersji manuskryptu. Pomagałem także w ulepszaniu manuskryptu na etapie recenzji.

20.02.2022 r.……
data i podpis

Załącznik nr 3

Andrzej Białowiec
imię i nazwisko

Wrocław, 26.02.2022
(miejscowość i data)

Katedr Biogospodarki Stosowanej
Uniwersytet Przyrodniczy we Wrocławiu
51-630 Wrocław, Chełmońskiego 37a
afiliacja

OŚWIADCZENIE

Oświadczam, że w pracy:
Paweł Stępień, Kacper Świechowski, Martyna Hnat, Szymon Kugler, Sylwia Stegenta-Dąbrowska, Jacek A. Koziel, Piotr Manczarski, Andrzej Białowiec. 2019. Waste to Carbon: Biocoal from Elephant Dung as New Cooking Fuel. Energies, 12, 4344; doi:10.3390/en12224344

mój udział polegał na:
Na pozyskaniu części środków na realizację badań, sprawdzeniu poprawności wygenerowanych danych eksperymentalnych jak i otrzymanych modeli. Byłem odpowiedzialny za wykonanie poprawek do pierwszej wersji manuskryptu przed wysłaniem go do recenzji jak i uczestniczyłem w tworzeniu odpowiedzi na recenzje i dalszych modyfikacjach manuskryptu. Pozyskałem także środki na opublikowanie artykułu.

26.02.2022
data i podpis

energies

MDPI

Article

Waste to Energy: Solid Fuel Production from Biogas Plant Digestate and Sewage Sludge by Torrefaction-Process Kinetics, Fuel Properties, and Energy Balance

Kacper Świechowski [1,*], Martyna Hnat [1], Paweł Stępień [1], Sylwia Stegenta-Dąbrowska [1], Szymon Kugler [2], Jacek A. Koziel [3] and Andrzej Białowiec [1,3]

1 Faculty of Life Sciences and Technology, Institute of Agricultural Engineering, Wrocław University of Environmental and Life Sciences, 37/41 Chełmońskiego Str., 51-630 Wrocław, Poland; hnat.martyna@gmail.com (M.H.); pawel.stepien@upwr.edu.pl (P.S.); sylwia.stegenta@upwr.edu.pl (S.S.-D.); andrzej.bialowiec@upwr.edu.pl or andrzejb@iastate.edu (A.B.)

2 Faculty of Chemical Technology and Engineering, Polymer Institute, West Pomeranian University of Technology, 10 Pułaskiego Str., 70-322 Szczecin, Poland; szymon.kugler@zut.edu.pl

3 Department of Agricultural and Biosystems Engineering, Iowa State University, Ames, IA 50011, USA; koziel@iastate.edu

* Correspondence: kacper.swiechowski@upwr.edu.pl

Received: 30 May 2020; Accepted: 15 June 2020; Published: 18 June 2020

Abstract: Sustainable solutions are needed to manage increased energy demand and waste generation. Renewable energy production from abundant sewage sludge (SS) and digestate (D) from biogas is feasible. Concerns about feedstock contamination (heavy metals, pharmaceuticals, antibiotics, and antibiotic-resistant bacteria) in SS and D limits the use (e.g., agricultural) of these carbon-rich resources. Low temperature thermal conversion that results in carbonized solid fuel (CSF) has been proposed as sustainable waste utilization. The aim of the research was to investigate the feasibility of CSF production from SS and D via torrefaction. The CSF was produced at 200~300 °C (interval of 20 °C) for 20~60 min (interval 20 min). The torrefaction kinetics and CSF fuel properties were determined. Next, the differential scanning calorimetry (DSC) and thermogravimetric analysis (TGA) of SS and D torrefaction were used to build models of energy demand for torrefaction. Finally, the evaluation of the energy balance of CSF production from SS and D was completed. The results showed that torrefaction improved the D-derived CSF's higher heating value (*HHV*) up to 11% ($p < 0.05$), whereas no significant *HHV* changes for SS were observed. The torrefied D had the highest *HHV* of 20 MJ·kg^{-1} under 300 °C and 30 min, (the curve fitted value from the measured time periods) compared to *HHV* = 18 MJ·kg^{-1} for unprocessed D. The torrefied SS had the highest *HHV* = 14.8 MJ·kg^{-1} under 200 °C and 20 min, compared to *HHV* 14.6 MJ·kg^{-1} for raw SS. An unwanted result of the torrefaction was an increase in ash content in CSF, up to 40% and 22% for SS and D, respectively. The developed model showed that the torrefaction of dry SS and D could be energetically self-sufficient. Generating CSF with the highest *HHV* requires raw feedstock containing ~15.4 and 45.9 MJ·kg^{-1} for SS and D, respectively (assuming that part of feedstock is a source of energy for the process). The results suggest that there is a potential to convert biogas D to CSF to provide renewable fuel for, e.g., plants currently fed/co-fed with municipal solid waste.

Keywords: renewable energy; sewage sludge; biogas digestate; waste to energy; waste to carbon; circular economy; sustainability; carbonized solid fuel

1. Introduction

1.1. Abundant Waste Resources for Solid Fuel Production

The energy use per capita grew from 1.3 to 1.9 Mg of oil equivalents in 1971–2014 [1]. The global energy demand is expected to grow by about 27% worldwide from 2017 to 2040 [2]. The increase in energy needs and consumption has an impact on the environment [3,4]. There is a need to refine technologies for clean, abundant, and renewable energy for sustainable development.

Waste production increases with development. In general, developed economies produce more waste (mainly plastic), whereas in emerging economies, citizens generate less waste that nonetheless has a high content of high organic biodegradables. Regardless of the development stage, sewage sludge (SS) is abundantly produced worldwide as a byproduct of wastewater treatment. For example, Poland generated over 584,000 Mg d.m. (dry mass) of SS and over 9,300,000 Mg d.m. was produced in the whole EU in 2017 [4].

Biogas digestate (D) is another abundant source of carbon-rich waste that is a byproduct of renewable energy production. Two billion m^3 (bcm) of biogas are produced annually in the EU, representing ~0.42% of the total natural gas consumed (470 bcm). It is estimated that the amount of biogas produced in 2050 will be 36~98 bcm [5,6]. Such a significant increase will be associated with a challenge to find sustainable waste management of the produced D. Currently, the European biogas market is concentrated in Germany, with more than half of all European biogas plants located there [5]. Thus, new plants are likely to be built throughout the EU, which will create a market for D utilization.

The EU generates ~180 mln Mg of D per year. Approximately 120 mln Mg is produced from agricultural substrates, ~46 mln Mg from mixed municipal solid waste, 7 mln Mg from separated biowaste, and the remainder from SS and other agro/food industry by-products [7]. These Ds are directly used as fertilizer [7].

1.2. Waste Management Policies Create an Opportunity for Sustainable Reuse of SS and D

The EU has introduced policies regarding the increase of the share of renewable energy in total energy consumption and to waste management. For example, Directive 2009/28/EC promoted renewable energy and assumed its growth to be at least 20% of the total energy consumption in 2020 [8]. Though it is known that some EU countries did not achieve this goal, the EU established a new target for 2030 that assumes at least a 32% share for renewable energy [9].

Transition to the circular economy has been promoted. Directive 2009/28/EC [8] laid down measures to prevent or reduce the adverse impacts of the generation and management of waste [8]. The directive established a waste hierarchy (article 4) that relegated conventional incineration and landfilling while promoting prevention and re-use [8]. This transition creates an opportunity to find sustainable re-uses of SS that is current landfilled or incinerated.

The technologies for thermal waste treatment need to adjust to the shift from incineration and high-energy input to the medium- and low-energy input of non-recyclable residual waste. It has been agreed that incineration plants will continue to be an important element of waste management and a proper mix should be maintained when it comes to the waste-to-energy capacity for the treatment of non-recyclable waste. This is critical to avoid potential economic losses or the creation of infrastructural barriers to the achievement of higher recycling rates [10]. However, the unintended effect of increased recycling will be less fuel for incineration plants and a lower fuel quality. This is because the biggest calorific fraction (e.g., plastic) will be sorted out from the waste stream.

The European Committee for Standardization (CEN) established quality standards for solid recovered fuels (SRFs) to address the high variability and heterogeneity of waste streams and to simplify the market of waste conversion to energy. The EN 15359:2012 divides fuels produced from waste into five classes based on their low heating value (*LHV*), chlorine, and mercury content. The *LHV* for the first through fifth classes are ≥25, ≥20, ≥15, ≥10, and ≥3 $MJ \cdot kg^{-1}$, respectively [11]. The chlorine content is responsible for the temperature in which SRF can be incinerated, whereas mercury is

a main environmental concern. Other SRF parameters include corrosion and deposits to build up compounds [12]. Unprocessed waste, like SRF, contain some biological shares (home for harmful mold, fungus, and microorganism, virus, etc.), as well as small plastics particles; for this reason, they can be sources of health problems for people having contact with these materials [13].

1.3. Valorization of Waste via Torrefaction

Large quantities of SS and D are still used in agriculture [14,15]. However, a large fraction of SS and D waste streams cannot be used for fertilization due to its contamination (e.g., heavy metals, pharmaceuticals, antibiotics, and antibiotic-resistant bacteria [16–20]). Contaminated SS needs to be stabilized and then landfilled or incinerated [14], i.e., approaches that are being phased out in the EU. Similarly, some Ds from municipal biogas plants do not meet fertilizer standards. Biological hazards, dust, and lower calorific values of waste from sorting plants can be overcome by the thermal conversion of SRF to carbonized solid fuel (CSF), followed by CSF densification via pelletization. Thermal treatment (e.g., via torrefaction) eliminates biological hazards and increases energy density, and the pelletization further improves the energy densification and reduction of volatile organic compound (VOC) emissions from CSF up to 86% [21,22].

Thus, there is an opportunity for SS valorization to high-quality fuel via torrefaction. Torrefaction is a thermal treatment known as 'mild pyrolysis', 'roasting', or 'high-temperature drying'. Torrefaction is known to upgrade the fuel characteristics of biomass [23]. Torrefaction can also overcome the disadvantages of raw biomass, such as high moisture content, degradation and decay, odor, pathogens, and low energy density. The torrefaction process increases hydrophobicity and reduces grinding energy demand [24]. Torrefaction is achieved via the relatively slow heating of biomass at 200~300 °C in a no or limited oxygen environment [23].

This research aimed to investigate the feasibility of producing CSF from dry SS and D and completing initial techno-economic analyses for CSF utilization in cement and power plants. In this work, dried SS and D were torrefied and then compared to other alternative CSFs. This research addresses the goals of (1) an increasing share of renewables, (2) providing additional options for solid fuel for power plants in the future, and (3) managing the growing volume of organic waste produced by energy recovery.

The torrefaction experiment and process modeling were done for dry SS and D, excluding the energy needed for a drying process. The torrefaction of dry materials instead of materials with natural moisture contents was chosen for several reasons: (i) The initial moisture content of SS and D is very high <90% and its direct torrefaction could be biased (i.e., SS could be incinerated autothermal when its moisture content is under 50% [25]; (ii) SS is already dried to avoid landfill costs so that it can be incinerated or used to produce solid fertilizer [25] in larger wastewater treatment plants (in selected EU countries); (iii) moreover, technologies for water removal from SS and D by mechanical or thermal treatment are available, including solar drying [26] and/or waste heat from other processes [27]—for example, waste heat from biogas incineration in combined heat and power (CHP) units can be used for D drying; finally (iv), it is assumed that the model developed for dry mass will be easier to use, i.e., by recalculating for site-specific SS and D conditions (taking into account the initial moisture and the energy cost of its removal).

2. Materials and Methods

The experiment setup is presented in Figure 1. A detailed description is below. First, samples of digestate and sewage sludge were collected from industrial plants. Next, the samples were dried and ground. Then, parts of the samples were processed to CSF sample generation. The dried samples of raw SS and D were tested by thermogravimetric analysis (TGA) and differential scanning calorimetry (DSC) analyses. In parallel, the dried raw SS and D and CSF samples were tested by proximate and process analyses. After that, data analysis was conducted. Finally, as a result of data analysis, empirical models of CSF fuel features, torrefaction kinetics, and energy balance were obtained.

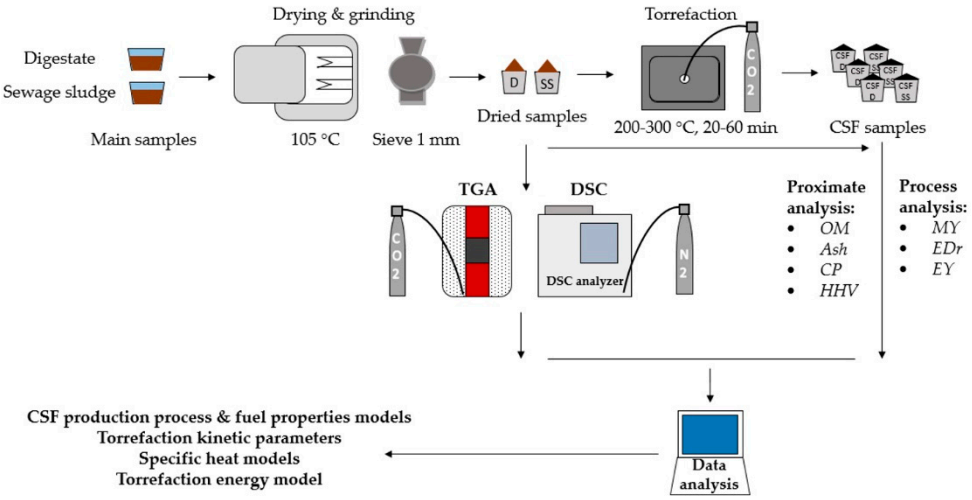

Figure 1. Experiment setup to convert sewage sludge and digestate to carbonized solid fuel (CSF) via torrefaction. The resulting CSF was analyzed for inputs to techno-economic analyses. D = biogas plant digestate; SS = sewage sludge. TGA = thermogravimetric analyses. DSC = differential scanning calorimeter analysis; *OM* = organic matter; *CP* = combustible parts; *HHV* = high heating value; *MY* = mass yield; *EDr* = energy densification ratio; and *EY* = energy yield.

2.1. Feedstock

2.1.1. Sewage Sludge

SS was collected at the 140,000 $m^3 \cdot d^{-1}$ wastewater treatment plant (WWTP) (Janówek, MPWiK S.A., Wrocław, Poland). The SS was a by-product of mechanical and biological wastewater treatment, with chemical additives for phosphorus removal. The 20 kg SS sample was collected from the secondary settling tank before the anaerobic digestion. Then, the sample was dried at 105 °C in a laboratory dryer (WAMED, model KBC-65W, Warsaw, Poland). Next, the dry SS was ground through a 1 mm screen with a laboratory knife mill (Testchem, model LMN-100, Pszów, Poland) and then stored before testing at −15 °C.

2.1.2. Digestate from the Biogas Plant

D originated from the 1 MW_{el} commercial biogas plant (Bio-Wat Sp. Z o. o., Świdnica, Poland). The biogas plant used the following feedstocks: a biodegradable fraction of municipal solid waste (34%), maize silage (30%), sugar beet pulp (30%), and yeast cake (6%). The 20 kg D sample was collected from the post-fermentation chamber. Next, the sample was dried, ground, and stored in identical conditions to that of SS.

2.2. CSF Production Method and Process Analysis

The CSF was produced in accordance with the previously described methodology [28]. A muffle furnace (Snol 8.1/1100, Utena, Lithuania) was used. CO_2 was delivered to the center of the furnace at ~2.5 $dm^3 \cdot min^{-1}$ to facilitate an inert atmosphere. Furnace setpoint temperatures of 200~300 °C (with 20 °C intervals) and 20~60 min (20 min intervals) residence times were used. The (10 ± 0.5 g) dry SS and D feedstock samples were heated in inert conditions from room temperature (20 °C) with a heating rate of 50 $°C \cdot min^{-1}$ to the setpoint. After the torrefaction process, CSF samples were removed from the muffle furnace when the interior temperature was lower than 200 °C. The approximate times of cooling from 300, 280, 260, 240, and 220–200 °C were ~38, 33, 29, 23, and 13.5 min, respectively. A process temperature vs. process time for 300 °C setpoint is presented in Figure 2. The mass of the sample before and after torrefaction was determined to calculate the mass loss and yield. The mass was measured within 0.1 g of accuracy.

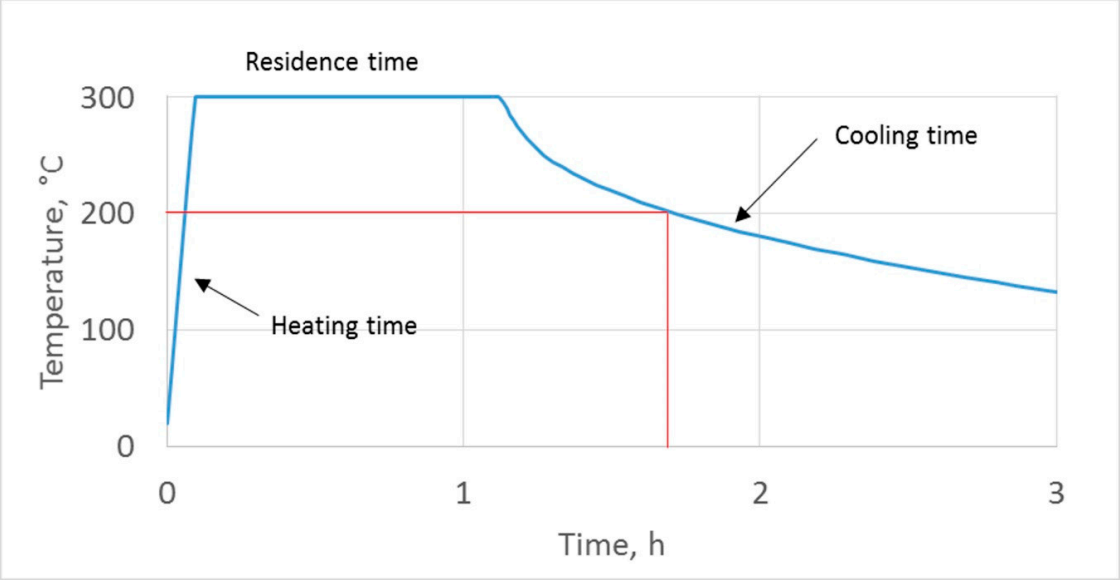

Figure 2. An example of temperature patterns during the torrefaction of sewage sludge and digestate.

The mass yield, energy densification ratio, and energy yield of CSF were determined based on Equations (1), (2), and (3) [29], respectively.

$$MY = m_b / m_a \cdot 100 \quad (1)$$

where MY is the mass yield (%), m_a is the mass of raw material before torrefaction (kg), and m_b is the mass of CSF after torrefaction (kg).

$$EDr = HHV_b / HHV_a \quad (2)$$

where EDr is the energy densification ratio, HHV_b is the high heating value of CSF (MJ·kg^{-1}), and HHV_a is the high heating value of raw material (MJ·kg^{-1}).

$$EY = MY \cdot EDr \quad (3)$$

where EY is the energy yield (%), MY is the mass yield (%), and EDr is the energy densification ratio.

2.3. Proximate Analysis of SS and D and their CSF

The physical–chemical properties of dry SS and D and CSF were tested in three replicates for:

- Organic matter (*OM*) content, a.k.a. a loss on ignition (*LOI*), using the method described elsewhere [30].
- Combustible part (*CP*) and ash content (ash) [31].
- High heating value (*HHV*) [32].

The (Snol 8.1/1100, Utena, Lithuania) furnace was used for *OM*, *CP*, and ash determination. The C200 calorimeter (IKA®Werke GmbH, Staufen, Germany) was used for *HHV* determination.

The Properties of Raw Feedstock

The *OM* content for dry SS and D was 61.9% and 86.6%, respectively. The ash content was 36.3% and 12.4% for SS and D (d.m.), respectively. The *CP* in dried SS and D were 63.7% and 87.6%, respectively. The *HHV* (14.6 MJ·kg^{-1}) of dried SS was lower than for dried D (18.1 MJ·kg^{-1}).

2.4. Thermogravimetric Analysis (TGA) of Raw Sewage Sludge and Digestate

The thermogravimetric analysis was performed in isothermal and non-isothermal conditions. First, isothermal conditions were used in order to determine the kinetics parameters (*k*—constant;

reaction rate; E_a—activation energy; and A—pre-exponential factor) of the torrefaction process. Next, non-isothermal conditions were used for tracking the thermal degradation from 50 to 850 °C.

The determination of kinetic parameters was completed in accordance with the previous methodology and reactor set-up [33]. Setpoint torrefaction temperatures and 1 h heating time in inert CO_2 ~10 $dm^3 \cdot h^{-1}$ flowrates were used for mass losses based on the initial mass of the dry sample (2.25 g) in three replicates. Next, the mass losses for each torrefaction temperature setpoints were used to determine constant reaction rates k. The first-order model was used (Equation (4)):

$$m_s = m_o \cdot e^{(-k \cdot t)} \tag{4}$$

where m_s is mass at time t (g), m_o is initial mass (g), k is the reaction rate constant (s^{-1}), and t is time (s).

The full methodology of kinetic parameters determination (k—constant reaction rate; Ea—activation energy; and A—pre-exponential factor) was presented in a previous work [34].

TGA in non-isothermal conditions was carried out at a heating rate of 10.8 °C·min^{-1}. Dry SS and D samples were placed in a tubular reactor and then heated to 850 °C, and they were kept there for 2 min.

The analysis of kinetic parameters and thermal degradation was done by means of the stand-mounted tubular furnace (Czylok, RST 40x200/100, Jastrzębie-Zdrój, Poland).

Data from non-isothermal TGA were subjected to mathematical manipulation in accordance with the following description. Raw TGA data were smoothed by using the locally weighted scatterplot smoothing (LOWESS) method [35] with *Span* (0–1) = 0.1. Next, based on the smoothed TGA curve, a derivative thermogravimetric curve (DTG) was created with the Savitzky–Golay smooth method (polynomial order = 2 and points of window = 20) [35]. The OriginPro 2017 software (OriginLab, Northampton, MA, USA) was used for data analysis.

2.5. Differential Scanning Calorimetry (DSC) of Raw Material

The DSC of SS and D was carried out in N_2 (3 $dm^3 \cdot h^{-1}$) atmosphere using a differential scanning calorimeter (TA Instruments, DSC Q2500, New Castle, DE, USA). The dry SS and D sample (~6 mg) was placed into the aluminum crucible, placed in the calorimeter, and heated from 20 to 500 °C (at 10 °C·min^{-1}) in n = 1 replicate.

2.6. Modeling of Torrefaction Process and CSF Fuel Properties

Polynomial models of the influence of torrefaction temperature and process (residence) time on the CSF parameters (*MY*, *EDr*, *EY*, *OM* content, *CP* content, ash content, and *HHV*) were developed. Models were based on measured data from the torrefaction and CSF properties for a particular torrefaction temperature and time using a similar modeling approach described in our previous work [36]. The general model is presented by Equation (5). Each model had one intercept (a_1) and six regression coefficients (a_2—a_7) (a confidence interval of 95% was assumed). Regression coefficients for which the p-value was <0.05 were assumed to be statistically significant. Correlation (R) and determination coefficients (R^2) were determined for each model.

$$f(T,t) = a_1 + a_2 \cdot T + a_3 \cdot T^2 + a_4 \cdot t + a_5 \cdot t^2 + a_6 \cdot T \cdot t + a_7 \cdot T^2 \cdot t^2 \tag{5}$$

where $f(T,t)$ is the variable (T, t, and combinations) being analyzed, a_1 is the intercept, a_2—a_7 are the regression coefficients, T is the torrefaction process temperature (°C), and t is torrefaction process time (min).

The standardized regression coefficients β for each regression coefficients (a_2—a_7) were standardized based on Equation (6). The βcoefficient determines how much its own standard deviations will change the dependent variable Y if the independent variable is changed by one (its own) standard deviation [36].

$$\beta = a_n \cdot SD_{Xi} / SD_{Yi} \tag{6}$$

where β is the standardized regression coefficient, a_n is the estimated regression coefficient, SD_{Xi} is the standard deviation of the independent variable x, xi represents the values of subsequent independent variables, SD_{Yi} is the standard deviation of the dependent variable y, and yi represents the values of subsequent dependent variables.

2.7. Energy Balance for Torrefaction

An energy balance of the torrefaction process was needed to determine if the process could be self-sustaining. The calculations were aimed to determine the energy needed to generate 1 g of CSF. The energy balance assumed:

- No heat losses of the reactor.
- The heat needed to dry SS and D were not included (due to site-specific variability in the feedstock and drying methods).
- All energy contained in torrgas was used to provide energy to the torrefaction process.
- The energy contained in torrgas was estimated based on Equation (8).

The energy balance model is presented in Figure 3. Material for torrefaction is given as the *HHV* of raw material multiplied by its mass needed (x) to obtain 1 g of CSF after the process. The x is calculated as:

$$x = 1/MY \cdot 100 \quad (7)$$

where x is a multiplier for an additional raw material mass to compensate for mass loss during torrefaction, MY is the mass yield of the torrefaction process (values based on the model, in %), and 100 is the value to remove the % unit from the equation.

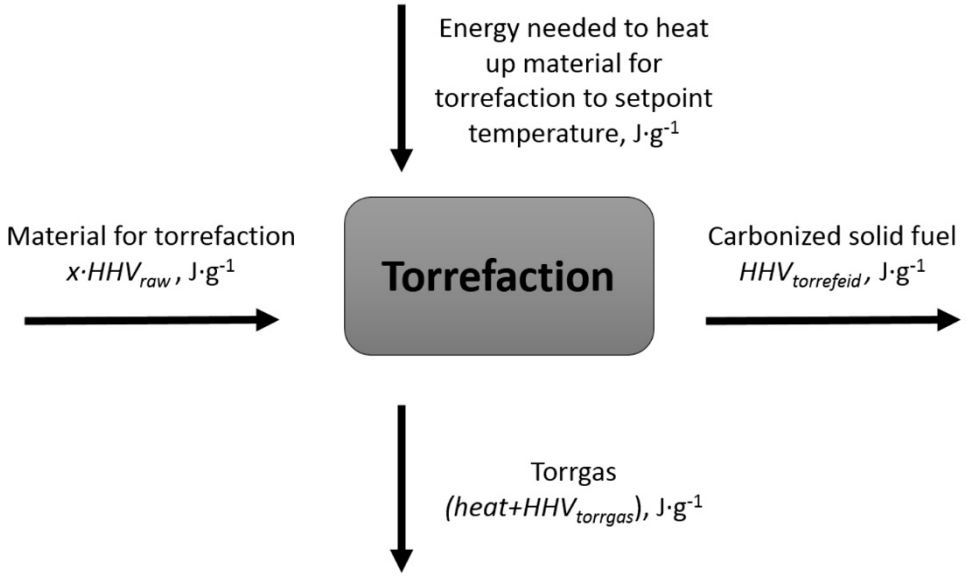

Figure 3. Energy balance of torrefaction to produce CSF (energy/mass).

The energy consumption of the torrefaction was estimated similarly to the model developed by Stępień et al. [37]. The model calculates energy needed to heat material to the setpoint temperature of torrefaction and uses the TGA and DSC analyses. In this research, the energy required to heat SS and D from 20 °C (room temperature) to 200, 220, 240, 260, 280, and 300 °C was estimated and then increased by multiplying it by x value to determine the energy needed to produce 1 g of CSF. The energy contained in a torrgas was calculated as Equation (8). Equation (8) was based on the assumption that total energy contained in torrgas (heat (energy contained in gas temperature) and chemical (energy contained in torrgas composition)) was a sum of external energy delivered to heat up material and energy contained in released volatiles minus the energy that remained in CSF. In reality,

the total energy potential of torrgas is lower than the calculated one due to the heat loss when CSF is removed from the reactor to the cooling stage (energy from the CSF cooling process was omitted for ease of calculations).

$$E_{torrgas} = E_{heat\ up} + E_{raw} - E_{CSF} \quad (8)$$

where $E_{torrgas}$ is the energy contained in torrgas (J·g^{-1}), $E_{heat\ up}$ is the energy needed to heat dry SS or D to setpoint temperature to produce 1 g of CSF (J·g^{-1}), E_{raw} is the energy contained in raw material (dry SS or D) before torrefaction used to obtain 1 g of CSF (J·g^{-1}), and E_{CSF} is the energy contained in 1 g of the obtained CSF (J·g^{-1}).

If the energy contained in torrgas was higher than the energy needed to heat materials SS or D to the setpoint temperature, it was assumed that the process of CSF generation was self-sufficient. The energy contained in 1 g of obtained CSF was calculated as *HHV* based on the *HHV* results.

3. Results

Raw data from the tests described in Sections 2.2–2.5 are presented in the Supplementary Materials. The results from the particular tests were tabulated on five excel sheets. The first sheet "Read Me" is a guide about how to find data. The sheet "Torrefaction Process" contains the results of process mass yield, energy densification ratio, and energy yield. The sheet "Proximate Analysis" contains results of moisture content, organic matter content, combustible part content, ash content, and high heating value of the tested materials. Next, the sheets named "TGA (Isothermal Condition)" and "TGA (Non-Isothermal Condition)" contain results from the thermogravimetric analysis. The last sheet "DSC" contains results from differential scanning calorimetry.

3.1. The Effect of Torrefaction Temperature and Time on CSF Properties

The mass yields (*MY*) for SS and D torrefaction decreased with an increase of process temperature (Figure 4). This trend was more apparent for the D than for SS. At 300 °C and 60 min torrefaction, *MY* was ~80% and 40% for SS and D, respectively. The highest *MY* values were obtained for CSFs generated at the lowest temperature (200 °C). For both models, all regression coefficients were statistically significant ($p < 0.05$) (Table A1), and determination coefficients (R^2) were >0.83, which indicates a reasonable fit to the experimental data. For the SS model, the most important coefficient was a_6 ($\beta = -6.27$), whereas, in the D model, it was a_6 ($\beta = -4.34$). The sum of standardized β coefficients (a_2—a_7) for these models was −0.4 and −0.52, respectively, for SS and D (Table A1), which means that generally, the *MY* value was decreasing with the increase of torrefaction temperature and process time.

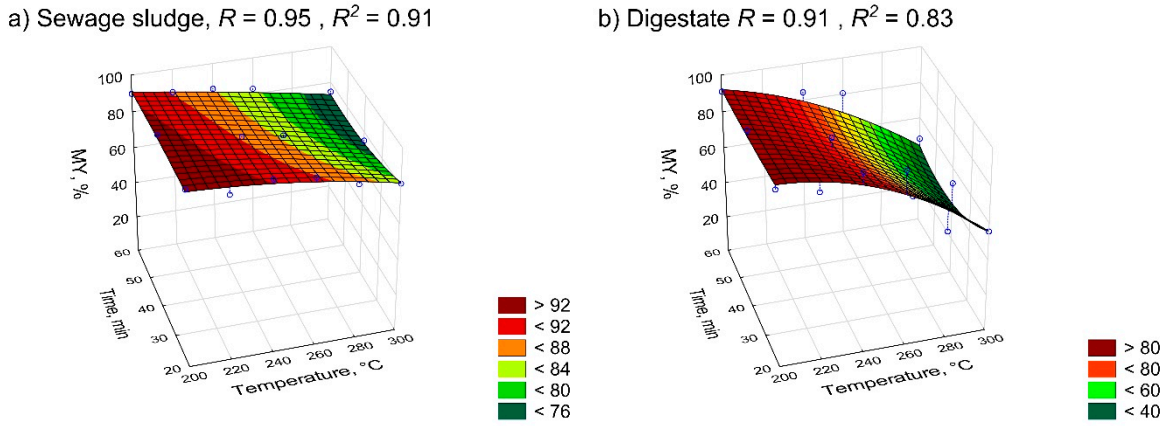

Figure 4. The influence of torrefaction temperature and residence time on the mass yield of CSF from (**a**) sewage sludge and (**b**) digestate. *R*—correlation coefficient; R^2—determination coefficient.

The *EDr* in CSF generated from SS decreased with an increase of process temperature, whereas it increased for D (Figure 5). CSFs from SS produced at 200 °C had an *EDr* of ~1.01, while CSFs

generated at 300 °C had an *EDr* of ~0.85. For CSFs generated from D, *EDr* values were ~1.01–1.10. It appears that CSF production from D was promoted by short residence time up to ~40 min and high torrefaction temperature (280–300 °C). For SS, time did not have an impact on *EDr* and was promoted at low temperatures (200–240 °C) (Figure 5). For both models, all regression coefficients were statistically significant ($p < 0.05$) (Table A2), while the R^2 was 0.85 and 0.68 for SS and D, respectively. The most important coefficient was a_3 ($\beta = -4.20$), whereas, in the D model, it was a_6 ($\beta = -12.91$) (Table A2). The sum of standardized β coefficients (a_2–a_7) was −0.56 and −0.49, respectively, for SS and D (Table A2). This means that generally, the *EDr* value decreased with the increase of torrefaction temperature and process time. It is somewhat surprising in the case of D where *EDr* increased, but this increase was not consistent across the studied range; the *EDr* decrease was apparent for torrefaction longer than ~40 min and higher than ~260 °C (Figure 5).

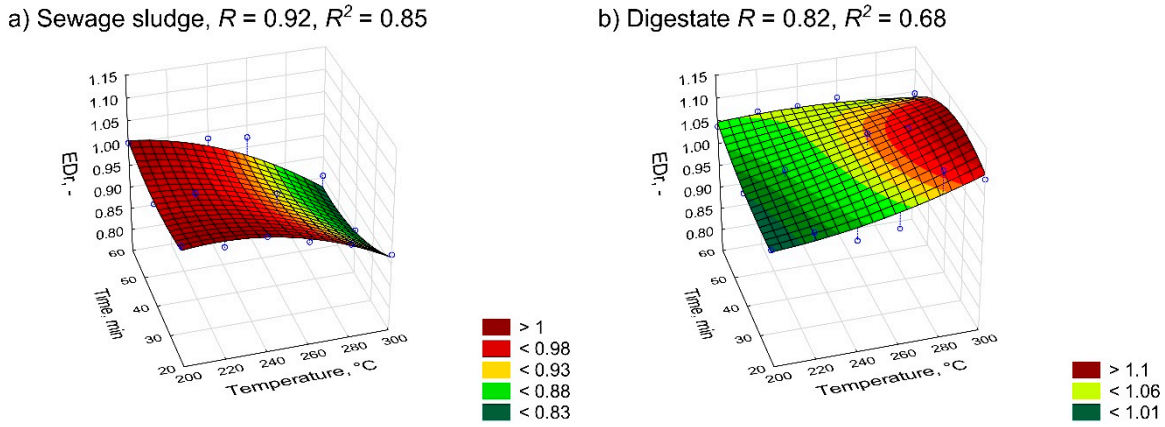

Figure 5. The influence of torrefaction temperature and residence time on the energy densification ratio of CSF from (**a**) sewage sludge and (**b**) digestate. *R*—correlation coefficient; R^2—determination coefficient.

The *EY* for CSF decreased with an increase in process temperature for both SS and D. The time had a lower impact on *EY* compared to the temperature (Figure 6). For SS, the *EY* decreased from ~100 to ~60%, whereas for D, it decreased from ~100 to ~45%. All regression coefficients were statistically significant ($p < 0.05$) (Table A3), with $R^2 = 0.9$ and 0.83 for SS and D, respectively. The most important coefficients were a_6 ($\beta = -4.55$) for SS and a_3 ($\beta = -3.79$) for D (Table A3). The sum of the standardized β coefficients (a_2–a_7) for these models was −0.55 and −0.59, respectively, for SS and D (Table A3), which means that generally, *EY* decreased with the increase of torrefaction temperature and process time.

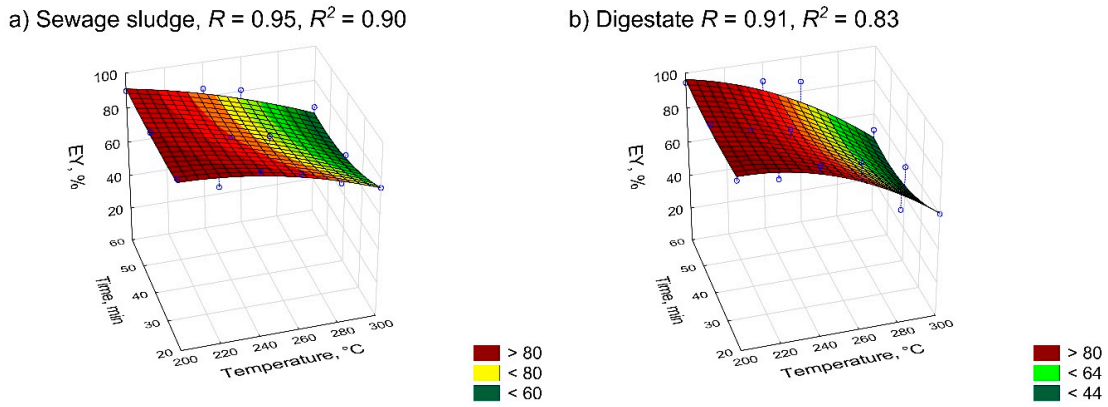

Figure 6. The influence of torrefaction temperature and residence time on the energy yield of CSF from (**a**) sewage sludge and (**b**) digestate. *R*—correlation coefficient; R^2—determination coefficient.

3.2. Result of Proximate Analysis of CSF

The *OM* content in CSFs decreased with an increase in temperature. CSF from SS was characterized by a lower *OM* (~57~47%) compared with D-derived CSF (~87%~75%) (Figure 7). The time and temperature had a significant impact ($p < 0.05$) on decreasing *OM*. Statistical differences between particular measurements are given in the Tables A8 and A9. There were no differences in *OM* ($p < 0.05$) for CSFs generated from SS in a range from 200 °C (20~60 min) to 220 (20~40 min) (Table A8). In the case of D, more differences between particular process ranges ($p < 0.05$) were found (Table A9). The R^2 values for SS and D were 0.89 and 0.83, respectively. All regression coefficients were statistically significant ($p < 0.05$) (Table A4). The most important coefficient was a_6 ($\beta = -5.15$) for SS and a_3 ($\beta = -2.83$) for D (Table A4). The sum of the standardized β coefficients (a_2–a_7) for these models was −0.42 and −0.77, respectively (Table A4). This means that, generally, the *OM* value decreased with the increase of torrefaction temperature and process time. The sum of the β coefficients for D was lower than for SS; the total loss in the organic matter was greater for D (Table A4).

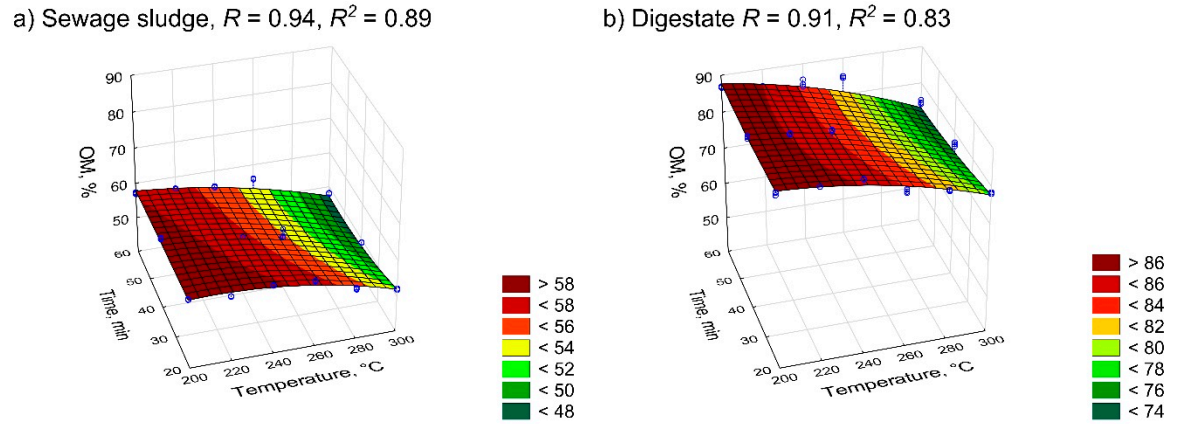

Figure 7. The influence of torrefaction temperature and residence time on the organic matter content in CSF from (**a**) sewage sludge and (**b**) digestate. *R*—correlation coefficient; R^2—determination coefficient.

The ash content ranged from ~40% to ~48% and from ~12% to ~24% for SS and D, respectively. Torrefaction increased the ash content in CSF from both SS and D, and it was significant with the increase in temperature and residence time ($p < 0.05$) (Figure 8). The statistical differences between ash content for particular conditions are given in Tables A10 and A11. There were no differences in ash content ($p < 0.05$) (Table A10) in CSFs from SS produced at 200 °C for 40~60 min, and up to 240 °C for 20~60 min. All regression coefficients were statistically significant ($p < 0.05$) (Table A5), and the models' R^2 values were 0.88 and 0.82 for SS and D, respectively. The most important coefficient for the SS model was a_6 ($\beta = 5.10$), whereas it was a_4 ($\beta = 2.47$) for the D model (Table A5). The sum of the standardized β coefficients (a_2–a_7) for these models was 0.42 and 1.22, respectively, for SS and D (Table A5). This means that the ash content generally increased with the increase of torrefaction temperature and process time. The sum of the β coefficients was higher for D than for SS; the CSF production from D was characterized by a faster increase in ash content (relative to the initial ash content of the raw material).

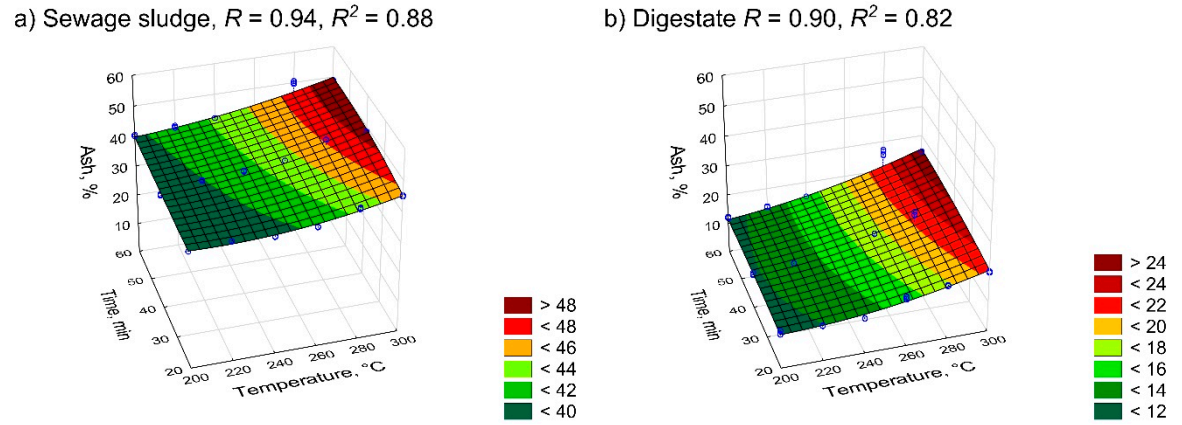

Figure 8. The influence of torrefaction temperature and residence time on ash content in CSF from (**a**) sewage sludge and (**b**) digestate. *R*—correlation coefficient; R^2—determination coefficient.

The content of *CP* had an opposite trend to ash content. *CP* decreased from ~60% to ~52% and from ~88% to ~76% for SS and D, respectively (Figure 9). There were no differences in *CP* in CSFs from SS produced at 200 °C for 40~60 min up to 240 °C for 20~60 min ($p < 0.05$) (Table A12), similar to the trend observed for the ash content. The statistical differences between the *CP* of D-derived CSFs were varied (Table A13). All regression coefficients were statistically significant ($p < 0.05$) (Table A6). Both models had high R^2 values of 0.88 and 0.82, for SS and D, respectively. The most important coefficient for the SS model was a_6 ($\beta = -5.10$), whereas it was a_4 ($\beta = -2.47$) for the D model (Table A6). The sum of the standardized β coefficients (a_2–a_7) for these models was −0.42 and −1.22, respectively, for SS and D (Table A6). This trend was the opposite one to observed for ash content.

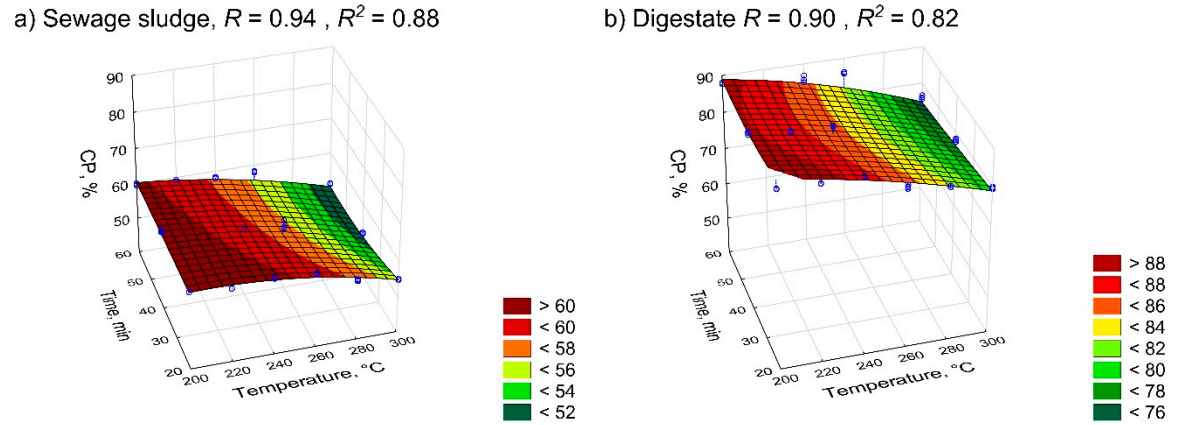

Figure 9. The influence of torrefaction temperature and residence time on combustible parts in CSF from (**a**) sewage sludge and (**b**) digestate. *R*—correlation coefficient; R^2—determination coefficient.

The torrefaction for SS resulted in a decrease of *HHV* from ~14 to ~13 MJ·kg^{-1} with an increase in residence time and process temperature (Figure 10a). However, an increase in *HHV* with temperature was observed for the D where the *HHV* increased up to 40 min. The longer torrefaction of D past 40 min caused the *HHV* to decrease again. The highest value of *HHV* for D-derived CSF was ~20 MJ·kg^{-1} at 300 °C and 40 min (Figure 10b). There were no statistical differences in *HHV* ($p < 0.05$) for D-derived CSFs produced from 200 °C for 40~60 min up to 280 °C for 20 min (Table A15). The statistical differences between the *HHV* of SS-derived CSFs are presented in Table A14. All regression coefficients were statistically significant ($p < 0.05$) (Table A7), and the R^2 of D was only 0.52; it was 0.81 for SS. The most important coefficient for the SS model was a_6 ($\beta = -4.09$), whereas it was a_6 ($\beta = 11.87$) for the D model (Table A7). The sum of standardized β coefficients (a_2–a_7) was −0.55 and −0.46, for SS and D,

respectively (Table A7). The trends observed here were similar to *EDr*, namely, despite the increase of the *HHV* from a certain point, it began to decrease, allowing for process optimization.

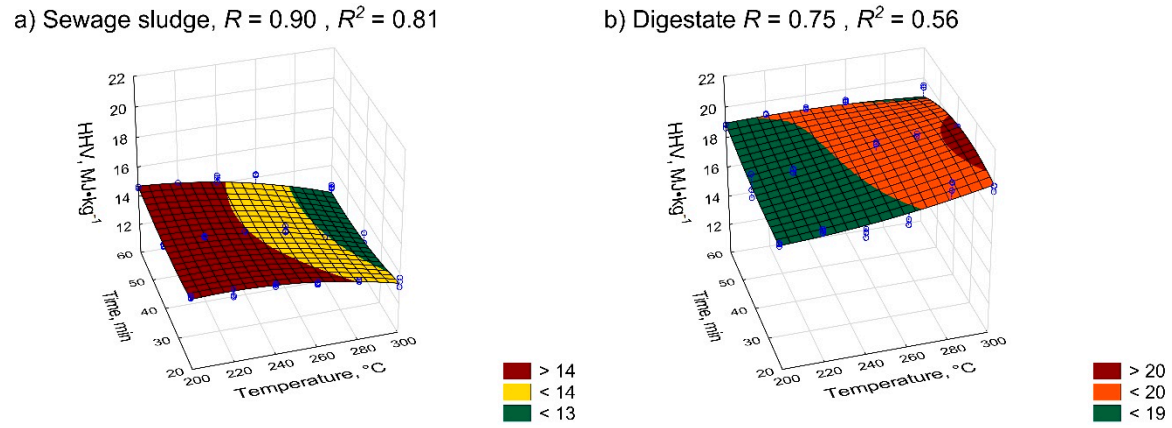

Figure 10. The influence of torrefaction temperature and residence time on the high heating value of CSF from (**a**) sewage sludge and (**b**) digestate. *R*—correlation coefficient; R^2—determination coefficient.

3.3. The Thermogravimetric Analysis

The reaction rates (*k*) constants for the first-order equation were calculated based on mass losses during torrefaction for each process temperatures (Figures 11 and 12 and Table 1). Next, an Arrhenius plot was created from *k* values, and then linear models were created (Figure 13), from which E_a and *A* values were calculated. The determination coefficient for SS was higher than for D (R^2 = 0.99 vs. R^2 = 0.90, respectively) (Figure 13). The *k* for 200~280 °C was higher for SS ($k = 8.71 \times 10^{-6}$~2.99×10^{-5}), whereas at 300 °C, the *k* value of D was greater ($k = 4.60 \times 10^{-5}$) (Table 1). The E_a and *A* parameters ranged from 46,700 to 52,230 and from 0.75 to 1.95, respectively (Table 1).

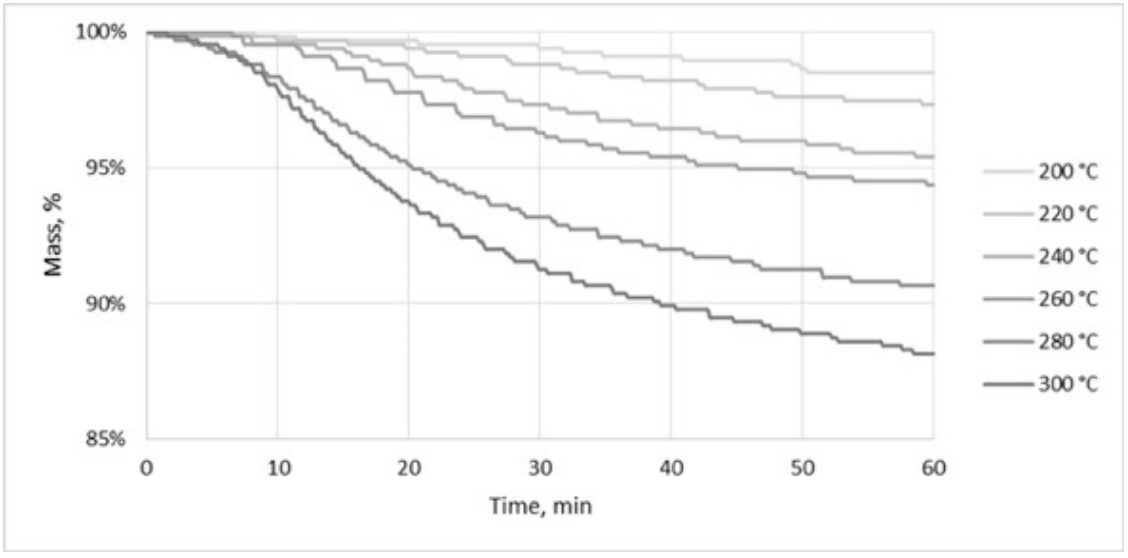

Figure 11. TGA of sewage sludge at torrefaction temperatures.

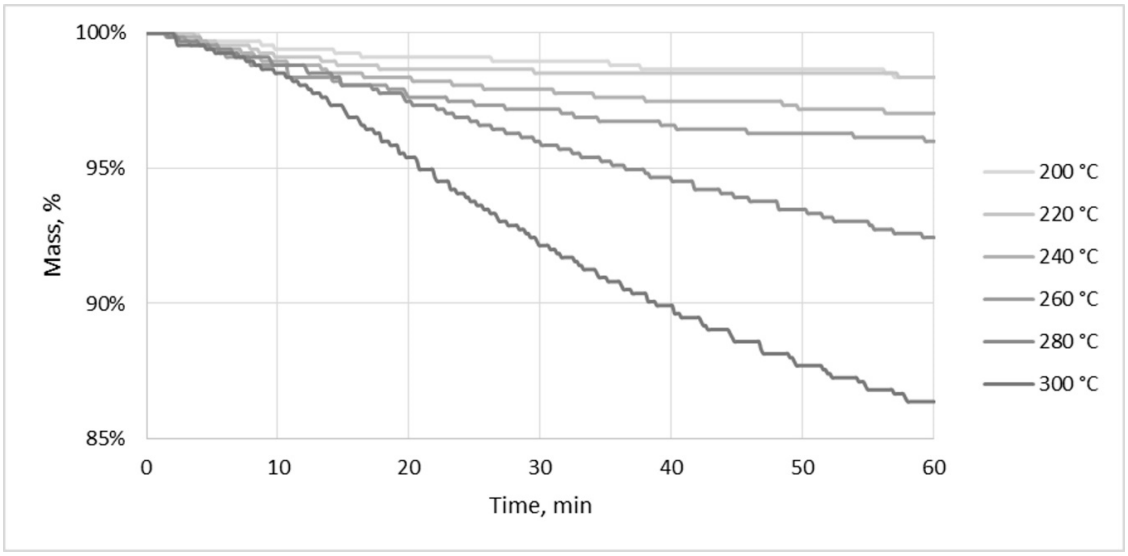

Figure 12. TGA of digestate at torrefaction temperatures.

Table 1. Summary of kinetic parameters of the torrefaction process.

Material	T, °C	T, K	k, s^{-1}	E_a, $J \cdot mol^{-1}$	A, s^{-1}
Sewage sludge	200	473	4.73×10^{-6}	46,700	0.75
	220	493	8.71×10^{-6}		
	240	513	1.52×10^{-5}		
	260	533	1.90×10^{-5}		
	280	553	2.99×10^{-5}		
	300	573	3.85×10^{-5}		
Digestate	200	473	4.91×10^{-6}	52,230	1.95
	220	493	4.46×10^{-6}		
	240	513	7.79×10^{-6}		
	260	533	1.09×10^{-5}		
	280	553	2.34×10^{-5}		
	300	573	4.60×10^{-5}		

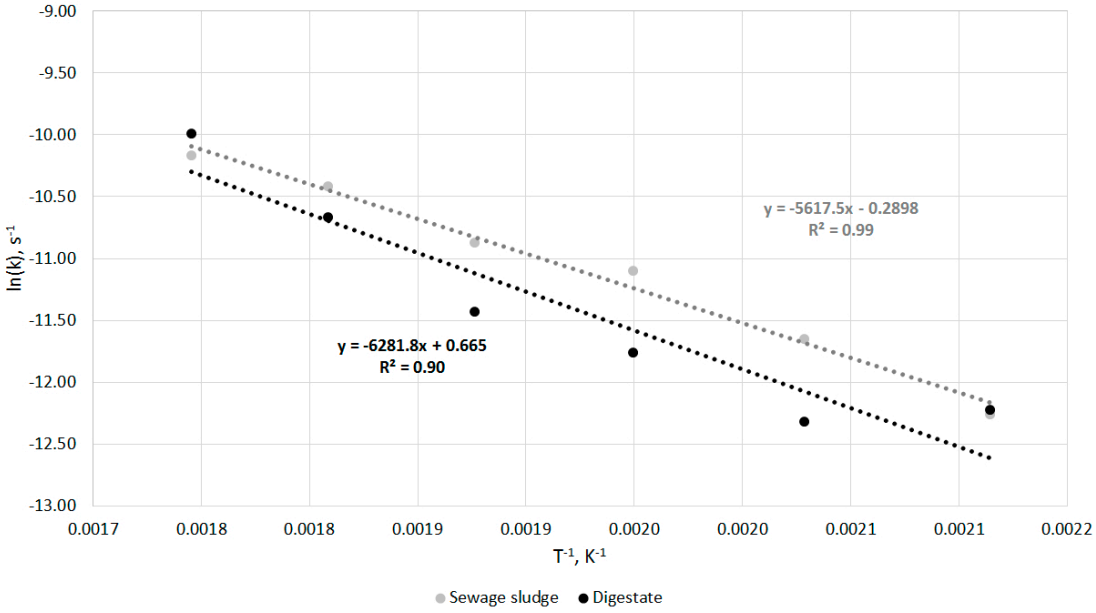

Figure 13. Arrhenius plot for sewage sludge and digestate.

Figure 14 presents a thermal decomposition in an inert condition under non-isothermal conditions for SS and D samples heated from 50 to 850 °C. The decomposition of SS started at ~200–240 °C, whereas the decomposition of D started at 260–270 °C. After ~450 °C, the thermal decomposition of D sped up compared to SS, and at the end (850 °C), D had an average weight loss of ~63%, whereas SS had one of ~50% (Figure 14). The principal decomposition of the D started at ~350 °C and ended at ~550 °C, with a maximum decomposition peak at ~475 °C (DTG = 0.5%). For SS, a principal thermal decomposition started earlier at ~300 °C and ended at ~700 °C, with a maximum decomposition peak at ~500 °C (DTG = 0.2%).

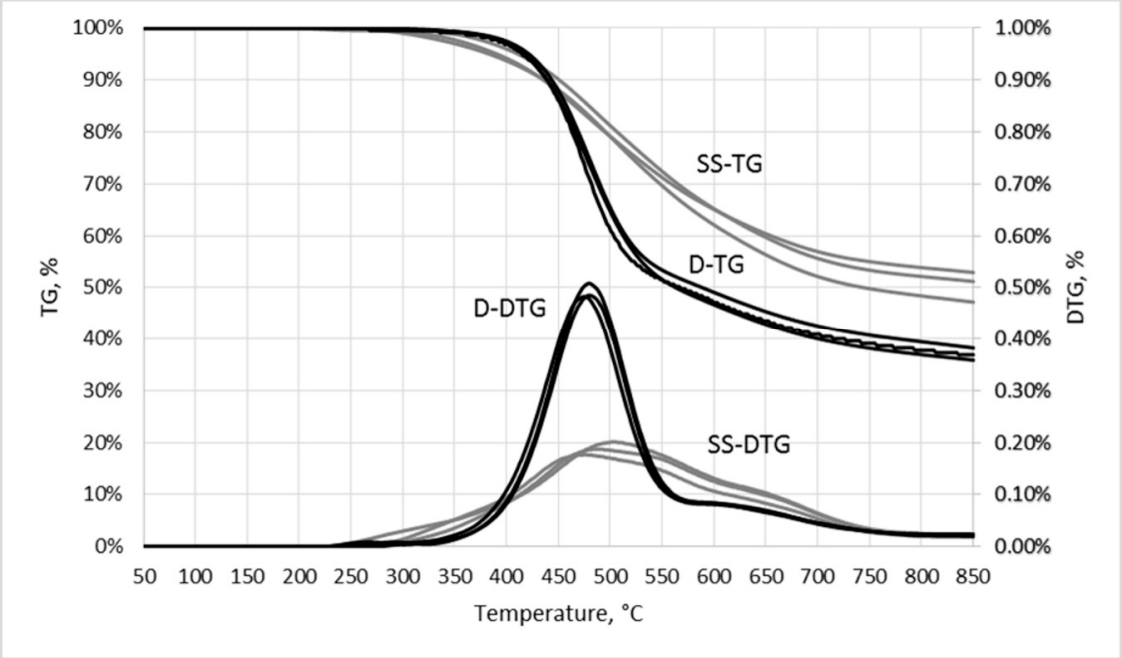

Figure 14. The thermogravimetric characteristic of sewage sludge (SS) and digestate (D) heated from 50 °C to 850 °C.

3.4. The Differential Scanning Calorimetry

Differential scanning calorimetry analysis revealed heat flow characteristics and energy needs to heat SS and D from 20 °C to 500 °C with a heating rate of 10 °C·min^{-1} in a nitrogen atmosphere. One endoenergetic transformation occurred for SS; the transformation started at 72 °C and ended at 170 °C (Figure 15). During transformation, two peaks occurred—first at 102 °C and second at 155 °C. The total energy needed for this transformation was 21.53 J·g^{-1}. After transformation, the energy needs for heating SS started to decrease. The decrease of heat flow with an increase of temperature from 170 to 500 °C was almost linear (Figure 15).

In the case of D, two transformations occurred. The first one was an endothermic transformation. It started at 36 °C and ended at 168 °C. The second transformation was exothermic. It started at 285 °C and ended at 351 °C, with a maximum peak at 327 °C. The total energy needed for the endothermic reaction was 115.19 J·g^{-1}, whereas the exothermic one emitted 39.84 J·g^{-1} (Figure 16).

The energy demand for heating SS and D to the setpoint of torrefaction was estimated based on results from the TGA analysis (Figure 14) and DSC analysis (Figures 15 and 16). Since the estimations were based on dried SS and D, the energy needed for water removal was not included. The energy demand estimation was completed based on the protocol proposed by Stępień et al. [37]. Then, the energy needed to produce 1 g of CSF was estimated as the "energy needed to heat 1 g of raw material" (Table 2) multiplied by x (Equation (7)). The results showed that heating 1 g of SS from 20 to 200–300 °C required more energy (449–643 J·g^{-1}) compared to the energy needed for heating of 1 g of digestate (381~492 J·g^{-1}) to the same torrefaction setpoint (Table 2). Due to the mass loss occurring

during the process, the *MY* decreased, and, therefore, the *x* value (Equation (7)) increased from 1.05 to 1.37 and 1.02 to 2.30 for SS and D, respectively (Table 2). The energy needed to produce 1 g of CSF increased with torrefaction temperature and time in the case of both SS and D. The decreasing trend of energy contained in CSF produced from SS in higher torrefaction temperatures and times conditions for SS was observed, whereas for D, the trend was opposite.

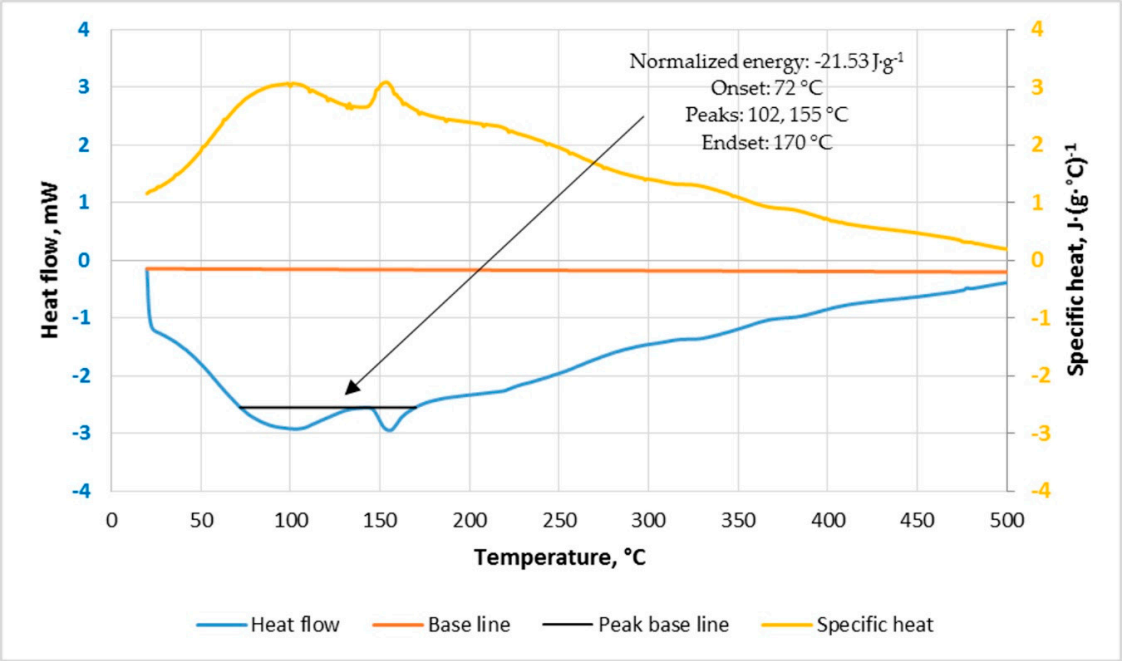

Figure 15. DSC analysis of sewage sludge.

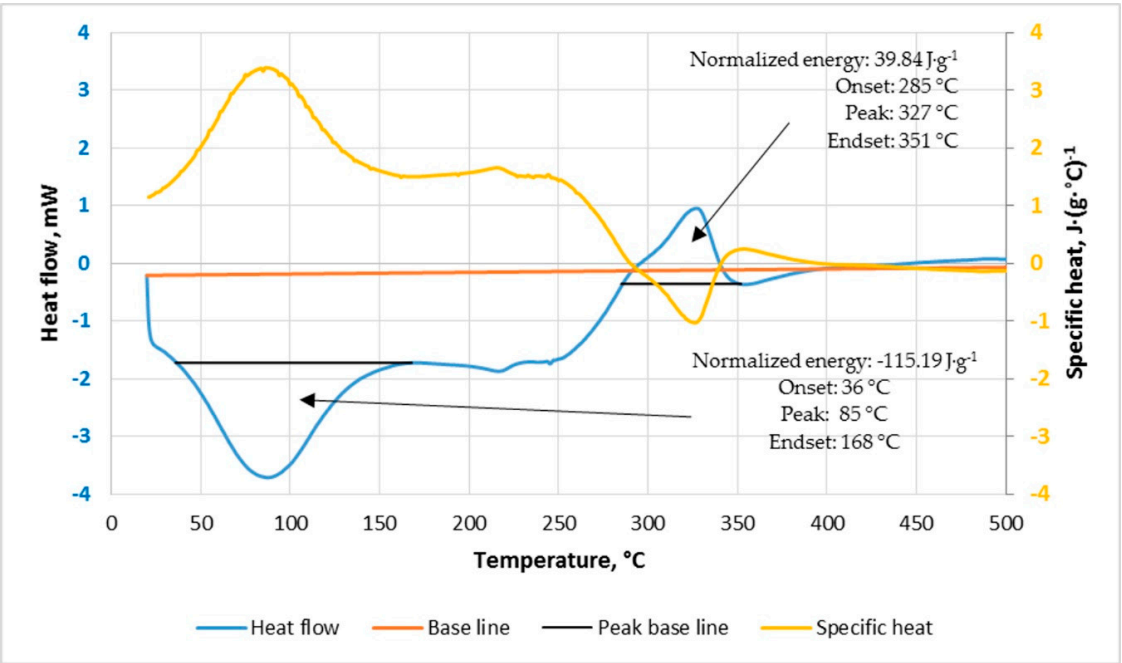

Figure 16. DSC analysis of digestate.

Table 2. Results of torrefaction energy balance.

Feedstock	Torrefaction temperature, °C	Torrefaction residence time, min	Energy needed to heat up 1 g of raw material, J·g^{-1}	*MY*, %	x, -	Energy needed to produce 1 g of CSF, J·g^{-1}	Energy contained in raw material used to produce 1 g of CSF, J·g^{-1}	Energy contained in 1 g of CSF, J·g^{-1}	Energy contained in torrgas (heat and $HHV_{torrgas}$), J·g^{-1}
Sewage sludge	200	20	449	94.94	1.05	473	15,368	14,692	1150
		40	449	93.54	1.07	480	15,597	14,414	1663
		60	449	90.42	1.11	497	16,135	14,668	1964
	220	20	496	93.86	1.07	529	15,544	14,758	1315
		40	496	90.71	1.10	547	16,084	14,322	2309
		60	496	87.35	1.14	568	16,704	14,456	2816
	240	20	540	92.00	1.09	587	15,859	14,655	1791
		40	540	87.30	1.15	619	16,712	14,066	3265
		60	540	84.06	1.19	642	17,358	14,088	3912
	260	20	579	89.34	1.12	648	16,330	14,383	2596
		40	579	83.32	1.20	695	17,512	13,646	4560
		60	579	80.55	1.24	719	18,113	13,565	5267
	280	20	613	85.90	1.16	714	16,986	13,941	3759
		40	613	78.76	1.27	779	18,525	13,062	6241
		60	613	76.83	1.30	798	18,989	12,887	6900
	300	20	643	81.66	1.22	787	17,868	13,330	5325
		40	643	73.62	1.36	873	19,817	12,314	8376
		60	643	72.90	1.37	882	20,013	12,054	8840
Digestate	200	20	381	98.14	1.02	388	18,432	18,122	698
		40	381	94.18	1.06	405	19,209	18,210	1404
		60	381	91.70	1.09	415	19,728	18,822	1322
	220	20	413	96.11	1.04	430	18,823	18,269	984
		40	413	88.95	1.12	465	20,336	18,521	2280
		60	413	86.34	1.16	479	20,952	18,900	2530
	240	20	444	90.76	1.10	489	19,931	18,505	1915
		40	444	80.86	1.24	549	22,371	18,864	4056
		60	444	78.85	1.27	563	22,944	18,915	4591
	260	20	472	82.12	1.22	575	22,029	18,828	3776
		40	472	69.91	1.43	676	25,877	19,238	7314
		60	472	69.21	1.44	683	26,138	18,868	7953
	280	20	490	70.17	1.43	699	25,779	19,240	7238
		40	490	56.09	1.78	875	32,254	19,644	13,485
		60	490	57.43	1.74	854	31,498	18,757	13,594
	300	20	492	54.92	1.82	895	32,936	19,740	14,091
		40	492	39.40	2.54	1248	45,918	20,082	27,085
		60	492	43.52	2.30	1130	41,571	18,584	24,117

4. Discussion

4.1. The Impact of Torrefaction Technological Parameters on the Efficiency of the Process and Fuel Properties

The *MY* of SS and D showed a decreasing trend during torrefaction. *MY* decreased with the increase of the process temperature. The *MY* of SS decreased to ~80%, whereas for D, it decreased up to ~40% at 300 °C (Figure 4). The decreasing trend for both tested materials was also shown in the case of *EY*. Despite twice differences for *MY*, the *EY* differences were smaller, i.e., the tested SS and D contained 60% and 50% of their initial energy content, respectively, for the maximum torrefaction temperature of 300 °C (Figure 6). The 10% difference in *EY* resulted from differences in the *EDr* (Figure 5). For SS, the value of *EDr* decreased, whereas for D, *EDr* increased with the increase of temperature. Differences in *EDr* were likely a result of differences in *OM* and the composition and thermal reactivity of SS and D. However, the *MY* of SS torrefaction was comparable to other studies (Table 3). Torrefaction is feasible for CSF production for additional types of abundant waste feedstock (refuse-derived fuel, sawdust, pruned biomass, walnut shells, spent mushroom compost, and elephant dung) [34,38–42].

Pulka et al. [38] torrefied a SS, originating from different wastewater treatment plants, by means of a tubular furnace at temperatures 200–300 °C for 1 h with a resulting *MY* of 90~80%. The *MY* of the torrefaction process of D can be compared to lignocellulose materials such as Oxytree pruning biomass or sawdust (*MY* 92~55% and 94~33%, respectively) (Table 3). The lower *MY* of D and lignocellulose materials resulted from much lower ash content in raw materials. There were over 30% of ash in the biomass waste (Table 3), which resulted in a decrease of *OM* content due to its decomposition during torrefaction (Table 3). The decreasing trend of *EDr* with temperature and time for SS (Figure 5) was also confirmed by Pulka et al. [38], where *EDr* was 0.96–0.29 (T = 200~300 °C, t = 1 h). Compared to the results in this study, *EDr* was ~1.0–0.83 for the same conditions (Figure 5). D-derived CSF showed an uptrend for *EDr* for 20 and 40 min, while for 60 min, *EDr* (1.05) was stable regardless of the process temperature (Figure 5). The uptrend of *EDr* resulted from the torrefied material energy densification. A similar uptrend was also visible in other materials such as Oxytree pruned biomass, reuse-derived fuel (RDF), and sawdust (Table 3).

The properties of the tested SS were *OM* = 61.9%, ash = 36.3%, *CP* = 63.7%, and *HHV* = 14.6 MJ·kg^{-1}. Similar values for SS-derived CSF were reported by Pulka et al. [38], where *OM*, ash, and *HHV* were 56.2%, 43.1%, and 13.5 MJ·kg^{-1}, respectively. For the tested D, proximate analyses showed *OM*, ash, *CP*, and *HHV* of 86.6%, 12.4%, 87.6%, and 18.1 MJ·kg^{-1}, respectively. The main outcome of the analysis was that SS had a higher ash content and, therefore, a lower *HHV* than D. In comparison to elephant dung (the product of methane fermentation in the elephant stomach) [34], the tested D from biogas plant had over five times less ash content and was comparable *HHV* (Table 3). It follows that the initial fermentation of substrates has a crucial influence on final product properties. In terms of energy content, SS and D were incomparable with typical energy biomass substrates, e.g., *Miscanthus x Giganteus*, *Rosa multiflora* (energetic rose), and *Salix viminalis* (willow) that have an *HHV* of 17.68, 17.54, and 17.5 MJ·kg^{-1}, respectively [43].

This study showed that *OM* (Figure 7) and *CP* (Figure 9) decreased with the increase of process temperature and time, whereas the ash content increased ($p < 0.05$) (Figure 8) (Tables A8–A13) for both SS and D. This effect was expected during biomass torrefaction and confirmed by other works. The organic compounds of biomass are degraded under high temperatures and are removed in the form of gas, whereas inorganic materials remain in biomass [36,38].

Ash acts as ballast; its higher concentration results in a decrease of energy fuel quality. In the tested SS, an initial high ash concentration (36.3%) contributed to a high ash concentration of ~40–50% in CSF (Figure 8). As a result of the devolatilization of *OM* and increased ash content, the *HHV* of SS-derived CSFs started to decrease with an increase of temperature and time (Figure 10). The *HHV* decreased from ~14 to ~13 MJ·kg^{-1} (200–300 °C). Similar findings were obtained for elephant dung, where ash content increased by ~50–71% and *HHV* decreased from 11.4 to 6.5 MJ·kg^{-1} (200~300 °C, 1 h) (Table 3). The reduction of energy content in solid residue after torrefaction was also reported by

Syguła et al. [40], where spent mushroom compost was torrefied. The calorific value of the torrefied biomass increased with process temperature up to 280 °C (13.8~17.8 MJ·kg^{-1}), whereas at 300 °C, *HHV* decreased to 14.3 MJ·kg^{-1}.

Table 3. Summarized results of the torrefaction process technological parameters for different waste materials (process time = 1 h).

Material	Temperature, °C	*MY*, %	*EDr*	*EY*, %	*OM*, %	Ash, %	*CP*, %	*HHV*, MJ·kg^{-1}	Reference
Sewage sludge	Raw	-	-	-	56.2	43.1	-	13.5	[38]
	200	90	0.96	86	56.4 ^{vm}	43.6	-	12.9	
	220	91	0.98	89	56.2 ^{vm}	43.8	-	13.2	
	240	89	0.99	88	55.9 ^{vm}	44.1	-	13.4	
	260	88	0.48	42	36.3 ^{vm}	63.7	-	6.5	
	280	87	0.30	26	27.7 ^{vm}	72.3	-	4.1	
	300	80	0.29	23	26.6 ^{vm}	73.4	-	3.9	
Elephant dung	Raw	-	-	-	48.9	50.8	49.2	11.4	[34]
	200	96	1.14	109	57.4	42.5	57.5	13.0	
	220	90	1.12	102	60.2	39.8	60.2	12.8	
	240	89	0.83	74	49.8	50.1	49.9	9.5	
	260	90	0.91	82	44.8	55.1	44.9	10.3	
	280	63	0.81	52	28.3	71.5	28.5	7.5	
	300	73	0.86	63	28.7	71.3	28.7	6.5	
Spent Mushroom Compost	Raw	-	-	-	71.6 ^{vm}	28.4	-	13.8	[40]
	200	97	1.07	103	69.7 ^{vm}	30.3	-	14.4	
	220	99	1.18	116	76.7 ^{vm}	23.3	-	15.9	
	240	96	1.10	105	71.5 ^{vm}	28.5	-	14.8	
	260	95	1.16	110	69.8 ^{vm}	30.2	-	15.5	
	280	93	1.33	123	68.2 ^{vm}	31.8	-	17.8	
	300	90	1.06	95	57.4 ^{vm}	42.6	-	14.3	
Pruning Oxytree biomass	Raw	-	-	-	90.2	8.1	91.9	18.3	[41]
	200	92	1.05	96	89.3	8.7	91.3	19.2	
	220	88	1.06	93	88.3	9.7	90.3	19.4	
	240	78	1.11	86	86.6	11.2	88.8	20.4	
	260	64	1.16	74	85.0	12.5	87.5	21.1	
	280	57	1.18	67	83.2	13.9	86.1	21.6	
	300	55	1.20	66	83.3	13.6	86.4	22.0	
Walnut Shells	Raw	-	-	-	81.4 ^{vm}	0.6	-	19.6	[42]
	200	87	1.05	91	78.4 ^{vm}	0.7	-	20.6	
	220	84	1.06	89	77.8 ^{vm}	0.9	-	20.7	
	240	70	1.08	75	75.4 ^{vm}	1.2	-	21.1	
	260	64	1.13	72	70.2 ^{vm}	1.5	-	22.1	
	280	39	1.18	46	60.2 ^{vm}	2.1	-	23.1	
	300	43	1.24	54	44.7 ^{vm}	2.2	-	24.3	
Refuse-Derived Fuel (RDF)	Raw	-	-	-	76.0 ^{vm}	14.3	-	26.9	[39]
	200	85	0.94	80	74.7 ^{vm}	14.1	-	28.2	
	220	73	1.07	78	72.9 ^{vm}	16.4	-	31.4	
	240	61	0.99	60	63.5 ^{vm}	21.6	-	29.9	
	260	55	1.04	57	56.9 ^{vm}	23.9	-	31.5	
	280	58	1.03	60	60.4 ^{vm}	23.1	-	31.5	
	300	62	1.13	70	61.9 ^{vm}	23.2	-	34.1	
Sawdust	Raw	-	-	-	77.6 ^{vm}	0.5	-	19.6	[39]
	200	94	0.99	93	76.9 ^{vm}	0.6	-	20.0	
	220	75	1.12	84	65.3 ^{vm}	0.9	-	21.2	
	240	58	1.17	68	58.8 ^{vm}	0.9	-	22.4	
	260	42	1.24	52	48.8 ^{vm}	1.3	-	23.5	
	280	40	1.26	51	44.3 ^{vm}	1.4	-	24.7	
	300	33	1.33	44	40.5 ^{vm}	1.6	-	25.8	

^{vm}—given as the volatile matter (%).

This research showed that SS torrefaction at the lowest temperature of 200 °C was sufficient due to the lack of significant return on the *HHV* increase (Figure 10), ash content increase (Figure 8), and energy consumption for the process (Table 2). On the other hand, the torrefied D showed the opposite trend, as *HHV* increased with process temperature and time (Figure 10), i.e., the CSF produced at 300 °C and 30 min (the curve fitted value from the measured time periods) had the highest *HHV* (20 MJ·kg^{-1}). This value was comparable to torrefied sawdust at 200 °C (19.6 MJ·kg^{-1}) [39] or the torrefied pruned biomass of the Oxytree at 240 °C (20.4 MJ·kg^{-1}) [41].

The energetic properties of SS and D-derived CSF were not as high as those associated with other alternative biowaste material used to torrefaction. For example, torrefied spent coffee grounds had an *HHV* of 21–22 MJ·kg^{-1} with an ash content of 1.4% [44], and the *HHV* for the de-oiled seed from biodiesel production was ~23 MJ·kg^{-1} with ash content of ~9.4% [45].

4.2. Thermogravimetric Analysis of Raw Materials and Kinetic Parameters of Torrefaction

The reported TGA analyses of SS and D showed that both materials have similar activation energies of 46.7 and 52.2 kJ·mol^{-1}, yet different pre-exponential factors of 0.75 and 1.95 s^{-1}, respectively (Table 4). Table 4 summarizes the kinetic parameters of materials for which these parameters were determined by the same method as in the study. The higher k values were associated with higher decomposition rates and higher mass losses during torrefaction. This was confirmed by *MY*, as *MY* for D was lower than for SS at the same process temperature (Figure 4). The tested materials were more thermally degradable than elephant dung ($k = 1.16 \times 10^{-6}$~2.73×10^{-5} s^{-1}) and spent mushroom compost ($k = 1.70 \times 10^{-5}$~4.60×10^{-5} s^{-1}), and they were less degradable from lignocellulose materials such pruned Oxytree biomass ($k = 1.43 \times 10^{-5}$~7.25×10^{-5} s^{-1}) (Table 4). This was likely due to the *OM* composition. SS and D have less lignin than woody materials. Lignin is harder to decompose than other biomass constituents such as hemicellulose or cellulose.

Table 4. Summary of the torrefaction kinetic parameters for different materials.

Material	Mass, g	Experimental k (200–300 °C), s^{-1}	E_a,J·mol^{-1}	*A*, s^{-1}	*OM*, %	Ash, %	Reference
Sewage sludge	2.25	4.73×10^{-6}–3.83×10^{-5}	46.70	7.48×10^{-1}	61.9	36.3	-
Digestate	2.25	4.91×10^{-6}–4.60×10^{-5}	52.23	1.94×10^{0}	86.6	12.4	-
Sewage sludge	2.25	4.02×10^{-5}–6.71×10^{-5}	12.02 *	6.97×10^{-4} *	59.7	40.3	[38]
Elephant dung	2.25	1.16×10^{-6}–2.73×10^{-5}	17.70 *	9.60×10^{-4} *	48.9	50.8	[34]
Spent mushroom compost	2.25	1.70×10^{-5}–4.60×10^{-5}	21.92 *	3.90×10^{-3} *	71.6	28.4	[40]
Pruning Oxytree biomass	3.00	1.43×10^{-5}–7.25×10^{-5} *	36.44 *	1.53×10^{-1} *	90.2	8.1	[41]
RDF	-	2.11×10^{-3}–1.75×10^{-3} *	3.67 *	3.50×10^{-5} *	85.8	13.3	[39]

* recalculated in accordance with Section 2.4. TGA of raw material based on means k value available in articles: [34,38–41].

The chemical SS composition differed depending on the origin. Hattori and Mukai [46] tested six SS materials with *OM* ranging from 32.3 to 94.1%, and the hemicelluloses, celluloses, and lignin content ranged from 5.1% to 9.8%, 0.2% to 5%, and 9.9% to 29.1%, respectively [46]. The tested D was mainly made from corn (30%), beet pulp (30%), and organic municipal waste (34%), so each constituent of D was a non-lignin material. For example, corn stover is mainly composed of cellulose (~35%), hemicellulose (~20%), and lignin (~12%) [47], and sugar beet pulp is primarily composed of hemicellulose (~23%), cellulose (~22%) and lignin (~2%) [48]. For comparison, wood is typically composed of ~25% hemicelluloses, 45% cellulose, and 25% lignin [49]. Ash content is almost always very low at <5% [50], i.e., over 95% of the mass is organic, and in result, the total amount of lignin was higher than in SS or D where ash decreased the amount of *OM*.

4.3. Differential Scanning Calorimetry Analysis

For both tested materials, a DSC analysis began with the endothermic reaction peaks at 102 (or 155) and 85 °C for SS and D, respectively (Figures 15 and 16). Because SS and D were dried before DSC analysis and reactions start at lower temperatures than drying temperature (105 °C), water evaporation could be excluded as a reason for this phenomenon. On the other hand, biomass samples may have absorbed some moisture from the air before the test. In the study of Bryś et al. [51], endothermic peaks were observed in the temperature range of 80–120 °C for dry and wet woody biomass (beech, willow, alder, and spruce). These peaks were assigned to moisture evaporation. For all wet woody biomass,

a large endothermic peak derived from the water was observed, while in the samples after drying, the peak was very small [51].

Chemical composition was not tested during this study; thus, the origin of particular transformations remains unclear. Peaks at 102, 155, and 85 °C were unlikely to belong to the degradation of proteins, fats, or sugars. Protein peaks took place at ~60–100 °C [52]. Fat melting and crystallization peaks were found at lower temperatures than ~40–45 °C [53,54]. In contrast, sugar transitions peaks tend to have sharper shapes than those found in this study and take place at different temperatures, e.g., fructose, glucose, and sucrose melt at 135~156, 159~180, and 194~203 °C, respectively [55].

In general, the charring process is exothermal, whereas volatilization is endothermic [56]. In our study, the results of the DSC analysis did not have an apparent link to the results of the TGA analysis. The occurrence of endothermic reactions did not make any apparent mass changes in the DTG plot (Figure 14). The endothermic reactions ended at ~170 °C, whereas a mass loss in the DTG plot started >200 °C. This might have been a result of insufficient precision in the use of the laboratory balance. The tested D had one exothermic transformation at 327 °C (Figure 16). This transformation may have been a result of lignin charring. A study by Yang et al. [57] revealed that separate DSC analyses of hemicellulose and lignin showed exothermic peaks at 275 and 365 °C, respectively, whereas the thermal degradation of cellulose was endothermic.

The calculated energy needed to heat up a 1 g of the dry mass of the tested materials from 20 to 300 °C in inert conditions was 643 and 492 $J \cdot g^{-1}$ for SS and D, respectively. On the other hand, the energy needed to produce 1 g of CSF in the same conditions (60 min) was, respectively, 882 and 1130 $J \cdot g^{-1}$. This was likely a result of mass losses during torrefaction, i.e., more than 1 g of raw material must be processed to produce 1 g of CSF.

Table 2 shows that the energy balance of dry SS and D torrefaction was energetically self-efficient due to the energy contained in torrgas. The heat of torrgas and $HHV_{torrgas}$ was greater than the energy needed to heat SS and D to the setpoint temperature. Consequently, torrgas can be used as a source of energy for a torrefaction process. Of course, these are only theoretical calculations based on small samples of SS and D that were torrefied in ideal conditions. Scaling up with more complex calculations—that should cover, e.g., heat losses during CSF cooling, the air temperature used to torrgas combustion, equipment efficiency—are still needed. Water evaporation (~2 257 $J \cdot g^{-1}$ at 100 °C and 1 atm) [58] from raw waste should be also included.

In terms of CSF energy content, the calculations showed that the best variant for SS torrefaction was 200 °C and 60 min, where the produced CSF had 14 692 $J \cdot g^{-1}$, whereas, for D, it was 300 °C and 40 min, which produced CSF with 20 082 $J \cdot g^{-1}$. The production of these CSFs consumed 15,368 and 45,918 $J \cdot g^{-1}$ of energy contained in raw SS and D, respectively. The differences between output and input energy increased by energy added to heat a raw material comprised energy that was converted to torrgas. For the best variants of CSF production, the values of energy contained in torrgas (heat and HHV_{torrgas}) were 1150 and 27 085 $J \cdot g^{-1}$ for SS and D, respectively.

The best variants of SS and D CSF had *HHV* values of 14.8 and 20 $MJ \cdot kg^{-1}$, respectively. Based on these values, SS and D can be classified in accordance with EN 15359:2012 standard to third and fourth classes, for which *LHV* has to be ≥15 and ≥10 $MJ \cdot kg^{-1}$, respectively. Thus, it is possible that D-derived CSF would be classified as second class (≥20 $MJ \cdot kg^{-1}$); nevertheless, moisture absorbed from the atmosphere during CSF storage can make torrefaction difficult. The content of chlorine and mercury was not measured in this study.

5. Conclusions

The following conclusions arise from this research:

- The torrefaction of dry sewage sludge and digestate is energetically self-sufficient.
- Torrefaction improved the higher heating value of the digestate, but it did not improve the *HHV* of sewage sludge. The torrefied digestate had the highest *HHV* = 20 $MJ \cdot kg^{-1}$ under 300 °C and 30 min (the curve fitted from the measured time periods) compared to *HHV* = 18 $MJ \cdot kg^{-1}$ for the

unprocessed digestate. The torrefied sewage sludge had the highest *HHV* = 14.8 MJ·kg^{-1} under 200 °C and 20 min, as compared to *HHV* 14.6 MJ·kg^{-1} for raw sewage sludge.

- An unwanted result of torrefaction is an increase in ash content in CSF. A higher ash content results in higher waste production during combustion on the incineration plant. Ash content in the torrefied digestate with the highest *HHV* was 22%, whereas sewage sludge was 40% ash.
- The kinetics parameters showed that both materials had similar thermal degradability.
- To heat a dried sewage sludge and digestate from 20 to 300 °C, 643 and 492 J·g^{-1} are needed, respectively.
- Approximately 15.4 and 45.9 MJ·kg^{-1} of energy contained in the dry sewage sludge and digestate are needed to produce CSF with the greatest *HHV*, respectively.

This research shows that there is a potential in using D as a substrate for torrefaction and its valorization as an improved fuel source, whereas the potential in using SS for fuel and is questionable due to a lack of *HHV* increase. The energetic potential of CSF can be enhanced by increasing the density of the material (pelletization), but this process requires additional energy [59]. Due to CSF's low energy value, it seems that it would be more profitable to find another application for this material, e.g., agriculture, because SS-derived CSF has a reduced heavy metal mobility for the reclamation of contaminated sites [60] or as a soil fertilizer [61].

The next step should be to identify the technological parameters for the torrefaction of D on a technical scale and to check the possibilities of further energy densification (e.g., by pelletization). This is important for the investment analysis and technology design of the process on the industrial scale.

Supplementary Materials: The following are available online at http://www.mdpi.com/1996-1073/13/12/3161/s1. Excel: data on the fuel properties of carbonized solid fuels (CSF) produced from sewage sludge and digestate.

Author Contributions: Conceptualization, K.Ś.; methodology, K.Ś., and P.S.; software, K.Ś.; validation, K.Ś., P.S., and M.H.; formal analysis, K.Ś., M.H., and S.K.; investigation, M.H., P.S., S.K., and K.Ś.; resources, P.S.; data curation, K.Ś.; writing—original draft preparation, K.Ś.; writing—review and editing, K.Ś., S.S.-D., A.B., and J.K.; visualization, K.Ś.; supervision, A.B., and J.A.K. All authors have read and agreed to the published version of the manuscript.

Funding: This research was funded by the Polish Ministry of Science and Higher Education (2015–2019), the Diamond Grant Program # 0077/DIA/2015/14. This research was partially supported by the Iowa Agriculture and Home Economics Experiment Station, Ames, Iowa. Project no. IOW05556 (Future Challenges in Animal Production Systems: Seeking Solutions through Focused Facilitation) sponsored by Hatch Act and State of Iowa funds.

Acknowledgments: The presented article results were obtained as part of the activity of the leading research team—Waste and Biomass Valorization Group (WBVG), https://www.upwr.edu.pl/research/50121/waste_and_biomass_valorization_group_wbvg.html.

Conflicts of Interest: The authors declare no conflict of interest. The funders had no role in the design of the study; in the collection, analyses, or interpretation of data; in the writing of the manuscript, or in the decision to publish the results.

Appendix A

Appendix A contains a statistical evaluation of empirical models presented in the article. Tables A1–A7 present the evaluations of the intercept and coefficients values presented for particular models. In these tables, standardized B coefficients are presented.

Tables A8–A15 show statistical evaluations of statistically significant differences for particular temperatures and residence times for particular observations.

Table A1. Statistical evaluation of model coefficients for the *MY* of CSF from sewage sludge and digestate.

Material	Intercept/ Coefficient	Value of Intercept/ Coefficient	Standard Error	*p*	Lower Limit of Confidence	Upper Limit of Confidence	Standardized β Coefficient
Sewage sludge	a_1	2.50×10^{-1}	6.67×10^{-1}	0.00	-1.22×10^{0}	1.72×10^{0}	–
	a_2	5.64×10^{-3}	4.40×10^{-3}	0.00	-4.05×10^{-3}	1.53×10^{-2}	2.76
	a_3	-1.08×10^{-5}	0.00×10^{0}	0.00	-1.08×10^{-5}	-1.08×10^{-5}	−2.65
	a_4	2.08×10^{-2}	1.89×10^{-2}	0.00	-2.08×10^{-2}	6.25×10^{-2}	4.88
	a_5	-1.12×10^{-4}	1.23×10^{-4}	0.00	-3.82×10^{-4}	1.57×10^{-4}	−2.12
	a_6	-1.01×10^{-4}	7.48×10^{-5}	0.00	-2.65×10^{-4}	6.40×10^{-5}	−6.27
	a_7	2.26×10^{-9}	0.00×10^{0}	0.00	2.26×10^{-9}	2.26×10^{-9}	3.00
Digestate	a_1	-1.28×10^{0}	2.48×10^{0}	0.00	-6.74×10^{0}	4.17×10^{0}	-
	a_2	2.02×10^{-2}	1.64×10^{-2}	0.00	-1.58×10^{-2}	5.63×10^{-2}	3.55
	a_3	-4.31×10^{-5}	2.72×10^{-5}	0.00	-1.03×10^{-4}	1.67×10^{-5}	−3.79
	a_4	3.57×10^{-2}	7.03×10^{-2}	0.00	-1.19×10^{-1}	1.91×10^{-1}	3.00
	a_5	-1.63×10^{-4}	4.56×10^{-4}	0.00	-1.17×10^{-3}	8.40×10^{-4}	−1.10
	a_6	-1.94×10^{-4}	2.78×10^{-4}	0.00	-8.07×10^{-4}	4.18×10^{-4}	−4.34
	a_7	4.54×10^{-9}	0.00×10^{0}	0.00	4.54×10^{-9}	4.54×10^{-9}	2.16

$MY = a_1 + a_2 \cdot T + a_3 \cdot T^2 + a_4 \cdot t + a_5 \cdot t^2 + a_6 \cdot T \cdot t + a_7 \cdot T^2 \cdot t^2$, T ranged from 200 °C to 300 °C, t ranged from 20 min to 60 min; more information in the 'CSF Production Method and Process Analysis' section.

Table A2. Statistical evaluation of model coefficients for the *EDr* of CSF from sewage sludge and digestate.

Material	Intercept/ Coefficient	Value of Intercept/ Coefficient	Standard Error	*p*	Lower Limit of Confidence	Upper Limit of Confidence	Standardized β coefficient
Sewage sludge	a_1	2.37×10^{-1}	7.31×10^{-1}	0.00	-1.37×10^{0}	1.85×10^{0}	-
	a_2	7.06×10^{-3}	4.83×10^{-3}	0.00	-3.56×10^{-3}	1.77×10^{-2}	4.04
	a_3	-1.47×10^{-5}	0.00×10^{0}	0.00	-1.47×10^{-5}	-1.47×10^{-5}	−4.20
	a_4	3.68×10^{-3}	2.07×10^{-2}	0.00	-4.20×10^{-2}	4.93×10^{-2}	1.01
	a_5	3.02×10^{-5}	1.34×10^{-4}	0.00	-2.66×10^{-4}	3.26×10^{-4}	0.67
	a_6	-3.68×10^{-5}	8.20×10^{-5}	0.00	-2.17×10^{-4}	1.44×10^{-4}	−2.67
	a_7	3.84×10^{-10}	0.00×10^{0}	0.00	3.84×10^{-10}	3.84×10^{-10}	0.59
Digestate	a_1	1.58×10^{0}	6.37×10^{-1}	0.00	1.79×10^{-1}	2.98×10^{0}	–
	a_2	-4.26×10^{-3}	4.21×10^{-3}	0.00	-1.35×10^{-2}	5.01×10^{-3}	−4.11
	a_3	7.42×10^{-6}	0.00×10^{0}	0.00	7.42×10^{-6}	7.42×10^{-6}	3.59
	a_4	-2.29×10^{-2}	1.81×10^{-2}	0.00	-6.27×10^{-2}	1.69×10^{-2}	−10.57
	a_5	1.67×10^{-4}	1.17×10^{-4}	0.00	-9.07×10^{-5}	4.25×10^{-4}	6.24
	a_6	1.05×10^{-4}	7.16×10^{-5}	0.00	-5.22×10^{-5}	2.63×10^{-4}	12.91
	a_7	-3.27×10^{-9}	0.00×10^{0}	0.00	-3.27×10^{-9}	-3.27×10^{-9}	−8.55

$EDr = a_1 + a_2 \cdot T + a_3 \cdot T^2 + a_4 \cdot t + a_5 \cdot t^2 + a_6 \cdot T \cdot t + a_7 \cdot T^2 \cdot t^2$, T ranged from 200 °C to 300 °C, t ranged from 20 min to 60 min; more information in the 'CSF Production Method and Process Analysis' section.

Table A3. Statistical evaluation of model coefficients for the *EY* of CSF from sewage sludge and digestate.

Material	Intercept/ Coefficient	Value of Intercept/ Coefficient	Standard Error	*p*	Lower Limit of Confidence	Upper Limit of Confidence	Standardized β coefficient
Sewage sludge	a_1	-1.94×10^{-1}	1.09×10^{0}	0.00	-2.59×10^{0}	2.20×10^{0}	-
	a_2	1.02×10^{-2}	7.19×10^{-3}	0.00	-5.62×10^{-3}	2.60×10^{-2}	3.10
	a_3	-2.08×10^{-5}	1.19×10^{-5}	0.00	-4.71×10^{-5}	5.43×10^{-6}	−3.18
	a_4	2.06×10^{-2}	3.09×10^{-2}	0.00	-4.74×10^{-2}	8.85×10^{-2}	2.99
	a_5	-7.24×10^{-5}	2.00×10^{-4}	0.00	-5.13×10^{-4}	3.68×10^{-4}	−0.85
	a_6	-1.18×10^{-4}	1.22×10^{-4}	0.00	-3.86×10^{-4}	1.51×10^{-4}	−4.55
	a_7	2.35×10^{-9}	0.00×10^{0}	0.00	2.35×10^{-9}	2.35×10^{-9}	1.94
Digestate	a_1	-1.08×10^{0}	2.37×10^{0}	0.00	-6.30×10^{0}	4.14×10^{0}	–
	a_2	1.90×10^{-2}	1.57×10^{-2}	0.00	-1.55×10^{-2}	5.35×10^{-2}	3.48
	a_3	-4.13×10^{-5}	2.60×10^{-5}	0.00	-9.85×10^{-5}	1.60×10^{-5}	−3.79
	a_4	2.28×10^{-2}	6.73×10^{-2}	0.00	-1.25×10^{-1}	1.71×10^{-1}	1.99
	a_5	-5.70×10^{-5}	4.36×10^{-4}	0.00	-1.02×10^{-3}	9.03×10^{-4}	−0.40
	a_6	-1.37×10^{-4}	2.66×10^{-4}	0.00	-7.23×10^{-4}	4.49×10^{-4}	−3.19
	a_7	2.66×10^{-9}	0.00×10^{0}	0.00	2.66×10^{-9}	2.66×10^{-9}	1.32

$EY = a_1 + a_2 \cdot T + a_3 \cdot T^2 + a_4 \cdot t + a_5 \cdot t^2 + a_6 \cdot T \cdot t + a_7 \cdot T^2 \cdot t^2$, T ranged from 200 °C to 300 °C, t ranged from 20 min to 60 min; more information in the 'CSF Production Method and Process Analysis' section.

Table A4. Statistical evaluation of model coefficients for the *OM* content in CSF from sewage sludge and digestate.

Material.	Intercept/ Coefficient	Value of Intercept/ Coefficient	Standard Error	*p*	Lower Limit of Confidence	Upper Limit of Confidence	Standardized β Coefficient
Sewage sludge	a_1	-2.18×10^{-2}	1.99×10^{-1}	0.00	-4.23×10^{-1}	3.79×10^{-1}	–
	a_2	5.07×10^{-3}	1.32×10^{-3}	0.00	2.42×10^{-3}	7.72×10^{-3}	4.45
	a_3	-1.01×10^{-5}	0.00×10^{0}	0.00	-1.01×10^{-5}	-1.01×10^{-5}	−4.43
	a_4	9.46×10^{-3}	5.65×10^{-3}	0.00	-1.92×10^{-3}	2.08×10^{-2}	3.97
	a_5	-4.42×10^{-5}	3.66×10^{-5}	0.00	-1.18×10^{-4}	2.95×10^{-5}	−1.50
	a_6	-4.62×10^{-5}	2.24×10^{-5}	0.00	-9.12×10^{-5}	-1.21×10^{-6}	−5.15
	a_7	9.40×10^{-10}	0.00×10^{0}	0.00	9.40×10^{-10}	9.40×10^{-10}	2.24
Digestate	a_1	5.49×10^{-1}	3.08×10^{-1}	0.00	-7.04×10^{-2}	1.17×10^{0}	–
	a_2	3.37×10^{-3}	2.03×10^{-3}	0.00	-7.17×10^{-4}	7.46×10^{-3}	2.33
	a_3	-8.17×10^{-6}	0.00×10^{0}	0.00	-8.17×10^{-6}	-8.17×10^{-6}	−2.83
	a_4	1.93×10^{-3}	8.73×10^{-3}	0.00	-1.56×10^{-2}	1.95×10^{-2}	0.64
	a_5	1.06×10^{-5}	5.66×10^{-5}	0.00	-1.03×10^{-4}	1.24×10^{-4}	0.28
	a_6	-1.57×10^{-5}	3.46×10^{-5}	0.00	-8.52×10^{-5}	5.38×10^{-5}	−1.38
	a_7	1.02×10^{-10}	0.00×10^{0}	0.00	1.02×10^{-10}	1.02×10^{-10}	0.19

$OM = a_1 + a_2 \cdot T + a_3 \cdot T^2 + a_4 \cdot t + a_5 \cdot t^2 + a_6 \cdot T \cdot t + a_7 \cdot T^2 \cdot t^2$, T ranged from 200 °C to 300 °C, t ranged from 20 min to 60 min; more information in the 'CSF production method and process analysis' section.

Table A5. Statistical evaluation of model coefficients for the ash content in CSF from sewage sludge and digestate.

Material	Intercept/ Coefficient	Value of Intercept/ Coefficient	Standard Error	*p*	Lower Limit of Confidence	Upper Limit of Confidence	Standardized β Coefficient
Sewage sludge	a_1	9.26×10^{-1}	1.94×10^{-1}	0.00	5.36×10^{-1}	1.32×10^{0}	–
	a_2	-4.46×10^{-3}	1.28×10^{-3}	0.00	-7.03×10^{-3}	-1.88×10^{-3}	−4.15
	a_3	8.83×10^{-6}	0.00×10^{0}	0.00	8.83×10^{-6}	8.83×10^{-6}	4.12
	a_4	-8.71×10^{-3}	5.49×10^{-3}	0.00	-1.98×10^{-2}	2.34×10^{-3}	−3.88
	a_5	3.81×10^{-5}	3.56×10^{-5}	0.00	-3.35×10^{-5}	1.10×10^{-4}	1.37
	a_6	4.31×10^{-5}	2.17×10^{-5}	0.00	-6.46×10^{-7}	8.68×10^{-5}	5.10
	a_7	-8.48×10^{-10}	0.00×10^{0}	0.00	-8.48×10^{-10}	-8.48×10^{-10}	−2.14
Digestate	a_1	-1.73×10^{-2}	3.26×10^{-1}	0.00	-6.74×10^{-1}	6.39×10^{-1}	–
	a_2	-5.53×10^{-4}	2.15×10^{-3}	0.00	-4.89×10^{-3}	3.78×10^{-3}	−0.38
	a_3	4.04×10^{-6}	0.00×10^{0}	0.00	4.04×10^{-6}	4.04×10^{-6}	1.37
	a_4	7.62×10^{-3}	9.25×10^{-3}	0.00	-1.10×10^{-2}	2.62×10^{-2}	2.47
	a_5	-6.43×10^{-5}	6.00×10^{-5}	0.00	-1.85×10^{-4}	5.63×10^{-5}	−1.69
	a_6	-2.01×10^{-5}	3.66×10^{-5}	0.00	-9.37×10^{-5}	5.36×10^{-5}	−1.73
	a_7	6.43×10^{-10}	0.00×10^{0}	0.00	6.43×10^{-10}	6.43×10^{-10}	1.18

Ash $= a_1 + a_2 \cdot T + a_3 \cdot T^2 + a_4 \cdot t + a_5 \cdot t^2 + a_6 \cdot T \cdot t + a_7 \cdot T^2 \cdot t^2$, T ranged from 200 °C to 300 °C, t ranged from 20 min to 60 min; more information in the 'CSF Production Method and Process Analysis' section.

Table A6. Statistical evaluation of model coefficients for the *CP* in CSF from sewage sludge and digestate.

Material	Intercept/ Coefficient	Value of Intercept/ Coefficient	Standard Error	*p*	Lower Limit of Confidence	Upper Limit of Confidence	Standardized β Coefficient
Sewage sludge	a_1	7.40×10^{-2}	1.94×10^{-1}	0.00	-3.15×10^{-1}	4.64×10^{-1}	–
	a_2	4.46×10^{-3}	1.28×10^{-3}	0.00	1.88×10^{-3}	7.03×10^{-3}	4.15
	a_3	-8.83×10^{-6}	0.00×10^{0}	0.00	-8.83×10^{-6}	-8.83×10^{-6}	−4.12
	a_4	8.71×10^{-3}	5.49×10^{-3}	0.00	-2.34×10^{-3}	1.98×10^{-2}	3.88
	a_5	-3.81×10^{-5}	3.56×10^{-5}	0.00	-1.10×10^{-4}	3.35×10^{-5}	−1.37
	a_6	-4.31×10^{-5}	2.17×10^{-5}	0.00	-8.68×10^{-5}	6.46×10^{-7}	−5.10
	a_7	8.48×10^{-10}	0.00×10^{0}	0.00	8.48×10^{-10}	8.48×10^{-10}	2.14
Digestate	a_1	1.02×10^{0}	3.26×10^{-1}	0.00	3.61×10^{-1}	1.67×10^{0}	–
	a_2	5.53×10^{-4}	2.15×10^{-3}	0.00	-3.78×10^{-3}	4.89×10^{-3}	0.38
	a_3	-4.04×10^{-6}	0.00×10^{-0}	0.00	-4.04×10^{-6}	-4.04×10^{-6}	−1.37
	a_4	-7.62×10^{-3}	9.25×10^{-3}	0.00	-2.62×10^{-2}	1.10×10^{-2}	−2.47
	a_5	6.43×10^{-5}	6.00×10^{-5}	0.00	-5.63×10^{-5}	1.85×10^{-4}	1.69
	a_6	2.01×10^{-5}	3.66×10^{-5}	0.00	-5.36×10^{-5}	9.37×10^{-5}	1.73
	a_7	-6.43×10^{-10}	0.00×10^{0}	0.00	-6.43×10^{-10}	-6.43×10^{-10}	−1.18

$CP = a_1 + a_2 \cdot T + a_3 \cdot T^2 + a_4 \cdot t + a_5 \cdot t^2 + a_6 \cdot T \cdot t + a_7 \cdot T^2 \cdot t^2$, T ranged from 200 °C to 300 °C, t ranged from 20 min to 60 min; more information in the 'CSF Production Method and Process Analysis' section.

Table A7. Statistical evaluation of model coefficients for the *HHV* of CSF from sewage sludge and digestate.

Material	Intercept/ Coefficient	Value of Intercept/ Coefficient	Standard Error	*p*	Lower Limit of Confidence	Upper Limit of Confidence	Standardized β Coefficient
Sewage sludge	a_1	3.46×10^{0}	5.95×10^{0}	0.00	-8.51×10^{0}	1.54×10^{1}	–
	a_2	1.03×10^{-1}	3.93×10^{-2}	0.00	2.40×10^{-2}	1.82×10^{-1}	3.94
	a_3	-2.14×10^{-4}	6.52×10^{-5}	0.00	-3.45×10^{-4}	-8.26×10^{-5}	−4.09
	a_4	5.37×10^{-2}	1.69×10^{-1}	0.00	-2.86×10^{-1}	3.93×10^{-1}	0.98
	a_5	4.40×10^{-4}	1.09×10^{-3}	0.00	-1.76×10^{-3}	2.64×10^{-3}	0.65
	a_6	$-5.37 \times 10-^{4}$	6.68×10^{-4}	0.00	-1.88×10^{-3}	8.06×10^{-4}	−2.61
	a_7	5.60×10^{-9}	0.00×10^{0}	0.00	5.60×10^{-9}	5.60×10^{-9}	0.58
Digestate	a_1	2.86×10^{1}	6.95×10^{0}	0.00	1.46×10^{1}	4.26×10^{1}	-
	a_2	-7.70×10^{-2}	4.59×10^{-2}	0.00	-1.69×10^{-1}	1.53×10^{-2}	−3.78
	a_3	1.34×10^{-4}	7.62×10^{-6}	0.00	-1.91×10^{-6}	2.87×10^{-4}	3.30
	a_4	-4.15×10^{-1}	1.97×10^{-1}	0.00	-8.11×10^{-1}	-1.82×10^{-2}	−9.72
	a_5	3.02×10^{-3}	1.28×10^{-3}	0.00	4.56×10^{-4}	5.59×10^{-3}	5.73
	a_6	1.90×10^{-3}	7.80×10^{-4}	0.00	3.36×10^{-4}	3.47×10^{-3}	11.87
	a_7	-5.91×10^{-8}	0.00×10^{0}	0.00	-5.91×10^{-8}	-5.91×10^{-8}	−7.86

$HHV = a_1 + a_2 \cdot T + a_3 \cdot T^2 + a_4 \cdot t + a_5 \cdot t^2 + a_6 \cdot T \cdot t + a_7 \cdot T^2 \cdot t^2$, T ranged from 200 °C to 300 °C, t ranged from 20 min to 60 min; more information in the 'CSF Production Method and Process Analysis' section.

Table A8. Analysis of variance for organic matter content of sewage sludge.

SS, Tukey test for *OM*, a bold font signifies statistically significant difference ($p < 0.05$)		200	200	200	220	220	220	240	240	240	260	260	260	280	280	280	300	300	300
		20	40	60	20	40	60	20	40	60	20	40	60	20	40	60	20	40	60
200	20		0.97	**0.00**	**0.02**	**0.00**	**0.00**	1.00	**0.00**	**0.00**	0.09	**0.00**	**0.00**	**0.00**	**0.00**	**0.00**	**0.00**	**0.00**	**0.00**
200	40	0.97		**0.00**	**0.00**	**0.00**	**0.00**	0.57	**0.00**	**0.00**	**0.00**	**0.00**	**0.00**	**0.00**	**0.00**	**0.00**	**0.00**	**0.00**	**0.00**
200	60	**0.00**	**0.00**		0.29	1.00	0.87	**0.00**	0.08	**0.00**	0.06	**0.00**	**0.02**	**0.00**	**0.00**	**0.00**	**0.00**	**0.00**	**0.00**
220	20	**0.02**	**0.00**	0.29		0.08	**0.00**	0.11	**0.00**	**0.00**	1.00	**0.00**	**0.00**	**0.00**	**0.00**	**0.00**	**0.00**	**0.00**	**0.00**
220	40	**0.00**	**0.00**	1.00	0.08		1.00	**0.00**	0.28	**0.00**	**0.01**	**0.00**	0.08	**0.00**	**0.00**	**0.00**	**0.00**	**0.00**	**0.00**
220	60	**0.00**	**0.00**	0.87	**0.00**	1.00		**0.00**	0.97	**0.01**	**0.00**	**0.00**	0.73	**0.00**	**0.00**	**0.00**	**0.00**	**0.00**	**0.00**
240	20	1.00	0.57	**0.00**	0.11	**0.00**	**0.00**		**0.00**	**0.00**	0.44	**0.00**	**0.00**	**0.00**	**0.00**	**0.00**	**0.00**	**0.00**	**0.00**
240	40	**0.00**	**0.00**	0.08	**0.00**	0.28	0.97	**0.00**		0.46	**0.00**	0.17	1.00	**0.00**	**0.00**	**0.00**	**0.00**	**0.00**	**0.00**
240	60	**0.00**	**0.00**	**0.00**	**0.00**	**0.00**	**0.01**	**0.00**	0.46		**0.00**	1.00	0.84	**0.03**	**0.00**	**0.00**	**0.00**	**0.00**	**0.00**
260	20	0.09	**0.00**	0.06	1.00	**0.01**	**0.00**	0.44	**0.00**	**0.00**		**0.00**	**0.00**	**0.00**	**0.00**	**0.00**	**0.00**	**0.00**	**0.00**
260	40	**0.00**	**0.00**	**0.00**	**0.00**	**0.00**	**0.00**	**0.00**	0.17	1.00	**0.00**		0.47	0.13	**0.00**	**0.00**	**0.00**	**0.00**	**0.00**
260	60	**0.00**	**0.00**	**0.02**	**0.00**	0.08	0.73	**0.00**	1.00	0.84	**0.00**	0.47		**0.00**	**0.00**	**0.00**	**0.00**	**0.00**	**0.00**
280	20	**0.00**	**0.00**	**0.00**	**0.00**	**0.00**	**0.00**	**0.00**	**0.00**	**0.03**	**0.00**	0.13	**0.00**		**0.00**	**0.00**	**0.00**	**0.00**	**0.00**
280	40	**0.00**	**0.00**	**0.00**	**0.00**	**0.00**	**0.00**	**0.00**	**0.00**	**0.00**	**0.00**	**0.00**	**0.00**	**0.00**		**0.00**	**0.00**	0.50	**0.00**
280	60	**0.00**	**0.00**	**0.00**	**0.00**	**0.00**	**0.00**	**0.00**	**0.00**	**0.00**	**0.00**	**0.00**	**0.00**	**0.00**	**0.00**		**0.00**	**0.00**	0.39
300	20	**0.00**	**0.00**	**0.00**	**0.00**	**0.00**	**0.00**	**0.00**	**0.00**	**0.00**	**0.00**	**0.00**	**0.00**	**0.00**	**0.00**	**0.00**		**0.00**	**0.00**
300	40	**0.00**	**0.00**	**0.00**	**0.00**	**0.00**	**0.00**	**0.00**	**0.00**	**0.00**	**0.00**	**0.00**	**0.00**	**0.00**	0.50	**0.00**	**0.00**		0.17
300	60	**0.00**	**0.00**	**0.00**	**0.00**	**0.00**	**0.00**	**0.00**	**0.00**	**0.00**	**0.00**	**0.00**	**0.00**	**0.00**	**0.00**	0.39	**0.00**	0.17	

Table A9. Analysis of variance for organic matter content of digestate.

D, Tukey test for *OM*, a bold font signifies statistically significant difference ($p < 0.05$)		200	200	200	220	220	220	240	240	240	260	260	260	280	280	280	300	300	300
		20	40	60	20	40	60	20	40	60	20	40	60	20	40	60	20	40	60
200	20		1.00	1.00	1.00	0.80	**0.00**	1.00	**0.01**	**0.00**	**0.00**	**0.00**	**0.00**	**0.00**	**0.00**	**0.00**	**0.00**	**0.00**	**0.00**
200	40	1.00		1.00	1.00	0.89	**0.01**	1.00	**0.02**	**0.00**	**0.00**	**0.00**	**0.00**	**0.00**	**0.00**	**0.00**	**0.00**	**0.00**	**0.00**
200	60	1.00	1.00		1.00	1.00	0.07	0.98	0.23	**0.00**	**0.00**	**0.00**	**0.00**	**0.00**	**0.00**	**0.00**	**0.00**	**0.00**	**0.00**
220	20	1.00	1.00	1.00		0.89	**0.01**	1.00	**0.02**	**0.00**	**0.00**	**0.00**	**0.00**	**0.00**	**0.00**	**0.00**	**0.00**	**0.00**	**0.00**
220	40	0.80	0.89	1.00	0.89		0.42	0.60	0.78	**0.00**	**0.00**	**0.00**	**0.01**	**0.00**	**0.00**	**0.00**	**0.00**	**0.00**	**0.00**
220	60	**0.00**	**0.01**	0.07	**0.01**	0.42		**0.00**	1.00	0.66	**0.00**	**0.00**	0.98	**0.00**	**0.00**	**0.00**	**0.00**	**0.00**	**0.00**
240	20	1.00	1.00	0.98	1.00	0.60	**0.00**		**0.01**	**0.00**	**0.00**	**0.00**	**0.00**	**0.00**	**0.00**	**0.00**	**0.00**	**0.00**	**0.00**
240	40	**0.01**	**0.02**	0.23	**0.02**	0.78	1.00	**0.01**		0.31	**0.00**	**0.00**	0.79	**0.00**	**0.00**	**0.00**	**0.00**	**0.00**	**0.00**
240	60	**0.00**	**0.00**	**0.00**	**0.00**	**0.00**	0.66	**0.00**	0.31		**0.00**	**0.00**	1.00	**0.00**	**0.00**	**0.00**	**0.00**	**0.00**	**0.00**
260	20	**0.00**	**0.00**	**0.00**	**0.00**	**0.00**	**0.00**	**0.00**	**0.00**	**0.00**		**0.00**	**0.00**	**0.02**	**0.00**	**0.00**	**0.00**	**0.00**	**0.00**
260	40	**0.00**	**0.00**	**0.00**	**0.00**	**0.00**	**0.00**	**0.00**	**0.00**	**0.00**	**0.00**		**0.00**	0.93	**0.00**	**0.00**	**0.00**	**0.00**	**0.00**
260	60	**0.00**	**0.00**	**0.00**	**0.00**	**0.01**	0.98	**0.00**	0.79	1.00	**0.00**	**0.00**		**0.00**	**0.00**	**0.00**	**0.00**	**0.00**	**0.00**
280	20	**0.00**	**0.00**	**0.00**	**0.00**	**0.00**	**0.00**	**0.00**	**0.00**	**0.00**	**0.02**	0.93	**0.00**		**0.00**	**0.00**	**0.00**	**0.00**	**0.00**
280	40	**0.00**	**0.00**	**0.00**	**0.00**	**0.00**	**0.00**	**0.00**	**0.00**	**0.00**	**0.00**	**0.00**	**0.00**	**0.00**		**0.00**	**0.00**	0.08	0.67
280	60	**0.00**	**0.00**	**0.00**	**0.00**	**0.00**	**0.00**	**0.00**	**0.00**	**0.00**	**0.00**	**0.00**	**0.00**	**0.00**	**0.00**		**0.00**	**0.00**	**0.00**
300	20	**0.00**	**0.00**	**0.00**	**0.00**	**0.00**	**0.00**	**0.00**	**0.00**	**0.00**	**0.00**	**0.00**	**0.00**	**0.00**	**0.00**	**0.00**		**0.03**	**0.00**
300	40	**0.00**	**0.00**	**0.00**	**0.00**	**0.00**	**0.00**	**0.00**	**0.00**	**0.00**	**0.00**	**0.00**	**0.00**	**0.00**	**0.08**	**0.00**	**0.03**		**0.00**
300	60	**0.00**	**0.00**	**0.00**	**0.00**	**0.00**	**0.00**	**0.00**	**0.00**	**0.00**	**0.00**	**0.00**	**0.00**	**0.00**	0.67	**0.00**	**0.00**	**0.00**	

Table A10. Analysis of variance for ash content of sewage sludge.

SS, Tukey test for Ash, a bold font signifies statistically significant difference ($p < 0.05$)		200	200	200	220	220	220	240	240	240	260	260	260	280	280	280	300	300	300
		20	40	60	20	40	60	20	40	60	20	40	60	20	40	60	20	40	60
200	20		0.98	**0.00**	0.16	**0.00**	**0.00**	1.00	**0.00**	**0.00**	0.09	**0.00**	**0.00**	**0.00**	**0.00**	**0.00**	**0.00**	**0.00**	**0.00**
200	40	0.98		**0.00**	**0.00**	**0.00**	**0.00**	0.76	**0.00**	**0.00**	**0.00**	**0.00**	**0.00**	**0.00**	**0.00**	**0.00**	**0.00**	**0.00**	**0.00**
200	60	**0.00**	**0.00**		0.87	0.94	0.15	**0.01**	**0.00**	**0.00**	0.96	**0.00**	**0.00**	**0.00**	**0.00**	**0.00**	**0.00**	**0.00**	**0.00**
220	20	0.16	**0.00**	0.87		0.05	**0.00**	0.48	**0.00**	**0.00**	1.00	**0.00**	**0.00**	**0.00**	**0.00**	**0.00**	**0.00**	**0.00**	**0.00**
220	40	**0.00**	**0.00**	0.94	0.05		0.98	**0.00**	0.17	**0.02**	0.10	**0.00**	**0.04**	**0.00**	**0.00**	**0.00**	**0.00**	**0.00**	**0.00**
220	60	**0.00**	**0.00**	0.15	**0.00**	0.98		**0.00**	0.96	0.45	**0.00**	0.17	0.63	**0.00**	**0.00**	**0.00**	**0.00**	**0.00**	**0.00**
240	20	1.00	0.76	**0.01**	0.48	**0.00**	**0.00**		**0.00**	**0.00**	0.31	**0.00**	**0.00**	**0.00**	**0.00**	**0.00**	**0.00**	**0.00**	**0.00**
240	40	**0.00**	**0.00**	**0.00**	**0.00**	0.17	0.96	**0.00**		1.00	**0.00**	0.98	1.00	**0.00**	**0.00**	**0.00**	**0.00**	**0.00**	**0.00**
240	60	**0.00**	**0.00**	**0.00**	**0.00**	**0.02**	0.45	**0.00**	1.00		**0.00**	1.00	1.00	**0.00**	**0.00**	**0.00**	**0.00**	**0.00**	**0.00**
260	20	0.09	**0.00**	0.96	1.00	0.10	**0.00**	0.31	**0.00**	**0.00**		**0.00**	**0.00**	**0.00**	**0.00**	**0.00**	**0.00**	**0.00**	**0.00**
260	40	**0.00**	**0.00**	**0.00**	**0.00**	**0.00**	0.17	**0.00**	0.98	1.00	**0.00**		1.00	**0.02**	**0.00**	**0.00**	**0.00**	**0.00**	**0.00**
260	60	**0.00**	**0.00**	**0.00**	**0.00**	**0.04**	0.63	**0.00**	1.00	1.00	**0.00**	1.00		**0.00**	**0.00**	**0.00**	**0.00**	**0.00**	**0.00**
280	20	**0.00**	**0.00**	**0.00**	**0.00**	**0.00**	**0.00**	**0.00**	**0.00**	**0.00**	**0.00**	**0.02**	**0.00**		**0.00**	**0.00**	**0.00**	**0.00**	**0.00**
280	40	**0.00**	**0.00**	**0.00**	**0.00**	**0.00**	**0.00**	**0.00**	**0.00**	**0.00**	**0.00**	**0.00**	**0.00**	**0.00**		**0.00**	**0.00**	1.00	**0.03**
280	60	**0.00**	**0.00**	**0.00**	**0.00**	**0.00**	**0.00**	**0.00**	**0.00**	**0.00**	**0.00**	**0.00**	**0.00**	**0.00**	**0.00**		**0.00**	**0.00**	**0.05**
300	20	**0.00**	**0.00**	**0.00**	**0.00**	**0.00**	**0.00**	**0.00**	**0.00**	**0.00**	**0.00**	**0.00**	**0.00**	**0.00**	**0.00**	**0.00**		**0.00**	**0.00**
300	40	**0.00**	**0.00**	**0.00**	**0.00**	**0.00**	**0.00**	**0.00**	**0.00**	**0.00**	**0.00**	**0.00**	**0.00**	**0.00**	1.00	**0.00**	**0.00**		0.32
300	60	**0.00**	**0.00**	**0.00**	**0.00**	**0.00**	**0.00**	**0.00**	**0.00**	**0.00**	**0.00**	**0.00**	**0.00**	**0.00**	**0.03**	**0.05**	**0.00**	0.32	

Table A11. Analysis of variance for ash content of digestate.

D, Tukey test for Ash, a bold font signifies statistically significant difference ($p < 0.05$)		200	200	200	220	220	220	240	240	240	260	260	260	280	280	280	300	300	300
		20	40	60	20	40	60	20	40	60	20	40	60	20	40	60	20	40	60
200	20		0.25	0.09	0.17	**0.02**	**0.00**	0.17	**0.01**	**0.00**	**0.00**	**0.00**	**0.00**	**0.00**	**0.00**	**0.00**	**0.00**	**0.00**	**0.00**
200	40	0.25		1.00	1.00	1.00	0.87	1.00	0.99	0.58	**0.01**	**0.00**	0.71	**0.00**	**0.00**	**0.00**	**0.00**	**0.00**	**0.00**
200	60	0.09	1.00		1.00	1.00	0.99	1.00	1.00	0.86	**0.02**	**0.00**	0.94	**0.00**	**0.00**	**0.00**	**0.00**	**0.00**	**0.00**
220	20	0.17	1.00	1.00		1.00	0.94	1.00	1.00	0.71	**0.01**	**0.00**	0.83	**0.00**	**0.00**	**0.00**	**0.00**	**0.00**	**0.00**
220	40	**0.02**	1.00	1.00	1.00		1.00	1.00	1.00	1.00	0.12	**0.00**	1.00	**0.00**	**0.00**	**0.00**	**0.00**	**0.00**	**0.00**
220	60	**0.00**	0.87	0.99	0.94	1.00		0.93	1.00	1.00	0.50	**0.00**	1.00	**0.02**	**0.00**	**0.00**	**0.00**	**0.00**	**0.00**
240	20	0.17	1.00	1.00	1.00	1.00	0.93		1.00	0.70	**0.01**	**0.00**	0.82	**0.00**	**0.00**	**0.00**	**0.00**	**0.00**	**0.00**
240	40	**0.01**	0.99	1.00	1.00	1.00	1.00	1.00		1.00	0.23	**0.00**	1.00	**0.00**	**0.00**	**0.00**	**0.00**	**0.00**	**0.00**
240	60	**0.00**	0.58	0.86	0.71	1.00	1.00	0.70	1.00		0.81	**0.02**	1.00	**0.06**	**0.00**	**0.00**	**0.00**	**0.00**	**0.00**
260	20	**0.00**	**0.01**	**0.02**	**0.01**	0.12	0.50	**0.01**	0.23	0.81		0.81	0.69	0.97	**0.00**	**0.00**	**0.04**	**0.00**	**0.00**
260	40	**0.00**	**0.00**	**0.00**	**0.00**	**0.00**	**0.00**	**0.00**	**0.00**	**0.02**	0.81		**0.01**	1.00	**0.01**	**0.00**	0.95	0.10	**0.00**
260	60	**0.00**	0.71	0.94	0.83	1.00	1.00	0.82	1.00	1.00	0.69	**0.01**		**0.04**	**0.00**	**0.00**	**0.00**	**0.00**	**0.00**
280	20	**0.00**	**0.00**	**0.00**	**0.00**	**0.00**	**0.02**	**0.00**	**0.00**	0.06	0.97	1.00	**0.04**		**0.00**	**0.00**	0.74	**0.03**	**0.00**
280	40	**0.00**	**0.00**	**0.00**	**0.00**	**0.00**	**0.00**	**0.00**	**0.00**	**0.00**	**0.00**	**0.01**	**0.00**	**0.00**		0.16	0.41	1.00	1.00
280	60	**0.00**	**0.00**	**0.00**	**0.00**	**0.00**	**0.00**	**0.00**	**0.00**	**0.00**	**0.00**	**0.00**	**0.00**	**0.00**	0.16		**0.00**	**0.01**	0.66
300	20	**0.00**	**0.00**	**0.00**	**0.00**	**0.00**	**0.00**	**0.00**	**0.00**	**0.00**	**0.04**	0.95	**0.00**	0.74	0.41	**0.00**		0.95	0.07
300	40	**0.00**	**0.00**	**0.00**	**0.00**	**0.00**	**0.00**	**0.00**	**0.00**	**0.00**	**0.00**	0.10	**0.00**	**0.03**	1.00	**0.01**	0.95		0.89
300	60	**0.00**	**0.00**	**0.00**	**0.00**	**0.00**	**0.00**	**0.00**	**0.00**	**0.00**	**0.00**	**0.00**	**0.00**	**0.00**	1.00	0.66	0.07	0.89	

Table A12. Analysis of variance for combustible parts content of sewage sludge.

SS, Tukey test for *CP*, a bold font signifies statistically significant difference ($p < 0.05$)		200	200	200	220	220	220	240	240	240	260	260	260	280	280	280	300	300	300
		20	40	60	20	40	60	20	40	60	20	40	60	20	40	60	20	40	60
200	20		0.98	**0.00**	0.16	**0.00**	**0.00**	1.00	**0.00**	**0.00**	0.09	**0.00**	**0.00**	**0.00**	**0.00**	**0.00**	**0.00**	**0.00**	**0.00**
200	40	0.98		**0.00**	**0.00**	**0.00**	**0.00**	0.76	**0.00**	**0.00**	**0.00**	**0.00**	**0.00**	**0.00**	**0.00**	**0.00**	**0.00**	**0.00**	**0.00**
200	60	**0.00**	**0.00**		0.87	0.94	0.15	**0.01**	**0.00**	**0.00**	0.96	**0.00**	**0.00**	**0.00**	**0.00**	**0.00**	**0.00**	**0.00**	**0.00**
220	20	0.16	**0.00**	0.87		0.05	**0.00**	0.48	**0.00**	**0.00**	1.00	**0.00**	**0.00**	**0.00**	**0.00**	**0.00**	**0.00**	**0.00**	**0.00**
220	40	**0.00**	**0.00**	0.94	0.05		0.98	**0.00**	0.17	**0.02**	0.10	**0.00**	**0.04**	**0.00**	**0.00**	**0.00**	**0.00**	**0.00**	**0.00**
220	60	**0.00**	**0.00**	0.15	**0.00**	0.98		**0.00**	0.96	0.45	**0.00**	0.17	0.63	**0.00**	**0.00**	**0.00**	**0.00**	**0.00**	**0.00**
240	20	1.00	0.76	**0.01**	0.48	**0.00**	**0.00**		**0.00**	**0.00**	0.31	**0.00**	**0.00**	**0.00**	**0.00**	**0.00**	**0.00**	**0.00**	**0.00**
240	40	**0.00**	**0.00**	**0.00**	**0.00**	**0.17**	0.96	**0.00**		1.00	**0.00**	0.98	1.00	**0.00**	**0.00**	**0.00**	**0.00**	**0.00**	**0.00**
240	60	**0.00**	**0.00**	**0.00**	**0.00**	0.02	0.45	**0.00**	1.00		**0.00**	1.00	1.00	**0.00**	**0.00**	**0.00**	**0.00**	**0.00**	**0.00**
260	20	0.09	**0.00**	0.96	1.00	0.10	**0.00**	0.31	**0.00**	**0.00**		**0.00**	**0.00**	**0.00**	**0.00**	**0.00**	**0.00**	**0.00**	**0.00**
260	40	**0.00**	**0.00**	**0.00**	**0.00**	**0.00**	0.17	**0.00**	0.98	1.00	**0.00**		1.00	**0.02**	**0.00**	**0.00**	**0.00**	**0.00**	**0.00**
260	60	**0.00**	**0.00**	**0.00**	**0.00**	**0.04**	0.63	**0.00**	1.00	1.00	**0.00**	1.00		**0.00**	**0.00**	**0.00**	**0.00**	**0.00**	**0.00**
280	20	**0.00**	**0.00**	**0.00**	**0.00**	**0.00**	**0.00**	**0.00**	**0.00**	**0.00**	**0.00**	**0.02**	**0.00**		**0.00**	**0.00**	**0.00**	**0.00**	**0.00**
280	40	**0.00**	**0.00**	**0.00**	**0.00**	**0.00**	**0.00**	**0.00**	**0.00**	**0.00**	**0.00**	**0.00**	**0.00**	**0.00**		**0.00**	**0.00**	1.00	**0.03**
280	60	**0.00**	**0.00**	**0.00**	**0.00**	**0.00**	**0.00**	**0.00**	**0.00**	**0.00**	**0.00**	**0.00**	**0.00**	**0.00**	**0.00**		**0.00**	**0.00**	**0.05**
300	20	**0.00**	**0.00**	**0.00**	**0.00**	**0.00**	**0.00**	**0.00**	**0.00**	**0.00**	**0.00**	**0.00**	**0.00**	**0.00**	**0.00**	**0.00**		**0.00**	**0.00**
300	40	**0.00**	**0.00**	**0.00**	**0.00**	**0.00**	**0.00**	**0.00**	**0.00**	**0.00**	**0.00**	**0.00**	**0.00**	**0.00**	1.00	**0.00**	**0.00**		0.32
300	60	**0.00**	**0.00**	**0.00**	**0.00**	**0.00**	**0.00**	**0.00**	**0.00**	**0.00**	**0.00**	**0.00**	**0.00**	**0.00**	**0.03**	**0.05**	**0.00**	0.32	

Table A13. Analysis of variance for combustible parts content of digestate.

D, Tukey test for *CP*, a bold font signifies statistically significant difference ($p < 0.05$)		200	200	200	220	220	220	240	240	240	260	260	260	280	280	280	300	300	300
		20	40	60	20	40	60	20	40	60	20	40	60	20	40	60	20	40	60
200	20		0.25	0.09	0.17	0.02	0.00	0.17	0.01	0.00	0.00	0.00	0.00	0.00	0.00	0.00	0.00	0.00	0.00
200	40	0.25		1.00	1.00	1.00	0.87	1.00	0.99	0.58	0.01	0.00	0.71	0.00	0.00	0.00	0.00	0.00	0.00
200	60	0.09	1.00		1.00	1.00	0.99	1.00	1.00	0.86	0.02	0.00	0.94	0.00	0.00	0.00	0.00	0.00	0.00
220	20	0.17	1.00	1.00		1.00	0.94	1.00	1.00	0.71	0.01	0.00	0.83	0.00	0.00	0.00	0.00	0.00	0.00
220	40	**0.02**	1.00	1.00	1.00		1.00	1.00	1.00	1.00	0.12	0.00	1.00	0.00	0.00	0.00	0.00	0.00	0.00
220	60	**0.00**	0.87	0.99	0.94	1.00		0.93	1.00	1.00	0.50	0.00	1.00	0.02	0.00	0.00	0.00	0.00	0.00
240	20	0.17	1.00	1.00	1.00	1.00	0.93		1.00	0.70	0.01	0.00	0.82	0.00	0.00	0.00	0.00	0.00	0.00
240	40	**0.01**	0.99	1.00	1.00	1.00	1.00	1.00		1.00	0.23	0.00	1.00	0.00	0.00	0.00	0.00	0.00	0.00
240	60	**0.00**	0.58	0.86	0.71	1.00	1.00	0.70	1.00		0.81	0.02	1.00	0.06	0.00	0.00	0.00	0.00	0.00
260	20	**0.00**	**0.01**	**0.02**	**0.01**	0.12	0.50	**0.01**	0.23	0.81		0.81	0.69	0.97	0.00	0.00	0.04	0.00	0.00
260	40	**0.00**	**0.00**	**0.00**	**0.00**	**0.00**	**0.00**	**0.00**	**0.00**	**0.02**	0.81		0.01	1.00	0.01	0.00	0.95	0.10	0.00
260	60	**0.00**	0.71	0.94	0.83	1.00	1.00	0.82	1.00	1.00	0.69	**0.01**		0.04	0.00	0.00	0.00	0.00	0.00
280	20	**0.00**	**0.00**	**0.00**	**0.00**	**0.00**	**0.02**	**0.00**	**0.00**	0.06	0.97	1.00	**0.04**		0.00	0.00	0.74	0.03	0.00
280	40	**0.00**	**0.00**	**0.00**	**0.00**	**0.00**	**0.00**	**0.00**	**0.00**	**0.00**	**0.00**	**0.01**	**0.00**	**0.00**		0.16	0.41	1.00	1.00
280	60	**0.00**	**0.00**	**0.00**	**0.00**	**0.00**	**0.00**	**0.00**	**0.00**	**0.00**	**0.00**	**0.00**	**0.00**	**0.00**	0.16		**0.00**	**0.01**	0.66
300	20	**0.00**	**0.00**	**0.00**	**0.00**	**0.00**	**0.00**	**0.00**	**0.00**	**0.00**	**0.04**	0.95	**0.00**	0.74	0.41	**0.00**		0.95	0.07
300	40	**0.00**	**0.00**	**0.00**	**0.00**	**0.00**	**0.00**	**0.00**	**0.00**	**0.00**	**0.00**	0.10	**0.00**	**0.03**	1.00	**0.01**	0.95		0.89
300	60	**0.00**	**0.00**	**0.00**	**0.00**	**0.00**	**0.00**	**0.00**	**0.00**	**0.00**	**0.00**	**0.00**	**0.00**	**0.00**	1.00	0.66	0.07	0.89	

Table A14. Analysis of variance for HHV of sewage sludge.

SS, Tukey test for *HHV*, a bold font signifies statistically significant difference ($p < 0.05$)		200	200	200	220	220	220	240	240	240	260	260	260	280	280	280	300	300	300
		20	40	60	20	40	60	20	40	60	20	40	60	20	40	60	20	40	60
200	20		0.46	1.00	0.99	0.88	0.32	1.00	**0.01**	0.51	0.33	**0.02**	0.12	**0.01**	**0.00**	**0.00**	**0.00**	**0.00**	**0.00**
200	40	0.46		1.00	1.00	1.00	1.00	0.94	0.90	1.00	1.00	0.98	1.00	0.93	**0.00**	**0.00**	**0.01**	**0.00**	**0.00**
200	60	1.00	1.00		1.00	1.00	0.98	1.00	0.18	1.00	0.98	0.34	0.81	0.21	**0.00**	**0.00**	**0.00**	**0.00**	**0.00**
220	20	0.99	1.00	1.00		1.00	0.99	1.00	0.21	1.00	0.99	0.39	0.86	0.25	**0.00**	**0.00**	**0.00**	**0.00**	**0.00**
220	40	0.88	1.00	1.00	1.00		1.00	1.00	0.50	1.00	1.00	0.74	0.99	0.57	**0.00**	**0.00**	**0.00**	**0.00**	**0.00**
220	60	0.32	1.00	0.98	0.99	1.00		0.86	0.97	1.00	1.00	1.00	1.00	0.98	**0.00**	**0.00**	**0.01**	**0.00**	**0.00**
240	20	1.00	0.94	1.00	1.00	1.00	0.86		0.07	0.96	0.87	0.15	0.54	0.09	**0.00**	**0.00**	**0.00**	**0.00**	**0.00**
240	40	**0.01**	0.90	0.18	0.21	0.50	0.97	0.07		0.88	0.96	1.00	1.00	1.00	**0.00**	**0.00**	0.39	**0.00**	**0.00**
240	60	0.51	1.00	1.00	1.00	1.00	1.00	0.96	0.88		1.00	0.98	1.00	0.91	**0.00**	**0.00**	**0.00**	**0.00**	**0.00**
260	20	0.33	1.00	0.98	0.99	1.00	1.00	0.87	0.96	1.00		1.00	1.00	0.98	**0.00**	**0.00**	**0.01**	**0.00**	**0.00**
260	40	**0.02**	0.98	0.34	0.39	0.74	1.00	0.15	1.00	0.98	1.00		1.00	1.00	**0.00**	**0.00**	0.20	**0.00**	**0.00**
260	60	0.12	1.00	0.81	0.86	0.99	1.00	0.54	1.00	1.00	1.00	1.00		1.00	**0.00**	**0.00**	**0.04**	**0.00**	**0.00**
280	20	**0.01**	0.93	0.21	0.25	0.57	0.98	0.09	1.00	0.91	0.98	1.00	1.00		**0.00**	**0.00**	0.33	**0.00**	**0.00**
280	40	**0.00**	**0.00**	**0.00**	**0.00**	**0.00**	**0.00**	**0.00**	**0.00**	**0.00**	**0.00**	**0.00**	**0.00**	**0.00**		**0.02**	**0.04**	0.97	1.00
280	60	**0.00**	**0.00**	**0.00**	**0.00**	**0.00**	**0.00**	**0.00**	**0.00**	**0.00**	**0.00**	**0.00**	**0.00**	**0.00**	**0.02**		**0.00**	0.51	0.24
300	20	**0.00**	**0.01**	**0.00**	**0.00**	**0.00**	**0.01**	**0.00**	0.39	**0.00**	**0.01**	0.20	**0.04**	0.33	**0.04**	**0.00**		**0.00**	**0.00**
300	40	**0.00**	**0.00**	**0.00**	**0.00**	**0.00**	**0.00**	**0.00**	**0.00**	**0.00**	**0.00**	**0.00**	**0.00**	**0.00**	0.97	0.51	**0.00**		1.00
300	60	**0.00**	**0.00**	**0.00**	**0.00**	**0.00**	**0.00**	**0.00**	**0.00**	**0.00**	**0.00**	**0.00**	**0.00**	**0.00**	1.00	0.24	**0.00**	1.00	

Table A15. Analysis of variance for HHV of digestate.

D, Tukey test for *HHV*, a bold font signifies statistically significant difference ($p < 0.05$)		200	200	200	220	220	220	240	240	240	260	260	260	280	280	280	300	300	300
		20	40	60	20	40	60	20	40	60	20	40	60	20	40	60	20	40	60
200	20		1.00	0.87	0.99	0.65	0.14	1.00	1.00	0.17	1.00	**0.00**	0.07	**0.00**	**0.00**	1.00	**0.00**	**0.00**	0.56
200	40	1.00		0.83	0.97	0.59	0.11	1.00	1.00	0.14	1.00	**0.00**	0.06	**0.00**	**0.00**	1.00	**0.00**	**0.00**	0.49
200	60	0.87	0.83		1.00	1.00	0.99	0.47	1.00	1.00	0.89	0.05	0.96	**0.00**	0.07	1.00	0.22	**0.01**	1.00
220	20	0.99	0.97	1.00		1.00	0.93	0.77	1.00	0.95	0.99	**0.02**	0.79	**0.00**	**0.02**	1.00	0.09	**0.00**	1.00
220	40	0.65	0.59	1.00	1.00		1.00	0.25	1.00	1.00	0.67	0.13	1.00	**0.00**	0.17	1.00	0.43	**0.03**	1.00
220	60	0.14	0.11	0.99	0.93	1.00		**0.03**	0.69	1.00	0.15	0.63	1.00	**0.03**	0.72	0.69	0.95	0.25	1.00
240	20	1.00	1.00	0.47	0.77	0.25	**0.03**		0.96	**0.04**	1.00	**0.00**	**0.01**	**0.00**	**0.00**	0.96	**0.00**	**0.00**	0.19
240	40	1.00	1.00	1.00	1.00	1.00	0.69	0.96		0.75	1.00	**0.00**	0.49	**0.00**	**0.01**	1.00	**0.03**	**0.00**	0.99
240	60	0.17	0.14	1.00	0.95	1.00	1.00	**0.04**	0.75		0.18	0.57	1.00	**0.03**	0.65	0.75	0.92	0.21	1.00
260	20	1.00	1.00	0.89	0.99	0.67	0.15	1.00	1.00	0.18		**0.00**	0.08	**0.00**	**0.00**	1.00	**0.00**	**0.00**	0.58
260	40	**0.00**	**0.00**	0.05	**0.02**	0.13	0.63	**0.00**	**0.00**	0.57	**0.00**		0.82	0.98	1.00	**0.00**	1.00	1.00	0.18
260	60	0.07	0.06	0.96	0.79	1.00	1.00	**0.01**	0.49	1.00	0.08	0.82		0.07	0.88	0.49	0.99	0.42	1.00
280	20	**0.00**	**0.00**	**0.00**	**0.00**	**0.00**	**0.03**	**0.00**	**0.00**	**0.03**	**0.00**	0.98	0.07		0.96	**0.00**	0.74	1.00	**0.00**
280	40	**0.00**	**0.00**	0.07	**0.02**	0.17	0.72	**0.00**	**0.01**	0.65	**0.00**	1.00	0.88	0.96		**0.01**	1.00	1.00	0.23
280	60	1.00	1.00	1.00	1.00	1.00	0.69	0.96	1.00	0.75	1.00	**0.00**	0.49	**0.00**	**0.01**		**0.03**	**0.00**	0.99
300	20	**0.00**	**0.00**	0.22	0.09	0.43	0.95	**0.00**	**0.03**	0.92	**0.00**	1.00	0.99	0.74	1.00	**0.03**		1.00	0.52
300	40	**0.00**	**0.00**	**0.01**	**0.00**	**0.03**	0.25	**0.00**	**0.00**	0.21	**0.00**	1.00	0.42	1.00	1.00	**0.00**	1.00		**0.04**
300	60	0.56	0.49	1.00	1.00	1.00	1.00	0.19	0.99	1.00	0.58	0.18	1.00	**0.00**	0.23	0.99	0.52	0.04	

References

1. World Bank Open Data. Available online: https://data.worldbank.org/ (accessed on 2 February 2020).
2. IEA (2018), World Energy Outlook 2018, IEA, Paris. Available online: https://doi.org/10.1787/weo-2018-en (accessed on 4 April 2020).
3. Martins, F.; Felgueiras, C.; Smitková, M. Fossil fuel energy consumption in European countries. *Energy Procedia* **2018**, *153*, 107–111. [CrossRef]
4. Sewage Sludge Production and Disposal. Eurostat. Available online: http://appsso.eurostat.ec.europa.eu/nui/show.do?lang=en&dataset=env_ww_spd (accessed on 24 February 2020).
5. Simon, F. The Future of Biogas in Europe: It's a Local Affair. Available online: https://www.euractiv.com/section/energy/news/the-future-of-biogas-in-europe-its-a-local-affair/ (accessed on 29 February 2020).
6. Terlouw, W.; Peters, D.; Tilburg, J.; Schimmel, M.; Berg, T.; Cihlar, T.; Ur Rehman Mir, G.; Spöttle, M.; Staats, M.; Villar Lejaretta, A. Gas for Climate The Optimal Role for Gas in a Net-Zero Emissions Energy System 2019. Available online: https://www.gasforclimate2050.eu/files/files/Navigant_Gas_for_Climate_The_optimal_role_for_gas_in_a_net_zero_emissions_energy_system_March_2019.pdf (accessed on 29 February 2020).
7. Corden, C.; Bougas, K.; Cunningham, E.; Tyrer, D.; Kreißig, J.; Zetti, E.; Gamero, E.; Wildey, R.; Crookes, M. Digestate and Compost as Fertilisers: Risk Assessment and Risk Management Options 2019. Available online: https://ec.europa.eu/environment/chemicals/reach/pdf/40039%20Digestate%20and%20Compost%20RMOA%20-%20Final%20report%20i2_20190208.pdf (accessed on 29 February 2020).
8. Official Journal of the European Union Directive 2009/28/EC of the European Parliament and of the Council of 23 April 2009 on the Promotion of the Use of Energy from Renewable Sources and Amending and Subsequently Repealing Directives 2001/77/EC and 2003/30/EC 2009. Available online: https://eur-lex.europa.eu/legal-content/EN/ALL/?uri=CELEX%3A32009L0028 (accessed on 29 February 2020).
9. 2030 Climate & Energy Framework. Available online: https://ec.europa.eu/clima/policies/strategies/2030_en (accessed on 29 February 2020).
10. European Commission, Communication from the Commission to the Europea Parliamentnt, the Council, the European Economic and Social Committee and the Committee of the Regions—The Role of Waste-to-Energy in the Circular Economy. 2017. Available online: https://ec.europa.eu/environment/waste/waste-to-energy.pdf (accessed on 2 February 2020).
11. PN-EN 15359:2012 Standard. Available online: https://sklep.pkn.pl/pn-en-15359-2012e.html?options=cart (accessed on 2 February 2020).
12. Ulewicz, M.; Maciejewski, P. Application of Alternative Fuels—Ecological Benefits. *Nauk. Chem.* **2011**, *2*, 384–402. Available online: http://yadda.icm.edu.pl/yadda/element/bwmeta1.element.baztech-article-BATA-0013-0084 (accessed on 2 February 2020).
13. O'Toole, J.J.; Wessels, T.E.; Lynch, J.F.; Fassel, V.A.; Lembke, L.L.; Kniseley, R.N.; Norton, G.A.; Junk, G.A.; Richard, J.J.; Dekalb, E.L.; et al. *Health and Environmental Effects of Refuse Derived Fuel (RDF) Production and RDF/Coal Co-Firing Technologies*; Ames Laboratory, U.S. DOE: Ames, IA, USA, 1981. [CrossRef]
14. Fytili, D.; Zabaniotou, A.Â. Utilization of sewage sludge in EU application of old and new methods—A review. *Renew. Sustain. Energy Rev.* **2008**, *12*, 116–140. [CrossRef]
15. Koszel, M.; Lorencowicz, E. Agricultural use of biogas digestate as a replacement fertilizers. *Agric. Agric. Sci. Procedia* **2015**, *7*, 119–124. [CrossRef]
16. Stańczyk-Mazanek, E.; Kępa, U.; Stępniak, L. Drug-Resistant Bacteria in Soils Fertilized with Sewage Sludge. *Annu. Set Environ. Prot.* **2015**, *17*, 125–142.
17. Kupper, T.; Bürge, D.; Jörg Bachmann, H.; Güsewell, S.; Mayer, J. Heavy metals in source-separated compost and digestates. *Waste Manag.* **2014**, *34*, 867–874. [CrossRef]
18. Feng, L.; Escolà Casas, M.; Ditlev Mørck Ottosen, L.; Bjarne Møller, H.; Bester, K. Removal of antibiotics during the anaerobic digestion of pig manure. *Sci. Total Environ.* **2017**, *603*, 219–225. [CrossRef]
19. Pšenička, P. Pollutants in digestate After Anaerobic Digestion of Organic Fraction of Municipal Solid Waste; Conference Paper 2011. Conference: FCUL, Faculdade de Ciências da Universidade de Lisboa. Available online: https://www.researchgate.net/publication/210140082 (accessed on 29 February 2020).
20. Fijalkowski, K.; Rorat, A.; Grobelak, A.; Kacprzak, M.J. The presence of contaminations in sewage sludge—The current situation. *J. Environ. Manage.* **2017**, *203*, 1126–1136. [CrossRef]

21. Białowiec, A.; Micuda, M.; Szumny, A.; Łyczko, J.; Koziel, J.A. Quantification of VOC Emissions from Carbonized Refuse-Derived Fuel Using Solid-Phase Microextraction and Gas Chromatography-Mass Spectrometry. *Molecules* **2018**, *23*. [CrossRef]
22. Białowiec, A.; Micuda, M.; Szumny, A.; Łyczko, J.; Koziel, J.A. Waste to Carbon: Influence of Structural Modification on VOC Emission Kinetics from Stored Carbonized Refuse-Derived Fuel. *Sustainability* **2019**, *11*. [CrossRef]
23. Gent, S.; Twedt, M.; Gerometta, C.; Almberg, E. Introduction to Thermochemical Conversion Processes. In *Theoretical and Applied Aspects of Biomass Torrefaction: For Biofuels and Value-Added Products*; Butterworth-Heinemann: Oxford, UK, 2017; pp. 1–16. ISBN 9780128094839. [CrossRef]
24. Cahyanti, M.N.; Rama Krishna, C.; Doddapaneni, T.; Kikas, T. Biomass torrefaction: An overview on process parameters, economic and environmental aspects and recent advancements. *Bioresour. Technol.* **2020**, *301*. [CrossRef] [PubMed]
25. Luft, J.-E.; Ojala, T.; Ruokanen, L.; Zinchuk, O. *Good Practices Related to Wastewater Management*; Union of Baltic Cities: Turku, Finland, 2012; ISBN 978-952-5725-96-4. Available online: https://www.ubc-sustainable.net/sites/www.ubc-environment.net/files/publications/book_polish_web.pdf (accessed on 11 June 2020).
26. Bennamoun, L. Solar drying of wastewater sludge: A review. *Renew. Sustain. Energy Rev.* **2012**, *16*, 1061–1073. [CrossRef]
27. Bianchini, A.; Bonfiglioli, L.; Pellegrini, M.; Saccani, C. Sewage sludge drying process integration with a waste-to-energy power plant. *Waste Manag.* **2015**, *42*, 159–165. [CrossRef] [PubMed]
28. Stępień, P.; Białowiec, A. Kinetic Parameters of Torrefaction Process of Alternative Fuel Produced from Municipal Solid Waste and Characteristic of Carbonized Refuse Derived Fuel. *Detritus* **2018**, *3*, 75–83. [CrossRef]
29. Chin, K.L.; H'ng, P.S.; Go, W.Z.; Wong, W.Z.; Lim, T.W.; Maminski, M.; Paridah, M.T.; Luqman, A.C. Optimization of torrefaction conditions for high energy density solid biofuel from oil palm biomass and fast growing species available in Malaysia. *Ind. Crops Prod.* **2013**, *49*, 768–774. [CrossRef]
30. Waste Characteristics. Content of Organic Matter. Polish Standard PN-EN 15169:2011. Available online: http://sklep.pkn.pl/pn-en-15169-2011p.html (accessed on 2 February 2020).
31. Municipal Solid Waste. Combustible and Non-Combustible Content. Polish Standard PN-Z-15008-04:1993. Available online: http://sklep.pkn.pl/pn-z-15008-04-1993p.html (accessed on 2 February 2020).
32. Solid Fuels. Determination of the Higher Heating Value and the Lower Heating Value. Polish Standard PN-G-04513:1981 Standard. Available online: http://sklep.pkn.pl/pn-g-04513-1981p.html (accessed on 2 February 2020).
33. Stępień, P.; Pulka, J.; Serowik, M.; Białowiec, A. Thermogravimetric and Calorimetric Characteristics of Alternative Fuel in Terms of Its Use in Low-Temperature Pyrolysis. *Waste Biomass Valori.* **2018**, *10*, 1–9. [CrossRef]
34. Stępień, P.; Świechowski, K.; Hnat, M.; Kugler, S.; Stegenta-Dąbrowska, S.; Koziel, J.A.; Manczarski, P.; Białowiec, A. Waste to Carbon: Biocoal from Elephant Dung as New Cooking Fuel. *Energies* **2019**, *12*, 1–32. [CrossRef]
35. OriginLab 18.1.2 Algorithms (Smooth). Available online: https://www.originlab.com/doc/Origin-Help/Smooth-Algorithm (accessed on 2 February 2020).
36. Świechowski, K.; Liszewski, M.; Bąbelewski, P.; Koziel, J.A.; Białowiec, A. Oxytree Pruned Biomass Torrefaction: Mathematical Models of the Influence of Temperature and Residence Time on Fuel Properties Improvement. *Materials* **2019**, *12*. [CrossRef]
37. Stępień, P.; Serownik, M.; Koziel, J.A.; Białowiec, A. Waste to Carbon Energy Demand Model and Data Based on the TGA and DSC Analysis of Individual MSW Components. *Data* **2019**, *4*, 1–6. [CrossRef]
38. Pulka, J.; Manczarski, P.; Koziel, J.A.; Białowiec, A. Torrefaction of Sewage Sludge: Kinetics and Fuel Properties of Biochars Torrefaction of Sewage Sludge: Kinetics and Fuel Properties of Biochars. *Energies* **2019**, *12*, 1–10. [CrossRef]
39. Białowiec, A.; Pulka, J.; Manczarski, P.; Stępień, P.; Gołaszewski, J. The RDF/SRF torrefaction: An effect of temperature on characterization of the product—Carbonized Refuse Derived Fuel. *Waste Manag.* **2017**, *70*, 91–100. [CrossRef] [PubMed]

40. Syguła, E.; Koziel, J.A.; Białowiec, A. Proof-of-Concept of Spent Mushrooms Compost Torrefaction—Studying the Process Kinetics and the Influence of Temperature and Duration on the Calorific Value of the Produced Biocoal. *Energies* **2019**, *12*, 1–19. [CrossRef]
41. Świechowski, K.; Liszewski, M.; Bąbelewski, P.; Koziel, J.A.; Białowiec, A. Fuel properties of torrefied biomass from pruning of Oxytree. *Data* **2019**, *112*, 1–9. [CrossRef]
42. Dyjakon, A.; Noszczyk, T.; Smędzik, M. The Influence of Torrefaction Temperature on Hydrophobic Properties of Waste Biomass from Food Processing. *Energies* **2019**, *12*, 1–17. [CrossRef]
43. Słupska, M.; Dyjakon, A.; Stopa, R. Determination of Strength Properties of Energy Plants on the Example of Miscanthus×Giganteus, Rosa Multiflora and Salix Viminalis. *Energies* **2019**, *12*, 1–19. [CrossRef]
44. Chen, Y.; Jhou, S. Integrating spent coffee grounds and silver skin as biofuels using torrefaction. *Renew. Energy* **2020**, *148*, 275–283. [CrossRef]
45. Gan, Y.Y.; Ong, H.C.; Ling, T.C.; Chen, W.; Chong, C.T. Torrefaction of de-oiled Jatropha seed kernel biomass for solid fuel production. *Energy* **2019**, *170*, 367–374. [CrossRef]
46. Hattori, H.; Mukai, S. Soil Science and Plant Nutrition Decomposition of Sewage Sludges in Soil as Affected by their Organic Matter Composition. *Soil Sci. Plant Nutr.* **1986**, *32*, 421–432. [CrossRef]
47. Pan, Z.; Zhang, R.; Zicari, S. *Integrated Processing Technologies for Food and Agricultural By-Products*; Elsevier: Cambridge, MA, USA, 2019.
48. Michel, F.; Thibault, J.; Barryb, J. Preparation and Characterisation of Dietary Fibre from Sugar Beet Pulp. *J. Sci. Food Agric.* **1988**, *42*, 77–85. [CrossRef]
49. Novaes, E.; Kirst, M.; Chiang, V.; Winter-Sederoff, H.; Sederoff, R. Lignin and Biomass: A Negative Correlation for Wood Formation and Lignin Content in Trees. *Futur. Perspect. Plant Biol. Lignin* **2010**, *154*, 555–561. [CrossRef] [PubMed]
50. Danish, M.; Ahmad, T. A review on utilization of wood biomass as a sustainable precursor for activated carbon production and application. *Renew. Sustain. Energy Rev.* **2018**, *87*, 1–21. [CrossRef]
51. Bryś, A.; Bryś, J.; Ostrowska-Ligęza, E.; Kaleta, A.; Górnicki, K.; Szymon, G.; Koczoń, P. Wood biomass characterization by DSC or FT-IR spectroscopy. *J. Therm. Anal. Calorim.* **2016**, 27–35. [CrossRef]
52. Durowoju, I.B.; Bhandal, K.S.; Hu, J.; Carpick, B.; Kirkitadze, M. Differential Scanning Calorimetry—A Method for Assessing the Thermal Stability and Conformation of Protein Antigen. *J. Vis. Exp.* **2017**, *121*, 1–8. [CrossRef]
53. Tomaszewska-Gras, J. Melting and crystallization DSC profiles of milk fat depending on selected factors. *J. Therm. Anal. Calorim.* **2013**, 199–208. [CrossRef]
54. Cassel, R.B. *Determining Percent Solid in an Edible Fat*; TA Instruments, Inc.: New Castle, DE, USA, 2002; Available online: http://www.tainstruments.com/pdf/literature/TA290.pdf (accessed on 20 February 2020).
55. Saavedra-Leos, Z.; Alavrez-Salas, C.; Esneider-Alcala, M.; Toxqui-Teran, A.; Perez-Garcia, S.; Ruiz-Cabrera, M. Towards an improved calorimetric methodology for glass transition temperature determination in amorphous sugars. *Cyta J. Food* **2012**, *10*, 258–267. [CrossRef]
56. Ball, R.; Mcintosh, A.C.; Brindley, J. Feedback processes in cellulose thermal decomposition: Implications for fire-retarding strategies and treatments. *Combust. Theory Model.* **2004**, *8*, 281–291. [CrossRef]
57. Yang, H.; Yan, R.; Chen, H.; Lee, H.D.; Zheng, C. Characteristics of hemicellulose, cellulose and lignin pyrolysis. *Fuel* **2007**, *86*, 1781–1788. [CrossRef]
58. Water—Heat of Vaporization. Available online: https://www.engineeringtoolbox.com/water-properties-d_1573.html (accessed on 2 February 2020).
59. Białowiec, A.; Micuda, M.; Koziel, J.A. Waste to Carbon: Densification of Torrefied Refuse-Derived Fuel. *Energies* **2018**, *11*. [CrossRef]
60. Medyńska-Juraszek, A.; Ćwieląg-Piasecka, I. Effect of Biochar Application on Heavy Metal Mobility in Soils Impacted by Copper Smelting Processes. *Pol. J. Environ. Stud.* **2020**, *29*, 1–9. [CrossRef]
61. Pulka, J.; Manczarski, P.; Stępień, P.; Marzena, S.; Koziel, J.A.; Białowiec, A. Waste-to-Carbon: Is the Torrefied Sewage Sludge with High Ash Content a Better Fuel or Fertilizer? *Materials* **2020**, *13*, 1–28. [CrossRef]

Załącznik nr 3

Kacper Świechowski
imię i nazwisko

WROCŁAW 18.02.2022
(miejscowość i data)

Katedr Biogospodarki Stosowanej
Uniwersytet Przyrodniczy we Wrocławiu
51-630 Wrocław, Chełmońskiego 37a
afiliacja

OŚWIADCZENIE

Oświadczam, że w pracy:

Kacper Świechowski, Martyna Hnat, Paweł Stępień, Sylwia Stegenta-Dąbrowska, Szymon Kugler, Jacek A. Koziel, Andrzej Białowiec. 2020. Waste to Energy: Solid Fuel Production from Biogas Plant Digestate and Sewage Sludge by Torrefaction-Process Kinetics, Fuel Properties, and Energy Balance. Energies, 13, 3161; doi:10.3390/en13123161.

mój udział polegał na:

Opracowaniu wyników z badań pod względem statystycznym przy wykorzystaniu oprogramowania Statistica. Opracowanie polegało w szczególności na wyznaczeniu modeli wpływu parametrów technologicznych (czasu i temperatury) toryfikacji na zmianę właściwości paliwowych badanych materiałów, wyznaczeniu parametrów kinetycznych toryfikacji w warunkach izotermicznych, wyznaczeniu ilości energii potrzebnej do toryfikacji na podstawie wyników z analizy DSC, wyznaczeniu bilansu masy i energii procesu. Ponadto byłem odpowiedzialny za napisanie pierwszej wersji manuskryptu, w szczególności metodyki oraz opisu i dyskusji wyników. Pełniłem także rolę autora korespondencyjnego.

18.02.2022 Świechowski
data i podpis

Załącznik nr 3

Głogów, 25.02.22r.
(miejscowość i data)

Martyna Hnat
imię i nazwisko

Instytut Inżynierii Rolniczej
Uniwersytet Przyrodniczy we Wrocławiu
51-630 Wrocław, Chełmońskiego 37
afiliacja

OŚWIADCZENIE

Oświadczam, że w pracy:
Kacper Świechowski, Martyna Hnat, Paweł Stępień, Sylwia Stegenta-Dąbrowska, Szymon Kugler, Jacek A. Koziel, Andrzej Białowiec. 2020. Waste to Energy: Solid Fuel Production from Biogas Plant Digestate and Sewage Sludge by Torrefaction-Process Kinetics, Fuel Properties, and Energy Balance. Energies, 13, 3161; doi:10.3390/en13123161.

mój udział polegał na:
Pozyskaniu materiałów badawczych – osadu ściekowego oraz pofermentu z biogazowni, a następnie na ich przygotowaniu do analiz (suszenie, rozdrabnianie, homogenizacja). Wykonałam także część analiz w tym wygenerowałam biowegle i poddałam je analizie technicznej w celu określenia właściwości paliwowych. Wykonałam także analizę TGA w warunkach izotermicznych i nieizotermicznych.

Hnat Martyna 25.02.22r.
data i podpis

Załącznik nr 3

Paweł Stępień
imię i nazwisko

Instytut Inżynierii Rolniczej
Uniwersytet Przyrodniczy we Wrocławiu
51-630 Wrocław, Chełmońskiego 37
afiliacja

Wrocław, 28.02.2022
(miejscowość i data)

OŚWIADCZENIE

Oświadczam, że w pracy:
Kacper Świechowski, Martyna Hnat, Paweł Stępień, Sylwia Stegenta-Dąbrowska, Szymon Kugler, Jacek A. Koziel, Andrzej Białowiec. 2020. Waste to Energy: Solid Fuel Production from Biogas Plant Digestate and Sewage Sludge by Torrefaction-Process Kinetics, Fuel Properties, and Energy Balance. Energies, 13, 3161; doi:10.3390/en13123161.

mój udział polegał na:

Opracowaniu metodyki w zakresie analizy DSC, oraz opracowaniu wyników uzyskanych z tej że analizy. Brałem udział także w procesie recenzji odpowiadając na pytania recenzentów i poprawiając manuskrypt. Byłem także kierownikiem projektu z którego sfinansowano część badań.

28.02.2022
data i podpis

PODPIS ZAUFANY
PAWEŁ JAKUB
STĘPIEŃ
28.02.2022 15:51:28 [GMT+1]
Dokument podpisany elektronicznie
podpisem zaufanym

Załącznik nr 3

Sylwia Stegenta-Dąbrowska
imię i nazwisko

Wrocław, 24.02.2022
(miejscowość i data)

Katedr Biogospodarki Stosowanej
Uniwersytet Przyrodniczy we Wrocławiu
51-630 Wrocław, Chełmońskiego 37a
afiliacja

OŚWIADCZENIE

Oświadczam, że w pracy:
Kacper Świechowski, Martyna Hnat, Paweł Stępień, Sylwia Stegenta-Dąbrowska, Szymon Kugler, Jacek A. Koziel, Andrzej Białowiec. 2020. Waste to Energy: Solid Fuel Production from Biogas Plant Digestate and Sewage Sludge by Torrefaction-Process Kinetics, Fuel Properties, and Energy Balance. Energies, 13, 3161; doi:10.3390/en13123161.

mój udział polegał na:
Jako promotor pomocniczy pomagałam doktorantowi zmodyfikować pierwszą wersję manuskryptu w szczególności rozdział dotyczący wprowadzenia, metodyki oraz dyskusji uzyskanych wyników badań. W trakcie recenzji uczestniczyłam w udzielaniu odpowiedzi do recenzentów oraz nanoszeniu poprawek do manuskryptu.

24.02.2022, Sylwia Stegenta-Dąbrowska
data i podpis

Załącznik nr 3

Szymon Kugler
imię i nazwisko

Szczecin, 26.02.2022
(miejscowość i data)

Wydział Technologii i Inżynierii Chemicznej
Zachodniopomorski Uniwersytet Technologiczny w Szczecinie
71-065 Szczecin, al. Piastów 42
afiliacja

OŚWIADCZENIE

Oświadczam, że w pracy:
Kacper Świechowski, Martyna Hnat, Paweł Stępień, Sylwia Stegenta-Dąbrowska, Szymon Kugler, Jacek A. Koziel, Andrzej Białowiec. 2020. Waste to Energy: Solid Fuel Production from Biogas Plant Digestate and Sewage Sludge by Torrefaction-Process Kinetics, Fuel Properties, and Energy Balance. Energies, 13, 3161; doi:10.3390/en13123161.

mój udział polegał na:
Wykonaniu analizy skaningowej kalorymetrii różnicowej (DSC) przy wykorzystaniu analizatora DSC Q2500 (TA Instruments, New Castle, DE, USA).

Szymon Kugler
Elektronicznie podpisany przez Szymon Kugler
Data: 2022.02.26 15:36:56 +01'00'

.....
data i podpis

Załącznik nr 3

Jacek Koziel 23-2-2022…….

imię i nazwisko (miejscowość i data)

Department of Agricultural and Biosystems Engineering
Iowa State University
Ames, IA 50011, USA
afiliacja

OŚWIADCZENIE

Oświadczam, że w pracy:

Kacper Świechowski, Martyna Hnat, Paweł Stępień, Sylwia Stegenta-Dąbrowska, Szymon Kugler, Jacek A. Koziel, Andrzej Białowiec. 2020. Waste to Energy: Solid Fuel Production from Biogas Plant Digestate and Sewage Sludge by Torrefaction-Process Kinetics, Fuel Properties, and Energy Balance. Energies, 13, 3161; doi:10.3390/en13123161.

mój udział polegał na:

Nadzorowaniu pracy nad tworzeniem manuskryptem w szczególności opracowywania graficznej prezentacji zastosowanych metod badawczych oraz uzyskanych wyników. Sprawdzałem poprawność wykonania pierwszej wersji manuskryptu pod względem merytorycznym oraz językowym. Aktywnie uczestniczyłem w procesie recenzji w tym wprowadzaniu poprawek do manuskryptu. Byłem także odpowiedzialny za pozyskanie części środków finansujących proces publikacji.

data i podpis

Załącznik nr 3

Andrzej Białowiec
imię i nazwisko

Wrocław, 26.02.2022
(miejscowość i data)

Katedr Biogospodarki Stosowanej
Uniwersytet Przyrodniczy we Wrocławiu
51-630 Wrocław, Chełmońskiego 37a
afiliacja

OŚWIADCZENIE

Oświadczam, że w pracy:
Kacper Świechowski, Martyna Hnat, Paweł Stępień, Sylwia Stegenta-Dąbrowska, Szymon Kugler, Jacek A. Koziel, Andrzej Białowiec. 2020. Waste to Energy: Solid Fuel Production from Biogas Plant Digestate and Sewage Sludge by Torrefaction-Process Kinetics, Fuel Properties, and Energy Balance. Energies, 13, 3161; doi:10.3390/en13123161.

mój udział polegał na:
Na nadzorowaniu procesu pisania i publikowania artykułu. Brałem także udział w przygotowywaniu odpowiedzi na pytania recenzentów i wprowadzaniu poprawek do manuskryptu.

26.02.2022
data i podpis

energies

MDPI

Article

Medical Peat Waste Upcycling to Carbonized Solid Fuel in the Torrefaction Process

Kacper Świechowski, Małgorzata Leśniak and Andrzej Białowiec *

Department of Applied Bioeconomy, Wrocław University of Environmental and Life Sciences, 37a Chełmońskiego Str., 51-630 Wrocław, Poland; kacper.swiechowski@upwr.edu.pl (K.Ś.); 110819@student.upwr.edu.pl (M.L.)
* Correspondence: andrzej.balowiec@upwr.edu.pl

Abstract: Peat is the main type of peloid used in Polish cosmetic/healing spa facilities. Depending on treatment and origin, peat waste can be contaminated microbiologically, and as a result, it must be incinerated in medical waste incineration plants without energy recovery (local law). Such a situation leads to peat waste management costs increase. Therefore, in this work, we checked the possibility of peat waste upcycling to carbonized solid fuel (CSF) using torrefaction. Torrefaction is a thermal treatment process that removes microbiological contamination and improves the fuel properties of peat waste. In this work, the torrefaction conditions (temperature and time) on CSF quality were tested. Parallelly, peat decomposition kinetics using TGA and torrefaction kinetics with lifetime prediction using macro-TGA were determined. Furthermore, torrefaction theoretical mass and energy balance were determined. The results were compared with reference material (wood), and as a result, obtained data can be used to adjust currently used wood torrefaction technologies for peat torrefaction. The results show that torrefaction improves the high heating value of peat waste from 19.0 to 21.3 MJ $\times$ kg^{-1}, peat main decomposition takes place at 200–550 °C following second reaction order (n = 2), with an activation energy of 33.34 kJ $\times$ mol^{-1}, and pre-exponential factor of 4.40 $\times$ 10^{-1} s^{-1}. Moreover, differential scanning calorimetry analysis revealed that peat torrefaction required slightly more energy than wood torrefaction, and macro-TGA showed that peat torrefaction has lower torrefaction constant reaction rates (k) than wood 1.05 $\times$ 10^{-5}–3.15 $\times$ 10^{-5} vs. 1.43 $\times$ 10^{-5}–7.25 $\times$ 10^{-5} s^{-1}.

Keywords: peloids; waste to energy; waste to carbon; circular economy; torrefied biomass; kinetics lifetime prediction; mass balance; energy balance; fuel properties

Citation: Świechowski, K.; Leśniak, M.; Białowiec, A. Medical Peat Waste Upcycling to Carbonized Solid Fuel in the Torrefaction Process. *Energies* **2021**, *14*, 6053. https://doi.org/10.3390/en14196053

Academic Editor: Szymon Szufa

Received: 28 August 2021
Accepted: 17 September 2021
Published: 23 September 2021

1. Introduction

Peloids are commonly used in spa treatment and cosmetology for cosmetic and healing purposes. Peloids refer to inorganic, organic, or a mixture matter that originated through geological and/or biological processes. Özay et al. [1] proposed to divide peloids by origin and composition into four groups: peat, sludge (bituminous or mineral), slime (sea or delta), and earth (rock or schist) [1]. The most used peloid in Poland is peat. Leśniak [2] shows that a typical SPA facility in Poland uses from 2.90 to 3.42 Mg of peat yearly. Assuming an average value of 3.16 Mg $\times$ year^{-1} and a current number of spa facilities (103), the annual peat waste (PW) production counts about 324 Mg [2]. The PW management depends on the specific situations in the country and its law regulations [3]. In general, waste peloids generated in beauty salons are safe, but ones from spa centers may be microbiologically contaminated, and in such a situation, PW must be considered as medical waste, requiring a special waste treatments method, e.g., waste incineration. However, other methods of PW recycling and upcycling should be developed. In this study, we check the validity of thermal upcycling of medical/cosmetic peat waste into high-quality solid fuel, free of possible infectious substances using the torrefaction process.

1.1. Peat Applications

Peat can be classified according to different factors such as fiber content or fiber decomposition, organic matter, and vegetation forming the organic content. In addition, ASTM D4427-13, "Standard Classification of Peat Samples by Laboratory Testing", can be used for peat classification. There is also a special von Post scale, which classifies peat soils based on the degree of its decomposition at 10 points (H_1–H_{10} with the interpretation from none to complete decomposition) [4]. For medical/cosmetic purposes, typically, peat with classes from H_6 to H_{10} is used [5]. Each class corresponds to 10% of decomposition (degree of humification). Where H_1 means peat, which squeezed releases almost clear water, plants are identifiable, and no amorphous material is present, while H_{10} means completely decomposed peat, which squeezed escape between fingers, without discernible plants structures [6]. Medical/cosmetic peat usage in Europe is dated to the 18th century, but external usage as poultices is dated to the early 19th century [7]. Peat in cosmetics is used, inter alia, for facial care treatments supporting the treatment of acne, and scars, and sun discoloration, as an antiaging treatment that improves the elasticity of the facial skin and so on [5]. On the other hand, in a healing spa (peat bath), peat is mainly used to overheat the body. It is possible thanks to high heat capacity and relatively flat cooling curve in comparison to water. As a result, baths improve blood circulation, effects myalgia, and chronic inflammation, and so on [7].

Using peat as fuel started earlier. Since the 12th-century, peat has become an important energy source in Europe. Nevertheless, currently using peat for energy production has ended in most countries [8]. Only six countries in the EU (Estonia, Finland, Ireland, Latvia, Lithuania, and Sweden) use peat for energy purposes excavating around 9.4 mln Mg per year of it. Among these countries, only 208 peat-fired energy plants exist, and only Finland uses peat in significant amounts, covering around 25% of its national heat needs [9]. Nevertheless, peat does not play a significant role in the energy sector of the EU (1.7%), and since 2010, its consumption has decreased. As a result, it is highly probable that peat's role in the EU energy sector will further decrease [10]. On the other hand, Russia, which has a significant peat reserve (~30% of the world's peat), is considered to go back to peat mining for energy uses as a more environmentally friendly alternative for coal and to diversify locals' energy sources. The main peat advantage is its abundance and low-cost mining in comparison to coal. Nevertheless, peat is characterized by high moisture content and relatively high ash content. Therefore, before energy use, peat required seasoning and pretreatment [11–13].

Besides medical/cosmetic and energy purposes, peat is also widely used in horticulture and agriculture. Peat-specific properties allow its use as a soil improver, growing medium, compost ingredient, etc. For example, peat mining for agricultural usage is common in such countries as Germany and Poland [10], which do not use it for energy purposes. On the other hand, peat and peatlands represent a valuable global carbon store and are critical for preserving biodiversity [14]. Moreover, the analysis of the European Commission from 2018 shows that limiting the use of peatlands is effective for CO_2 emission mitigation [11]. Therefore, peat replacement materials are sought. The opportunity for such replacement material is looking in biochars and hydro-chars obtained from organic waste [15,16]. Since carbon materials alone or in mixtures with organic substances have the potential to substitutes (partially or full) peat for agricultural usages. For example, some biochars (depending on substrate and process conditions) have higher pH, increased surface area, excellent water, and nutrient retention properties in comparison to peat. Moreover, biochars may contain different forms of nitrogen and have a considerable amount of potassium [15]. That suggests that biochar from medical/cosmetic peat waste may partially replace fresh peat usage in agriculture/horticulture or other emerging applications such as odors mitigation [17].

1.2. Peat Thermal-Upgrading Methods

Some studies show that peat can be upgraded thermally by various methods, i.e., torrefaction [18], pyrolysis [19], gasification [20], or hydrothermal carbonization [21]. Each process favors different input substrates, process conditions, and end products. Torrefaction is typically used to improve the calorific value and storage properties (increased hydrophobicity) of biomass. It takes place at 200–320 °C in the absence of oxygen. Solids are the main process products [22]. The pyrolysis also takes place in the absence of oxygen but at temperatures over 320 °C. As a result, depending on pyrolysis conditions main products are liquid, gas, or solid; nevertheless, amounts of solids obtained from pyrolysis always are lower than from torrefaction. On the other hand, gasification takes place in a partially oxidative atmosphere and converts substrates mainly into gases. This process requires temperatures from ~800 to 1150 °C [23,24]. The main drawback of mentioned processes is the fact that materials need to be dry, or additional energy needs to be spent on water removal. Moreover, in the case of pyrolysis and gasification, high process temperatures required much more energy in comparison to torrefaction [25]. Partially, these drawbacks can be overcome by hydrothermal carbonization (HTC), which favors wet substrates, and low temperatures 150–320 °C. Nevertheless, HTC required sophisticated reactors that can stand high pressure up to 50 bars or more [26,27].

Some studies show the prospect of thermal peat upgrading to fuels (gases or solids) using the overmentioned processes [18–21,28]. Nevertheless, none of them focus on medical/cosmetic peat waste particularly. In addition, none of the studies alone provide comprehensive data of peat upcycling to carbonized solid fuel by torrefaction, including the effect of process conditions on CSF fuel qualities, torrefaction kinetics, energy, and mass balance of the whole process. Especially that peat is not homogenous material, and its composition varies significantly around the world. As a result, adopting data from different studies to make any conclusion may not be fully successful and precise.

The torrefaction is a well-known and world-wise used process for wood energy properties upgrading [29]. Besides energy densification in a solid product, torrefaction removes water, increases hydrophobic characteristics, decreases energy to grind, and decreases biodegradability [30]. As a result, torrefied material becomes easier to transport, manage, and storage [31]. Such positive effects are mainly due to hemicellulose decomposition. The hemicellulose is rich in hydroxyl groups (including carboxylic and phenolic groups), which can form a hydrogen bond with water increasing bonded water content [30,32]. When hemicellulose is decomposed because of depolymerization, demethoxylation, and bond cleavage reactions, these groups are removed as well. As a result, fuel becomes hydrophobic and more fungal-resistant [32]. In addition, changes in chemical composition (decrease in available nutrients and production of toxic chemicals) the resistance to biodegradation increases [30]. The end effect and properties of torrefied material depend on used feedstock, reactor type, and process conditions, i.e., temperature, time, heating rate, feedstock particle size, pressure, etc. [33].

1.3. Aim of the Study

In this study, we performed initial laboratory analyses on medical/cosmetic peat waste upcycling using torrefaction. The analyses covered the effects of process conditions on carbonized solid fuel quality, thermal decomposition kinetics, torrefaction kinetics with lifetime prediction, and theoretical mass and energy balance determination. The analyses were performed following our previous research related to wood biomass torrefaction. Therefore, obtained data are comparable to well-described wood material. As a result, obtained data may be used for adjusting the existing technology used for wood torrefaction to peat torrefaction.

2. Materials and Methods

2.1. Materials

The medical/cosmetic peat come from a peat bog "Kołobrzeg" owned by Uzdrowisko Kołobrzeg S.A. The peat bog is located around 3.5 km from Kołobrzeg, Poland. The peatland is classified as a low type [2,34], and the medical properties of the peat are confirmed by the National Institute of Public Health. The natural moisture content of peat obtained from the peat bog was 89.9%, and organic dry mass was 92.5% of dry mass. The peat had a degree of humification (according to the van Post scale) between H_4 and H_6 [2,35].

2.2. Methods

2.2.1. Torrefaction Process—CSF Production

The carbonized solid fuel (CSF) was produced using a muffle furnace (Snol 8.1/1100, Utena, Lithuania). The dry peat samples of ~20 g were placed at ceramic trays and put in the muffle furnace. To keep the inert atmosphere, CO_2 was introduced into the furnace. The furnace was heated from room temperature to setpoint temperature (200–300 °C, intervals 20 °C). When the temperature inside reached the setpoint, it was kept for 20, 40, or 60 min. After this time, the furnace was left to self-cooling, and when the temperature dropped below 100 °C, samples were removed. For the CSF production process, mass yield (MY), energy densification ratio (EDr), and energy yield (EY) were determined using Equations (1)–(3).

$$MY = m_{CSF}/m_{raw} \times 100 \quad (1)$$

$$EDr = HHVCSF/HHVraw \quad (2)$$

$$EY = MY \times EDr \quad (3)$$

where:

MY—mass yield, %; m_{CSF}—mass of produced CSF, g; m_{raw}—a mass of substrate used for CSF production, g; EDr—energy densification ratio, -; HHV_{CSF}—high heating value of CSF, J × g^{-1}; HHV_{raw}—high heating value of substrate used for CSF production, J × g^{-1}; EY—energy yield, %.

2.2.2. Proximate Analysis and High Heating Value Determination

Proximate analysis and high heating value determination were performed for raw peat and produced CSF. The proximate analysis consisted of moisture content (MC), volatile matter (VM), ash content (AC), and fixed carbon (FC). Additionally, volatile solids (VS) and combustible parts (CP) were determined. The proximate analysis with additional parameters was determined according to methods presented in previous work [36]. The high heating value (HHV) was determined using a calorimeter (IKA, C200, Staufen, Germany). Each sample was tested in three repetitions. Used standards, methods, and equipment are listed in Appendix A, Table A1.

2.2.3. Statistical Analyses

CSF production data and results of the proximate analysis with HHV were subjected to regression analysis. The regression analysis aimed to provide useful empirical models for easy determination of CSF properties and CSF production process in function of torrefaction temperature and time. The regression was performed according to the methodology described in previous work [37]. In short, empirical data were subjected to four main regression equations (linear, second-order polynomial, factorial regression, and response surface regression). Then, models were compared using the determination coefficient (R^2) and the Akaike information criterion (AIC). Then, models with the highest R^2 and the lowest AIC were chosen as the best fitted to the experimental data. Next, coefficients significance was checked. When some coefficients turned out to be not significant, it was removed from the model, and rest of the coefficients were recalculated again.

To check if there is an effect of process temperature and the treatment time on CSF properties, ANOVA analyses were performed at ($p < 0.05$). Then, to check between which groups the difference occurs, a Tukey post-hoc test was performed.

2.2.4. Thermal Decomposition Analysis

The thermal decomposition of dry peat and wood (as reference material) was studied using two different approaches and equipment, TG/DTG-DSC analyzer and macroTG/DTG analyzer. The mentioned abbreviation means TG—thermogravimetry; DTG—difference thermogravimetry; DSC—differential scanning calorimetry. The macro term refers to sample size. In standard TG, the sample is measured in mg, while in macro-TG, the sample mass is measured in g.

Firstly, samples were subjected to TG/DTG-DSC analysis, where samples were decomposed at a range of 30–800 °C. In this test, the temperature increased with a constant rate of 10 °C × min^{-1}. For this analysis, a sample of ~3.6 mg was subjected to a simultaneous thermal analyzer (Netzsch, 449 F1 Jupiter, Selb, Germany) in a nitrogen atmosphere to prevent Boudouard reaction at >700 °C that occur when CO_2 is used [38]. Experiment results showed material decomposition in the function of time and allowed for the determination of decomposition kinetics. Moreover, TG-DSC results were used for the calculation of the theoretical mass and energy balance of the torrefaction process (Section 2.2.5) according to previous work [39]. The decomposition kinetics were determined using the well-known Coats–Redfern method (CR) [40]. For the CR method, the kinetic triplet consists of activation energy (Ea), pre-exponential factor (A), and reaction order (n). In this study, kinetic triplets were determined for the whole process as well as decomposition peaks. The full methodology of kinetic triplet determination is described elsewhere [36].

Secondly, dry peat samples were subjected for macroTG/DTG analysis at torrefaction temperature range 200–300 °C. For this test, stand-mounted tubular furnace (Czylok, RST 40 × 200/100, Jastrzębie-Zdrój, Poland) coupled with the laboratory balance (RADWAG, PS 750.3Y, Radom, Poland) was used. The samples of ~3 g were heated by 60 min at 200, 220, 240, 260, 280, and 300 °C in the CO_2 atmosphere to imitate conditions of setpoint temperatures of CSF production (Section 2.2.1). The results showed thermal decomposition at specific torrefaction temperature in function of time. Moreover, results were used for torrefaction kinetics determination for isothermal temperature according to previous work [41]. In short, for each torrefaction temperature, the constant reaction rate (k) was determined by experimental data fitting to the first-order reaction. Then, using determined k values, the Arrhenius plot, ln(k) vs. 1/T, was drawn. Next, from the obtained slope and intercept, the activation energy and pre-exponential factor for the torrefaction process were obtained. Then, using obtained kinetic triplet, the prediction of the lifetime of material exposed to isothermal conditions may be performed for any temperatures in the range of 200–300 °C. In this study, kinetic triplet was used for the prediction of the temperatures, which was used for kinetic determination. The result of wood subjected to this method is presented in previous work [41].

2.2.5. Theoretical Mass and Energy Balance of the Torrefaction Process

Theoretical mass and energy balance of the torrefaction process were calculated for peat and wood (as reference material) using data from some of the analyses. The balances were calculated to produce 1 g of CSF. The balance calculations include the mass of substrate needed to produce 1 g pf CSF; external energy needed to heat this mass of substrate to the setpoint temperature (DSC results) (including mass change during the heating); the energy contained in 1 g of CSF (HHV results); a mass of gas produced during the production of 1 g of CSF, and energy contained in this gas. To calculate the mentioned values, results of MY, HHV, and TG/DSC were used. The graph of balances determination is shown in Figure 1. The green squares represent the order of preformed calculations, the gray squares represent experimental/calculated data used for balances determination, and the blue squares stand for input and output data.

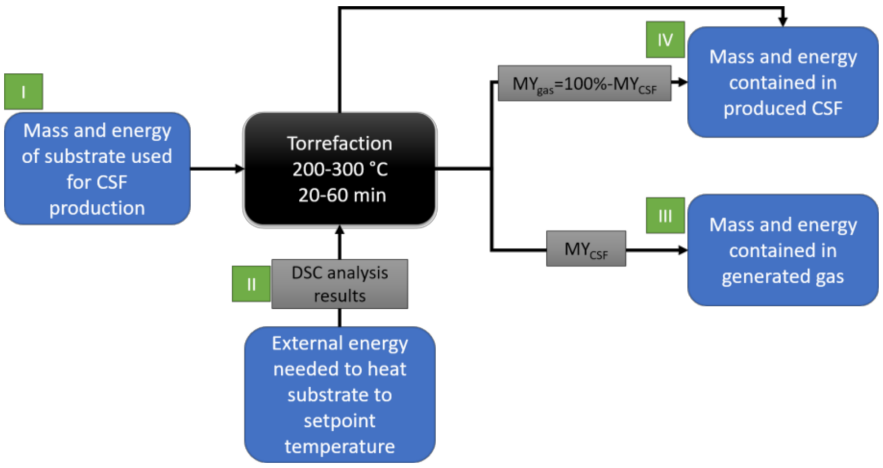

Figure 1. Theoretical mass and energy balance of the torrefaction process, calculations procedure.

The calculations were performed in four steps. First (I), knowing MY of CSF production, a mass of substrate needed for 1 g of CSF was calculated. Then, knowing the HHV of a substrate, energy contained in the input substrate was calculated. Secondly (II), the results of DSC were used to determine the amount of energy needed to heat a proper amount of substrate to the setpoint temperature. Here, DSC results were given by thermal analyzer software right away in mW per mg. Therefore, by multiplication DSC results by time, the external energy provided to the sample was calculated. Thirdly (III), the energy contained in CSF was determined by experimental HHV determination. Fourthly (IV), the mass and energy contained in the gas produced alongside the production of 1 g of CSF were determined. The mass of gas was calculated as the difference between the used substrate and the mass of obtained CSF, while the energy was calculated as the difference between energy contained in substrate and CSF increased by external energy provided to heat substrate to the setpoint temperature. Here it was assumed that CSF is completely cooled before it is removed from the reactor, and this energy goes to the gas phase (Figure 1).

To keep calculations as simple as possible, the following assumptions were adopted:

(i) Processed material is completely dry, MC = 0%;
(ii) Only external energy is used to provide heat for the process;
(iii) The process has 100% efficiency, no heat losses;
(iv) All external energy after the process goes to gaseous products.

3. Results and Discussion

3.1. CSF Production and Proximate Analysis

All raw data generated in this study were given in Supplementary Materials. The result of the raw peat and CSF properties were summarized in Table 1. The 3D models with equations presenting occurring changes in the function of torrefaction temperature and time are presented in Appendix A (Figure A1a–i).

The raw peat used in this study had 84.8% of moisture content, and its dry mass was characterized by 59.3%, 26.3%, and 14.4% content of VM, FC, and AC, respectively. Moreover, the average high heating value was 19,013 J $\times$ g^{-1}. The peat composition varies in a wide range. For example, Canadian peat has only 36% of MC, but almost 70% of VM, around 30% of FC, and only 2% of AC [42], while Bangladesh peat was characterized by 20–50% of MC, 7–48% of VM and ash content up to 90% [43]. Therefore, direct data comparison needs to be performed carefully.

Table 1. Results of CSF production and CSF properties.

Temp.	Time	MY, %	EDr, -	EY, %	VM, %	AC, %	FC, %	VS, %	CP, %	HHV, J × g^{-1}
0	0	-	-	-	59.3	14.4	26.3	83.0	85.6	19,013
	20	97.6	1.03	100.6	56.0	14.1	29.9	83.1	85.9	19,598
200	40	97.3	1.05	102.1	55.8	14.2	30.0	82.9	85.8	19,941
	60	97.1	1.04	101.4	57.2	14.6	28.2	82.7	85.4	19,841
	20	98.4	1.03	101.5	56.8	14.1	29.0	83.2	85.9	19,619
220	40	95.4	1.07	101.7	56.3	14.3	29.4	82.8	85.7	20,272
	60	91.2	1.06	97.0	55.0	15.2	29.7	81.9	84.8	20,217
	20	96.7	1.02	98.9	55.3	14.2	30.5	83.0	85.8	19,444
240	40	90.7	1.07	97.0	54.0	14.8	31.2	82.2	85.2	20,341
	60	87.7	1.07	93.7	53.0	15.1	31.9	81.9	84.9	20,318
	20	93.1	1.05	97.5	54.3	14.7	31.0	82.4	85.3	19,922
260	40	83.4	1.10	91.3	49.3	16.9	33.8	80.0	83.1	20,836
	60	83.4	1.13	93.9	49.1	17.0	33.9	79.8	83.0	21,419
	20	81.1	1.08	87.4	47.5	16.8	35.7	79.9	83.2	20,495
280	40	79.9	1.12	89.6	44.6	17.7	37.7	78.8	82.3	21,324
	60	77.6	1.11	86.2	45.6	17.6	36.8	79.0	82.4	21,124
	20	81.8	1.11	91.0	44.7	17.3	38.0	79.4	82.7	21,163
300	40	73.4	1.12	82.2	40.3	18.5	41.2	77.7	81.5	21,315
	60	69.1	1.10	75.9	38.1	20.3	41.6	75.8	79.7	20,873

The results showed that increasing process temperature and time causes the decrease in peat MY from 97.6% to 69.1% at 200 °C and 20 min and 300 °C and 60 min, respectively (Figure A1a). The opposite trend was observed for EDr, where, with the increase in temperature and process time, the EDr values increased from 1.03 for CSF produced at 200 °C and 20 min to 1.12 for CSF produced at 300 °C and 40 min (Figure A1b). Moreover, with increasing temperature, the EY decreased from 100.6% to 75.9% (Figure A1c) for CSF produced at 200 °C and 20 min and 300 °C and 60 min, respectively. The obtained results have a typical tendency of lignocellulosic materials. For comparison, the wood torrefied at the same conditions is characterized by MY of 92–55%, 1.05–1.20 of EDr, and 96–66% of EY [44]. Since peat showed to has smaller mass losses, comparable EDr, and higher EY than wood, it suggests that it is a suitable material for torrefaction. Weight losses are an inevitable element of each torrefaction, and mass losses are related to water removal and partial devolatilization. When during devolatilization, more oxygen than carbon leaves processed material, its high heating value increases, and as a result increase in EDr is observed. The EDr presents how much energy is in the CSF when compared to not torrefied material, and when EDr is higher than 1, the CSF contains more energy than not torrefied material. Typically, torrefaction leads to EDr increase [45] but some materials, mostly not lignocellulosic, have the opposite trend, e.g., sewage sludge [46]. In this study, EY was over 100% at 200–220 °C (Table 1), which is a result of the inaccuracy of empirical measurements. Theoretically, EY cannot be higher than 100% because it would mean that the produced CSF is more energy than in substrate used for its production. As was mentioned above, during torrefaction, devolatilization always occurs, and they take away some chemical energy and move it to gas and liquid fractions.

Devolatilization is a process where large molecules are thermally decomposed by temperature into smaller ones, and when molecules are small enough, they are released from the material by convection forces. During this phenomenon occurs, inter alia, decarbonization, dehydrogenation, deoxygenation [47]. As a result, volatile matter decreases, and ash and fixed carbon content increase. Typical biomass consists of cellulose, hemicellulose, and lignin, and these components affect the properties of biomass and torrefied biomass. The hemicellulose (xylan) consists of 78.57% of VM, 2.11% of AC, and 19.33% of FC. The cellulose consists of 95.21% of VM and only 4.79% of FC. Ash is not present in cellulose. The lignin has the lowest VM of 54.61% but the highest FC of 29.25%, and AC of 16.15 [48].

Since in the torrefaction temperatures, mainly hemicellulose decomposes, its properties have the highest effect on torrefied material properties.

The torrefaction process resulted in a decrease in VM from 59.3% for dry unprocessed peat to 38.1% for CSF produced at 300 °C and 60 min (Table 1). At the same conditions, AC increased by ~6% from 14.4% to 20.3%, and FC by ~15% from 26.3% to 41.6%. These changes are characterized by smooth trends, where the temperature has much more effect on observed change than the time (Figure A1d–f). In addition, increasing temperature resulted in a decrease in VS and CP from 83% to 75.8% and from 85.6% to 79.7%, respectively (Figure A1g–h). For comparison, the energetic non-woody biomass is characterized by VM of 70–94%, AC of 1.3–17%, and FC of 2.4–17.2% [49,50], while wood biomass has much homogeneous composition, 82–84%, 15.5–16.4, and 0.3–0.8%, respectively [51]. That means the torrefied peat has less VM and more FC than typical wooden biomasses, but it also has much more AC. Peat, torrefied at 300 °C, becomes like lignite (VM of 39.8%, AC of 8.5%, FC of 51.6%) [52].

3.2. Process Kinetics

3.2.1. TG/DTG and DSC Results

In Figure 2, the results of TG/DTG and DSC analysis are presented. The TG/DTG curves show that the main decomposition of peat and wood starts at similar temperatures, around 200–220 °C; nevertheless, peat turns out to be more resistant for thermal degradation and is characterized by a much lower mass losses in comparison to wood. It is obvious, as peat is more decomposed material than wood. The used peat has a degree of humification (according to the van Post scale) between H_4 and H_6 [35], meaning that it may be characterized by moderate decomposition. DTG results also showed that peat main decomposition occurred at 200–550 °C and was characterized by two peaks, the first maximum at ~325 °C and the second at ~450 °C. In contrast, wood main decomposition occurred at ~200–380 °C with a maximum at ~330 °C. DSC results are presented in Figure 2b. For both materials. DSC curves are similar up to 300 °C. First, they have one endothermal reaction at ~100 °C and then one exothermal at ~300 °C. At temperatures higher than 300 °C, the peat curve increases more than a woods curve. Moreover, during peat decomposition, one exothermic reaction occurs at 600 °C, while for wood, two endothermic reactions at 478 and 730 °C may be seen.

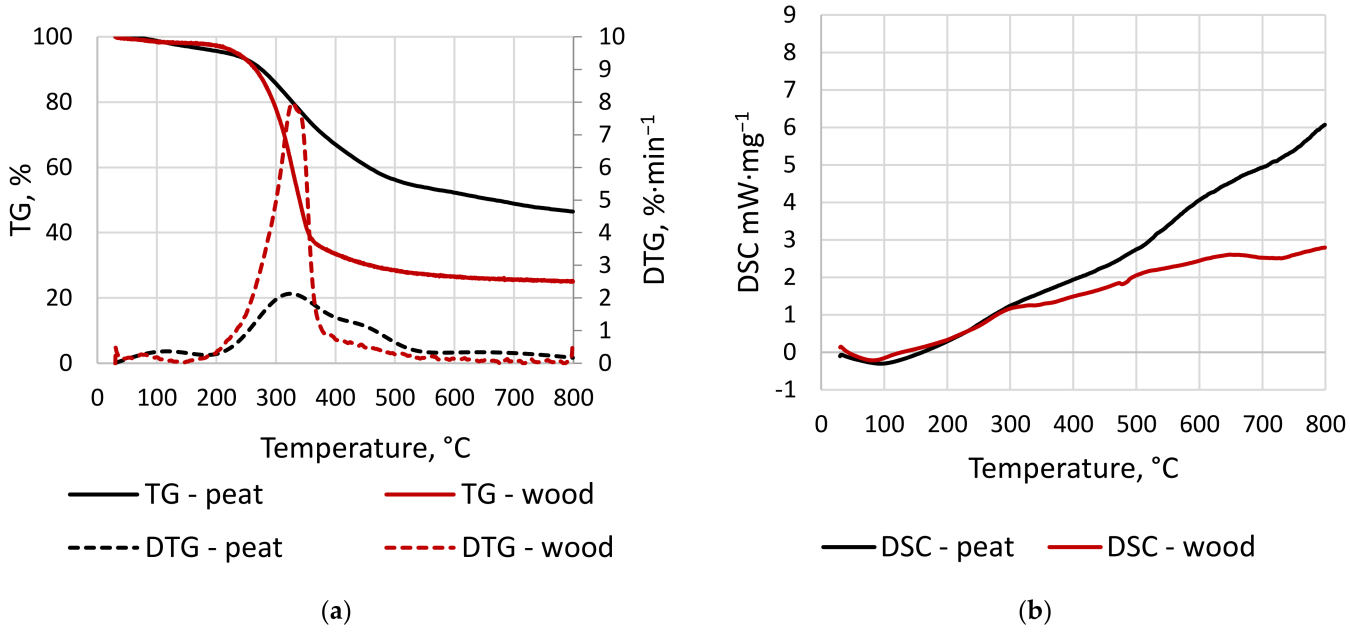

Figure 2. Thermal analysis results of (**a**) TG/DTG, (**b**) DSC.

The observed differences are related to the chemical composition and degree of humification of tested materials. The wood is made of five elements: lignin (18–35%), carbohydrates such as cellulose (40–50%), hemicelluloses (25–35%), organic extractives, and minerals (ash) [53], while peat is an organic matter mixture consists of partially decomposed plants grown in bogs, swamps, and marshes [54]. The organic matter mixture may vary significantly depending on peat age, depth, groundwater level, and so on [55]. For example, Iglovikov et al. [55] analyzed peat soil that consists of bitumens (6–10%), hemicellulose (14–18%), cellulose (1–1.5%), humic acids (28–34%), fulvic acid (15.5–19%), lignin (5–7%), and other organic and inorganic compounds. The study of Brown et al. [56] showed that cellulose and lignin content vary from 14.9% to 46.7% and from 1.1% to 5.2%, respectively.

Typically, the thermal decomposition of hemicellulose, cellulose, and lignin in an inert atmosphere takes place at 220–315, 290–400, and 100–900 °C, respectively [57,58]. Hemicellulose decomposes with two characteristic peaks at ~245 and ~296 °C, while cellulose decomposes at one stage with a maximum of ~345 °C. This means that the decomposition of cellulose occurs intensively in a shorter time than hemicellulose decomposition [48]. This suggests that visible on Figure 2a wood main decomposition at ~200–380 °C with a maximum at ~330 °C is related to hemicellulose and cellulose decomposition, wherein hemicellulose peak is not visible (lack of left shoulder). Some cellulose presence in the peat sample is also visible in the first main decomposition peak at ~325 °C. Nevertheless, lower mass losses in the peat sample at these temperatures suggest that there is a much lower amount of cellulose than in the wood. On the other hand, the studies [55,56] showed much different cellulose concentrations in the peats (1.5% vs. 46.7%). Therefore, there is a need to take caution to state that this decomposition was mainly related to cellulose. Nevertheless, continuous mass losses in both samples at temperatures higher than 400 °C are mainly related to lignin decomposition.

Because peat has a more complex organic matrix, its thermal degradation cannot be described only by three components such as typical biomass. The bitumens that may be constituents up to 10% of the peat [55] decompose in two stages [59]. The study of Murugan et al. [59] shows that the first stage starts at 80 °C and ends at 360 °C with a maximum peak at 295 °C, while the second stage starts at 360 °C and end at 540 °C with a maximum at 445 °C [59]. On the other hand, Santos et al. [60] analyzed humic and fulvic acid thermal degradation. The humic acid was characterized by multiple decomposition peaks at 280, 500, 575, 620, and 800 °C. In contrast, fulvic acid showed to be more resistant to thermal decomposition than humic acids. Fulvic acid was characterized by continuous mass loss with small decomposition peaks at 200, 310, and 545 °C, and one big decomposition peak at 920 °C [60]. These results suggest that bitumens and humic acids were partially responsible for the main decomposition of peat alongside cellulose and hemicellulose at 200–400 °C, and they are the main reason for visible right shoulder at 400–500 °C (Figure 2a). Moreover, Spedding [54] suggests that up to 110 °C free and absorbed water is evaporated from the peat. Above 110 °C, polymerizations of waxes and resins start and lead to a decrease in peat hydrophilic character. At temperatures higher than 160 °C, gases such as CO_2 and CO and colloidally bound water start to be released. From 200 to 320 °C, cellulose, pentosans, and pectin decompose. Since these components contain bound oxygen in their structure, it results in additional water releasing during thermal decomposition, and next, at 280 °C, tars start to be generated alongside other gases.

3.2.2. Peat Thermal Decomposition Kinetics by Coats–Redfern

Table 2 contains kinetic data of peat thermal conversion. The analysis was performed in a nitrogen environment at a heating rate of 10 °C × min^{-1} using the Coats–Redfern method. The kinetic triplets were calculated for the whole process 30–800 °C and the decomposition peaks. The first peak in both samples is related to water and light volatile organic constituents' removal [61]. The second peak is related to the main decomposition of compounds that were described in the previous paragraphs. The kinetics analysis revealed that for peat and wood, the first decomposition related to water evaporation was charac-

terized by a reaction order of 3, with an activation energy of 27.11 and 6.67 kJ × mol^{-1}, respectively. The analysis also showed that the main decomposition of peat had second reaction order with an activation energy of 33.34 kJ × mol^{-1}, while wood main decomposition had a 1.68 reaction order with an activation energy of 65.47 kJ × mol^{-1}. The overall whole decomposition process of peat turns out to have n of 1.33 with an Ea of 21.1 kJ × mol^{-1}, while wood has n of 1.68 with 65.47 kJ × mol^{-1}. All kinetic triplets had a high determination coefficient over 0.9. Only the first peat peak had a slightly lower value. The high value of determination coefficients means that the order of reactions and the activation energy were calculated properly.

Table 2. Kinetic triplets determined at β = 10 °C × min^{-1} using the Coats–Redfern method.

Material, -	Note, -	Temperature Range, °C	n, -	Ea, kJ × mol^{-1}	A, s^{-1}	R^2, -
Peat	Whole process	30–800	1.33	21.10	1.97×10^{-2}	0.97
Peat	First peak	30–200	3.00	27.11	1.92×10^{-1}	0.89
Peat	Main decomposition peak	200–550	2.00	33.34	4.40×10^{-1}	0.99
Wood	Whole process	30–800	1.54	27.91	2.08×10^{-1}	0.91
Wood	First peak	30–200	3.00	6.67	6.86×10^{-5}	0.99
Wood	Main decomposition peak	215–430	1.68	65.47	9.05×10^{2}	0.98

The provided data cannot be directly compared with other kinetic studies because the peat composition is a complex matrix, and there are many different approaches for kinetics determination. For example, Chen et al. [62] analyzed decomposition kinetics of forest peat under nitrogen atmosphere and described it using reactions of four fractions: moisture, hemicellulose, cellulose, and lignin. The moisture removal had Ea of 61 kJ × mol^{-1} and n of 2.18. The hemicellulose, cellulose, and lignin had Ea of 90, 121, and 65 kJ × $mol^{-1,}$ respectively, while the reaction orders were 0.96, 0.85, and 2.31, respectively [62]. On the other hand, Wen et al. [63] analyzed peat moss decomposition and distinguished six stages related to observed decomposition peaks. For β = 10 °C × min^{-1} and CR method only stages 2–4 were determined at 136–309, 309–379, 379–611, and 611–652 °C. For these stages, the Ea changed from 71.3 to 1018.8 kJ × mol^{-1}, while the reaction order changed from 0.6 to 2.6 [63]. Similarly, it is with wood. For example, Fraga et al. [64] analyzed the decomposition of wood using the CR method considering only a first-order reaction model (n = 1). The result showed that wood decomposes in two stages. The first stage occurred at 250–390 °C, while the second one was at 390–612 °C. The Ea for these stages were 190 and 117 kJ × mol^{-1}, respectively [64]. Nevertheless, despite the differences in the observed values, and approaches, the results suggest relatively suitable predictions of conversion in these works.

3.2.3. Peat Torrefaction Kinetics by an Isothermal Method

To compare the kinetics of tested peat at torrefaction temperature range, an isothermal experiment using macro-TGA (sample mass of 3 g) was performed according to previous work [41]. The dry peat was heated at temperatures of 200–300 °C (interval 20 °C) in 60 min, and then TG data were subjected for constant reaction rates with assumptions of the first-order decomposition. As a result, constant reaction rates (k) for specific temperatures were determined. The higher k, the higher mass losses are observed, or the same mass loss is obtained at a shorter time. Moreover, determined Ea and A can be used to calculate k for any torrefaction temperature. It was found that k values changed from 1.05×10^{-5} to 3.15×10^{-5} s^{-1} and that Ea and A were 22.02 kJ × mol^{-1} and 3.41×10^{-3} s^{-1}, respectively (Table 3). The experimental mass loss in specific temperatures can be seen in Figure A2a, while mass loss predicted using calculated k values in Figure A2b. In the previous work [39], we summarized and recalculated serval waste material torrefaction kinetics by the same method. The graphic of k values at specific temperatures for wood refuse-derived fuel (RDF), sewage sludge, and digestate is shown in Figure A3. The result shows that peat decomposition is much slower than wood but faster than sewage sludge and digestate up to 260 °C. Torrefaction at over 260 °C is slower for peat than sewage sludge and

digestate (Figure A3). Meanwhile, RDF torrefaction is slower than peat at all torrefaction temperatures (Figure A3). These results suggest that the thermal decomposition of peat is comparable with other waste materials but differs from the torrefaction of wood.

Table 3. Torrefaction kinetic triplets for isothermal conditions (T = 200–300 °C, t = 60 min) considering a first-order reaction model.

	Temperature, °C	k, s^{-1}	Ea, kJ × mol^{-1}	A, s^{-1}	R^2, -	Reference
Peat	200	1.05×10^{-5}	22.02	3.41×10^{-3}	0.894	This study
	220	1.82×10^{-5}				
	240	2.24×10^{-5}				
	260	2.39×10^{-5}				
	280	2.70×10^{-5}				
	300	3.15×10^{-5}				
Wood	200	1.43×10^{-5}	36.44	1.53×10^{-1}	0.996	[41]
	220	2.04×10^{-5}				
	240	3.19×10^{-5}				
	260	4.15×10^{-5}				
	280	5.37×10^{-5}				
	300	7.25×10^{-5}				

3.3. Theoretical Mass and Energy Balance

Table 4 consists of data regarding theoretical torrefaction energy and mass balance. The calculations were performed for peat and wood as reference material. The main goal of the calculations was to show the energy and mass fate during the production of 1 g of CSF at specific conditions. The first and second headings show torrefaction's specific conditions for which calculations were performed. The third heading contains data of substrate mass used to produce 1 g of CSF at specific conditions. The fourth headings contain data of chemical energy contained in this substrate. The fifth heading is related to external energy provided to the substrate to perform the torrefaction process (here calculated using DSC results). The next one shows the energy contained in 1 g of CSF (here as HHV result). The seventh heading shows the mass of produced gas, and the last heading shows the energy contained in this gas.

The results show that with increasing temperature and time, the mass of substrate needed to produce 1 g of CSF increases. Demand for peat ranged from 1.025 to 1.446 g for 200 and 300 °C, while for wood substrate, demand range from 1.042 to 1.831 g. The required mass of peat is lower than in the case of the wood for all torrefaction conditions. It means that to produce the same amount of CSF, less peat is needed than wood. This is the result of mass yield and decomposition differences between processed materials, as raw peat is more humified material than wood.

With increasing substrate mass, increase the energy of the substrate used to produce a unit of CSF. Up to 260 °C, the differences in substrate chemical energy for peat and wood are negligible, but over 260 °C, much more chemical energy in the wood is consumed to produce 1 g of CSF. The biggest difference occurs at 280 °C in 60 min (24,497 $J_{sub} \times J^{-1}_{CSF}$ vs. 32,177 $J_{sub} \times J^{-1}_{CSF}$ for peat and wood, respectively). This is a result of the high decomposition rate of wood at these temperatures.

The DSC results showed that the external energy required to heat the substrate to setpoint temperature is slightly higher for peat than for wood. The external energy for peat differs from 179 to 633 $J \times J^{-1}_{CSF}$, while for wood differs from 136 to 578 $J \times J^{-1}_{CSF}$. The differences probably result from a difference in substrates composition and its specific heat. The specific heat of peat and wood depends on temperature and moisture. Assuming that both materials were completely dried, the peat should have a higher specific heat than wood because it required more energy. Nevertheless, results of specific heat in the literature provide overlapping data for peat and wood. For example, specific heat for dry peat differs from 0.9 to 1.3 $J \times (g \times K)^{-1}$ [65] and for dry wood from 1.1 to 1.45 $J \times (g \times K)^{-1}$ [66,67].

Table 4. Theoretical torrefaction mass and energy balance.

Temp. °C	Time, min	Mass of Substrate Used to Produce 1 g of CSF, g		Energy Contained in the Raw Material Used to Produce 1 g of CSF, J		External Energy Needed to Produce 1 g of CSF, J *		Energy Contained in 1 g of CSF, J **		Mass Of Gas Generated during the Production of 1 g of CSF, g		Energy Contained in Gas after Production of 1 g of CSF, J ***	
		Peat	Wood	Peat	Wood	Peat	Wood	Peat	Wood	Peat	Wood	Peat	Wood
200	20	1.025	1.042	19,491	19,068	179	136	19,598	18,551	0.025	0.042	71	654
	40	1.027	1.071	19,533	19,596	179	136	19,941	18,960	0.027	0.071	−229	773
	60	1.030	1.088	19,576	19,898	179	136	19,841	19,178	0.030	0.088	−87	856
220	20	1.016	1.063	19,326	19,440	224	185	19,619	18,753	0.016	0.063	−70	871
	40	1.049	1.125	19,939	20,589	224	185	20,272	19,312	0.049	0.125	−109	1462
	60	1.097	1.139	20,849	20,830	224	185	20,217	19,440	0.097	0.139	857	1575
240	20	1.034	1.144	19,666	20,931	289	251	19,444	19,498	0.034	0.144	511	1684
	40	1.103	1.256	20,965	22,981	289	251	20,341	20,077	0.103	0.256	913	3155
	60	1.141	1.290	21,685	23,604	289	251	20,318	20,371	0.141	0.290	1657	3484
260	20	1.074	1.133	20,425	20,720	379	336	19,922	19,456	0.074	0.133	883	1600
	40	1.199	1.391	22,804	25,442	379	336	20,836	20,767	0.199	0.391	2347	5011
	60	1.200	1.554	22,809	28,428	379	336	21,419	21,136	0.200	0.554	1770	7627
280	20	1.233	1.308	23,447	23,932	495	446	20,495	20,467	0.233	0.308	3447	3911
	40	1.252	1.531	23,809	28,012	495	446	21,324	21,432	0.252	0.531	2980	7026
	60	1.288	1.759	24,497	32,177	495	446	21,124	21,646	0.288	0.759	3868	10,976
300	20	1.223	1.621	23,248	29,653	633	578	21,163	21,457	0.223	0.621	2718	8773
	40	1.363	1.829	25,918	33,454	633	578	21,315	22,034	0.363	0.829	5236	11,998
	60	1.446	1.831	27,498	33,493	633	578	20,873	22,002	0.446	0.831	7257	12,069

* Value determined using DSC analysis result; ** value determined using calorimetric analysis result (HHV); *** value is the sum of chemical energy contained in gas and heat from external energy, if no external energy stays in CSF.

The results showed that for both materials, the energy contained in CSF increases with process temperature, which is mainly a result of oxygen removal in the devolatilization process [47]. As a result of progressing mass loss during torrefaction at higher temperatures, an increase in gas production is visible. The gas production for peat ranges from 0.025 to 0.446 g of gas per 1 g of CSF, while for wood, from 0.042 to 0.831 g of gas is produced per 1 g of CSF made from wood. Although, gas constitutes a significant amount as a by-product, especially at 300 °C. It contains much less energy than CSF. Nevertheless, when gas energy is higher than the external energy needed to produce CSF, the process may be self-sufficient (assuming gas combustion). In this study, the results suggest that the production of CSF from wood can be self-sufficient at any torrefaction conditions, while peat requires temperatures higher than 240 °C. However, cautions should be kept with that result interpretation because data show theoretical calculations for dry material and lack of energy losses related to the use of specific torrefaction technology. The peat used in this study had around 85% moisture content, and it can be easily calculated by using latent heat of evaporation (2257 J $\times$ $g^{-1}{}_{H2O}$ at 100 °C). For water evaporation of 1% from any material, there is a demand for 22.57 J of additional energy (assuming dryer efficiency at 100%). It means that for the presented case (peat with 85% of moisture content) for each torrefaction condition, over 1918.5 J per processed gram of fresh peat should be added. As a result, any torrefaction conditions do not provide a self-sufficient process.

For the above, presented results are the initial step and base for future calculations when specific conditions and technology (moisture of processed substrate, drying technology, e.g., mechanical, conventional, solar, mixed drying, torrefaction process, e.g., batch or continuous reactors) will be considered. Furthermore, because the calculations were made with wood materials as a reference, currently available technology for wood torrefaction/pyrolysis can be easier recalculated and redesigned (if needed) for peat.

This paper presents the initial test on medical waste peat torrefaction. We intended to check the influence of temperature and residence time on the basic fuel properties of CSF. However, here we intend to draw the possible applications and needs for additional characterization of CSF. We recommend that the next experimental work should also cover more detailed characterization of CSF following techniques FTIR, XRD, SEM, TEM, and BET, to check other possible applications of CSF, i.e., soil additive, adsorbent.

4. Conclusions

In this work, for the first time, medical/cosmetic peat waste was torrefied, and the effect of torrefaction temperature and time on CSF quality was determined. Parallelly, decomposition of peat waste was determined according to the CR method using TGA equipment (temperature range 30–800 °C) and torrefaction kinetics using macro-TGA equipment (temperature range 200–300 °C) were determined. In addition, macro-TGA was used for lifetime prediction. Moreover, theoretical torrefaction mass and energy balances of peat waste were determined. As a result, the full process of peat torrefaction with its effects was presented. The main findings of performed analyses were:

- Torrefaction improves fuel properties of peat, HHV increase from 19.0 to 21.3 MJ $\times$ kg^{-1};
- Peat main decomposition takes place at 200–550 °C following second reaction order (n = 2), with an activation energy of 33.34 kJ $\times$ mol^{-1} and pre-exponential factor of 4.40 $\times$ 10^{-1} s^{-1};
- Macro-TGA shows that peat decomposition at torrefaction temperature is comparable with other waste materials but differs from wood, for which the constant reaction rates (k) are much lower;
- Theoretically, torrefaction of dry peat can be self-sufficient at temperatures higher than 240 °C, but future calculations with specific technology need to be performed to find real conditions of self-sufficient peat processing.

Since peat has already been used worldwide, technologies of its use exist. Therefore, there should be no problem finding a place for CSF made from medical/cosmetic peat

waste. Moreover, CSF has similar energetic properties to lignite, and as a result, it can be considered as co-fuel to the lignite incineration plant or for gasification for energy or hydrogen purposes. In addition, since biochars are used as partial replacements in agriculture, it may be an additional place for biochar made from peat. Whether medical peat waste will be used for energetic uses or agricultural one, the work provides useful information about its processing and main properties.

Another problem, which has not been arisen here, but should be further studied, is that the distribution of peat waste is very dispersed; therefore, small-scale torrefaction systems should be designed and tested.

Supplementary Materials: The following are available online at https://www.mdpi.com/article/10.3390/en14196053/s1.

Author Contributions: Conceptualization, K.Ś.; methodology, K.Ś.; software, K.Ś.; validation, K.Ś.; formal analysis, M.L.; investigation, M.L.; resources, A.B. and K.Ś.; data curation, K.Ś. and A.B.; writing—original draft preparation, K.Ś., M.L., and A.B.; writing—review and editing, K.Ś. and A.B.; visualization, K.Ś.; supervision, A.B. All authors have read and agreed to the published version of the manuscript.

Funding: The presented article results were obtained as part of the activity of the leading research team—Waste and Biomass Valorization Group (WBVG). The publication is financed under the Leading Research Groups support project from the subsidy increased for the period 2020–2025 in the amount of 2% of the subsidy referred to Art. 387 (3) of the Law of 20 July 2018 on Higher Education and Science, obtained in 2019.

Institutional Review Board Statement: Not applicable.

Informed Consent Statement: Not applicable.

Data Availability Statement: All data generated and used in the study is available in the article and Supplementary Materials.

Conflicts of Interest: The authors declare no conflict of interest.

Abbreviations

A	Pre-exponential factor
AC	Ash content
AIC	Akaike information criterion
ASTM	American Society for Testing and Materials
CSF	Carbonized solid fuel
CP	Combustible parts
CR	Coats–Redfern method
DSC	Differential scanning calorimetry
Ea	Activation energy
EDr	Energy densification ratio
EU	The European Union
EY	Energy yield
FC	Fixed carbon
HHV	High heating value
HTC	Hydrothermal carbonization
MC	Moisture content
MY	Mass yield
n	Reaction order
PW	Peat waste
R^2	Determination coefficient
SPA facility	A place devoted to a renewal of mind, body, and spirit by different methods
TGA	Thermogravimetric analysis
VM	Volatile matter
VS	Volatile solids

Appendix A

Table A1. Standards and methods used for fuel properties determination.

Properties	Standard/Method	Equipment (Manufacturer, Model, City, Country)	Ref.
Moisture content (MC)	PN-EN 14346:2011	Dryer (WAMED, model KBC-65W, Warsaw, Poland)	[36]
Volatile matter (VM)	TGA method	TGA—tubular furnace (Czylok, RST 40 × 200/100, Jastrzębie-Zdrój, Poland) coupled with a laboratory balance (RADWAG, PS 750.3Y, Warsaw, Poland)	
Ash content (AC)	PN-Z-15008-04:1993	Muffle furnace (Snol 8.1/1100, Utena, Lithuania)	
Fixed carbon (FC)	by difference (calculation)	-	
Volatile solids (VS)	PN-EN 15169:2011	Muffle furnace (Snol 8.1/1100, Utena, Lithuania)	
Combustible parts (CP)	PN-Z-15008-04:1993	Muffle furnace (Snol 8.1/1100, Utena, Lithuania)	
High heating value (HHV)	PN-Z-15008-04:1993	Calorimeter (IKA, C200, Staufen, Germany)	

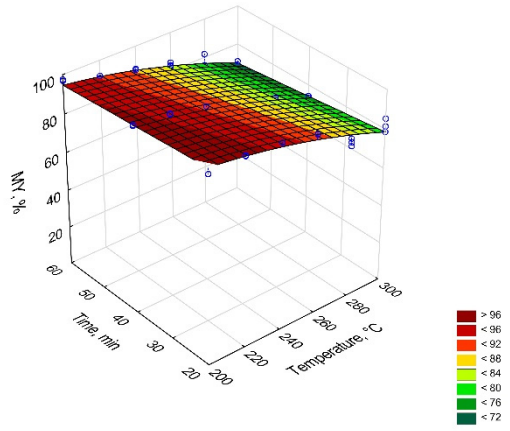

$MY(T,t) = 71.8242 + 0.400445 \times T - 0.00121217 \times T^2 - 0.000727896 \times T \times t$

$R^2 = 0.94$, $AIC = 311.04$

(**a**)

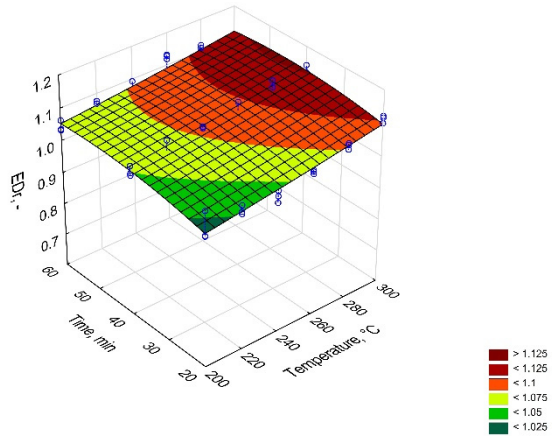

$EDr(T,t) = 0.829846 + 0.000326428 \times T + 1.16354 \times 10^{-6} \times T^2 + 0.00521945 \times t - 4.40994 \times 10^{-5} \times t^2 - 3.65412 \times 10^{-6} \times T \times t$

$R^2 = 0.67$, $AIC = -188.95$

(**b**)

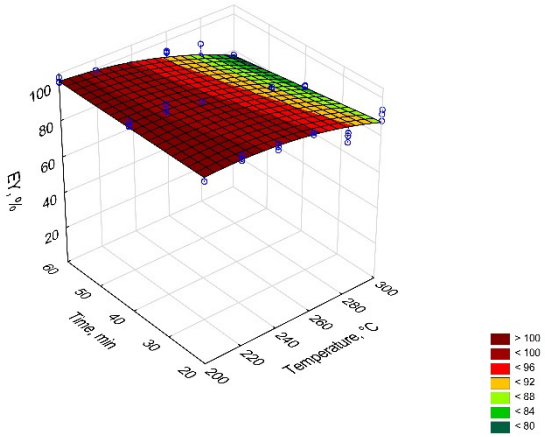

$EY(T,t) = 0.880983 \times T - 0.0019112 \times T^2 + 0.567866 \times t - 0.00274661 \times T \times t$

$R^2 = 0.86$, $AIC = 331.71$

(**c**)

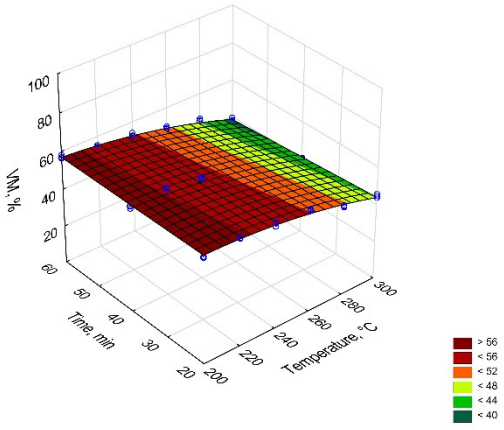

$VM(T,t) = 0.543524 \times T - 0.00129347 \times T^2 + 0.273621 \times t - 0.00137518 \times T \times t$

$R^2 = 0.96$, $AIC = 238.01$

(**d**)

Figure A1. *Cont.*

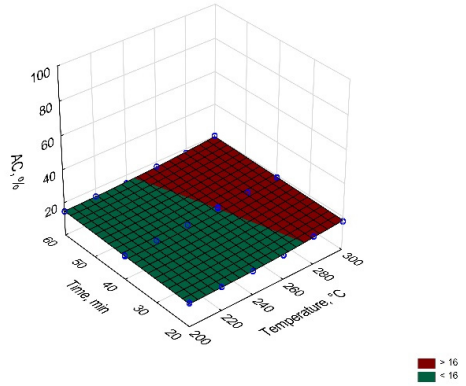

$$AC(T,t) = 30.2156 - 0.169301 \times T + 0.00041784 \times T^2 + 0.000148139 \times T \times t$$

$R^2 = 0.92$, $AIC = 148.04$

(**e**)

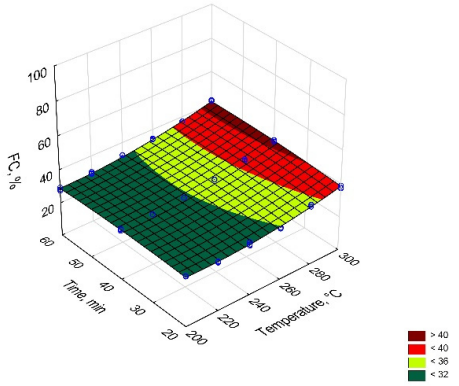

$$FC(T,t) = 80.5359 - 0.500491 \times T + 0.00114964 \times T^2 - 0.00248963 \times t^2 + 0.00093469 \times T \times t$$

$R^2 = 0.96$, $AIC = 204.27$

(**f**)

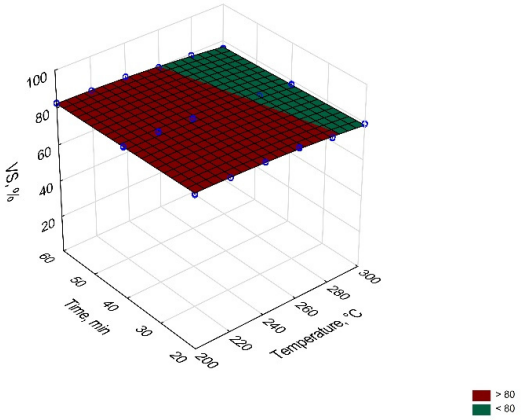

$$VS(T,t) = 63.5139 + 0.205531 \times T - 0.0005065 \times T^2 - 0.000172719 \times T \times t$$

$R^2 = 0.93$, 159.81

(**g**)

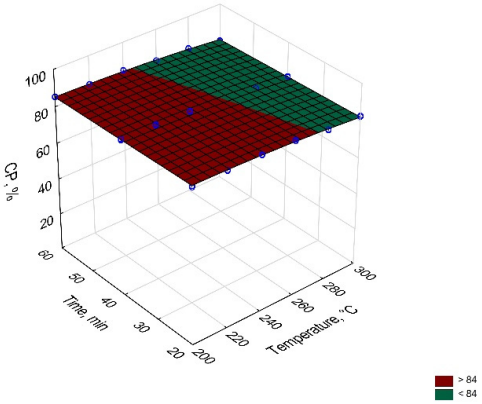

$$CP(T,t) = 69.7844 + 0.169301 \times T - 0.00041784 \times T^2 - 0.000148139 \times T \times t$$

$R^2 = 0.92$, $AIC = 148.04$

(**h**)

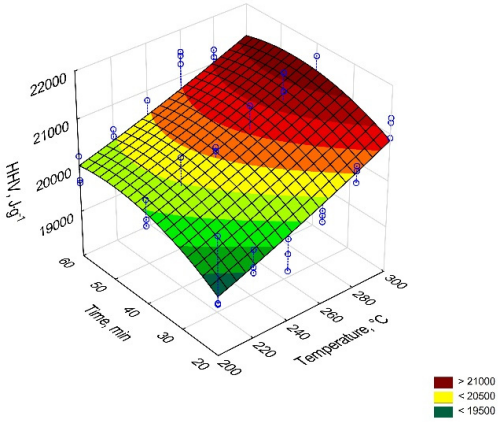

$$HHV(T,t) = 15778.1 + 6.20633 \times T + 0.0221229 \times T^2 + 99.2385 \times t - 0.838472 \times t^2 - 0.0694761 \times T \times t$$

$R^2 = 0.67$, $AIC = 875.16$

(**i**)

Figure A1. Torrefaction temperature and time effect on properties of CSF produced from medical/cosmetic peat waste, the equations boundary, T = 200–300 °C, t = 20–60 min. (**a**) mass yield, (**b**) energy densification ratio, (**c**) energy yield, (**d**) volatile matter, (**e**) ash content, (**f**) fixed carbon, (**g**) volatile solids, (**h**) combustible parts, (**i**) high heating value.

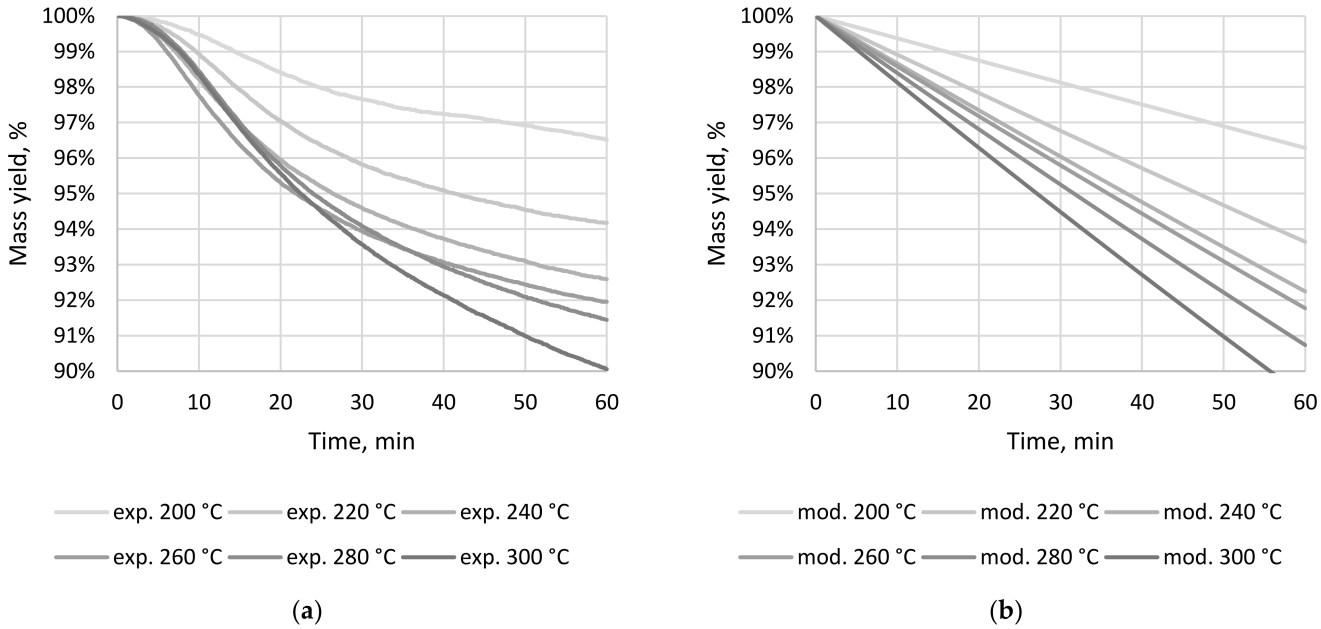

Figure A2. Results of macro-TGA, the effect of isothermal temperatures in time (**a**) experimental data, (**b**) lifetime prediction.

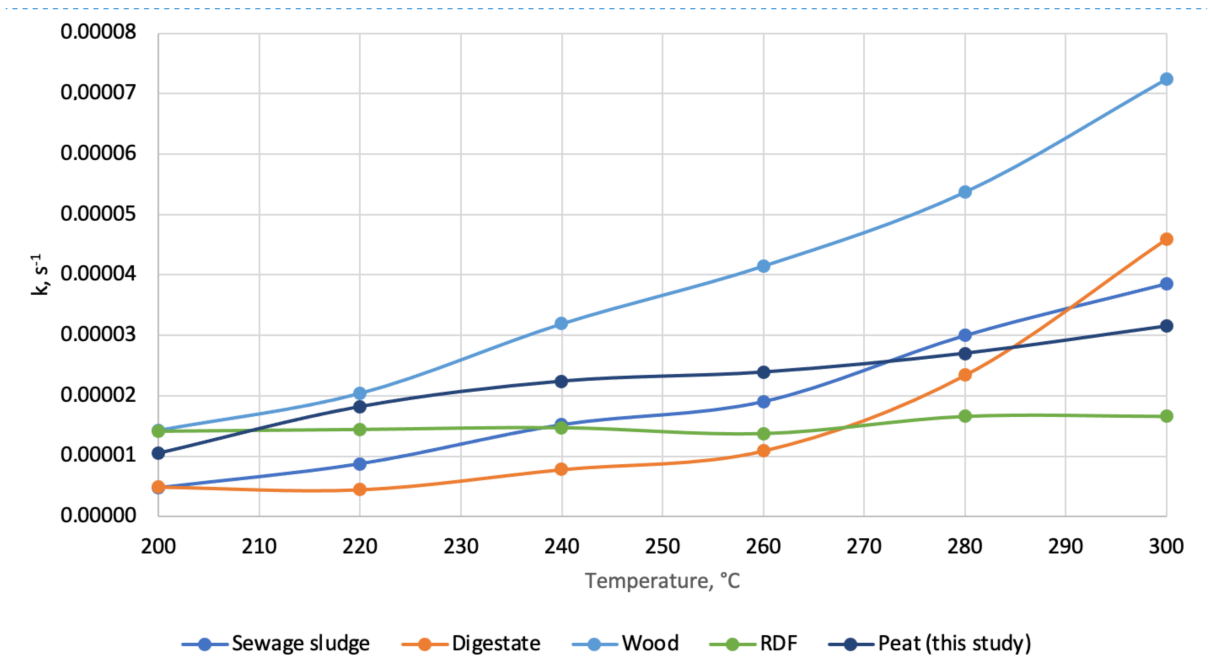

Figure A3. The constant reaction rates (k) in function of temperature for different materials at specific temperatures [39].

References

1. Özay, P.; Karagülle, M.; Kardeş, S.; Karagülle, M.Z. Chemical and mineralogical characteristics of peloids in Turkey. *Environ. Monit. Assess.* **2020**, *192*, 805. [CrossRef] [PubMed]
2. Leśniak, M. Management of Waste from Cosmetic Industry. Bachelor's Thesis, Wrocław Univesristy of Envrionmental and Life Sciences, Wroclaw, Poland, 2021.
3. Dudkiewicz, E. Disposal of the post-treatment mud in Polish spas. *Gaz Woda i Technika Sanitarna* **2015**, *1*, 25–28. [CrossRef]
4. Sutejo, Y.; Saggaff, A.; Rahayu, W. Hanafiah physical and chemical characteristics of fibrous peat. In Proceedings of the 3rd International Conference on Construction and Building Engineering (Iconbuild) 2017: Smart Construction Towards Global Challenges, Palembang, Indonesia, 14–17 August 2017; AIP Conference Proceedings. American Institute of Physics Inc.: College Park, MD, USA, 2017; Volume 1903, p. 090006.

5. Majcher-Kozieł, M. Borowina-właściwości lecznicze i kosmetologiczne. *Chemia w Szkole* **2013**, *4*, 42–44.
6. Von Post Humification Scale. Available online: https://www.blacklandcentre.org/the-science/von-post-humification-scale/ (accessed on 8 August 2021).
7. Drobnik, J.; Stebel, A. Central European ethnomedical and officinal uses of peat, with special emphasis on the Tołpa Peat Preparation (TPP): An historical review. *J. Ethnopharmacol.* **2020**, *246*, 112248. [CrossRef]
8. History of Peat. Available online: https://peatmoss.com/what-is-peat-moss/the-history-of-peat/ (accessed on 11 August 2021).
9. Kapetaki, Z.; Moya, J. *Recent Trends in EU Coal, Peat and Oil Shale Regions*; Publications Office of the European Union: Luxembourg, 2021.
10. Kapetaki, Z.; Alves Dias, P.; Conte, A.; Kanellopoulos, K.; Mandras, G.; Medarac, H.; Nijs, W.; Ruiz, P.; Somers, J.; Tarvydas, D. *Recent Trends in EU Coal, Peat and Oil Shale Regions*; Publications Office of the European Union: Luxembourg, 2021.
11. Tcvetkov, P.S. The history, present status and future prospects of the Russian fuel peat industry. *Mires and Peat* **2017**, *19*, 1–12. [CrossRef]
12. Krysanova, K.O.; Krylova, A.Y.; Zaichenko, V.M. Application of hydrothermal carbonization to improve the energy properties of peat. *Solid Fuel Chem.* **2021**, *55*, 123–128. [CrossRef]
13. Misnikov, O. Basic technologies and equipment used for peat deposits development in foreign countries. In *E3S Web of Conferences, Proceedings of the 3rd International Innovative Mining Symposium, Kemerovo, Russia, 3–5 October 2018*; EDP Sciences: Les Ulis, France, 2018; Volume 41.
14. Dalias, P.; Prasad, M.; Mumme, J.; Kern, J.; Stylianou, M.; Christou, A. Low-cost post-treatments improve the efficacy of hydrochar as peat replacement in growing media. *J. Environ. Chem. Eng.* **2018**, *6*, 6647–6652. [CrossRef]
15. Chrysargyris, A.; Prasad, M.; Kavanagh, A.; Tzortzakis, N. Biochar type and ratio as a peat additive/partial peat replacement in growing media for cabbage seedling production. *Agronomy* **2019**, *9*, 693. [CrossRef]
16. Neumaier, D.; Lohr, D.; Voßeler, R.; Girmann, S.; Kolbinger, S.; Meinken, E. Hydrochars as peat substitute in growing media for organically grown potted herbs. *Acta Hortic.* **2017**, *1168*, 377–386. [CrossRef]
17. Chen, B.; Koziel, J.A.; Lee, M.; O'Brien, S.C.; Li, P.; Brown, R.C. Mitigation of acute hydrogen sulfide and ammonia emissions from swine manure during three-hour agitation using pelletized biochar. *Atmosphere* **2021**, *12*, 825. [CrossRef]
18. Kosov, V.V.; Sinelshchikov, V.A.; Sytchev, G.A.; Zaichenko, V.M. Effect of torrefaction on properties of solid granulated fuel of different biomass types. *High Temp.* **2014**, *52*, 907–912. [CrossRef]
19. Tabakaev, R.; Astafev, A.; Dubinin, Y.; Yazykov, N.; Yakovlev, V. Evaluation of autothermal peat pyrolysis realization for fuel processing technologies. *Waste Biomass Valorization* **2019**, *10*, 1021–1027. [CrossRef]
20. Zaitsev, A.S.; Taburchinov, R.I.; Ozerova, I.P.; Pereira, A.O.; Egorov, R.I. Allothermal gasification of peat and lignite by a focused light flow. *Appl. Sci.* **2020**, *10*, 2640. [CrossRef]
21. Krysanova, K.; Krylova, A.; Zaichenko, V. Properties of biochar obtained by hydrothermal carbonization and torrefaction of peat. *Fuel* **2019**, *256*, 115929. [CrossRef]
22. Dyjakon, A.; Noszczyk, T. Alternative fuels from forestry biomass residue: Torrefaction process of horse chestnuts, oak acorns, and spruce cones. *Energies* **2020**, *13*, 2468. [CrossRef]
23. Chen, W.H.; Wang, C.W.; Ong, H.C.; Show, P.L.; Hsieh, T.H. Torrefaction, pyrolysis and two-stage thermodegradation of hemicellulose, cellulose and lignin. *Fuel* **2019**, *258*, 116168. [CrossRef]
24. Wei, R.; Li, H.; Chen, Y.; Hu, Y.; Long, H.; Li, J.; Xu, C.C. Environmental issues related to bioenergy. In *Reference Module in Earth Systems and Environmental Sciences*; Elsevier: Amsterdam, The Netherlands, 2020.
25. Basu, P. *Biomass Gasification, Pyrolysis and Torrefaction*; Elsevier: Amsterdam, The Netherlands, 2013; ISBN 9780123964885.
26. Nizamuddin, S.; Baloch, H.A.; Griffin, G.J.; Mubarak, N.M.; Bhutto, A.W.; Abro, R.; Mazari, S.A.; Ali, B.S. An overview of effect of process parameters on hydrothermal carbonization of biomass. *Renew. Sustain. Energy Rev.* **2017**, *73*, 1289–1299. [CrossRef]
27. Funke, A.; Ziegler, F. Hydrothermal carbonization of biomass: A summary and discussion of chemical mechanisms for process engineering. *Biofuels Bioprod. Biorefining* **2010**, *4*, 160–177. [CrossRef]
28. Zaitchenko, V.M.; Krysanova, K.O.; Krysanov, O.N.; Sychev, G.A.; Krylova, A.Y. Effect of temperature on the torrefaction of peat. *Solid Fuel Chem.* **2018**, *52*, 70–72. [CrossRef]
29. Nunes, L.J.R. A case study about biomass torrefaction on an industrial scale: Solutions to problems related to self-heating, difficulties in pelletizing, and excessive wear of production equipment. *Appl. Sci.* **2020**, *10*, 2546. [CrossRef]
30. Shoulaifar, T.K. *Chemical Changes in Biomass during Torrefaction*; Åbo Akademi University: Turku, Finland, 2016.
31. Rudolfsson, M.; Borén, E.; Pommer, L.; Nordin, A.; Lestander, T.A. Combined effects of torrefaction and pelletization parameters on the quality of pellets produced from torrefied biomass. *Appl. Energy* **2017**, *191*, 414–424. [CrossRef]
32. Wang, L.; Riva, L.; Skreiberg, Ø.; Khalil, R.; Bartocci, P.; Yang, Q.; Yang, H.; Wang, X.; Chen, D.; Rudolfsson, M.; et al. Effect of torrefaction on properties of pellets produced from woody biomass. *Energy Fuels* **2020**, *34*, 15343–15354. [CrossRef]
33. Agar, D.; DeMartini, N.; Hupa, M. Influence of elevated pressure on the torrefaction of wood. *Energy Fuels* **2016**, *30*, 2127–2136. [CrossRef]
34. Ilnicki, P. Torfowiska i Torf. *Recenzje* **2004**, *50*, 203–207.
35. Uzdrowisko Kołobrzeg, S.A. Medical Peat Brochure. Available online: https://spa.uzdrowisko.kolobrzeg.pl/borowina-lecznicza-1-kg-p-7.html (accessed on 26 August 2021).

36. Syguła, E.; Świechowski, K.; Hejna, M.; Kunaszyk, I.; Białowiec, A. Municipal solid waste thermal analysis—Pyrolysis kinetics and decomposition reactions. *Energies* **2021**, *14*, 4510. [CrossRef]
37. Świechowski, K.; Stępień, P.; Syguła, E.; Koziel, J.; Białowiec, A. Lab-scale study of temperature and duration effects on carbonized solid fuels properties produced from municipal solid waste components. *Materials* **2021**, *14*, 1191. [CrossRef] [PubMed]
38. Hunt, J.; Ferrari, A.; Lita, A.; Crosswhite, M.; Ashley, B.; Stiegman, A.E. Microwave-specific enhancement of the carbon−carbon dioxide (Boudouard) reaction. *J. Phys. Chem.* **2013**, *117*, 26871–26880. [CrossRef]
39. Świechowski, K.; Hnat, M.; Stępień, P.; Stegenta-Dąbrowska, S.; Kugler, S.; Koziel, J.A.; Białowiec, A. Waste to energy: Solid fuel production from biogas plant digestate and sewage sludge by torrefaction-process kinetics, fuel properties, and energy balance. *Energies* **2020**, *13*, 3161. [CrossRef]
40. Noszczyk, T.; Dyjakon, A.; Koziel, J.A. Kinetic parameters of nut shells pyrolysis. *Energies* **2021**, *14*, 682. [CrossRef]
41. Świechowski, K.; Stegenta-Dabrowska, S.; Liszewski, M.; Babelewski, P.; Koziel, J.A.; Białowiec, A. Oxytree pruned biomass torrefaction: Process kinetics. *Materials* **2019**, *12*, 3334. [CrossRef]
42. Badour, C.; Gilbert, A.; Xu, C.; Li, H.; Shao, Y.; Tourigny, G.; Preto, F. Combustion and air emissions from co-firing a wood biomass, a Canadian peat and a Canadian lignite coal in a bubbling fluidised bed combustor. *Can. J. Chem. Eng.* **2012**, *90*, 1170–1177. [CrossRef]
43. Al Tanjil, H.; Akter, S. Characterization of peat for identifying the effectiveness as energy source by proximate analysis. *Petronelum Coal* **2020**, *62*, 63–70.
44. Świechowski, K.; Liszewski, M.; Babelewski, P.; Koziel, J.A.; Białowiec, A. Oxytree pruned biomass torrefaction: Mathematical models of the influence of temperature and residence time on fuel properties improvement. *Materials* **2019**, *12*, 2228. [CrossRef] [PubMed]
45. Nunes, L.J.R.; Matias, J.C.O.; Loureiro, L.M.E.F.; Sá, L.C.R.; Silva, H.F.C.; Rodrigues, A.M.; Causer, T.P.; Devallance, D.B.; Ciolkosz, D.E. Evaluation of the potential of agricultural waste recovery: Energy densification as a factor for residual biomass logistics optimization. *Appl. Sci.* **2021**, *11*, 20. [CrossRef]
46. Pulka, J.; Wiśniewski, D.; Gołaszewski, J.; Białowiec, A. Is the biochar produced from sewage sludge a good quality solid fuel? *Arch. Environ. Prot.* **2016**, *42*, 125–134. [CrossRef]
47. Zhang, C.; Ho, S.-H.; Chen, W.-H.; Xie, Y.; Liu, Z.; Chang, J.-S. Torrefaction performance and energy usage of biomass wastes and their correlations with torrefaction severity index. *Appl. Energy* **2018**, *220*, 598–604. [CrossRef]
48. Zhou, H.; Long, Y.; Meng, A.; Chen, S.; Li, Q.; Zhang, Y. A novel method for kinetics analysis of pyrolysis of hemicellulose, cellulose, and lignin in TGA and macro-TGA. *RSC Adv.* **2015**, *5*, 26509–26516. [CrossRef]
49. Bhavsar, P.A.; Jagadale, M.H.; Khandetod, Y.P.; Mohod, A.G. Proximate analysis of selected non woody biomass. *Int. J. Curr. Microbiol. Appl. Sci.* **2018**, *7*, 2846–2849. [CrossRef]
50. Słupska, M.; Dyjakon, A.; Stopa, R. Determination of strength properties of energy plants on the example of Miscanthus-Giganteus, Rosa Multiflora and Salix Viminalis. *Energies* **2019**, *12*, 3660. [CrossRef]
51. Telmo, C.; Lousada, J.; Moreira, N. Proximate analysis, backwards stepwise regression between gross calorific value, ultimate and chemical analysis of wood. *Bioresour. Technol.* **2010**, *101*, 3808–3815. [CrossRef]
52. Donahue, C.J.; Rais, E.A. Proximate analysis of coal. *J. Chem. Educ.* **2009**, *86*, 222. [CrossRef]
53. Pettersen, R.C. The chemical composition of wood. In *The Chemistry of Solid Wood*; American Chemical Society: Washington, DC, USA, 1984; pp. 57–126.
54. Spedding, P.J. Peat. *Fuel* **1988**, *67*, 883–900. [CrossRef]
55. Iglovikov, A.; Motorin, A. Composition of organic matter in peat soils of the northern trans-Urals depending on groundwater level. In *E3S Web of Conferences, Proceedings of the Innovative Technologies in Environmental Science and Education (ITESE-2019), Divnomorskoe Village, Russia, 9–14 September 2019*; EDP Sciences: Les Ulis, France, 2019; Volume 135, p. 01004. [CrossRef]
56. Brown, A.; Mathur, S.P.; Kauri, T.I.; Kushner, D.J. Measurement and significance of cellulose in peat soils. *Can. J. Soil Science* **1988**, *68*, 681–685. [CrossRef]
57. Zhang, J.; Chen, T.; Wu, J.; Wu, J. A novel gaussian-DAEM-reaction model for the pyrolysis of cellulose, hemicellulose and lignin. *RSC Adv.* **2014**, *4*, 17513. [CrossRef]
58. Yang, H.; Yan, R.; Chen, H.; Lee, D.H.; Zheng, C. Characteristics of hemicellulose, cellulose and lignin pyrolysis. *Fuel* **2007**, *86*, 1781–1788. [CrossRef]
59. Murugan, P.; Mani, T.; Mahinpey, N.; Dong, M. Pyrolysis kinetics of athabasca bitumen using a TGA under the influence of reservoir sand. *Can. J. Chem. Eng.* **2012**, *90*, 315–319. [CrossRef]
60. Santos, A.; Bertoli, A.; Borges, A.C.; Gomes, R.; Garcia, J.; Trevisan, M. New organomineral complex from humic substances extracted from poultry wastes: Synthesis, characterization and controlled release study. *J. Braz. Chem. Soc.* **2017**, *29*, 140–150. [CrossRef]
61. Łyczko, J.; Masztalerz, K.; Lipan, L.; Iwiński, H.; Lech, K.; Carbonell-Barrachina, Á.A.; Szumny, A. Coriandrum Sativum L.—Effect of multiple drying techniques on volatile and sensory profile. *Foods* **2021**, *10*, 403. [CrossRef]
62. Chen, H.; Zhao, W.; Liu, N. Thermal analysis and decomposition kinetics of Chinese forest peat under nitrogen and air atmospheres. *Energy Fuels* **2011**, *25*, 797–803. [CrossRef]
63. Wen, Y.; Wang, S.; Mu, W.; Yang, W.; Jönsson, P.G. Pyrolysis performance of peat moss: A simultaneous in-situ thermal analysis and bench-scale experimental study. *Fuel* **2020**, *277*, 118173. [CrossRef]

64. Fraga, L.G.; Silva, J.; Teixeira, S.; Soares, D.; Ferreira, M.; Teixeira, J. Thermal conversion of pine wood and kinetic analysis under oxidative and non-oxidative environments at low heating rate. *Proceedings* **2020**, *58*, 23. [CrossRef]
65. Grishin, A.M.; Golovanov, A.N.; Sukov, Y.V. Experimental determination of thermophysical, thermokinetic, and filtration characteristics of peat. *J. Eng. Phys. Thermophys.* **2006**, *79*, 557–562. [CrossRef]
66. Anusha, S.; Samarasekara, L.; Coorey, R.V. Thermal capacity as a function of moisture content of Sri Lankan wood species: Wheatstone bridge method. *Proc. Tech. Sess.* **2011**, *27*, 9–16.
67. Nopens, M.; Sazama, U.; Krause, A.; Fröba, M. Specific heat capacity of wood between −140 and 50 °C in dry and wet state. *Holzforschung* **2021**, *75*, 779–785. [CrossRef]

Załącznik nr 3

Kacper Świechowski
imię i nazwisko

WROCŁAW 28.02.2022
(miejscowość i data)

Katedr Biogospodarki Stosowanej
Uniwersytet Przyrodniczy we Wrocławiu
51-630 Wrocław, Chełmońskiego 37a
afiliacja

OŚWIADCZENIE

Oświadczam, że w pracy:

Kacper Świechowski, Małgorzata Leśniak, Andrzej Białowiec. 2021. Medical Peat Waste Upcycling to Carbonized Solid Fuel in the Torrefaction Process. Energies, 14, 6053. doi.org/10.3390/en14196053.

mój udział polegał na:

Opracowaniu wyników z badań pod względem statystycznym przy wykorzystaniu oprogramowania Statistica. Opracowanie polegało w szczególności na wyznaczeniu modeli wpływu parametrów technologicznych (czasu i temperatury) toryfikacji na zmianę właściwości paliwowych badanych materiałów, wyznaczeniu parametrów kinetycznych toryfikacji w warunkach izotermicznych, wyznaczeniu ilości energii potrzebnej do toryfikacji. Ponadto byłem odpowiedzialny za napisanie pierwszej wersji manuskryptu, w szczególności metodyki oraz opisu i dyskusji wyników. Podczas procesu recenzji stworzyłem pierwszą wersję odpowiedzi dla recenzentów i wykonywałem poprawki w manuskrypcie.

28.02.2022 Świechowski
data i podpis

Załącznik nr 3

Małgorzata Leśniak
imię i nazwisko

Katedr Biogospodarki Stosowanej
Uniwersytet Przyrodniczy we Wrocławiu
51-630 Wrocław, Chełmońskiego 37a
afiliacja

Wrocław 28.02.2022
(miejscowość i data)

OŚWIADCZENIE

Oświadczam, że w pracy:
Kacper Świechowski, Małgorzata Leśniak, Andrzej Białowiec. 2021. Medical Peat Waste Upcycling to Carbonized Solid Fuel in the Torrefaction Process. Energies, 14, 6053. doi.org/10.3390/en14196053.

mój udział polegał na:
Pozyskaniu materiału badawczego – borowiny i przygotowaniu ich do dalszych badań (suszenie, rozdrobnienie). Do wykonanych przeze mnie badań należało wykonanie biowęgli i poddanie ich wraz z nieprzetworzonym materiałem analizie technicznej oraz analizie TGA w warunkach izotermicznych. Byłam odpowiedzialna za opracowanie pierwszej wersji wstępu w języku polskim.

28.02.2022
data i podpis

Załącznik nr 3

Andrzej Białowiec
imię i nazwisko

Wrocław, 26.02.2022
(miejscowość i data)

Katedr Biogospodarki Stosowanej
Uniwersytet Przyrodniczy we Wrocławiu
51-630 Wrocław, Chełmońskiego 37a
afiliacja

OŚWIADCZENIE

Oświadczam, że w pracy:
Kacper Świechowski, Małgorzata Leśniak, Andrzej Białowiec. 2021. Medical Peat Waste Upcycling to Carbonized Solid Fuel in the Torrefaction Process. Energies, 14, 6053. doi.org/10.3390/en14196053.

mój udział polegał na:
Nadzorowaniu pracy nad pisaniem manuskryptu i sprawdzeniu poprawności pierwszej wersji manuskryptu pod względem merytorycznym. Do moich obowiązków należało także sprawdzenie poprawności uzyskanych danych eksperymentalnych. Jako autor korespondencyjny byłem odpowiedzialny za proces recenzji. We współpracy z pozostałymi współautorami przygotowałem odpowiedzi dla recenzentów i wprowadzałem część poprawek do manuskryptu.

26.02.2022
data i podpis

materials

MDPI

Article

Carbonized Solid Fuel Production from Polylactic Acid and Paper Waste Due to Torrefaction

Kacper Świechowski [1,*], Christian Zafiu [2] and Andrzej Białowiec [1]

[1] Department of Applied Bioeconomy, Wrocław University of Environmental and Life Sciences, 37a Chełmońskiego Str., 51-630 Wrocław, Poland; andrzej.bialowiec@upwr.edu.pl
[2] Department of Water, Atmosphere and Environment, Institute of Waste Management, University of Natural Resources and Life Sciences, Muthgasse 107, 1190 Wien, Austria; christian.zafiu@boku.ac.at
* Correspondence: kacper.swiechowski@upwr.edu.pl

Abstract: The quantity of biodegradable plastics is increasing steadily and taking a larger share in the residual waste stream. As the calorific value of biodegradable plastic is almost two-fold lower than that of conventional ones, its increasing quantity decreases the overall calorific value of municipal solid waste and refuse-derived fuel which is used as feedstock for cement and incineration plants. For that reason, in this work, the torrefaction of biodegradable waste, polylactic acid (PLA), and paper was performed for carbonized solid fuel (CSF) production. In this work, we determined the process yields, fuel properties, process kinetics, theoretical energy, and mass balance. We show that the calorific value of PLA cannot be improved by torrefaction, and that the process cannot be self-sufficient, while the calorific value of paper can be improved up to 10% by the same process. Moreover, the thermogravimetric analysis revealed that PLA decomposes in one stage at ~290–400 °C with a maximum peak at 367 °C, following a 0.42 reaction order with the activation energy of 160.05 kJ·(mol·K)$^{-1}$.

Keywords: torrefaction; solid fuel; waste to carbon; circular economy; biodegradable materials; calorific value

Citation: Świechowski, K.; Zafiu, C.; Białowiec, A. Carbonized Solid Fuel Production from Polylactic Acid and Paper Waste Due to Torrefaction. *Materials* **2021**, *14*, 7051. https://doi.org/10.3390/ma14227051

Academic Editors: Rossana Bellopede and Lorena Zichella

Received: 23 October 2021
Accepted: 16 November 2021
Published: 20 November 2021

1. Introduction

1.1. Background of Current Situation

The negative impact of plastic waste accumulated in the environment (in oceans, soils, and air), including the form of microplastics, is undeniable. Most of the commonly used polymers are based on fossil resources and resistant to biodegradation, which means that once released to the environment, they will persist for a long time. Currently, there is a risk of the release of chemicals from all plastic that is unproperly landfilled into the soil and groundwater. Plastic waste that has leaked into oceans is a cause of death of marine life and is a source of microplastic that pollutes the air we breathe and water we drink [1–4].

Geyer et al. [5] estimated in 2017 that, since the 1950s, over 8300 Mt of plastics were ever produced globally, out of which 56% (ca. 4700 Mt) of the ever-produced plastics were landfilled or ended up in the environment [5]. In 2019 alone, 368 Mt of plastic were produced [6], and it is estimated that that annual production will increase by four times in 2050 [7]. To date, to cover plastic production, around 4% of the total extracted fossil fuels (e.g., natural gas, oil, and coal), are needed annually, and by 2050 this number could increase to 20% [8]. Currently, the largest plastic producers are China (31%), North America (19%), and the European Union (EU) (16%) [6]. According to "Global Plastic Flow 2018" that was prepared by Conversio Market & Strategy GmbH [9], the global plastic consumption was 385 Mt which consisted of 172 Mt of packaging waste and 213 Mt of non-packaging waste. At the same time, 250 Mt of plastic waste was generated, of which only 175 Mt was collected, and hence 75 Mt was improperly disposed or released to the environment. Only

~28.5% of the collected plastic waste was recycled; a similar amount was incinerated, and 43% was landfilled [9].

A large share of plastic materials (almost 40% in the EU) is used for packaging, which has the shortest life cycle. Other sectors that consume large amounts of plastic are building and construction (~20%) and automotive (~10%) [6]. These shares are most probably similar for the rest of the world. According to the Ellen Macarthur Foundation [10], only 14% of produced packaging plastic globally was collected for recycling purposes, wherein 4% was lost during recycling processes, 8% was recycled in cascaded recycling (waste plastic was converted into other, lower-value products), and only 2% of produced plastic had a closed-recycling loop (wasted plastic was converted into the same or similar quality products) [10].

At the first glance, the presented data show that the most abundant type of plastic waste (packaging) is hard to recycle, or its recycling is not economical yet. The reasons for this are the low quality of the recycled plastics in comparison to the virgin material, cost-intensive recycling processes, and lack of proper infrastructure [1]. Some plastic materials, such as high-density polyethylene (HD-PE), or polyethylene terephthalate (PET) can be recycled economically, due to their high market value, whereas low-density polyethylene (LD-PE), and other foil materials are used for refuse-derived fuel (RDF) production [1,11]

1.2. The Problem of Bioplastic Solution

With increasing awareness of citizens about ecology and sustainability, an increasing number of producers replace conventional packing plastic with biobased and biodegradable plastics. In 2020, around 47% of all produced bioplastic was used in the packaging sector. According to the European Bioplastics organization, bioplastic (biodegradable and non-biodegradable) represents about 1% of all produced plastic. The organization also estimates that, due to the rising demand, the bioplastic market will increase by ~40% up to 2025 [11,12].

Bio-based plastics are a potential solution for problems related to fossil-based plastic. In theory, bioplastics open new end-of-life scenarios, such as composting or anaerobic digestion, and lead to a reduction in conventional plastics pollution. In practice, however, there are problems with proper management [11]. Different biodegradable plastics need different environmental conditions to be biodegraded, e.g., biodegradable PLA-based biowaste bags need relatively high temperatures for overcoming the glass transition temperature (~70 °C) and initiating biodegradability. Such temperatures can be achieved in industrial composting plants, but not in home composters. In practice, biodegradable plastic is not usually decomposed during anaerobic digestion [13]. As a result, some countries, and some municipalities in the EU, allow the use of biodegradable bags for kitchen waste collection, while others do not [13]. At the same time, the bioplastic products also increase their share in the municipal solid waste (MSW) stream as, to date, no strategies exist for the collection and processing of bioplastic wastes. The reason for this is that these plastics are still a minority in the waste stream, are difficult to detect, and require sophisticated methods for proper separation [14]. Therefore, most of the bioplastic waste goes to residual fraction of municipal solid waste or is collected with conventional plastic. In both cases, biodegradable plastics are used for RDF production or are landfilled, if the local regulations allow it. As a result, biodegradable plastics do not lead to a decrease in plastic pollutions and additionally decrease the calorific value of RDF made from waste. The calorific value of the most abundant plastic (PE-LD) used for RDF production is ca. 40 $MJ \cdot kg^{-1}$ [15], while the most common biodegradable plastic used to replace it, is PLA with ~19 $MJ \cdot kg^{-1}$. A simple simulation in Figure A1 shows that when biodegradable plastic share increases, the high heating value of RDF decreases from 28 to 18 $MJ \cdot kg^{-1}$.

1.3. The RDF Quality Importance

Refused-derived fuel (RDF), also known as solid recovered fuel (SRF), is mainly made from MSW. The RDF can also be made from other waste such as used tires, sewage sludges,

textiles, wood, and others. The main properties of RDF decisive of its quality are calorific value and ash content. The higher the calorific value and lower ash content, the better quality of RDF. The calorific value of RDF depends on the share of RDF components and can differ from 11 MJ·kg^{-1} [16] to 36 MJ·kg^{-1} [17]. From a calorific point of view, the most valuable materials are plastics such as PP and PE ~46 MJ·kg^{-1}, PS ~41 MJ·kg^{-1}, and PET ~26 MJ·kg^{-1} [18], whereas organic waste, paper, and fabrics lead to a decrease in RDF energetic potential [19]; however, this increases the renewable energy availability. Organic waste such as kitchen and food wastes are also the main source of moisture that further decreases the energetic potential of RDF [19]. Similarly, the ash content of RDF depends on materials share, and the ash amount in plastic wastes is much lower than in other waste.

The high-quality RDF is needed for specialized incineration plants and for cement plants where RDF replaces coal and provides cleaner and partly renewable energy. In particular, cement plants need high calorific value RDF to keep the cement production process stable and safe for the environment. During waste incineration (also applies to RDF), there is a need to keep the temperature of exhaust gases above 850 °C for at least 2 s to eliminate the formation of harmful compounds. In the case of a cement plant, the waste needs to generate higher temperatures for clinker burning, and when the RDF calorific value is not high enough, the required temperature will not be obtained [20].

The RDF is usually produced in the mechanical-biological treatment plant (MBT), where MSW are valorized by various mechanical and biological methods. Mechanical methods include material separation, screening, and grinding [21]. These methods are applied to increase calorific value, increase homogeneity, and decrease ash and other pollutants (Hg, Cl) content. On the other hand, a biological method such as bio-drying is used to remove water from MSW. If RDF, produced in the MBT plant, does not meet the required quality, it can be upgraded in the future by mixing other more energetic industrial materials, by the densification process (pelletization), or by thermal processing such as torrefaction or carbonization in low temperatures [21,22]. Thermal processing in conventional pyrolysis temperatures is not applicable, as most plastics are concerting into oil and gas instead of solid carbonized fuel; as result, the calorific value of solid carbonized fuel starts to decrease [23]. Furthermore, mixing, densification, and thermal processing can be combined to maximize the quality of RDF. Here, it is important to note that each of the mentioned processes requires energy, and the legitimacy of the use of these methods depends on a specific situation.

While conventional plastics PP, PE, and PET are usually subjected to mechanical recycling after separate collection, biodegradable plastics recycling has not been developed yet. Therefore, the decreasing share of conventional plastics and increasing share of bioplastics in RDF induces a need for research on the torrefaction of these biodegradable materials, as a perspective for CSF production from MSW in the future.

1.4. Study Aim

In this work, PLA wastes, PLA-made cups, and paper-made cups with the addition of PLA were subjected to thermal processing-torrefaction. The main aim was to check the legitimacy of low-temperature processing of PLA wastes for fuel parameters improvement. PLA wastes were processed at 200–300 °C to check the possibilities of thermal upgrading. As torrefaction and low-temperature pyrolysis of mixed waste turned out to increase the calorific value of RDF [23], we assumed that similar results will be obtained for PLA wastes. As result, a decreasing calorific value of MSW and RDF with an increasing biodegradable plastic share will be overcome. For this reason, the fuel properties of torrefied PLA wastes, torrefaction kinetics, and theoretical energy required for torrefaction were determined.

1.5. Methods of Thermal Processes Analysis

There are many various methods and techniques for thermal study performance and thermal process analysis. The most common are studies using small, lab-scale reactors made for specific situations, or by adopting other equipment such as muffle furnaces or

autoclaves. These types of equipment allow performing thermal conversion of materials to produce enough carbonized material used for other analyses such as proximate analysis, elemental analysis, etc. Such small reactors are in favor of testing new and non-standard materials as they provide a lot of information about process efficiency and product quality [24]. On the other hand, these reactors have limited potential for thermal process reaction analysis. Most of them work similar to a black-box and only the beginning and the final product is measured, without intermediates. For that reason, thermal analysis is also performed using thermogravimetric equipment, allowing us to measure changes in materials mass, occurred reactions, quality, and chemical compositions of intermediate products. The basic thermogravimetric analysis is TGA that provides information about mass losses during a time at a defined temperature, and differential scanning calorimetry (DSC) provides information about energy flow through sample. Additionally, TGA/DSC equipment can be coupled with other instruments that identify released gasses and their chemical composition. As result, emissions and evolved pollution during the process can be quantified and managed [25–27].

2. Materials and Methods

2.1. Materials

The samples of biodegradable materials for the experiment were prepared from commercially available one-use cups. Paper (PAP) served as reference material and was obtained from cups that were made of 99% of paper, and 1% of PLA. The PLA material was obtained from cups made of 100% PLA plastic. The paper cups were ground using a laboratory knife mill (Testchem, model LMN-100, Pszów, Poland), through a 3 mm sieve, while the PLA cups were cut manually into pieces of ~1 cm^2 as the PLA was melting and blocked the mill. Then, the crumbled material was subjected to a torrefaction process. Samples of raw and torrefied materials were stored in plastic containers at room temperature (~20 °C).

2.2. Methods

Before the experiment, raw, crumbled materials were dried at 105 °C using a laboratory dryer (WAMED, KBC-65W, Warsaw, Poland) until a constant mass was obtained. These dry materials were used for CSF production. After that, the materials and produced CSFs were subjected to proximate analysis and higher heating value (HHV) determination analysis. Next, dry raw samples of raw materials were subjected to thermogravimetric analysis (TGA) for kinetic parameters determination and differential scanning calorimetry analysis (DSC) for determination of endo and exothermal reaction presence. Next, data from the CSF production process and proximate analysis were used to build regression models that show and describe quantitatively the effect of process temperature and time on CSF properties.

2.2.1. Torrefaction Process—CSF Production

The CSF was produced at different temperatures of 200–300 °C in intervals of 20 °C and kept for 20, 40, and 60 minutes each. For the torrefaction procedure, 10 g of dry samples were placed in ceramic crucibles. These crucibles were placed into the chamber of the muffle furnace (Snol 8.1/1100, Utena, Lithuania), which was purged with CO_2 gas to create an inert atmosphere before the samples were heated to the setpoint temperature. During the torrefaction process, CO_2 gas was continuously supplied to the chamber to prevent sample ignition. The CO_2 flow was shut off after the treatment period and when the temperature of the chamber declined to <150 °C. The mass of samples before and after the process was used to calculate mass yield following Equation (1). Then, using the results of HHV, the energy densification ratio was calculated (Equation (2)), and then the energy yield of CSF was determined according to Equation (3).

$$MY = \frac{m_b}{m_r} \cdot 100 \quad (1)$$

where $MY.$ is the mass yield, %; m_b is the mass of material after torrefaction, g (CSF); and m_r is the mass of material before torrefaction, g.

$$EDr = \frac{HHV_b}{HHV_r} \quad (2)$$

Where $EDr.$ is the energy densification ratio; $HHV_b.$ is the high heating value of material after torrefaction ($J \cdot g^{-1}$) (CSF); and m_r is the high heating value of material before torrefaction ($J \cdot g^{-1}$).

$$EY = MY \cdot EDr \quad (3)$$

where EY is the energy yield, %; $MY.$ is the mass yield, %; and EDr is the energy densification ratio.

2.2.2. Proximate Analysis and HHV Determination

For all samples, the proximate analysis was performed. The moisture content (MC) was determined by the drying method at 105 °C using a laboratory dryer (WAMED, KBC-65W, Warsaw, Poland) according to PN-EN 14346:2011 standard [28]. The volatile matter (VM) was measured by a thermogravimetric method using a tubular furnace (Czylok, RST 40 × 200/100, Jastrzębie-Zdrój, Poland), according to [29]. The ash content (AC) was measured by sample incineration in a muffle furnace (Snol 8.1/1100, Utena, Lithuania) according to PN-Z-15008-04:1993 standard [30], and fixed carbon was measured by difference. Additionally, samples were tested for volatile solids content (VS) and combustible part content (CP) using the muffle furnace (Snol 8.1/1100, Utena, Lithuania) according to PN-EN 15169:2011 [31] and PN-Z-15008-04:1993 [30] standards, respectively. All samples were tested for high heating value using a calorimeter (IKA, C200, Staufen, Germany), according to PN EN ISO 18125:2017-07 [32]. To ensure repeatability, each experiment was triplicated.

2.2.3. Statistical Analyses

Results of CSF production and proximate analysis were subjected to regression analyses to provide empirical equations. These equations are used to describe the following properties of CSF: MY, EDr, EY, VM, AC, FC, VS, CP, and HHV depending on process temperature and time. The regression was performed according to previous work [19]. In brief, experimental data were subjected to four regression models: (I) linear equation, (II) second-order polynomial equation, (III) factorial regression equation, and (IV) response surface regression equation. Then, determination coefficient (R^2) and Akaike value (AIC) were calculated for each model. Next, models with the greatest R^2 and the lowest AIC value were chosen as the best fit to experimental data; the other models were rejected. In the case chosen model had some insignificant regression coefficients (a_n), they were removed, and regression analysis was performed again.

To check if process conditions have an impact on fuel properties, ANOVA was performed, with a post hoc Tukey test to test the pairwise significance ($p < 0.05$).

2.2.4. Thermal Analysis

The dry samples were subjected to TG/DTG/DSC thermal analysis using a simultaneous thermal analyzer (Netzsch, 449 F1 Jupiter, Selb, Germany). Term TG/DTG/DSC stands for thermogravimetry/difference thermogravimetry/differential scanning calorimetry. TG/DTG results present how material decomposes in the function of temperature, while the DSC results show transformations and reactions occurring at a particular temperature.

The sample was placed into a corundum crucible. The mixture of nitrogen and argon 4:1 was used as an inert gas. The sample was heated 10 °C·min^{-1} from 30–800 °C. As a reference, an empty crucible was used. TGA/DTG/DSC analyzer automatically recalculated DSC data to mW·mg^{-1} and determined DTG from TG.

The TG data was used to determine kinetic parameters according to the Coats–Redfern (CR) method. The CR's kinetic triplet is activation energy (Ea), pre-exponential factor (A), and order of reaction (n). The methodology of CR determination was presented elsewhere [24].

2.2.5. Theoretical Mass and Energy Balance of the Torrefaction Process

Using part of the data from analyses that have been mentioned in the earlier paragraphs, theoretical energy balance for the torrefaction of PLA and paper waste was calculated. The calculations refer to the production of 1 g of CSF and include the determination of the:

- Mass of substrate used to produce 1 g of CSF;
- Energy contained in the raw material used to produce 1 g of CSF;
- External energy provided to the reactor to heat the proper amount of substrate to setup temperature, to produce 1 g of CSF;
- Energy contained in 1 g of CSF;
- Mass of gas generated during the production of 1 g of CSF;
- Energy contained in gas after production of 1 g of CSF.

For calculations, data of MY, HHV, and DSC results were used. The scheme of energy balance determination is shown in Figure 1. The green squares represent the order of calculations, the grey squares represent experimental/calculated data used for energy balance determination, and the blue squares stand for input and output data results.

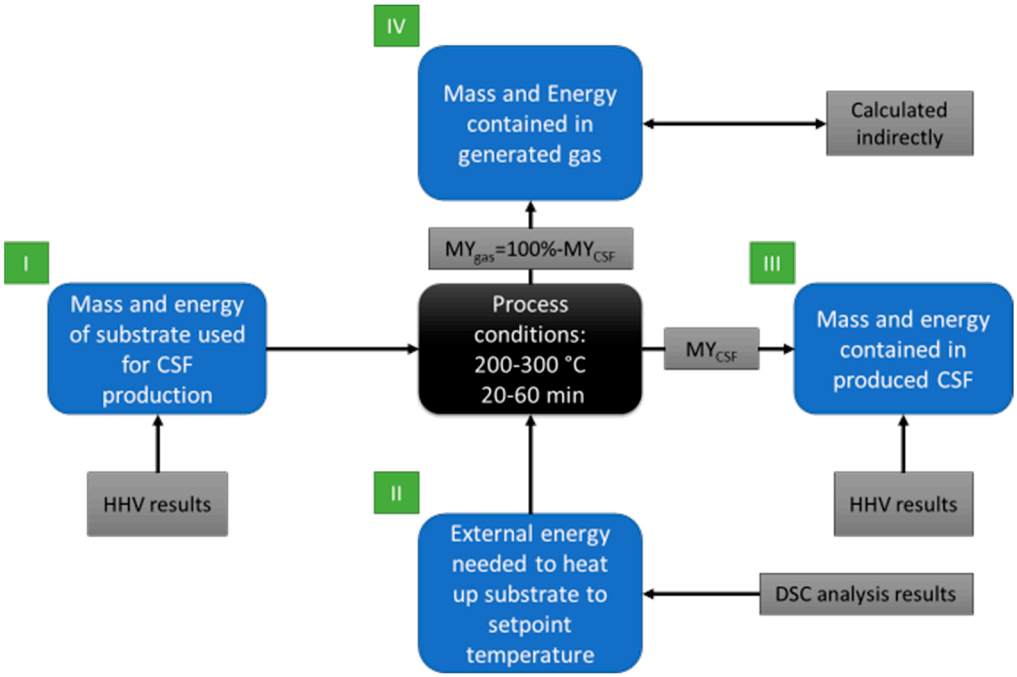

Figure 1. Scheme of mass and energy balance determination.

In step I, the mass yield of CSF production was used to determine the mass of substrate to produce 1 g of CSF by Equation (4), which allowed us to calculate the energy contained in the substrate used to produce 1 g of CSF by Equation (5).

$$M_s = \frac{Mr_{CSF}}{MY_{CSF}} \quad (4)$$

where: M_s—mass of substrate used to produce the required amount of CSF, (here 1 g), g; Mr_{CSF}—required mass of CSF, (here 1 g), g; and MY_{CSF}—mass yield of CSF production, % (Equation (1)).

$$E_s = M_s \cdot HHV_s \quad (5)$$

where: E_s—energy contained in the substrate used to produce CSF, J; M_s—mass of substrate used to produce CSF, g; and HHV_s—high heating value of substrate, $J \cdot g^{-1}$.

For step II, the results from DSC were used as input in the form of a power flow by the sample during heating. The DSC was converted from $mW \cdot mg^{-1}$ to J mg^{-1} by the multiplication by time in seconds, providing information about the energy in J used to increase the temperature for 1 g of substrate. The energy demand to heat to setpoint temperature and mass of substrate demand produce CSF per g were used to calculate the demand of external energy to produce 1 g of CSF.

For step III, it is assumed, that the energy contained in 1 g of CSF equals the HHV, which was determined by the experiment.

In step IV, the energy contained in the gas was calculated indirectly. The energy in the gas is assumed to be a sum of external energy from step II, and the difference between energy contained in substrate and energy contained in CSF obtained from torrefaction, following Equation (6).

$$E_{gas} = E_{external} + E_{substrate} - E_{CSF} \quad (6)$$

where: E_{gas}—energy contained in the gas, J; $E_{external}$—external energy provided to the-reactor to heat the substrate to setup temperature, J; $E_{substrate}$—energy contained in the substrate used to produce CSF, J; and E_{CSF}—energy contained in produced CSF, J.

To keep calculations as simple as possible, the calculations were performed following assumptions:

- Moisture content in substrate = 0%;
- External energy is used to provide heat for the process;
- No heat losses of the reactor;
- The energy contained in the gas is a sum of chemical energy related to the chemical composition of gas and heat; here it was assumed that CSF is cooled down after the process, and all heat goes to gas.

3. Results and Discussion

3.1. Torrefaction Process—CSF Production

In Figures 2–4, process temperature and time effect on mass yield, energy densification ratio, and energy yield of carbonized solid fuel made from PLA and PAP were presented. The equations for these models were summarized in Table A1.

The mass yield of CSF made from PLA was almost not affected by process conditions. Small weight loss was observed in CSF produced at 300 °C in 60 minutes, where the MY decrease to 92%. For comparison, MY of CSF started to decrease from the lowest temperatures, at 200 °C and 20 min, the MY had around 80%, which decreased to 40% at 300 °C and 60 min (Figure 2). The reason for the very high MY of CSF made from PLA is the PLA decomposition resistances in the torrefaction temperatures range. It has been confirmed later in this work by TG/DTG results, that PLA decomposition began around 290 °C, and peaked at 367 °C (Figure 5a). For comparison, the PAP's main decomposition started already around 240 °C and peaked at 326 °C (Figure 5a). Although TG/DTG results are useful to investigate the thermochemical characteristics of a material, such as the temperature of decomposition, it is insufficient to determine the mass yield in certain temperature regimes or reaction times for different reactors due to different geometries, sample sizes, or thermal properties. Depending on the temperature regime, which has the main effect on decomposition, the time can result in less or more significant mass losses, especially in temperature regimes that include the main decomposition reactions and long residence time [33]. Therefore, empirical models for MY of PLA and PAP samples were developed (Table A1) to correct the challenges of the experiments.

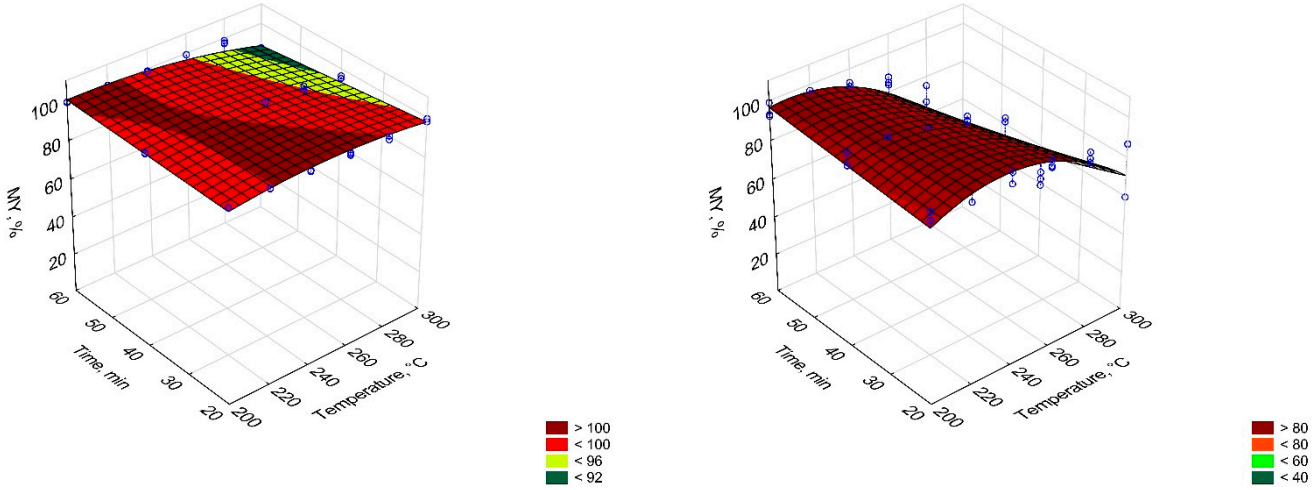

(**a**) (**b**)

Figure 2. Temperature and time effect on the mass yield (MY) of carbonized solid fuel made from (**a**) PLA, (**b**) PAP.

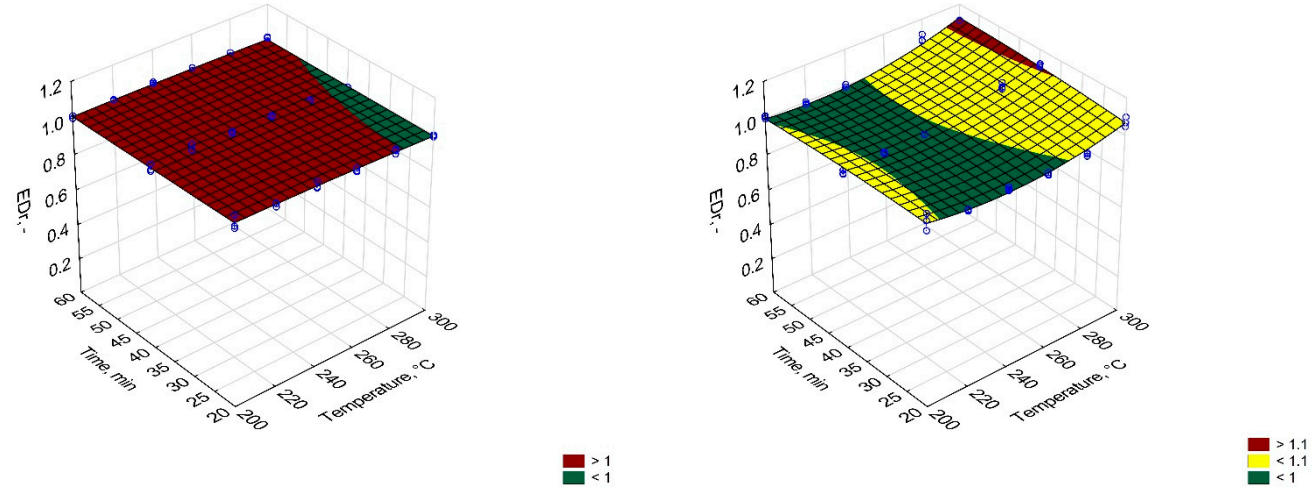

(**a**) (**b**)

Figure 3. Temperature and time effect on the energy densification ratio (EDr) of carbonized solid fuel made from (**a**) PLA and (**b**) PAP.

Figure 2 shows the process temperature and time effects on the energy densification ratio (EDr). The EDr shows how much more energy is contained in the CSF in comparison to unprocessed material. When EDr is equal to 1, no effect of a process for energy improvement is observed. When EDr is lower than 1, it means that there is less energy in CSF than it was initially in a substrate, and when EDr is higher than 1, it means that there is more energy in CSF than it was in a substrate. In this study, no statistically significant ($p > 0.05$) effect of torrefaction on EDr of PLA could be observed. However, a small effect of CSF made from paper could be observed. Here, EDr increased at a statistically significant level ($p < 0.05$) at setpoint temperatures higher than 280 °C.

The studied material was characterized by low enhancement in EDr. Typically, processed biomass is characterized by EDr from 1.2 to 1.4 [34]. The EDr increase was a result of the increase in HHV. The calorific value increase was probably a result of higher deoxygenation in comparison to the less intense decarbonization of material. When torrefaction temperature increases, the relative oxygen content decreases, in favor of relative carbon content which leads to an increase in HHV of CSF [35]. In the case of PLA, the process was below decomposed temperature so proper deoxygenation could not take place, while

the PAP probably did not release enough oxygen compared to carbon to significantly increase HHV.

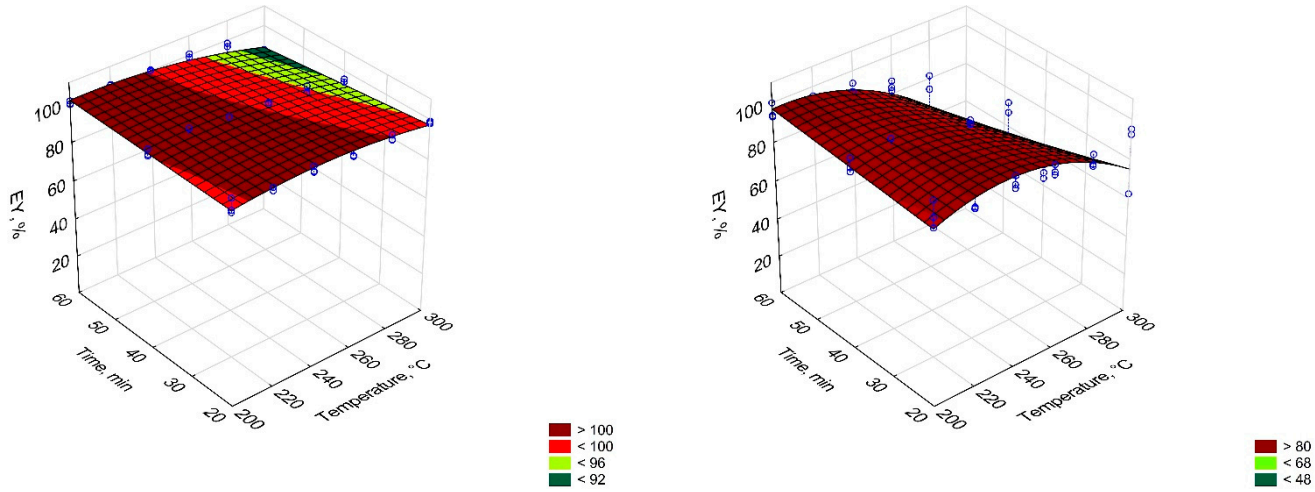

(**a**) (**b**)

Figure 4. Temperature and time effect on the energy yield (EY) of carbonized solid fuel made from (**a**) PLA and (**b**) PAP.

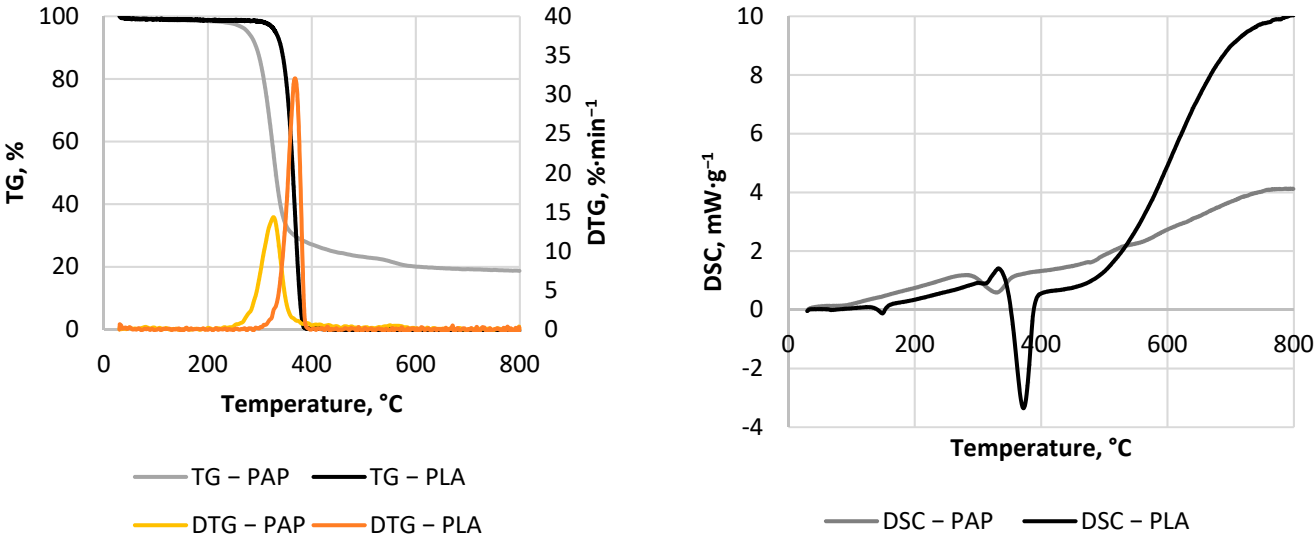

(**a**) (**b**)

Figure 5. Thermal analysis results, (**a**) TG/DTG, (**b**) DSC.

The energy yield (EY) shows how much energy that is contained in the substrate remains in the CSF after the process. With the increasing process temperature and time, the solid mass of substrate decreases as more gases and later also liquids are formed. Each of the products needs some chemical energy for its formation, which results in a decrease in the EY of CSF. Therefore, carbon and oxygen migration is an important factor during torrefaction [35]. The EY of CSF made from PLA was not affected by the process conditions for experimental conditions that were lower than 300 °C and 40 min (Figure 4). Under these conditions, MY remained constant and at lower temperatures, no significant changes in the HHV of torrefied PLA could be found. Therefore, the trend for EY was similar to MY. In the case of PAP, an EY decrease at temperatures higher than 280 °C was found, which resulted in a carbon migration to gas and liquid products [35,36].

3.2. Proximate Analysis and HHV Results

The samples of materials used to produce CSF were also analyzed for volatile matter (VM), ash content (AC), fixed carbon (FC), volatile solids (VS), combustibles parts (CP), and high heating value (HHV). The PLA materials had 100%, 0%, 0%, 100%, and 100% of VM, AC, FC, VS, and CP, respectively, while the PAP material had 88.2%, 3.6%, 8.2%, 96.3%, and 96.4% of VM, AC, FC, VS, and CP, respectively. The HHV of PLA and PAP were 19,420 and 17,525 J·g^{-1}, respectively (Table 1).

Table 1. Results of proximate analysis and calorific value of CSF, as dry basis.

Material	Temp., °C	Time, min	VM, %	FC, %	AC, %	VS, %	CP, %	HHV, J·g^{-1}
PLA	-	-	100.0	0.0	0.0	100.0	100.0	19,420
	200	20	100.0	0.0	0.0	100.0	100.0	19,675
		40	100.0	0.0	0.0	100.0	100.0	19,598
		60	100.0	0.0	0.0	100.0	100.0	19,512
	220	20	100.0	0.0	0.0	100.0	100.0	19,631
		40	100.0	0.0	0.0	100.0	100.0	19,799
		60	100.0	0.0	0.0	100.0	100.0	19,613
	240	20	100.0	0.0	0.0	100.0	100.0	19,703
		40	100.0	0.0	0.0	100.0	100.0	19,654
		60	100.0	0.0	0.0	100.0	100.0	19,682
	260	20	100.0	0.0	0.0	100.0	100.0	19,399
		40	100.0	0.0	0.0	100.0	100.0	19,372
		60	100.0	0.0	0.0	100.0	100.0	19,592
	280	20	100.0	0.0	0.0	100.0	100.0	19,529
		40	100.0	0.0	0.0	100.0	100.0	19,510
		60	100.0	0.0	0.0	100.0	100.0	19,410
	300	20	100.0	0.0	0.0	100.0	100.0	19,346
		40	100.0	0.0	0.0	100.0	100.0	19,294
		60	100.0	0.0	0.0	100.0	100.0	19,571
PAP	-	-	88.2	8.2	3.6	96.3	96.4	17,525
	200	20	86.6	9.9	3.4	96.6	96.6	17,889
		40	86.2	10.1	3.6	96.3	96.4	17,283
		60	86.7	9.8	3.5	96.5	96.5	17,653
	220	20	88.0	8.6	3.4	96.5	96.6	17,185
		40	86.7	10.0	3.3	96.4	96.7	17,504
		60	86.4	10.1	3.5	96.4	96.5	17,368
	240	20	85.5	10.9	3.5	96.3	96.5	17,446
		40	84.7	11.8	3.6	96.2	96.4	17,366
		60	84.8	11.7	3.5	96.2	96.5	17,434
	260	20	86.2	10.2	3.6	96.1	96.4	17,163
		40	84.0	12.4	3.6	96.0	96.4	17,389
		60	81.9	14.1	4.0	95.7	96.0	17,220
	280	20	83.6	12.7	3.7	96.3	96.3	17,352
		40	67.9	26.0	6.1	93.7	93.9	19,048
		60	66.9	26.2	7.0	92.8	93.0	19,146
	300	20	69.3	24.8	5.9	93.9	94.1	18,758
		40	60.8	31.5	7.7	91.8	92.3	19,520
		60	55.7	34.6	9.7	89.9	90.3	19,346

For PLA samples, an unexpected result was found for FC and AC, 0%, while VM, VS, and CP were 100%. The same results were obtained for all CSF made from PLA (Table 1). Moreover, the Tukey test shows that there were no significant changes between the HHV of CSF made from PLA. Therefore, it can be stated that torrefaction does not affect PLA fuel properties. These unexpected results can be explained in two ways: (I) The amount of ash (minerals) in PLA was too small to be detected by equipment that was used, or (II) there were no minerals in the PLA material at all. In case of a lack of minerals (case II), the results would be correct, as all organic matter was incinerated/devoltalized during experiments. In the other case (I), a correction for the undetected mass would have to be

performed. However, the error of the undetected mass is ±0.1 mg at an input of 1 g and therefore negligible.

In the literature, both cases can be found for PLA. In favor of assumption (II) were results from Camacho-Muñoz et al. [37] that showed 100% of vs. in a PLA sample. However, Jing et al. [38] showed that PLA is a type of thermally degradable material that burns at a relatively rapid heat release rate with negligible chars, suggesting that at least some FC should remain.

For CSF made of PAP, a decrease in VM with increasing temperature and time was observed. With increasing process temperature and time from 200 °C and 20 min to 300 °C and 60 min, the VM decreases from 86.6% to 55.7%, while FC and AC increase from 9.9% to 34.6%, and from 3.4% to 9.7%, respectively (Table 1). The observed decrease in VM is related to the devoltalization of materials. On a molecular level, large cellulose molecules in PAP are broken into smaller ones until they are small enough to be removed by convection [39]. Depending on the chemical composition, more or fewer of such small molecules are released and, as a result, different values of VM can be observed. Unlike VM, the AC and FC content increase mainly as a result of the loss in VM. Unlike AC, which is related to the mineral present in the sample, additional FC can be produced during secondary reactions [40]. Nevertheless, for biomass, the presence of components such as hemicellulose and cellulose is the main contributor of VM production, while lignin is the same for FC production [41].

Both tested materials were characterized by a relatively high level of VM, and low and zero content of FC (PAP and PLA, respectively). For comparison, wood biomass has 86% of VM, 15% of FC, and 0.4% of AC [42], torrefied wood at 300 °C in 30 min has 71% of VM, 29% of FC, and 0.4% of AC [43], while high-rank bituminous (coal) has 27.6% of VM, 65% of FC, and 7.4% of AC [44]. It is clear that fuel properties of torrefied paper and biodegradable plastic are not close to conventional solid fuels. Nevertheless, the positive aspect of PLA material is its zero-ash content, which decreases the costs for managing the ash.

The high heating value of 19.4 $MJ \cdot kg^{-1}$ for PLA is more than twice lower than that of conventional plastics such as polyethylene [45]. Moreover, torrefaction does not increase the HHV of PLA (Table 1). On the other hand, torrefaction was found to be suitable for PAP. The HHV of PAP increased from 17.5 $MJ \cdot kg^{-1}$ to 19.5 $MJ \cdot kg^{-1}$ in CSF produced at 300 °C; 40 min. Though these values seem to suffice when they are compared to energetic biomasses (HHV ~ 18 $MJ \cdot kg^{-1}$) [46], they are still small in comparison with coals 30 $MJ \cdot kg^{-1}$ [47] or conventional plastics 40 $MJ \cdot kg^{-1}$ [45].

3.3. Thermal Analysis Results

Figure 5a shows the TG/DTG results. The PLA mass was almost constant up to around 290 °C, where thermal decomposition started. The PLA decomposed totally in one step at temperatures of ~300–400 °C, with the maximum peak at 367 °C. Backes et al. [48] show that PLA composition (additive presence) affects thermal degradation, and some components reduce the activation energy of initiation of thermo-degradation reactions. As a result, the decomposition onset temperature and maximum peak can differ up to 40 °C depending on the processed PLA [48]. Additionally, maximum decomposition peaks occur at 353–385 °C [48]. The DSC analysis results are shown in Figure 5b. The analysis shows that during PLA pyrolysis several reactions related to polymer phase transition occurred. The first phase transition at 64 °C is the glass transition of PLA. At 149 °C, the endothermal melting transformation was observed and finally, at 372 °C, the main endothermal decomposition peak was found. These findings agreed well with the result of Sousa et al. [49]. The results show that, for some reason, the DSC decomposition peak was shifted in comparison to DTG at about 5 °C (Figure 5a,b). Nevertheless, these findings explain that torrefaction could not significantly change the properties of PLA, as the temperature was too low for efficient devolatilization.

For PAP, three peaks were observed by DTG. First at 80 °C, second at 326 °C, and third at 550 °C with 1.3%, 74.6%, and 5.4% mass change (Figure 5a, grey curve), respectively. The first and third peaks are almost not visible in Figure 5a. The first peak is related to residual water evaporation, while the second peak is probably related to cellulose decomposition. This is due to the fact that white paper is made mainly from cellulose, (85–99%) with the addition of lignin of 0–15% [50]. Nevertheless, reprocessed paper (e.g., newspaper) has less cellulose (40–55%), more lignin (18–30%), and comparable content hemicellulose (25–40%) in comparison to white paper [50]. Additionally, the previously mentioned substances could affect the PAP sample decomposition. Typically, the hemicellulose, cellulose, and lignin decompose at 225–325 °C, 305–375 °C, and 250–500 °C, respectively [51]. According to Porshnov et al. [52], the temperature range of 250–300 °C is a characteristic interval for hemicellulose decomposition, 300–350 °C for cellulose decomposition, while above 400 °C the residue of lignocellulosic substances decomposed at a very slow rate. Lignin decomposition reactions were reported to occur at up to 900 °C [52]. Therefore, it is highly probable that PAP's third peak is related to lignin decomposition. The DSC results showed that, during PAP pyrolysis, four endothermal transformations occurred. The first transformation at 91.4 °C was probably related to residual moisture removal [53], and the following transformations were related to the decomposition of elements of the PAP sample. Similar results were obtained by Yang et al. [53], who tested clean cellulose and found the main endothermal peak related to decomposition at 355 °C. In this study, this peak was found at 329.6 °C (Figure 5b) and, similarly to the PLA, the DSC peak of PAP was shifted in comparison to DTG at about 3.6 °C.

The kinetic parameters were determined at β = 10 °C·min^{-1} using the Coats–Redfern method. The kinetic triplets were determined for the whole process (30–800 °C) and the main peaks observed at TG/DTG plots (Figure 5a). The whole decomposition process for PAP and PLA were described by a reaction order of 1.56 and 2.02, respectively, and relative low activation energy of 33.11 kJ·(mol·K)$^{-1}$, and 46.24 kJ·(mol·K)$^{-1}$, respectively (Table 2). Here, it is worth noting that, for PLA, the determination coefficient was low, at 0.66, which was a result of the one-stage decomposition process, which occurred at 290–400 °C. Additionally, other kinetic triplets were determined with high determination coefficients (Table 2). The main PLA decomposition reaction was described by a reaction order of 0.42 and 160.05 kJ·(mol·K)$^{-1}$ activation energy, while PAP exhibited an order of 2.12, and 122.55 kJ·(mol·K)$^{-1}$ (Table 2). The first peak for PAP was omitted, as it was only residual water evaporation. It is worth noting that the suspected lignin decomposition at the third peak of the PAP sample had the highest activation energy of 173.05 kJ·(mol·K^{-1}), which was about 51 kJ·(mol·K)$^{-1}$ larger than the main decomposition of cellulose. This finding is contrary to Noszczyk et al. [54] who studied several types of biomass materials and noticed that the cellulose content had a significant impact on the E_a, and the highest E_a was observed at the second stage of reaction, which was related to the cellulose decomposition [54].

Table 2. Kinetic triplets determined at β = 10 °C·min^{-1} using Coats-Redfern method.

Material	Note	Temperature, °C	n	Ea, kJ·(mol·K)$^{-1}$	A, s^{-1}	R^2
PLA	Whole process	30–800	2.02	46.24	2.91×10	0.66
	Main decomposition peak	290–400	0.42	160.05	2.37×10^{10}	0.96
PAP	Whole process	30–800	1.56	33.11	5.88×10^{-1}	0.89
	Main decomposition peak	240–400	2.12	122.55	1.74×10^{8}	0.96
	Third decomposition peak	668–760	3.00	173.05	4.90×10^{10}	0.91

3.4. Theoretical Mass and Energy Balance of the Torrefaction Process

Table 3 summarizes the theoretical mass and energy balance to produce 1 g CSF s given. The table compares the temperature and time. The third and fourth headings present the input mass needed to produce 1 g of CSF, and the chemical energy contained in

this material. The fifth heading presents external heat provided to the torrefaction process. The sixth heading shows energy contained in 1 g of CSF. The seventh heading present a mass of gas released from the substrate during torrefaction, and the last heading show energy contained in this gas. The energy in gas was calculated as a sum of external energy provided to conduct a process and energy of substrate that was not converted into CSF.

Table 3. Torrefaction mass and energy balance for production of 1 g of CSF from PLA and Paper wastes.

Temp., °C	Time, min	Mass of Substrate Used to Produce 1 g of CSF, g		Energy Contained in the Raw Material Used to Produce 1 g of CSF, J		External Energy Needed to Produce 1 g of CSF, J *		Energy Contained in 1 g of CSF, J **		Mass of Gas Generated during the Production of 1 g of CSF, g		Energy Contained in Gas after Production of 1 g of CSF, J ***	
		PLA	PAP	PLA	PAP	PLA	PAP	PLA	PAP	PLA	PAP	PLA	PAP
200	20	1.004	1.054	19,500	18,475	86	328	19,675	17,889	0.004	0.054	−89	914
	40	1.006	1.048	19,540	18,367	86	328	19,598	17,283	0.006	0.048	27	1412
	60	1.006	1.055	19,538	18,482	86	328	19,512	17,653	0.006	0.055	112	1157
220	20	1.003	1.074	19,483	18,817	133	425	19,631	17,185	0.003	0.074	−15	2056
	40	1.004	1.053	19,505	18,459	133	425	19,799	17,504	0.004	0.053	−161	1380
	60	1.007	1.060	19,552	18,582	133	425	19,613	17,368	0.007	0.060	72	1639
240	20	1.005	1.053	19,512	18,454	194	536	19,703	17,446	0.005	0.053	3	1543
	40	1.007	1.078	19,562	18,886	194	536	19,654	17,366	0.007	0.078	101	2056
	60	1.013	1.096	19,676	19,207	194	536	19,682	17,434	0.013	0.096	188	2309
260	20	1.010	1.066	19,608	18,683	267	663	19,399	17,163	0.010	0.066	477	2184
	40	1.011	1.102	19,642	19,308	267	663	19,372	17,389	0.011	0.102	537	2583
	60	1.007	1.170	19,562	20,499	267	663	19,592	17,220	0.007	0.170	237	3942
280	20	1.014	1.131	19,685	19,822	355	803	19,529	17,352	0.014	0.131	510	3273
	40	1.025	1.357	19,909	23,778	355	803	19,510	19,048	0.025	0.357	754	5534
	60	1.022	1.550	19,839	27,163	355	803	19,410	19,146	0.022	0.550	784	8820
300	20	1.012	1.288	19,646	22,571	458	940	19,346	18,758	0.012	0.288	758	4753
	40	1.043	2.357	20,247	41,303	458	940	19,294	19,520	0.043	1.357	1,410	22,722
	60	1.227	2.485	23,833	43,551	458	940	19,571	19,346	0.227	1.485	4,719	25,144

* value determined using DSC analysis result. ** value determined using calorimetric analysis result (HHV). *** value is the sum of chemical energy contained in gas and heat from external energy, assuming that no external energy stays in CSF.

The result shows that more PAP than PLA substrate is needed to produce 1 g of CSF. In the case of 300 °C at 60 min, the double mass of PAP is needed compared to PLA (Table 3). The reason for this large input substrate demand originates from the low mass yield of PAP torrefaction (Figure 2b). As a result, much more chemical energy contained in PAP is put into the process to produce 1 g of CSF (23,833 J for PLA vs. 43,551 J for PAP). Additionally, the DSC results showed that more energy was needed to heat PAP than PLA to 300 °C, (458 $J \cdot g^{-1}_{CSF}$ vs. 940 $J \cdot g^{-1}_{CSF}$) (Table 3). This is caused probably by the mostly higher specific heat value (Sp) of PAP in comparison to PLA. Depending on chemical composition, Sp of PAP varies from 1150 to 1650 $J \cdot (g \cdot K)^{-1}$ [55] while, for PLA, the value varies from 1180 to 1210 $J \cdot (g \cdot K)^{-1}$ [56]. On the other hand, PLA has a higher thermal conductivity, 0.12–0.15 $W \cdot (m \cdot K)^{-1}$ than PAP 0.08–0.11 $W \cdot (m \cdot K)^{-1}$ [55,56].

During torrefaction, torrgas are produced. The analysis showed that a small mass of torrgas is produced from PLA and, depending on process conditions, these vary from 0.004 $g \cdot g^{-1}_{CSF}$ to 0.227 $g \cdot g^{-1}_{CSF}$. As the production of 1 g of CSF from PAP needs far more substrate, much more torrgas is produced and varies from 0.054 $g \cdot g^{-1}_{CSF}$ to 1.485 $g \cdot g^{-1}_{CSF}$ (Table 3). As a result, during torrefaction at 300 °C, for each gram of produced CSF, around 1.5 g of torrgas is generated, and these torrgas contain more energy than produced CSF, while for PLA it is only 0.23 g of torrgas with around four times less energy than produced CSF (Table 3).

When energy contained in torrgas is higher than the external energy needed to produce CSF, it theoretically can be assumed that the process is self-sufficient. This is true when torrgas are incinerated to provide heat for a substrate. With that assumption can be stated that PLA torrefaction can be self-sufficient at process temperatures higher than 300 °C and 40 min, while PAP is similar from 200 °C and 20 min (Table 3). Nevertheless, these results do not include heat losses, process efficiency, and energy needed for water evaporation that is in the real feedstock. Due to many different approaches to reactors design, it is hard to assume any heat losses and process efficiency. However, the contribution of water can be calculated and added to the results obtained in this study. To remove 1% of the water from solid fuel, at least 22.57 J (2257 $J \cdot g^{-1}_{H2O}$ is the latent heat of water evaporation at 100 °C) is needed, as well as the energy needed to heat this water to 100 °C [57]. For this

reason, the herein presented calculations serve as a starting point that has to be adapted for a particular reactor system and different feedstocks.

4. Summary

The results of this study showed that PLA's fuel properties cannot be improved by torrefaction, as no calorific values increase were observed with increasing process temperature and time. The reason is that PLA hardly decomposes, with negligible charring effects at torrefaction temperatures. On the other hand, PAP's fuel properties can be improved up to 10% by applying temperatures higher than 280 °C, which is probably caused by a partial cellulose decomposition. Additionally, the kinetic analysis revealed that PLA is decomposed in a one-stage process, that takes place at ~290–400 °C, with Ea of 160.05 kJ·(mol·K)$^{-1}$, while PAP is decomposed in a two-stage process, at ~240–400 °C, and ~668–760 °C, with Ea of 122.55 kJ·(mol·K)$^{-1}$ and 173.05 kJ·(mol·K)$^{-1}$, respectively. Moreover, the calculations showed that PLA torrefaction cannot be self-sufficient for CSF production and external energy is required, while CSF production from PAP proves to be self-sufficient under assumptions of no heat loss.

These results provide the first step towards an understanding of the PLA torrefaction process, but further research is needed to investigate higher temperatures of thermal PLA processing embracing gaseous and liquid products rather than solids, as PLA decomposes entirely into volatile components. Moreover, future studies should focus on PLA co-pyrolysis with conventional plastic, as a separation in waste management facilities is currently not possible from the MSW stream. Such a separation may be possible for separately collected and clean plastic wastes, but will fail in the case of plastics with organic adhesions, which are typical for plastic in MSW.

Regarding waste management scenarios, our study showed that the thermal properties of PLA qualify this material neither as a fuel surrogate in waste incinerators nor for an improvement by torrefaction process when we compare PLA with conventional high energy plastics. Therefore, a successive substitution of high caloric plastics by PLA may be reasonable when the end-of-life-scenario for the material is composting, but will raise the demand of conventional fuel when its thermally treated.

Supplementary Materials: The following are available online at https://www.mdpi.com/article/10.3390/ma14227051/s1, Table S1: CSF Production, Table S2: Proximate Analysis, Table S3: TG-DTG-DSC.

Author Contributions: Conceptualization, K.Ś; methodology, K.Ś.; software, K.Ś.; validation, K.Ś. and A.B, formal analysis, K.Ś.; investigation, K.Ś.; resources, K.Ś and A.B.; data curation, K.Ś.; writing—original draft preparation, K.Ś; writing—review and editing, K.Ś., C.Z., and A.B; visualization, K.Ś.; supervision, C.Z. and A.B.; project administration, K.Ś.; and funding acquisition, A.B. All authors have read and agreed to the published version of the manuscript.

Funding: This research received no external funding.

Institutional Review Board Statement: Not applicable.

Informed Consent Statement: Not applicable.

Data Availability Statement: All data derived during the experiments are given in the paper or the Supplementary Materials.

Acknowledgments: The presented article results were obtained as part of the activity of the leading research team—Waste and Biomass Valorization Group (WBVG). Paper has been prepared during research scholarship of Kacper Świechowski at BOKU financed under the Leading Research Groups support project from the subsidy increased for the period 2020–2025 in the amount of 2% of the subsidy referred to Art. 387 (3) of the Law of 20 July 2018 on Higher Education and Science, obtained in 2019—project number N040/0012/20.

Conflicts of Interest: The authors declare no conflict of interest.

Glossary

PLA	polylactic acid
PAP	paper
CSF	carbonized solid fuel
EU	European Union
HD-PE	high-density polyethylene
PET	polyethylene terephthalate
LD-PE	low-density polyethylene
RDF	refuse-derived fuel
MSW	municipal solid waste
SRF	solid recovered fuel
MBT	mechanical-biological treatment plant for waste
PP	Polypropylene
PE	Polyethylene
PS	Polystyrene
HHV	higher heating value
TGA	thermogravimetric analysis
DSC	differential scanning calorimetry analysis
MY	mass yield
EDr	energy densification ratio
EY	energy yield
MC	moisture content
VM	volatile matter
AC	ash content
VS	volatile solids content
CP	combustible part content
R^2	determination coefficient
AIC	Akaike value
a_n	regression coefficients,
DTG	differential thermogravimetry
CR	Coats–Redfern method
Ea	activation energy
A	pre-exponential factor
n	order of reaction
Sp	specific heat value

Appendix A

In Figure A1, the predictions of RDFs HHV depending on biodegradable plastic share in conventional plastic was presented. The calculation was completed using data from previous work [58]. Predictions were made based on the following assumptions: RDF components (component name, component share, components HHV): carton, 10%, 14.6 $MJ \cdot kg^{-1}$; fabric 10%, 17.6 $MJ \cdot kg^{-1}$; kitchen waste 5%, 16,4 $MJ \cdot kg^{-1}$; paper 10%, 13.8 $MJ \cdot kg^{-1}$; plastic 50%, 38.5 $MJ \cdot kg^{-1}$; rubber 5%, 31 $MJ \cdot kg^{-1}$; tetrapack 5%, 21.6 $MJ \cdot kg^{-1}$; and wood 5%, 18.7 $MJ \cdot kg^{-1}$ [58]. The HHV of biodegradable plastic 19 $MJ \cdot kg^{-1}$ [this study].

In Table A1, torrefaction temperature and time effect on process yields and fuel properties are summarized. Presented equations are valid for CSF properties determination at T = 200–300 °C and t = 20–60 min. The R^2 stands for the determination coefficient. The higher = better.

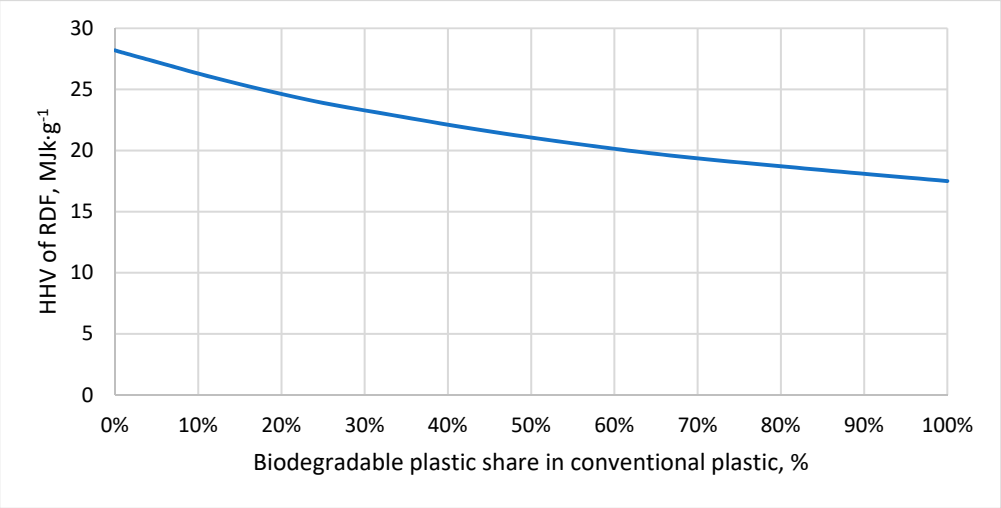

Figure A1. Effect of biodegradable plastic share in conventional plastic on RDF quality.

Table A1. Empirical equations for determination of torrefaction process and fuel properties of CSF produced from PLA and PAP; the equations boundary, T = 200–300 °C, t = 20–60 min.

Material	Equation	R^2
PLA	$MY(T,t), \% = 0.759 \times T - 0.00139 \times T^2 + 0.678 \times t - 0.00303 \times T \times t$	0.55
	$EDr(T,t), \% = 0.975 + 0.000545 \times T - 0.00000160 \times T^2 - 0.00101 \times t + 0.00000220 \times t^2 + 0.00000340 \times T \times t$	0.13
	$EY(T,t), \% = 0.792 \times T - 0.00151 \times T^2 + 0.596 \times t - 0.00270 \times T \times t$	0.58
	$VM, \% = 100$	1.00
	$FC, \% = 0$	1.00
	$AC, \% = 0$	1.00
	$VS, \% = 100$	1.00
	$CP, \% = 100$	1.00
	$HHV, J \cdot g^{-1} = 19549 \pm 140$	1.00
PAP	$MY(T,t), \% = -340.901 + 3.558 \times T - 0.00712 \times T^2 + 2.079 \times t - 0.00952 \times T \times t$	0.86
	$EDr(T,t), \% = 2.404 - 0.0119 \times T + 0.0000243 \times T^2 - 0.00189 \times t - 0.0000268 \times t^2 + 0.0000184 \times T \times t$	0.77
	$EY(T,t), \% = -260.469 + 2.876 \times T - 0.00570 \times T^2 + 1.946 \times t - 0.00889 \times T \times t$	0.78
	$VM(T,t), \% = -153.308 + 2.021 \times T - 0.00418 \times T^2 + 0.899 \times t - 0.00421 \times T \times t$	0.92
	$FC(T,t), \% = 184.153 - 1.583 \times T + 0.00336 \times T^2 - 0.00609 \times t^2 + 0.00245 \times T \times t$	0.90
	$AC(T,t), \% = 53.879 - 0.409 \times T + 0.000815 \times T^2 - 0.232 \times t + 0.00105 \times T \times t$	0.94
	$VS, \% = 47.732 + 0.396 \times T - 0.000790 \times T^2 + 0.239 \times t - 0.00109 \times T \times t$	0.94
	$CP(T,t), \% = 46.120 + 0.409 \times T - 0.000815 \times T^2 + 0.232 \times t - 0.00105 \times T \times t$	0.94
	$HHV(T,t), J \cdot g^{-1} = 39{,}926.103 - 198.210 \times T + 0.425 \times T^2 + 0.0447 \times T \times t$	0.77

References

1. Narancic, T.; O'Connor, K.E. Plastic waste as a global challenge: Are biodegradable plastics the answer to the plastic waste problem? *Microbiology* **2019**, *165*, 129–137. [CrossRef] [PubMed]
2. North, E.J.; Halden, R.U. Plastics and environmental health: The road ahead. *Rev. Environ. Health* **2013**, *28*, 1–8. [CrossRef]
3. Jambeck, J.R.; Geyer, R.; Wilcox, C.; Siegler, T.R.; Perryman, M.; Andrady, A.; Narayan, R.; Lavender Law, K. Plastic waste inputs from land into the ocean. *Science* **2015**, *347*, 768–771. [CrossRef]
4. Katyal, D.; Kong, E.; Villanueva, J. Microplastics in the environment: Impact on human health and future mitigation strategies. *Environ. Health Rev.* **2020**, *63*, 27–31. [CrossRef]
5. Geyer, R.; Jambeck, J.R.; Law, K.L. Production, use, and fate of all plastics ever made. *Sci. Adv.* **2017**, *3*, e1700782. [CrossRef]
6. PlascticsEurope. Plastics—The Facts 2020 An analysis of European Plastics Production, Demand and Waste Data. 2020. Available online: https://plasticseurope.org/knowledge-hub/plastics-the-facts-2020/ (accessed on 15 November 2021).
7. Qureshi, M.S.; Oasmaa, A.; Pihkola, H.; Deviatkin, I.; Tenhunen, A.; Mannila, J.; Minkkinena, H.; Pohjakallioc, M.; Laine-Ylijokid, J. Pyrolysis of plastic waste: Opportunities and challenges. *J. Anal. Appl. Pyrolysis* **2020**, *152*, 104804. [CrossRef]
8. Rujnić-Sokele, M.; Pilipović, A. Challenges and opportunities of biodegradable plastics: A mini review. *Waste Manag. Res.* **2017**, *35*, 132–140. [CrossRef] [PubMed]

9. Conversio Market & Strategy. Global Plastic Flow 2018. 2020. Available online: https://www.carboliq.com/pdf/19_conversio_global_plastics_flow_2018_summary.pdf (accessed on 15 November 2021).
10. Ellen Macarthur Foundation. The New Plastics Economy: Rethinking the Future of Plastics & Catalysing Action. 2017. Available online: https://ellenmacarthurfoundation.org/the-new-plastics-economy-rethinking-the-future-of-plastics-and-catalysing (accessed on 15 November 2021).
11. Dilkes-Hoffman, L.S.; Pratt, S.; Lant, P.A.; Laycock, B. The role of biodegradable plastic in solving plastic solid waste accumulation. In *Plastics to Energy: Fuel, Chemicals, and Sustainability Implications*; Elsevier: Amsterdam, The Netherlands, 2018; pp. 469–505. [CrossRef]
12. European Bioplastic Conference. Bioplastics Market Development 2020. 2020. Available online: https://docs.european-bioplastics.org/conference/Report_Bioplastics_Market_Data_2020_short_version.pdf (accessed on 15 November 2021).
13. European Environment Agency. *Bio-Waste in Europe-Turning Challenges into Opportunities*; Van der Linden, A., Almut, R., Eds.; European Environment Agency: Copenhagen, Denmark, 2020. [CrossRef]
14. Singh, N.; Hui, D.; Singh, R.; Ahuja, I.P.S.; Feo, L.; Fraternali, F. Recycling of plastic solid waste: A state of art review and future applications. *Compos. Part B Eng.* **2017**, *115*, 409–422. [CrossRef]
15. Eriksson, O.; Finnveden, G. Plastic waste as a fuel—CO_2-neutral or not? *Energy Environ. Sci.* **2009**, *2*, 907–914. [CrossRef]
16. Boumanchar, I.; Chhiti, Y.; M'hamdi Alaoui, F.E.; Sahibed-dine, A.; Bentiss, F.; Jama, C.; Bensitel, M. Municipal solid waste higher heating value prediction from ultimate analysis using multiple regression and genetic programming techniques. *Waste Manag. Res.* **2019**, *37*, 578–589. [CrossRef]
17. Dianda, P.; Mahidin, M.; Munawar, E. Production and characterization refuse derived fuel (RDF) from high organic and moisture contents of municipal solid waste (MSW). In *IOP Conference Series: Materials Science and Engineering*; Institute of Physics Publishing: Banda Aceh, Indonesia, 2018; Volume 334. [CrossRef]
18. Gug, J.I.; Cacciola, D.; Sobkowicz, M.J. Processing and properties of a solid energy fuel from municipal solid waste (MSW) and recycled plastics. *Waste Manag.* **2015**, *35*, 283–292. [CrossRef] [PubMed]
19. Świechowski, K.; Stępień, P.; Syguła, E.; Koziel, J.; Białowiec, A. Lab-Scale Study of Temperature and Duration Effects on Carbonized Solid Fuels Properties Produced from Municipal Solid Waste Components. *Materials* **2021**, *14*, 1191. [CrossRef] [PubMed]
20. Wielgosiński, G. Thermal Waste Conversion. Racibórz: Nowa Energia. 2020. Available online: https://nowa-energia.com.pl/wydawnictwa-ksiazkowe/ (accessed on 15 November 2021).
21. Caputo, A.C.; Pelagagge, P.M. RDF production plants: I Design and costs. *Appl. Therm. Eng.* **2002**, *22*, 423–437. [CrossRef]
22. Nobre, C.; Vilarinho, C.; Alves, O.; Mendes, B.; Gonçalves, M. Upgrading of refuse derived fuel through torrefaction and carbonization: Evaluation of RDF char fuel properties. *Energy* **2019**, *181*, 66–76. [CrossRef]
23. Syguła, E.; Świechowski, K.; Stępień, P.; Koziel, J.A.; Białowiec, A. The Prediction of Calorific Value of Carbonized Solid Fuel Produced from Refuse-Derived Fuel in the Low-Temperature Pyrolysis in CO_2. *Materials* **2020**, *14*, 49. [CrossRef]
24. Syguła, E.; Świechowski, K.; Hejna, M.; Kunaszyk, I.; Białowiec, A. Municipal Solid Waste Thermal Analysis—Pyrolysis Kinetics and Decomposition Reactions. *Energies* **2021**, *14*, 4510. [CrossRef]
25. Miranda, T.; Nogales, S.; Román, S.; Montero, I.; Arranz, J.I.; Sepúlveda, F.J. Control of several emissions during olive pomace thermal degradation. *Int. J. Mol. Sci.* **2014**, *15*, 18349–18361. [CrossRef]
26. Abd-Elghany, M.; Klapötke, T.M. A review on differential scanning calorimetry technique and its importance in the field of energetic materials. *Phys. Sci. Rev.* **2018**, *3*, 103. [CrossRef]
27. Mansa, R.; Zou, S. Thermogravimetric analysis of microplastics: A mini review. *Environ. Adv.* **2021**, *5*, 100117. [CrossRef]
28. PN-EN 14346:2011 Standard. Waste Characteristics. Calculation of Dry Mass on the Basis of Dry Residue or Water Content. Available online: https://sklep.pkn.pl/pn-en-14346-2011p.html (accessed on 15 November 2021).
29. Torquato, L.D.M.; Crnkovic, P.M.; Ribeiro, C.A.; Crespi, M.S. New approach for proximate analysis by thermogravimetry using CO_2 atmosphere: Validation and application to different biomasses. *J. Therm. Anal. Calorim.* **2017**, *128*, 1–14. [CrossRef]
30. PN-Z-15008-04:1993 Standard. Municipal Solid Waste. Analysis of Combustible and Non-Combustible Content. Available online: https://sklep.pkn.pl/pn-z-15008-04-1993p.html (accessed on 15 November 2021).
31. PN-EN 15169:2011 Standard. Waste Characteristics. Determination of Organic Matter Content for Waste, Slurry and Sludge. Available online: https://sklep.pkn.pl/pn-en-15169-2011p.html (accessed on 15 November 2021).
32. PN EN ISO 18125:2017-07 Solid Biofuels—Determination of Calorific Value. Available online: https://sklep.pkn.pl/pn-en-iso-18125-2017-07p.html (accessed on 15 November 2021).
33. Poudel, J.; Karki, S.; Oh, S.C. Valorization of waste wood as a solid fuel by torrefaction. *Energies* **2018**, *11*, 1641. [CrossRef]
34. Dyjakon, A.; Noszczyk, T. Alternative fuels from forestry biomass residue: Torrefaction process of horse chestnuts, oak acorns, and spruce cones. *Energies* **2020**, *13*, 2468. [CrossRef]
35. Chen, D.; Gao, A.; Cen, K.; Zhang, J.; Cao, X.; Ma, Z. Investigation of biomass torrefaction based on three major components: Hemicellulose, cellulose, and lignin. *Energy Convers. Manag.* **2018**, *169*, 228–237. [CrossRef]
36. Tumuluru, J.S.; Sokhansanj, S.; Hess, J.R.; Wright, T.C.; Boardman, R.D. A review on biomass torrefaction process and product properties for energy applications. *Ind. Biotechnol.* **2011**, *7*, 384–401. [CrossRef]
37. Camacho-Muñoz, R.; Villada-Castillo, H.S.; Solanilla-Duque, J.F. Anaerobic biodegradation under slurry thermophilic conditions of poly(lactic acid)/starch blend compatibilized by maleic anhydride. *Int. J. Biol. Macromol.* **2020**, *163*, 1859–1865. [CrossRef]

38. Jing, J.; Zhang, Y.; Tang, X.; Fang, Z. Synthesis of a highly efficient phosphorus-containing flame retardant utilizing plant-derived diphenolic acids and its application in polylactic acid. *RSC Adv.* **2016**, *6*, 49019–49027. [CrossRef]
39. Caillat, S.; Vakkilainen, E. Large-scale biomass combustion plants: An overview. In *Biomass Combustion Science, Technology and Engineering*; Woodhead Publishing Limited: Sawston, UK, 2013; pp. 189–224. [CrossRef]
40. Elyounssi, K.; Blin, J.; Halim, M. High-yield charcoal production by two-step pyrolysis. *J. Anal. Appl. Pyrolysis* **2010**, *87*, 138–143. [CrossRef]
41. Narzari, R.; Borkotoki, B. Chapter 2-Biochar: An Overview on its Production, Properties and Potential Benefits. In *Biology, Biotechnology and Sustainable Development*; Research India Publications: Delhi, India, 2015.
42. Tong, S.; Xiao, L.; Li, X.; Zhu, X.; Liu, H.; Luo, G.; Worasuwannarak, N.; Kerdsuwan, S.; Fungtammasan, B.; Yao, H. A gas-pressurized torrefaction method for biomass wastes. *Energy Convers. Manag.* **2018**, *173*, 29–36. [CrossRef]
43. Ramos-Carmona, S.; Pérez, J.F.; Pelaez-Samaniego, M.R.; Barrera, R.; Garcia-Perez, M. Effect of torrefaction temperature on properties of patula pine. *Maderas: Cienc. Y Tecnol.* **2017**, *19*, 39–50. [CrossRef]
44. Yi, L.; Feng, J.; Qin, Y.H.; Li, W.Y. Prediction of elemental composition of coal using proximate analysis. *Fuel* **2017**, *193*, 315–321. [CrossRef]
45. Zhou, H.; Meng, A.; Long, Y.; Li, Q.; Zhang, Y. An overview of characteristics of municipal solid waste fuel in China: Physical, chemical composition and heating value. *Renew. Sustain. Energy Rev.* **2014**, *36*, 107–122. [CrossRef]
46. Słupska, M.; Dyjakon, A.; Stopa, R. Determination of strength properties of energy plants on the example of miscanthus-giganteus, rosa multiflora and salix viminalis. *Energies* **2019**, *12*, 3660. [CrossRef]
47. Parikh, J.; Channiwala, S.A.; Ghosal, G.K. A correlation for calculating HHV from proximate analysis of solid fuels. *Fuel* **2005**, *84*, 487–494. [CrossRef]
48. Backes, E.H.; Pires, L.d.N.; Costa, L.C.; Passador, F.R.; Pessan, L.A. Analysis of the degradation during melt processing of pla/biosilicate® Composites. *J. Compos. Sci.* **2019**, *3*, 52. [CrossRef]
49. Sousa, S.; Costa, A.; Silva, A.; Simões, R. Poly(lactic acid)/Cellulose films produced from composite spheres prepared by emulsion-solvent evaporation method. *Polymers* **2019**, *11*, 66. [CrossRef] [PubMed]
50. Byadgi, S.A.; Kalburgi, P.B. Production of Bioethanol from Waste Newspaper. *Procedia Environ. Sci.* **2016**, *35*, 555–562. [CrossRef]
51. Van der Stelt, M.J.C. *Chemistry and Reaction Kinetics of Biowaste Torrefaction*; Technische Universiteit Eindhoven: Eindhoven, The Netherlands, 2011.
52. Porshnov, D.; Ozols, V.; Ansone-Bertina, L.; Burlakovs, J.; Klavins, M. Thermal decomposition study of major refuse derived fuel components. *Energy Procedia* **2018**, *147*, 48–53. [CrossRef]
53. Yang, H.; Yan, R.; Chen, H.; Lee, D.H.; Zheng, C. Characteristics of hemicellulose, cellulose and lignin pyrolysis. *Fuel* **2007**, *86*, 1781–1788. [CrossRef]
54. Noszczyk, T.; Dyjakon, A.; Koziel, J.A. Kinetic parameters of nut shells pyrolysis. *Energies* **2021**, *14*, 682. [CrossRef]
55. Lavrykov, S.A.; Ramarao, B.V. Thermal Properties of Copy Paper Sheets. *Dry. Technol.* **2012**, *30*, 297–311. [CrossRef]
56. Zmeskal, O.; Marackova, L.; Lapcikova, T.; Mencik, P.; Prikryl, R. Thermal properties of samples prepared from polylactic acid by 3D printing. *AIP Conf. Proc.* **2020**, *2305*, 020022. [CrossRef]
57. Water-Heat of Vaporization Online Water Heat of Vaporization Calculator. Available online: https://www.engineeringtoolbox.com/water-properties-d_1573.html (accessed on 15 November 2021).
58. Świechowski, K.; Syguła, E.; Koziel, J.A.; Stępień, P.; Kugler, S.; Manczarski, P.; Białowiec, A. Low-Temperature Pyrolysis of Municipal Solid Waste Components and Refuse-Derived Fuel—Process Efficiency and Fuel Properties of Carbonized Solid Fuel. *Data* **2020**, *5*, 48. [CrossRef]

Załącznik nr 3

Kacper Świechowski
imię i nazwisko

WROCŁAU 28.02.2022
(miejscowość i data)

Katedr Biogospodarki Stosowanej
Uniwersytet Przyrodniczy we Wrocławiu
51-630 Wrocław, Chełmońskiego 37a
afiliacja

OŚWIADCZENIE

Oświadczam, że w pracy:

Kacper Świechowski, Christian Zafiu, Andrzej Białowiec. 2021. Carbonized Solid Fuel Production from Polylactic Acid and Paper Waste Due to Torrefaction. Materials, 14, 7051. doi.org/10.3390/ma14227051.

mój udział polegał na:

Pozyskanie materiałów badawczych i przeprowadzeniu badań zgodnie z metodyką zawartą w artykule. Opracowaniu wyników z badań pod względem statystycznym przy wykorzystaniu oprogramowania Statistica. Opracowanie polegało w szczególności na wyznaczeniu modeli wpływu parametrów technologicznych (czasu i temperatury) toryfikacji na zmianę właściwości paliwowych badanych materiałów, wyznaczeniu parametrów kinetycznych toryfikacji w warunkach nieizotermicznych, wyznaczeniu ilości energii potrzebnej do toryfikacji. Ponadto byłem odpowiedzialny za napisanie pierwszej wersji manuskryptu. Jako autor korespondencyjny byłem odpowiedzialny za wykonywanie recenzji.

28.02.2022 Świechowski
data i podpis

Appendix No. 3

Christian Zafiu
name and surname

23.02.22
(place and date)

Department of Water, Atmosphere and Environment
Institute of Waste Management
University of Natural Resources and Life Sciences,
Muthgasse 107, 1190 Wien, Austria
affiliation

STATEMENT

I declare that in publication:
Kacper Świechowski, Christian Zafiu, Andrzej Białowiec. 2021. Carbonized Solid Fuel Production from Polylactic Acid and Paper Waste Due to Torrefaction. Materials, 14, 7051. doi.org/10.3390/ma14227051.

my participation in work was:
I actively supervised the work of Kacper Świechowski during the preparation of the part of the manuscript related to the bioplastics, and plastics. I revised the initial manuscript and I took part in reviewing process.

.....
(date and signature)

Załącznik nr 3

Andrzej Białowiec
imię i nazwisko

Wrocław, 26.02.2022
(miejscowość i data)

Katedr Biogospodarki Stosowanej
Uniwersytet Przyrodniczy we Wrocławiu
51-630 Wrocław, Chełmońskiego 37a
afiliacja

OŚWIADCZENIE

Oświadczam, że w pracy:
Kacper Świechowski, Christian Zafiu, Andrzej Białowiec. 2021. Carbonized Solid Fuel Production from Polylactic Acid and Paper Waste Due to Torrefaction. Materials, 14, 7051. doi.org/10.3390/ma14227051.

mój udział polegał na:
Nadzorowaniu poprawności wykonywanych badań, sprawdzeniu poprawności uzyskanych wyników oraz sprawdzeniu pierwszej wersji manuskryptu. Pozyskałem także część finansowania na wykonanie badań. Brałem udział w procesie recenzji.

26.02.2022
data i podpis